

Universiteit
Leiden
The Netherlands

Immunogenicity and tumorigenicity of pluripotent stem cells

Kooreman, N.G.

Citation

Kooreman, N. G. (2020, February 13). *Immunogenicity and tumorigenicity of pluripotent stem cells*. Retrieved from https://hdl.handle.net/1887/85322

Version:	Publisher's Version
License:	Licence agreement concerning inclusion of doctoral thesis in the Institutional Repository of the University of Leiden
Downloaded from:	https://hdl.handle.net/1887/85322

Note: To cite this publication please use the final published version (if applicable).

Cover Page

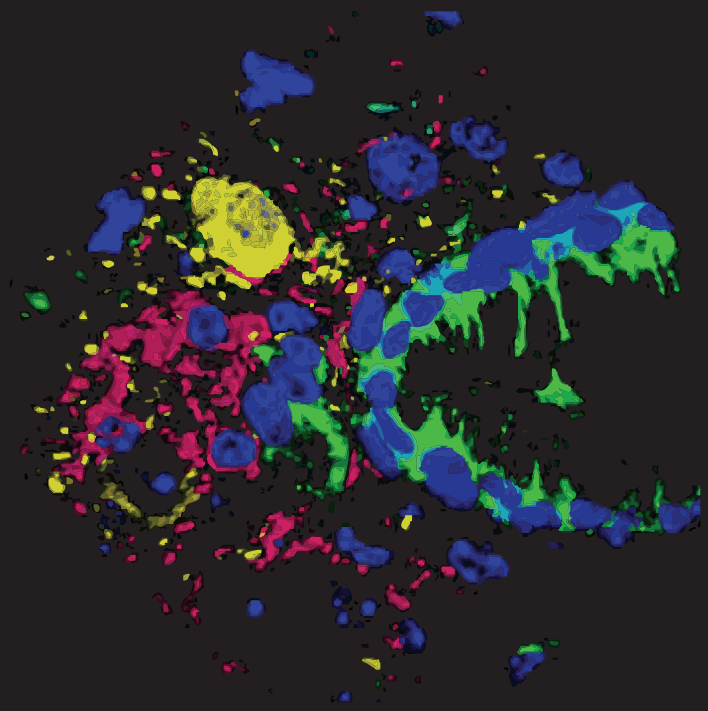


Universiteit Leiden



The handle http://hdl.handle.net/1887/85322 holds various files of this Leiden University dissertation.

Author: Kooreman, N.G.
Title: Immunogenicity and tumorigenicity of pluripotent stem cells
Issue Date: 2020-02-13



Immunogenicity and Tumorigenicity of Pluripotent Stem Cells

N.G. Kooreman

Immunogenicity and Tumorigenicity of Pluripotent Stem Cells

Nigel G. Kooreman

Immunogenicity and Tumorigenicity of Pluripotent Stem Cells

Image on cover: Courtesy of Sonja Schrepfer

ISBN: 978-94-6361-373-6
Layout and printed by: Optima Grafische Communicatie (www.ogc.nl)
Publication of this thesis was financially supported by: Haaglanden Medisch Centrum, Chipsoft, Pfizer, Servier Nederland Pharma, Khloris Biosciences, Living With Hope Foundation

© 2020 N.G. Kooreman
All rights reserved. No part of this thesis may be reproduced or transmitted in any form, by any means, electronic or mechanical, without the prior permission of the author, or where appropriate, of the publisher of the articles.

Immunogenicity and Tumorigenicity of Pluripotent Stem Cells

PROEFSCHRIFT

ter verkrijging van
de graad van Doctor aan de Universiteit Leiden,
op gezag van Rector Magnificus prof. mr. C.J.J.M. Stolker,
volgens besluit van het College voor Promoties
te verdedigen op donderdag 13 februari 2020
klokke 16.15 uur

door

Nigel Geoffrey Kooreman

geboren te Rotterdam
in 1986

Promotores:
Prof. dr. J.F. Hamming
Prof. dr. P.H.A. Quax
Prof. dr. J.C. Wu (Stanford University, USA)

Leden promotiecommissie:
Prof. dr. C.L. Mummery
Prof. dr. M.C. Verhaar (UMC Utrecht)
Prof. dr. S. Schrepfer (UC San Francisco, USA)
Prof. dr. M.J.T.H. Goumans
Dr. A.L. Vahrmeijer

The research as described in this thesis has been a collaborative effort of the Department of Radiology and Medicine at Stanford University, the Stanford Cardiovascular Institute, the Stanford Institute for Stem Cell Biology and Regenerative Medicine (California, USA) and the Department of Surgery, Leiden University Medical Center (The Netherlands). The research was financially partly supported by grants from the VSBfund, the Prof. Michael-van Vloten Foundation, Ketel 1 funds, Hendrik Muller foundation, Minerva Scholarship Fund, Jo-Keur Foundation, Leiden University Foundation (LUF), Leiden University Medical Center.

Financial support by the Dutch Heart Foundation for the publication of this thesis is gratefully acknowledged.

To my parents

CONTENTS

Chapter 1 **General introduction** 9

Part 1 **Regenerative therapies**

Chapter 2 **Tracking gene and cell fate** 23
Kooreman N.G., Ransohoff J.D. and Wu J.C.
Nature Materials. 2014; 13, 106-109

Chapter 3 **Optimization of iPSC technology** 39
Diecke S., Lu J., Lee, J., Termglinchan V.,
Kooreman N.G., et al. *Scientific Reports*. 2015; 5, 8081

Part 2 **Applications of regenerative therapies**

Chapter 4 **Gene therapy for vascular disease** 95
Kooreman N.G., Adam M., Jagger A., Wagenhauser M., Mehrkens D.,
et al. *Arteriosclerosis, Thrombosis and Vascular Biology (ATVB)*. 2018;
38, 1796-1805.

Chapter 5 **Pluripotent stem cell therapy for vascular disease** 119
Gu M., Mordwinkin N.M., Kooreman N.G., Lee J.,
Wu S., et al. *European Heart Journal*. 2015; 36, 806-816

Part 3 **Tumorigenity and Immunogenicity of PSCs**

Chapter 6 **Tumorigenicity of iPSCs** 159
Kooreman, N.G., and Wu, J.C. *Journal Royal Society Interface*. 2010;
7s6, S753-763

Chapter 7 **Immunogenicity of PSCs and PSC-derived cell grafts** 179
Kooreman, N.G., de Almeida, P.E., Meyer, E.H.,
Diecke, S., Dey, D., et al. *Nature Communications*.
2014; 5, 3903

Chapter 8 **Modeling PSC alloimmunity using humanized mice** 219
Kooreman N.G., de Almeida P.E., Stack J.P., Nelakanti R.V., Diecke S., et al. *Cell Reports.* 2017; 20, 8, 1978-1990.

Chapter 9 **Utilizing the tumorigenic and immunogenic properties of iPSCs into a cancer vaccine** 257
Kooreman N.G., Kim Y., de Almeida P.E., Termglichan V., Diecke S., et al. *Cell Stem Cell*. 2018; 22, 501-513.e7

Part 4 **General discussion**

Chapter 10 **General discussion and summary** 303

Chapter 11 **Future Perspectives** 313

Summary (in Dutch) 323

Acknowledgements (Dankwoord) 333
Curriculum Vitae 337
List of publications 339

Chapter 1

General Introduction

REGENERATIVE MEDICINE

With the increasing life expectancy of humankind, chronic illnesses will likely become more prevalent (Mathers and Loncar 2006). In this setting, tissue damage to organs with a limited regenerative capacity, such as the heart and the brain, will become large contributors to increases in morbidity. To address this issue, various avenues are being pursued to regenerate these tissues with, among others, gene or cell therapies.

The ways in which gene therapy could regenerate and or "correct" diseased tissue is, 1) by gene therapy *in vivo* or, 2) by gene-editing a specific diseased cell line *ex vivo* and then transplanting the corrected cells back into the same patient.

Cell therapy is mainly focused around progenitor or stem cells, with the use of multipotent adult stem cells dating back as early as two decades ago as a regenerative therapy for neurologic, immunological and cardiac diseases, amongst others (Asahara et al. 1997, Traynor et al. 2000, Tateishi-Yuyama et al. 2002, Burt et al. 2006, Honmou et al. 2011, Savitz et al. 2011, Prasad et al. 2014). With the first isolation of embryonic stem cells (ESCs) and the creation of induced pluripotent stem cells (iPSCs), together referred to as pluripotent stem cells (PSCs), researchers now have access to a cell type that could potentially be differentiated into every cell of the human body.

With regard to regenerative medicine, the main focus of this thesis will be on the use of gene and PSC therapy for the treatment of vascular diseases. Over the years, the management of arterial disease is primarily targeted towards lifestyle changes and supportive medicative therapies to control blood pressure and serum cholesterol levels. Disease progression under these therapies ultimately leads to invasive strategies, either by endovascular PT(C)A and stenting or (bypass) surgery. Between these two stages in treatment, the field of regenerative medicine might be effective in decreasing disease progression or potentially treating it altogether.

Accepting vascular disease as a chronic inflammatory disease, regenerative medicine has proven useful in stabilizing aortic aneurysms by using immunomodulatory mesenchymal stem cells to inhibit elastin-degrading enzymes (Hashizume et al. 2011). Another example is the use of gene therapy for the treatment of peripheral artery disease (PAD). Therefore, many clinical trials have looked into increasing neo-vascularization using plasmids or adenovirus overexpressing vascular endothelial growth factor (VEGF), fibroblast growth factor (FGF), developmental endothelial locus-1 (Del-1), hypoxia-inducible factor 1 alpha (Hif-1α) and hepatocyte growth factor (HGF) (Makinen et al. 2002, Rajagopalan et al. 2003, Matyas et al. 2005, Kusumanto et al. 2006, Grossman et al. 2007, Rajagopalan et al. 2007, Nikol et al. 2008, Powell et al. 2008, Shigematsu et al. 2010, Anghel et al. 2011, Belch et al. 2011, Creager et al. 2011). Although the VEGF and FGF trials did not show a significant reduction in the number of amputations or time to amputation, HGF studies have shown

efficacy by increasing tissue oxygenation in addition to improvements in peak walking time, ulcer healing and a reduction of amputation rate.

PLURIPOTENT STEM CELLS

After the first isolation of human ESCs in 1998 (Thomson et al. 1998), researchers have been exploring the potential of these pluripotent cells for regenerative therapies (Soto-Gutierrez et al. 2006, Pagliuca et al. 2014, Nguyen et al. 2016). Since then, many cell lines have been derived from ESCs, but ethical concerns surrounding the use of embryonic tissue or cells, as well as the immune response that these cells might trigger as an allogeneic transplant, limit the therapeutic potential for regenerative medicine.

In 2006, Shinya Yamanaka discovered that adult somatic murine cells could be reprogrammed to a pluripotent state, similar to ESCs (Takahashi and Yamanaka 2006). In brief, he looked into the gene expression profile of ESCs and distilled from this, the key regulators that are important to maintaining pluripotency. By overexpressing these genes (Oct4, cMyc, KLF4 and Sox2) in somatic cells with a lentiviral vector, his group was able to push the somatic cells into a pluripotent state. These iPSCs are similar to ESCs in morphology, characteristics and their potential to form cells from all three germ layers.

A year later, Yamanaka's group showed the same principle to be true for human cells (Takahashi et al. 2007), giving rise to a potentially groundbreaking field of regenerative medicine. Over the years, several groups published on the different cell lines that were successfully derived from these iPSCs (Burridge et al. 2012, Homma et al. 2013, Takebe et al. 2013, Pagliuca et al. 2014). The premise of iPSCs was that these cells could be derived from the patient's own cells, thereby taking away the ethical concerns surrounding the use of ESCs.

The therapeutic and regenerative potential of pluripotent cells are now being explored in pre-clinical and clinical trials (Alper 2009, Schwartz et al. 2012, Garber 2015, Cyranoski 2018), but their intrinsic properties, as well as the method of derivation, have raised considerable safety concerns.

CLINICAL HURDLES ASSOCIATED WITH REGENERATIVE MEDICINE

Tumorigenicity

The use of gene and cell therapies for regenerative medicine has been explored for several decades. During this time, critical safety issues have emerged, leading to serious adverse events, including the death and illness of participants in clinical trials (Thomas et al. 2003).

This resulted in more stringent policies surrounding gene and cell therapies and led to further evaluation of the effects of both therapies. However, even with stricter regulations and a better understanding of the therapies, setbacks still occur. For instance, the first human clinical trial in Riken Japan using iPSC-derived retinal cells had been temporarily halted due to mutagenesis in the transplanted cells for macula degeneration (Garber 2015).

One key risk factor, both for gene therapy as well as the generation of iPSCs, is insufficient knowledge of the effects of incorporated genes on the function of the genome. Especially in cases where the vector integrates into the genome, the site of integration might result in the activation of pro-oncogenes. This is true for gene therapy, but also for the generation of iPSCs, where the first generation of iPSCs had a reactivation of the cMyc gene with subsequent tumorigenesis (Okita et al. 2007). Also, the field of regenerative medicine should remain vigilant when using the differentiated population that is derived from pluripotent cells. For example, reports on atypical cell configurations in transplanted grafts raised the question whether this is the result of a plasticity in the epigenetic state of differentiated cells within the graft or possibly the non-specific differentiation of the small amount of remnant undifferentiated cells. Even though no disconcerting evidence was found with regards to the presence of these cells, these findings do warrant wariness when using these therapies in future clinical practice (Riegler et al. 2015).

Immunogenicity

One of the major limitations of gene and cell therapy is the immune response to vectors or cell types. As described in the previous section, the immunogenicity of gene vectors can have significant adverse effects, even resulting in the death of a participant in a safety trial (Raper et al. 2003). In this trial, a retroviral vector was used to treat a metabolic disorder. However, the vector caused a cytokine release storm in the patient which resulted in his death. Although such severe immune responses are rare, varying degrees of immunity can be expected towards gene vectors, but also cell transplants. Most of the allogeneic stem cell-based therapies therefore require immunosuppressive therapies (Kim et al. 2003, Schwartz et al. 2012, Selden et al. 2013), and even though good results have been achieved in preclinical animal models (Swijnenburg et al. 2008, Pearl et al. 2011), little is known about the optimal immunosuppressive therapies in humans to ensure cell engraftment. Thus far, some engraftment of pluripotent cells has been achieved in pre-clinical trials in large animal models using co-stimulatory blockade therapies (Chong et al. 2014), indicating an important role of the immune system in the survival of these cells. However, to further advance and optimize immunosuppressive strategies for humans, the immunogenic properties of stem cell grafts should be described in detail.

The premise of PSC therapies was that they could be performed without or with minimal immunosuppressive therapy. For ESCs, this is because of the low expression of MHC mol-

ecules on ESCs (Drukker et al. 2002). However, upon transplantation, ESCs seem to upregulate MHC class I and class II and become more immunogenic, which will be discussed in this thesis. With the discovery of iPSCs, the thought was that creating PSCs from a patients' own tissue would abolish the need for immunosuppressive regiments. However, as will be addressed in this thesis, this last concept needs to be re-evaluated.

OUTLINE OF THIS THESIS

The scope of the current thesis is to highlight different forms of regenerative therapies for vascular diseases and to investigate the immunogenic and tumorigenic properties of PSCs. Specifically, how these properties should be addressed and monitored within the field of regenerative medicine, but also how we could use them to enhance the field of cancer immunotherapy.

An overview of the applications of gene and cell therapy in regenerative medicine is provided in **Chapter 2**, along with means to monitor these therapies *in vivo*. In **Chapter 3**, a new method to reprogram somatic cells to iPSCs is described, called a codon-optimized mini-intronic plasmid (CoMiP). This vector is inexpensive to generate and increases the transfection efficiency compared to other DNA-based reprogramming methods by having the bacterial replication origin and selectable marker while maintaining the juxtaposition of the 5' and the 3' ends of the transgene expression cassette. As an appendix to this chapter, we discuss a vector called a non-viral minicircle (MC) that consist of supercoiled DNA molecules containing the reprogramming factors needed for establishing iPSCs. They are smaller than conventional plasmids and lack a bacterial origin of replication. The small size increases the transfection efficiency and the lack of bacterial backbone makes the vector non-immunogenic. Both of these properties also make this vector a good candidate for *in vivo* gene therapy.

In **Chapter 4**, the application of gene therapy for arterial disease is explored. Using a different minicircle vector, carrying the transgene IL-10, we assess the effect of MC IL-10 infusion into angiotensin II-infusion-ApoE-/- AAA mice on aneurysm diameter and dissection rate. In **Chapter 5**, another major field of interest will be addressed: PSC therapy. We focus on the use of iPSCs as a regenerative therapy for peripheral artery disease in subjects with diabetes. An important question that is answered here is whether the source of iPSCs is important for the outcome of the cell product. Therefore, iPSCs from diabetic and non-diabetic mice were created and differentiated into endothelial cells (ECs) to assess the regenerative potential in a hindlimb ischemia model.

Even though the potential of PSC-based therapies is enormous, the immunogenic and tumorigenic properties of PSCs are of concern in the clinical translation of these cells for regenerative medicine.

In **Chapter 6**, therefore, we describe the tumorigenic properties of PSCs. Particularly, the pro-oncogenic factors that are used to induce pluripotency in adult cells, the mutations gained during the culture of PSCs and the cancer-resembling properties. In **Chapter 7**, the immunogenicity of iPSCs is addressed in an autologous murine transplant model. The immune responses to autologous iPSC grafts are described in great detail with, among others, single-cell PCR analysis as well as T-cell Receptor (TCR) sequencing of graft infiltrating cells. To further model immunity of PSCs in a human setting, we explored the use of various types of humanized mice, including the human bone marrow, liver and thymus (hBLT) mouse model in **Chapter 8**. To this purpose, we transplanted humanized mice with GFP and luciferase labeled human ESC-derived endothelial cells (ESC-ECs) for *in vitro* and *in vivo* tracking of the cells. The human immune responses in the hBLT model are described in great detail and ways to improve the model are discussed.

Even though the field of regenerative medicine has concerns about the tumorigenic and immunogenic properties of PSCs, the field of immunotherapy might benefit from it. In **Chapter 9** both these qualities of iPSCs are used to prime several mouse strains and protect them against the development of various types of cancer. The cancer vaccine described here is able to prime mice effectively and provide an adequate immune response *in vitro* as well as *in vivo* against cancer and has the potential to be translated to clinical practice as a (neo) adjuvant immunotherapy in the treatment of various types of cancer.

REFERENCES

Alper, J. (2009). "Geron gets green light for human trial of ES cell-derived product." Nat Biotechnol 27(3): 213-214.

Anghel, A., G. Taranu, E. Seclaman, A. Rata, L. Tamas, H. Moldovan, . . . A. Popa-Wagner (2011). "Safety of vascular endothelial and hepatocyte growth factor gene therapy in patients with critical limb ischemia." Curr Neurovasc Res 8(3): 183-189.

Asahara, T., T. Murohara, A. Sullivan, M. Silver, R. van der Zee, T. Li, . . . J. M. Isner (1997). "Isolation of putative progenitor endothelial cells for angiogenesis." Science 275(5302): 964-967.

Belch, J., W. R. Hiatt, I. Baumgartner, I. V. Driver, S. Nikol, L. Norgren, . . . Investigators (2011). "Effect of fibroblast growth factor NV1FGF on amputation and death: a randomised placebo-controlled trial of gene therapy in critical limb ischaemia." Lancet 377(9781): 1929-1937.

Burridge, P. W., G. Keller, J. D. Gold and J. C. Wu (2012). "Production of de novo cardiomyocytes: human pluripotent stem cell differentiation and direct reprogramming." Cell Stem Cell 10(1): 16-28.

Burt, R. K., A. Traynor, L. Statkute, W. G. Barr, R. Rosa, J. Schroeder, . . . Y. Oyama (2006). "Nonmyeloablative hematopoietic stem cell transplantation for systemic lupus erythematosus." JAMA 295(5): 527-535.

Chong, J. J., X. Yang, C. W. Don, E. Minami, Y. W. Liu, J. J. Weyers, . . . C. E. Murry (2014). "Human embryonic-stem-cell-derived cardiomyocytes regenerate non-human primate hearts." Nature 510(7504): 273-277.

Creager, M. A., J. W. Olin, J. J. Belch, G. L. Moneta, T. D. Henry, S. Rajagopalan, . . . W. R. Hiatt (2011). "Effect of hypoxia-inducible factor-1alpha gene therapy on walking performance in patients with intermittent claudication." Circulation 124(16): 1765-1773.

Cyranoski, D. (2018). "'Reprogrammed' stem cells approved to mend human hearts for the first time." Nature 557(7707): 619-620.

Drukker, M., G. Katz, A. Urbach, M. Schuldiner, G. Markel, J. Itskovitz-Eldor, . . . N. Benvenisty (2002). "Characterization of the expression of MHC proteins in human embryonic stem cells." Proc Natl Acad Sci U S A 99(15): 9864-9869.

Garber, K. (2015). "RIKEN suspends first clinical trial involving induced pluripotent stem cells." Nat Biotechnol 33(9): 890-891.

Grossman, P. M., F. Mendelsohn, T. D. Henry, J. B. Hermiller, M. Litt, J. F. Saucedo, . . . K. Rocha-Singh (2007). "Results from a phase II multicenter, double-blind placebo-controlled study of Del-1 (VLTS-589) for intermittent claudication in subjects with peripheral arterial disease." Am Heart J 153(5): 874-880.

Hashizume, R., A. Yamawaki-Ogata, Y. Ueda, W. R. Wagner and Y. Narita (2011). "Mesenchymal stem cells attenuate angiotensin II-induced aortic aneurysm growth in apolipoprotein E-deficient mice." J Vasc Surg 54(6): 1743-1752.

Homma, K., S. Okamoto, M. Mandai, N. Gotoh, H. K. Rajasimha, Y. S. Chang, . . . M. Takahashi (2013). "Developing rods transplanted into the degenerating retina of Crx-knockout mice exhibit neural activity similar to native photoreceptors." Stem Cells 31(6): 1149-1159.

Honmou, O., K. Houkin, T. Matsunaga, Y. Niitsu, S. Ishiai, R. Onodera, . . . J. D. Kocsis (2011). "Intravenous administration of auto serum-expanded autologous mesenchymal stem cells in stroke." Brain 134(Pt 6): 1790-1807.

Kim, H. J., C. Y. Park, Y. H. Park, Y. J. Kim, D. W. Kim, W. S. Min and C. C. Kim (2003). "Successful allogeneic hematopoietic stem cell transplantation using triple agent immunosuppression in severe aplastic anemia patients." Bone Marrow Transplant 31(2): 79-86.

Kusumanto, Y. H., V. van Weel, N. H. Mulder, A. J. Smit, J. J. van den Dungen, J. M. Hooymans, . . . G. A. Hospers (2006). "Treatment with intramuscular vascular endothelial growth factor gene compared with placebo for patients with diabetes mellitus and critical limb ischemia: a double-blind randomized trial." Hum Gene Ther 17(6): 683-691.

Makinen, K., H. Manninen, M. Hedman, P. Matsi, H. Mussalo, E. Alhava and S. Yla-Herttuala (2002). "Increased vascularity detected by digital subtraction angiography after VEGF gene transfer to human lower limb artery: a randomized, placebo-controlled, double-blinded phase II study." Mol Ther 6(1): 127-133.

Mathers, C. D. and D. Loncar (2006). "Projections of global mortality and burden of disease from 2002 to 2030." PLoS Med 3(11): e442.

Matyas, L., K. L. Schulte, J. A. Dormandy, L. Norgren, O. Sowade, G. Grotzbach, . . . E. Wahlberg (2005). "Arteriogenic gene therapy in patients with unreconstructable critical limb ischemia: a randomized, placebo-controlled clinical trial of adenovirus 5-delivered fibroblast growth factor-4." Hum Gene Ther 16(10): 1202-1211.

Nguyen, P. K., E. Neofytou, J. W. Rhee and J. C. Wu (2016). "Potential Strategies to Address the Major Clinical Barriers Facing Stem Cell Regenerative Therapy for Cardiovascular Disease: A Review." JAMA Cardiol 1(8): 953-962.

Nikol, S., I. Baumgartner, E. Van Belle, C. Diehm, A. Visona, M. C. Capogrossi, . . . F. Meyer (2008). "Therapeutic Angiogenesis With Intramuscular NV1FGF Improves Amputation-free Survival in Patients With Critical Limb Ischemia." Mol Ther 16(5): 972-978.

Okita, K., T. Ichisaka and S. Yamanaka (2007). "Generation of germline-competent induced pluripotent stem cells." Nature 448(7151): 313-317.

Pagliuca, F. W., J. R. Millman, M. Gurtler, M. Segel, A. Van Dervort, J. H. Ryu, . . . D. A. Melton (2014). "Generation of functional human pancreatic beta cells in vitro." Cell 159(2): 428-439.

Pearl, J. I., A. S. Lee, D. B. Leveson-Gower, N. Sun, Z. Ghosh, F. Lan, . . . J. C. Wu (2011). "Short-term immunosuppression promotes engraftment of embryonic and induced pluripotent stem cells." Cell Stem Cell 8(3): 309-317.

Powell, R. J., M. Simons, F. O. Mendelsohn, G. Daniel, T. D. Henry, M. Koga, . . . B. H. Annex (2008). "Results of a double-blind, placebo-controlled study to assess the safety of intramuscular injection of hepatocyte growth factor plasmid to improve limb perfusion in patients with critical limb ischemia." Circulation 118(1): 58-65.

Prasad, K., A. Sharma, A. Garg, S. Mohanty, S. Bhatnagar, S. Johri, . . . S. T. S. G. Inve (2014). "Intravenous autologous bone marrow mononuclear stem cell therapy for ischemic stroke: a multicentric, randomized trial." Stroke 45(12): 3618-3624.

Rajagopalan, S., E. R. Mohler, 3rd, R. J. Lederman, F. O. Mendelsohn, J. F. Saucedo, C. K. Goldman, . . . B. H. Annex (2003). "Regional angiogenesis with vascular endothelial growth factor in peripheral arterial disease: a phase II randomized, double-blind, controlled study of adenoviral delivery of vascular endothelial growth factor 121 in patients with disabling intermittent claudication." Circulation 108(16): 1933-1938.

Rajagopalan, S., J. Olin, S. Deitcher, A. Pieczek, J. Laird, P. M. Grossman, . . . N. Chronos (2007). "Use of a constitutively active hypoxia-inducible factor-1alpha transgene as a therapeutic strategy in no-option critical limb ischemia patients: phase I dose-escalation experience." Circulation 115(10): 1234-1243.

Raper, S. E., N. Chirmule, F. S. Lee, N. A. Wivel, A. Bagg, G. P. Gao, . . . M. L. Batshaw (2003). "Fatal systemic inflammatory response syndrome in a ornithine transcarbamylase deficient patient following adenoviral gene transfer." Mol Genet Metab 80(1-2): 148-158.

Riegler, J., M. Tiburcy, A. Ebert, E. Tzatzalos, U. Raaz, O. J. Abilez, . . . J. C. Wu (2015). "Human Engineered Heart Muscles Engraft and Survive Long Term in a Rodent Myocardial Infarction Model." Circ Res 117(8): 720-730.

Savitz, S. I., V. Misra, M. Kasam, H. Juneja, C. S. Cox, Jr., S. Alderman, . . . J. C. Grotta (2011). "Intravenous autologous bone marrow mononuclear cells for ischemic stroke." Ann Neurol 70(1): 59-69.

Schwartz, S. D., J. P. Hubschman, G. Heilwell, V. Franco-Cardenas, C. K. Pan, R. M. Ostrick, . . . R. Lanza (2012). "Embryonic stem cell trials for macular degeneration: a preliminary report." Lancet 379(9817): 713-720.

Selden, N. R., A. Al-Uzri, S. L. Huhn, T. K. Koch, D. M. Sikora, M. D. Nguyen-Driver, . . . R. D. Steiner (2013). "Central nervous system stem cell transplantation for children with neuronal ceroid lipofuscinosis." J Neurosurg Pediatr 11(6): 643-652.

Shigematsu, H., K. Yasuda, T. Iwai, T. Sasajima, S. Ishimaru, Y. Ohashi, . . . R. Morishita (2010). "Randomized, double-blind, placebo-controlled clinical trial of hepatocyte growth factor plasmid for critical limb ischemia." Gene Ther 17(9): 1152-1161.

Soto-Gutierrez, A., N. Kobayashi, J. D. Rivas-Carrillo, N. Navarro-Alvarez, D. Zhao, T. Okitsu, . . . I. J. Fox (2006). "Reversal of mouse hepatic failure using an implanted liver-assist device containing ES cell-derived hepatocytes." Nat Biotechnol 24(11): 1412-1419.

Swijnenburg, R. J., S. Schrepfer, J. A. Govaert, F. Cao, K. Ransohoff, A. Y. Sheikh, . . . J. C. Wu (2008). "Immunosuppressive therapy mitigates immunological rejection of human embryonic stem cell xenografts." Proc Natl Acad Sci U S A 105(35): 12991-12996.

Takahashi, K., K. Tanabe, M. Ohnuki, M. Narita, T. Ichisaka, K. Tomoda and S. Yamanaka (2007). "Induction of pluripotent stem cells from adult human fibroblasts by defined factors." Cell 131(5): 861-872.

Takahashi, K. and S. Yamanaka (2006). "Induction of pluripotent stem cells from mouse embryonic and adult fibroblast cultures by defined factors." Cell 126(4): 663-676.

Takebe, T., K. Sekine, M. Enomura, H. Koike, M. Kimura, T. Ogaeri, . . . H. Taniguchi (2013). "Vascularized and functional human liver from an iPSC-derived organ bud transplant." Nature 499(7459): 481-484.

Tateishi-Yuyama, E., H. Matsubara, T. Murohara, U. Ikeda, S. Shintani, H. Masaki, . . . I. Therapeutic Angiogenesis using Cell Transplantation Study (2002). "Therapeutic angiogenesis for patients with limb ischaemia by autologous transplantation of bone-marrow cells: a pilot study and a randomised controlled trial." Lancet 360(9331): 427-435.

Thomas, C. E., A. Ehrhardt and M. A. Kay (2003). "Progress and problems with the use of viral vectors for gene therapy." Nat Rev Genet 4(5): 346-358.

Thomson, J. A., J. Itskovitz-Eldor, S. S. Shapiro, M. A. Waknitz, J. J. Swiergiel, V. S. Marshall and J. M. Jones (1998). "Embryonic stem cell lines derived from human blastocysts." Science 282(5391): 1145-1147.

Traynor, A. E., J. Schroeder, R. M. Rosa, D. Cheng, J. Stefka, S. Mujais, . . . R. K. Burt (2000). "Treatment of severe systemic lupus erythematosus with high-dose chemotherapy and haemopoietic stem-cell transplantation: a phase I study." Lancet 356(9231): 701-707.



Part I

Regenerative therapies

Chapter 2

Tracking gene and cell fate

Kooreman, N.G., Ransohoff, J.D., and Wu, J.C. (2014). Tracking gene and cell fate for therapeutic gain. **Nature Materials,** *13, 106-109*

SUMMARY

The preclinical intersection of molecular imaging and gene- and cell-based therapies will enable more informed and effective clinical translation. We discuss how imaging can monitor cell and gene fate and function *in vivo* and overcome barriers associated with these therapies.

In recent years, impressive progress has been made in the bench-to-bedside translation of gene and cell-based treatments to address a wide range of pathologies in preclinical and clinical settings. Similar advances in bioimaging have provided powerful tools to monitor their *in vivo* fate and function. Here, we provide an overview of relevant gene and cell-based therapies and highlight the applications of molecular imaging technologies to evaluate graft function, regulation and interaction with host tissue. Moreover, we emphasize particular strategies to facilitate the continued, collaborative synergy between molecular imaging technologies and these therapies, which will expedite their assessment and development.

CLINICAL AND PRECLINICAL STUDIES

Significant progress has been made in clinical and preclinical arenas towards the development of gene and cell therapies.

Corrective gene therapy

Gene and stem cell-based therapies have the potential to treat a variety of diseases. Investigators have successfully illustrated the principle of isolating, engineering and re-introducing a 'corrected' graft for a variety of diseases with lineage-restricted phenotypes, including X-linked (Hacein-Bey-Abina et al. 2002) and adenosine deaminase deficient (Aiuti et al. 2009) severe combined immunodeficiency disease, chronic granulomatous disease (Ott et al. 2006), adrenoleukodystrophy (Cartier et al. 2009) and Wiskott–Aldrich syndrome (Boztug et al. 2010). These therapies, largely limited experimentally to retroviral insertion of the corrected gene product in autologously derived hematopoietic stem cells (HSCs), have been met with widely publicized and appropriately directed concerns regarding their safety, despite encouraging demonstrations of phenotype correction. Follow-up reports have shown leukemic (Hacein-Bey-Abina et al. 2003) and pre-leukemic (Stein et al. 2010) induction, clonal T-cell expansion (Howe et al. 2008), and genomic instability (Stein et al. 2010) secondary to retroviral-mediated insertional mutagenesis in or near proto-oncogenes. Such events, as a consequence of untargeted genome editing, served as an impetus for the temporary ban by the Food and Drug Administration on gene therapy in 2002. The subsequent lifting of the ban in 2003 heralded a more skeptical and slow-progressing era that has continued to the present, leaving the field yet to realize its full potential.

Allogeneic stem cell transplantation

Although the aforementioned near pause in gene therapy led to more cautious development in this arena, interest in autologous or allogeneic stem cell-based approaches strengthened significantly. However, despite wide interest in the use of bone-marrow-derived mesenchymal stem cells (MSCs) for a range of regenerative therapies, including those for inflammatory (Griffin et al. 2013), joint (Barry and Murphy 2013) and cardiac diseases (Sheikh et al. 2012), among others, questions regarding the clinical efficacy of various stem cell protocols remain. In addition to marginal improvement observed in several stem cell trials, there is also evidence of detrimental side effects as seen with skeletal myoblast therapy for cardiac repair (Menasche et al. 2008). The discrepancy between the more definitive preclinical success of stem cell therapies and their less promising early clinical results may be partly attributed to a lack of knowledge regarding in vivo graft behaviour.

Promising new therapeutic products are now emerging, in particular those making use of human embryonic stem cell (hESC) and induced pluripotent stem cell (iPSC) derivatives. These include the now defunct Geron trial using allogeneic hESC-derived oligodendrocyte

progenitor cells for spinal cord repair (Strauss 2010), the Advanced Cell Technology trial using hESC-derived retinal pigment epithelium cells (RPEs) for Stargardt's macular dystrophy (Schwartz et al. 2012), and the RIKEN Japan trial using autologous iPSC-derived RPEs for age-related macular degeneration (Cyranoski 2013). As with earlier somatic cell therapies, pluripotent stem cell therapeutics will also need to be extensively tested and evaluated by bioimaging technologies to better understand their fate in vivo.

Genetically engineered stem cells

With the goal of optimizing clinical impact, the most promising approaches combine gene and cell therapy to deliver a corrected or beneficial gene in a therapeutically relevant cell. As an emerging paradigm, T-cell immunotherapy offers hope for more targeted chemotherapy by genetically instructing T-cell trafficking, direction, or redirection towards tumor cells, with the potential to engineer bispecific T cells with engineered proliferation and antitumor specificities (Kershaw et al. 2002). A noteworthy, single- patient-case example of using positron emission tomography (PET) imaging to track the fate of genetically labelled and therapeutically manipulated cytolytic T lymphocytes (CTLs) has demonstrated a valuable platform for integrating gene and cell therapy with molecular imaging (Yaghoubi et al. 2009). In this report, CTLs labelled with the PET reporter gene herpes simplex virus thymidine kinase (HSV-tk) were infused intracranially after resection of a glioblastoma multiforme. PET imaging after administration of the PET reporter probe 9-(4-[18F]-fluoro-3-hydroxymethylbutyl)- guanine ([18F]FHBG) revealed not only accumulation of the engineered CTLs in the patient's primary tumor but also homing to another metastatic site.

In addition to studying the in vivo fate of transplanted engineered cells, ex vivo edited cells also offer a valuable investigative platform. For instance, the ability to reprogram patient-specific adult somatic cells to iPSCs by overexpression of pluripotent transcription factors (Takahashi et al. 2007) has been used for ex vivo disease modelling. Notable examples of recapitulating disease phenotypes in a dish include amyotrophic lateral sclerosis (Dimos et al. 2008), spinal muscular atrophy (Ebert et al. 2009), long QT syndrome (Moretti et al. 2010) and inherited cardiomyopathies (Sun et al. 2012, Lan et al. 2013), among others. Beyond disease modelling, this platform has also expedited development of high-throughput drug screening (Mordwinkin et al. 2013) as well as gene correction in monogenic diseases (Simara et al. 2013).

BIOIMAGING

Molecular imaging technologies can importantly further the progress of gene- and cell-based therapies.

Disease modelling and monitoring

Gene- and cell-based approaches have suffered from a lack of knowledge and control over *in vivo* graft behavior. Requiring years of preclinical testing, their combined progression will need to overcome the obstacles that have impeded these approaches independently and should benefit significantly from insights gained from bioimaging of gene and cell fate. Historically, lineage mapping by physical or genetic labelling has contributed extensively to our understanding of developmental processes and stem cell behavior and assisted in the isolation of important stem cell populations. To better understand why gene and cell therapies have fallen short of their potential so far, an approach similar to that taken by developmental biologists should be more fully adopted by molecular imaging specialists and translational researchers. The coupling of therapeutic cells or vectors to reporter cassettes to permit live, longitudinal imaging of cellular processes may provide key insights that will help elucidate and harness their full regenerative and corrective capacities, while simultaneously addressing safety and regulatory concerns (Wang et al. 2012, Joung and Sander 2013).

LABELLING THE THERAPEUTIC POPULATION

A diverse range of cell labelling and tracking modalities are available to investigators.

Imaging modalities

For regenerative medicine, several cell types are of interest because of their multipotent (for example, MSCs) or pluripotent (for example, hESCs and iPSCs) nature (Fig. 1a). Therapeutic applications of some of these cells have been explored through clinical trials, but unresolved concerns surrounding safety and efficacy are limiting their full clinical implementation (de Almeida et al. 2013). The principal barriers to full regulatory acceptance of pluripotent stem cell-based therapeutics are their immunogenic and tumorigenic potential; addressing these will require *in vivo* tracking of transplanted grafts (Kooreman and Wu 2010). *In vivo* tracking of cell fate involves either 'direct' physical labelling of cells by incubating them with a contrast agent, or 'indirect' genetic labelling of cells by transfecting them with reporter gene construct(s) (Fig. 1b). The position of and signal from these labels can then be tracked using a CCD (charged coupled device) camera for bioluminescence imaging (BLI) or fluorescence imaging (FLI), single photon emission computed tomography (SPECT), PET and magnetic resonance imaging (MRI), among other modalities. Selection of the optimal labelling technique and imaging modality depends on the cellular processes that need to be studied as well as the readouts that are most desirable, with each labelling and imaging strategy having distinct advantages and disadvantages (Youn and Chung 2013). Until now, most clinical studies have relied on direct labelling strategies to track homing and migration of multipotent stem cells or engineered cells (see Table 1). These studies have answered critical

questions in regenerative medicine, such as the importance of early stem cell engraftment on predicting late functional improvement (Vrtovec et al. 2013) and the optimal route of cell delivery (comparing transendocardial versus intracoronary routes) into the heart (Vrtovec et al. 2013). Furthermore, these cardiac regenerative studies highlight the importance of combining bioimaging of organ function with that of cell homing to assess which part of a diseased organ might benefit most from cell therapy (Musialek et al. 2013). For immunotherapy using modified CTLs or tumor-specific dendritic cells (DCs), bioimaging has provided clinicians with important insight into the kinetics of antitumor cell infiltration into tumor tissue (de Vries et al. 2005, Yaghoubi et al. 2009). By using fluorinated (^{19}F) contrast agents to label human DCs for MRI, preclinical studies have further demonstrated

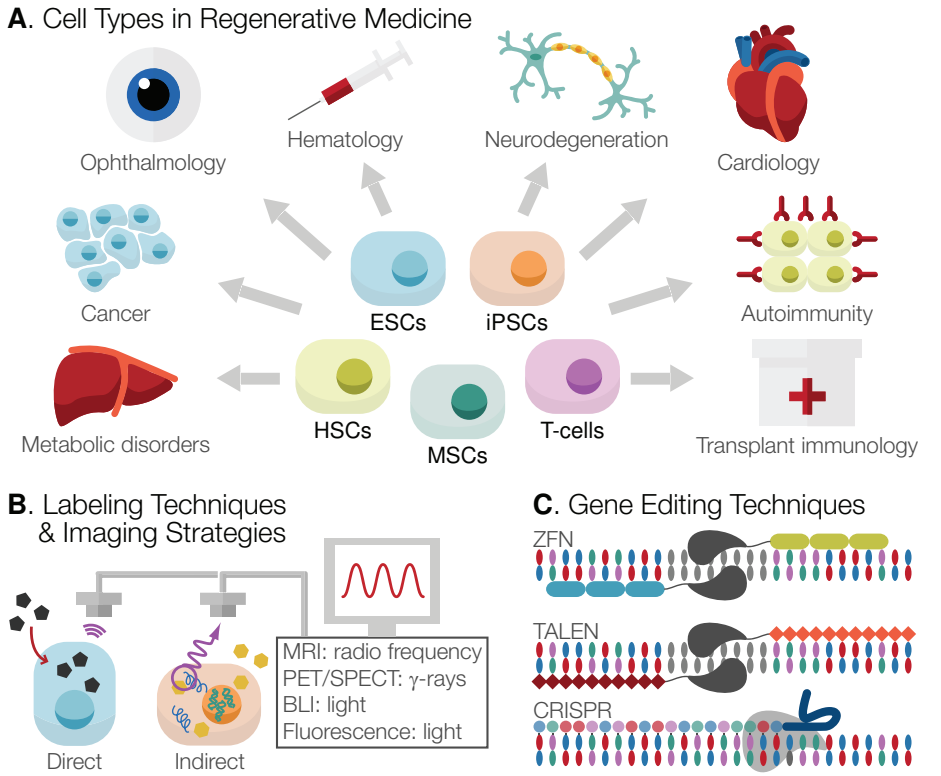


Figure 1. a, A variety of cell types, including somatic cells (T cells), adult stem cells (HSCs, MSCs) and pluripotent stem cell (ESCs, iPSCs) derivatives, are available to researchers to address a wide range of pathologies across fields. b, To enable *in vivo* monitoring of transplanted cells by protein, enzyme and receptor-based platforms, cells can be labelled either 'directly' (with a physical compound such as iron particles or radiotracers) or 'indirectly' (by genetic integration of reporter gene(s)). c, Targeted genome editing can be achieved by several techniques, including ZFN, TALEN and CRISPR approaches. Dual editing of cells to integrate corrected gene products with reporter cassettes will facilitate informed assessment of their safety and efficacy by bioimaging. Image courtesy of Ryan Tucker and Christina Sicoli (Manuscript by Design).

DC migration to draining lymph nodes, with superior assessment of cell quantity compared with that obtained by other MRI labels (Helfer et al. 2010, Bonetto et al. 2011).

With the current focus on moving pluripotent stem cell derivatives to the clinic (Garber 2013), *in vivo* tracking of these cells is critical in assessing their homing and proliferative potential over time, as well as the exclusion of teratoma formation (Lee et al. 2013). In preclinical studies, more emphasis is placed on indirect genetic labelling over direct physical labelling because the former technique is not subject to signal dilution on cell division nor discordance between signal intensity and cell viability on graft loss (Li et al. 2008, Higuchi et al. 2009). Of note, label uptake by inflammatory cells may produce a false positive readout of graft persistence, as a consequence of uncoupling of the label from its original host cell (Amsalem et al. 2007). Preclinical genetic labelling of stem cells with fluorescent proteins or bioluminescent enzymes has provided researchers with important information regarding graft behavior in small animal models, offering both fast readouts of longitudinal cell survival and low costs per imaging study. However, the penetrance of these signals is too low for detection in humans, hence largely limiting their application to small animal models (Contag and Bachmann 2002). By contrast, PET and SPECT provide higher sensitivity than optical techniques, making them better suited for monitoring biological processes in large animal and human studies (Kang et al. 2006, Schachinger et al. 2008, Yaghoubi et al. 2009, Vrtovec et al. 2013, Vrtovec et al. 2013), while also sensitively permitting visualization of as low as 1×10^5 engrafted cells (Templin et al. 2012). Although spatial resolution remains a limitation with nuclear medicine imaging, it could be overcome by combining with computed tomography (CT) (Doyle et al. 2007) or with MRI. However, the combined PET–CT or SPECT–CT approaches may not be ideal for repetitive assessment of gene or cell fate because of the high exposure to ionizing radiation. Hence, the combined PET–MRI approach may be an attractive alternative because it offers decreased radiation and high spatial resolution qualities (Wehrl et al. 2009).

Cell labelling strategies

Labelling cells to enable a combined PET–MRI approach will be of great clinical value for gene and cell therapies. Numerous PET reporter systems have been previously described, including those using dopamine receptor D2 and somatostatin receptors. These systems, however, suffer from low sensitivity, as endogenous receptor expression leads to high background signal (MacLaren et al. 1999, Liang et al. 2002, Kwekkeboom et al. 2010). The sodium iodide symporter (NIS) has been proposed as an alternative reporter gene as a result of its wide substrate availability, labelling stability, and well-understood metabolism and substrate clearance (Chung 2002). However, the presence of NIS in other tissues such as the thyroid, stomach and urinary tract reduces its reporter specificity. For PET imaging in gene- and cell-based therapies, the most widely used label so far has been the *HSV-tk* reporter gene (Black et al. 1996, Wu et al. 2003, Cao et al. 2006, Yaghoubi et al. 2009). This

Table 1.
Human clinical trials or case reports using direct and indirect labelling strategies for *in vivo* bioimaging to monitor homing and migration of transplanted cells. ^{18}F-FHBG, fluorine 18-9-[4-fluoro-3-(hydroxymethyl)butyl]guanine; ^{18}F-FDG, fluorine 18-fluorodeoxyglucose; SPIO, superparamagnetic iron oxide; ^{111}In-oxine, indium oxine; ^{99m}Tc-HMPAO, ^{99m}Tc-hexamethylpropyleneamine oxime; *HSV-tk*, herpes simplex virus thymidine kinase; LVEF, left ventricular ejection fraction; PBMC, peripheral blood mononuclear cells.

Labeling:	Imaging Modality	Cell type	Treatment	Procedure	Outcome	Source
^{18}F–FHBG	PET/MRI	Cytolytic T-cells (CTL) *($1x10^9$ cells)*	Immunotherapy for glioblastoma multiforme	-Genetically modified CTLs with *HSV-tk* to target glioblastoma -Administration of CTLs (after tumor resection) with Rickham reservoir	-Tracking of CTLs up to 2 hours after infusion -Possibility to induce programmed cell death of CTLs after ganciclovir administration	Yaghoubi, Jensen et al. 2009
^{18}F-FDG	PET/CT	Hematopoietic stem cells (HSC) *($4.5x10^8$ cells)*	Cell therapy after myocardial infarction	-HSC isolation via spectra apheresis -40 min incubation with ^{18}F-FDG -Administration via balloon catheter	-High resolution assessment of retention in myocardium (1.5% of cells) -Short half-life of ^{18}F-FDG limits usefulness after 20 hours	Kang, et al. 2006
SPIO + ^{111}In-oxine	MRI and scintigraphy	Dendritic cells (DC) *($15x10^6$ cells)*	Immunotherapy for melanoma	-DC isolation from PBMC -15 min incubation with ^{111}In-oxine -SPIO added to culture media -Injection into draining lymph node of resected area	-Similar sensitivity between scintigraphy and MRI -Scintigraphy allows quantification of cells -MRI superior in assessing location and migration of labeled cells	de Vries, Lesterhuis et al. 2005
SPIO	MRI	Neural stem cells (NSC)	Cell therapy for brain damage	-NSC isolation from exposed neural tissue -60 min incubation with SPIO -Stereotactic implantation in region of brain damage	-Non-invasive tracking of engraftment and migration of labeled cells up to 7 weeks	Zhu et al. 2006
^{111}In-oxine	PET	Circulating progenitor cells (CPC) *(~10^6 cells)*	Cell therapy after myocardial infarction (MI)	-CPC isolation from PBMC -60 min incubation with ^{111}In-oxine -Administration via balloon catheter	-Reduced homing of cells in chronic MI (> 1 year) versus acute MI (<14 days)	Schachinger, Aicher et al. 2008
^{99m}Tc-HMPAO	SPECT	Bone marrow mononuclear cells (BMMNC) *(~100×10^6)*	Cell therapy for non-ischemic dilated cardiomyopathy	-BMMNC isolation via apheresis -Labeling of $CD34^+$ cells with ^{99m}Tc-HMPAO before injection -Intracoronary or transendocardial injection in affected myocardium	-Better homing of cells leads to increase in LVEF at 3 and 12 months after procedure -Superior engraftment with transendocardial injection	Vrtovec, Poglajen et al. 2013; Vrtovec, Poglajen et al. 2013

construct offers several benefits, including quantitative and anatomic evaluation of reporter gene expression (Gambhir et al. 2000). It also has the ability to function as a suicide gene on administration of exogenous acycloguanosine substrates in pharmacological amounts, making it particularly ideal for ablating unwanted tumorigenic findings (Cao et al. 2006).

For MRI, chemical exchange saturation transfer (CEST) has been used to improve detection sensitivity. It is based on the principle that mobile protons resonate at a frequency distinct from those in bulk fluid. A proton signal specific to a molecule or CEST substrate is selectively saturated with signal. These protons' movement towards, exchange with, and subsequent signal transfer to bulk water results in the exchange transfer of signal loss (Ward et al. 2000). Whereas all ^{1}H-based magnetic resonance reporter genes rely on (super) paramagnetic substances and water relaxation for contrast (Louie et al. 2000, Moore et al. 2001, Genove et al. 2005), the contrast produced by CEST agents can additionally be switched on and off by frequency selection. Using a lysine-rich protein (LRP) reporter, Gilad *et al.* demonstrated this principle by creating a contrast material that is detectable in the micromolar range, biodegradable and capable of distinguishing live from dead cells, thus enabling the constant monitoring of endogenous expression levels in daughter cells (Gilad et al. 2007). Newer CEST contrast agents, such as human protamine-1, address immunogenic concerns regarding the use of animal reporter proteins, and are being investigated for *in vivo* imaging applications (Bar-Shir et al. 2013). Another advantage is that the separation of signals from different CEST contrast agents enable multiple, simultaneous measurements possible from distinct target populations (McMahon et al. 2008, Liu et al. 2012). In contrast to fusion reporter genes, the use of a single reporter gene for multimodal imaging with photoacoustics, MRI and PET is also being explored (Qin et al. 2013).

Targeted genome editing

Significant advances have been made with respect to genome editing technologies, but these advances have not yet been extensively integrated with bioimaging technologies (Fig. 1c). The majority of genetic engineering to a targeted locus so far has been accomplished by use of zinc- finger nucleases (ZFNs). More recently, transcription activator-like effector nucleases (TALENs) have offered a similarly promising tool, coupling a generic *Fok*I nuclease domain with a specific DNA- binding domain. For ZFNs and TALENs, DNA-binding modules are engineered to match a target DNA sequence. There, they direct double strand breaks and facilitate potential DNA alterations and repair under non-homologous end joining or homology-directed repair. A third genome editing system also offers strong potential for improving targeted gene therapies: the clustered regularly interspaced short palindromic repeats (CRISPR) system uses RNA-guided Cas9 DNAse activity to generate sequence-specific target cleavage (Horii et al. 2013).

So far, these three genome editing approaches have been used for correction or modelling of α1-antitrypsin disease (Yusa et al. 2011), sickle cell anemia (Sebastiano et al. 2011)

and Parkinson's disease (Soldner et al. 2011). Recently, Wang *et al.* demonstrated how ZFN technology can introduce a triple fusion reporter cassette into the safe-harbor AAVS1 locus of hESCs and iPSCs with readout capacity by three independent systems: BLI (firefly luciferase), PET (*HSV-tk*), and FLI (monomeric red fluorescent protein) (Wang et al. 2012). This work provides a platform for future introduction of a dual reporter gene and corrected cassette under the control of the target site promoter, providing important insights into temporal and spatial activity of cell fate. Collectively, these three approaches (ZFN, TALEN and CRISPR) make potent tools for genomic targeting. Investigators now have the ability to guide genomic integration of reporter genes and corrected genes, and to monitor the behavior of edited grafts with bioimaging platforms.

CONCLUSIONS

Gene and stem cell therapies, individually or integrated into one therapeutic product, have yet to realize their full potential. Two significant hurdles are the lack of regulatory confidence in the safety and specificity of genomic manipulations in gene correction or in cell differentiation, and a lack of understanding into the long-term survival kinetics and behavior of transplanted cells or integrated gene products. We propose here that bioimaging will play a critical role in overcoming these barriers by providing more quantitative and longitudinal readouts of graft and vector behavior, and lead to more informed and comprehensive patient care. The use of bioimaging in an integrated, collaborative approach will offer valuable insight into the delivery, engraftment, survival and host tissue interactions of vectors and cells, as well as early knowledge of off-target behavior and oncogenic events. By providing powerful tools for guiding clinical practice and scientific development, bioimaging is assured of a bright future as a research field.

REFERENCES

Aiuti, A., F. Cattaneo, S. Galimberti, U. Benninghoff, B. Cassani, L. Callegaro, . . . M. G. Roncarolo (2009). "Gene therapy for immunodeficiency due to adenosine deaminase deficiency." N Engl J Med 360(5): 447-458.

Amsalem, Y., Y. Mardor, M. S. Feinberg, N. Landa, L. Miller, D. Daniels, . . . J. Leor (2007). "Iron-oxide labeling and outcome of transplanted mesenchymal stem cells in the infarcted myocardium." Circulation 116(11 Suppl): I38-45.

Bar-Shir, A., G. Liu, K. W. Chan, N. Oskolkov, X. Song, N. N. Yadav, . . . A. A. Gilad (2013). "Human Protamine-1 as an MRI Reporter Gene Based on Chemical Exchange." ACS Chem Biol.

Barry, F. and M. Murphy (2013). "Mesenchymal stem cells in joint disease and repair." Nat Rev Rheumatol 9(10): 584-594.

Black, M. E., T. G. Newcomb, H. M. Wilson and L. A. Loeb (1996). "Creation of drug-specific herpes simplex virus type 1 thymidine kinase mutants for gene therapy." Proc Natl Acad Sci U S A 93(8): 3525-3529.

Bonetto, F., M. Srinivas, A. Heerschap, R. Mailliard, E. T. Ahrens, C. G. Figdor and I. J. de Vries (2011). "A novel (19)F agent for detection and quantification of human dendritic cells using magnetic resonance imaging." Int J Cancer 129(2): 365-373.

Boztug, K., M. Schmidt, A. Schwarzer, P. P. Banerjee, I. A. Diez, R. A. Dewey, . . . C. Klein (2010). "Stem-cell gene therapy for the Wiskott-Aldrich syndrome." N Engl J Med 363(20): 1918-1927.

Cao, F., S. Lin, X. Xie, P. Ray, M. Patel, X. Zhang, . . . J. C. Wu (2006). "In vivo visualization of embryonic stem cell survival, proliferation, and migration after cardiac delivery." Circulation 113(7): 1005-1014.

Cartier, N., S. Hacein-Bey-Abina, C. C. Bartholomae, G. Veres, M. Schmidt, I. Kutschera, . . . P. Aubourg (2009). "Hematopoietic stem cell gene therapy with a lentiviral vector in X-linked adrenoleukodystrophy." Science 326(5954): 818-823.

Chung, J. K. (2002). "Sodium iodide symporter: its role in nuclear medicine." J Nucl Med 43(9): 1188-1200.

Contag, C. H. and M. H. Bachmann (2002). "Advances in in vivo bioluminescence imaging of gene expression." Annu Rev Biomed Eng 4: 235-260.

Cyranoski, D. (2013). "Stem cells cruise to clinic." Nature 494(7438): 413.

de Almeida, P. E., J. D. Ransohoff, A. Nahid and J. C. Wu (2013). "Immunogenicity of pluripotent stem cells and their derivatives." Circ Res 112(3): 549-561.

de Vries, I. J., W. J. Lesterhuis, J. O. Barentsz, P. Verdijk, J. H. van Krieken, O. C. Boerman, . . . C. G. Figdor (2005). "Magnetic resonance tracking of dendritic cells in melanoma patients for monitoring of cellular therapy." Nat Biotechnol 23(11): 1407-1413.

Dimos, J. T., K. T. Rodolfa, K. K. Niakan, L. M. Weisenthal, H. Mitsumoto, W. Chung, . . . K. Eggan (2008). "Induced pluripotent stem cells generated from patients with ALS can be differentiated into motor neurons." Science 321(5893): 1218-1221.

Doyle, B., B. J. Kemp, P. Chareonthaitawee, C. Reed, J. Schmeckpeper, P. Sorajja, . . . N. M. Caplice (2007). "Dynamic tracking during intracoronary injection of 18F-FDG-labeled progenitor cell therapy for acute myocardial infarction." J Nucl Med 48(10): 1708-1714.

Ebert, A. D., J. Yu, F. F. Rose, Jr., V. B. Mattis, C. L. Lorson, J. A. Thomson and C. N. Svendsen (2009). "Induced pluripotent stem cells from a spinal muscular atrophy patient." Nature 457(7227): 277-280.

Gambhir, S. S., E. Bauer, M. E. Black, Q. Liang, M. S. Kokoris, J. R. Barrio, . . . H. R. Herschman (2000). "A mutant herpes simplex virus type 1 thymidine kinase reporter gene shows improved sensitivity for imaging reporter gene expression with positron emission tomography." Proc Natl Acad Sci U S A 97(6): 2785-2790.

Garber, K. (2013). "Inducing translation." Nat Biotechnol 31(6): 483-486.

Genove, G., U. DeMarco, H. Xu, W. F. Goins and E. T. Ahrens (2005). "A new transgene reporter for in vivo magnetic resonance imaging." Nat Med 11(4): 450-454.

Gilad, A. A., M. T. McMahon, P. Walczak, P. T. Winnard, Jr., V. Raman, H. W. van Laarhoven, . . . P. C. van Zijl (2007). "Artificial reporter gene providing MRI contrast based on proton exchange." Nat Biotechnol 25(2): 217-219.

Griffin, M. D., S. J. Elliman, E. Cahill, K. English, R. Ceredig and T. Ritter (2013). "Concise review: Adult mesenchymal stromal cell therapy for inflammatory diseases: How well are we joining the dots?" Stem Cells 31(10): 2033-2041.

Hacein-Bey-Abina, S., F. Le Deist, F. Carlier, C. Bouneaud, C. Hue, J. P. De Villartay, . . . M. Cavazzana-Calvo (2002). "Sustained correction of X-linked severe combined immunodeficiency by ex vivo gene therapy." N Engl J Med 346(16): 1185-1193.

Hacein-Bey-Abina, S., C. Von Kalle, M. Schmidt, M. P. McCormack, N. Wulffraat, P. Leboulch, . . . M. Cavazzana-Calvo (2003). "LMO2-associated clonal T cell proliferation in two patients after gene therapy for SCID-X1." Science 302(5644): 415-419.

Helfer, B. M., A. Balducci, A. D. Nelson, J. M. Janjic, R. R. Gil, P. Kalinski, . . . R. B. Mailliard (2010). "Functional assessment of human dendritic cells labeled for in vivo (19)F magnetic resonance imaging cell tracking." Cytotherapy 12(2): 238-250.

Higuchi, T., M. Anton, K. Dumler, S. Seidl, J. Pelisek, A. Saraste, . . . M. Schwaiger (2009). "Combined reporter gene PET and iron oxide MRI for monitoring survival and localization of transplanted cells in the rat heart." J Nucl Med 50(7): 1088-1094.

Horii, T., D. Tamura, S. Morita, M. Kimura and I. Hatada (2013). "Generation of an ICF Syndrome Model by Efficient Genome Editing of Human Induced Pluripotent Stem Cells Using the CRISPR System." Int J Mol Sci 14(10): 19774-19781.

Howe, S. J., M. R. Mansour, K. Schwarzwaelder, C. Bartholomae, M. Hubank, H. Kempski, . . . A. J. Thrasher (2008). "Insertional mutagenesis combined with acquired somatic mutations causes leukemogenesis following gene therapy of SCID-X1 patients." J Clin Invest 118(9): 3143-3150.

Joung, J. K. and J. D. Sander (2013). "TALENs: a widely applicable technology for targeted genome editing." Nat Rev Mol Cell Biol 14(1): 49-55.

Kang, W. J., H. J. Kang, H. S. Kim, J. K. Chung, M. C. Lee and D. S. Lee (2006). "Tissue distribution of 18F-FDG-labeled peripheral hematopoietic stem cells after intracoronary administration in patients with myocardial infarction." J Nucl Med 47(8): 1295-1301.

Kershaw, M. H., J. A. Westwood and P. Hwu (2002). "Dual-specific T cells combine proliferation and antitumor activity." Nat Biotechnol 20(12): 1221-1227.

Kooreman, N. G. and J. C. Wu (2010). "Tumorigenicity of pluripotent stem cells: biological insights from molecular imaging." J R Soc Interface 7 Suppl 6: S753-763.

Kwekkeboom, D. J., B. L. Kam, M. van Essen, J. J. Teunissen, C. H. van Eijck, R. Valkema, . . . E. P. Krenning (2010). "Somatostatin-receptor-based imaging and therapy of gastroenteropancreatic neuroendocrine tumors." Endocr Relat Cancer 17(1): R53-73.

Lan, F., A. S. Lee, P. Liang, V. Sanchez-Freire, P. K. Nguyen, L. Wang, . . . J. C. Wu (2013). "Abnormal calcium handling properties underlie familial hypertrophic cardiomyopathy pathology in patient-specific induced pluripotent stem cells." Cell Stem Cell 12(1): 101-113.

Lee, A. S., C. Tang, M. S. Rao, I. L. Weissman and J. C. Wu (2013). "Tumorigenicity as a clinical hurdle for pluripotent stem cell therapies." Nat Med 19(8): 998-1004.

Li, Z., Y. Suzuki, M. Huang, F. Cao, X. Xie, A. J. Connolly, . . . J. C. Wu (2008). "Comparison of reporter gene and iron particle labeling for tracking fate of human embryonic stem cells and differentiated endothelial cells in living subjects." Stem Cells 26(4): 864-873.

Liang, Q., J. Gotts, N. Satyamurthy, J. Barrio, M. E. Phelps, S. S. Gambhir and H. R. Herschman (2002). "Noninvasive, repetitive, quantitative measurement of gene expression from a bicistronic message by positron emission tomography, following gene transfer with adenovirus." Mol Ther 6(1): 73-82.

Liu, G., M. Moake, Y. E. Har-el, C. M. Long, K. W. Chan, A. Cardona, . . . M. T. McMahon (2012). "In vivo multicolor molecular MR imaging using diamagnetic chemical exchange saturation transfer liposomes." Magn Reson Med 67(4): 1106-1113.

Louie, A. Y., M. M. Huber, E. T. Ahrens, U. Rothbacher, R. Moats, R. E. Jacobs, . . . T. J. Meade (2000). "In vivo visualization of gene expression using magnetic resonance imaging." Nat Biotechnol 18(3): 321-325.

MacLaren, D. C., S. S. Gambhir, N. Satyamurthy, J. R. Barrio, S. Sharfstein, T. Toyokuni, . . . H. R. Herschman (1999). "Repetitive, non-invasive imaging of the dopamine D2 receptor as a reporter gene in living animals." Gene Ther 6(5): 785-791.

McMahon, M. T., A. A. Gilad, M. A. DeLiso, S. M. Berman, J. W. Bulte and P. C. van Zijl (2008). "New "multicolor" polypeptide diamagnetic chemical exchange saturation transfer (DIACEST) contrast agents for MRI." Magn Reson Med 60(4): 803-812.

Menasche, P., O. Alfieri, S. Janssens, W. McKenna, H. Reichenspurner, L. Trinquart, . . . A. A. Hagege (2008). "The Myoblast Autologous Grafting in Ischemic Cardiomyopathy (MAGIC) trial: first randomized placebo-controlled study of myoblast transplantation." Circulation 117(9): 1189-1200.

Moore, A., L. Josephson, R. M. Bhorade, J. P. Basilion and R. Weissleder (2001). "Human transferrin receptor gene as a marker gene for MR imaging." Radiology 221(1): 244-250.

Mordwinkin, N. M., P. W. Burridge and J. C. Wu (2013). "A review of human pluripotent stem cell-derived cardiomyocytes for high-throughput drug discovery, cardiotoxicity screening, and publication standards." J Cardiovasc Transl Res 6(1): 22-30.

Moretti, A., M. Bellin, A. Welling, C. B. Jung, J. T. Lam, L. Bott-Flugel, . . . K. L. Laugwitz (2010). "Patient-specific induced pluripotent stem-cell models for long-QT syndrome." N Engl J Med 363(15): 1397-1409.

Musialek, P., L. Tekieli, M. Kostkiewicz, T. Miszalski-Jamka, P. Klimeczek, W. Mazur, . . . W. Wojakowski (2013). "Infarct size determines myocardial uptake of CD34+ cells in the peri-infarct zone: results from a study of (99m)Tc-extametazime-labeled cell visualization integrated with cardiac magnetic resonance infarct imaging." Circ Cardiovasc Imaging 6(2): 320-328.

Ott, M. G., M. Schmidt, K. Schwarzwaelder, S. Stein, U. Siler, U. Koehl, . . . M. Grez (2006). "Correction of X-linked chronic granulomatous disease by gene therapy, augmented by insertional activation of MDS1-EVI1, PRDM16 or SETBP1." Nat Med 12(4): 401-409.

Qin, C., K. Cheng, K. Chen, X. Hu, Y. Liu, X. Lan, . . . Z. Cheng (2013). "Tyrosinase as a multifunctional reporter gene for Photoacoustic/MRI/PET triple modality molecular imaging." Sci Rep 3: 1490.

Schachinger, V., A. Aicher, N. Dobert, R. Rover, J. Diener, S. Fichtlscherer, . . . A. M. Zeiher (2008). "Pilot trial on determinants of progenitor cell recruitment to the infarcted human myocardium." Circulation 118(14): 1425-1432.

Schwartz, S. D., J. P. Hubschman, G. Heilwell, V. Franco-Cardenas, C. K. Pan, R. M. Ostrick, . . . R. Lanza (2012). "Embryonic stem cell trials for macular degeneration: a preliminary report." Lancet 379(9817): 713-720.

Sebastiano, V., M. L. Maeder, J. F. Angstman, B. Haddad, C. Khayter, D. T. Yeo, . . . J. K. Joung (2011). "In situ genetic correction of the sickle cell anemia mutation in human induced pluripotent stem cells using engineered zinc finger nucleases." Stem Cells 29(11): 1717-1726.

Sheikh, A. Y., B. C. Huber, K. H. Narsinh, J. M. Spin, K. van der Bogt, P. E. de Almeida, . . . J. C. Wu (2012). "In vivo functional and transcriptional profiling of bone marrow stem cells after transplantation into ischemic myocardium." Arterioscler Thromb Vasc Biol 32(1): 92-102.

Simara, P., J. A. Motl and D. S. Kaufman (2013). "Pluripotent stem cells and gene therapy." Transl Res 161(4): 284-292.

Soldner, F., J. Laganiere, A. W. Cheng, D. Hockemeyer, Q. Gao, R. Alagappan, . . . R. Jaenisch (2011). "Generation of isogenic pluripotent stem cells differing exclusively at two early onset Parkinson point mutations." Cell 146(2): 318-331.

Stein, S., M. G. Ott, S. Schultze-Strasser, A. Jauch, B. Burwinkel, A. Kinner, . . . M. Grez (2010). "Genomic instability and myelodysplasia with monosomy 7 consequent to EVI1 activation after gene therapy for chronic granulomatous disease." Nat Med 16(2): 198-204.

Strauss, S. (2010). "Geron trial resumes, but standards for stem cell trials remain elusive." Nat Biotechnol 28(10): 989-990.

Sun, N., M. Yazawa, J. Liu, L. Han, V. Sanchez-Freire, O. J. Abilez, . . . J. C. Wu (2012). "Patient-specific induced pluripotent stem cells as a model for familial dilated cardiomyopathy." Sci Transl Med 4(130): 130ra147.

Takahashi, K., K. Tanabe, M. Ohnuki, M. Narita, T. Ichisaka, K. Tomoda and S. Yamanaka (2007). "Induction of pluripotent stem cells from adult human fibroblasts by defined factors." Cell 131(5): 861-872.

Templin, C., R. Zweigerdt, K. Schwanke, R. Olmer, J. R. Ghadri, M. Y. Emmert, . . . U. Martin (2012). "Transplantation and tracking of human-induced pluripotent stem cells in a pig model of myocardial infarction: assessment of cell survival, engraftment, and distribution by hybrid single photon emission computed tomography/computed tomography of sodium iodide symporter transgene expression." Circulation 126(4): 430-439.

Vrtovec, B., G. Poglajen, L. Lezaic, M. Sever, D. Domanovic, P. Cernelc, . . . J. C. Wu (2013). "Effects of intracoronary CD34+ stem cell transplantation in nonischemic dilated cardiomyopathy patients: 5-year follow-up." Circ Res 112(1): 165-173.

Vrtovec, B., G. Poglajen, L. Lezaic, M. Sever, A. Socan, D. Domanovic, . . . J. C. Wu (2013). "Comparison of transendocardial and intracoronary CD34+ cell transplantation in patients with nonischemic dilated cardiomyopathy." Circulation 128(11 Suppl 1): S42-49.

Wang, Y., W. Y. Zhang, S. Hu, F. Lan, A. S. Lee, B. Huber, . . . J. C. Wu (2012). "Genome editing of human embryonic stem cells and induced pluripotent stem cells with zinc finger nucleases for cellular imaging." Circ Res 111(12): 1494-1503.

Ward, K. M., A. H. Aletras and R. S. Balaban (2000). "A new class of contrast agents for MRI based on proton chemical exchange dependent saturation transfer (CEST)." J Magn Reson 143(1): 79-87.

Wehrl, H. F., M. S. Judenhofer, S. Wiehr and B. J. Pichler (2009). "Pre-clinical PET/MR: technological advances and new perspectives in biomedical research." Eur J Nucl Med Mol Imaging 36 Suppl 1: S56-68.

Wu, J. C., I. Y. Chen, G. Sundaresan, J. J. Min, A. De, J. H. Qiao, . . . S. S. Gambhir (2003). "Molecular imaging of cardiac cell transplantation in living animals using optical bioluminescence and positron emission tomography." Circulation 108(11): 1302-1305.

Yaghoubi, S. S., M. C. Jensen, N. Satyamurthy, S. Budhiraja, D. Paik, J. Czernin and S. S. Gambhir (2009). "Noninvasive detection of therapeutic cytolytic T cells with 18F-FHBG PET in a patient with glioma." Nat Clin Pract Oncol 6(1): 53-58.

Youn, H. and J. K. Chung (2013). "Reporter gene imaging." AJR Am J Roentgenol 201(2): W206-214.

Yusa, K., S. T. Rashid, H. Strick-Marchand, I. Varela, P. Q. Liu, D. E. Paschon, . . . L. Vallier (2011). "Targeted gene correction of alpha1-antitrypsin deficiency in induced pluripotent stem cells." Nature 478(7369): 391-394.

Zhu, J., L. Zhou and F. XingWu (2006). "Tracking neural stem cells in patients with brain trauma." N Engl J Med 355(22): 2376-2378.

Chapter 3

Optimization of iPSC technology

Diecke, S., Lu, J., Lee, J., Termglinchan, V., Kooreman, N.G., Burridge, P.W., Ebert, A.D., Churko, J.M., Sharma, A., Kay, M.A., et al. (2015). Novel codon-optimized mini-intronic plasmid for efficient, inexpensive, and xeno-free induction of pluripotency. **Scientific Reports,** *5, 8081.*

ABSTRACT

The development of human induced pluripotent stem cell (iPSC) technology has revolutionized the regenerative medicine field. This technology provides a powerful tool for disease modeling and drug screening approaches. To circumvent the risk of random integration into the host genome caused by retroviruses, non-integrating reprogramming methods have been developed. However, these techniques are relatively inefficient or expensive. The mini-intronic plasmid (MIP) is an alternative, robust transgene expression vector for reprogramming. Here we developed a single plasmid reprogramming system which carries codon-optimized (Co) sequences of the canonical reprogramming factors (Oct4, Klf4, Sox2, and c-Myc) and short hairpin RNA against p53 ("4-in-1 CoMiP"). We have derived human and mouse iPSC lines from fibroblasts by performing a single transfection. Either independently or together with an additional vector encoding for LIN28, NANOG, and GFP, we were also able to reprogram blood-derived peripheral blood mononuclear cells (PBMCs) into iPSCs. Taken together, the CoMiP system offers a new highly efficient, integration-free, easy to use, and inexpensive methodology for reprogramming. Furthermore, the CoMiP construct is color-labeled, free of any antibiotic selection cassettes, and independent of the requirement for expression of the Epstein-Barr Virus nuclear antigen (EBNA), making it particularly beneficial for future applications in regenerative medicine.

INTRODUCTION

The groundbreaking studies of Shinya Yamanaka and James Thomson showed that certain combinations of different pluripotency and oncogenic transcription factors (OCT4, SOX2, NANOG, MYC, and LIN28) were able to initiate the molecular circuitry of pluripotency and convert somatic cells into induced pluripotent stem cells (iPSCs) (Takahashi et al. 2007, Yu et al. 2007). Based on morphology, growth characteristics, and gene expression profiles, these iPSCs are nearly indistinguishable from embryonic stem cells (ESCs) (Bock et al. 2011, Lee et al. 2014). Like ESCs, iPSCs have the potential to differentiate into all three germ layers of the human body, opening new opportunities for drug discovery approaches and stem cell-based therapies. The first iPSCs were derived using viruses that integrate into the host genome, potentially altering the gene expression of the target cell (Takahashi and Yamanaka 2006, Takahashi et al. 2007). To circumvent the subsequent risk of oncogene mutation and potential tumor formation, various non-integrating reprogramming techniques using Sendai virus, mRNAs, and protein- or DNA-based methods have been developed (Jia et al. 2010, Warren et al. 2010, Chou et al. 2011, Okita et al. 2011, Mandal and Rossi 2013). Because mRNA and protein-dependent methods are labor intensive and have a low reprogramming efficiency, most laboratories currently use Sendai virus or different episomal plasmids for the induction of pluripotency. Although Sendai virus-mediated iPSC conversion is the most efficient non-integrating reprogramming technique, there are considerable drawbacks such as high costs and viral biosafety concerns that must be addressed. To that end, we focused on developing an alternative, inexpensive, and user-friendly episomal reprogramming method.

We have recently shown that using a special episomal vector devoid of any bacterial plasmid backbone is an alternative method to generate transgene-free iPSCs from human adult cells (Jia et al. 2010, Narsinh et al. 2010, Diecke et al. 2014). These so-called minicircles are smaller in size than standard plasmids, which also enhance their transfection and expression rate. To produce high-quality minicircle DNA, we used a new simple, rapid, and inexpensive minicircle production system (Kay et al. 2010). However, because the minicircle production and purification methodology is relatively complex and time consuming compared to viral methods, we aimed to develop a novel and user-friendly reprogramming plasmid to overcome these drawbacks. Recently, a mini-intronic plasmid (MIP) vector has been reported as an alternative, robust, non-silencing transgene expression DNA vector in vitro and in vivo (Lu et al. 2013). The defining feature of MIP vectors is the presence of pUC replication origin and the RNA-OUT antibiotic- free selectable marker in a designated noncoding exon. The MIP vector overcomes the transgene silencing observed with plasmids and provides at least 2–10 times higher levels of transgene expression compared to a minicircle vector containing the same expression cassette in vitro and in vivo (Lu et al. 2013). To convert a differentiated cell into a pluripotent state, it is necessary to express high levels of the reprogramming factors with the right stoichiometry within

a transfected cell (Tiemann et al. 2011). The usage rates of codons vary among different organisms and genes, which in turn can influence the levels of protein expression (Aggen et al. 2011). Codon optimization increases protein expression by substitution of rare codons with more frequent codons in the amino acid sequence of the protein of interest. Therefore, our objective here was to investigate the possibility of using a MIP vector backbone together with the codon optimized (Co) reprogramming factors to induce pluripotency efficiently. We introduced a codon-optimized polycistronic expression cassette, in which the four reprogramming factors are controlled by one promoter separated by different self-cleaving 2a peptide sequences and are integrated into a MIP vector. By combining two independent techniques, we were able to generate a novel, single plasmid reprogramming system called CoMiP, which is highly efficient, integration-free, and cost-effective.

RESULTS

Higher transfection and expression efficiencies by using the 4-in-1 CoMiP episomal plasmid

In our previous study, we showed that the transfection and expression efficiencies of episomal plasmids are dependent on their overall size and the length of the DNA sequence required for their bacterial amplification (Lu et al. 2012). Therefore, we first compared the transfection efficiency of our novel 4-in-1 CoMiP plasmids with already established reprogramming techniques, namely minicircle and EBNA/OriP-based episomal plasmids carrying the canonical Yamanaka factors (Jia et al. 2010, Okita et al. 2011). Because the EBNA/ OriP-based episomal plasmids do not express any fluorescence marker genes, we co-transfected an additional plasmid of similar size expressing GFP in order to analyze the transfection efficiencies. Our results showed that the 4-in-1 CoMiP (9.4 kb) vector had the highest transfection efficiency (21.45 ± 9.4%) as well as the best cell survival after the transfection compared to the other 2 techniques (Fig. 1A) and Supplementary Fig. 1. The minicircle transfection efficiency (7.6 kb; 15.05 ± 6.86%) analyzed using FACS was comparable to the EBNA/OriP episomal plasmids (~12 kb; 16.35 ± 5.87%), but we observed an increased level of cell death in the minicircle-transfected cells (Fig. 1B) and Supplementary Figs. 1 and 2. One potential reason for this might be residual chromosomal bacterial DNA after the minicircle preparation (Diecke et al. 2014). Furthermore, by comparing the level of the transgene expression among the independent constructs, we were able to show that the 4-in-1 CoMiP plasmid had the highest Oct4 protein expression level among the reprogramming transgenes (1.6x higher than minicircle and 2.3x higher than regular plasmids) (Supplementary Fig. 3A).

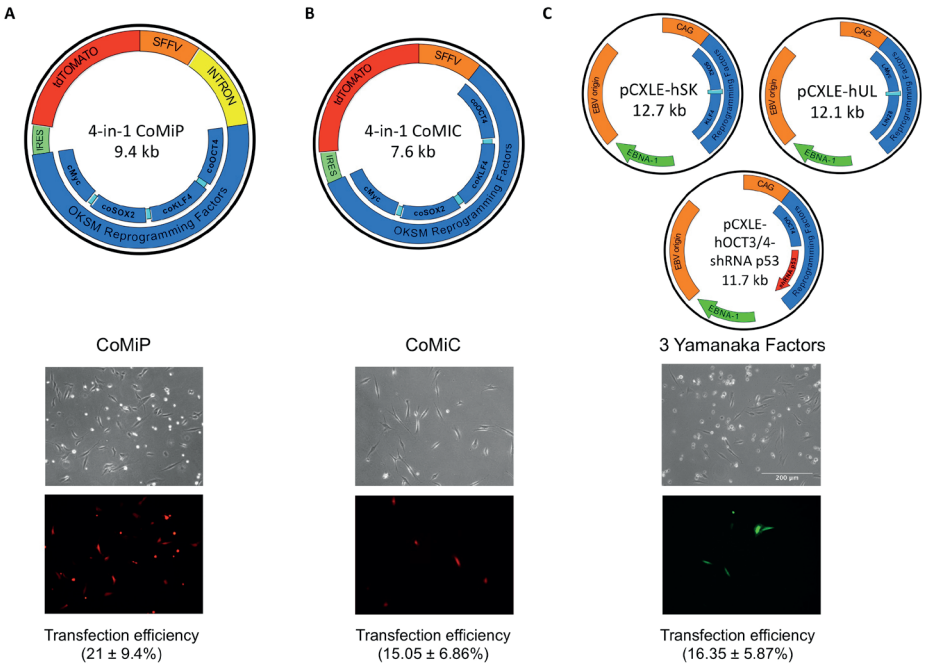


Figure 1. The reprogramming vectors include (A) 4-in-1 CoMiP, (B) 4-in-1 Minicircle, and (C) 3 Yamanaka episomal plasmids. The highest transfection, expression efficiencies, and survival rate were observed with the 4-in-1 CoMiP reprogramming plasmid (A). Lower but moderate transfection efficiency and cell survival rates were observed by using either minicircle (B) or episomal (C) reprogramming plasmids.

Single transfection of the 4-in-1 CoMiP plasmid is sufficient to induce pluripotency

Initially, our goal here was to optimize our minicircle reprogramming technique (Jia et al. 2010). Therefore, we took advantage of a codon-optimized expression cassette of the four canonical reprogramming factors OCT4, KLF4, SOX2, and c-MYC (OKSM) described previously, and combined this cassette with shRNA targeting p53 (Warlich et al. 2011). Using this codon-optimized minicircle (CoMiC) construct, we were able to reprogram adult human fibroblasts via a single nucleofection event (Diecke et al. 2014). However, the minicircle production process is difficult and time consuming, and the overall reprogramming efficiency was below 0.005%. To overcome these limitations, we used our recently developed expression vector system called mini-intronic plasmid (MIP) (Lu et al. 2013). The MIP vector system prevents transgene silencing, which is observed with regular plasmids, by using an engineered intron sequence within the eukaryotic expression cassette. This intronic sequence contains the essential elements required for the bacterial replication and selection of the MIP plasmid (Supplementary Fig. 4). Moreover, we found that the inclusion of the intron into the eukaryotic expression cassette significantly increased the transgene expression for MIP compared to canonical plasmids (2.3-fold lower protein expression) or

minicircle (1.6-fold lower protein expression) constructs (Supplementary Fig. 3) (Lu et al. 2013). Accordingly, we introduced the codon-optimized reprogramming cassette OKSM together with a tdTomato construct and the p53 shRNA into the MIP backbone vector. Using this 4-in-1 codon-optimized mini-intronic plasmid (4- in-1 CoMiP), we were able to reprogram human adult fibroblasts in less than 2 weeks under feeder-free conditions using chemically-defined media (E7, E8) (Fig. 2). Nearly all emerging iPSC clones were true iPSC colonies and not intermediate "pre-iPSCs," which randomly differentiated during the reprogramming process (Papp and Plath 2011). After starting the reprogramming experiment with one million human fibroblasts, a single nucleofection was sufficient to derive approximately 250 iPSC colonies (0.025±0.005%).

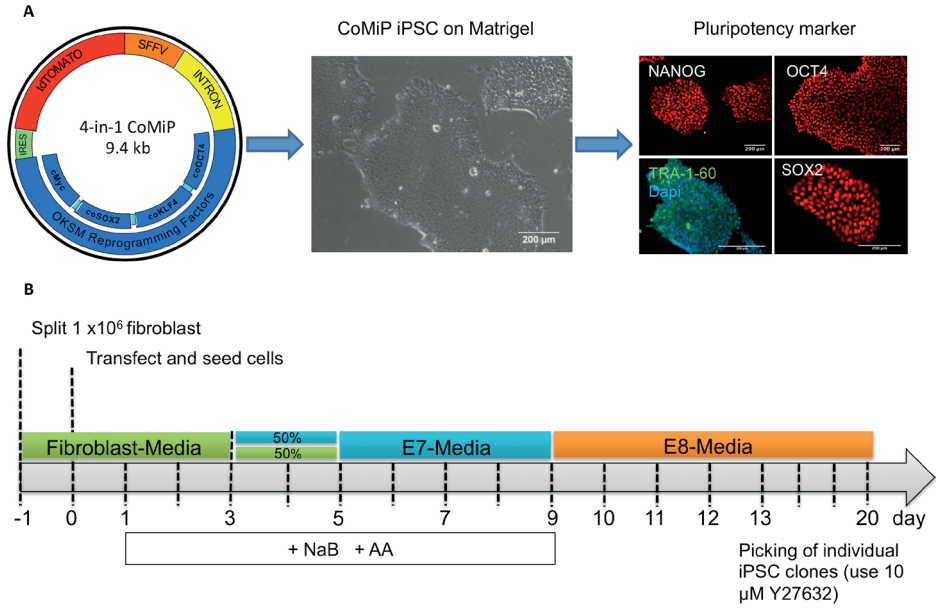


Figure 2. (A) Representative brightfield and fluorescent images demonstrating the pluripotent phenotype of the 4-in-1 CoMiP-derived human iPSCs. (B) Detailed timeline shows the media requirements and chemical treatments used for the reprogramming of human fibroblasts, as well as the time frame in which the first iPSCs are ready for further expansion through individual picking.

CoMiP plasmid is more efficient than the minicircle or EBNA/ OriP episomal plasmid

We next compared the reprogramming efficiency of our newly developed 4-in-1 CoMiP vector against the minicircle and the Yamanaka EBNA/OriP-based episomal plasmids (Fig. 3). From each reprogramming method, we established at least 5 different iPSC clones and confirmed the pluripotent phenotype of those cells via immunostaining and teratoma assays (Supplementary Fig. 5). To compare the different reprogramming methods, we

transfected 1x10^6 fibroblasts from either younger (18–23 years old; n=5) or older (50–70 years old; n=5) human subjects with 12 mg total DNA of the different reprogramming plasmids. Afterwards, we plated 5x10^5 of the transfected cells onto a Matrigel-coated plate and changed the media every other day. After 12 days, a significant number of alkaline phosphatase (AP) positive colonies (97 ± 6, per 500,000 transfected cells) appeared in the culture transfected with the 4-in-1 CoMiP vector (Fig. 3A). By contrast, fewer number of AP-positive colonies were evident in the culture transfected with the Yamanaka EBNA/OriP episomal reprogramming plasmids after 16 days (49 ± 9, per 500,000 transfected cells) (Fig. 3A). A comparison of these two different techniques and time points shows a greater than two-fold superior reprogramming efficiency for the 4-in-1 CoMiP vector (Fig. 3B). Moreover, it appears that the higher expression rates of the 4-in-1 CoMiP transgenes led to an early establishment of the pluripotent state within the transfected cells. As shown before, the reprogramming efficiency of the minicircle technique was low for human fibroblasts and highly variable in each individual experiment, resulting in 3–10 potential iPSC clones per transfection (one million cells, below 0.005%) (Figs. 3A, 3B) (Jia et al. 2010). Interestingly, we were able to reprogram human fibroblasts using the 4-in-1 CoMiP vector with a single Lipofectamine LTX-mediated transfection, albeit with significantly lower ef-

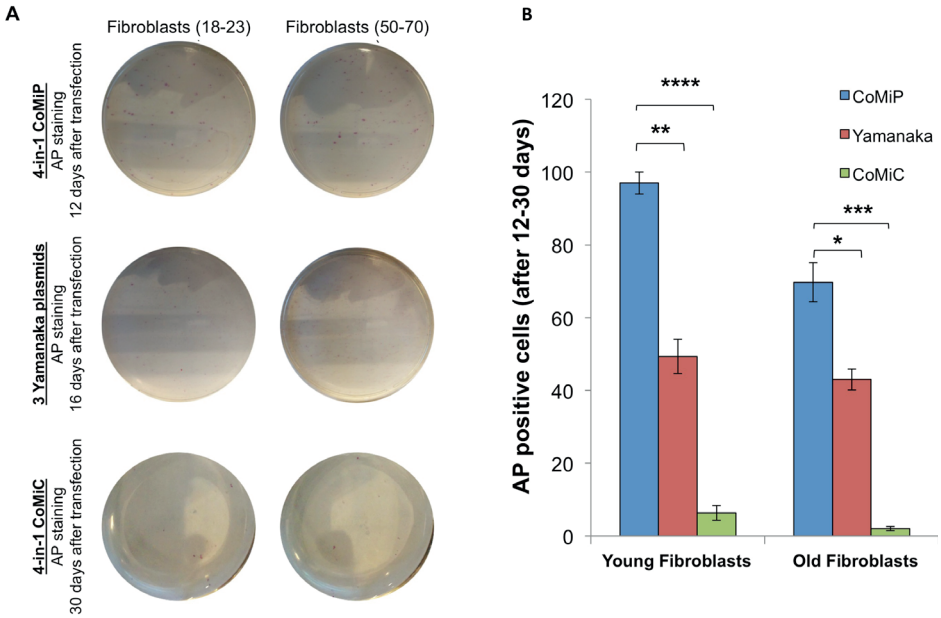


Figure 3. (A) Alkaline phosphatase (AP) staining revealed faster and superior reprogramming efficiency of the 4-in-1 CoMiP plasmid compared to the 3 Yamanaka episomal plasmids in younger and older human subjects within the first 20 days. (B) The chart summarizes the quantification of the AP-positive iPSC colonies observed in panel (A). Statistical significance was analyzed using the Student's t-test and expressed as a P-value. *P < 0.05; **P < 0.01; ***P < 0.001; ****P < 0.0001; ns, not significant.

ficiency (0.002%) (Supplementary Fig. 6). By contrast, we could not derive any iPSC clones performing a single lipofection with either the minicircle or the 3 individual Yamanaka reprogramming vectors (Supplementary Fig. 6).

Induction of pluripotency under chemically-defined conditions and the influence of the innate immune response on the reprogramming efficiency

Because iPSCs or iPSC-derived specialized cell types are potentially relevant for clinical application, it is important to see if we could reprogram human fibroblasts under chemically-defined culture conditions. Therefore, we compared the reprogramming efficiencies of 4-in-1 CoMiP-transfected human fibroblasts initially cultivated in fibroblast media with cells grown under chemically defined conditions (E8 medium plus hydrocortisone on the defined matrix Synthemax) (Chen et al. 2011). Although the use of fully chemically- defined conditions reduced the overall number of AP-positive colonies (by at least 50%), we were able to obtain more than 50 colonies by transfecting 250,000 fibroblasts (Supplementary Fig. 7A). Recently, two publications described a significant effect of the innate immune response on reprogramming efficiency by activating either the Toll-like receptor 3 pathway using Polyinosinic- polycytidylic acid (Poly I:C) or by suppressing interferon-induced apoptosis with the Vaccinia virus protein B18R (Lee et al. 2012, Mandal and Rossi 2013). These studies utilized either protein (Poly I:C) or mRNA (B18R) reprogramming approaches. Because cytosolic DNA also triggers the innate immune response (Stetson and Medzhitov 2006), we therefore analyzed the 4-in-1 CoMiP-mediated reprogramming efficiency after manipulating the immune response by either Poly I:C or B18R. Our experiments showed a slightly reduced number of AP-positive colonies following activation of the innate immune response by Poly I:C, and a slightly increased number of AP-positive colonies following inhibition of the innate immune response by B18R. However, neither activation nor the inhibition of the innate immune response significantly influenced the CoMiP reprogramming efficiency (Supplementary Fig. 7B).

CoMiP-derived iPSCs are pluripotent and similar to human ESCs. We next established multiple 4-in-1 CoMiP-derived iPSC lines using either lipofection or electroporation and confirmed their pluripotency. iPSCs demonstrate the expression of the key pluripotency genes OCT4, NANOG, SOX2, and TRA-1-81, whereas cardiac genes were not expressed compared to differentiated iPSC-derived cardiomyocytes (Fig. 4A). Furthermore, chromatin immunoprecipitation (ChiP) followed by qRT-PCR demonstrated that the newly established iPSCs had similar epigenetic pattern as the human ESC line H7 (Fig. 4B). Promoters of pluripotency genes (OCT4, SOX2, NANOG, and REX1) exhibited histone methylation patterns associated with active gene transcription (H3K4me3), whereas promoter regions of lineage specific genes (NKX2.5) exhibited repressive methylation patterns (H4K27me3). All 4-in-1 CoMiP-derived iPSCs showed pluripotent immunostaining and normal karyotype, and were able to differentiate in vivo into all three germ layers (Fig. 5A–C). Using a small

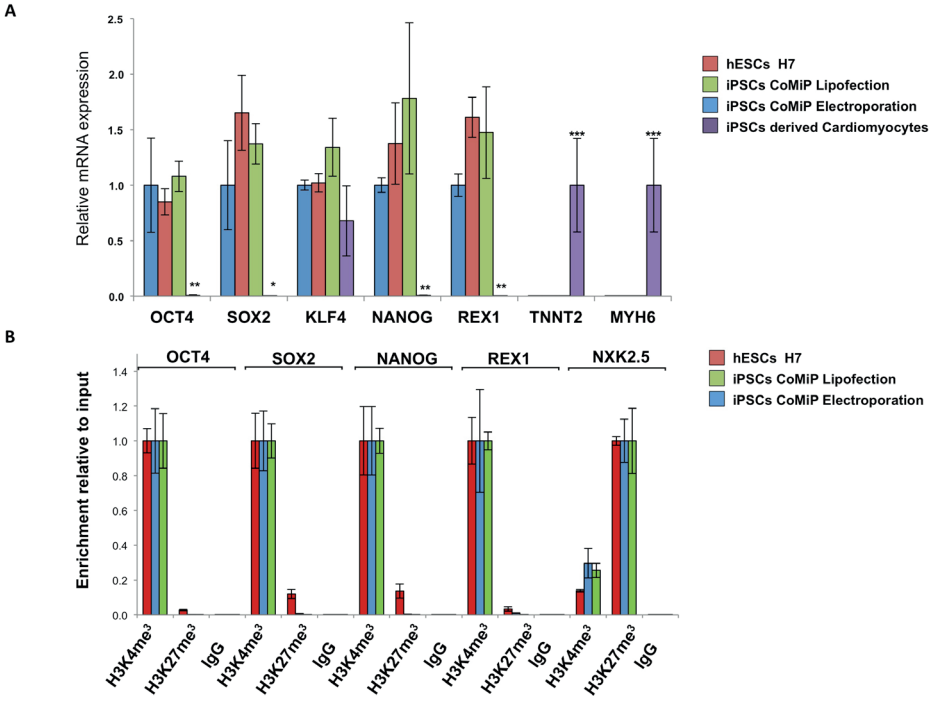


Figure 4. (A–B) 4-in-1 CoMiP-derived iPSCs generated by either electroporation or lipofection showed a similar gene expression and promoter methylation patterns as those observed in the standard human ESC line H7. The 4-in-1 CoMiP-derived iPSCs were negative for the expression of cardiac specific markers such as TNNT2 and MYH6, which were used as a negative control. Statistical significance was analyzed using the student's t-test and expressed as a P-value. *P < 0.05; **P < 0.01; ***P < 0.001; ****P < 0.0001; ns, not significant.

molecule-based monolayer differentiation protocol, we were also able to differentiate the 4-in-1 CoMiP-derived iPSCs effectively in vitro into cardiomyocytes, endothelial cells, and neurons (Fig. 5D) (Chambers et al. 2009, Burridge et al. 2014). A specific PCR assay using primers targeting a 2A-linked junction region between the codon optimized OCT4 and KLF4 regions, and a separate Southern blot analysis using a portion of the tdTomato gene as a probe, confirmed that 4-in-1 CoMiP-derived iPSCs are mainly integration-free (Supplementary Fig. 8). However, some of the CoMiP-derived iPSCs showed traces of plasmid integration or episomal persistence until passage 15 (data not shown). The rate of genomic integration of the 4-in-1 CoMiP plasmid was comparable to the integration rate reported for other reprogramming plasmids (González et al. 2011). Interestingly, we noticed that the PCR-based screening method for integration is not sufficient. With this method, it is not possible to distinguish among residual episomal persistence, partial plasmid integration, and complete plasmid integration. Therefore, we recommend using the PCR primer as a pre-screening method followed by verification by Southern blot. This combined approach enabled us to identify some iPSCs that showed no sign of integration using PCR primer but

were positive for integration in a Southern blot experiment (Supplementary Figs. 8A and 8B).

Induction of pluripotency in other human somatic cell types and in mouse fibroblasts. For purposes of clinical application, it is easier to obtain cells for reprogramming via phlebotomy than skin biopsy. For this reason, we next attempted to reprogram freshly isolated peripheral blood mononuclear cells (PBMCs) using the 4-in-1 CoMiP plasmid. Previous studies already described the successful reprogramming of PBMCs with different episomal vectors expressing the canonical reprogramming factors OCT4, KLF4, SOX2, and c-MYC, either together with NANOG and LIN28 or in different combinations (Chou et al. 2011, Mack et al. 2011, Dowey et al. 2012). Therefore, we transfected $2x10^6$ cells with either the 4-in-1 CoMiP plasmid independently or with an additional plasmid expressing LIN28, NANOG, and GFP (CoMiP LNG). As expected, the reprogramming efficiency of the 4-in-1 CoMiP plasmid alone was relatively low (5–7 colonies, 0.00025%), but was up to 3-fold

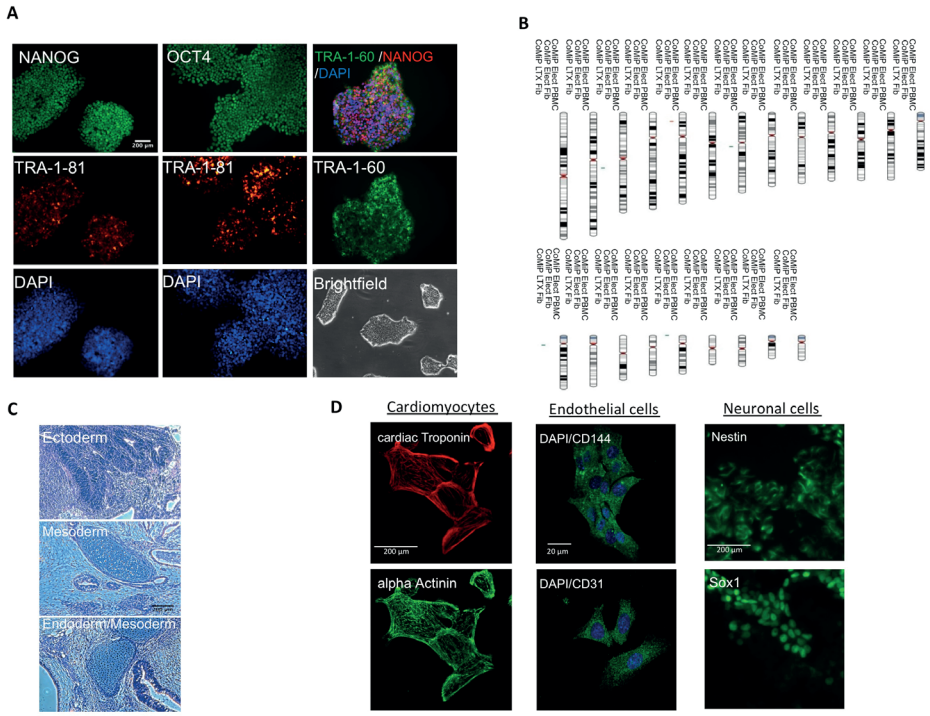


Figure 5. Confirmation of pluripotency of the 4-in-1 CoMiP-derived iPSCs. (A) Immunofluorescence staining on the pluripotency markers NANOG, OCT4, TRA-1-60, and TRA-1-81. DAPI and brightfield images are also shown. (B) 4-in-1 CoMiP-derived iPSCs showed a normal karyotype and (C) from formed in vivo teratomas consisting of ectoderm, mesoderm, and endoderm lineages on H&E staining. (D) Directed in vitro differentiation into cardiomyocytes, endothelial cells, and neuronal cell using specific monolayer differentiation protocols further confirmed the pluripotent nature of the 4-in-1 CoMiP-derived iPSCs.

higher when we transfected both plasmids simultaneously (10–17 colonies, 0.00085%). The subsequently isolated iPSC colonies were positive for the expression of the pluripotency markers OCT4, NANOG, and TRA-1-81 (Fig. 6) and demonstrated a normal karyotype (Fig. 5B). Furthermore, we confirmed the pluripotent phenotype of these cells using either the teratoma or the Scorecard assay. The teratoma assay demonstrated the potential of PBMC-derived iPSCs to differentiate in vivo into all 3 germ layers (Supplementary Fig. 9A). The Scorecard assay is a real-time PCR-based method comparing pluripotency and differentiation data sets derived with multiple hESC cell (Bock et al. 2011). Using this gene expression panel, we also confirmed the pluripotency of our PBMC-derived iPSCs. Furthermore, upon spontaneous differentiation we observed a massive down-regulation of pluripotency-related marker genes and in parallel a strong up-regulation of genes specific for the 3 germ layers (Supplementary Fig. 10A). Based on a previously published robust data set, the Scorecard

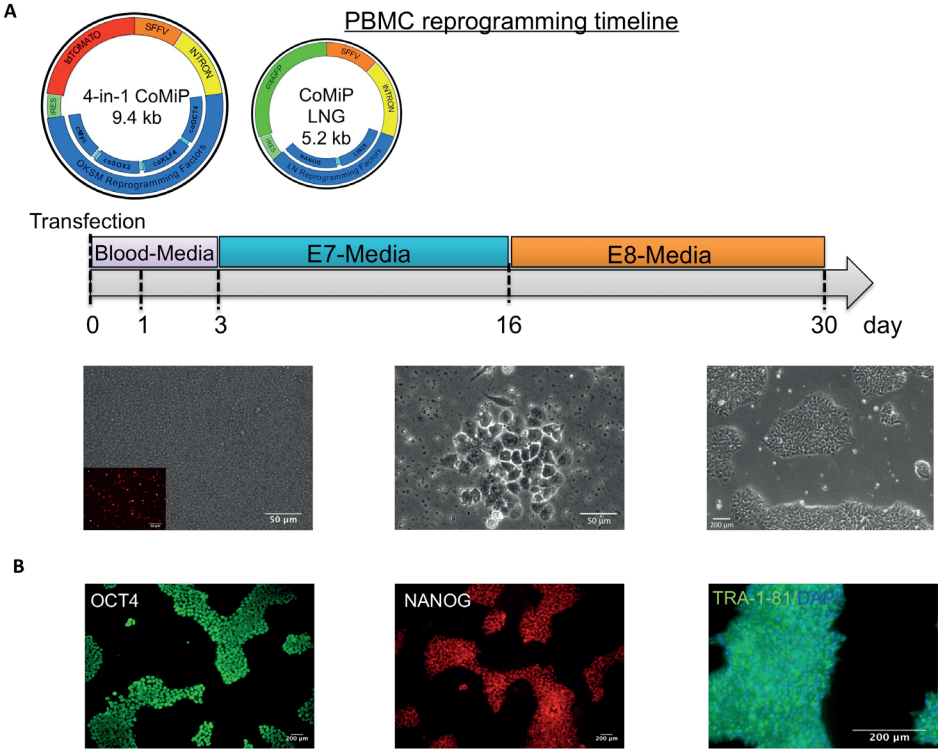


Figure 6. Human peripheral blood mononuclear cells (PBMCs) were successfully reprogrammed using the 4-in-1 CoMiP vector in combination with a Yamanaka vector co-expressing human c-Myc, LIN28, and NANOG. A single transfection of $2x10^6$ PBMCs and subsequent cultivation in blood media and chemical defined media was sufficient to generate multiple iPSC colonies. Representative brightfield (A) and fluorescent (B) pictures exemplified the expected outcome of normal PBMC reprogramming experiment. A robust transfection efficiency (tdTomato expression in PBMCs observed 2 days after the electroporation) and optimal culture condition supporting the initial proliferation of the PBMCs are crucial for a successful experimental outcome.

assay could predict the differentiation propensity of the newly derived iPSCs compared to standardized hESCs (Bock et al. 2011). According to those results, our PBMC-derived iPSC clones 1 and 2 have a comparable endoderm and an increased mesoderm and ectodermal differentiation propensity (Supplementary Fig. 10B). Other clinically relevant and easily obtainable cell types for deriving patient-specific iPSCs include keratinocytes and renal-derived epithelial cells (Zhou et al. 2012, Piao et al. 2014). Therefore, we also tested our new reprogramming plasmid on these cell types. Similar to what was seen with fibroblasts, a single transfection was enough to reprogram these cells, although with a much lower efficiency in the case of the keratinocytes (5–7 colonies, 0.00025%; Supplementary Fig 11). Interestingly, we observed an accelerated reprogramming time course when transfecting renal epithelial cells obtained from clean catch urine sample, with early iPSCs appearing only 3–5 days after transfection (80–100 colonies, 0.008%; data not shown). Finally, we were also able to derive mouse iPSC colonies from tail fibroblasts of C57Bl6 mice with our 4-in-1 CoMiP construct. This might be of special interest because EBV plasmid-based reprogramming vectors cannot replicate in murine cells, which reduces their reprogramming efficiency (Hu 2014). Teratoma assays and immunostaining experiments confirmed the pluripotency of these mouse iPSCs (de Almeida et al. 2014) (Supplementary Fig. 12). A schematic diagram of overall study design and summary of results is shown in Supplementary Fig. 13.

DISCUSSION

When Shinya Yamanaka and colleagues described the first successful induction of pluripotency in somatic cells in 2006, their reprogramming technique utilized retroviruses that integrated into the host cell genome (Takahashi and Yamanaka 2006). Over time, several non-integrating reprogramming techniques based on protein expression, mRNA, or DNA transfection, as well as non-integrating viruses, have been developed (González et al. 2011). However, most of these alternative techniques are either laborious or relatively expensive. Therefore, the initial aim of our study was to simplify and optimize our previously described minicircle reprogramming technique (Jia et al. 2010). To reduce the number of transfections required for the derivation of iPSCs, we introduced a codon-optimized reprogramming cassette carrying the factors OCT4, KLF4, SOX2, and c-MYC together with a tdTomato color marker (coOKSM-IRES-tdTomato) in our minicircle backbone. Using this construct, we were able to reprogram human adult fibroblasts by performing only one transient transfection. However, the reprogramming efficiency of the new 4-in-1 codon optimized minicircle construct (4-in-1 CoMiC) was still extremely low (below 0.002%) (Diecke et al. 2014). Therefore, we decided to evaluate our newly developed transgene expression vector MIP as an alternative shuttle system for the delivery of the reprogramming factors (Lu et al. 2013). We introduced the coOKSM-IRES-tdTomato transgene expression cassette into

the MIP backbone, creating the 4-in-1 CoMiP vector. We were able to reprogram numerous somatic human somatic cells (fibroblasts, PBMCs, keratinocytes, and renal epithelial cells) and mouse cell lines (C57Bl6) via a single electroporation. Furthermore, when the 4-in-1 CoMiP vector was cotransfected with a second plasmid expressing LIN28 and NANOG, a single transfection was sufficient to reprogram blood-derived erythroblasts.

Compared to other established non-integrating reprogramming methods, the 4-in-1 CoMiP has multiple advantages. It is color-labeled, time-efficient, inexpensive, and easy-to-use, thus providing an attractive alternative for use in regenerative medicine. In contrast to most of the previously published reprogramming plasmids, the CoMiP system is based on a single plasmid, which does not require the EBNA1 and OriP elements of the Epstein-Barr virus (EBV) for its function (Gonzalez et al. 2009, Okita et al. 2011). In addition, because of the engineered intronic region of the polycistronic 4-in-1 CoMiP plasmid, the overall size of our construct was significantly reduced, which in turn increased the transfection efficiency in different somatic cell types. Moreover, the smaller size allowed us to include a RFP marker gene to track the transfection efficiency of our target cell lines. We hypothesize that the higher exogenous transgene expression rate mediated by the intronic sequence and the codon optimization of the 4-in-1 CoMiP plasmid are sufficient to reactivate the endogenous circuit of pluripotency within the first few days, whereas more persistent transgene expression would require other EBNA1- and OriP-based episomal vectors.

Interestingly, we observed a significantly reduced time course for the induction of pluripotency using the 4-in-1 CoMiP, which allowed us to select the first iPSC colonies 12 days after the initial transfection. Furthermore, the 4-in-1 CoMiP reprogramming protocol is compatible to fully chemically defined culture conditions using E7 and E8 media, which may prove to be important for future clinical applications of iPSCs. By contrast, the EBNA1 and OriP sequences used in the Yamanaka episomal reprogramming system are derived from the human pathogenic EBV, and thus carry the risk of possibly altering the innate immune response-triggered gene expression of the subsequently derived iPSCs and may limit their clinical applications (Jia et al. 2010). Moreover, the generation and/or function of iPSCs derived from patients carrying an acute or latent infection with EBV (a common occurrence) may be affected by virus-induced overexpression of EBNA1, which in turn could lead to a hyper-expression of the exogenous reprogramming genes (Young and Rickinson 2004).

The use of DNA-based reprogramming methods always carries the potential risk of random genomic integration of the transfected DNA into the host cell genome (Stadtfeld and Hochedlinger 2010). Thus, the transfection of fewer plasmids (1 plasmid in the case of the 4-in-1 CoMiP vs. 3 Yamanaka episomal plasmids) is a less risky method for generating integration-free iPSCs. Compared to other single reprogramming plasmids described so far, our 4-in-1 CoMiP protocol is more efficient and is highly reproducible in a broad variety of somatic cell types (Gonzalez et al. 2009, Kaji et al. 2009, Yu et al. 2009, Chou et

al. 2011). Keratinocytes, however, were relatively difficult to reprogram, resulting in only a few iPSC colonies, probably due to the change from specialized keratinocyte media into more chemically-defined conditions of the E7 or E8 media. By contrast, the reason for the enhanced reprogramming process of the renal epithelial cells may be their propensity for mesenchymal-to-epithelial transition and their higher expression levels of E-Cadherin (Li et al. 2010, Redmer et al. 2011, Esteban et al. 2012, Liu et al. 2013). Therefore, we believe that the reprogramming efficiencies of the different constructs used in this study also depend on the cell type used for the reprogramming experiment (Jia et al. 2010, Narsinh et al. 2010).

Aside from the aforementioned DNA-based reprogramming methods, there are three other commonly used integration-free techniques for inducing pluripotency: protein addition, mRNA transfection, and Sendai virus infection. The disadvantages of the protein reprogramming technique are that it is expensive, inefficient, and slow (Kim et al. 2009, Lee et al. 2012). Using modified mRNA for the induction of pluripotency is an elegant and unique approach that guarantees derivation of integration-free iPSCs without any further screening experiments. However, this method is laborious and requires a repetitive series of daily mRNA transfections for up to 14 days and the pre-treatment of the initial cell types with the expensive interferon alpha antagonist B18R (Colamonici et al. 1995). This molecule is crucial for enhancing cell survival during the series of mRNA transfections and for efficient reprogramming (Mandal and Rossi 2013). Another limitation of this technique is its dependency on the feeder cell and conditioned media, which brings an extra risk of potentially transmitting undetected human pathogens (Amit et al. 2005). One publication addressed the aforementioned disadvantages of mRNA based reprogramming. Using synthetic, self-replicative RNA, Yoshioka and colleagues showed that a single mRNA transfection was sufficient to derive iPSCs from newborn or adult human fibroblasts (Yoshioka et al. 2013). However, further validation is required to establish how robust and reproducible this particular method is. By comparison, the Sendai virus is perhaps the most efficient integration-free reprogramming method currently available. However, it is also the most expensive method, and requires more stringent biosafety containment measures and a separate tissue culture room. The persistence of residual viral material requires an extended period of tissue culture time (10 to 20 passages) to establish virus-free iPSC lines for further downstream analysis and differentiation experiments (González et al. 2011). Finally, another recently published approach used small-molecule compounds to reprogram mouse somatic cells (Hou et al. 2013). However, the efficiency of this technique is also quite low, and the study must be reproduced using human somatic cells in order to be of broader clinical interest.

In summary, the 4-in-1 CoMiP is an effective alternative reprogramming method for deriving integration-free iPSCs from various donor tissue sources, including PBMCs under chemically defined conditions without using animal-derived products. Compared to other DNA-based reprogramming methods like the minicircle or the Yamanaka three individual

plasmids system, the CoMiP construct is faster and less expensive for inducing pluripotency in a somatic cell type (Supplementary Fig. 13). Furthermore, the cost effectiveness of our new reprograming technique should be emphasized because of the current impetus for major research institutions to generate large-scale iPSC banks. For example, the estimated cost for the consumables per derived iPSC line is, $80 for 4-in-1 CoMiP versus $500 for Sendai virus. Hence this CoMiP construct will allow novice and inexperienced researchers alike to easily obtain bona fide iPSCs within 14 days. Aside from being the fastest reprogramming method, the 4-in-1 CoMiP plasmid does not result in intermediate iPSCs and, due to its color label, the entire reprogramming process is easy to monitor. With all these superior qualities, we believe that this new technology is of special interest given the great potential of iPSCs in regenerative medicine.

METHODS

Construction of the 4-in-1 CoMiP construct

The 4-in-1 CoMiP construct was constructed from the 4-in-1 CoMiC vector. The 1.4 kb OIPR intron carrying pUC origin and RNA-OUT selectable marker was PCR-amplified from the MIP parental plasmid by using forward primer "5'ATTGGGATCTTCACACAGCA3'" and reverse primer "5'TTAGCTAGTCAGCTAGTGGAC3'". *AgeI* sites were incorporated into the 5' end of both primers. The PCR product was digested with *AgeI* restriction enzyme and then ligated with *AgeI*-digested 4-in-1 CoMiC. The *AgeI* cut 4-in-1 CoMiC once at the 3' end of SFFV promoter. The ligation was selected on LB solid media with 6% sucrose (the condition for RNA-OUT selection). The positive colonies were then selected for sequencing to determine the insertion orientation in the resultant 4-in-1 CoMiP plasmid. The U6-driven p53 expression cassette was PCR-amplified from the pCXLE-hOCT3/4-shp53-F vector by using the forward primer "5'GACGCCGCCATCTCTAGG3'" and reverse primer "5'CCCGGGCTGCAGGAATTC3'". *SpeI* sites were incorporated into the 5' end of both primers. The *SpeI*-digested U6-p53 PCR product was then ligated with *XbaI* digested 4-in-1 CoMiP. *XbaI* cut 4-in-1 CoMiP once in the short (36 bp) spacer backbone region. The ligation was then selected on LB solid media with 6% sucrose and the positive colonies were selected for sequencing. However, only the backward insertion was able to grow in this experiment design. This provided the final version of 4-in-1 CoMiP vector.

Production of minicircle, episomal plasmid, and CoMiP vectors

The minicircle plasmids were produced as described previously (Jia et al. 2010, Diecke et al. 2014). The episomal reprogramming plasmids used for this study were purified using the QIAGEN Plasmid Maxi Kit (QIAGEN, USA). The 4-in-1 CoMiP construct was transformed into NTC4862 DH5α competent cells and then plated on 6% sucrose solid media (see

Nature Technology's NTC vector User's Manual) and propagated at 30°C for 24–48 hours. Individual colonies were picked and miniprep was performed (QIAprep Spin Miniprep Kit, USA). Thereafter, a 100 µl aliquot of the 4-in-1 CoMiP bacterial culture was inoculated with 100 ml of 6% sucrose liquid media and incubated for 16–18 hr at 37°C. This culture was then used to isolate the 4-in-1 CoMiP vector by using the QIAGEN Plasmid MAXI Kit.

Reprogramming using 4-in-1 CoMiC, 4-in-1 CoMiP, or episomal plasmids

Reprogramming using the minicircle technique was performed as previously described with an optimized minicircle backbone (4-in-1 CoMiC) and some changes in the reprogramming procedure (Narsinh et al. 2010). To increase cell survival after electroporation, the minicircle DNA was purified using Zymoclean Gel DNA Recovery Kit (Zymo Research, USA). The DNA of either the 4-in-1 CoMiP plasmid or the 3 individual Yamanaka episomal plasmids was isolated according to the QIAGEN Plasmid Plus Maxi Kit instructions. The following paragraph describes the fibroblast transfection procedure, which was identical for all reprogramming plasmids used in this study. One day before the reprogramming experiment, 1×10^6 human fibroblasts were plated onto a 10 cm dish. On the ensuing day, the cells were trypsinized and electroporated with 12 µg DNA of the reprogramming plasmids (12 µg of 4-in-1 minicircle CoMiC or 4-in-1 CoMiP, 4 µg each of the individual Yamanaka episomal plasmids) using the Invitrogen Neon system (1600 volt, 10 ms, and 3 pulses, transfection efficiency should be more than 50%). Subsequently, these cells were equally distributed onto one or two Matrigel-coated plates (5.5×10^5 cells) in fibroblast media. On the following morning (day 1), the media was changed to fibroblast media with the addition of 0.2 mM sodium butyrate plus 50 µg/mL ascorbic acid. On day 3, the media was changed to Essential 7 media supplemented with 0.2 mM sodium butyrate and 50 µg/mL ascorbic acid. Between day 6 (4-in-1 CoMiP) and day 20 (4-in-1 minicircle CoMiC, Yamanaka episomal plasmids) the first iPSC-like colonies appeared, after which we switched the culture conditions to Essential 8 medium and hypoxic conditions. Around days 12–30, the iPSC colonies were large enough for manual selection under the microscope. In general, we selected 6 individual iPSC clones using the Vitrolife stem cell cutting tool with a 10 µL tip, and transferred them into 6 different wells of a Matrigel-coated plate with Essential 8 media in the presence of 10 µM ROCK inhibitor (Y-27632). After 5–7 days, the individual colonies became big enough to dissociate into single cells using 0.5 mL TrypLE for 8 minutes. Thereafter, we washed the cells once and passaged them into one well of a Matrigel-coated 6-well plate containing 2 mL Essential 8 media and 10 µM ROCK inhibitor (Y-27632).

Karyotype analysisof human iPSCs

The iPSC lines were detached from the culture plate using Accutase for 8 min and centrifuged at 300 g for 3 min. iPSC pellets were resuspended in 200 µL of PBS and DNA was isolated using the DNeasy blood and tissue kit (Qiagen, Valencia, CA). DNA was submitted to the

Stanford Functional Genomics Facility for SNP karyotyping using the HuCytoSNP-12 chip (Illumina). CNV and SNP visualization were performed using KaryoStudio v1.4 (Illumina).

RNA extraction and quantitative real-time PCR

Total RNA was isolated using RNeasy Plus Mini Kit (Qiagen 74134). The reverse transcriptase PCR was performed using the iScript™ cDNA Synthesis Kit (Bio-rad 170-8891). The quantitative real-time PCR was performed using the iQ SYBR Green Supermix (Bio-rad 170-8882) and a CFX96™ real-time PCR detector (Bio-Rad). The relative mRNA levels were normalized to the values of 18S mRNA for each reaction. Primer information shown in Supplementary Table 2.

Chromatin immunoprecipitation assays

The antibodies used in ChIP assays were 39159 for H3 tri-methylation lysine4 (Active Motif), 39155 for H3 tri-methylation lysine27 (Active Motif), and sc-2027 for control IgG (Santa Cruz Biotechnology). Antibodies were incubated with Dynabeads (Invitrogen, 10003D) for 12hr at 4°C. The main fraction of the crosslinked and sheared chromatin was incubated with the antibody-conjugated Dynabeads and a small aliquot of the chromatin was used as an input control. After an overnight incubation at 4°C, the incubated beads were rinsed with sonication buffer (50 mM Hepes pH 7.9, 140 mM NaCl, 1 mM EDTA, 1% Triton X-100, 0.1% Na-deoxycholate, 0.1% SDS, 0.5 mMPMSF), high salt buffer (50 mM Hepes pH 7.9, 500 mM NaCl, 1 mM EDTA, 1% Triton X-100, 0.1% Na-deoxycholate, 0.1% SDS, 0.5 mM PMSF), and LiCl buffer (20 mM Tris, pH 8.0, 1 mM EDTA, 250 mM LiCl, 0.5% NP-40, 0.5% Na-deoxycholate, 0.5 mM PMSF). The washed beads were incubated with an elution buffer (50 mM Tris, pH 8.0, 1 mM EDTA, 1% SDS, 50 mM NaHCO3) for 1hr at 65°C and then de-crosslinked overnight with 5M NaCl at 65°C. The immunoprecipitated DNA was treated with Rnase A and Proteinase K, and purified by ChIP DNA clean and concentrator (Zymo Research D5205). The immunoprecipitated and input DNA wa sanalyzed by quantitative real-time PCR. Primer information is shown in Supplementary Table 3.

Fluorescent activated cell sorting (FACS)

Transfected fibroblasts were detached using TrypLE (Life Technologies) and stained when indicated with propidium iodide (PI) to determine the percentage of viable cells. Samples were analyzed using a LSR Fortessa Analyzer and BD FACSDiva, as well as FlowJo softwares.

Scorecard pluripotency and differentiation panel

iPSC or iPSC-derived embryoid bodies (10 days old) were harvested either using Trizol or RNeasy Mini Kit (QIAGEN). Subsequently, samples were further processed as described in TaqMan® hPSC Scorecard™ Panel User Guide (Life Technologies). Samples were prepared in a384-well plate and analyzed by 7900HT System.

Screening for potential plasmid integration by Southern blot or PCR

Genomic DNA was extracted from CoMiP-transfected cell line, lentivirus-infected control cell line, and negative control fibroblast cell line. Twenty µg of genomic DNA from each sample was digested with SpeI overnight at 37 °C. SpeI cut the CoMiP expression cassette once and linearized the vector. Digested DNA samples were separated by electrophoresis on a 1% agarose gel and blotted onto a nitrocellulose membrane. 0.1ng SpeI-digested or non-digested CoMiP vector DNA was incorporated into the same Southern gel as linearized or non-linearized non-integrating control. Twenty µg SpeI-digested genomic DNA of negative control fibroblasts were mixed with one CoMiP vector linearized non-integrating control sample to imitate genomic DNA extracted from cell lines. The Southern blot membrane was hybridized with [P-32] dCTP-labeled 702bp tdTomato probe (PCR product by using forward primer "5'GTGAGCAAGGGCGAGGAGG3'" and reverse primer "5'CTTGTACAGCTCGTCCATGC3'") overnight at 65°C. CoMiP signals were detected through phosphoimaging. The PCR screening was performed by using the standard Taq polymerase protocol and primers summarized in Supplementary Table 1.

Analysis of protein expression differences by Western blot

Cells were harvested in RIPA lysis buffer (Sigma) supplemented with protease (Complete Mini; Roche) and phosphatase inhibitors (Phosphatase Inhibitor Cocktail I and II; Sigma). Five to twenty µg of total protein were separated by SDS-PAGE and transferred to polyvinylidene fluoride membranes following the protocol of the manufacturer (Invitrogen XCell SureLock™ Mini Cell Electrophoresis and Wet Blot System). Membranes were incubated overnight with the primary antibodies and with appropriate peroxidase-conjugated secondary antibodies for 45 min. Chemiluminescence (PerkinElmer) reaction was carried out. Primary antibodies used were against OCT4 (R&D Systems, AF1759) and α-tubulin (Sigma). Secondary antibodies were anti-goat and anti-mouse horseradish peroxidase (Jackson Laboratories).

Immunofluorescence of human iPSCs

Human iPSCs ($1x10^4$ cells/chamber) derived with the different methods were seeded on Matrigel coated 8-chamber slides in a final volume of 200µL of E8 medium. After 24-72 hr, cells were washed 3X with PBS and fixed for 20 min at RT using 100 µL 4% paraformaldehyde (PFA) in PBS. Thereafter, cells were washed with 200 µL PBS (3X) and incubated for 15 min at RT with 100µL of permeabilization solution (0.2% Triton X-100 in PBS). Next, cells were washed twice with PBS and incubated with blocking solution (2% BSA or 4% goat serum or 2% FBS in PBS), for 1 hr at RT or overnight at 4°C. After another wash step (PBS), cells were covered overnight at 4°C with primary antibody diluted appropriately in blocking solution (100 µL per chamber). The following day, slides were washed 4X for 10 min using 1% goat serum, 0.1% Tween-20 in PBS. Afterwards, cells were incubated with

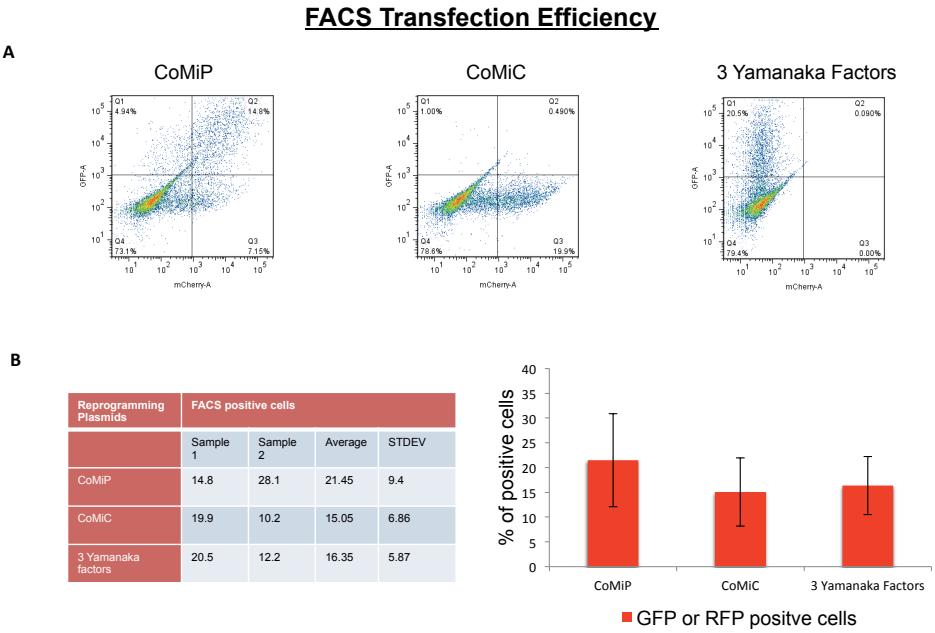
the appropriate secondary antibody diluted in blocking solution, for 1 hr at RT (100 µL per chamber). After a final wash step (4X, 1% goat Serum, 0.1% Tween-20 in PBS, for 10 min), chambers were removed and cells were incubated with a small amount of Vectashield mounting medium with DAPI. Afterwards, cells were covered and sealed using nail varnish.

Immunofluorescence of human iPSC-derived cardiomyocytes

iPSC-CMs were passaged onto Matrigel-coated coverslips and immunohistochemistry was performed as described before (Lan et al., 2013). Samples were analyzed using a LSM 510 Meta inverted confocal microscope (Carl Zeiss) and ZEN software (Carl Zeiss).

Statistical Analysis

Data shown are presented as mean ± standard error mean (SEM) of four or more independent experiments. Differences are considered statistically significant at $P<0.05$, and assessed using the Student's t test (for paired samples).

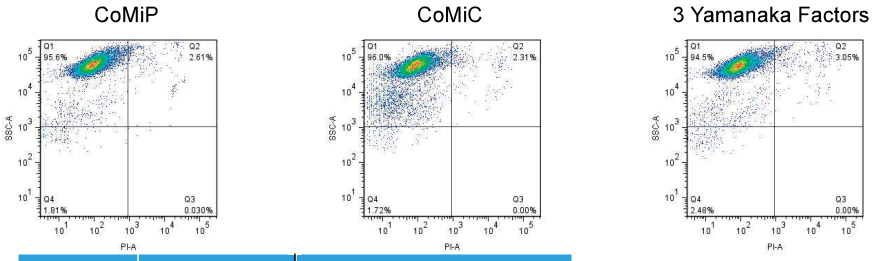


Reprogramming Plasmids	FACS positive cells			
	Sample 1	Sample 2	Average	STDEV
CoMiP	14.8	28.1	21.45	9.4
CoMiC	19.9	10.2	15.05	6.86
3 Yamanaka factors	20.5	12.2	16.35	5.87

Supplementary Figure 1. Comparison of the transfection efficiencies using different reprogramming plasmids. (A-B) FACS blot showing the comparable transfection efficiencies of CoMiP, CoMiC, and 3 Yamanaka factors.

FACS Viability – Propidium Iodide Staining

A

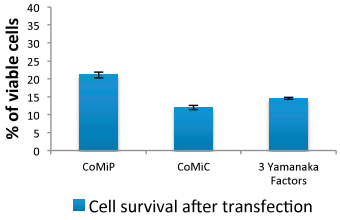


B

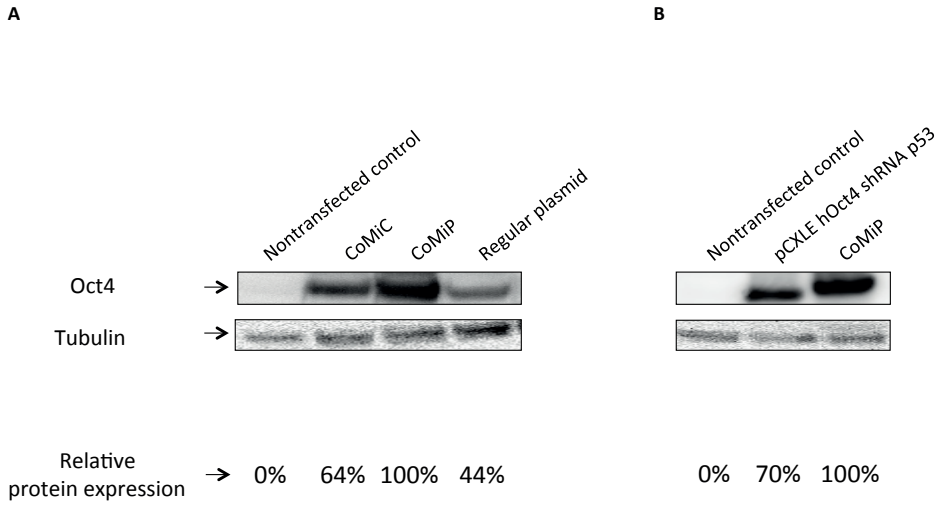
Reprogramming Plasmids	Cell number		FACS			
	Sample 1	Sample 2	Sample 1		Sample 2	
			PI negative	PI positive	PI negative	PI positive
CoMiP	245000	230000	96.9	3.1	97.8	2.2
CoMiC	167500	162500	97.7	2.3	97.4	2.6
3 Yamanaka factors	130000	140000	97.0	3.0	96.4	3.6

C

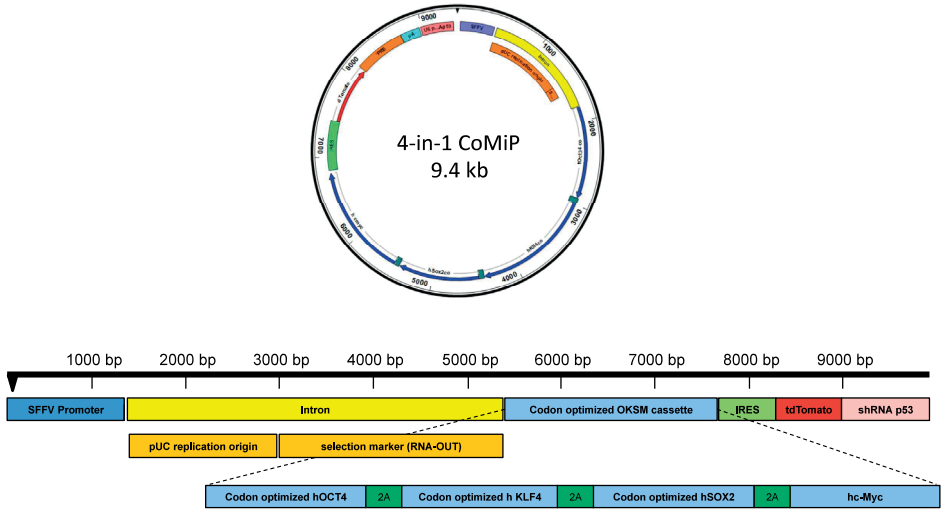
Reprogramming Plasmids	Relative number of cells alive after transfection (1100000 cell transfected)			
	Sample 1	Sample 2	Average	STDEV
CoMiP	21.58	20.45	21.02	0.80
CoMiC	11.55	12.39	11.97	0.60
3 Yamanaka factors	14.77	14.33	14.55	0.31



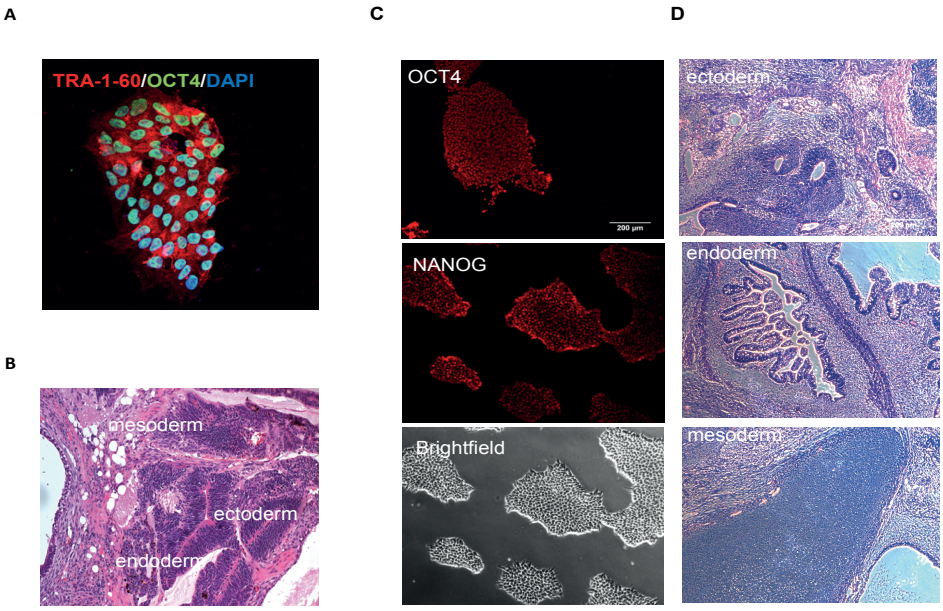
Supplementary Figure 2. Cell viability after transfection of the individual reprogramming plasmids. (A-C) Using propidium iodide staining followed by FACS analysis, we observed the highest cell survival after transfecting with the CoMiP reprogramming plasmid.



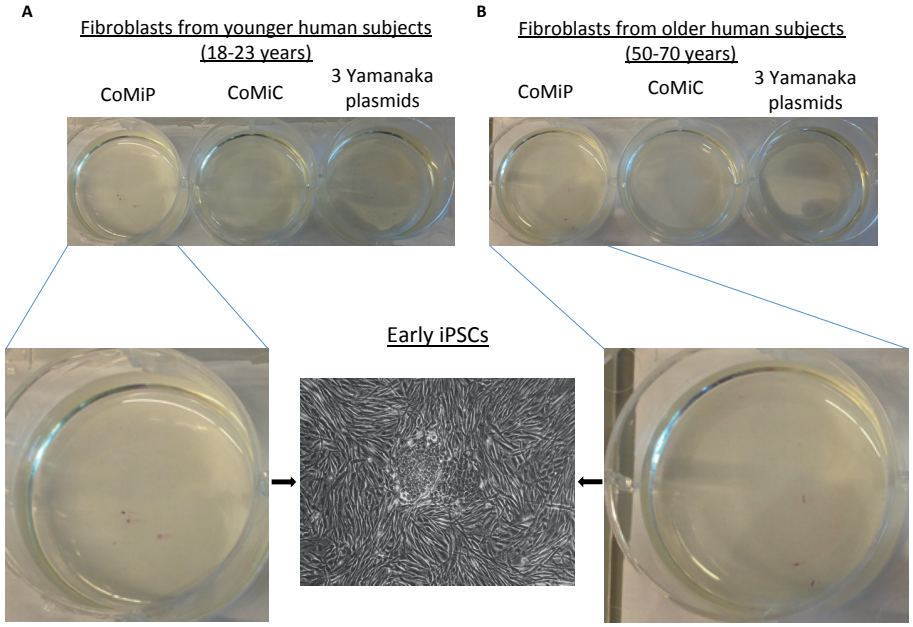
Supplementary Figure 3. Analysis of the transient transgene expression levels in HEK 293 cells produced by the different constructs used in this study (minicircle, CoMiP, and regular Plasmid). (A) Codon-optimized reprogramming cassette OKSM cloned into minicircle, mini-intronic plasmid (MiP), or regular plasmid backbone were transfected into HEK 293 cells. Western blot illustrates that the level of protein expression is dependent on the plasmid backbone. All constructs had the same SFFV promoter sequence driving the OKSM expression. (B) Comparison of the transgene expression efficiency mediated by different constructs (Yamanaka episomal plasmids, pCXL, and the 4-in-1 CoMiP) showed superior OCT4 protein expression (Western blot) levels by the CoMiP construct.



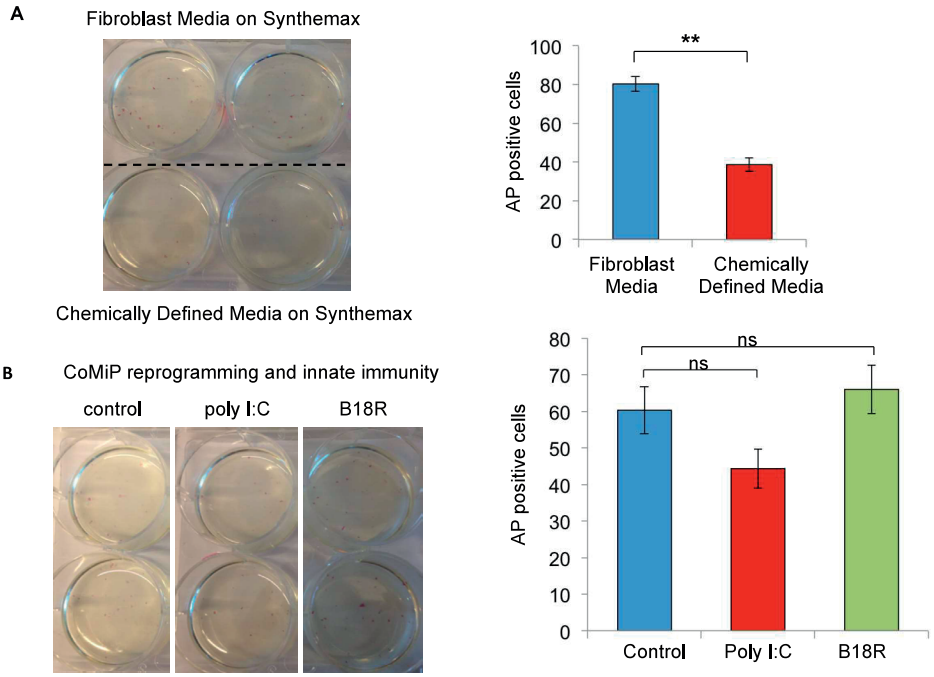
Supplementary Figure 4. Schematic overview of the 4-in-1 codon-optimized reprogramming plasmid (CoMiP). The plasmid-defining intronic sequence contains the antibiotic-free bacterial selection cassette. The strong spleen focus forming virus (SFFV) promoter drives the expression of the reprogramming factors that are linked to a fluorescent marker (tdTomato) through an internal ribosomal entry site (IRES) site. Addition of a p53 shRNA further increased the reprogramming efficiency.



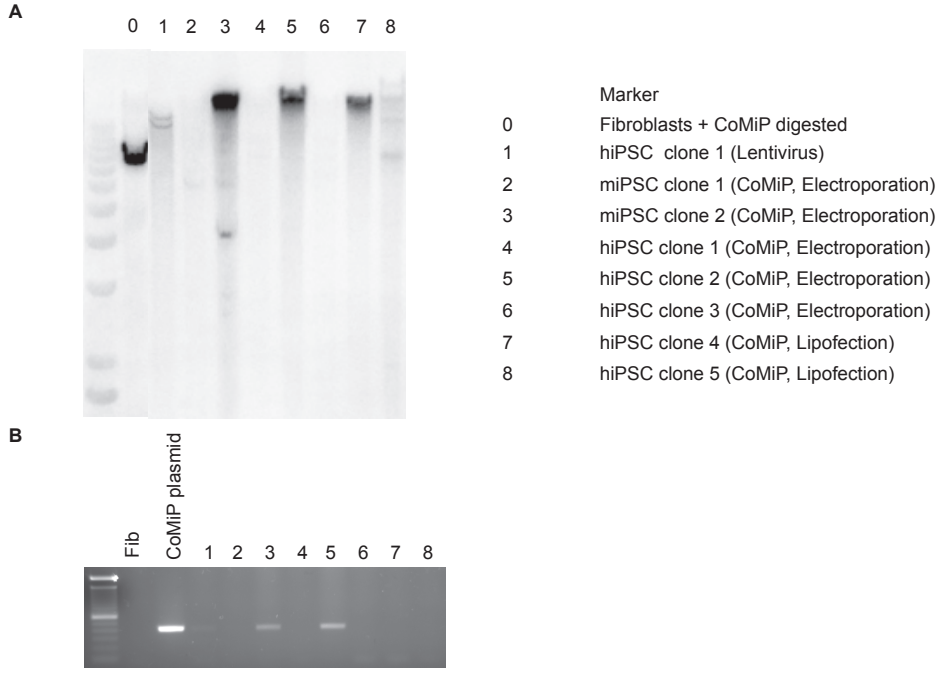
Supplementary Figure 5. (A) Immunofluorescence staining (TRA-1-60, OCT4 and nuclear DAPI staining) and (B) in vivo teratoma differentiation assays confirmed pluripotency of the iPSCs derived with the 3 individual Yamanaka episomal plasmids pCXLE-hOCT3/4-shRNA p53, pCXLE-hl-Myc/LIN28, and pCXLE-hSOX2/KLF4. (C) The pluripotent identity of the iPSCs derived with the 4-in-1 minicircle (CoMiC) was confirmed by Brightfield picture Immunofluorescence staining (OCT4 and NANOG) and (D) in vivo teratoma differentiation assays.



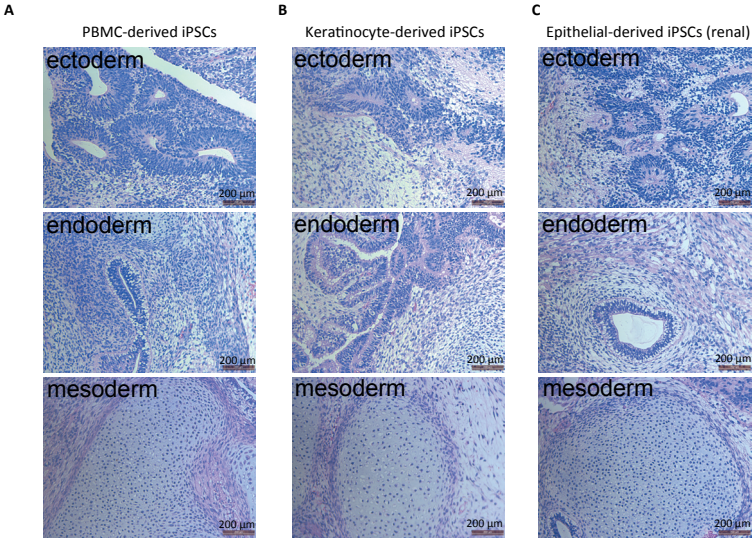
Supplementary Figure 6. Comparison of the three different plasmid-based reprogramming strategies on human fibroblasts. CoMiC, CoMiP, and episomal plasmids were transiently introduced into fibroblasts of (A) young (18-23 years) versus (B) old (50-70 years) human subjects using lipofection. Using the 4-in-1 CoMiP plasmid, we were able to derive 3-10 iPSC colonies after transfecting $2x10^5$ cells in a single attempt, whereas we could not generate any iPSCs by using a single-pass lipofection with the minicircle or episomal plasmid. Representative pictures showing different AP positive cell colonies (magnification) and a proliferating pre-iPSC clone.



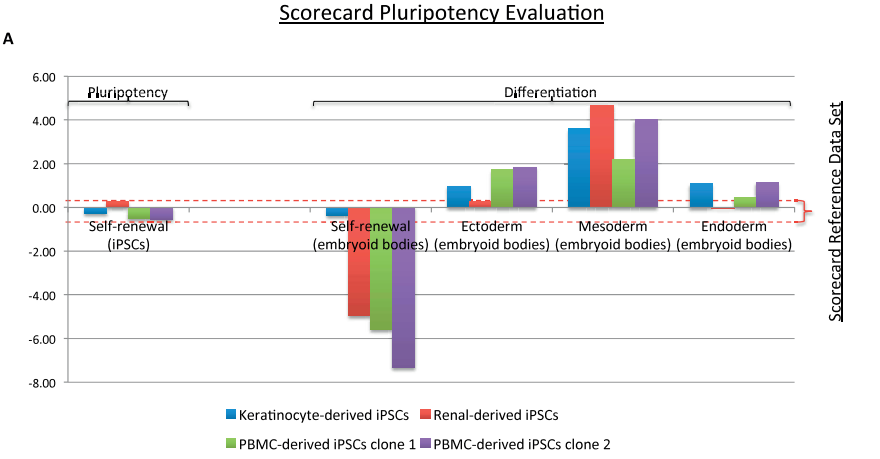
Supplementary Figure 7. Analysis of the reprogramming efficiencies under chemical defined condition and influences of the innate immune response. (A) Robust 4-in-1 CoMiP-mediated reprogramming efficiency under chemical defined conditions using Synthemax and chemical defined media E7. However, reprogramming using fully chemical defined condition reduced the overall number of AP-positive colonies by roughly 50%. (B) Manipulating the innate immune response had no statistically significant influence on the 4-in-1 CoMiP-mediated reprogramming efficiency. Activation of the innate immune response by poly I:C slightly reduced the number of AP-positive cells, whereas inhibition of the innate immune response by B18R slightly enhanced the number of AP-positive cells. Statistical significance was analyzed using the student's t-test and expressed as a P-value. *P < 0.05; **P < 0.01; ns, not significant



Supplementary Figure 8. Reprogramming with 4-in-1 CoMiP plasmid allows derivation of integration-free iPSCs. (A) Southern blot experiments were used to screen different 4-in-1 CoMiP-derived iPSCs for potential integrations. Lanes 0 and 1 represent control DNA either from untransfected 4-in-1 CoMiP plasmid DNA (internal control for the Southern blot probe targeting the tdTomato sequence, 0) or from a lentiviral-derived iPSC line (1, integration control). Clones 2, 4, and 6 were integration-free and also free of residual plasmid DNA. Clones 3, 5 and 7 might be free of integration but still had residual CoMiP DNA within the individual clones as circulating episomes. The clone at line 8 shows multiple genomic integrations. (B) PCR-based screening method for potential integration using primers targeting the junction region between OCT4 and KLF4 within the 4-in-1 CoMiP plasmid mainly confirms the Southern blot results, albeit with a lower specificity (clones 7 and 8 appear negative).

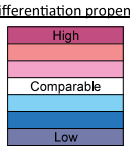


Supplementary Figure 9. PBMC, keratinocytes, and renal epithelia-derived iPSCs are pluripotent. After injection into nude mice, all of the individual iPSCs generated teratomas representing all 3 germ layers.

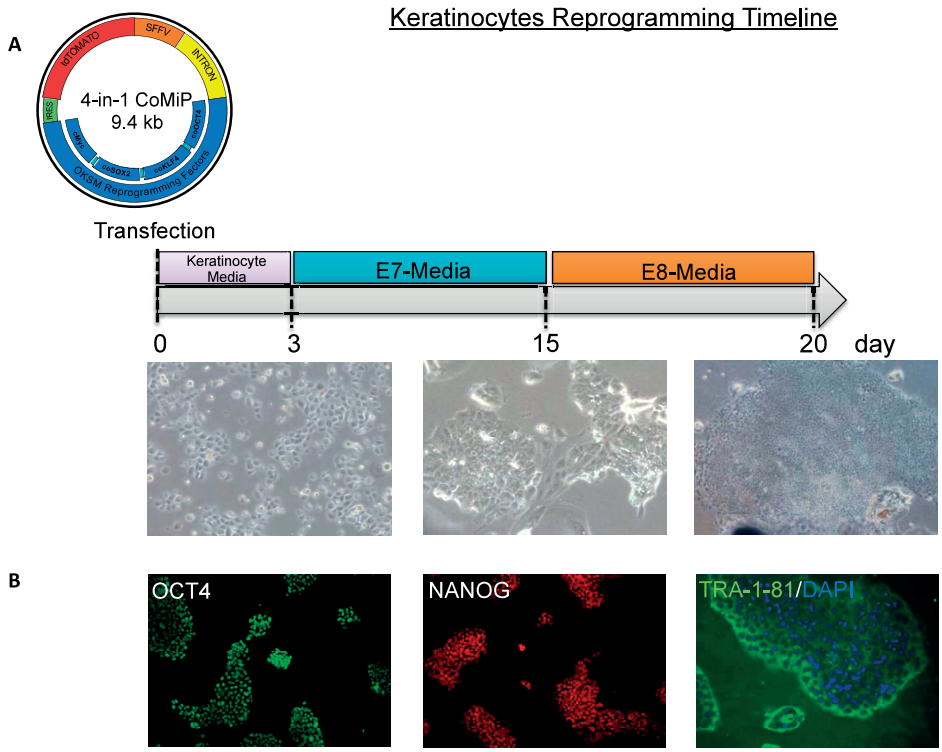


B

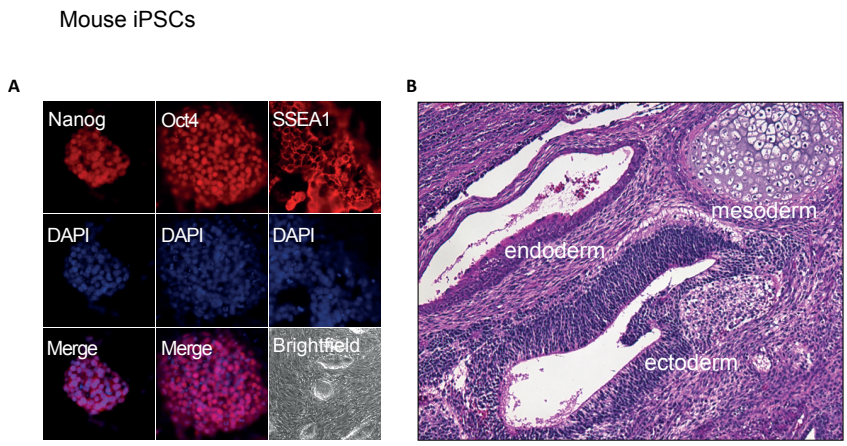
iPSC line	Ectoderm Germ layer	Mesoderm Germ layer	Endoderm Germ layer
Keratinocyte-derived iPSCs	0,97	3,61	1,09
Renal-derived iPSCs	0,24	4,67	-0,03
PBMC-derived iPSCs clone 1	1,71	2,17	0,43
PBMC-derived iPSCs clone 2	1,83	4,00	1,12



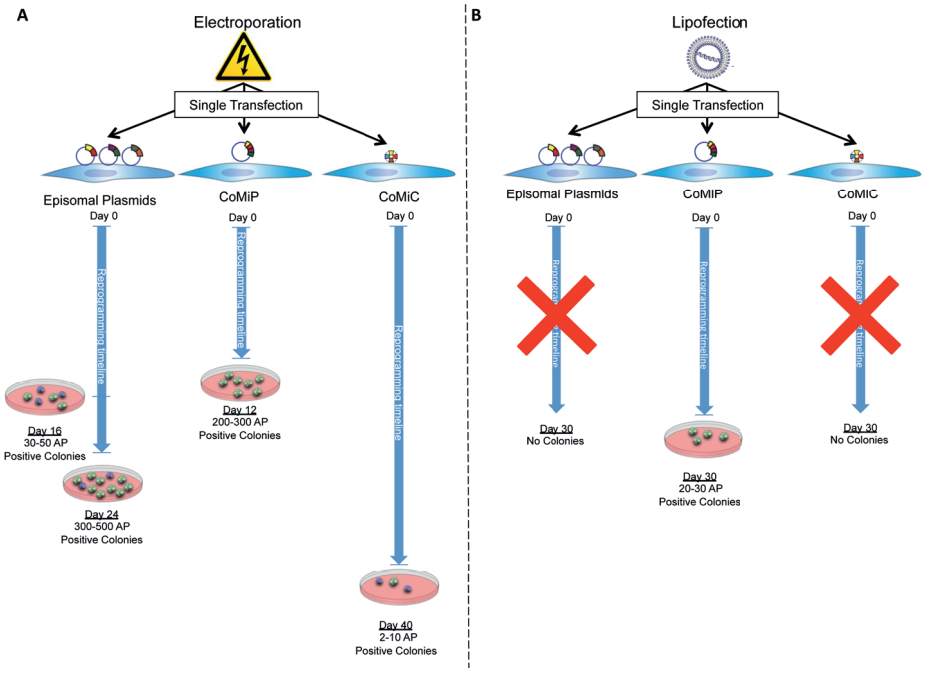
Supplementary Figure 10. Pluripotency analysis of the PBMC, keratinocytes and renal epithelia-derived iPSCs using the TaqMan® hPSC ScorecardTM Panel. (A) The individual iPSC lines showed overall expression scores of pluripotency genes that were comparable to the reference. After spontaneous differentiation into embryoid bodies, the expression of the self- renewal genes were down-regulated and the expression of genes of the 3 germ layers were up- regulated. (B) All cell lines showed a high propensity to differentiate into the 3 germ layers.



Supplementary Figure 11. CoMiP reprogramming of human keratinocytes. (A) Timeline shows the expected morphological changes of 4-in-1 CoMiP-transfected and reprogrammed human keratinocytes. (B) The expression of different pluripotency related marker genes within the keratinocyte-derived iPSCs was confirmed by immunofluorescence staining for OCT4, NANOG, and TRA-1-81.



Supplementary Figure 12. The pluripotency of the 4-in-1 CoMiP-derived murine iPSC cell lines were confirmed by *in vitro* and *in vivo* experiments. (A) Immunofluorescence staining showed the expression of different pluripotency associated marker genes (Nanog, Oct4, and SSEA-1). (B) Teratoma assay confirmed the pluripotent potential of murine iPSCs to form ectoderm, endoderm, and mesoderm layers *in vivo*.



Supplementary Figure 13. Summarizing the study design of the comparison of the three reprogramming methods. (A) One single nucleofection was sufficient enough to reprogram human adult fibroblast using any one of the three methods. Using the 4-in-1 CoMiP vector system was faster than the episomal or minicircle reprogramming methods without generating intermediate iPSCs (blue cell cluster) but only fully reprogrammed iPSCs (green cell cluster). (B) Interestingly, only the 4-in-1 CoMiP vector system was able to induce pluripotency in adult human fibroblasts by using one single lipofection to deliver the reprogramming plasmids. AP, alkaline phosphatase.

SUPPLEMENTARY TABLES

Supplementary Table 1

Primer sequences for integration test:

OCT4-KLF4 Set2	**F**: GGCAGAAGGGCAAGAGAAG
	R: CTCCCGCCATCTGTTGTTAG

Supplementary Table 2

Primer sequences for qPCR:

NANOG	**F**: TTCACTGTGTTAGCCAGGATG	**R**: ATGTCTTTTCTAGGCAGGGC
SOX2	**F**:GAGAAGTTTGAGCCCCAGG	**R**: AGAGGCAAACTGGAATCAGG
REX1	**F**: TTCTCCTTTGTTTTACGTTTGGG	**R**: AGATCACACCATTGCACTCC
KFL4	**F**: ACCTACACAAAGAGTTCCCATC	**R**: TGTGTTTACGGTAGTGCCTG
OCT4	**F**: CCATGCATTCAAACTGAGGTG	**R**: CCTTTGTGTTCCCAATTCCTTC
TNNT2	**F**: AGCGGAAAAGTGGGAAGAG	**R**: TCCAAGTTATAGATGCTCTGCC
MYH6	**F**: GGGACAGTGGTAAAAGCAAAG	**R**: ACAAAGTGAGGATGGGTGG
18s	**F**: GAGACTCTGGCATGCTAACTAG	**R**: GGACATCTAAGGGCATCACAG

Supplementary Table 3

Primer sequences for ChIP-qPCR:

NANOG-ChIP	**F**: AGAGAAGGAGAGAGGGTTAAGG
	R: GCAGGTGCCACCAAGTTAT
OCT4-ChIP	**F**: CTTGGGTCTGATAAGGGTCAAA
	R: CAGGGTCTCTCACATCTCCTA
SOX2-ChIP	**F**: CATGAACGGCTGGAGCAA
	R: GCTGGTCATGGAGTTGTACTG
REX1-ChIP	**F**: AAGTGTCTGGCGGTGATTT
	R: CTCCAGAGATAAGAGGAGAGGAA
NKX2.5-ChIP	**F**: GTAAGAGCGGCTTGACCTAC
	R: CTGACTTTCTACAAATGCTGAGTG

Supplementary Table 4 (Scorecard results)

Scorecard Analysis of iPSC Lines (Fold-change)

Target Name	Category	PBMC CI1	Keratinocyte	Renal	PBMC CI2
CDH9	Ectoderm	0,30	0,07	0,18	0,36
COL2A1	Ectoderm	3,43	0,39	1,57	2,18
DMBX1	Ectoderm	0,06	0,09	0,46	0,13
DRD4	Ectoderm	0,08	0,01	0,09	0,06
EN1	Ectoderm	1,51	0,63	7,21	1,38
LMX1A	Ectoderm	0,37	0,12	1,50	0,43
MAP2	Ectoderm	5,65	0,58	0,18	6,06
MYO3B	Ectoderm	2,89	0,61	1,13	2,85
NOS2	Ectoderm	0,15	0,22	0,26	0,11
NR2F1/NR 2F2	Ectoderm	0,39	0,04	0,08	0,46
NR2F2	Ectoderm	19,76	0,75	4,93	19,91
OLFM3	Ectoderm	0,46	0,51	0,52	0,48
PAPLN	Ectoderm	0,89	0,23	1,45	0,84
PAX3	Ectoderm	111,11	1,73	4,04	73,80
PAX6	Ectoderm	2,17	0,15	0,27	2,62
POU4F1	Ectoderm	0,64	0,72	1,90	0,07
PRKCA	Ectoderm	0,37	0,28	0,27	0,36
SDC2	Ectoderm	9,79	6,22	16,61	10,69
SOX1	Ectoderm	0,03	0,04	0,07	0,20
TRPM8	Ectoderm	25,24	2,40	1,28	28,11
WNT1	Ectoderm	0,22	0,24	0,47	0,18
ZBTB16	Ectoderm	0,64	0,25	1,27	0,72
AFP	Endoderm	0,01	0,01	0,01	0,00
CABP7	Endoderm	0,00	0,04	0,83	0,00
CDH20	Endoderm	1,04	0,47	0,46	1,00
CLDN1	Endoderm	1,01	0,47	0,56	1,22
CPLX2	Endoderm	0,02	0,05	0,02	0,01
ELAVL3	Endoderm	0,07	0,70	4,88	0,07
EOMES	Endoderm	0,03	0,02	0,06	0,04
FOXA1	Endoderm	0,45	0,14	0,64	0,05
FOXA2	Endoderm	0,00	0,60	0,01	0,00
FOXP2	Endoderm	0,37	0,37	0,42	0,33
GATA4	Endoderm	0,02	0,04	0,24	0,01
GATA6	Endoderm	0,00	0,01	0,03	0,01
HHEX	Endoderm	0,07	0,09	0,48	0,07
HMP19	Endoderm	0,42	1,24	1,74	0,34
HNF1B	Endoderm	0,21	0,03	0,17	0,12
HNF4A	Endoderm	0,00	0,27	0,06	0,00
KLF5	Endoderm	1,39	1,95	3,05	1,30
LEFTY1	Endoderm	0,04	1,07	0,52	0,05

LEFTY2	Endoderm	0,22	0,95	0,60	0,24
NODAL	Endoderm	0,01	0,26	0,27	0,01
PHOX2B	Endoderm	0,13	0,14	0,28	0,11
POU3F3	Endoderm	0,53	0,06	0,67	0,51
PRDM1	Endoderm	0,14	0,03	0,07	0,13
RXRG	Endoderm	1,93	0,20	0,05	1,47
SOX17	Endoderm	0,02	0,17	1,97	0,18
SST	Endoderm	12,84	4,76	1,63	16,16
FGF4	Mesendoderm	0,12	13,55	51,21	0,08
GDF3	Mesendoderm	0,68	11,90	8,75	0,87
NPPB	Mesendoderm	0,02	0,08	0,01	0,09
NR5A2	Mesendoderm	159,74	372,92	532,81	160,16
PTHLH	Mesendoderm	1,58	0,29	0,58	1,41
T	Mesendoderm	0,00	0,00	0,00	0,01
ABCA4	Mesoderm	1,64	1,58	2,80	1,90
ALOX15	Mesoderm	0,12	0,21	0,41	0,15
BMP10	Mesoderm	0,28	0,29	0,58	0,22
CDH5	Mesoderm	54,01	1,98	1,73	54,66
CDX2	Mesoderm	0,32	0,26	0,25	0,26
COLEC10	Mesoderm	0,57	0,48	2,21	0,77
ESM1	Mesoderm	0,50	1,02	1,81	0,66
FCN3	Mesoderm	1,12	1,41	6,03	1,13
FOXF1	Mesoderm	0,91	2,22	5,59	1,47
HAND1	Mesoderm	0,02	0,38	1,31	0,09
HAND2	Mesoderm	1,62	2,85	3,59	0,48
HEY1	Mesoderm	0,82	0,27	0,37	0,79
HOPX	Mesoderm	0,28	2,36	4,67	4,87
IL6ST	Mesoderm	1,17	0,73	1,32	1,11
NKX2-5	Mesoderm	0,87	4,64	1,96	0,38
ODAM	Mesoderm	0,25	2,53	3,29	1,42
PDGFRA	Mesoderm	0,09	1,02	0,74	0,10
PLVAP	Mesoderm	0,89	0,32	0,77	0,81
RGS4	Mesoderm	0,15	1,06	0,45	0,15
SNAI2	Mesoderm	3,40	0,29	0,20	3,79
TBX3	Mesoderm	0,02	0,08	0,20	0,02
TM4SF1	Mesoderm	11,15	0,60	0,21	14,61
CXCL5	Self-renewal	23,67	4,46	5,59	31,89
DNMT3B	Self-renewal	omitted	omitted	omitted	omitted
HESX1	Self-renewal	omitted	omitted	omitted	omitted
IDO1	Self-renewal	0,15	0,30	0,33	0,17
LCK	Self-renewal	1,67	1,66	2,59	1,27
NANOG	Self-renewal	0,49	1,07	1,55	0,40
POU5F1	Self-renewal	0,31	0,70	0,92	0,30
SOX2	Self-renewal	0,53	0,52	1,07	0,69
TRIM22	Self-renewal	0,91	0,37	0,81	1,00

Fold-change legend	
fc > 100	Upregulated
10 < fc <= 100	
2 < fc <= 10	
0.5 <= fc <= 2	Comparable
0.1 <= fc < 0.5	
0.01 <= fc < 0.1	
fc < 0.01	Downregulated
omitted	

Scorecard Analysis of Embryoid Bodies (Fold-change)

Experiment Filename				
Target Name	**Category**	**PBMC CI1**	**Renal**	**PBMC CI2**
CDH9	Ectoderm	0,26	0,02	0,51
COL2A1	Ectoderm	31,89	0,65	21,25
DMBX1	Ectoderm	1,05	0,01	0,74
DRD4	Ectoderm	0,33	0,27	1,39
EN1	Ectoderm	102,37	3,75	5,81
LMX1A	Ectoderm	157,80	0,22	81,69
MAP2	Ectoderm	25,76	0,21	10,09
MYO3B	Ectoderm	21,22	20,75	25,59
NOS2	Ectoderm	0,11	14,22	0,40
NR2F1/NR2F2	Ectoderm	84,81	0,17	133,13
NR2F2	Ectoderm	890,29	1.357,35	872,57
OLFM3	Ectoderm	48,53	0,52	44,44
PAPLN	Ectoderm	0,31	0,46	0,31
PAX3	Ectoderm	672,77	7,25	2.505,62
PAX6	Ectoderm	26,99	0,12	151,11
POU4F1	Ectoderm	39,66	1,16	15,34
PRKCA	Ectoderm	1,52	0,26	0,29
SDC2	Ectoderm	52,75	2,52	10,21
SOX1	Ectoderm	0,94	0,06	1,96
TRPM8	Ectoderm	86,50	1,01	12,72
WNT1	Ectoderm	3.542,76	65,58	3.343,77
ZBTB16	Ectoderm	9,25	0,40	18,89
AFP	Endoderm	18,80	1,46	0,01
CABP7	Endoderm	3,26	0,32	4,00
CDH20	Endoderm	7,75	0,39	53,48
CLDN1	Endoderm	3,39	10,65	7,20
CPLX2	Endoderm	10,33	0,13	1,36
ELAVL3	Endoderm	13,76	0,30	5,42
EOMES	Endoderm	0,03	0,37	0,09
FOXA1	Endoderm	3,22	0,38	0,24

FOXA2	Endoderm	0,81	0,49	0,01
FOXP2	Endoderm	19,19	0,64	10,72
GATA4	Endoderm	0,79	1,13	0,06
GATA6	Endoderm	0,74	2,07	0,35
HHEX	Endoderm	0,89	0,19	0,06
HMP19	Endoderm	50,30	5,74	8,28
HNF1B	Endoderm	5,70	1,22	2,80
HNF4A	Endoderm	2,79	1,13	0,06
KLF5	Endoderm	2,74	15,93	12,36
LEFTY1	Endoderm	0,01	0,03	0,02
LEFTY2	Endoderm	0,23	0,11	0,74
NODAL	Endoderm	0,01	0,06	0,06
PHOX2B	Endoderm	10,11	0,24	7,21
POU3F3	Endoderm	3,03	0,01	1,77
PRDM1	Endoderm	0,42	1,29	0,47
RXRG	Endoderm	94,86	12,02	35,09
SOX17	Endoderm	36,51	13,05	0,26
SST	Endoderm	133,19	32,06	132,01
FGF4	Mesendoderm	0,04	4,87	0,21
GDF3	Mesendoderm	0,07	3,76	0,46
NPPB	Mesendoderm	0,58	3,25	9,02
NR5A2	Mesendoderm	17,90	9,67	98,89
PTHLH	Mesendoderm	120,07	15,16	52,43
T	Mesendoderm	0,00	0,04	0,01
ABCA4	Mesoderm	12,06	30,33	26,86
ALOX15	Mesoderm	3,21	6,63	1,33
BMP10	Mesoderm	111,32	264,25	21,54
CDH5	Mesoderm	25,86	3.381,32	15,19
CDX2	Mesoderm	6,60	13,44	5,34
COLEC10	Mesoderm	10,68	0,82	3,15
ESM1	Mesoderm	68,94	8,96	19,25
FCN3	Mesoderm	8,69	14,21	0,29
FOXF1	Mesoderm	25,80	70,37	3,14
HAND1	Mesoderm	49,83	144,92	34,07
HAND2	Mesoderm	183,24	242,43	18,45
HEY1	Mesoderm	7,99	107,20	9,13
HOPX	Mesoderm	125,69	131.646,05	34,24
IL6ST	Mesoderm	12,05	12,50	4,29
NKX2-5	Mesoderm	8,41	1,69	1,61
ODAM	Mesoderm	14,39	752,49	7,16
PDGFRA	Mesoderm	4,56	1,93	1,64
PLVAP	Mesoderm	18,24	5,26	1,05
RGS4	Mesoderm	69,10	71,92	7,93
SNAI2	Mesoderm	235,71	28,52	41,22
TBX3	Mesoderm	5,81	190,57	9,69
TM4SF1	Mesoderm	72,18	22,96	6,56
CXCL5	Self-renewal	0,23	0,07	0,87
DNMT3B	Self-renewal	0,00	0,04	0,01

HESX1	Self-renewal	0,02	0,02	0,02
IDO1	Self-renewal	0,00	0,03	0,00
LCK	Self-renewal	0,00	0,05	0,01
NANOG	Self-renewal	0,00	0,06	0,04
POU5F1	Self-renewal	0,02	0,13	0,08
SOX2	Self-renewal	0,18	0,02	0,18
TRIM22	Self-renewal	0,32	0,20	0,29

Experiment Filename		
Target Name	**Category**	**Keratinocyte**
CDH9	Ectoderm	0,50
COL2A1	Ectoderm	0,14
DMBX1	Ectoderm	0,42
DRD4	Ectoderm	0,27
EN1	Ectoderm	32,66
LMX1A	Ectoderm	0,76
MAP2	Ectoderm	1,49
MYO3B	Ectoderm	26,88
NOS2	Ectoderm	0,20
NR2F1/NR2F2	Ectoderm	0,25
NR2F2	Ectoderm	17,67
OLFM3	Ectoderm	5,33
PAPLN	Ectoderm	1,76
PAX3	Ectoderm	11,03
PAX6	Ectoderm	0,40
POU4F1	Ectoderm	4,19
PRKCA	Ectoderm	1,03
SDC2	Ectoderm	3,44
SOX1	Ectoderm	1,77
TRPM8	Ectoderm	4,45
WNT1	Ectoderm	11,42
ZBTB16	Ectoderm	0,69
AFP	Endoderm	0,26
CABP7	Endoderm	3,39
CDH20	Endoderm	1,37
CLDN1	Endoderm	3,31
CPLX2	Endoderm	0,56
ELAVL3	Endoderm	2,16
EOMES	Endoderm	1,53
FOXA1	Endoderm	0,45
FOXA2	Endoderm	0,75
FOXP2	Endoderm	8,91
GATA4	Endoderm	1,35
GATA6	Endoderm	0,70
HHEX	Endoderm	0,07
HMP19	Endoderm	2,54

HNF1B	Endoderm	3,36
HNF4A	Endoderm	0,21
KLF5	Endoderm	89,05
LEFTY1	Endoderm	1,13
LEFTY2	Endoderm	7,04
NODAL	Endoderm	0,19
PHOX2B	Endoderm	6,81
POU3F3	Endoderm	0,37
PRDM1	Endoderm	2,07
RXRG	Endoderm	14,37
SOX17	Endoderm	22,06
SST	Endoderm	14,66
FGF4	Mesendoderm	0,61
GDF3	Mesendoderm	4,36
NPPB	Mesendoderm	0,81
NR5A2	Mesendoderm	155,79
PTHLH	Mesendoderm	33,61
T	Mesendoderm	0,09
ABCA4	Mesoderm	28,43
ALOX15	Mesoderm	1,22
BMP10	Mesoderm	14,04
CDH5	Mesoderm	37,38
CDX2	Mesoderm	6,26
COLEC10	Mesoderm	22,04
ESM1	Mesoderm	3,90
FCN3	Mesoderm	1,10
FOXF1	Mesoderm	5,87
HAND1	Mesoderm	257,23
HAND2	Mesoderm	4,03
HEY1	Mesoderm	3,16
HOPX	Mesoderm	1.856,77
IL6ST	Mesoderm	8,06
NKX2-5	Mesoderm	27,79
ODAM	Mesoderm	518,18
PDGFRA	Mesoderm	1,56
PLVAP	Mesoderm	1,14
RGS4	Mesoderm	7,03
SNAI2	Mesoderm	5,20
TBX3	Mesoderm	21,16
TM4SF1	Mesoderm	8,56
CXCL5	Self-renewal	5,17
DNMT3B	Self-renewal	0,04
HESX1	Self-renewal	1,44
IDO1	Self-renewal	1,11
LCK	Self-renewal	3,26
NANOG	Self-renewal	2,90
POU5F1	Self-renewal	1,75
SOX2	Self-renewal	2,88

TRIM22	Self-renewal	5,29

Fold change legend

fc > 100	Upregulated
10 < fc <= 100	
2 < fc <= 10	
0.5 <= fc <= 2	Comparable
0.1 <= fc < 0.5	
0.01 <= fc < 0.1	
fc < 0.01	Downregulated
omitted	

Appendix

Second generation codon-optimized minicircle (CoMiC) for non-viral reprogramming of human adult fibroblasts

Adapted from:
Diecke, S., Lisowski, L., Kooreman, N.G., Wu, J.C. (2014). Second generation codon-optimized minicircle (CoMiC) for non-viral reprogramming of human adult fibroblasts. **Methods Mol Biol,** *1181, 1-13.*

Somatic cells, such as human adult fibroblasts, can be reverted to an embryonic stem cell (ESC)-like state by inducing the expression of specific genes and transcription factors that regulate the maintenance of pluripotency in embryonic stem cells (Takahashi et al. 2007). These so-called core factors of pluripotency, namely OCT4, SOX2, NANOG, and two oncogenes (c-MYC and LIN28), initiate the resetting of the epigenetic profile of a terminal differentiated somatic cell and activate the molecular circuitry of pluripotency (Maherali et al. 2007, Feng et al. 2009, Mitalipov and Wolf 2009). The resultant induced pluripotent stem cells (iPSCs) have similar morphology, growth characteristics, and gene expression profiles as hESCs (Wernig et al. 2007). Furthermore, the capacity of iPSCs to differentiate into all other cell types of the human body has opened up new clinical opportunities for developing successful personalized stem cell-based therapies and drug discovery approaches. Initially iPSCs were produced using retroviral and lentiviral vectors that are known to integrate into the chromosomes of the target cells, potentially causing disruption of gene transcription and subsequent tumor formation (Sommer et al. 2010). Therefore, various laboratories have developed additional non-integrating reprogramming techniques such as Sendai virus, mRNA, and protein- or DNA-based methods (Stadtfeld et al. 2008, Zhou et al. 2009, Stadtfeld and Hochedlinger 2010, Warren et al. 2010, Okita et al. 2011).

In order to induce the transformation of a nullipotent somatic cell into a pluripotent state, it is necessary to express the right stoichiometry of the reprogramming factors within the same transfected cell (Tiemann et al. 2011). One elegant approach to achieve this requirement uses polycistronic constructs in which the four reprogramming factors are controlled by one promoter separated by a different self-cleaving 2a peptide sequence (Warlich et al. 2011). The disadvantage of such polycistronic plasmids is their large size, which might decrease the transfection efficiency in the adult human fibroblast. To overcome this problem, we cloned the polycistronic expression cassette into a minicircle plasmid backbone. Minicircles are special episomal DNA vectors devoid of any bacterial plasmid backbone (Fig. 1a). Therefore, minicircles are significantly smaller than standard plasmids, which in turn enhances their transfection efficiency and the survival rate of the target cells (Jia et al. 2010). Furthermore, it has been shown that minicircle constructs sustain a higher expression rate of their harboring transgenes over a longer period of time. Although the minicircle theoretically should not integrate into the genome of the target cell, there is still a relatively small chance of integration. Therefore, it is important to screen the derived iPSCs for random integration using specific PCR primers or Southern blot experiments (Gonzalez et al. 2011). The following protocol details the entire process of reprogramming human adult fibroblasts into human iPSCs: from dissociating fibroblasts from patient skin biopsy samples, to the reprogramming and characterization of the newly derived iPSC line. The time from induction of pluripotency to expansion of the subsequent iPSC line to passage 3 is approximately 1 month (Fig. 2b). The workflow of the reprogramming process is summarized in Fig. 3. The final part of the protocol explains the pluripotency of the iPSCs

is confirmed using immunostaining (Fig. 4a). However, it will also be necessary to perform further experiments, including directed differentiation into specific germ layers and teratoma formation assay, to verify pluripotency (Fig. 4b, c) (Lan et al. 2013). It should also be mentioned that the minicircle reprogramming technique still has a very low efficiency and therefore should be only used by researchers with iPSC experience as an alternative method for obtaining integration-free induced pluripotent stem cells, or if it is necessary to compare different reprogramming techniques.

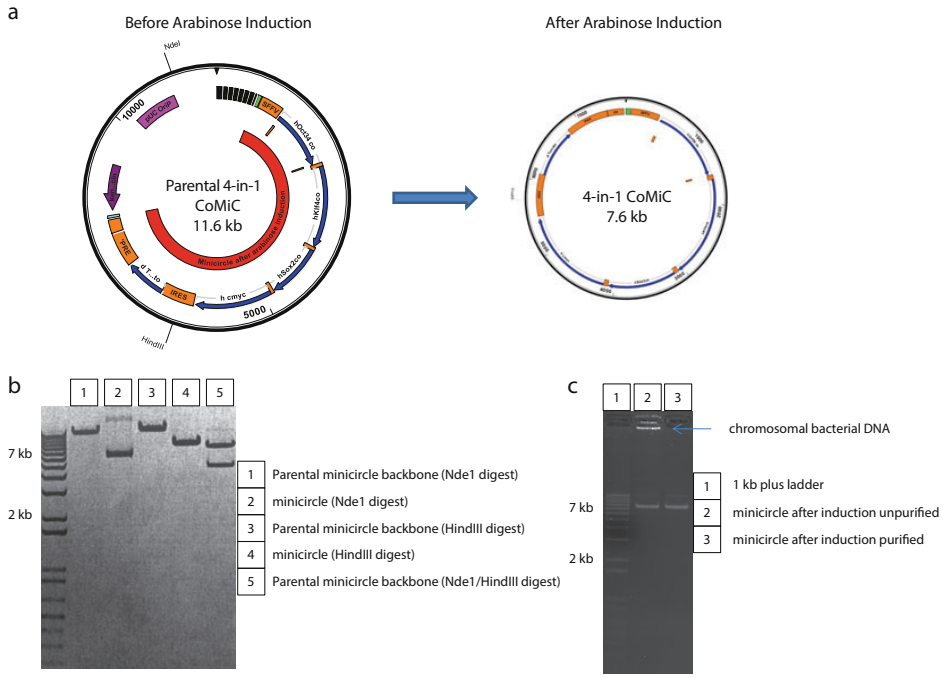


Figure 1. (a) Map of parental 4-in-1 reprogramming minicircle before and after arabinose induction. (b) Control digest to verify quality of the minicircle production. (c) Gel showing bands representing the minicircle after induction, both before and after purification steps

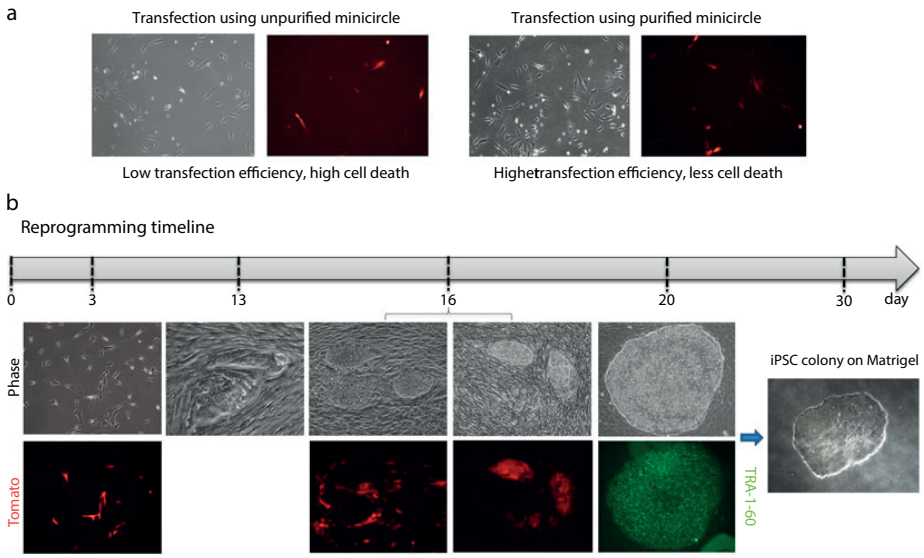


Figure 2. (a) Representative bright field and fluorescent (Tomato) images demonstrating the transfection efficiency and cell survival of unpurified and purified minicircle. (b) Timeline showing the expected phase contrast and fluorescent images at various stages of the reprogramming process. At day 20, pluripotency was confirmed by TRA-1-60 immunofluorescent staining

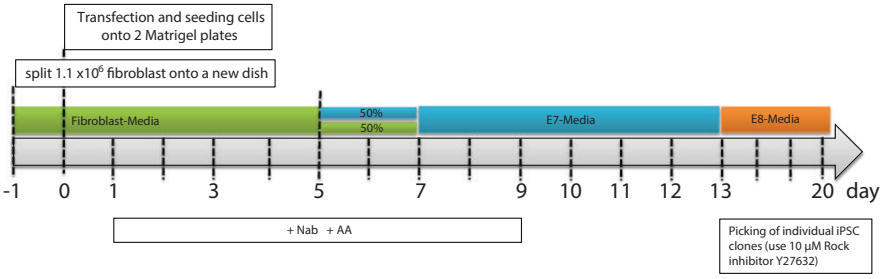


Figure 3. Timeline for reprogramming adult human fibroblasts into induced pluripotent stem cells using CoM-iC

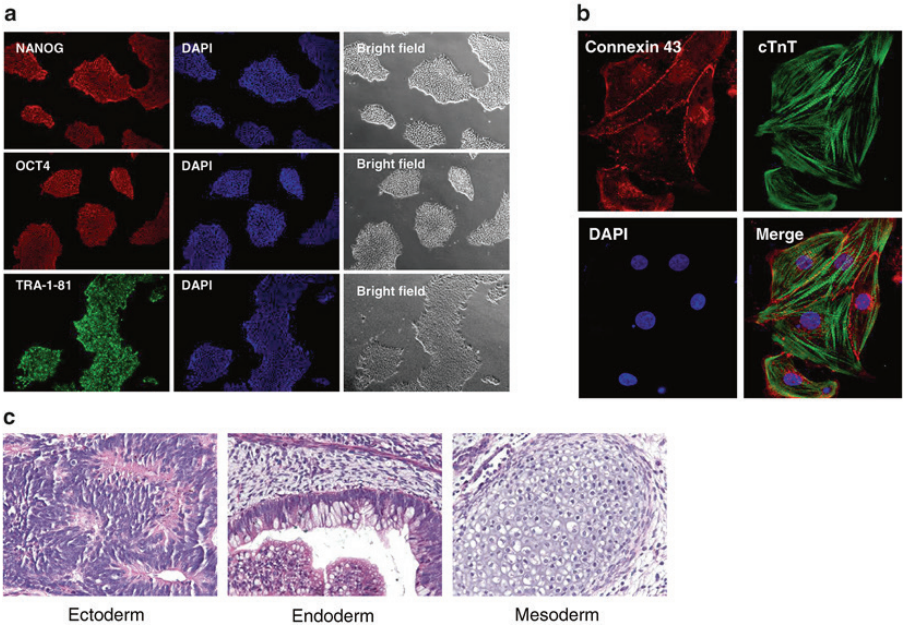


Figure 4. Immunofluorescence staining demonstrating (a) pluripotency markers NANOG, OCT4 and TRA-1-81, DAPI, and bright field images. (b) Immunofluorescent staining of iPSC-derived cardiomyocytes demonstrating positive staining of cardiac markers connexin 43 and cardiac troponin as well as DAPI. (c) Representative H&E staining from teratomas to confirm the pluripotency status of the generated iPSCs

Table 1. List of antibodies and dilutions used for characterization of human induced pluripotent stem cells and differentiated cardiomyocytes. Staining protocols were optimized with the antibodies from the listed suppliers. Optimization may be required if different antibodies are used

Antigen	Supplier	Product no.	Dilution	Raised in	Secondary (1:400)	Supplier	Product no.
Connexin-43	SIGMA	C6219	1:400	rabbit	Alexa Fluor® 488 Goat Anti-Rabbit IgG (H+L)	Life Technologies	A-11037
c Troponin-T	Thermo Scientific	MS-295-P	1:400	mouse	Alexa Fluor® 488 Goat Anti-Mouse IgG (H+L)	Life Technologies	A-11001
NANOG	Santa Cruz	SC-33759	1:100	rabbit	Alexa Fluor® 488 Goat Anti-Rabbit IgG (H+L)	Life Technologies	A-11037
OCT4	Santa Cruz	SC-9081	1:100	rabbit	Alexa Fluor® 488 Goat Anti-Rabbit IgG (H+L)	Life Technologies	A-11037
Tra-1–81	Millipore	mab4381	1:250	mouse	Alexa Fluor® 488 Goat Anti-Mouse IgG (H+L)	Life Technologies	A-11001

MATERIALS

Media

1. Fibroblast media: Low glucose Dulbecco's Modified Eagle Media (DMEM low glucose) with 20% fetal bovine serum (FBS).
2. iPSC media: Essential 8 (combine supplement with base media) and Essential 7 (Essential 6 combined with base media and supplemented with 100 ng/mL FGF2).

Reagents

1. Phosphate buffered saline (PBS).
2. Collagenase IV.
3. Penicillin/streptomycin.
4. Lennox L Broth (LB) base.
5. Sodium hydroxide (NaOH) solution, 1 M.
6. L-(+)-Arabinose ≥99%, distilled water (dH2O).
7. Kanamycin sulfate, 100×.
8. Matrigel-Growth factor reduced, hESC-qualified.
9. DMEM/F12.
10. TrypLE Express, store at room temperature (RT), there is no need to warm to 37°C before use.
11. 0.25 % Trypsin/Ethylenediaminetetraacetic acid (EDTA).
12. Accutase.
13. Y27632 (ROCK inhibitor): 10 mM stock in Ultrapure water, store at −20°C.
14. Ultrapure water.
15. Sodium butyrate (NaB).
16. Qiagen Plasmid Plus Maxi Kit.
17. DNAase (2,000 U/ml).
18. Gelatin.
19. Neon Buffer R.
20. Qiagen Plasmid Plus Maxi kit.
21. 4 % Paraformaldehyde (PFA).
22. New England biolabs enzymes HindIII and Nde1.

METHODS

Minicircle production

1. Prepare 1,200 mL of LB Broth media by adding 24 g of LB
   Broth Base to 1,200 mL of distilled water (hH2O) and divide this over the three culture flasks.
2. Autoclave the flasks using the "liquid cycle."
3. After cooling down of the flasks to room temperature, add 4 mL of Kanamycin 100x to each one of the culture flasks.
4. In the morning, pick one clone from a parental plasmid transformed bacterial plate in 5 mL LB media containing kanamycin (50 μg/mL) and grow this pre-culture until the evening at 37°C with shaking at 250 rpm.
5. In the evening, grow an overnight culture by combining 100 μL of the pre-culture with each of the flasks containing media with kanamycin and culture overnight (16–18 h) at 37°C with shaking at 250 rpm (see Note 1).
6. The optical density (OD, absorbance) of the overnight culture should be between 3.75 and 4.25.
7. Prepare a minicircle induction mix comprising 1 volume of fresh LB Broth (1,200 mL), 4 % 1 N NaOH (48 mL), and 1% L-Arabinose (12 g) and mix well.
8. Add 400 mL of the induction mix to each of the three flasks with the overnight culture and mix well.
9. Incubate the combined mix at 32 °C with shaking at 250 rpm for 6–8 h.
10. Harvest all the culture flasks, transfer them to centrifuge bottle, and pellet the bacteria (6,000 × g).
11. Isolate minicircles according to the Qiagen Plasmid Plus Maxi kit instructions with certain modifications (see Notes 2 and 3).
12. Confirm the successful minicircle induction by digestion using HindIII and Nde1. Nde1 linearizes only the parental backbone but not the minicircle. Therefore, you should expect one band around 7.7 kb when digesting the minicircle with both enzymes (Fig. 1b).

Fibroblast isolation from a patient skin punch biopsy

1. All of these steps should be performed in a sterile tissue culture hood. Prepare a fibroblast digestion solution by dissolving 1 mg/mL Collagenase IV in DMEM/F12 and sterile filter it through a 0.2 μm pore size filter.
2. Transfer the skin punch biopsy into a 15mL conical tube containing 3 mL PBS + penicillin/streptomycin (1:100), repeat this step three times.
3. Transfer the tissue into a sterile 10 cm plate and add 1 mL Collagenase IV. Use two scalpels to cross cut the tissue into small pieces while keeping the tissue immersed in Collagenase IV.

4. Additionally, add 2 mL Collagenase IV solution to the minced tissue and pipette it up and down. Transfer the Collagenase IV/tissue suspension into a 15mL conical tube and add 25µL of 0.5 M EDTA and 20µL of DNase. Afterwards, incubate the mixture for 3 h in a tissue culture incubator at 37°C.
5. Following the 3-h incubation time, pipette the tissue pieces up and down several times to obtain single-cell fibroblasts.
6. Add 12 mL fibroblast media containing 1× penicillin/ streptomycin to stop the Collagenase IV digestion.
7. Centrifuge for 4 min at 300 x g.
8. Resuspend the pellet in 2 mL fibroblast media containing 1× penicillin/streptomycin solution, and plate it in one well of a 0.1% gelatin-coated 6-well plate. Depending on the size of your tissue sample, you may need to plate the cells in more than one well of a 6-well plate. To prepare gelatin-coated plates, gelatin stock (10%) is dissolved in PBS, 1 ml of this solution is pipetted into a well of a 6-well plate and incubated for 1 h at 37°C.
9. Incubate the cells for at least 4 days without changing the media, until some of the fibroblasts start to attach and propagate. After this, change the media every other day.
10. Once the cells become confluent, split using 0.25% Trypsin–EDTA for 10 min. Plate the cells onto a 0.1% gelatin-coated T225 flask to further expand and freeze multiple vials of fibroblast after the flask becomes confluent.

Prepare Matrigel plates

1. Thaw stock bottle of Matrigel at 4°C overnight.
2. Keep Matrigel on ice, and add 300 µL Matrigel to 50 mL of cold DMEM/F12 media. Add 2 mL to each well of a 6 well plate. (Alternatively use one Matrigel aliquot per 20 mL cold DMEM/F12 media and cover four 10 cm plates using 5 mL.)
3. Place the plates in the fridge and allow the Matrigel to polymerize overnight.

Reprogramming of human fibroblasts using Neon transfection and CoMiC

1. The target fibroblast cell line should be thawed and cultured for at least 3 days before starting the reprogramming experiment. Additionally, it is beneficial to further purify the minicircle DNA using the Zymoclean Gel DNA Recovery Kit to eliminate residual chromosomal bacterial DNA of the minicircle preparation (Fig. 1c). This step will increase the cell survival after the electroporation (Fig. 2a).
2. Plate 1.1×10^6 human fibroblast in a 10cm tissue culture plate 1 day before starting the reprogramming experiment.
3. On the following day (day 0), trypsinize the cells using Trypsin 0.25% EDTA for 10 min to obtain a single cell suspension.
4. Wash off the trypsin using 10 mL of DMEM plus 20% FBS and centrifuge for 3 min at 300 × g.

5. Aspirate the media, and dissolve the cell pellet in 100–105 µL Neon Buffer R (the volume depends on the amount of plasmid you have to use to get 10–12 µg DNA). The final volume of buffer, DNA, and cells should be around 110 µL.
6. Perform the transfection using a 100 µL Neon tip and the following settings: 1,600 V, 10 ms, and 3 pulses (transfection efficiency should be more than 50%).
7. Plate the cells equally distributed onto two Matrigel-coated plates (5.5×10^5 cells) in fibroblast media.
8. On the following morning (day 1), change the media to fibroblast media and add sodium butyrate (0.2 mM) plus 50 µg/mL ascorbic acid.
9. On day 3, change the media to fibroblast media and add sodium butyrate (0.2 mM) plus 50 µg/mL ascorbic acid.
10. On day 5, change the media to 50:50 fibroblast media:Essential 7 media and add sodium butyrate (0.2 mM) plus 50 µg/mL ascorbic acid.
11. On days 7–13, change the media every other day until the first pre-iPSC colonies appear. Change the media to Essential 7 and add sodium butyrate (0.2 mM) plus 50 µg/mL ascorbic acid.
12. Between days 14 and 20, after you recognize the first colonies, switch to Essential 8 media and hypoxic culture conditions. Around day 20, the iPSC colonies should be big enough for manual picking under the microscope. Pick six individual iPSC clones using the Vitrolife stem cell cutting tool with a 10 µL tip and transfer them into six different wells of a Matrigel-coated plate with Essential 8 media in presence of 10 µM ROCK Inhibitor (Y-27632). If it is difficult to detach the iPSC colonies from the surrounding fibroblasts, you also can scrape those fibroblasts away to make room for the outgrowing iPSC colony. After 2 days, the iPSC clone should be large enough to pick.

Colony purification and expansion

1. After 5–7 days, the individual colonies become big enough to dissociate into single cells using 0.5 mL TrypLE for 8min. Detach the remaining colonies by pipetting them up and down with a 1 mL pipette.
2. Wash the cells once with 5 mL Essential 8 media.
3. Centrifuge for 3 min at 300 × g.
4. Passage the cells into one well of a Matrigel-coated 6-well plate containing 2 mL Essential 8 media.
5. After 5–7 days, colonies will have grown out and become dense enough to split onto a Matrigel-coated 10 cm plate. Therefore, incubate the cells with 1 mL Accutase for 8 min, wash using 9 mL Essential 8 media, and centrifuge for 3 min at 300 × g.
6. Seed the cells onto a Matrigel-coated 10 cm plate in Essential 8 media in the presence of 10µM Y27632.

7. Once the 10cm plate become confluent, freeze down 5 vials (passage 3 iPS cells) and continue to grow at a 1:6 split ratio, freezing vials every 10 passages.
8. Grow cells to at least passage 5 to test for the expression of the pluripotency marker genes and to passage 15 before testing for efficient differentiation.

NOTES

1. Do not start off with too much parental plasmid, as an overgrown culture will limit the induction efficiency.
2. To ensure a high yield, make sure that the pellet is completely resuspended in Qiagen Maxi Kit P1 buffer and use the same volume of P2 and S3. For example, when using 400 mL spinning tubes, resuspend the pellet in 10 mL P1, P2, and S3 buffer instead of 8mL.
3. To avoid bacterial genomic DNA contamination, avoid excessive shaking of the resuspended pellet when adding buffer P2.

REFERENCES

Aggen, D. H., A. S. Chervin, T. M. Schmitt, B. Engels, J. D. Stone, S. A. Richman, . . . D. M. Kranz (2011). "Single-chain VαVβ T-cell receptors function without mispairing with endogenous TCR chains." Gene Therapy 19(4): 365-374.

Amit, M., M. E. Winkler, S. Menke, E. Brüning, K. Büscher, J. Denner, . . . U. Martin (2005). "No Evidence for Infection of Human Embryonic Stem Cells by Feeder Cell-Derived Murine Leukemia Viruses." Stem Cells 23(6): 761-771.

Bock, C., E. Kiskinis, G. Verstappen, H. Gu, G. Boulting, Z. D. Smith, . . . A. Meissner (2011). "Reference Maps of Human ES and iPS Cell Variation Enable High-Throughput Characterization of Pluripotent Cell Lines." Cell 144(3): 439-452.

Burridge, P. W., E. Matsa, P. Shukla, Z. C. Lin, J. M. Churko, A. D. Ebert, . . . J. C. Wu (2014). "Chemically defined generation of human cardiomyocytes." Nature Methods 11(8): 855-860.

Chambers, S. M., C. A. Fasano, E. P. Papapetrou, M. Tomishima, M. Sadelain and L. Studer (2009). "Highly efficient neural conversion of human ES and iPS cells by dual inhibition of SMAD signaling." Nat Biotechnol 27(3): 275-280.

Chen, G., D. R. Gulbranson, Z. Hou, J. M. Bolin, V. Ruotti, M. D. Probasco, . . . J. A. Thomson (2011). "Chemically defined conditions for human iPSC derivation and culture." Nature Methods 8(5): 424-429.

Chou, B.-K., P. Mali, X. Huang, Z. Ye, S. N. Dowey, L. M. S. Resar, . . . L. Cheng (2011). "Efficient human iPS cell derivation by a non-integrating plasmid from blood cells with unique epigenetic and gene expression signatures." Cell Res 21(3): 518-529.

Colamonici, O. R., P. Domanski, S. M. Sweitzer, A. Larner and R. M. L. Buller (1995). "Vaccinia Virus B18R Gene Encodes a Type I Interferon-binding Protein That Blocks Interferon Transmembrane Signaling." Journal of Biological Chemistry 270(27): 15974-15978.

de Almeida, P. E., E. H. Meyer, N. G. Kooreman, S. Diecke, D. Dey, V. Sanchez-Freire, . . . J. C. Wu (2014). "Transplanted terminally differentiated induced pluripotent stem cells are accepted by immune mechanisms similar to self-tolerance." Nat Commun 5: 3903.

Diecke, S., L. Lisowski, N. G. Kooreman and J. C. Wu (2014). "Second generation codon optimized minicircle (CoMiC) for nonviral reprogramming of human adult fibroblasts." Methods Mol Biol 1181: 1-13.

Dowey, S. N., X. Huang, B.-K. Chou, Z. Ye and L. Cheng (2012). "Generation of integration-free human induced pluripotent stem cells from postnatal blood mononuclear cells by plasmid vector expression." Nat Protoc 7(11): 2013-2021.

Esteban, M. A., X. Bao, Q. Zhuang, T. Zhou, B. Qin and D. Pei (2012). "The mesenchymal-to-epithelial transition in somatic cell reprogramming." Current Opinion in Genetics & Development 22(5): 423-428.

Feng, B., J. H. Ng, J. C. Heng and H. H. Ng (2009). "Molecules that promote or enhance reprogramming of somatic cells to induced pluripotent stem cells." Cell Stem Cell 4(4): 301-312.

Gonzalez, F., M. Barragan Monasterio, G. Tiscornia, N. Montserrat Pulido, R. Vassena, L. Batlle Morera, . . . J. C. I. Belmonte (2009). "Generation of mouse-induced pluripotent stem cells by transient expression of a single nonviral polycistronic vector." Proceedings of the National Academy of Sciences 106(22): 8918-8922.

González, F., S. Boué and J. C. I. Belmonte (2011). "Methods for making induced pluripotent stem cells: reprogramming à la carte." Nat Rev Genet 12(4): 231-242.

Gonzalez, F., S. Boue and J. C. Izpisua Belmonte (2011). "Methods for making induced pluripotent stem cells: reprogramming a la carte." Nat Rev Genet 12(4): 231-242.

Hou, P., Y. Li, X. Zhang, C. Liu, J. Guan, H. Li, . . . H. Deng (2013). "Pluripotent Stem Cells Induced from Mouse Somatic Cells by Small-Molecule Compounds." Science 341(6146): 651-654.

Hu, K. (2014). "All Roads Lead to Induced Pluripotent Stem Cells: The Technologies of iPSC Generation." Stem Cells and Development 23(12): 1285-1300.

Jia, F., K. D. Wilson, N. Sun, D. M. Gupta, M. Huang, Z. Li, . . . J. C. Wu (2010). "A nonviral minicircle vector for deriving human iPS cells." Nat Methods 7(3): 197-199.

Kaji, K., K. Norrby, A. Paca, M. Mileikovsky, P. Mohseni and K. Woltjen (2009). "Virus-free induction of pluripotency and subsequent excision of reprogramming factors." Nature 458(7239): 771-775.

Kay, M. A., C.-Y. He and Z.-Y. Chen (2010). "A robust system for production of minicircle DNA vectors." Nat Biotechnol 28(12): 1287-1289.

Kim, D., C.-H. Kim, J.-I. Moon, Y.-G. Chung, M.-Y. Chang, B.-S. Han, . . . K.-S. Kim (2009). "Generation of Human Induced Pluripotent Stem Cells by Direct Delivery of Reprogramming Proteins." Cell Stem Cell 4(6): 472-476.

Lan, F., A. S. Lee, P. Liang, V. Sanchez-Freire, P. K. Nguyen, L. Wang, . . . J. C. Wu (2013). "Abnormal calcium handling properties underlie familial hypertrophic cardiomyopathy pathology in patient-specific induced pluripotent stem cells." Cell Stem Cell 12(1): 101-113.

Lee, J., Y. Kim, H. Yi, S. Diecke, J. Kim, H. Jung, . . . J. Ju (2014). "Generation of disease-specific induced pluripotent stem cells from patients with rheumatoid arthritis and osteoarthritis." Arthritis Res Ther 16(1): R41.

Lee, J., N. Sayed, A. Hunter, Kin F. Au, Wing H. Wong, Edward S. Mocarski, . . . John P. Cooke (2012). "Activation of Innate Immunity Is Required for Efficient Nuclear Reprogramming." Cell 151(3): 547-558.

Li, R., J. Liang, S. Ni, T. Zhou, X. Qing, H. Li, . . . D. Pei (2010). "A Mesenchymal-to-Epithelial Transition Initiates and Is Required for the Nuclear Reprogramming of Mouse Fibroblasts." Cell Stem Cell 7(1): 51-63.

Liu, X., H. Sun, J. Qi, L. Wang, S. He, J. Liu, . . . H. Zheng (2013). "Sequential introduction of reprogramming factors reveals a time-sensitive requirement for individual factors and a sequential EMT-MET mechanism for optimal reprogramming." Nat Cell Biol 15(7): 829-838.

Lu, J., F. Zhang and M. A. Kay (2013). "A mini-intronic plasmid (MiP): a novel robust transgene expression vector in vivo and in vitro." Mol Ther 21(5): 954-963.

Lu, J., F. Zhang, S. Xu, A. Z. Fire and M. A. Kay (2012). "The Extragenic Spacer Length Between the 5' and 3' Ends of the Transgene Expression Cassette Affects Transgene Silencing From Plasmid-based Vectors." Mol Ther 20(11): 2111-2119.

Mack, A. A., S. Kroboth, D. Rajesh and W. B. Wang (2011). "Generation of Induced Pluripotent Stem Cells from CD34+ Cells across Blood Drawn from Multiple Donors with Non-Integrating Episomal Vectors." PLoS ONE 6(11): e27956.

Maherali, N., R. Sridharan, W. Xie, J. Utikal, S. Eminli, K. Arnold, . . . K. Hochedlinger (2007). "Directly reprogrammed fibroblasts show global epigenetic remodeling and widespread tissue contribution." Cell Stem Cell 1(1): 55-70.

Mandal, P. K. and D. J. Rossi (2013). "Reprogramming human fibroblasts to pluripotency using modified mRNA." Nat Protoc 8(3): 568-582.

Mitalipov, S. and D. Wolf (2009). "Totipotency, pluripotency and nuclear reprogramming." Adv Biochem Eng Biotechnol 114: 185-199.

Narsinh, K. H., F. Jia, R. C. Robbins, M. A. Kay, M. T. Longaker and J. C. Wu (2010). "Generation of adult human induced pluripotent stem cells using nonviral minicircle DNA vectors." Nat Protoc 6(1): 78-88.

Okita, K., Y. Matsumura, Y. Sato, A. Okada, A. Morizane, S. Okamoto, . . . S. Yamanaka (2011). "A more efficient method to generate integration-free human iPS cells." Nat Methods 8(5): 409-412.

Okita, K., Y. Matsumura, Y. Sato, A. Okada, A. Morizane, S. Okamoto, . . . S. Yamanaka (2011). "A more efficient method to generate integration-free human iPS cells." Nature Methods 8(5): 409-412.

Papp, B. and K. Plath (2011). "Reprogramming to pluripotency: stepwise resetting of the epigenetic landscape." Cell Res 21(3): 486-501.

Piao, Y., S. S. C. Hung, S. Y. Lim, R. C. B. Wong and M. S. H. Ko (2014). "Efficient Generation of Integration-Free Human Induced Pluripotent Stem Cells From Keratinocytes by Simple Transfection of Episomal Vectors." Stem Cells Translational Medicine 3(7): 787-791.

Redmer, T., S. Diecke, T. Grigoryan, A. Quiroga-Negreira, W. Birchmeier and D. Besser (2011). "E-cadherin is crucial for embryonic stem cell pluripotency and can replace OCT4 during somatic cell reprogramming." EMBO Rep 12(7): 720-726.

Sommer, C. A., A. G. Sommer, T. A. Longmire, C. Christodoulou, D. D. Thomas, M. Gostissa, . . . G. Mostoslavsky (2010). "Excision of reprogramming transgenes improves the differentiation potential of iPS cells generated with a single excisable vector." Stem Cells 28(1): 64-74.

Stadtfeld, M. and K. Hochedlinger (2010). "Induced pluripotency: history, mechanisms, and applications." Genes & Development 24(20): 2239-2263.

Stadtfeld, M., M. Nagaya, J. Utikal, G. Weir and K. Hochedlinger (2008). "Induced pluripotent stem cells generated without viral integration." Science 322(5903): 945-949.

Stetson, D. B. and R. Medzhitov (2006). "Recognition of Cytosolic DNA Activates an IRF3-Dependent Innate Immune Response." Immunity 24(1): 93-103.

Takahashi, K., K. Okita, M. Nakagawa and S. Yamanaka (2007). "Induction of pluripotent stem cells from fibroblast cultures." Nat Protoc 2(12): 3081-3089.

Takahashi, K., K. Tanabe, M. Ohnuki, M. Narita, T. Ichisaka, K. Tomoda and S. Yamanaka (2007). "Induction of pluripotent stem cells from adult human fibroblasts by defined factors." Cell 131(5): 861-872.

Takahashi, K. and S. Yamanaka (2006). "Induction of pluripotent stem cells from mouse embryonic and adult fibroblast cultures by defined factors." Cell 126(4): 663-676.

Tiemann, U., M. Sgodda, E. Warlich, M. Ballmaier, H. R. Scholer, A. Schambach and T. Cantz (2011). "Optimal reprogramming factor stoichiometry increases colony numbers and affects molecular characteristics of murine induced pluripotent stem cells." Cytometry A 79(6): 426-435.

Tiemann, U., M. Sgodda, E. Warlich, M. Ballmaier, H. R. Schöler, A. Schambach and T. Cantz (2011). "Optimal reprogramming factor stoichiometry increases colony numbers and affects molecular characteristics of murine induced pluripotent stem cells." Cytometry 79A(6): 426-435.

Warlich, E., J. Kuehle, T. Cantz, M. H. Brugman, T. Maetzig, M. Galla, . . . A. Schambach (2011). "Lentiviral Vector Design and Imaging Approaches to Visualize the Early Stages of Cellular Reprogramming." Mol Ther 19(4): 782-789.

Warren, L., P. D. Manos, T. Ahfeldt, Y.-H. Loh, H. Li, F. Lau, . . . D. J. Rossi (2010). "Highly Efficient Reprogramming to Pluripotency and Directed Differentiation of Human Cells with Synthetic Modified mRNA." Cell Stem Cell 7(5): 618-630.

Warren, L., P. D. Manos, T. Ahfeldt, Y. H. Loh, H. Li, F. Lau, . . . D. J. Rossi (2010). "Highly efficient reprogramming to pluripotency and directed differentiation of human cells with synthetic modified mRNA." Cell Stem Cell 7(5): 618-630.

Wernig, M., A. Meissner, R. Foreman, T. Brambrink, M. Ku, K. Hochedlinger, . . . R. Jaenisch (2007). "In vitro reprogramming of fibroblasts into a pluripotent ES-cell-like state." Nature 448(7151): 318-324.

Yoshioka, N., E. Gros, H.-R. Li, S. Kumar, Dekker C. Deacon, C. Maron, . . . Steven F. Dowdy (2013). "Efficient Generation of Human iPSCs by a Synthetic Self-Replicative RNA." Cell Stem Cell 13(2): 246-254.

Young, L. S. and A. B. Rickinson (2004). "Epstein–Barr virus: 40 years on." Nature Reviews Cancer 4(10): 757-768.

Yu, J., K. Hu, K. Smuga-Otto, S. Tian, R. Stewart, I. I. Slukvin and J. A. Thomson (2009). "Human Induced Pluripotent Stem Cells Free of Vector and Transgene Sequences." Science 324(5928): 797-801.

Yu, J., M. A. Vodyanik, K. Smuga-Otto, J. Antosiewicz-Bourget, J. L. Frane, S. Tian, . . . J. A. Thomson (2007). "Induced pluripotent stem cell lines derived from human somatic cells." Science 318(5858): 1917-1920.

Zhou, H., S. Wu, J. Y. Joo, S. Zhu, D. W. Han, T. Lin, . . . S. Ding (2009). "Generation of induced pluripotent stem cells using recombinant proteins." Cell Stem Cell 4(5): 381-384.

Zhou, T., C. Benda, S. Dunzinger, Y. Huang, J. C. Ho, J. Yang, . . . M. A. Esteban (2012). "Generation of human induced pluripotent stem cells from urine samples." Nat Protoc 7(12): 2080-2089.



Part II

Applications of regenerative therapies

ABBREVIATIONS:

AAA - abdominal aortic aneurysm
AngII - Angiotensin II
BLI - Bioluminescence imaging
FOXP3 - forkhead box P3
GRZB - Granzyme B
IL-10 - Interleukin-10
IL-6 - Interleukin-6
MC - Minicircle
MRC1 - Mannose Receptor, C type 1
PBMC - Peripheral Blood Mononuclear Cell;
SMC - Smooth muscle cell
TNFa - Tumor necrosis factor alpha
Treg - Regulatory T cell

Chapter 4

Gene therapy for vascular disease

Kooreman N.G[*], Adam M.[*], Jagger A., Wagenhäuser M., Mehrkens D., Wang Y., Kayama Y., Toyama K., Raaz U., Schellinger I.N., Maegdefessel L., Spin J.M., Hamming J.F., Quax P.H.A., Baldus S., Wu J.C., Tsao P.S. (2018). Systemic upregulation of IL-10 using a non-immunogenic vector reduces abdominal aortic aneurysm growth and dissection rate **ATvB**, *8:1796-1805.*

[*] *authors contributed equally*

ABSTRACT

Objective

Recruitment of immunologic competent cells to the vessel wall is a crucial step in formation of abdominal aortic aneurysms (AAA). Innate immunity effectors (eg, macrophages), as well as mediators of adaptive immunity (eg, T cells), orchestrate a local vascular inflammatory response. IL-10 (interleukin-10) is an immune-regulatory cytokine with a crucial role in suppression of inflammatory processes. We hypothesized that an increase in systemic IL-10-levels would mitigate AAA progression.

Approach and Results

Using a single intravenous injection protocol, we transfected an IL-10 transcribing non-immunogenic minicircle vector into the Ang II (angiotensin II)-ApoE$^{-/-}$ infusion mouse model of AAA. IL-10 minicircle transfection significantly reduced average aortic diameter measured via ultrasound at day 28 from 166.1±10.8% (control) to 131.0±5.8% (IL-10 transfected). Rates of dissecting AAA were reduced by IL-10 treatment, with an increase in freedom from dissecting AAA from 21.5% to 62.3%. Using flow cytometry of aortic tissue from minicircle IL-10-treated animals, we found a significantly higher percentage of CD4^{+}/CD25^{+}/Foxp3 (forkhead box P3)$^{+}$ regulatory T cells, with fewer CD8^{+}/GZMB^{+} (granzyme B) cytotoxic T cells. Furthermore, isolated aortic macrophages produced less TNF-α (tumor necrosis factor-α), more IL-10, and were more likely to be MRC1 (mannose receptor, C type 1)–positive alternatively activated macrophages. These results concurred with gene expression analysis of lipopolysaccharide-stimulated and Ang II-primed human peripheral blood mononuclear cells.

Conclusions

Taken together, we provide an effective gene therapy approach to AAA in mice by enhancing anti-inflammatory and dampening proinflammatory pathways through minicircle-induced augmentation of systemic IL-10 expression.

INTRODUCTION

Human abdominal aortic aneurysm (AAA) is defined as a pathologic dilatation that exceeds the normal diameter by 50%, or that has an antero-posterior diameter of over 30 mm. AAAs are a significant cause of morbidity and mortality in the United States and worldwide. The average incidence in Western civilizations is 0.4-0.67% (Nordon et al. 2011). Although mortality numbers are slowly decreasing due to better endovascular and open surgical repair techniques as well as better risk factor management (Schermerhorn et al. 2012), AAAs still accounted for up to 10,000 deaths per year in the US in 2014, or approximately 3.1 deaths per 100,000 people(Centers for Disease Control and Prevention). Infiltration of monocytes/macrophages, polymorphonuclear leukocytes (PMNs), and T- and B-lymphocytes mark the early phases of aneurysm development (Thomas et al. 2006). With further progression, a variety of cytokines, leukotrienes and immunoglobulins attract additional inflammatory cells and establish a local vascular inflammatory response. Matrix degeneration with disruption of local collagen and elastin follows, accompanied by smooth muscle cell (SMC) apoptosis in the aortic media, and ultimately leading to AAA expansion and rupture (Kunieda et al. 2006, Ailawadi et al. 2009). With vascular inflammation being one of the major initial hallmarks of AAA formation, mechanisms that dampen the immune response might be leveraged to prevent progressive tissue damage. Interleukin-10 (IL-10) is a well described anti-inflammatory cytokine, with a crucial role in suppression of inflammatory processes in diseases such as environmental allergy, asthma or inflammatory bowel disease. There is evidence that the immune-regulatory capacities of IL-10 might also be crucial in aneurysm development, as the IL-10-1082 'A' polymorphism (associated with lower IL-10 production (Turner et al. 1997)) is more common in patients with AAA (Bown et al. 2007), and patients with this polymorphism are at an increased risk of developing AAA (McColgan et al. 2009). IL-10 plasma concentrations in patients with AAA are significantly decreased compared to matched patients with coronary artery disease (Kadoglou et al. 2012). Also, IL-10-knockout mice show increased susceptibility to Angiotensin II (AngII)-induced aortic aneurysm and aortic rupture (Ait-Oufella et al. 2013). To our knowledge, no studies have to-date been conducted utilizing transgenic IL-10 animals. IL-10 treatment has already been successfully performed in inflammatory bowel disease and glomerulosclerosis in rodents. However, recent studies have encountered major pitfalls. Intravenous or intraperitoneal injections of recombinant IL-10 need to be performed close to the time point of disease induction, or be repeated daily, due to IL-10's short plasma half-life (Duchmann et al. 1996, Grool et al. 1998, Rachmawati et al. 2011). In humans, outcomes in the treatment of inflammatory bowel disease did not demonstrate efficacy (Buruiana et al. 2010). While disease-specific reasons for these limited results may exist, one major drawback is the lack of sufficient IL-10 bioavailability at the tissue of interest (Marlow et al. 2013). To increase IL-10 bioavailability and to overcome IL-10 delivery issues, here we applied

a non-viral minicircle transfection approach to the AngII-infusion-ApoE-/- AAA model. Minicircles (MC) are episomal DNA vectors lacking a bacterial plasmid backbone. Due to their small size compared to standard plasmids, they display higher transfection efficiency and survival rate of the target cells. In addition, MC constructs sustain a higher expression rate of their harboring transgenes over a longer period of time. This, combined with their low immunogenicity, makes them intriguing vectors for gene therapy (Chen et al. 2008, Huang et al. 2009, Lijkwan et al. 2014).

MATERIAL AND METHODS

Mouse model

B6.129P2-*Apoetm1Unc*/J male mice (ApoE-/-) were transfected via intravenous injection of 25µg MC into the retro-orbital venous plexus at a concentration of 25µg/100µl containing either a transgenic transcript for murine IL-10 or GFP (control). MC GFP was deliberately chosen as a control vector against MC IL10, as we wanted to adjust for the effects of actual translation of proteins from minicircle DNA to protein in transfected cells. Based on this approach, we designed the experiment in Supp. figure 1, to prove that our MC GFP was not altering aneurysm formation unexpectedly and randomly compared to AngII + PBS treatment alone.

Seven days after transfection, aortic aneurysm formation was induced using continuous subcutaneous angiotensin II (AngII) – infusion. Osmotic pumps (model 2004, Alzet) containing either AngII (1 µg/kg/min, Sigma-Aldrich) or saline were introduced in ApoE-/- male mice (C57BL/6J background) as previously described (Daugherty et al. 2000). Pump implantation occurred at 3-6 months of age (mean age 168 ± 7.6 days, total n=78), mice were age-matched before starting the experiment.

Suprarenal aortic diameter was followed via ultrasound measurements on a VisualSonics Vevo2100 over 28 days as previously described (Maegdefessel et al. 2012, Maegdefessel et al. 2012, Maegdefessel et al. 2014) and validated (Azuma et al. 2011). Diameter was assessed using the leading edge-to-leading edge method (Gurtelschmid et al. 2014). Lesions were classified as aortic dissections if intramural hematoma was visible in ultrasound or at autopsy.

Bioluminescence imaging (BLI) was performed with the Xenogen In Vivo Imaging System on days 1, 3, 9, and 15 after transfection. D-Luciferin (Promega) was administered intraperitoneally at a dose of 375 mg/kg of body weight.

Murine plasma was collected with a standardized method via mandibular vein and centrifuged at 15 min at 3000 rpm at 4°C. ELISA for IL-10 was performed according to the manufacturer's instructions (Quantikine ELISA Mouse IL-10 Immunoassay).

Construction and amplification of MC-IL-10 plasmids

For minicircle amplification, a single colony E. coli was grown at 37°C overnight and subsequently spun down. The pellet was re-dissolved with broth (pH 7.0) containing 1% L-(+)-arabinose and incubated at 30°C for 2 hours. MC constructs were isolated from the culture using plasmid purification kits (Qiagen, Venlo, Netherlands). Primers (cactagtcgcgcccggggag/gacccatgggggcccgcc) were used to PCR minicircle DNA with attB/attP elements and obtain DNA fragment A. The CMV promoter, multiple cloning site and poly A elements were PCR-amplified from pcDNA3.1/zeo(+) (Invitrogen) with primers aattgcatgaagaatctgct/ctggttctttccgcctcaga to obtain DNA fragment B. Ligation of DNA fragment A and DNA fragment B resulted in vector C. The IL-10 coding sequence was synthesized and subcloned into the KpnI/XhoI site of vector C, resulting in pMC-IL10. For detailed methods please see Huang et al. (Huang et al. 2009) and Supp. Figure 4.

Similar minicircles bearing transcripts for green fluorescent protein and firefly luciferase were used for control purposes (Jia et al. 2010).

Tissue harvesting

Mice were euthanized with an inhalation overdose of isoflurane (Vet One). Aortas were immediately flushed via the left ventricle with ice-cold PBS and then dissected from fat and connective tissue from the renal arteries to the diaphragm (via Microscope, Leica). Specimens were snap-frozen in liquid nitrogen and stored at −80°C.

Histological staining

Histological staining after harvesting was performed in the correlating suprarenal region of the AAA. Using already evaluated techniques (Azuma et al. 2011) aortic tissue was cut in 7-µm-thick serial sections and subsequently stained with hematoxylin and eosin (Sigma-Aldrich) and Picrosirius red (Sigma-Aldrich) according to standard protocols. All histological analyses were obtained at room temperature using a Keyence BZ-9000 microscope with BZ2 Analyzer software.

Flow cytometry

Flow cytometry analysis for markers of T-cell and macrophage polarization was performed in suprarenal aortic tissue at day 7 after AngII-infusion. Control mice were injected with saline instead of MC-GFP to avoid interference with flow cytometry, untreated animals received neither AngII nor MC IL-10 treatment. Aortic tissue was digested with Liberase (27 WU/ml) and DNase I (0.1 %) in DMEM media. Cells were counted and prepared for flow cytometry and 1×10^6 cells were used for staining. For intra- and extra-cellular staining, cells were fixed and permeabilized using BD Cytofix/Cytoperm™ Fixation. Fluorophore-conjugated monoclonal antibodies against mouse CD3, CD4, CD8, CD25, CD45, FoxP3, GranzymeB, F4/80, IL10, MRC1, TNF-α and viablitiy (1:100; BD Bioscience, Biolegend,

eBioscience) were used. Cells were assayed using a LSRII flow cytometer (BD Biosciences) and further analyzed with FlowJo software (Tree Star, Ashland, OR, USA).

Human PBMC experiments

Human PBMCs were isolated from the blood of healthy volunteers using a standard Ficoll protocol. Subsequently, cells were treated with AngII (100uM) for 24 hours followed by LPS induction (100ng/ml) for an additional 24 hours. IL-10 (20ng/ml) or control treatment (PBS) was performed in combination with AngII priming and before LPS stimulation. Cells were harvested using Qiazol and RNA was isolated using the Qiagen miRNeasy kit. RNA was quantified by Nanodrop (Thermo Fisher Scientific). mRNA was reverse transcribed using the SuperScript III RT kit (Thermo Fisher Scientific) according to the manufacturer's instructions and expression levels were quantified with standard qRT-PCR (TaqMan) with the following assays: GAPDH (internal control), TNF, IL6, TGFB1, MRC1, CD163, FOXP3, GZMB, IL10 (all Thermo Fisher Scientific). Amplification took place on Quantstudio 12K Flex Real-Time PCR system (Thermo Fisher Scientific). Results were normalised to GAPDH.

Statistical analysis

All calculations were made with GraphPad Prism 6.01. Normal distribution was tested by Kolmogorov-Smirnov-Test and led to pairwise testing with Students unpaired t-test. Otherwise the Mann-Whitney rank sum test was performed. For multiple comparisons, post-hoc Fisher's Least Significant Difference (LSD) tests were calculated after one-way repeated measures analysis of variance. For curve comparisons of Kaplan-Meier survival curves a Log-rank (Mantel-Cox) test was performed. For *in vitro* experiments, obvious outliers were removed using the Robust regression and Outlier removal method (ROUT) with a coefficient Q of 2% (Motulsky and Brown 2006).

A p value of <0.05 was considered statistically significant. Data are presented as mean ± SEM or median ± interquartile range if data were not normally distributed or not interval scaled.

RESULTS

To evaluate transfection efficacy of our intravenous MC injection approach, we first utilized minicircles expressing a firefly luciferase reporter construct (MC-Luc). MC-Luc was injected and subsequent bioluminescence imaging (BLI) was performed at days 1, 3, 9, and 15. We found a noticeable increase in luciferase activity in regions corresponding to the lungs at 1-3 days after transfection, with increasing activity in the liver and kidney regions over the

course of the first 9 days (Fig. 1A). By 15 days after transfection, the luciferase signal had significantly dropped, indicating a considerable loss of activity (Fig. 1B).

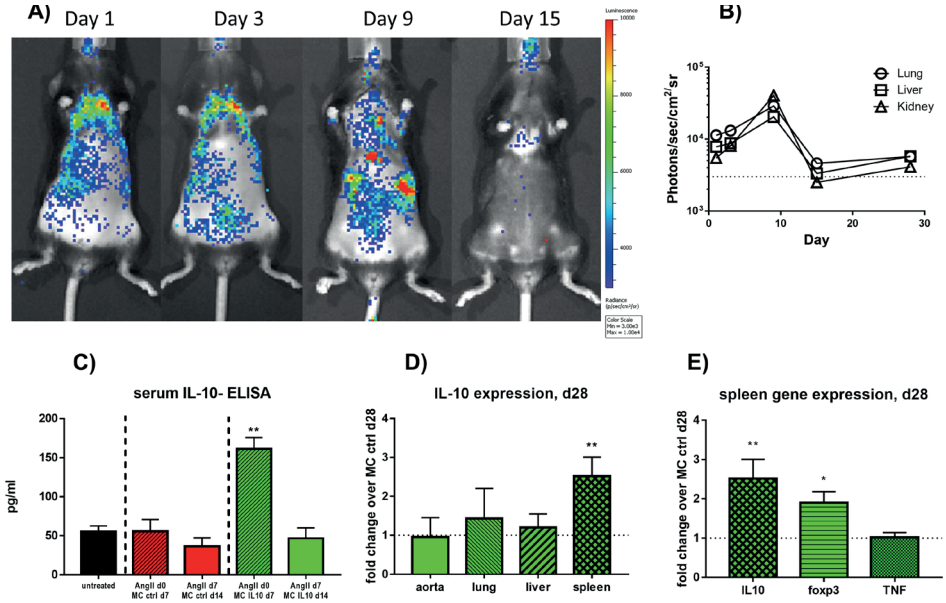


Figure 1. Vector expression and efficiency in vivo.
Bioluminescence imaging (BLI) was performed at days 1, 3, 9, and 15 after intravenous injection of MC-Luc. Subsequently, BLI was performed with the Xenogen In Vivo Imaging System with administration of D-Luciferin at a dose of 375 mg/kg of body weight. (A) Localization and intensity of bioluminescence. (B) Quantification of bioluminescence per organ (C) IL-10 plasma levels of mice at d7 after transfection with MC IL-10; n=5 per group, ** = p≤0.01. (D) Gene expression analysis (q-rtPCR) of IL-10 after 28days of AngII treatment in homogenized tissue. (E) Gene expression of splenic tissue for IL-10, foxp3 and TNF at d28 after AngII infusion.

AngII-treatment began at day 7 after MC transfection, to ensure active vector expression during aneurysm induction. We also evaluated IL-10 plasma levels of mice at 7 and 14 days after injection with MC IL-10 or MC control, confirming expression and production of IL-10 in a similar fashion to MC-Luc. We found a significant increase in plasma IL-10 levels in MC IL-10-treated mice (vs. matched controls) at day 7 after transfection (161.3 ± 14.6 pg/ml vs. 55.5 ± 15.4 pg/ml, $p < 0.01$, n=5, Figure 1C). At day 14 after MC injection, no differences could be found for IL-10 expression in MC IL-10 vs. MC control (46.8 ± 13.4 pg/ml vs. 36.8 ± 10.6 pg/ml, p = n.s., n=4/5). To further evaluate the long-term effects of MC IL-10 injection regarding tissue levels of IL-10, expression in peripheral tissues were quantified with qRT-PCR at day 28 after AngII infusion. Here, IL-10 did not show significantly higher expression in aortic tissue, lung tissue or hepatic tissue in comparison to MC control (Figure 1D). Interestingly however, splenic IL-10 expression was significantly higher in MC IL-10 than in controls (2.52 ± 0.5-fold increase vs. MC control, $p<0.01$, n=10). This was ac-

companied by higher splenic Foxp3 expression at day 28 after AngII (1.9 ± 0.3-fold, p<0.05, n=10, Fig. 1E), but not increased TNF levels.

Subcutaneous AngII pump implantation at day 7 after transfection led to significant suprarenal aortic aneurysm formation in ApoE -/- mice as previously described (Daugherty et al. 2000), with 78% of the mice having a diameter of more than 150% of baseline in the control group. Aneurysm formation was attenuated in mice that had been injected with MC IL-10, as only 10% of these animals had a diameter increase of ≥150% (average diameter 166.1 ± 10.8 % in control vs. 131.0 ± 5.8 % in IL-10 treated animals, p < 0.01, n = 9 vs. 10, Figure 2A). Differences in diameter remained throughout the time course of aneurysm formation, starting at day 7 (Fig. 2A). These findings were supported by H&E and Picrosirius Red stainings, which showed a relevant decrease in AAA diameter after MC IL-10 treatment (Figure 2B).

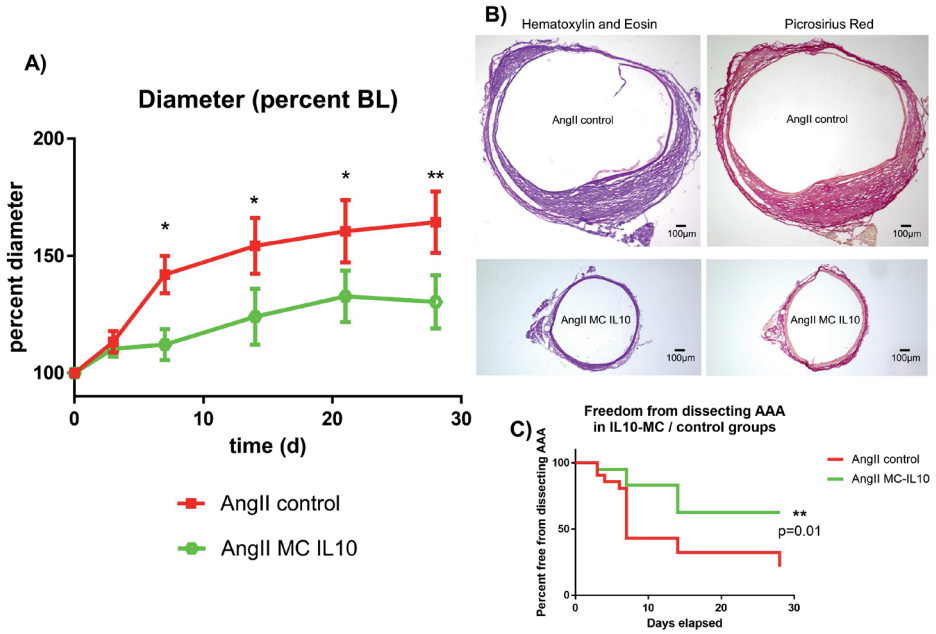


Figure 2. Aortic diameter and rate of dissecting AAAs after MC IL-10 transfection.
Ultrasound measurements of ApoE-/- mice after subcutaneous infusion of AngII (1 µg/kg/min). (A) Aortic diameter in percent of baseline diameter over a time course of 28 days; n = 15 vs. 15, * = p≤0.05, ** = p≤0.01 vs. AngII MC control. (B) Representative H&E and Picrosirius Red staining of suprarenal aortic sections harvested d28 after AngII infusion. (C) Kaplan-Meier curve for freedom from dissecting AAA; n = 15 vs. 15, ** = p≤0.01 vs. AngII MC control.

In the murine ApoE-/- AngII infusion AAA model, aneurysm formation is tipically driven by intramural hematoma or myointimal dissection of the aortic wall. Therefore, in addition to aneurysm size, the presence of a 'dissecting AAA' is also an important aspect of

AAA formation (Trachet et al. 2015). In concert with the significantly decreased diameter after MC IL-10 treatment, we found improved dissecting AAA-free survival in animals transfected with the IL-10 vector (21.5 % vs. 62.3 % at day 28 in AngII vs. AngII MC-IL10, p = 0.01, n = 41, Fig. 2C).

Next, we evaluated the number and polarization of CD45+ / CD3+ lymphocytes and F4/80+ macrophages in suprarenal aortic tissue 7 days after aneurysm induction via flow cytometry. AngII MC IL-10-treated animals showed a significantly higher percentage of regulatory T cells (T_{reg} cells) than AngII-control or non-AngII-treated animals (CD4+/CD25+/Foxp3+, 1.8 ± 0.1 % of CD45+/CD3+ vs. 0.6 ± 0.08 % in AngII-control vs. 0.7 ± 0.05 % in non-AngII-animals, p < 0.01 vs. AngII-control and non-AngII, n=5/6/5 per group, Fig. 3A). In contrast, AngII-control treated animals had an increased percentage of cytotoxic T cells compared to AngII MC IL-10 or non-AngII treated mice (CD8+ / GranzymeB+, 3.9 ± 0.2 % of CD45+/CD3+ vs. 2.3 ± 0.3 % in AngII-control and 2.6 ± 0.3 % in non-AngII, p < 0.01 vs. AngII MC IL-10 and non-AngII, n= 6/5/5 per group, Fig. 3B). As a result, the T_{reg} cell to cytotoxic T cell ratio (CD4+/CD25+/FOXP3+ per CD8+/GranzymeB+) was highly and significantly increased in the AngII MC IL-10-treated animals (Fig. 3C).

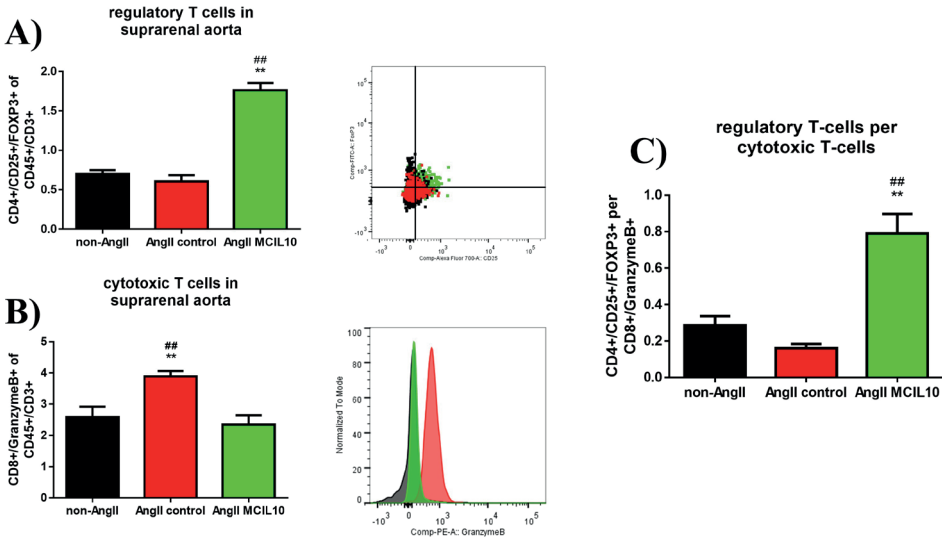


Figure 3. T lymphocyte presence and differentiation in aortic tissue.
At day 7 after aneurysm induction (d14 after transfection with MC) aortic tissue was harvested, lysed and analyzed via flow cytometry to characterize T cell differentiation. A and B include representative flow cytometry graphs and histograms; n=4/5/4; n=5/6/5
(A) Percentage of CD4+/CD25+/Foxp3 of CD45+/CD3+ cells in untreated animals, AngII-infused controls and AngII-infused/MC-IL10 transfected animals; ** = p≤0.01 vs. AngII, ## = p≤0.01 vs. untreated. (B) Percentage of CD8+/GranzymeB+ of CD45+/CD3+ cells; ** = p≤0.01 vs. AngII MC IL-10, ## = p≤0.01 vs. untreated. (C) Ratio of CD4+/CD25+/Foxp3 over CD8+/GranzymeB+ cell (T_{reg} to cytotoxic T cell ratio), ** = p≤0.01 vs. AngII, ## = p≤0.01 vs. untreated.

We did not find a significant difference in absolute cell number in aortic tissue (CD4+ or CD8+ or CD3+/CD45+ or F4/80+ cells of single cells) between the three experimental groups, indicating that there was a difference in cell polarization, rather than cell number (Supp. Figure 2).

Peripheral blood quantification did not reveal significant differences in T cell polarization regarding T_{reg} and cytotoxic T cells. CD4+ cells were significantly more present in peripheral blood in AngII-treated animals, independent of MC IL-10 treatment (CD4+ of single cells, 2.2 ± 0.3 % in non-AngII-animals vs. 3.5 ± 0.4% in AngII-control vs. 3.7 ± 0.4 % in AngII MC IL-10, $p < 0.01$ vs. non-AngII, n=5/6/5 per group, Supp. Fig. 3D)

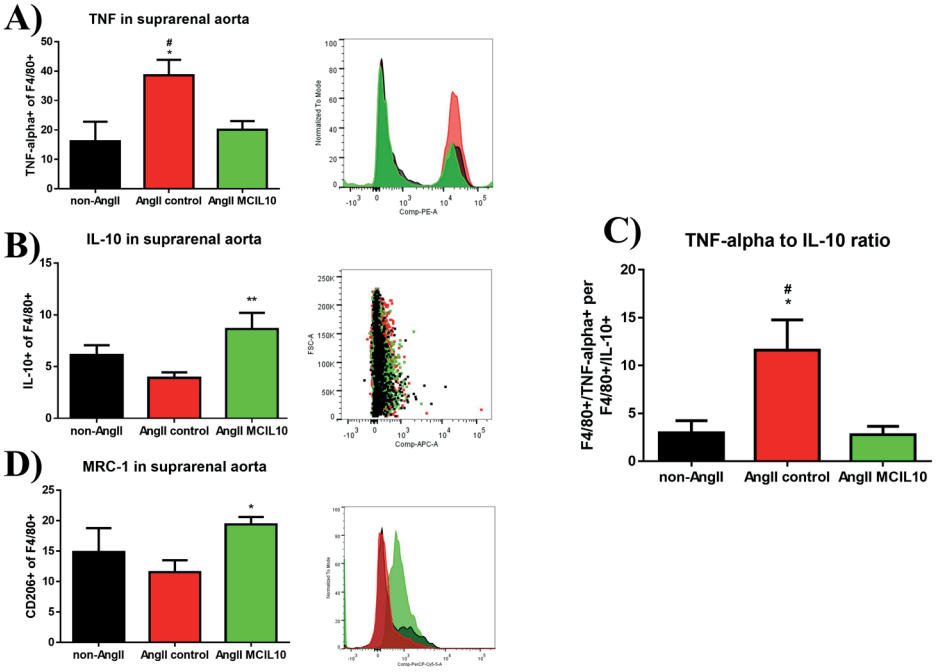


Figure 4. Macrophage presence and differentiation in aortic tissue.
At day 7 after aneurysm induction (d14 after transfection with MC) aortic tissue was harvested, lysed and analyzed via flow cytometry to characterize macrophage differentiation markers. A, B, D include representative flow cytometry graphs and histograms; n=4/5/4. (A) Percentage of TNF-α+ of F4/80+ cells in untreated, AngII-infused, and AngII-infused/MC-IL10 transfected animals; * = p≤0.05 vs. AngII MC-IL10, # = p≤0.05 vs. untreated. (B) Percentage of IL-10+ of F4/80+ cells; ** = p≤0.01 vs. AngII. (C) Ratio of TNF-α+ over IL-10+ cells; * = p≤0.05 vs. AngII MC-IL10, # = p≤0.05 vs. untreated. (D) Percentage of MRC1+ of F4/80+ cells; * = p≤0.05 vs. AngII

F4/80-positive macrophages in suprarenal aortic tissue were more prone to Tumor necrosis factor alpha (TNF-α) production (38.6 ± 5.3 percent of F4/80+ cells) without MC IL-10 application than after transfection with IL-10 (20.0 ± 3 percent of F4/80+, $p < 0.05$,

n= 4/5/4 per group, Fig. 4A), and also showed decreased IL-10 signal (3.9 ± 0.5 % of F4/80+ cells vs. 8.6 ± 1.6 % of F4/80+ cells, p < 0.01 vs. AngII-control, n= 4/5/4 per group, Fig. 4B). Notably, the increased TNF-α/IL-10 ratio in AngII-treated control animals was reversed with IL-10 transfection (Fig. 4C). Intriguingly, suprarenal aortic macrophages showed increased differentiation into the more anti-inflammatory M2-like phenotype with MC IL-10 treatment (19.4 ± 1.2 % of Mannose Receptor C type 1 (MRC1)+ over F4/80+ cells vs. 11.6 ± 1.9 % in AngII control, p < 0.05 vs. control, n= 4/5/4 per group, Fig. 4D).

To further investigate translational potential in human cells, we primed human PBMCs with AngII or AngII/IL-10 before stimulation with LPS and evaluated expression of inflammatory markers. There was a significant reduction in inflammatory gene expression with AngII/IL-10 vs. AngII alone for all markers except *FOXP3* (0.07 ± 0.01 vs. 0.31 ± 0.05 vs. 0.19 ± 0.04 relative expression vs. GAPDH in cells not primed with AngII vs. AngII primed cells vs. AngII/IL-10 treated cells, p = 0.07 vs. (+) AngII, n = 9/18/19, Fig. 5A). Granzyme B (*GRZB)*-expression was lower in AngII/IL-10 treated cells (0.19 ± 0.05 vs. 0.2 ± 0.02 vs. 0.14 ± 0.01 04 relative expression vs. GAPDH in cells with (-) AngII vs. (+) AngII vs. (+) AngII/IL-10, p < 0.05 vs. (+) AngII, n = 9/18/19, Fig. 5B), resulting in no significant change of *FOXP3* to *GRZB* ratio in AngII (+) vs. AngII (+) / IL-10 (0.47 ± 0.1 vs. 1.55 ± 0.25 vs. 1.48 ± 0.3 fold, p = n.s. vs. (+) AngII, n = 9/18/19, Fig 5C).

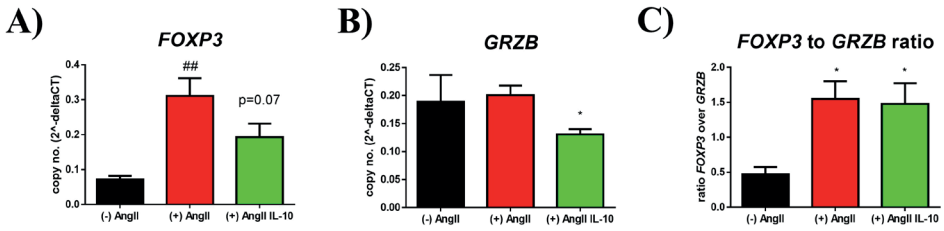


Figure 5. T lymphocyte differentiation in human PBMCs after AngII priming and stimulation.
Human PBMCs were isolated and primed with AngII or AngII/IL-10 for 24 hours before cells were activated with LPS (24h) to further evaluate gene expression of T cell characterizing markers; n=9/18/19. (A) Relative expression of FOXP3 over GAPDH in unprimed, AngII-primed, and AngII/IL-10 primed PBMCs; ## = p≤0.01 vs. untreated; p=.0.07 in AngII IL-10 vs. AngII. (B) Relative expression of GranzymeB (GZMB) in unprimed, AngII, AngII/IL-10 PBMCs; * = p≤0.05 vs. AngII. (C) Ratio (relative expression) of FOXP3 over GRZB; * = p≤0.05 vs. AngII.

Looking at macrophage markers revealed beneficial effects for (+) AngII/IL-10 vs. (+) AngII alone. TNF-α (TNF) expression dropped significantly with MC IL-10 treatment (0.15 ± 0.01 vs. 0.09 ± 0.03 vs. 0.004 ± 0.002; p < 0.05 vs. (+) AngII, n = 9/18/19, Fig. 6A). IL-10 expression was increased in (+) AngII / IL-10 (0.24 ± 0.03 vs. 0.36 ± 0.06 vs. 0.62 ± 0.12; p < 0.05 vs. (+) AngII, n = 9/15/11, Fig. 6B), resulting overall in a significantly decreased TNF-α to IL-10 ratio (0.62 ± 0.05 vs. 0.18 ± 0.07 vs. 0.01 ± 0.01; p < 0.01 vs. (+) AngII and vs. (-) AngII, n = 6/14/11, Fig. 6C). Markers of alternatively activated M2-macrophages, such as

MRC1 (0.005 ± 0.001 vs. 0.005 ± 0.001 vs. 0.01 ± 0.002; $p < 0.05$ vs. (+) AngII, n = 9/15/17, Fig. 6D) and CD163 (1.04 ± 0.16 vs. 0.8 ± 0.09 vs. 39.92 ± 21.79; $p < 0.01$ vs. (+) AngII, n = 9/18/11, Fig. 6E) were significantly up-regulated. Conversely, IL-6 expression was reduced in cells that were treated with IL-10 (0.32 ± 0.08 vs. 0.37 ± 0.06 vs. 0.05 ± 0.01; $p < 0.01$ vs. (+) AngII and vs. (-) AngII, n = 6/15/14, Fig. 6F).

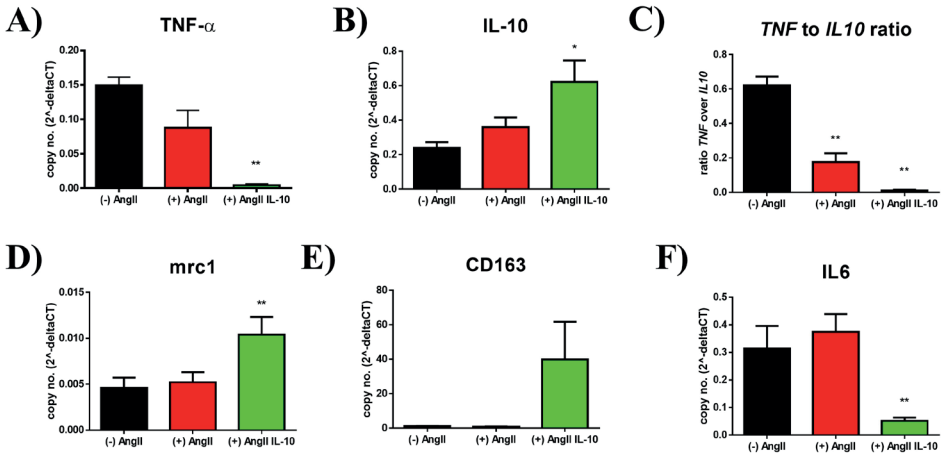


Figure 6. Macrophage differentiation in human PBMCs after AngII priming and stimulation.
Human PBMCs were isolated and primed with AngII or AngII/IL-10 for 24 hours before cells were activated with LPS (24h) to further evaluate macrophage activation (n=9/18/19). (A) Relative expression of TNF-α (TNF) over GAPDH in unprimed, AngII-primed, and AngII/IL-10 primed PBMCs; ** = p≤0.01 vs. AngII. (B) Relative expression of IL-10 in unprimed, AngII, and AngII/IL-10 PBMCs; * = p≤0.05 vs. AngII. (C) Ratio (relative expression) of TNF over IL-10; ** = p≤0.01 vs. AngII, ## = p≤0.01 vs. unprimed. (D) Relative expression of MRC1 in unprimed, AngII, and AngII/IL-10 PBMCs; ** = p≤0.01 vs. AngII. (E) Relative expression of CD163 in unprimed, AngII, and AngII/IL-10 PBMCs; ** = p≤0.01 vs. AngII. (F) Relative expression of IL-6 in unprimed, AngII, and AngII/IL-10 PBMCs; ** = p≤0.01 vs. AngII.

DISCUSSION

Here, we show that systemic transfection with a non-immunogenic delivery method using IL-10 expressing minicircles is feasible and effective in a murine model of AAA disease. Plasma IL-10 levels were significantly increased at 1 week after transfection in Apo E-/- mice, and IL-10 induction significantly decreased aneurysm size and likelihood of suprarenal dissecting AAA formation. These beneficial effects upon aneurysm development were accompanied by a significant increase in T_{reg} cells and a decrease in cytotoxic T cells. Furthermore, local macrophages were more likely to differentiate into the alternatively activated M2-macrophages and express less TNF-α as well as more IL-10. Human PBMCs with IL-10 treatment after AngII-incubation showed ameliorated expression of differentia-

tion markers Granzyme B (GZMB), TNF-α, MRC1, CD163 and IL-6, indicating possible translational potential in the application of IL-10.

One major IL-10-induced anti-inflammatory process in tissue is the induction of CD4+ CD25+ FOXP3+ T_{reg} cells (Saraiva and O'Garra 2010). In general, their mechanism of action also involves production of Interleukin-10 (IL-10) itself (Saraiva and O'Garra 2010, Steinke and Lawrence 2014), providing a self-amplifying feedback loop, which we also identified. The induction of a subset of more anti-inflammatory macrophages by T_{reg} cells (Tiemessen et al. 2007), particularly the so-called 'deactivated' M2c-macrophages which are believed to be important for tissue remodelling and matrix deposition, is also regulated by IL-10 (Liu et al. 2011, Martinez and Gordon 2014). In AAA disease, M2-macrophages are present in the later phases of development (Rateri et al. 2011) and are involved in healing and prevention of further AAA growth. By contrast, activation and clonal expansion of CD8+ cytotoxic T cells induces cell damage and apoptosis potentially worsening AAA disease, if not properly regulated (Henderson et al. 1999, Lindeman et al. 2009). As IL-10 has been shown to contribute to CD8+ cytotoxic T cell (CTL) expansion under certain conditions, we monitored the CD8+ GranzymeB+ CTL amount in tissue and calculated the ratio of T_{reg} / CTL ratio to further characterize the impact of IL-10 on the T cell population in the aortic wall.

Using the AngII-induced AAA model, we observed that systemic overexpression of IL-10 via single timepoint MC transfection led to aortic cell polarization into T_{reg} cells and anti-inflammatory M2-macrophages expressing MRC1. These changes in adaptive and innate immune cell differentiation were associated with a clear reduction in aneurysm formation. We did not find a significant change in CD3+/CD45+, CD4+, CD8+ or macrophage cell number in aortic tissue after MC injection. Therefore, our results suggest a polarization effect, rather than a recruitment. Considering the limited expression period of the MC-delivered plasmids of, at most, 2 weeks with regard to IL-10 plasma levels (when compared to the four-week period of aneurysm development), it could be that this treatment might have sparked self-amplifying cascades and cell-cell interactions that maintain the anti-inflammatory response. At 28 days after aneurysm induction, only splenic tissue showed increased expression of IL-10 (Figure 1D). This was accompanied by higher Foxp3 expression, possibly indicating pronounced T_{reg} polarization (Figure 1E). This is especially intriguing, as flow cytometry analysis of spleens at day 7 after AngII showed significantly fewer CD4+ cells and a tendency towards fewer Foxp3-positive T_{reg} cells (Supp. Figure 4 A and D). This might indicate an initial mobilization of CD4+ cells from the spleen in response to AngII, a redistribution process to non-lymphoid tissue known to occur after recognition of certain antigens (Bronte and Pittet 2013). Subsequently, splenic IL-10 and Foxp3 expression might increase again over the next 3 weeks if MC IL-10 expression had successfully induced anti-inflammatory processes in the aorta.

In patients with AAA, both the number and function of T_{reg} cells as well as the expression of FOXP3 are significantly decreased in peripheral blood (Yin et al. 2010, Zhou et al. 2015),

suggesting that the lack of T_{reg} immunomodulation may accelerate AAA formation. Indeed, adoptive transfer of T_{reg} cells to AngII-treated ApoE-/- mice reduced AAA incidence and severity in a dose-dependent manner (Meng et al. 2014). Further, direct treatment with T_{reg} cells decreased macrophage number and the expression of pro-inflammatory cytokines in local aortic tissue. After T_{reg} treatment *in vitro*, macrophages had a more pronounced M2-like phenotype, consistent with previous reports (Tiemessen et al. 2007, Liu et al. 2011). As such, the beneficial effects of T_{reg} cells are likely mediated via direct cell-cell contact as well as paracrine effects.

Yodoi et al. (Yodoi et al. 2015) demonstrated that expansion of Foxp3+ T_{reg} cells by IL-2 complex treatment resulted in a marked decrease in the incidence and mortality of AAA, and that this effect could be reversed by genetic depletion of Foxp3+ T_{reg} cells, further underlining the importance of T_{reg} cells in the prevention of aneurysm disease. Moreover, Zhou and colleagues (Zhou et al. 2015) further clarified the importance of IL-10 in mediating the beneficial effects of T_{reg} cells in AAA formation. Transfusion of T_{reg} cells from WT animals suppressed macrophage activation and reduced lesion macrophage and T cell counts in the murine AngII AAA model. However, this was not the case in mice that were infused with T_{reg} cells from IL-10-/- animals, suggesting that the presence of IL-10 is imperative for cell-cell interaction of T_{reg} cells with the surrounding tissue. IL-10 has also been shown to be a crucial regulator of inflammation-matrix interaction, as T_{reg} cells from IL-10 competent mice suppress MMP-9 and MMP-13 activity more strongly than T_{reg} cells from IL-10 -/- mice (Zhou et al. 2015). Notably, IL-10-/- mice show increased elastin degradation (Ait-Oufella et al. 2013) and, T_{reg} treatment inhibits apoptosis of aortic wall cells in the AngII-induced aneurysm model (Meng et al. 2014). Our data support a critical role for the mediator IL-10 in prevention of AAA formation, and suggest that a transient increase in IL-10 might be sufficient to induce a critical mass of anti-inflammatory T_{reg} cells and regulatory macrophages at the site of lesion, thereby possibly decreasing AAA growth by positively modulating the inflammatory response, with potential downstream effects on extracellular matrix degradation and apoptosis via IL-10.

Recent work highlights the special considerations that need to be taken into account regarding the role of aortic dissection in the AngII-AAA model (Saraff et al. 2003, Trachet et al. 2015). Inflammatory cell infiltration tends to localize to sites of aortic dissection (Cao et al. 2010). It is believed that classical activation of macrophages induces vascular dissection, thereby promoting AAA formation at least in part by an IL-6 dependent mechanism (Tieu et al. 2009). Our work suggests that re-adjusting the macrophage activation cascades using IL-10 treatment suppresses IL-6 as well as TNF-α expression and promotes MRC1 and CD163 transcription. The IL-10-induced increase in T_{reg} cells and the shift from classical to alternatively activated macrophages in aortic tissue is therefore likely to be an important mechanism in the prevention of dissecting AAA. We assume that our anti-inflammatory treatment primarily suppresses both micro- and macro-ruptures, as these hemorrhagic

events are thought to drive AAA growth in the AngII-model. This is further underscored by the early separation of our AAA diameter and dissecting AAA-free survival curves (Fig. 2 A and B) at day 7 with a subsequently similar growth rate.

In PBMCs from healthy controls stimulated with AngII, we observed minimal impact on inflammatory gene expression in the absence of IL-10 treatment. Our cells of interest, mainly monocytes/macrophages and T cells, all express receptors for AngII (Yanagitani et al. 1999, Crowley et al. 2010, Yodoi et al. 2015) and should therefore be susceptible to AngII priming. However, effects of AngII on leukocytes appear to be context-sensitive (Yanagitani et al. 1999, Crowley et al. 2008) and are difficult to duplicate *in vitro*(Keidar et al. 2001). We acknowledge that our understanding of AngII-induced effects on mononuclear cells is not complete, nevertheless, IL-10 treatment was beneficial after PBMCs were primed with AngII, supporting our main hypothesis that IL-10 initiates an anti-inflammatory and self-amplifying polarization towards T_{reg} cells and M2-macrophages.

There are limitations to our study. We applied the MC IL-10 vector systemically, once, and did not seek to control the site of expression nor the effect duration. It is possible that observed effects might be even stronger, and display less off-target impact if a more specific approach to the vasculature or immune cells had been chosen (Mayer et al. 2008, Sapet et al. 2012). Additionally, we cannot definitively conclude whether systemic or local increases of IL-10 are more important to prevent AAA formation, as the cellular changes we induced in aortic tissue were observed after systemic IL-10 delivery with an initial increase of plasma IL-10. With regard to clinical applicability and the known methodological shortcomings of cell-specific transfections, we deliberately chose this approach, intending to maintain translational potential and seeking to prove that MCs are feasible non-immunogenic vectors for the treatment of AAAs in this mouse model. We did not seek to provide deeper mechanistic insights as the interaction of IL-10 with lymphocytes and myeloid cells has been extensively studied before. While we do not provide hemodynamic data (such as blood pressure) in these animals, and therefore cannot exclude differences in MC-IL10 treated vs. non-MC-IL-10 treated animals, a recent publication suggests no prognostic value of hemodynamic markers on aneurysm growth (Prins et al. 2014). Also, initial characterization of the model did not show any alteration in arterial blood pressure after AngII infusion (Daugherty et al. 2000). The recently published prevention of blood pressure increase by continuous IL-10 infusion has only been shown in combination with significantly higher doses of AngII (90ng/min) and vastly higher IL-10 levels (0.5ng/min) when compared to our plasma IL-10 concentration (Lima et al. 2016).

In summary, we provide evidence that a one-time application of an IL-10 transcribing minicircle vector successfully limits aneurysm formation in a mouse model of AAA, while increasing regulatory T cells and alternatively activated macrophages in the aortic wall. IL-10 treatment of PBMCs partially recapitulated the anti-inflammatory effects of IL-10, indicating possible translational potential in humans.

REFERENCES

Ailawadi, G., C. W. Moehle, H. Pei, S. P. Walton, Z. Yang, I. L. Kron, . . . G. K. Owens (2009). "Smooth muscle phenotypic modulation is an early event in aortic aneurysms." J Thorac Cardiovasc Surg 138(6): 1392-1399.

Ait-Oufella, H., Y. Wang, O. Herbin, S. Bourcier, S. Potteaux, J. Joffre, . . . Z. Mallat (2013). "Natural Regulatory T Cells Limit Angiotensin II–Induced Aneurysm Formation and Rupture in Mice." Arteriosclerosis, Thrombosis, and Vascular Biology 33(10): 2374-2379.

Azuma, J., L. Maegdefessel, T. Kitagawa, R. L. Dalman, M. V. McConnell and P. S. Tsao (2011). "Assessment of elastase-induced murine abdominal aortic aneurysms: comparison of ultrasound imaging with in situ video microscopy." J Biomed Biotechnol 2011: 252141.

Bown, M. J., G. M. Lloyd, R. M. Sandford, J. R. Thompson, N. J. London, N. J. Samani and R. D. Sayers (2007). "The interleukin-10-1082 'A' allele and abdominal aortic aneurysms." J Vasc Surg 46(4): 687-693.

Bronte, V. and M. J. Pittet (2013). "The spleen in local and systemic regulation of immunity." Immunity 39(5): 806-818.

Buruiana, F. E., I. Sola and P. Alonso-Coello (2010). "Recombinant human interleukin 10 for induction of remission in Crohn's disease." Cochrane Database Syst Rev(11): CD005109.

Cao, R. Y., T. Amand, M. D. Ford, U. Piomelli and C. D. Funk (2010). "The Murine Angiotensin II-Induced Abdominal Aortic Aneurysm Model: Rupture Risk and Inflammatory Progression Patterns." Frontiers in Pharmacology 1: 9.

Centers for Disease Control and Prevention, N. C. f. H. S. (2016). "Underlying Cause of Death 1999-2015." CDC WONDER Online Database.

Chen, Z.-Y., E. Riu, C.-Y. He, H. Xu and M. A. Kay (2008). "Silencing of Episomal Transgene Expression in Liver by Plasmid Bacterial Backbone DNA Is Independent of CpG Methylation." Mol Ther 16(3): 548-556.

Crowley, S. D., C. W. Frey, S. K. Gould, R. Griffiths, P. Ruiz, J. L. Burchette, . . . T. M. Coffman (2008). "Stimulation of lymphocyte responses by angiotensin II promotes kidney injury in hypertension." American Journal of Physiology - Renal Physiology 295(2): F515-F524.

Crowley, S. D., Y.-S. Song, G. Sprung, R. Griffiths, M. Sparks, M. Yan, . . . P. Ruiz (2010). "A Role for Angiotensin II Type 1 Receptors on Bone Marrow-Derived Cells in the Pathogenesis of Angiotensin II–Dependent Hypertension." Hypertension 55(1): 99-108.

Daugherty, A., M. W. Manning and L. A. Cassis (2000). "Angiotensin II promotes atherosclerotic lesions and aneurysms in apolipoprotein E-deficient mice." J Clin Invest 105(11): 1605-1612.

Duchmann, R., E. Schmitt, P. Knolle, K. H. Meyer zum Buschenfelde and M. Neurath (1996). "Tolerance towards resident intestinal flora in mice is abrogated in experimental colitis and restored by treatment with interleukin-10 or antibodies to interleukin-12." Eur J Immunol 26(4): 934-938.

Grool, T. A., H. van Dullemen, J. Meenan, F. Koster, F. J. ten Kate, A. Lebeaut, . . . S. J. van Deventer (1998). "Anti-inflammatory effect of interleukin-10 in rabbit immune complex-induced colitis." Scand J Gastroenterol 33(7): 754-758.

Gurtelschmid, M., M. Bjorck and A. Wanhainen (2014). "Comparison of three ultrasound methods of measuring the diameter of the abdominal aorta." Br J Surg 101(6): 633-636.

Henderson, E. L., Y.-J. Geng, G. K. Sukhova, A. D. Whittemore, J. Knox and P. Libby (1999). "Death of Smooth Muscle Cells and Expression of Mediators of Apoptosis by T Lymphocytes in Human Abdominal Aortic Aneurysms." Circulation 99(1): 96-104.

Huang, M., Z. Chen, S. Hu, F. Jia, Z. Li, G. Hoyt, . . . J. C. Wu (2009). "Novel Minicircle Vector for Gene Therapy in Murine Myocardial Infarction." Circulation 120(11 suppl 1): S230-S237.

Jia, F., K. D. Wilson, N. Sun, D. M. Gupta, M. Huang, Z. Li, . . . J. C. Wu (2010). "A nonviral minicircle vector for deriving human iPS cells." Nat Methods 7(3): 197-199.

Kadoglou, N. P., I. Papadakis, K. G. Moulakakis, I. Ikonomidis, M. Alepaki, P. Moustardas, . . . C. D. Liapis (2012). "Arterial stiffness and novel biomarkers in patients with abdominal aortic aneurysms." Regul Pept 179(1-3): 50-54.

Keidar, S., R. Heinrich, M. Kaplan, T. Hayek and M. Aviram (2001). "Angiotensin II Administration to Atherosclerotic Mice Increases Macrophage Uptake of Oxidized LDL: A Possible Role for Interleukin-6." Arteriosclerosis, Thrombosis, and Vascular Biology 21(9): 1464-1469.

Kunieda, T., T. Minamino, J. Nishi, K. Tateno, T. Oyama, T. Katsuno, . . . I. Komuro (2006). "Angiotensin II induces premature senescence of vascular smooth muscle cells and accelerates the development of atherosclerosis via a p21-dependent pathway." Circulation 114(9): 953-960.

Lijkwan, M. A., A. A. Hellingman, E. J. Bos, K. E. van der Bogt, M. Huang, N. G. Kooreman, . . . J. C. Wu (2014). "Short hairpin RNA gene silencing of prolyl hydroxylase-2 with a minicircle vector improves neovascularization of hindlimb ischemia." Hum Gene Ther 25(1): 41-49.

Lima, V. V., S. M. Zemse, C. W. Chiao, G. F. Bomfim, R. C. Tostes, R. Clinton Webb and F. R. Giachini (2016). "Interleukin-10 limits increased blood pressure and vascular RhoA/Rho-kinase signaling in angiotensin II-infused mice." Life Sci 145: 137-143.

Lindeman, J. H. N., H. Abdul-Hussien, J. H. van Bockel, R. Wolterbeek and R. Kleemann (2009). "Clinical Trial of Doxycycline for Matrix Metalloproteinase-9 Inhibition in Patients With an Abdominal Aneurysm: Doxycycline Selectively Depletes Aortic Wall Neutrophils and Cytotoxic T Cells." Circulation 119(16): 2209-2216.

Liu, G., H. Ma, L. Qiu, L. Li, Y. Cao, J. Ma and Y. Zhao (2011). "Phenotypic and functional switch of macrophages induced by regulatory CD4+CD25+ T cells in mice." Immunol Cell Biol 89(1): 130-142.

Maegdefessel, L., J. Azuma, R. Toh, A. Deng, D. R. Merk, A. Raiesdana, . . . P. S. Tsao (2012). "MicroRNA-21 blocks abdominal aortic aneurysm development and nicotine-augmented expansion." Sci Transl Med 4(122): 122ra122.

Maegdefessel, L., J. Azuma, R. Toh, D. R. Merk, A. Deng, J. T. Chin, . . . P. S. Tsao (2012). "Inhibition of microRNA-29b reduces murine abdominal aortic aneurysm development." J Clin Invest 122(2): 497-506.

Maegdefessel, L., J. M. Spin, U. Raaz, S. M. Eken, R. Toh, J. Azuma, . . . P. S. Tsao (2014). "miR-24 limits aortic vascular inflammation and murine abdominal aneurysm development." Nat Commun 5: 5214.

Marlow, G. J., D. van Gent and L. R. Ferguson (2013). "Why interleukin-10 supplementation does not work in Crohn's disease patients." World J Gastroenterol 19(25): 3931-3941.

Martinez, F. O. and S. Gordon (2014). "The M1 and M2 paradigm of macrophage activation: time for reassessment." F1000Prime Rep 6: 13.

Mayer, C. R., N. A. Geis, H. A. Katus and R. Bekeredjian (2008). "Ultrasound targeted microbubble destruction for drug and gene delivery." Expert Opin Drug Deliv 5(10): 1121-1138.

McColgan, P., G. E. Peck, R. M. Greenhalgh and P. Sharma (2009). "The genetics of abdominal aortic aneurysms: a comprehensive meta-analysis involving eight candidate genes in over 16,700 patients." Int Surg 94(4): 350-358.

Meng, X., J. Yang, K. Zhang, G. An, J. Kong, F. Jiang, . . . C. Zhang (2014). "Regulatory T Cells Prevent Angiotensin II–Induced Abdominal Aortic Aneurysm in Apolipoprotein E Knockout Mice." Hypertension 64(4): 875-882.

Motulsky, H. J. and R. E. Brown (2006). "Detecting outliers when fitting data with nonlinear regression - a new method based on robust nonlinear regression and the false discovery rate." BMC Bioinformatics 7: 123.

Nordon, I. M., R. J. Hinchliffe, I. M. Loftus and M. M. Thompson (2011). "Pathophysiology and epidemiology of abdominal aortic aneurysms." Nat Rev Cardiol 8(2): 92-102.

Prins, P. A., M. F. Hill, D. Airey, S. Nwosu, P. R. Perati, H. Tavori, . . . U. K. Sampson (2014). "Angiotensin-induced abdominal aortic aneurysms in hypercholesterolemic mice: role of serum cholesterol and temporal effects of exposure." PLoS One 9(1): e84517.

Rachmawati, H., L. Beljaars, C. Reker-Smit, H. I. Bakker, A. M. Van Loenen-Weemaes, M. N. Lub-De Hooge and K. Poelstra (2011). "Intravenous administration of recombinant human IL-10 suppresses the development of anti-thy 1-induced glomerulosclerosis in rats." PDA J Pharm Sci Technol 65(2): 116-130.

Rateri, D. L., D. A. Howatt, J. J. Moorleghen, R. Charnigo, L. A. Cassis and A. Daugherty (2011). "Prolonged Infusion of Angiotensin II in apoE−/− Mice Promotes Macrophage Recruitment with Continued Expansion of Abdominal Aortic Aneurysm." The American Journal of Pathology 179(3): 1542-1548.

Sapet, C., N. Laurent, E. Bertosio, M. Bertuzzi and F. Sicard (2012). "Targeted transfection of cells/tissue in vivo."

Saraff, K., F. Babamusta, L. A. Cassis and A. Daugherty (2003). "Aortic Dissection Precedes Formation of Aneurysms and Atherosclerosis in Angiotensin II-Infused, Apolipoprotein E-Deficient Mice." Arteriosclerosis, Thrombosis, and Vascular Biology 23(9): 1621-1626.

Saraiva, M. and A. O'Garra (2010). "The regulation of IL-10 production by immune cells." Nat Rev Immunol 10(3): 170-181.

Schermerhorn, M. L., R. P. Bensley, K. A. Giles, R. Hurks, J. O'Malley A, P. Cotterill, . . . B. E. Landon (2012). "Changes in abdominal aortic aneurysm rupture and short-term mortality, 1995-2008: a retrospective observational study." Ann Surg 256(4): 651-658.

Steinke, J. W. and M. G. Lawrence (2014). "T-cell biology in immunotherapy." Annals of Allergy, Asthma & Immunology 112(3): 195-199.

Thomas, M., D. Gavrila, M. L. McCormick, F. J. Miller, Jr., A. Daugherty, L. A. Cassis, . . . N. L. Weintraub (2006). "Deletion of p47phox attenuates angiotensin II-induced abdominal aortic aneurysm formation in apolipoprotein E-deficient mice." Circulation 114(5): 404-413.

Tiemessen, M. M., A. L. Jagger, H. G. Evans, M. J. C. van Herwijnen, S. John and L. S. Taams (2007). "CD4+CD25+Foxp3+ regulatory T cells induce alternative activation of human monocytes/macrophages." Proceedings of the National Academy of Sciences 104(49): 19446-19451.

Tieu, B. C., C. Lee, H. Sun, W. LeJeune, A. Recinos, 3rd, X. Ju, . . . A. R. Brasier (2009). "An adventitial IL-6/MCP1 amplification loop accelerates macrophage-mediated vascular inflammation leading to aortic dissection in mice." The Journal of Clinical Investigation 119(12): 3637-3651.

Trachet, B., R. A. Fraga-Silva, A. Piersigilli, A. Tedgui, J. Sordet-Dessimoz, A. Astolfo, . . . N. Stergiopulos (2015). "Dissecting abdominal aortic aneurysm in Ang II-infused mice: suprarenal branch ruptures and apparent luminal dilatation." Cardiovascular Research 105(2): 213-222.

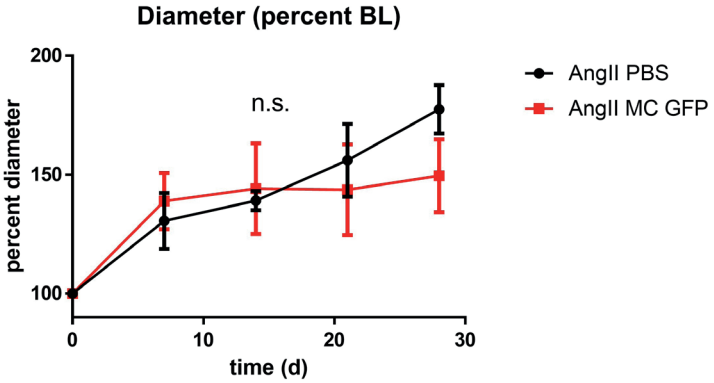
Turner, D. M., D. M. Williams, D. Sankaran, M. Lazarus, P. J. Sinnott and I. V. Hutchinson (1997). "An investigation of polymorphism in the interleukin-10 gene promoter." Eur J Immunogenet 24(1): 1-8.

Yanagitani, Y., H. Rakugi, A. Okamura, K. Moriguchi, S. Takiuchi, M. Ohishi, . . . T. Ogihara (1999). "Angiotensin II Type 1 Receptor–Mediated Peroxide Production in Human Macrophages." Hypertension 33(1): 335-339.

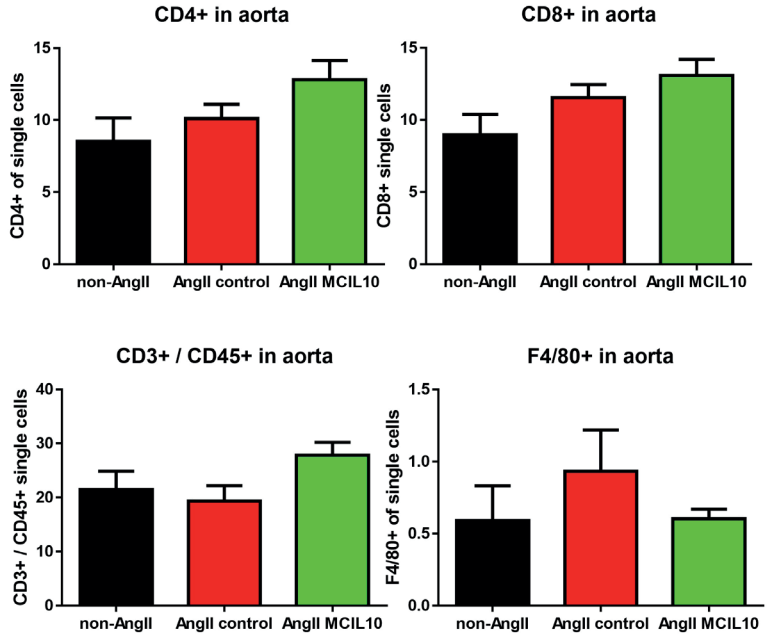
Yin, M., J. Zhang, Y. Wang, S. Wang, D. Böckler, Z. Duan and S. Xin (2010). "Deficient CD4+CD25+ T Regulatory Cell Function in Patients With Abdominal Aortic Aneurysms." Arteriosclerosis, Thrombosis, and Vascular Biology 30(9): 1825-1831.

Yodoi, K., T. Yamashita, N. Sasaki, K. Kasahara, T. Emoto, T. Matsumoto, . . . K.-i. Hirata (2015). "Foxp3+ Regulatory T Cells Play a Protective Role in Angiotensin II–Induced Aortic Aneurysm Formation in Mice." Hypertension 65(4): 889-895.

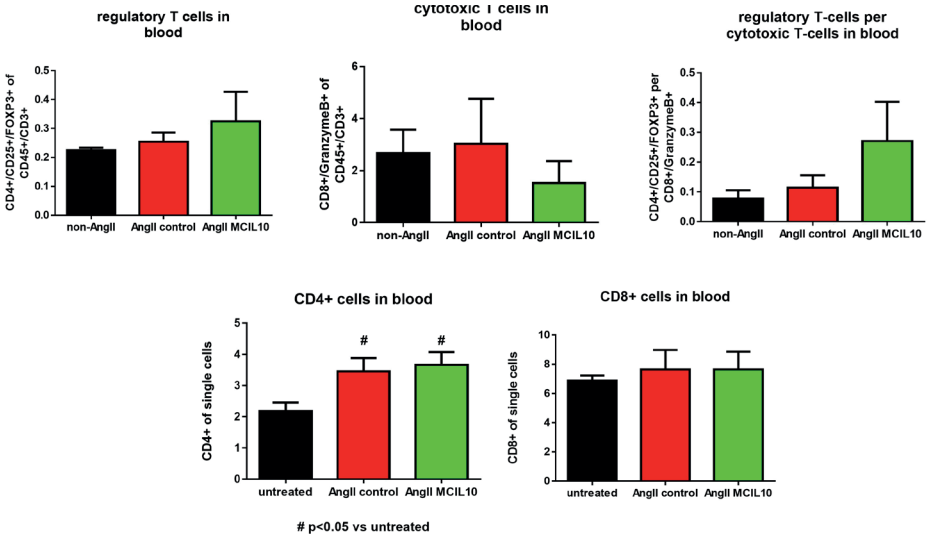
Zhou, Y., W. Wu, J. S. Lindholt, G. K. Sukhova, P. Libby, X. Yu and G.-P. Shi (2015). "Regulatory T cells in human and angiotensin II-induced mouse abdominal aortic aneurysms." Cardiovascular Research 107(1): 98-107.



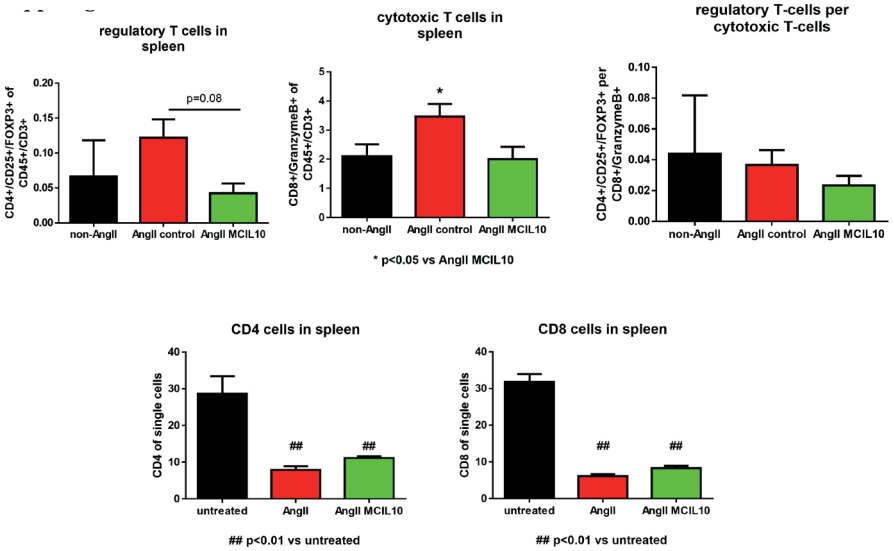
Supp. Figure 1. Aortic diameter of MC-GFP vs. saline transfected animals.
Ultrasound measurements of ApoE-/- mice after subcutaneous infusion of AngII (1 µg/kg/min) 7 days after MC-GFP or saline was infused. Aortic diameter in percent of baseline diameter over timecourse of 28 days; n = 5 vs. 5, p= n.s.



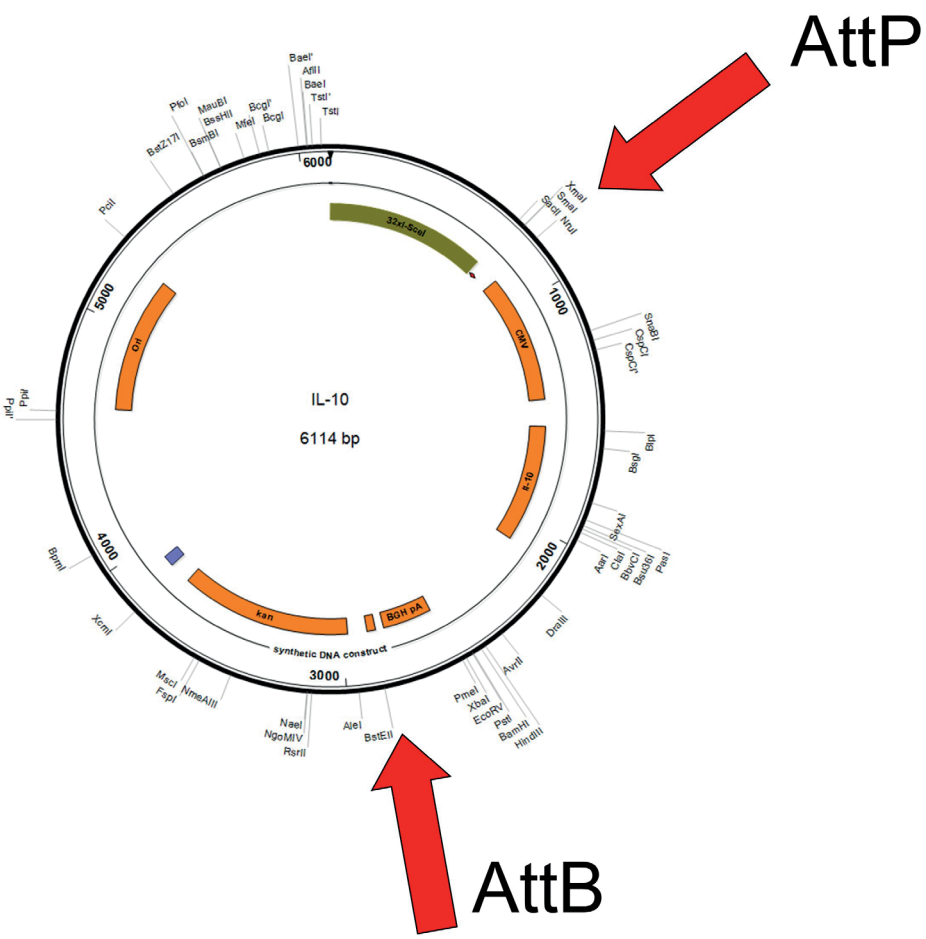
Supp. Figure 2. Presence of CD3+/CD45+ or F4/80+ cells in aortic tissue (ratio to single cells).
At day 7 after aneurysm induction (d14 after transfection with MC) aortic tissue was harvested, lysed and analyzed via flow cytometry to characterize amount and polarization of T cells and Macrophages. Data shown as CD4+, CD8+, CD3+/CD45+ or F4/80+ cells as percentage of all single cells; p= n.s.



Supp. Figure 3. T lymphocyte presence and differentiation in peripheral blood.
At day 7 after aneurysm induction (d14 after transfection with MC) peripheral blood (with subsequent RBC lysis) was harvested and analyzed via flow cytometry to characterize T cell differentiation; n=5/6/5. (A) Percentage of CD4+/CD25+/Foxp3 of CD45+/CD3+ cells in untreated, AngII – infused and AngII infused / MC-IL10 transfected animals, in blood; p= n.s. (B) Percentage of CD8+/GranzymeB+ of CD45+/CD3+ cells, in blood; p=n.s. (C) ratio of CD4+/CD25+/Foxp3 over CD8+/GranzymeB+ cell (T_{reg} to cytotoxic T cell ratio), in blood; p=n.s. (D) Percentage of CD4+ cells of single cells in untreated, AngII – infused and AngII infused / MC-IL10 transfected animals, in blood; p= n.s. (E) Percentage of CD8+ cells of single cells in untreated, AngII – infused and AngII infused / MC-IL10 transfected animals, in blood; p= n.s.



Supp. Figure 4. T lymphocyte presence and differentiation in spleen.
At day 7 after aneurysm induction (d14 after transfection with MC), spleens (with subsequent lysis according to standard protocol) were harvested and analyzed via flow cytometry to characterize T cell differentiation; n=5/6/5. (A) Percentage of CD4+/CD25+/Foxp3 of CD45+/CD3+ cells in untreated, AngII – infused and AngII infused / MC-IL10 transfected animals, in spleen; p= n.s. (B) Percentage of CD8+/GranzymeB+ of CD45+/CD3+ cells, in spleen; p<0.05 in AngII control vs. AngII MC IL10. (C) ratio of CD4+/CD25+/Foxp3 over CD8+/GranzymeB+ cell (T_{reg} to cytotoxic T cell ratio), in spleen; p=n.s. (D) Percentage of CD4+ cells of single cells in untreated, AngII – infused and AngII infused / MC-IL10 transfected animals, in spleen; p<0.01 vs. untreated (E) Percentage of CD8+ cells of single cells in untreated, AngII – infused and AngII infused / MC-IL10 transfected animals, in spleen; p<0.01 vs. untreated.



Supp. Figure 5. Schematics of Interleukin-10 expressing minicircle vector.

Chapter 5

Pluripotent stem cell therapy for vascular disease

Gu, M.[*]*, Mordwinkin, N.M.*[*]*, Kooreman, N.G., Lee, J., Wu, H., Hu, S., Churko, J.M., Diecke, S., Burridge, P.W., He, C., et al. (2015). Pravastatin reverses obesity-induced dysfunction of induced pluripotent stem cell-derived endothelial cells via a nitric oxide-dependent mechanism.* **European Heart Journal,** *36, 806-816.*

[*] *authors contributed equally*

ABSTRACT

Aims

High-fat diet-induced obesity (DIO) is a major contributor to type II diabetes and micro- and macro-vascular complications leading to peripheral vascular disease (PVD). Metabolic abnormalities of induced pluripotent stem cell-derived endothelial cells (iPSC-ECs) from obese individuals could potentially limit their therapeutic efficacy for PVD. The aim of this study was to compare the function of iPSC-ECs from normal and DIO mice using comprehensive *in vitro* and *in vivo* assays.

Methods and results

Six-week-old C57Bl/6 mice were fed with a normal or high-fat diet. At 24 weeks, iPSCs were generated from tail tip fibroblasts and differentiated into iPSC-ECs using a directed monolayer approach. *In vitro* functional analysis revealed that iPSC-ECs from DIO mice had significantly decreased capacity to form capillary-like networks, diminished migration, and lower proliferation. Microarray and ELISA confirmed elevated apoptotic, inflammatory, and oxidative stress pathways in DIO iPSC-ECs. Following hindlimb ischaemia, mice receiving intramuscular injections of DIO iPSC-ECs had significantly decreased reperfusion compared with mice injected with control healthy iPSC-ECs. Hindlimb sections revealed increased muscle atrophy and presence of inflammatory cells in mice receiving DIO iPSC-ECs. When pravastatin was co-administered to mice receiving DIO iPSC-ECs, a significant increase in reperfusion was observed; however, this beneficial effect was blunted by co-administration of the nitric oxide synthase inhibitor, N^{ω}-nitro-l-arginine methyl ester.

Conclusion

This is the first study to provide evidence that iPSC-ECs from DIO mice exhibit signs of endothelial dysfunction and have suboptimal efficacy following transplantation in a hindlimb ischaemia model. These findings may have important implications for future treatment of PVD using iPSC-ECs in the obese population.

INTRODUCTION

Obesity is a rapidly growing threat to global healthcare, with 1.5 billion adults overweight and 400 million of them considered obese. Increasing evidence indicates a high-caloric high-fat diet is a significant risk factor for causing deleterious effects on metabolism and heart function, and has been strongly linked to the progression of heart disease and type 2 diabetes (Szendroedi and Roden 2009, Birse et al. 2010, Flegal et al. 2010). Dysglycaemia associated with obesity, insulin resistance and subsequent diabetes mellitus can lead to decreased nitric oxide (NO) bioavailability, endothelial nitric oxide synthase (eNOS) uncoupling, and increased levels of reactive oxygen species (ROS) (Du et al. 2006). Left unchecked, this oxidative stress can result in an increased production of pro-inflammatory cytokines, leading to oxidative DNA damage and the activation nof cellular apoptotic signals and pathways (Esposito et al. 2002, Galassetti 2012). The hallmark of endothelial dysfunction involved in obesity and its vascular complications is thought to be the result of interplay between apoptosis, inflammation, and oxidative stress, including a reduced bioavailability of NO (Hink et al. 2001). Statins are 3-hydroxy-3-methyl-glutaryl-CoA reductase inhibitors used primarily to lower cholesterol levels. Statins have also been shown to have beneficial effects on endothelial progenitor cells, improve endothelial function, increase NO production, augment neovascularization, and decrease ROS and inflammatory cytokines (Liu et al. 2012). In recent years, embryonic stem cell-derived endothelial cells (ESC-ECs) have been evaluated in models of myocardial infarction and hindlimb ischaemia as a potential therapeutic option to promote angiogenesis and neovascularization (Cho et al. 2007, Li et al. 2007, Yu et al. 2009). At present, therapies derived from ESCs are associated with significant ethical and political concerns. The recent discovery of induced pluripotent stem cells (iPSCs) has provided an alternative for the treatment of ischaemic vascular disease (Takahashi et al. 2007). However, little is known about the function of induced pluripotent stem cell-derived endothelial cells (iPSC-ECs) derived from obese or overweight individuals, specifically whether they exhibit properties of endothelial dysfunction and impaired vascular function similar to native ECs from these individuals. This could potentially limit the use of iPSC-ECs from patients with diabetes as a therapeutic option for peripheral vascular disease (PVD) unless coadminister with low-dose pravastatin therapy.

METHODS

Experimental animals

Animal study protocols were approved by the Animal Research Committee at Stanford University. All mice were obtained from The Jackson Laboratories (Bar Harbor, ME, USA), and quarantined for one week prior to the initiation of treatment. They were kept on a

12-hour light/dark cycle, and food and water were available ad libitum. For derivation of murine iPSCs, donor tail tip fibroblasts were isolated from 24-week old male C57Bl/6 mice fed a normal diet (10% kcal from fat; control mice) or high-fat diet (60% kcal from fat; DIO mice) beginning at 6 weeks of age (n=5/group; Jackson Laboratories, Bar Harbor, ME, USA) (Wang and Liao 2012). Recipient animals undergoing hindlimb ischemia surgery consisted of 10-12 week old male NOD/SCID mice. To verify the presence of diabetes, intraperitoneal (IP) glucose tolerance tests (GTT) and insulin tolerance tests (ITT) were performed as described previously (Bruning et al. 1997, Andrikopoulos et al. 2008). Donor animals were then euthanized. In order to serve as internal controls for comparisons with iPSC-ECs, aortic endothelial cells (aortic-ECs) were also isolated from both control and DIO mice as previously described (Kobayashi et al. 2005).

Derivation and culture of murine iPSCs

Murine tail tip fibroblasts were dissociated and isolated with collagenase type IV (Life Technologies, Grand Island, NY, USA) and maintained with Dulbecco's modified Eagle medium (DMEM) containing 10% fetal bovine serum (FBS), L- glutamine, 4.5 g/L glucose, 100 U/mL penicillin, and 100 g/mL streptomycin at 37°C, 20% O2, and 5% CO2 in a humidified incubator. Murine fibroblasts (passage 1-2) were reprogrammed using a codon optimized 4-in-1 lentiviral vector encoding Oct4, Klf4, Sox2, and c-Myc as previously described (Warlich et al. 2011). Murine iPSC clones were transferred to irradiated murine embryonic fibroblast (MEF) feeder layers and subsequently maintained in DMEM containing 20% FBS, L-glutamine, non-essential amino acids (NEAA), β-mercaptoethanol, and 10 ng/mL leukemia inhibitory factor (LIF) at 37°C, 5% O2, and 10% CO2 in a humidified incubator and passaged every 3-4 days with trypsin. After 2 passages, iPSCs were transferred onto Matrigel-coated plates for further expansion.

Characterization of murine iPSCs

The pluripotency potential of iPSCs was determined by immunohistochemical staining for markers of the three germ layers following embryoid body (EB) formation (Burridge et al. 2007). At day 30, differentiated EBs were fixed with 4% paraformaldehyde for 15 minutes, permeabilized with 0.2% Triton X-100 in phosphate-buffered saline (PBS) for 30 minutes, and blocked with 1% bovine serum albumin (BSA) in PBS for 1 hour. The cells were then incubated with primary antibodies specific for markers representing the three germ layers: β-III-tubulin (TUJ-1) for ectoderm, SOX17 for endoderm, and smooth muscle actin (SMA) for mesoderm (Abcam, Cambridge, MA, USA). In addition, RT-PCR was performed on RNA isolated from fibroblasts, iPSCs, and EBs to evaluate the expression of genes specific to the three germ layers. TaqMan primers (Life Technologies) for ectoderm (Gbx, TJF), endoderm (α- fetoprotein [AFP], Foxa2), and mesoderm (GATA4, GATA6, MLC, Nkx) were used in this study, with 18s used as the endogenous control (Supplemental Table 1). Karyotype

analyses of passage 15 tail tip fibroblast-derived iPSCs were performed at the Cytogenetics Laboratory in the Department of Pathology at Stanford Hospital and Clinics. Cells were treated with 0.1 mg/mL colcemid for induction of mitotic arrest and were subsequently harvested by trypsin dispersal, hypotonic shock, and fixation with 3:1 methanol:acetic acid. For each cell line, 20 metaphases were analyzed by the standard G-banding method.

In vitro monolayer endothelial differentiation of murine iPSCs

To induce endothelial differentiation, approximately $1x10^5$ undifferentiated iPSCs were seeded in each well of Matrigel-coated 6-well plates and cultured in differentiation medium containing RPMI and B-27 supplement minus insulin (Life Technologies) with 5 μM CHIR-99021 (a glycogen synthase kinase [GSK]-3 inhibitor; Selleck Chemicals, Houston, TX, USA) for 2 days, followed by RPMI and B-27 supplement minus insulin with 2 μM CHIR-99021 for 2 additional days. The medium was then changed to RPMI and B-27 supplement minus insulin with 50 ng/mL vascular endothelial growth factor (VEGF; R&D Systems, Minneapolis, MN, USA), 10 ng/mL fibroblast growth factor basic (FGFb; R&D Systems), and 10 μM Y-27632 (a rho-associated protein kinase [ROCK] inhibitor; Sigma-Aldrich, Saint Louis, MO, USA) for 3 days. For the subsequent 7 days, the medium was changed to RPMI and B-27 supplement (with insulin) with 50 ng/mL VEGF, 10 ng/mL FGFb, 10 μM Y-27632, and 1 μM SB 431542 (a transforming growth factor [TGF]-β inhibitor; Sigma-Aldrich). At day 14, iPSC-ECs were sorted for $CD31^+/CD144^+$ markers using FACS and expanded on 0.2% gelatin coated plates. After sorting, iPSC-ECs were cultured in EBM-2 Basal Medium supplemented with the EGM-2 BulletKit (Lonza, Basel, Switzerland) at 37°C, 20% O2, and 5% CO2 in a humidified incubator with medium changes every 48 hours, and cells were passaged once they reached 80-90% confluence. Murine iPSC- ECs used for in vitro and in vivo characterizations were between passages 3 and 5.

Immunofluorescence staining of cultured murine iPSCs and iPSC-ECs

Cells were fixed with 4% paraformaldehyde for 15 minutes, permeabilized with 0.2% Triton X-100 in PBS for 30 minutes, and blocked with 1% BSA in PBS for 1 hour. Cells were then stained with appropriate primary antibodies and AlexaFluor-conjugated secondary antibodies (Life Technologies) and co-stained with DAPI (Vector Laboratories, Burlingame, CA, USA). The primary antibodies for SSEA-1 (EMD Millipore), Oct3/4 (Santa Cruz Biotechnology, Santa Cruz, CA, USA), Sox2 (BioLegend, San Diego, CA, USA), c-Myc (Abcam), CD31 (Life Technologies), and CD144 (BD Biosciences) were used in the staining. Murine iPSC-ECs were also incubated with 10 μg/mL DiI-Ac-LDL (Life Technologies) at 37°C for 6 hours. After washing twice with PBS, DiI- Ac-LDL uptake was detected with fluorescence microscopy as previously described (Voyta et al. 1984). Imaging was performed on a Zeiss LSM510 Meta inverted confocal microscope and processed with ZEN microscope software

(Carl Zeiss, Oberkochen, Germany) at the Stanford University Neuroscience Microscopy Service facility.

Biological characterization of murine iPSC-ECs

To determine the characteristics of aortic-ECs and iPSC-ECs in vitro, the formation of cord-like structures was assessed by seeding cells in 24-well plates coated with Matrigel and incubating them at 37°C for 24 hours as previously described (Yamashita et al. 2000). Cell proliferation was measured using the BrdU Cell Proliferation Assay Kit according to the manufacturer's protocol (Cell Signaling Technology, Danvers, MA, USA). EC adhesion and migration/wound-healing were determined using assays as previously described (Liang et al. 2007, Reinhart-King 2008). Wound-healing assay images were quantified using ImageJ (National Institutes of Health, Bethesda, MD, USA). In vitro apoptosis analysis was performed in a hypoxia chamber to mimic ischemic conditions, and measured via terminal deoxynucleotidyl transferase dUTP nick end labeling (TUNEL) using the Fluorescein In Situ Cell Death Detection Kit (Roche Applied Science, Penzberg, Germany) according to the manufacturer's protocol. Measurement of cell culture supernatant nitrite levels was determined using a Griess Reagent System according to the manufacturer's protocol (Promega, Madison, WI, USA). Enzyme-linked immunosorbent assay (ELISA) was performed on control and DIO iPSC-ECs cultured under hypoxic conditions for 24 hours using a Mouse Inflammatory Cytokines Multi-Analyte ELISArray Kit (Qiagen, Valencia, CA, USA) following the manufacturer's instructions. For pravastatin treatment, the dose was determined by adding pravastatin daily into the cell culture medium at 0.1, 1, and 10μM concentrations. No effect was seen using the 0.1 μM concentration, while cell death occurred at the 10μM concentration. The most significant effects were observed using 1μM pravastatin. Therefore, for all in vitro experiments in this study, pravastatin was used at this dose.

Surgical model for hindlimb ischaemia and cell delivery

The surgical procedure for the induction of unilateral hindlimb ischaemia was performed following a previously published protocol (Limbourg et al. 2009). Briefly, mice were anesthetized in an induction chamber containing 1–2% isoflurane (Baxter HealthCare, Deerfield, IL, USA) in 100% oxygen at a flow rate of 1 L/min. Ischaemia was induced by two separate ligations of the femoral artery, one distal and one proximal to the origin of the deep femoral branch. Subsequently, the skin was closed using 5-0 Vicryl sutures. Following the operation, animals were randomized into seven groups (n = 10 per group) and each was administered a single gastrocnemius intramuscular (IM) injection containing: (i) 50 μL of 1 : 1 Matrigel/EBM2 (vehicle), (ii) vehicle plus intraperitoneal (IP) pravastatin co-administration daily, (iii) 1×10^6 pooled iPSC-ECs from control donors in 50 μL of 1 : 1 Matrigel/EBM2, (iv) 1×10^6 pooled iPSC-ECs from DIO donors in 50 μL of 1 : 1 Matrigel/EBM2, (v) a single injection of 1×10^6 pooled iPSC-ECs fromDIOdonors plus co-administration of pravastatin

(20 mg/kg body weight; injected volume, 0.02 mL/g body weight, IP), (vi) a single injection of 1×10^6 pooled iPSC-ECs from DIO donors pre-incubated with 1 mM pravastatin for 7 days, and (vii) a single injection of 1×10^6 pooled iPSC-ECs from DIO donors plus co-administration of pravastatin and NO synthase inhibitor N^w-nitro-L-arginine methyl ester (L-NAME) daily. Prior to cell injection, iPSC-ECs were labelled with Cell- Tracker CM-DiI cell-labelling solution (Life Technologies) according to themanufacturer's instructions sothat the injected cells couldbe visualized post-mortem (Weir et al. 2008). To inhibit NO synthesis, L-NAME was administered in the drinking water at a concentration of 1 mg/mL during days 1 through 14 post cell delivery. Laser Doppler imaging (LDI) was performed on Days 0, 3, 7, 10, and 14 following cell injection.

Determination of the SDS-resistant eNOS dimers and monomers

SDS-resistant eNOS dimers and monomers were assayed using low-temperature NuPAGE® Novex® 3-8% Tris-Acetate Protein Gels as described previously (Leber et al. 1999, Zou et al. 2002), but with modifications. After treatment, samples were harvested and added to NuPAGE® LDS Sample Buffer (4X) directly without boiling. Samples were subjected to SDS-PAGE on 3-8% gels, and the whole western blot system were kept in ice bath at 4°C throughout the running and transfer procedures. After transfer, PVDF membranes were incubated with first antibodies against Phospho-Akt (Ser473) (1:1000, cell signaling #9271), Akt (1:1000, cell signaling #9272), eNOS (1:1000; cell signaling #9586), Phospho-eNOS (Ser1177) (1:1000, cell signaling #9571), Phospho-eNOS (Thr495) (1:1000, cell signaling #9574) in 5% fat-free milk overnight at 4°C. The blot was further incubated with a second horseradish peroxidase conjugated antibody against rabbit IgG (1:3000, life technology # G-21234) for 45 minutes at room temperature. The protein bands were visualized using the ECL Chemiluminescent Substrate Reagent Kit according to the manufacturer's instructions. The intensity (area times density) of the individual bands was quantitated by densitometry (GS-700 Imaging Densitometer; Bio-Rad Laboratories Inc.). Background was subtracted from the calculated area.

Microarray hybridization, data acquisition, and analysis

Microarray hybridization and data acquisition were performed at the Stanford Protein and Nucleic Acid Facility. Total RNA was isolated from biological duplicates of control and DIO iPSC-ECs using the RNeasy Mini Plus Kit (Qiagen). From the RNA samples, cDNA was reverse transcribed, and cRNA was then transcribed and hybridized to GeneChip Mouse Genome 430 2.0 microarrays (Affymetrix, Santa Clara, CA, USA) and processed according to the manufacturer's instructions. The array was scanned using an Affymetrix GeneChip Scanner 3000 7G, and data were normalized and annotated using Affymetrix Expression Console software. Gene expression intensity was generated from raw files and normalized by Robust Multi-array Average (RMA) using Partek Genomics Suite (Partek, Saint Louis,

MO, USA). One-way ANOVA P-value (<0.05) and fold- change (>1.5) was applied to select the significant differentially expressed genes. Canonical pathway analysis in Ingenuity Pathway Analysis software (Ingenuity Systems, Redwood City, CA, USA) was used to perform the gene pathway enrichment. TM4 Microarray Software Suite (Dana-Farber Cancer Institute, Boston, MA, USA) was used for hierarchical clustering and generating heat maps for significant differentially expressed genes and pathways.

Quantitative reverse-transcription polymerase chain reaction (qRT-PCR)

qRT-PCR of iPSC-ECs was performed using RT^2 Profiler Murine Apoptosis and Oxidative Stress Arrays and RT^2 SYBR Green/ROX qPCR Master Mix (Qiagen) on an ABI StepOnePlus Real-Time PCR System (Applied Biosystems) using biological triplicates. For data analysis, the ΔΔCt method was used and fold-change was calculated for each gene (DIO versus control group).

Histology and immunofluorescence staining

Two weeks following induction of hindlimb ischemia, mice were euthanized, hindlimbs snap frozen in O.C.T. compound (Sakura Finetek, Tokyo, Japan) and cryosectioned for histological and immunofluorescence assessment. Samples were sectioned longitudinally at a thickness of 5μm. Representative tissue sections were processed for routine hematoxylin and eosin (H&E) staining and reviewed by a pathologist blinded to the study groups. Incorporation of exogenous cells into the microvasculature of the ischemic tissue was assessed using immunofluorescence for CM-DiI (Life Technologies). For capillary density, sections were stained with a FITC-conjugated primary antibody specific for CD31 (BD Biosciences) and co-stained with DAPI (Vector Laboratories). At least 5 tissue sections were analyzed for each animal, with 5 high-powered images taken for each tissue section using a Leica DM IL LED inverted microscope equipped with a Leica DFC500 digital camera and processed with Leica LAS EZ software (Leica Microsystems, Buffalo Grove, IL, USA) and Image J software (NIH, Bethesda, MD, USA).

Statistical analysis

Statistics were calculated using GraphPad Prism (GraphPad Software, La Jolla, CA, USA). In vitro data were obtained from at least three independent experiments. Statistical significance between two groups was determined by paired or unpaired Student's t-test. For simple comparison between groups, one-way ANOVA was applied if the data were normally distributed, otherwise nonparametric Kruskal–Wallis test was used. For drug treatment experiments, two-way ANOVA followed by Bonferroni or Tukey's post hoc tests were applied. P-values were considered statistically significant if $P<0.05$ and all actual P-value are shown in the figures. All data are expressed as mean+SD.

RESULTS

Reprogramming of fibroblasts from control and diet-induced obesity mice into induced pluripotent stem cells

A previously published study has demonstrated that iPSCs can be generated from individuals with type 1 diabetes (Maehr et al. 2009). However, this study did not report the reprogramming efficiency of these cells. Hence, to test whether there is an inherent difference in the capacity of fibroblasts from control and DIO mice to be reprogrammed into iPSCs, tail tip fibroblasts were isolated from 24-week-old C57Bl/6 mice fed either a normal (10 kcal% from fat) or high-fat (60 kcal% from fat) diet beginning at 6 weeks of age. At 24 weeks of age, high-fat DIO mice had significantly increased body weight ($P = 0.001$), fasting glucose ($P = 0.016$), and showed a significant decrease in glucose and insulin tolerance compared to control mice ($P < 0.0001$; Supplementary material, Figure S1A–D). Next, we successfully reprogrammed tail tip fibroblasts into murine iPSCs using a codon optimized 4-in-1 lentiviral vector encoding Oct-4, Klf4, Sox2, and c-Myc. On Day 15 after reprogramming, we mechanically dissociated the individual iPSC colonies and transferred them onto irradiated MEF feeder layers for clonal expansion into multiple cell lines (3 lines/mouse, 5 mice/group) (Figure 1A). All murine iPSC colonies stained positive for alkaline phosphatase, as well as pluripotency markers SSEA-1, Oct4, Sox2, and c-Myc (Figure 1B–D). Interestingly, reprogramming efficiency was significantly lower in iPSCs derived from DIO mice compared with those derived from control mice ($P = 0.003$; Figure 1E). Immunohistochemistry and real-time polymerase chain reaction (RT-PCR) confirmed that the established iPSC lines were able to form cells derived from all three germ layers in vitro, expressed markers specific for endoderm, ectoderm, and mesoderm (Supplementary material, Figure S2A and B and Table S1), and also maintained a normal karyotype after extended passage (Supplementary material, Figure S3A and B).

Control and diet-induced obesity induced pluripotent stem cells can be successfully differentiated into induced pluripotent stem cell-derived endothelial cells

Next, we successfully differentiated iPSCs (at passage 15) from control and DIO mice into iPSC-ECs via a chemically defined monolayer differentiation protocol (Figure 2A). On Day 10 after induction of differentiation, iPSC-ECs were stained using antibodies against CD31 and CD144 and subsequently sorted by FACS. Double positive ($CD31^+/CD144^+$) cells were then plated on 0.2% gelatin coated plates for further expansion and characterization. Isolated iPSC-ECs showed Dil-Ac-LDL uptake and stained positive for endothelial markers CD31 and CD144 (Figure 2B). Flow cytometry showed no significant difference in EC differentiation capacity between iPSCs generated from DIO mice or healthy mice (18.80+1.51% vs. 20.47+1.75%, respectively; $P = 0.28$) (Supplementary material, Figure S4).

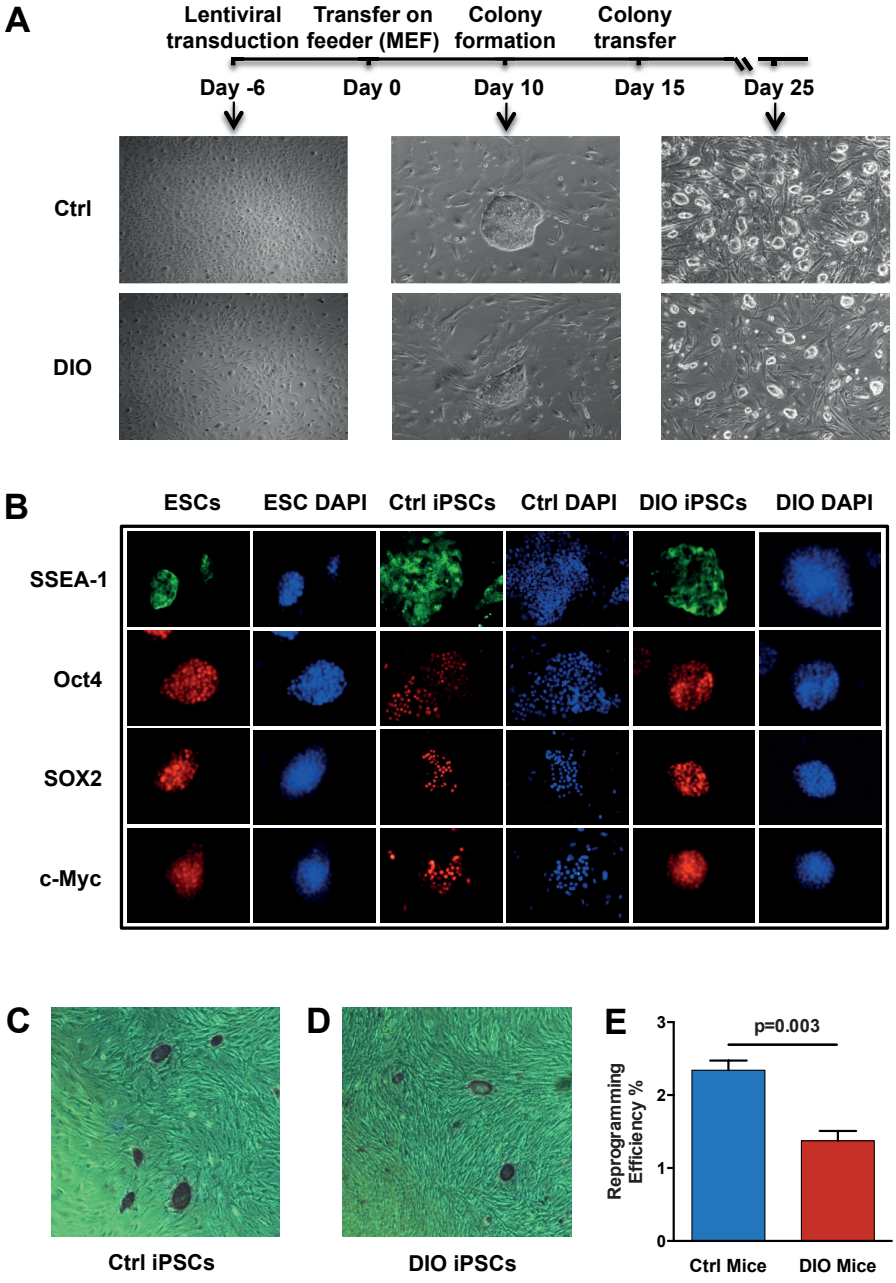


Figure 1. Generation and characterization of induced pluripotent stem cells. (A) Representative timeline of murine induced pluripotent stem cell generation. (B) Immunofluorescence of pluripotency markers SSEA-1, Oct4, Sox2, and c-Myc in mouse induced pluripotent stem cells. Mouse embryonic stem cells were used as positive control. (C–E) All murine induced pluripotent stem cell colonies stained positive for alkaline phosphatase. Reprogramming efficiency was significantly lower in induced pluripotent stem cells derived from diet-induced obesity tail tip fibroblasts compared with those derived from control mice (n = 5/group, P = 0.003).

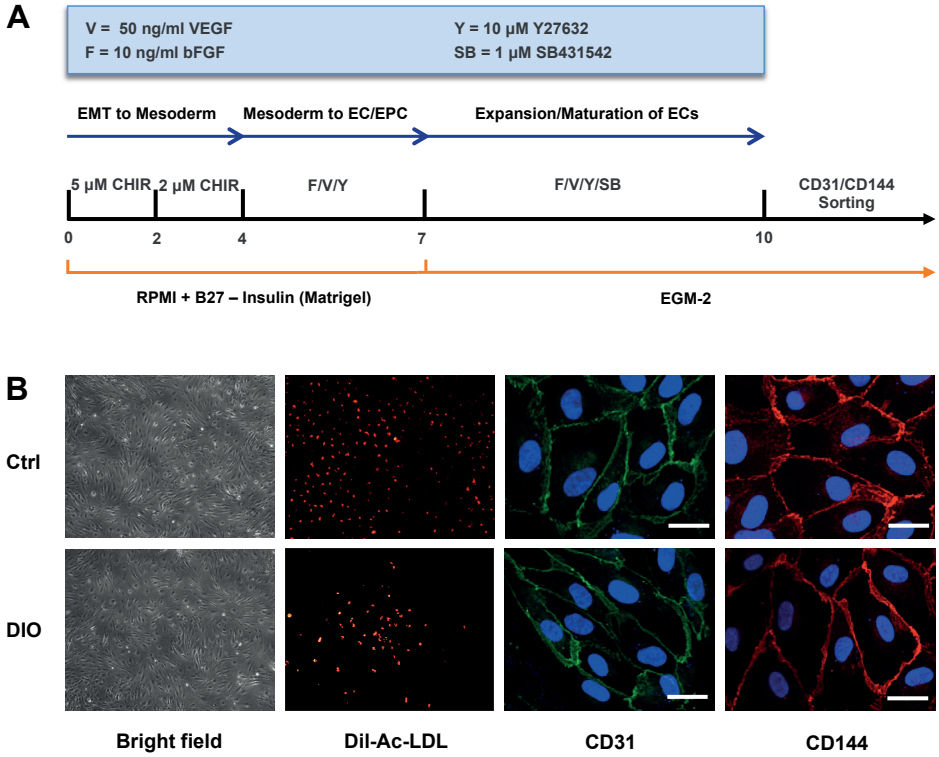


Figure 2. Differentiation of induced pluripotent stem cells into induced pluripotent stem cell-derived endothelial cells. (A) An outline of the protocol used for the differentiation of murine induced pluripotent stem cells to induced pluripotent stem cell-derived endothelial cells. At Day 14, induced pluripotent stem cell-derived endothelial cells were stained for CD31 and CD144, and double-positive ($CD31^+/CD144^+$) cells were expanded on 0.2% gelatin-coated plates in EGM-2 medium. (B) Representative brightfield images and positive immunofluorescence of differentiated induced pluripotent stem cell-derived endothelial cells for CD31 and CD144 at 63×. Differentiated induced pluripotent stem cell-derived endothelial cells also exhibited DiI-Ac-LDL uptake.

Diet-induced obesity induced pluripotent stem cell-derived endothelial cells exhibit endothelial dysfunction phenotype in vitro

Endothelial cells isolated from obese individuals have been shown to demonstrate properties of endothelial dysfunction in vitro (Caballero 2003). Similarly, we found cell migration and proliferation were significantly reduced among both aortic-ECs (data not shown) and iPSC-ECs from DIO mice compared with aortic-ECs and iPSC-ECs from control mice ($P < 0.05$; Figure 3A, B and E). Additionally, iPSC-ECs from DIO but not control mice showed a significant increase in apoptosis when cultured in a hypoxic environment ($P = 0.007$; Figure 3C and D). iPSC-ECs from DIO mice had significantly reduced capacity to form cord-like structures on Matrigel compared with control cells after 24 h ($P < 0.001$; Figure 3F). Incubation of iPSC-ECs from DIO mice with 1μM pravastatin for 24 h resulted in significant increases in cell migration ($P < 0.001$), proliferation ($P = 0.003$), and number of cord-like

structures on Matrigel ($P < 0.001$), and significant decrease in apoptosis ($P = 0.019$). Finally, DIO iPSC-ECs had significantly lower levels of NO production compared with control iPSC-ECs ($P = 0.019$); incubation of DIO iPSC-ECs with 1μM pravastatin for 24 h resulted in significantly higher levels of NO ($P = 0.016$). However, the effect of pravastatin in DIO iPSC-ECs was blocked by co-incubation with the NO synthase inhibitor L-NAME ($P = 0.001$) (Figure 3G). Interestingly, incubation of DIO iPSC-ECs with other statins including rosuvastatin (R-statin) and atorvastatin (A-statin) resulted in much less functional recovery compared with pravastatin (P-statin) (Supplementary material, Figure S5), which might be due to their different pharmacokinetic properties (Hamelin and Turgeon 1998).

Activation of Akt-endothelial nitric oxide synthase signalling pathway is suppressed in diet-induced obesity induced pluripotent stem cell-derived endothelial cells

As shown in Figure 3G, a hallmark of DIO iPSC-EC dysfunction was reduced NO production, which could be caused by reduced expression of endothelial or cytokine-inducible forms of NO synthase (eNOS and iNOS), impairment of eNOS activation, and/or increased eNOS uncoupling (Guzik 2002, Sansbury et al. 2012). Previous studies have shown that statins can rapidly promote the activation of Akt in endothelial cells leading to eNOS phosphorylation and increased NO production (Kureishi et al. 2000). To address our hypothesis that Akt and eNOS activation by statins was involved in improvement of DIO iPSC-EC function, we assessed eNOS and iNOS gene expressions as well as protein levels in control iPSC-ECs, DIO iPSC-ECs, and DIO iPSC-ECs with pravastatin preincubation. We found that DIO iPSC-ECs had significantly lower eNOS expression compared with control iPSC-ECs, which was reversed by pravastatin treatment for 24 h (Supplementary material, Figure S6A and B). Compared with eNOS expression, iNOS gene expression and protein levels were much lower in both control and DIO iPSC-ECs, suggesting a less important role in regulation of endothelial function (Supplementary material, Figure S7). We next assessed the modulation of Akt phosphorylation, eNOS phosphorylation, and eNOS coupling status by western blot analysis. A previous study showed that PKC signalling in endothelial cells inhibits eNOS activity by phosphorylating Thr-495 and dephosphorylating Ser-1177, whereas PKA signalling acts in reverse by increasing phosphorylation of Ser-1177 and dephosphorylation of Thr-495 to activate eNOS (Michell 2001). We found that iPSC-ECs from DIO mice showed significantly decreased phospho-Akt and phosphorylation of eNOS at the Ser1177 residue, which was reversed by pravastatin treatment. In contrast, the phosphorylation of eNOS at the Thr495 residue in DIO iPSC-ECs was significantly increased compared with control iPSC-ECs, indicating the deactivation of eNOS is associated with DIO (Supplementary material, Figure S6A, C–E). Finally, the percentage of the dimer-to-monomer ratio, an indicator of eNOS uncoupling which could lead to reduction of enzymatic activity (Rodríguez-Crespo et al. 1997, Zou et al. 2002), also showed a significant

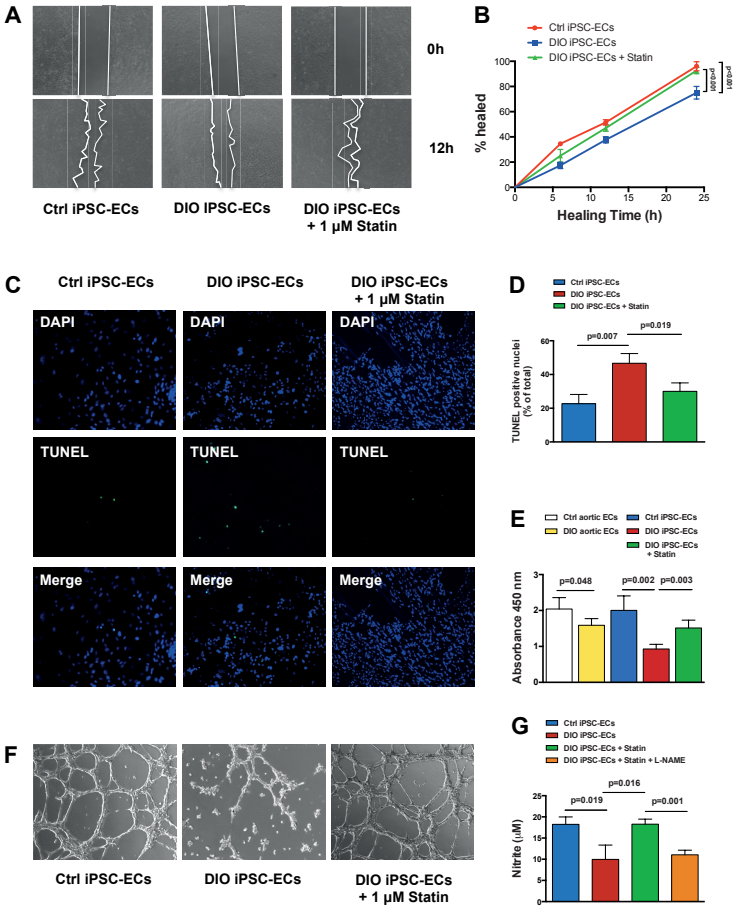


Figure 3. Characterization of induced pluripotent stem cell-derived endothelial cells in vitro. (A and B) Induced pluripotent stem cell-derived endothelial cells from diet-induced obesity mice demonstrated significant reduction in cell migration ($P < 0.001$). (C and D) TUNEL staining of diet-induced obesity induced pluripotent stem cell-derived endothelial cells demonstrated significant increase in apoptosis compared with control induced pluripotent stem cell-derived endothelial cells when cultured in hypoxic conditions ($P = 0.007$). (E) Both aortic-endothelial cells and induced pluripotent stem cell-derived endothelial cells from diet-induced obesity mice showed significant decrease in cell proliferation compared with control mice ($P = 0.048$ in aortic endothelial cells; $P = 0.002$ in induced pluripotent stem cell-derived endothelial cells). (F) Diet-induced obesity induced pluripotent stem cell-derived endothelial cells also demonstrated a reduced capacity to form cord-like network on Matrigel after 24 h compared with control induced pluripotent stem cell-derived endothelial cells ($P < 0.001$). The addition of 1 μM pravastatin to diet-induced obesity induced pluripotent stem cell-derived endothelial cells for 24 h resulted in significant increases in cell migration ($P < 0.001$), proliferation ($P = 0.003$), and the number of cord-like structures ($P < 0.001$), while significantly decreasing endothelial cell apoptosis ($P = 0.019$). (G) Measurement of nitrite levels in cell culture supernatant by Griess reaction demonstrated that diet-induced obesity induced pluripotent stem cell-derived endothelial cells had significantly lower levels of nitric oxide production compared with control induced pluripotent stem cell-derived endothelial cells ($P = 0.019$). Incubation of diet-induced obesity induced pluripotent stem cell-derived endothelial cells with 1 μM pravastatin for 24 h resulted in significantly higher levels of nitric oxide ($P = 0.016$). The effect of pravastatin on nitrite levels in diet-induced obesity induced pluripotent stem cell-derived endothelial cell was blocked by co-incubation with N^{ω}-nitro-l-arginine methyl ester ($P = 0.001$).

decrease in DIO iPSC-ECs, and was increased by pravastatin treatment (Supplementary material, Figure S6A, F).

Elevated apoptotic, inflammatory, and oxidative stress pathways in diet-induced obesity induced pluripotent stem cell-derived endothelial cells

Previous studies have shown endothelial dysfunction in patients with obesity is in part related to increased levels of oxidative stress, inflammation, cell apoptosis, and decreased NO production (Bruyndonckx et al. 2013). In order to investigate the mechanisms underlying the in vitro functional differences observed between DIO iPSC-ECs and control iPSC-ECs, we next performed microarray analysis. Our results indicate that 472 genes were differentially regulated in pathways related to apoptosis, inflammation, oxidative stress, and cellular senescence (Figure 4A; Supplementary material, Figure S8). We performed RT-PCR on a panel of genes involved in apoptosis and oxidative stress in control iPSC-ECs, DIO iPSC-ECs, and DIO iPSC-ECs after 1μM pravastatin treatment for 24 h. Of the genes investigated in these panels, 33 were significantly up-regulated (>three-fold) in DIO iPSC-ECs when compared with control iPSC-ECs (Figure 4B; Supplementary material, Table S2A and B). After pravastatin treatment, 28 apoptotic and oxidative genes were down-regulated in DIO iPSC-ECs. We next performed ELISA assays to determine levels of pro- and anti-inflammatory cytokines in cell culture supernatants following hypoxia for 24 h to mimic an ischaemic environment. Compared with control iPSC-ECs, DIO iPSC-ECs had significantly higher levels of inflammatory cytokines, including IL-1α, IL-1β, IL-4, IFN-γ, and TNF-α. Similarly, incubation of DIO iPSC-ECs with 1μM pravastatin for 24 h resulted in significant decreases in the pro-inflammatory cytokines IL-1α, IL-1β, IL-4, and TNF-α, as well as significant increases in the anti-inflammatory cytokines IL-6, IL-10, and IL 17A (Supplementary material, Figure S9).

Dysfunction of diet-induced obesity induced pluripotent stem cell-derived endothelial cells in a hindlimb ischaemia model is reversed by pravastatin co-administration

Several groups have demonstrated that healthy iPSC-ECs are effective in promoting angiogenesis and neovascularization in a hindlimb ischaemia model (Huang et al. 2010, Lai et al. 2013). However, it is unknown if DIO iPSC-ECs will also function properly in vivo. To characterize the functional differences between iPSC-ECs from control and DIO mice, we next induced hindlimb ischaemia and used LDI to quantify perfusion. Mice were randomized into seven groups (n = 10 per group) and each was administered a single gastrocnemius IM injection of a different treatment regimen (see Supplementary material). Beginning at Day 7 post-surgery, mice injected with control iPSC-ECs showed a significant increase in hindlimb reperfusion compared with mice injected with vehicle (0.38±0.04 vs. 0.61±0.04, vehicle vs. Ctrl iPSC-ECs, $P < 0.001$) or pravastatin only (0.45±0.06 vs. 0.61±0.04, vehicle

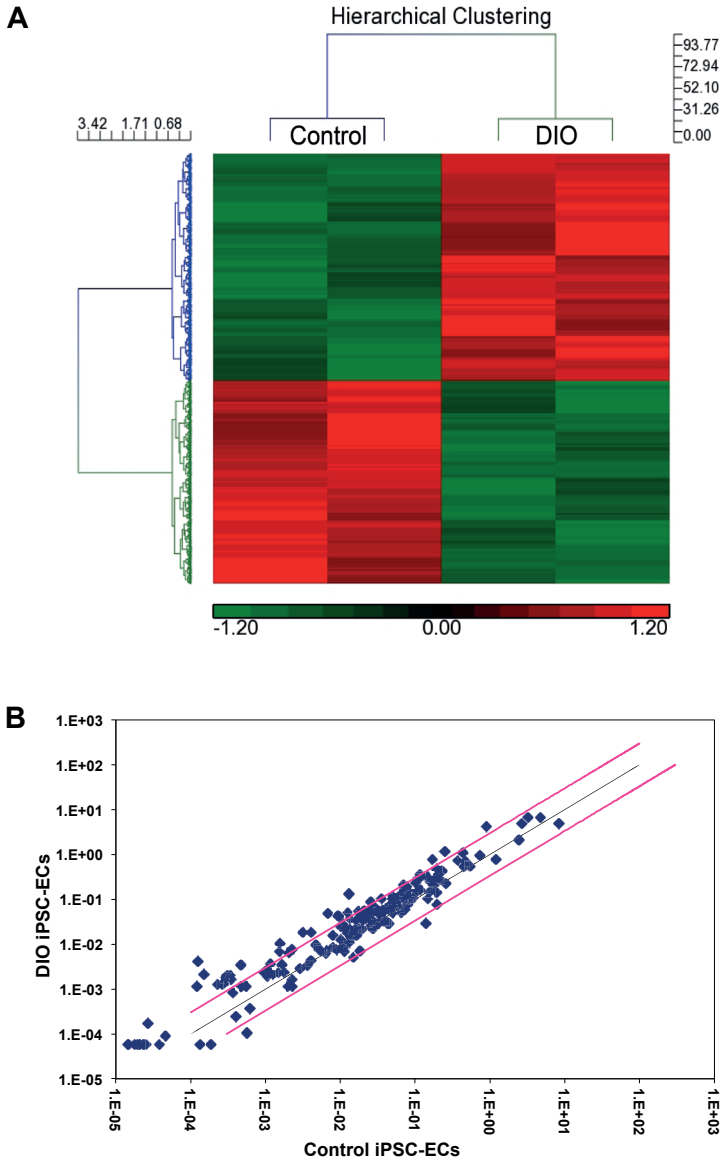


Figure 4. Microarray and RT-PCR gene expression profiling of induced pluripotent stem cell-derived endothelial cells from control and diet-induced obesity mice. (A) Heat map of the 472 significantly differentially regulated genes between diet-induced obesity induced pluripotent stem cell-derived endothelial cells and control induced pluripotent stem cell-derived endothelial cells. Enriched pathway analysis identified the involvement of biological pathways including metabolism, cell cycle, immune function, inflammation, cell adhesion, oxidative stress, senescence, and apoptosis. (B) RT-PCR for a panel of genes involved in apoptosis and cellular oxidative demonstrated a significant increase in many of these genes in diet-induced obesity induced pluripotent stem cell-derived endothelial cells compared with control induced pluripotent stem cell-derived endothelial cells (n = 5/group). Data expressed as fold-change with the black line indicating a one-fold-change and pink line indicating a three-fold change.

+ statin vs. Ctrl iPSC-ECs, P = 0.001) (Figure 5A and B). However, animals injected with DIO iPSC-ECs achieved significantly less hindlimb reperfusion compared with animals injected with control iPSC-ECs (0.61±0.04 vs. 0.46±0.06, Ctrl iPSC-ECs vs. DIO iPSC-ECs, P = 0.002). In addition, mice randomized to receive DIO iPSC-ECs combined with daily IP administration of pravastatin (beginning at Day 7) and mice randomized to receive DIO iPSC-ECs pre-incubated with pravastatin (beginning at Day 10) both had significantly higher levels of hindlimb reperfusion compared with mice that received DIO iPSC-ECs alone (Day 7: 0.62±0.02 vs. 0.46±0.06, DIO iPSC-ECs + IP statin vs. DIO iPSC-ECs, P < 0.001; Day 10: 0.66±0.04 vs. 0.53±0.02, DIO iPSC-ECs + prestatin vs.DIO iPSC-ECs, P = 0.004), and the level of perfusion was similar to that of mice receiving control iPSC-ECs. When mice that received DIO iPSC-ECs plus daily pravastatin also received the NO synthase inhibitor L-NAME in their drinking water, the increases in hindlimb reperfusion were significantly blunted from Day 7 onwards (0.62±0.02 vs. 0.54±0.09, DIO iPSC-ECs + IP statin vs. DIO iPSC-ECs + statin + L-NAME, P = 0.004), suggesting that the effect of pravastatin was via an NO-dependent pathway. Finally, we found that starting at Day 7, mice that received DIO iPSC-ECs combined with pravastatin treatment (either systemic treatment or pre-incubation) showed better hindlimb reperfusion than mice receiving pravastatin alone (0.45±0.06 vs. 0.62±0.02, vehicle + statin vs. DIO iPSC-ECs + IP statin, P < 0.001; 0.45±0.06 vs. 0.57±0.03, vehicle + statin vs. DIO iPSC-ECs + pre statin, P = 0.019), confirming the necessity of co-administration of pravastatin with DIO iPSC-ECs.

Histological evaluation of ischaemic hindlimbs confirms an apoptotic and inflammatory phenotype

We next performed histological evaluation of the ischaemic hindlimbs on Day 14 following cell injections. Hematoxylin & eosin (H&E) stained sections of hindlimbs from mice injected with DIO iPSC-ECs showed evidence of muscle atrophy and degeneration, as well as infiltration of inflammatory cells. In contrast, animals injected with control iPSC-ECs or DIO iPSC-ECs plus daily IP injections of pravastatin were protected from this damage. Animals injected with pre-treated DIO iPSC-ECs also showed reduced infiltration of neutrophils; however, the difference between DIO iPSC-ECs and DIO iPSC-ECs pre-treated with pravastatin did not reach statistical significance (P = 0.112) (Figure 6A and C). Immunostaining revealed that $CD31^+$ capillary density was significantly lower in the hindlimbs of mice injected with DIO iPSC-ECs compared with control iPSC-ECs (P = 0.006) (Figure 6B and D). Increased $CD31^+$ capillary density was observed in mice injected with DIO iPSC-ECs plus daily IP injections of pravastatin compared with mice injected with DIO iPSC-ECs alone (P = 0.047). Co-administration of the NO synthase inhibitor L-NAME with pravastatin blocked this effect (P = 0.001). Moreover, there was a trend showing that injection of DIO iPSC-ECs pre-treated with pravastatin for 7 days could also increase the capillary density compared with injection of untreated DIO iPSC-ECs; however, this did not

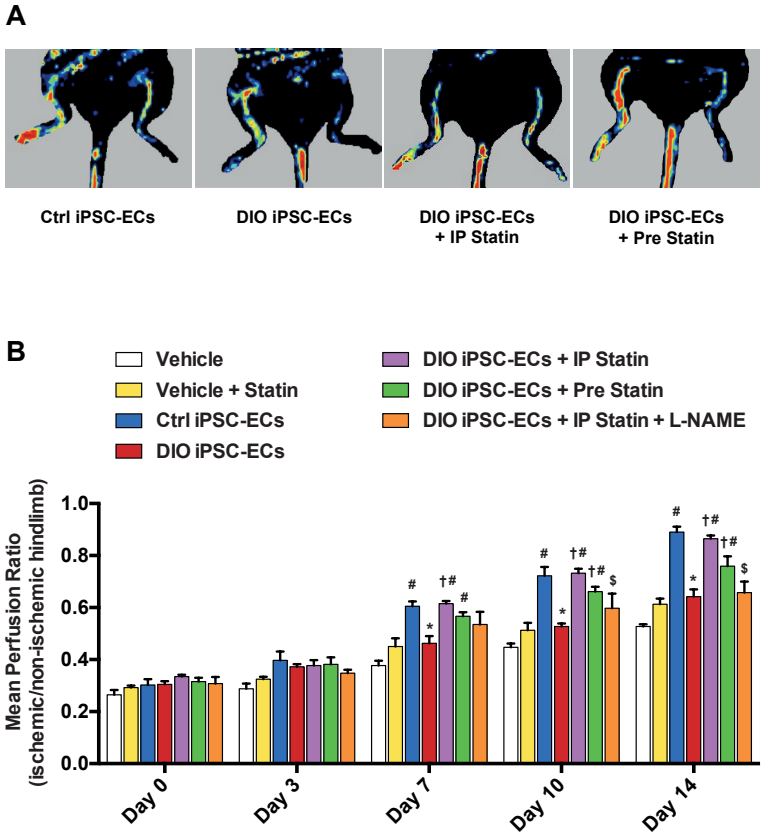


Figure 5. Laser Doppler imaging of ischaemic hindlimbs following intramuscular injection with vehicle, control induced pluripotent stem cell-derived endothelial cells, diet-induced obesity induced pluripotent stem cell-derived endothelial cells, and diet-induced obesity induced pluripotent stem cell-derived endothelial cells with treatments. (A) Graphic representation and (B) quantification by laser Doppler imaging show a significant increase in perfusion in the affected hindlimbs of mice injected with 1×10^6 control induced pluripotent stem cell-derived endothelial cells compared with vehicle alone and vehicle plus statin beginning at Day 7 post-injection ($P < 0.001$ vehicle vs. Ctrl induced pluripotent stem cell-derived endothelial cells; $P = 0.001$ vehicle + statin vs. Ctrl induced pluripotent stem cell-derived endothelial cells). Mice injected with 1×10^6 diet-induced obesity induced pluripotent stem cell-derived endothelial cells had a significant reduction in hindlimb perfusion compared with mice injected with control induced pluripotent stem cell-derived endothelial cells beginning at Day 7 post-injection ($P = 0.002$). Co-administration of pravastatin 20 mg/kg via daily intraperitoneal injections resulted in a significant increase in hindlimb reperfusion in mice that received diet-induced obesity induced pluripotent stem cell-derived endothelial cells starting from Day 7 ($P < 0.001$), while co-administration of N^{ω}-nitro-l-arginine methyl ester in these mice blocked this effect ($P = 0.004$). Injection with diet-induced obesity induced pluripotent stem cell-derived endothelial cells pre-treated with pravastatin in vitro also resulted in a significant increase in hindlimb reperfusion compared with injection of untreated diet-induced obesity induced pluripotent stem cell-derived endothelial cells starting from Day 10 ($P = 0.004$). n = 10/group, '†' vs. diet-induced obesity induced pluripotent stem cell-derived endothelial cells, "#" vs. vehicle + statin, "*" vs. control induced pluripotent stem cell-derived endothelial cells, "$" vs. diet-induced obesity induced pluripotent stem cell-derived endothelial cells + intraperitoneal statin

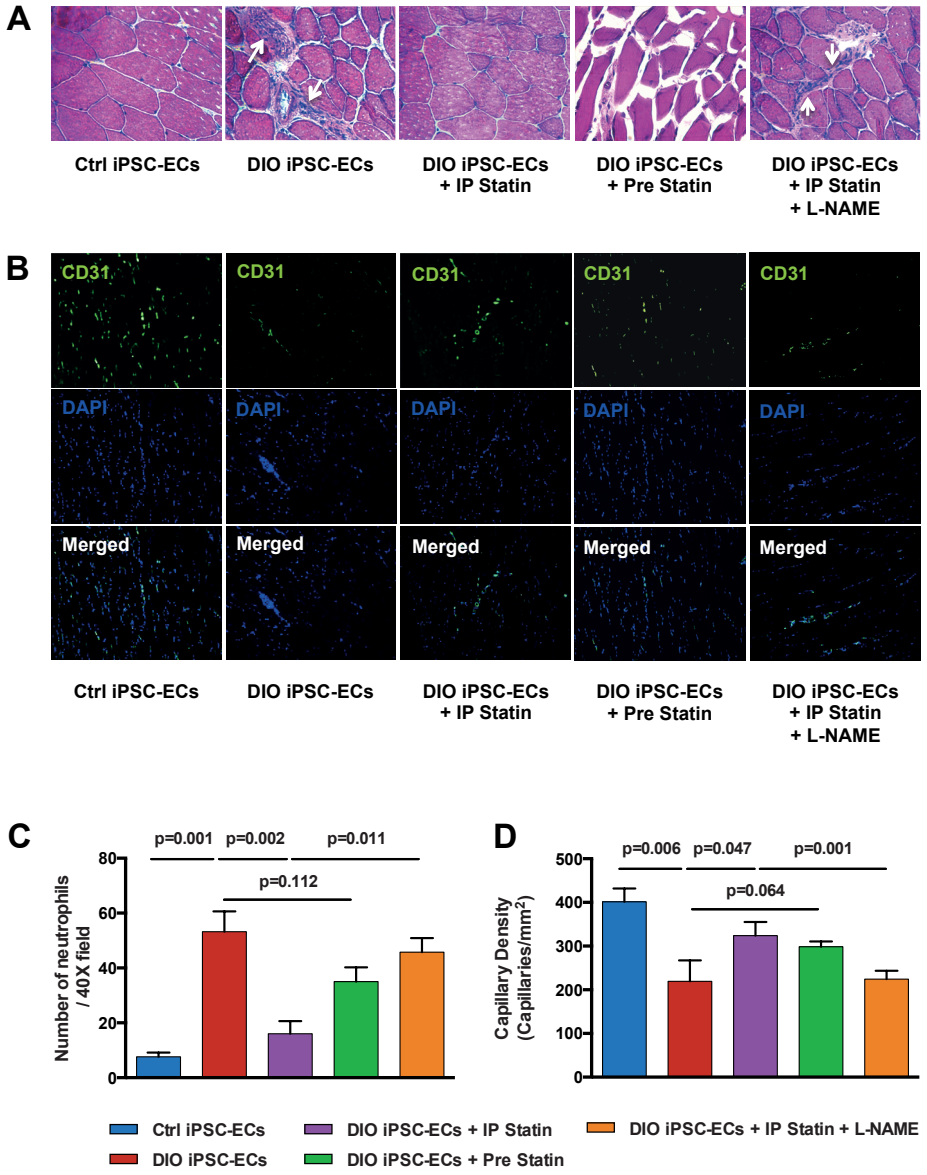


Figure 6. Histological evaluation of transplanted induced pluripotent stem cell-derived endothelial cells in the ischaemic hindlimb at Day 14.

Figure 6. Histological evaluation of transplanted induced pluripotent stem cell-derived endothelial cells in the ischaemic hindlimb at Day 14.
(A) H&E staining revealed evidence of muscle degeneration and inflammatory cell infiltration (indicated by white arrows) in animals injected with diet-induced obesity induced pluripotent stem cell-derived endothelial cells compared with animals injected with control induced pluripotent stem cell-derived endothelial cells, whereas animals injected with diet-induced obesity induced pluripotent stem cell-derived endothelial cells with intraperitoneal pravastatin treatment were protected from this damage. Co-administration of the nitric oxide inhibitor N^{ω}-nitro-l-arginine methyl ester blocked the effect of pravastatin in mice receiving diet-induced obesity induced pluripotent stem cell-derived endothelial cells (images at 40×). (B) Representative images of hindlimb frozen sections stained with mouse CD31 antibody. (C) Infiltration of the inflammatory cells was quantified by counting the number of neutrophils per high power field (40×). Three fields/animal and n = 5 animals per group were counted. Mice receiving diet-induced obesity induced pluripotent stem cell-derived endothelial cells showed significantly more neutrophil infiltration compared with mice injected with control induced pluripotent stem cell-derived endothelial cells (8 ± 2 vs. 54 ± 8, Ctrl induced pluripotent stem cell-derived endothelial cells vs. diet-induced obesity induced pluripotent stem cell-derived endothelial cells, P = 0.001), which was reversed by co-administration of diet-induced obesity induced pluripotent stem cell-derived endothelial cells and intraperitoneal pravastatin (54 ± 8 vs. 17 ± 5, diet-induced obesity induced pluripotent stem cell-derived endothelial cells vs. diet-induced obesity induced pluripotent stem cell-derived endothelial cells + intraperitoneal statin, P = 0.002). When mice that received diet-induced obesity induced pluripotent stem cell-derived endothelial cells plus daily pravastatin also received the nitric oxide synthase inhibitor N^{ω}-nitro-l-arginine methyl ester in their drinking water, the decrease in neutrophil infiltration was significantly blunted (17 ± 5 vs. 44 ± 5, diet-induced obesity induced pluripotent stem cell-derived endothelial cells + intraperitoneal statin vs. diet-induced obesity induced pluripotent stem cell-derived endothelial cells + intraperitoneal statin + N^{ω}-nitro-l-arginine methyl ester, P = 0.011). (D) Quantification of $CD31^{+}$ staining showed decreased number of capillaries per high power field in the hindlimbs of mice receiving diet-induced obesity induced pluripotent stem cell-derived endothelial cells compared with mice receiving control induced pluripotent stem cell-derived endothelial cells (P = 0.006). Co-administration of diet-induced obesity induced pluripotent stem cell-derived endothelial cells with pravastatin for 14 days resulted in a significant increase in capillary density compared with diet-induced obesity induced pluripotent stem cell-derived endothelial cells alone (P = 0.047), while co-administration of pravastatin with N^{ω}-nitro-l-arginine methyl ester blocked the effect of pravastatin in animals administered diet-induced obesity induced pluripotent stem cell-derived endothelial cells (P = 0.001).

reach statistical significance (P = 0.064). Immunofluorescent staining for CM-DiI-labelled iPSC-ECs verified engraftment of control iPSC-ECs in the ischaemic hindlimbs at Day 14 (Supplementary material, Figure S10). There was less detectable fluorescent signal in sectioned ischaemic hindlimbs of mice injected with labelled DIO iPSC-ECs compared with mice injected with DIO iPSC-ECs combined with daily IP injections of pravastatin.

DISCUSSION

Following hindlimb ischaemia injury, transplantation of ESC-ECs or iPSC-ECs can result in their incorporation into the host vasculature and increase reperfusion (Cho et al. 2007, Yamahara et al. 2008, Yu et al. 2009). However, since cells used in these studies were derived from healthy donors, it remains unknown if iPSC-ECs derived from DIO donors will function in the same way. Since patients who will require intervention to restore normal perfusion are likely to have significant morbidity such as obesity, identifying, and reversing endothelial dysfunction would be important before future application in regenerative medicine. The current study is the first to compare the functional capacity of iPSC-ECs from control healthy mice vs. DIO mice in vitro and in vivo. We first showed that DIO iPSC-ECs had impaired function in vitro compared with control iPSC-ECs. DIO iPSC-ECs had a reduced capacity to form cord-like structures on Matrigel after 24 h, as well as decreased migration and proliferation in vitro. When cultured in hypoxic conditions, DIO iPSC-ECs showed an increase in apoptosis compared with control iPSC-ECs. Second, by using a murine hindlimb ischaemia model, we showed that DIO iPSC-ECs exhibit impaired vascular function in vivo. Mice injected with DIO iPSC-ECs achieved significantly less reperfusion beginning at Day 10 compared with mice injected with control iPSC-ECs. While inflammation is often observed following surgical induction of hindlimb ischaemia (Silvestre et al. 2008), we observed significantly more inflammatory cells as well as muscle atrophy in mice injected with DIO iPSC-ECs compared with those injected with control iPSC-ECs. Immunostaining for $CD31^{+}$ cells also revealed significantly lower capillary density counts in the hindlimbs of mice injected with DIO iPSC-ECs compared with control iPSC-ECs. Microarray gene expression analysis comparing iPSC-ECs from control and DIO mice revealed 472 differentially regulated genes involved in biological pathways, including apoptosis, inflammation, immune function, oxidative stress, and cell senescence. Previous studies have demonstrated that statin treatment can promote angiogenesis in murine models of hindlimb ischaemia (Kureishi et al. 2000, Sata et al. 2001). In addition to their lipid lowering effects, statins can decrease inflammation and increase eNOS expression, resulting in a subsequent increase in NO bioavailability (Ni et al. 2001, Davignon 2004, Mason et al. 2004, Schonbeck and Libby 2004). In keeping with these observations, another important finding of this study is that co administration of low-dose pravastatin is able to reverse much of the dysfunc-

tion observed with DIO iPSC-ECs both in vitro and in vivo. Mechanistically, pravastatin therapy had significant beneficial effects in vitro on apoptosis, inflammation, and oxidative stress in DIO iPSC-ECs (Supplementary material, Figure S11). Pravastatin also resulted in a significant improvement in hindlimb reperfusion following ischaemia compared with mice receiving iPSC-ECs without pravastatin co-administration. These effects were inhibited by concurrent administration of L-NAME, an NO synthase inhibitor, suggesting the effects of pravastatin were via an NO-dependent mechanism. Taken together, these results correlate with a large body of evidence demonstrating that in pre-diabetes and DIO, abnormally high levels of inflammatory and oxidative stress biomarkers are associated with increased cellular apoptosis, leading to subsequent long-term complications such as endothelial dysfunction (van den Oever et al. 2010). These prolonged periods of heightened oxidative stress and inflammation can result in dysfunctional progenitor and stem cell populations, which have been implicated in increased risk of cardiovascular disease and PVD in patients with diabetes (Ohshima et al. 2009, Magenta et al. 2014). The observation that DIO iPSC-ECs show impaired function both in vitro and in vivo suggests one of the consequences of the altered metabolic state is the induction of global epigenetic changes that contribute to impaired EC function seen in these animals. These results are relevant and significant for cell therapy approaches. While autologous iPSC-ECs derived from obese patients might obviate issues associated with immunological rejection, these iPSC-ECs may be inadequate for restoring normal vascular function compared with iPSC-ECs derived from healthy donors. Based on these results, low-dose statin therapy may be a useful adjuvant when co-administered with dysfunctional DIO iPSC-ECs. Finally, the current iPSC-EC platform can also be used to identify additional novel drug targets that can alter the diabetes-induced dysfunctional state (Matsa et al. 2014).

In summary, our study is the first to show that iPSC-ECs derived from DIO mice exhibit decreased vascular function in vitro, and reduced function and incorporation into the host vasculature in vivo. Histological evaluation revealed muscle atrophy and increased infiltration of inflammatory cells in the ischaemic hindlimbs of mice receiving DIO iPSC-ECs. The EC dysfunction may be related to apoptosis, inflammation, and oxidative stress due to decreased NO production. Co administration with low-dose pravastatin therapy reversed EC dysfunction both in vitro and in vivo. Collectively, these findings may have important implications and caveats for future patient-specific iPSC-EC therapy, especially in pre-diabetic or DIO patients with PVD.

REFERENCES

Andrikopoulos, S., A. R. Blair, N. Deluca, B. C. Fam and J. Proietto (2008). "Evaluating the glucose tolerance test in mice." American journal of physiology. Endocrinology and metabolism 295(6): E1323-1332.

Birse, R. T., J. Choi, K. Reardon, J. Rodriguez, S. Graham, S. Diop, . . . S. Oldham (2010). "High-fat-diet-induced obesity and heart dysfunction are regulated by the TOR pathway in Drosophila." Cell Metab 12(5): 533-544.

Bruning, J. C., J. Winnay, B. Cheatham and C. R. Kahn (1997). "Differential signaling by insulin receptor substrate 1 (IRS-1) and IRS-2 in IRS-1-deficient cells." Molecular and cellular biology 17(3): 1513-1521.

Bruyndonckx, L., V. Hoymans, A. Van Craenenbroeck, D. Vissers, C. Vrints, J. Ramet and V. Conraads (2013). Assessment of Endothelial Dysfunction in Childhood Obesity and Clinical Use. Prevalence, Pathophysiology, and Management, Informa UK Limited: 165-206.

Burridge, P. W., D. Anderson, H. Priddle, M. D. Barbadillo Munoz, S. Chamberlain, C. Allegrucci, . . . C. Denning (2007). "Improved human embryonic stem cell embryoid body homogeneity and cardiomyocyte differentiation from a novel V-96 plate aggregation system highlights interline variability." Stem Cells 25(4): 929-938.

Caballero, A. E. (2003). "Endothelial dysfunction in obesity and insulin resistance: a road to diabetes and heart disease." Obes Res 11(11): 1278-1289.

Cho, S. W., S. H. Moon, S. H. Lee, S. W. Kang, J. Kim, J. M. Lim, . . . H. M. Chung (2007). "Improvement of postnatal neovascularization by human embryonic stem cell derived endothelial-like cell transplantation in a mouse model of hindlimb ischemia." Circulation 116(21): 2409-2419.

Davignon, J. (2004). "Beneficial cardiovascular pleiotropic effects of statins." Circulation 109(23 Suppl 1): III39-43.

Du, X., D. Edelstein, S. Obici, N. Higham, M. H. Zou and M. Brownlee (2006). "Insulin resistance reduces arterial prostacyclin synthase and eNOS activities by increasing endothelial fatty acid oxidation." J Clin Invest 116(4): 1071-1080.

Esposito, K., F. Nappo, R. Marfella, G. Giugliano, F. Giugliano, M. Ciotola, . . . D. Giugliano (2002). "Inflammatory cytokine concentrations are acutely increased by hyperglycemia in humans: role of oxidative stress." Circulation 106(16): 2067-2072.

Flegal, K. M., M. D. Carroll, C. L. Ogden and L. R. Curtin (2010). "Prevalence and trends in obesity among US adults, 1999-2008." JAMA 303(3): 235-241.

Galassetti, P. (2012). "Inflammation and oxidative stress in obesity, metabolic syndrome, and diabetes." Exp Diabetes Res 2012: 943706.

Guzik, T. J. (2002). "Mechanisms of Increased Vascular Superoxide Production in Human Diabetes Mellitus: Role of NAD(P)H Oxidase and Endothelial Nitric Oxide Synthase." Circulation 105(14): 1656-1662.

Hamelin, B. A. and J. Turgeon (1998). "Hydrophilicity/lipophilicity: relevance for the pharmacology and clinical effects of HMG-CoA reductase inhibitors." Trends Pharmacol Sci 19(1): 26-37.

Hink, U., H. Li, H. Mollnau, M. Oelze, E. Matheis, M. Hartmann, . . . T. Munzel (2001). "Mechanisms underlying endothelial dysfunction in diabetes mellitus." Circ Res 88(2): E14-22.

Huang, N. F., H. Niiyama, C. Peter, A. De, Y. Natkunam, F. Fleissner, . . . J. P. Cooke (2010). "Embryonic stem cell-derived endothelial cells engraft into the ischemic hindlimb and restore perfusion." Arterioscle-rosis, thrombosis, and vascular biology 30(5): 984-991.

Kobayashi, M., K. Inoue, E. Warabi, T. Minami and T. Kodama (2005). "A simple method of isolating mouse aortic endothelial cells." Journal of atherosclerosis and thrombosis 12(3): 138-142.

Kureishi, Y., Z. Luo, I. Shiojima, A. Bialik, D. Fulton, D. J. Lefer, . . . K. Walsh (2000). "The HMG-CoA reductase inhibitor simvastatin activates the protein kinase Akt and promotes angiogenesis in normocholesterolemic animals." Nat Med 6(9): 1004-1010.

Lai, W.-H., J. C. Y. Ho, Y.-C. Chan, J. H. L. Ng, K.-W. Au, L.-Y. Wong, . . . H.-F. Tse (2013). "Attenuation of Hind-Limb Ischemia in Mice with Endothelial-Like Cells Derived from Different Sources of Human Stem Cells." PLoS ONE 8(3): e57876.

Leber, A., B. Hemmens, B. Klosch, W. Goessler, G. Raber, B. Mayer and K. Schmidt (1999). "Characterization of recombinant human endothelial nitric-oxide synthase purified from the yeast Pichia pastoris." J Biol Chem 274(53): 37658-37664.

Li, Z., J. C. Wu, A. Y. Sheikh, D. Kraft, F. Cao, X. Xie, . . . J. P. Cooke (2007). "Differentiation, survival, and function of embryonic stem cell derived endothelial cells for ischemic heart disease." Circulation 116(11 Suppl): I46-54.

Liang, C. C., A. Y. Park and J. L. Guan (2007). "In vitro scratch assay: a convenient and inexpensive method for analysis of cell migration in vitro." Nature protocols 2(2): 329-333.

Limbourg, A., T. Korff, L. C. Napp, W. Schaper, H. Drexler and F. P. Limbourg (2009). "Evaluation of postnatal arteriogenesis and angiogenesis in a mouse model of hind-limb ischemia." Nature protocols 4(12): 1737-1746.

Liu, Y., J. Wei, S. Hu and L. Hu (2012). "Beneficial effects of statins on endothelial progenitor cells." Am J Med Sci 344(3): 220-226.

Maehr, R., S. Chen, M. Snitow, T. Ludwig, L. Yagasaki, R. Goland, . . . D. A. Melton (2009). "Generation of pluripotent stem cells from patients with type 1 diabetes." Proc Natl Acad Sci U S A 106(37): 15768-15773.

Magenta, A., S. Greco, M. C. Capogrossi, C. Gaetano and F. Martelli (2014). "Nitric Oxide, Oxidative Stress, andp66ShcInterplay in Diabetic Endothelial Dysfunction." BioMed Research International 2014: 1-16.

Mason, R. P., M. F. Walter and R. F. Jacob (2004). "Effects of HMG-CoA reductase inhibitors on endothelial function: role of microdomains and oxidative stress." Circulation 109(21 Suppl 1): II34-41.

Matsa, E., P. W. Burridge and J. C. Wu (2014). "Human Stem Cells for Modeling Heart Disease and for Drug Discovery." Science Translational Medicine 6(239): 239ps236-239ps236.

Michell, B. J. (2001). "Coordinated Control of Endothelial Nitric-oxide Synthase Phosphorylation by Protein Kinase C and the cAMP-dependent Protein Kinase." Journal of Biological Chemistry 276(21): 17625-17628.

Ni, W., K. Egashira, C. Kataoka, S. Kitamoto, M. Koyanagi, S. Inoue and A. Takeshita (2001). "Antiinflammatory and antiarteriosclerotic actions of HMG-CoA reductase inhibitors in a rat model of chronic inhibition of nitric oxide synthesis." Circ Res 89(5): 415-421.

Ohshima, M., T.-S. Li, M. Kubo, S.-L. Qin and K. Hamano (2009). "Antioxidant Therapy Attenuates Diabetes-Related Impairment of Bone Marrow Stem Cells." Circulation Journal 73(1): 162-166.

Reinhart-King, C. A. (2008). "Endothelial cell adhesion and migration." Methods in enzymology 443: 45-64.

Rodríguez-Crespo, I., P. Moënne-Loccoz, T. M. Loehr and P. R. Ortiz de Montellano (1997). "Endothelial Nitric Oxide Synthase: Modulations of the Distal Heme Site Produced by Progressive N-Terminal Deletions †." Biochemistry 36(28): 8530-8538.

Sansbury, B. E., T. D. Cummins, Y. Tang, J. Hellmann, C. R. Holden, M. A. Harbeson, . . . B. G. Hill (2012). "Overexpression of Endothelial Nitric Oxide Synthase Prevents Diet-Induced Obesity and Regulates Adipocyte Phenotype." Circulation Research 111(9): 1176-1189.

Sata, M., H. Nishimatsu, E. Suzuki, S. Sugiura, M. Yoshizumi, Y. Ouchi, . . . R. Nagai (2001). "Endothelial nitric oxide synthase is essential for the HMG-CoA reductase inhibitor cerivastatin to promote collateral growth in response to ischemia." FASEB J 15(13): 2530-2532.

Schonbeck, U. and P. Libby (2004). "Inflammation, immunity, and HMG-CoA reductase inhibitors: statins as antiinflammatory agents?" Circulation 109(21 Suppl 1): II18-26.

Silvestre, J. S., Z. Mallat, A. Tedgui and B. I. Levy (2008). "Post-ischaemic neovascularization and inflammation." Cardiovascular Research 78(2): 242-249.

Szendroedi, J. and M. Roden (2009). "Ectopic lipids and organ function." Curr Opin Lipidol 20(1): 50-56.

Takahashi, K., K. Tanabe, M. Ohnuki, M. Narita, T. Ichisaka, K. Tomoda and S. Yamanaka (2007). "Induction of pluripotent stem cells from adult human fibroblasts by defined factors." Cell 131(5): 861-872.

van den Oever, I. A., H. G. Raterman, M. T. Nurmohamed and S. Simsek (2010). "Endothelial dysfunction, inflammation, and apoptosis in diabetes mellitus." Mediators Inflamm 2010: 792393.

Voyta, J. C., D. P. Via, C. E. Butterfield and B. R. Zetter (1984). "Identification and isolation of endothelial cells based on their increased uptake of acetylated-low density lipoprotein." J Cell Biol 99(6): 2034-2040.

Wang, C. Y. and J. K. Liao (2012). "A mouse model of diet-induced obesity and insulin resistance." Methods in molecular biology 821: 421-433.

Warlich, E., J. Kuehle, T. Cantz, M. H. Brugman, T. Maetzig, M. Galla, . . . A. Schambach (2011). "Lentiviral vector design and imaging approaches to visualize the early stages of cellular reprogramming." Molecular therapy : the journal of the American Society of Gene Therapy 19(4): 782-789.

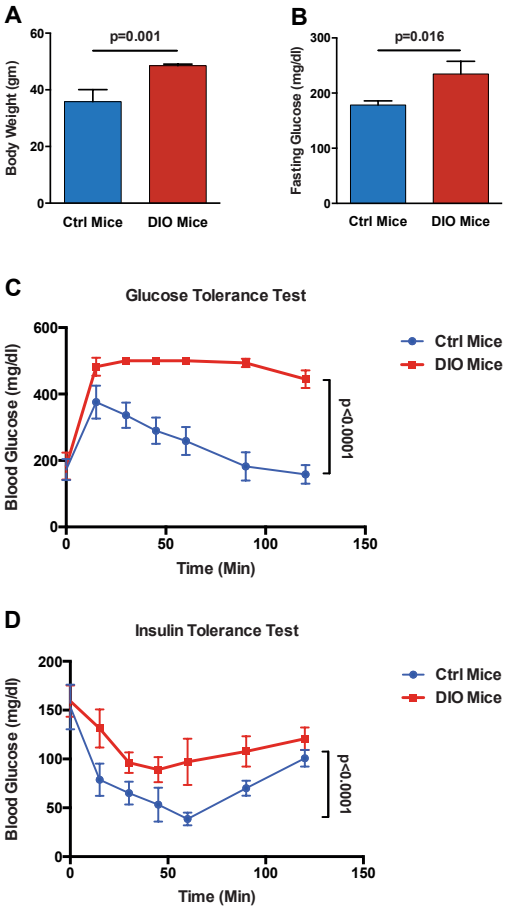
Weir, C., M. C. Morel-Kopp, A. Gill, K. Tinworth, L. Ladd, S. N. Hunyor and C. Ward (2008). "Mesenchymal stem cells: isolation, characterisation and in vivo fluorescent dye tracking." Heart, lung & circulation 17(5): 395-403.

Yamahara, K., M. Sone, H. Itoh, J. K. Yamashita, T. Yurugi-Kobayashi, K. Homma, . . . K. Nakao (2008). "Augmentation of Neovascularizaiton in Hindlimb Ischemia by Combined Transplantation of Human Embryonic Stem Cells-Derived Endothelial and Mural Cells." PLoS ONE 3(2): e1666.

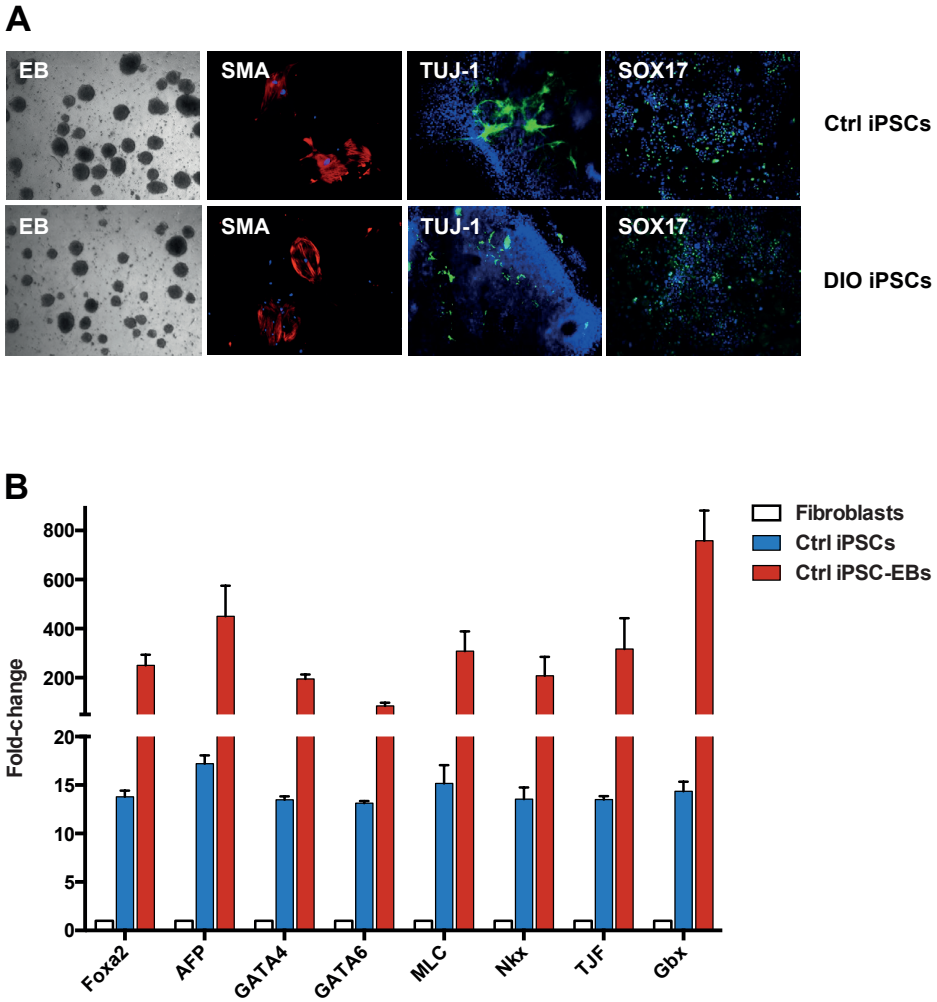
Yamashita, J., H. Itoh, M. Hirashima, M. Ogawa, S. Nishikawa, T. Yurugi, . . . S. Nishikawa (2000). "Flk1-positive cells derived from embryonic stem cells serve as vascular progenitors." Nature 408(6808): 92-96.

Yu, J., N. F. Huang, K. D. Wilson, J. B. Velotta, M. Huang, Z. Li, . . . J. C. Wu (2009). "nAChRs mediate human embryonic stem cell-derived endothelial cells: proliferation, apoptosis, and angiogenesis." PLoS One 4(9): e7040.

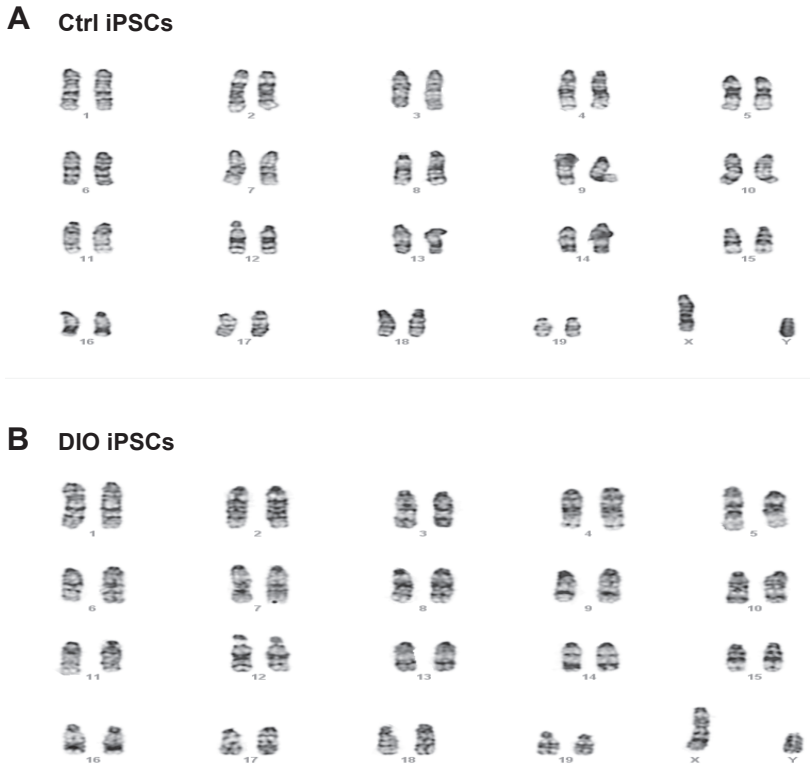
Zou, M.-H., C. Shi and R. A. Cohen (2002). "Oxidation of the zinc-thiolate complex and uncoupling of endothelial nitric oxide synthase by peroxynitrite." Journal of Clinical Investigation 109(6): 817-826.



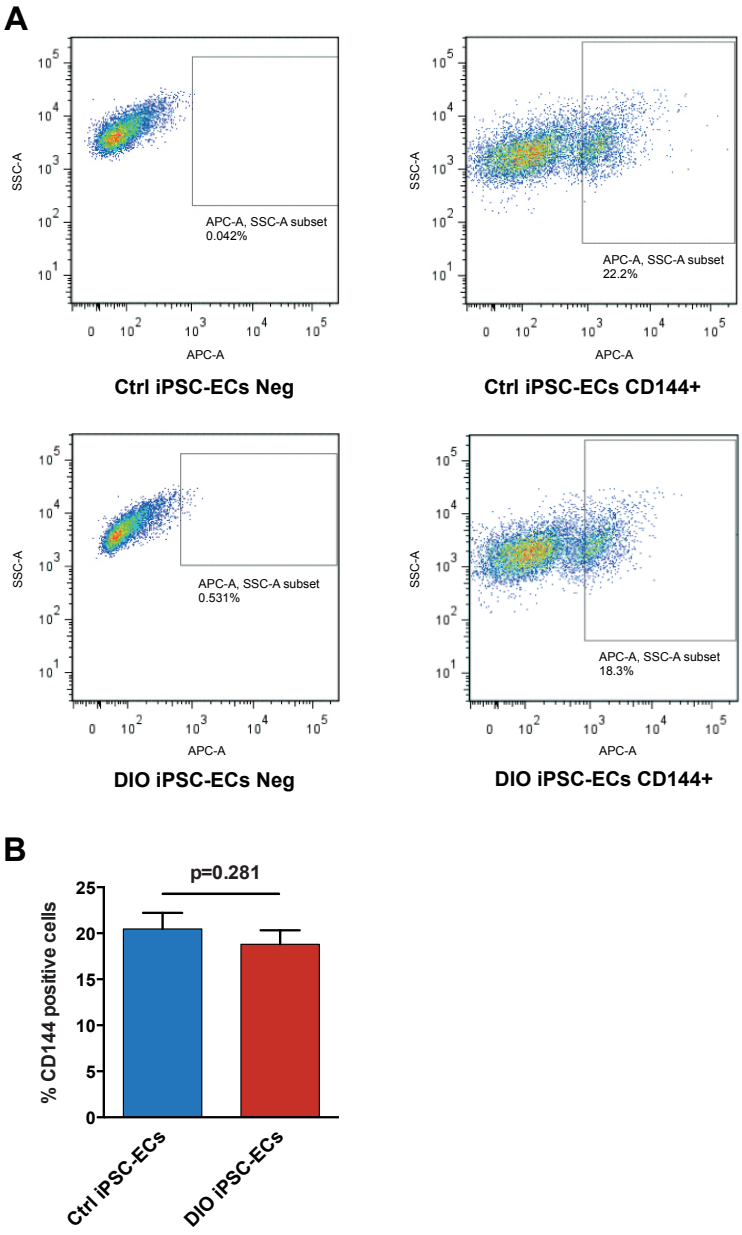
Supplementary Figure 1. Comparisons of control and DIO mice. (A) DIO mice had a significantly higher body weight (p=0.001) and (B) fasting blood glucose (p=0.016) compared to control mice. (C) DIO mice exhibited a significant decrease in glucose tolerance (p<0.001) and (D) insulin tolerance compared to control mice (p<0.001).



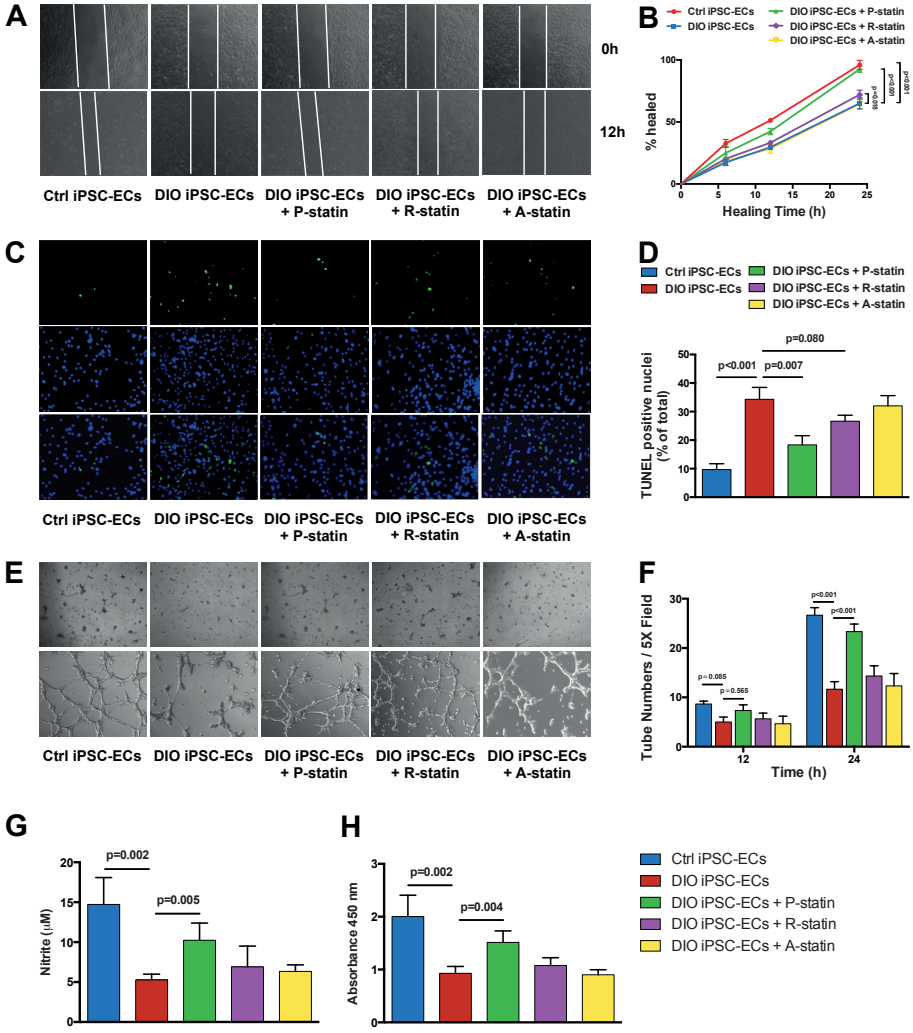
Supplementary Figure 2. Characterization of murine iPSCs. (A) Following embryoid body (EB) formation, outgrowths generated from iPSCs derived from control and DIO mice expressed markers of the three germ layers: mesoderm (SMA), ectoderm (TUJ-1), and endoderm (SOX17). (B) RT-PCR performed on RNAs isolated from differentiated EBs of control iPSCs confirmed expression of genes specific for the three germ layers (mesoderm, ectoderm, and endoderm). Fold-change compared to fibroblasts.



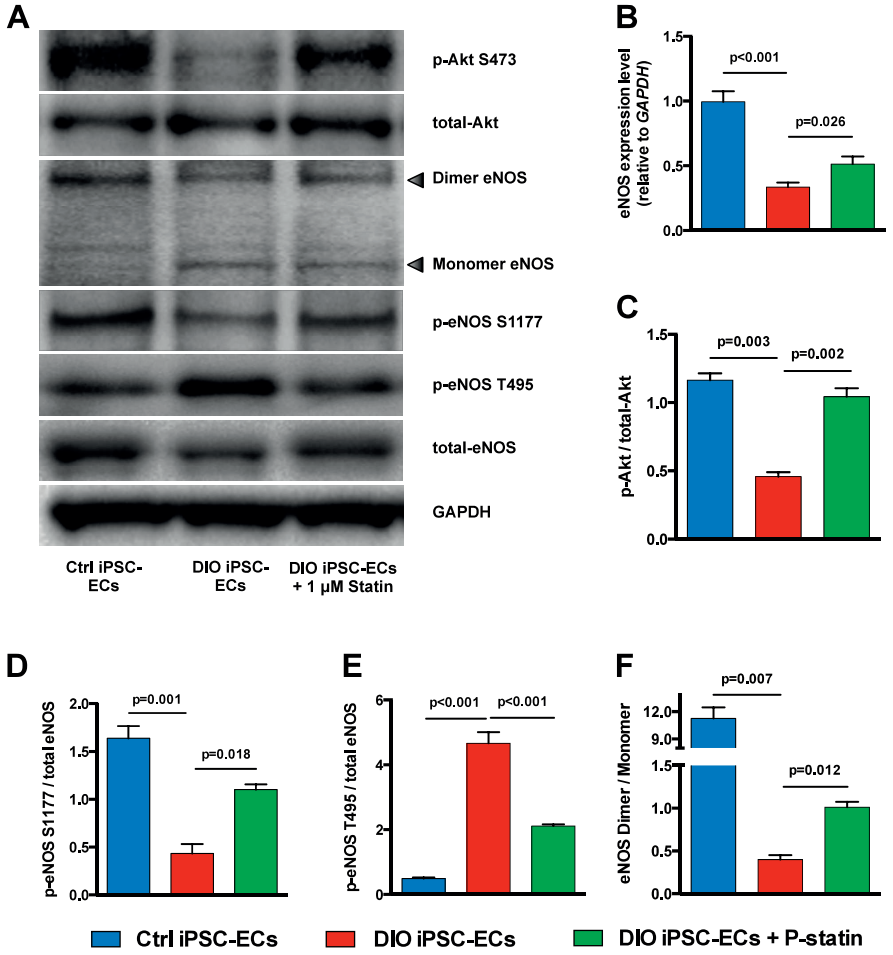
Supplementary Figure 3. Karyotype analysis of murine iPSCs. (A) iPSC lines derived from control and (B) DIO mice maintained a normal karyotype after extended passage.



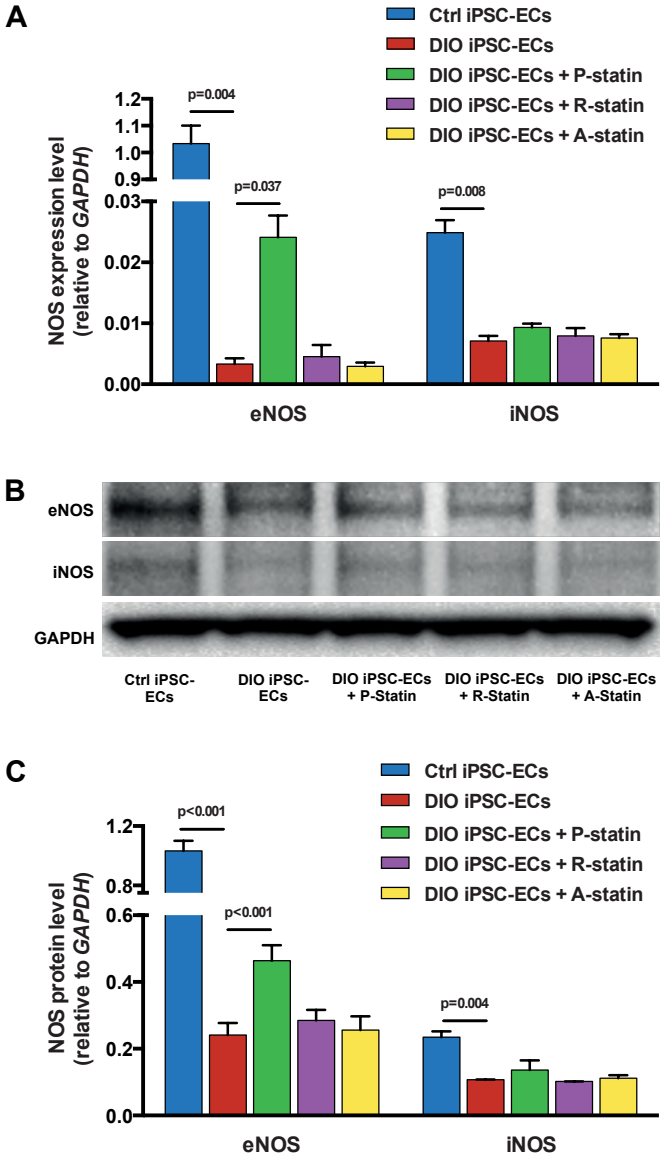
Supplementary Figure 4. Flow cytometry analysis of iPSC-EC differentiation efficiency. (A) Dot plots of iPSC-ECs stained with anti CD144-APC conjugated antibody in both control mice (upper panel) and DIO mice (lower panel). (B) Quantification of flow cytometry showed no significant differences in iPSC-EC differentiation efficiency between control and DIO group (20.47%±1.75% vs. 18.80%±1.51%, Ctrl iPSC-ECs vs. DIO iPSC-ECs, p=0.281).



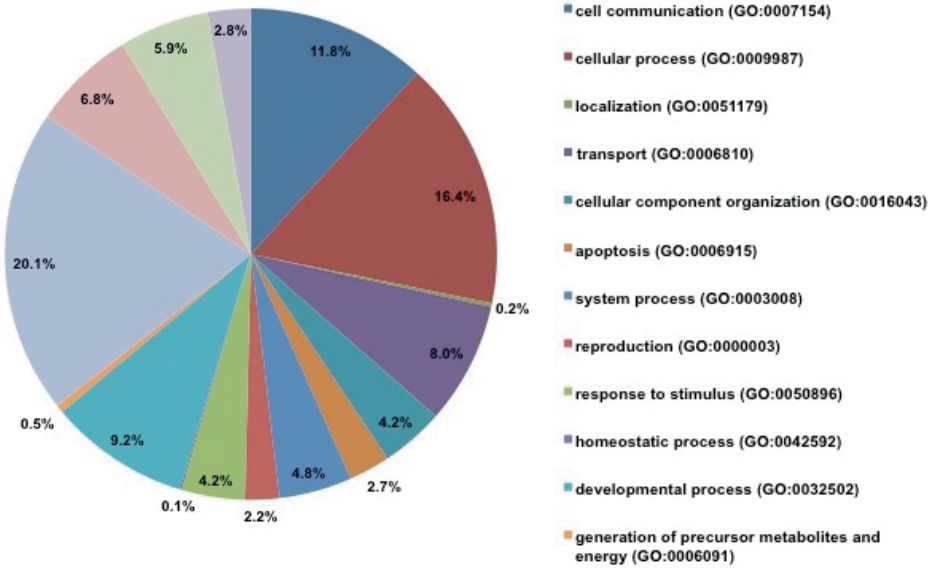
Supplementary Figure 5. Comparison of endothelial function recovery after pravastatin, rosuvastatin, and atorvastatin treatment in DIO iPSC-ECs. (A-B) iPSC-ECs from DIO mice demonstrated significant reductions in cell migration ($p<0.001$). Treatment with pravastatin (P- Statin) and rosuvastatin (R-Statin) reversed this phenotype ($p<0.001$ DIO iPSC-ECs vs. DIO iPSC-ECs + P-statin; $p=0.018$ DIO iPSC-ECs vs. DIO iPSC-ECs + R-statin). (C-D) TUNEL staining showed that P-statin and R-statin protected DIO iPSC-ECs from hypoxia-induced apoptosis ($p=0.007$ DIO iPSC-ECs vs. DIO iPSC-ECs + P-statin; $p=0.08$ DIO iPSC-ECs vs. DIO iPSC-ECs + R-statin). (E-F) P-statin treatment increased capacity to form a capillary-like network on Matrigel after 24 hours compared to DIO iPSC-ECs ($p<0.001$). However, the addition of R-statin and A-statin failed to significantly increase the capillary-like network in DIO iPSC-ECs. (G) Measurement of nitrite levels in cell culture supernatant by Griess reaction demonstrated that DIO iPSC-ECs had significantly lower levels of nitric oxide production compared to control iPSC-ECs ($p=0.002$), where incubation of DIO iPSC-ECs with P-statin for 24 hours resulted in significantly higher levels of NO ($p=0.005$). Incubation with R-statin and A- statin did not significantly change the NO production in DIO iPSC-ECs. (H) P-statin treatment significantly increased the cell proliferation rate in DIO iPSC-ECs ($p=0.004$), while R-statin and A-statin showed no significant protective effect.



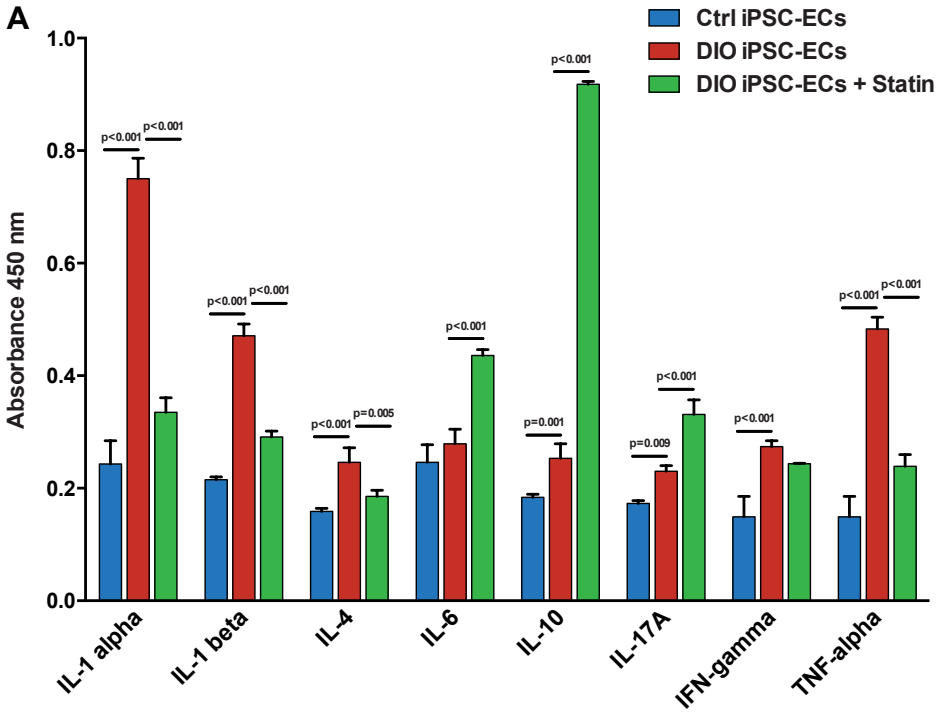
Supplementary Figure 6. eNOS protein levels, phosphorylation status, and dimerization in control iPSC-ECs and DIO iPSC-ECs. (A) Representative western blots and quantification of protein from control iPSC-ECs, DIO iPSC-ECs, and DIO iPSC-ECs with pravastatin treatment for 24 hours probed with (B) antibodies recognizing total eNOS protein, (C) antibodies recognizing serine phosphorylation of residue 473 of Akt protein and total Akt protein, (D) serine phosphorylation of residue 1177 of eNOS, or (E) threonine phosphorylation of residue 495 of eNOS. (F) eNOS dimers and monomers were separated by low-temperature SDS-PAGE (3- 8%) and the membrane was probed with eNOS antibody. The intensity (area times density) of dimers and monomers was determined by densitometry as described in Supplementary Methods. The results were expressed as eNOS dimer to monomer ratio. All blots were stripped and re- probed with an antibody to GAPDH (bottom) and blot shown is representative of three independent experiments.



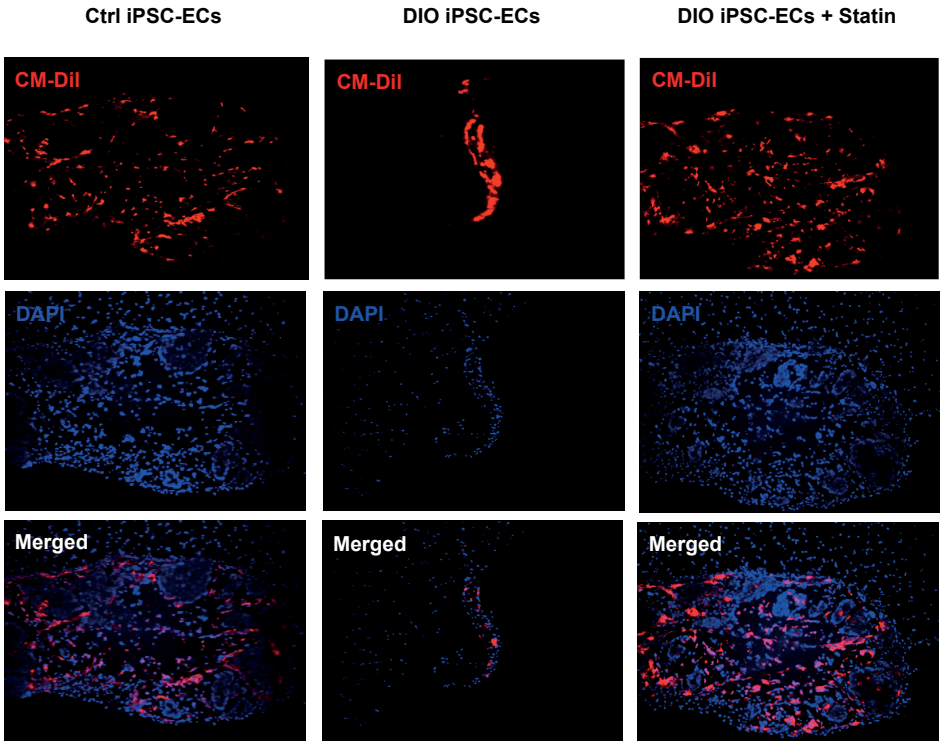
Supplementary Figure 7. eNOS and iNOS gene expression in control and DIO iPSC-ECs. (A) Real-time PCR was performed on cDNAs from control iPSC-ECs, DIO iPSC-ECs, and DIO iPSC-ECs following statin treatments. At basal level, control iPSC-ECs expressed more eNOS (p=0.004) and iNOS (p=0.008) compared with DIO iPSC-ECs. Incubation with pravastatin for 24 hours significantly increased eNOS gene expression in DIO iPSC-ECs (p=0.037 DIO iPSC- ECs vs. DIO iPSC-ECs + P-statin). None of the three statins showed any significant effect on iNOS gene expression in DIO iPSC-ECs at the transcriptional level. (B) Representative western blot images and (C) quantification of protein bands showed consistent results as gene expression assay. Both eNOS (p<0.001) and iNOS (p=0.004) protein levels were significantly reduced in DIO iPSC-ECs compared with control iPSC-ECs, while P-statin treatment only increased eNOS protein level in DIO iPSC-ECs (p<0.001, DIO iPSC-ECs vs. DIO iPSC-ECs + P-statin).



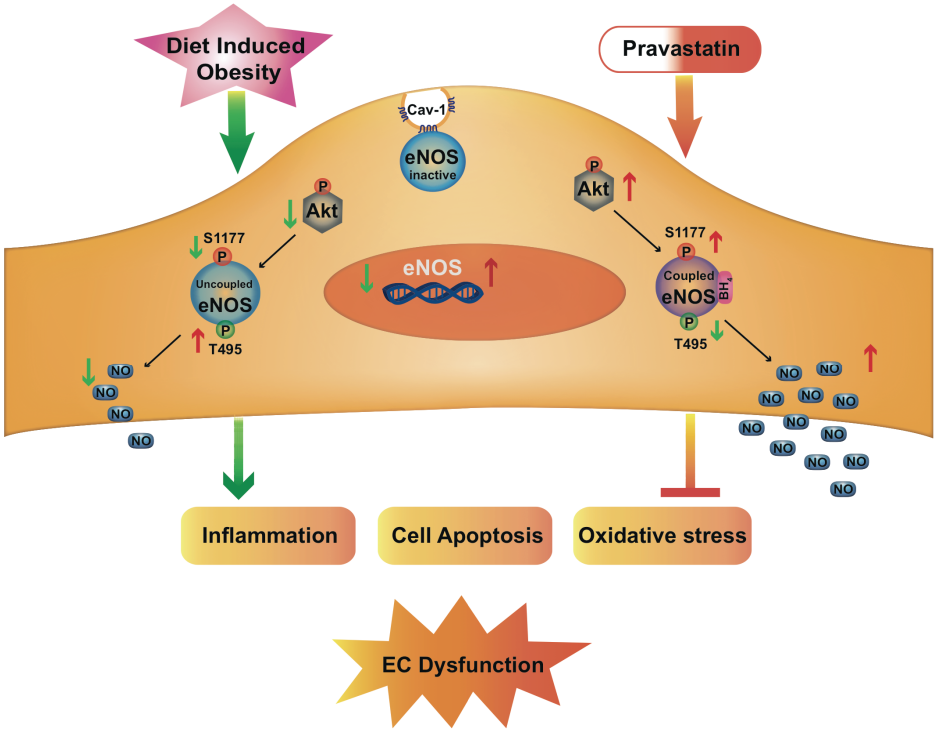
Supplementary Figure 8. Gene ontology (GO) biological pathway analysis. When comparing iPSC-ECs from control and DIO mice, GO biological pathway analysis identified the involvement of biological pathways including metabolism, cell cycle, immune function, inflammation, cell adhesion, oxidative stress, and apoptosis.



Supplementary Figure 9. Cell culture supernatants from DIO iPSC-ECs in hypoxia for 24 hours had significantly higher levels of the pro-inflammatory cytokines IL-1α, IL-1β, IL-4, IFN-γ, and TNF-α compared to control iPSC-ECs. Treatment of DIO iPSC-ECs with 1 uM pravastatin for 24 hours resulted in significant decreases in the pro-inflammatory cytokines IL-1α, IL-1β, IL-4, and TNF-α, and significant increases in anti-inflammatory cytokines IL-6, IL-10, and IL-17A (n=5/group).



Supplementary Figure 10. Immunofluorescent staining for CM-DiI labeled iPSC-ECs. At day 14, there was significantly less fluorescent signal detected in all of the ischemic hindlimbs of mice injected with DIO iPSC-ECs compared to those injected with control iPSC-ECs.



Supplementary Figure 11. Schematic representation of endothelial dysfunction associated with diet-induced obesity. Compared with iPSC-ECs from control mice, iPSC-ECs derived from obese mice showed 1) decreased Akt phosphorylation, which led to the reduction of eNOS phosphorylation at ser1177 residue; 2) increased eNOS phosphorylation at thr495 residue; 3) decreased eNOS gene expression and protein level; and 4) increased eNOS uncoupling. All of the above led to the deactivation of eNOS and reduced NO production in DIO iPSC-ECs, causing increased endothelial inflammation, cell apoptosis, and oxidative stress, thus resulting in EC dysfunction. Co-administration of 1 μM pravastatin therapy with DIO iPSC-ECs reversed this EC dysfunction through activation of eNOS signaling pathway.

Primers	Sequences (5'-3')
Foxa2	F: TAAGCGAGCTAAAGGGAGCA R: GTGGTTGAAGGCGTAATGGT
AFP	F: CGCGTTTCTGGTTGCTTACAC R: ACTTCTTGCTCTTGGCCTTGG
GATA4	F: TCTCACTATGGGCACAGCAG R: GCGATGTCTGAGTGACAGGA
GATA6	F: CATTTGGAGGAAACCGTGAA R: CCAGCAAATGCAGATTCCTT
MLC	F: CCACTCTGGGTGAGAGGCTA R: GGGCTGCCGTAGGATTCTC
Nkx	F: CCAAGGACCCTCGAGCTGA R: CGACAGATACCGCTGCTGCT
TJF	F: CGAGACCTACTGCATCGACA R: CATTGAGCTGACCAGGGAAT
Gbx	F: TGCAGGCGTCGCTCGTAG R: TCCGAGCTGTAGTCCAGATCA
18s	F: AAACGGCTACCACATCCAAG R: CCTCCAATGGATCCTCGTTA

Supplementary Table 1. Primer sequences for evaluating pluripotency by RT-PCR. A list of primer sequences used to confirm murine iPSCs can successfully differentiate into the three embryonic germ layers.

A

Gene	DIO iPSC-ECs / Ctrl iPSC-ECs	DIO iPSC-ECs + Statin / DIO iPSC-ECs	DIO iPSC-ECs + Statin / Ctrl iPSC-ECs
Bcl2a1a	5.57	-13.59	-2.44
Bcl2l10	14.06	-22.81	-1.62
Birc5	3.11	-4.73	-1.52
Bnip3	4.65	-17.59	-3.78
Bnip3l	4.68	-3.86	1.21
Casp3	3.52	-4.17	-1.18
Casp4	3.17	-3.35	-1.06
Cd40	4.30	-187.12	-43.53
Cd40lg	32.92	-43.92	-1.33
Cd70	4.62	-17.16	-3.72
Cidea	4.39	-72.11	-16.42
Dffb	4.08	-37.07	-9.08
Fas	6.98	-1.41	4.96
Fasl	4.68	-13.74	-2.93
Lhx4	5.98	-21.62	-3.62
Naip1	9.58	-12.42	-1.30
Nme5	3.12	-1.67	1.86
Polb	3.02	-4.51	-1.49
Prdx2	4.67	-7.88	-1.69
Pycard	4.64	2.03	9.41
Tnfsf10	6.60	-4.37	1.51
Traf1	4.90	-2.00	2.46

B

Gene	DIO iPSC-ECs / Ctrl iPSC-ECs	DIO iPSC-ECs + Statin / DIO iPSC-ECs	DIO iPSC-ECs + Statin / Ctrl iPSC-ECs
Als2	7.46	2.12	7.88
Atr	4.63	-161.92	-34.91
Duox1	6.80	-23.19	-3.40
Ehd2	3.27	1.69	6.56
Ercc2	3.99	2.01	8.02
Ercc6	3.40	-1.07	1.70
Gpx6	3.15	-473.39	-150.70
Gpx7	10.14	-9.50	1.07
Nqo1	3.00	-1.10	1.98
Vim	3.92	-1.97	1.15
Xpa	5.77	2.58	7.41

Supplementary Table 2. RT-PCR analysis of control, DIO iPSC-ECs, and DIO iPSC-ECs treated with 1 μM pravastatin for 24 hours. Of the genes investigated in panels consisting of (A) apoptotic and (B) oxidative stress pathway genes, 33 genes were significantly up-regulated (>3- fold) in DIO iPSC-ECs compared to control iPSC-ECs. After pravastatin treatment, 28 apoptotic and oxidative genes were down-regulated in DIO iPSC-ECs compared with untreated cells.



Part III

Tumorigenicity and Immunogenicity of PSCs

Chapter 6

Tumorigenicity of PSCs

Kooreman, N.G., and Wu, J.C. (2010). Tumorigenicity of pluripotent stem cells: biological insights from molecular imaging. **J. R. Soc. Interface,** *7 Suppl 6, S753-763.*

ABSTRACT

Embryonic stem cells (ESCs) and induced pluripotent stem cells (iPSCs) have the ability (i) to duplicate indefinitely while maintaining pluripotency and (ii) to differentiate into cell types of all three embryonic germ layers. These two properties of ESCs and iPSCs make them potentially suitable for tissue engineering and cell replacement therapy for many different diseases, including Parkinson's disease, diabetes and heart disease. However, one critical obstacle in the clinical application of ESCs or iPSCs is the risk of teratoma formation. The emerging field of molecular imaging is allowing researchers to track transplanted ESCs or iPSCs *in vivo*, enabling early detection of teratomas.

INTRODUCTION

In 1981, mouse embryonic stem cells (ESCs) were first isolated from the mouse blastocyst (Evans and Kaufman 1981, Martin 1981). A decade later, human ESCs (hESCs) were isolated from the human blastocyst (Thomson et al. 1998). ESC lines are created from the in vitro culture and expansion of the inner cell mass of the blastocyst stage embryo (Evans and Kaufman 1981, Martin 1981, Thomson et al. 1998). Subsequent studies found that it was possible to confer totipotency or pluripotency to somatic cells by transferring the nuclear contents of somatic cells into oocytes (Wilmut et al. 1997), or by fusion with hESCs (Tada et al. 2001, Cowan et al. 2005). This led Takahashi and Yamanaka to believe that certain factors, important in the maintenance of ESCs, could induce pluripotency in somatic cells and create mouse induced pluripotent stem cells (iPSCs), a process termed cellular reprogramming (Takahashi & Yamanaka 2006). It was first described using the exogenous expression of four genes, including two pluripotency transcription factors (i.e. Oct4 and Sox2) and two proto oncogenes (i.e. c-Myc and Klf4; (Takahashi and Yamanaka 2006)). The first mouse iPSC line was created in 2006 (Takahashi and Yamanaka 2006), and a year later human iPSC lines were created independently by James Thomson's and Shinya Yamanaka's groups (Takahashi et al. 2007, Yu et al. 2007).

The pluripotent state of hESCs and iPSCs is indicated by several cellular characteristics, including the following: (i) expression of transcription factors (e.g. Nanog, Oct4 and Sox2), and cell surface molecules (e.g. SSEA3, SESA4, Tra-1-60 and Tra-1-81), (ii) high activity of the enzymes alkaline phosphatase and telomerase, and (iii) typical cell morphology (e.g. small cells with a high nucleus to cytoplasm ratio and prominent nucleoli growing in flat colonies; (Thomson et al. 1998, Amit et al. 2000, Takahashi et al. 2007). The gold standard for pluripotency is to demonstrate a cell line's ability to form tissue of all three germ layers by creating chimeras (Okita et al. 2007) or tetraploid complementation (Zhao et al. 2009) with mouse iPSCs, or by forming teratomas with human iPSCs. Teratomas are defined as benign germ cell tumors (GCTs), which consist of mature, well-differentiated tissues (mature teratomas), or embryonic, less-differentiated tissues (immature teratomas) with a normal karyotype (Pierce et al. 1960, Oosterhuis and Looijenga 2005). The ability of the first hESC line to form tissue composed of all three germ layers was demonstrated by teratoma assay in immunodeficient SCID mice. Histology showed that every mouse had developed tumors composed of gut epithelium (endoderm); cartilage, bone, smooth muscle and striated muscle (mesoderm); and neural epithelium, embryonic ganglia, and stratified squamous epithelium (ectoderm; (Thomson et al. 1998). This assay was later used to test pluripotency in vivo for human iPSCs (Takahashi et al. 2007, Yu et al. 2007). Owing to the pluripotency of ESCs and iPSCs, they are considered to possess great potential for regenerative medicine, including possible treatment of Parkinson's disease (Yang et al. 2008), diabetes (D'Amour et al. 2006) and heart disease (Cao et al. 2008). Pre-clinical studies in

animal models, however, have reported teratoma formation occurring upon injection of mouse ESC (mESC)-derived beating embryoid bodies (EBs; (Cao et al. 2006, Xie et al. 2007) and ESC-derived neuroprogenitors (Chaudhry et al. 2009), highlighting a major hurdle that we have to overcome before clinical translation of pluripotent cells can be realized. The issue being addressed now is how teratoma formation occurs within differentiated ESC- or iPSC derived cell lines. Although not fully understood, it is believed to be the result of remnant, undifferentiated cells present within the transplanted cell population. This hypothesis is further reinforced by findings that transplantation of a fairly pure hESC derived cardiomyocyte population (82.6±6.6%, range 71–95%) into immunosuppressed rats did not result in teratoma formation after four weeks (Laflamme et al. 2007), whereas intracardiac injection of undifferentiated mESCs into immunodeficient rats resulted in teratoma formation in all of them after only three to four weeks (Cao et al. 2006, Nussbaum et al. 2007). Taking pluripotent cells from bench to bedside will therefore partly depend on the ability to purify the cell population and to detect teratoma formation early. The latter can be achieved with the non-invasive tracking of pluripotent cells in vivo with molecular imaging as discussed later.

The link between pluripotency and tumorigenicity

The link between pluripotency and tumorigenicity was discovered as early as the 1960s. At that time, researchers studied teratocarcinomas, the malignant form of teratomas (Pierce et al. 1960). The malignancy of teratocarcinomas lies in the presence of embryonic carcinoma (EC) cells, which are capable of self-renewal as well as differentiation into a variety of tissues (Andrews et al. 2005). Transplantation of a single EC cell resulted in the formation of a teratocarcinoma, which is composed of many differentiated tissues (Kleinsmith and Pierce 1964, Andrews et al. 2005). Subsequent studies showed that teratomas and teratocarcinomas could also be formed by the transplantation of normal mouse embryos or embryonic genital ridges to the adult host, demonstrating that tumor-initiating cells were also present within normal embryos (Stevens and Hummel 1957, Stevens 1964, Stevens 1967, Stevens 1968). When the first hESCs were isolated in 1998, similarities were observed between the newly isolated ESCs and EC cells, including the expression of the pluripotency markers (e.g. SSEA3, SSEA4, TRA 1–60, TRA 1–81, telomerase and alkaline phosphatase) and the ability to form teratomas in immunodeficient mice (Thomson et al. 1998). Furthermore, Andrews and co-workers hypothesized that EC cells might have a stronger selection for mutations that would increase self-renewal capacities and limit differentiation. Similarly, mutations have been observed when growing hESCs in culture over longer passages (Andrews et al. 2005). For example, unbalanced chromosomal translocation involving the long arm of chromosomes 1 and 9, resulting in karyotypic change 46,XX,der(9)t(1;9)(q31;q22), has been reported in H9 cells at passage 120 compared with passage 48 (Xie et al. 2010). Passaging of three subcultures of hESC line H7 (H7.S0, H7.S6, H7.S9) and the hESC line H14 over a period of several months resulted in a gain of the complete long arm of chromosome 17

(17q; (Draper et al. 2004)), which is also very commonly seen in EC cells derived from teratocarcinomas (Andrews et al. 2005). In addition to a gain of chromosome 17, a gain of chromosome 12 has also been observed in a few subpopulations of these cells. The pluripotency marker Nanog is sited on this chromosome (Draper et al. 2004). The gain of one or more isochromosomes on the short arm of chromosome 12 is associated with testicular GCTs in humans (Mostert et al. 1998). Further evidence for the role in chromosome 12 in the tumorgenicity of pluripotent cells was provided by Sperger and co-workers, who compared the gene expression of five hESC lines, 36 GCT cell lines, 14 samples of normal testis and 17 somatic cell lines. Significance analysis of microarrays in this study identified 1760 cDNAs in ESCs, 1299 cDNAs in EC cells and 1518 cDNAs in seminomas that were significantly more highly expressed than the control group of differentiated cells. They found 330 genes that were shared by ESCs, EC cells and seminomas, and among these genes was POU5F1 (Oct4). Furthermore, genes sited on chromosome 12 were highly represented ($p < 0.00001$) among the genes highly overexpressed in EC cells when compared directly with ESCs (Sperger et al. 2003). The molecular basis of the tumorigenicity of pluripotent cells lies in their cancer-resembling properties, namely their ability to self-renew and proliferate, which are promoted by several molecular processes and have been described in detail (Blum and Benvenisty 2008, Blum and Benvenisty 2009). These properties include self-renewal, rapid proliferation, lack of contact inhibition and telomerase activity (figure 1). On closer examination of the karyotype of ESCs, polyploidy has been observed in mESCs despite an intact spindle assembly checkpoint (SAC; (Malashicheva et al. 2002)). Mantel and coworkers demonstrated that mESCs and hESCs have an intact SAC, but that mitotic failure-induced polyploidy does not lead to apoptosis of these cells (Mantel et al. 2007). Mitotic errors often occur in rapidly proliferating cells and the SAC, typically leading to apoptosis of these cells and the necessity for genome maintenance. Uncoupling of this mechanism will lead to karyotypic abnormalities in ESC culture (figure 1). In addition, when inducing double-strand breaks in the DNA of mouse ESCs and mouse EBs by the DNA-damaging agent etoposide, ESCs were resistant to apoptosis whereas the EBs underwent caspase-3-dependent apoptosis. This suggests that polyploidy tolerance in ESCs will give way to apoptosis upon lineage-specific differentiation. This hypothesis has been confirmed for mouse as well as human mononuclear polyploidy/aneupoloid cells, indicating that checkpoint–apoptosis uncoupling is an intrinsic behavior of mESCs and hESCs (Mantel et al. 2007). The examination of gene expression in several human tumors has shown that the pluripotency markers used in reprogramming somatic cells to iPSCs are directly oncogenic (e.g. c-Myc and Klf4) or are involved in tumorigenesis (e.g. Sox2, Nanog, (Knoepfler 2009); and Oct3/4 (Palma et al. 2008)), Targets of Nanog, Sox2 and Oct4 that encode for transcription regulators, are overexpressed and prove especially active in high-grade breast tumors (Ben-Porath et al. 2008). Upregulation of Nanog and Oct4 is also associated with poor outcomes in patients with oral cancer (Chiou et al. 2008). The pluripotent genes Oct3/4,

Sox2, Nanog, c-Myc and Klf4 were also present in prostate tumor cell lines, as well as in primary prostate tumor tissue. Furthermore, injection of these tumor cells containing the pluripotent genes created strong tumorigenicity in immunodeficient mice (Bae et al. 2010). Using a mouse model in which Oct4 could be activated by doxycycline administration, Hochedlinger and co-workers evaluated the effects of Oct4 overexpression in somatic differentiation and tumorigenesis. Oct4-induced dysplasia of the epithelial tissues could be seen as early as 5 days after initiating doxycycline. Dysplasia was only seen in the epithelial progenitor and/or stem cells, and Oct4 overexpression had no effect on the cellular phenotype of differentiated cells. Withdrawal of doxycycline caused a complete reversal of the tumor phenotype, again showing the association of Oct4 with tumorigenesis (Hochedlinger et al. 2005). The biological link between pluripotency and tumorigenicity can perhaps best be described by c-Myc. Although not required for the induction of pluripotency in iPSCs, c-Myc augments the reprogramming ability of Oct4, Sox2 and Klf4 (Takahashi et al. 2007), inhibits differentiation and promotes proliferation (figure 1). Myc proteins have been shown by Eilers & Eisenman (Eilers and Eisenman 2008). The majority of these are upregulated and involved in cell growth; the few genes that are downregulated are involved in cell cycle arrest, cell adhesion and cell–cell communication. The influence of Myc on these nuclear processes is oncogenic as shown by the many tumors described in this review (Eilers and Eisenman 2008). However, not all members of the Myc family possess the same properties. L-Myc for instance has a decreased transformation activity and only few human cancers are associated with an aberrant expression of L-Myc. A recent study reported the creation of iPSCs with L-Myc instead of c-Myc and chimeric mice derived from these L-Myc iPSCs showed reduced tumorigenicity (Nakagawa et al. 2010). Recently, 21 genes were found to be highly expressed in hESCs as well as in teratomas (Blum and Benvenisty 2009). These genes were then credited as known oncogenes, if they were involved in cell-cycle progression, inhibition of apoptosis, signal transduction, transcription or translation. Of these 21 genes, Survivin (BIRC5) was found to be the strongest candidate gene. Survivin is an anti-apoptotic gene that is also involved in mitotic regulation and is expressed in the majority of cancers (Ambrosini et al. 1997, Li et al. 1998); figure 1). It was highly expressed in hESCs and teratomas and downregulated in mature EBs (Blum et al. 2009). From these insights into the gene expression of hESCs and iPSCs, it can be concluded that tumor formation is not dependent on the presence of EC-like cells, but is more an intrinsic property of pluripotent cells. Furthermore, this tumorigenicity of pluripotent cells is reduced upon differentiation. The dilemma now facing investigators is that in reducing the tumorigenicity of stem cells, the very essence of stem cells that makes them useful also has to be reduced, namely self-renewal and pluripotency.

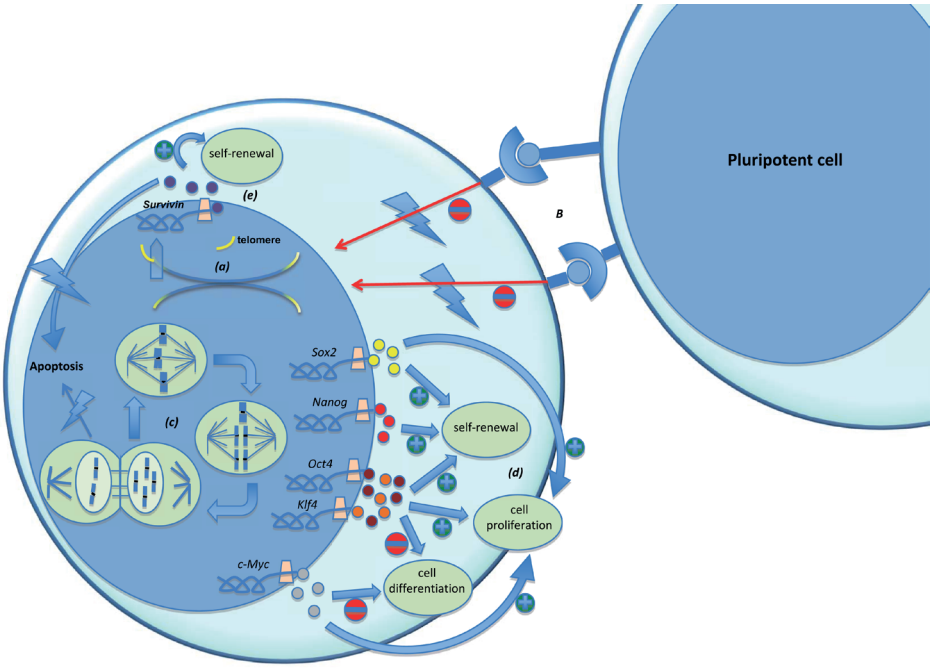


Figure 1. The molecular basis of the tumorigenicity of pluripotent cells. (a) Increased telomerase activity results in extended lifespan of the pluripotent cells by adding telomere ends to the chromosomes. (b) Lack of contact inhibition allows for proliferation and cell growth, even if pluripotent cells are in contact with neighbouring pluripotent cells. (c) Spindle assembly checkpoint (SAC) uncoupling results in failure to induce apoptosis of ESCs with karyotypic abnormalities such as mitotic failure-induced polyploidy. (d,e) Overexpression of the pluripotency markers leads to a highly proliferative, undifferentiated and self-renewal state. *Survivin (BIRC5)*, in addition to the self-renewal properties, functions as an anti-apoptotic gene.

Molecular imaging for tracking cell fate

In the last few decades, the field of medical imaging has advanced enormously, giving rise to different in vivo imaging technologies such as magnetic resonance imaging (MRI), computed tomography (CT), positron emission tomography (PET), single photon emission computed tomography (SPECT), ultrasound and the chargecoupled device (CCD) camera (Blasberg and Tjuvajev 2003). These modalities have been used in the field of nuclear medicine, in which radiolabelled imaging probes are injected into living subjects to provide information about structure and functionality of different organ systems. Although the field of nuclear medicine gave physicians non-invasive insights into the anatomy of organs, a better understanding of changes in biological processes at the cellular and molecular levels in disease was needed. This need gave rise to the field of molecular imaging, in which the interaction of an imaging probe with a molecular target (DNA, RNA or protein) can be detected using the appropriate imaging system. In addition to cardiovascular, neuronal and oncological applications, molecular imaging is also used in tracking the survival and

proliferation of stem cells in vivo. For the latter purpose, two approaches can be used to label the stem cells before transplantation. The first approach is directly labelling the cells by incubation with a contrast agent such as nanoparticles, magnetic particles or radionuclides. The second approach is by a reporter-gene construct transferred into the cells by a vector delivery system. Transcription and translation of the reporter gene will result in a reporter protein that can either be an intracellular enzyme, a cell surface receptor, a transmembrane protein or an intracellular storage protein.

Nanoparticle imaging

Semiconductor quantum dots (QDs) can be manipulated to emit different wavelengths of light and are very photostable, making them interesting options for in vivo tracking of stem cells. In addition, QDs provide brighter and more stable signals for molecular and cellular imaging (Dubertret et al. 2002, Jaiswal et al. 2003, Lin et al. 2007). However, QDs tend to aggregate in the cytosol, are difficult to deliver to the cells and have non-specific binding to multiple molecules.

Iron particle imaging

The monitoring of stem cells with MRI is mostly based on endocytosis of a contrast agent such as superparamagnetic iron oxide particles (SPIOs) or ultrasmall superparamagnetic iron oxide particles (USPIOs) that can elicit changes in T2 relaxivity, which allows their detection in vivo. Usage of MRI for the tracking of mesenchymal stem cells labelled by furomoxides has been described by several groups (Kraitchman et al. 2003, Amado et al. 2005, Arai et al. 2006). MRI signals in these studies could be detected from three weeks to two months. However, one concern is that the MRI signals can still be present even when the transplanted cells are no longer alive. This is because the iron particles can be engulfed by nearby cells, especially macrophages (figure 2;(Li et al. 2008)).

Radionuclide imaging

Stem cell imaging by directly labelling cells with radionuclides is the only direct labelling approach that has been used in human studies, using either bone marrow-derived stem cells (Hofmann et al. 2005) or circulating progenitor cells (Kang et al. 2006, Schachinger et al. 2008). Tracking these cells using SPECT, PET and gamma camera imaging is realized by a labeling agent that is introduced into the cells of interest before transplantation. The major advantage of radionuclide imaging over MRI is its higher imaging sensitivity. However, these cells can only be tracked for several hours to days, depending on their individual decay half-lives (e.g. 99mTc: 6 h; 111In: 2.8 days; 18F: 109 min). Another problem is that radionuclides can leak into other non-target cells and hence give rise to false-positive signals.

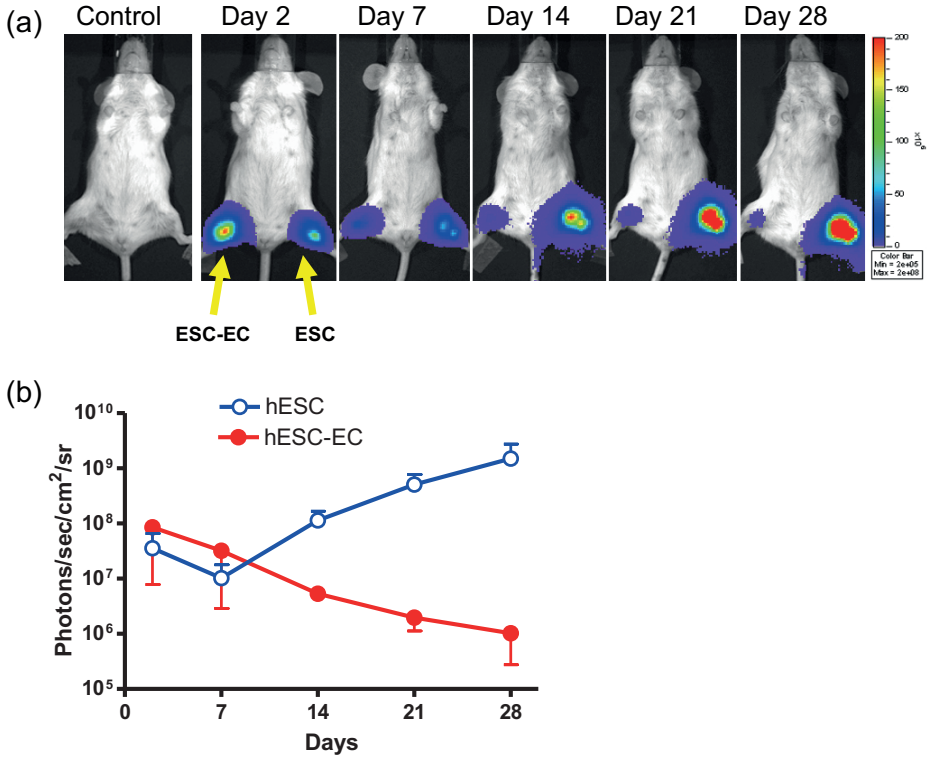


Figure 2. Comparison of physical labelling versus reporter gene labelling for tracking cell fate. Human ESCs were stably transduced with Fluc-eGFP double-fusion reporter gene as well as incubated with superparamagnetic iron oxide (SPIO). Immunodeficient SCID mice were injected with either undifferentiated ESCs or ESCs differentiated into endothelial cells (ESC–EC). (a) Representative animal injected with 1×10^6 ESC–ECs (right hind limb) shows significant bioluminescence activity at day 2, which decreases progressively over the next four weeks owing to acute donor cell death. In contrast, undifferentiated ESCs (left hind limb) proliferated dramatically over four weeks owing to teratoma formation. (b) Detailed quantitative analysis of bioluminescence signals from all animals transplanted with hESCs (blue open circles) versus hESC–ECs (red filled circles). Signal activity is expressed as photons s^{-1} cm^{-2} sr^{-1}. Note that the y-axis is shown as a logarithmic scale. (c) Representative in vivo gradient-recalled echo (GRE) imaging of the animals as shown in (a) and (b). MR signals showed no significant difference between undifferentiated ESCs and differentiated human ESC–ECs from day 2 to day 28. MR image by GRE at day 28 shows bulking expansion of the left hind limb injected with undifferentiated ESCs owing to teratoma formation (arrow head). (d) Detailed quantitative analysis of GRE signals from all animals transplanted with hESCs (blue open circles) and hESC–ECs (red filled circles) (signal activity is expressed as authority unit (AU)). The persistent MRI signal is owing to macrophages engulfing SPIO particles from transplanted cells that have died. Overall, unlike reporter gene imaging, MRI was unable to distinguish cell viability from cell proliferation as its signals remained relatively constant over the four-week time span. Reprinted with permission from Li et al (2008).

Reporter gene imaging

Reporter gene imaging is based on a reporter gene linked to a promotor/enhancer. These DNA sequences are transcribed into mRNAs and will lead to the production of reporter proteins that will interact with exogenously administered reporter probes. This reaction will lead to a detectable signal, which can be visualized by a CCD camera, SPECT, PET or MRI. As mentioned earlier, this can be (i) an intracellular enzyme that interacts with an exogenous reporter probe to give rise to a detectable signal (Cao et al. 2006), (ii) a cell surface receptor that binds to an exogenously delivered probe (e.g. dopamine 2 like receptor (MacLaren et al. 1999)), (iii) a transmembrane protein that mediates in the intracellular uptake of radioisotopes (e.g. sodium/iodide symporter; (Miyagawa et al. 2005), or (iv) an intracellular storage protein that actively concentrates endogenous contrast elements (e.g. intracellular iron in ferritin bound form; (Liu et al. 2009). For small animal imaging, several reporter gene constructs have been developed. A double-fusion construct containing the firefly luciferase (Fluc) and enhanced green fluorescence protein (eGFP) reporter gene has been used in several studies (van der Bogt et al. 2006, Cao et al. 2007, Lee et al. 2009). In these studies, the Fluc enzyme interacts with the reporter probe D-luciferin to generate low energy photons (2–3 eV) that can be detected by an ultrasensitive CCD camera. In addition, the eGFP allows confirmation of in vivo imaging signals with traditional ex vivo post-mortem histology. A triple-fusion construct for monitoring the in vivo survival, proliferation and migration of mESCs after intramyocardial transplantation was reported by Cao et al. (2006). This triple-fusion construct used Fluc for high-throughput bioluminescence imaging (BLI), monomeric red fluorescent protein (mRFP) for fluorescence-activated cell sorting and fluorescence microscopy, and herpes simplex virus truncated thymidine kinase (HSVttk) for deep tissue PET imaging (Cao et al. 2006). For PET reporter gene imaging, the HSVttk phosphorylates its radioactive substrate, 9-(4-[18F] fluoro-3-[hydroxymethyl]butyl) guanine ([18F]-FHBG), intracellularly. The [18F] generates two 511 keV photons that can be detected by PET. Compared with BLI, PET imaging provides higher anatomical details and allows imaging in large animals and humans (Yaghoubi et al. 2009). Finally, it should be mentioned that stable integration of the various reporter genes (Fluc, eGFP, mRFP and HSVttk) into cellular chromosomes allows the mother cell to pass on the reporter genes to daughter cells. Hence, this genetic approach can truly evaluate survival and proliferation, unlike physical approaches such as iron particle, QD or radionuclide labelling. However, the main disadvantage here is the risk of altering cellular behaviours from gene insertion. Although previous genomic (Wu et al. 2006) and proteomic (Wu et al. 2006) studies have not shown any significant adverse effects of mouse ESCs expressing the triple-fusion reporter genes, further optimization using safer site-specific integration approaches is probably needed in the future (Keravala et al. 2009).

Imaging for tumorigenicity

Several imaging modalities have been described here to track the survival and proliferation of pluripotent cells. Owing to the apparent risk of teratoma formation after transplantation of pluripotent cells, it is imperative that molecular imaging be used to detect these tumors at an early stage. In this pre-clinical setting of transplanting pluripotent cells, several groups have looked at the different imaging modalities for the detection of tumor formation in small animals. BLI of mice and rats using Fluc is most commonly used for tumor detection, because it is easy to use and very sensitive (figure 3). Teratoma formation can be detected by a strong BLI signal, even before a palpable tumor is formed (van der Bogt et al. 2006, Lee et al. 2009). Using BLI, Lee et al. have found that they could inject a maximum of $1x10^3$ undifferentiated ESCs in the skeletal muscle and $1x10^4$ undifferentiated hESCs in the cardiac muscle of immunodeficient mice without teratoma formation (Lee et al. 2009). These findings provided important pre-clinical insights into the effects of hESC numbers and local niches on teratoma development as well as the kinetics of teratoma formation.

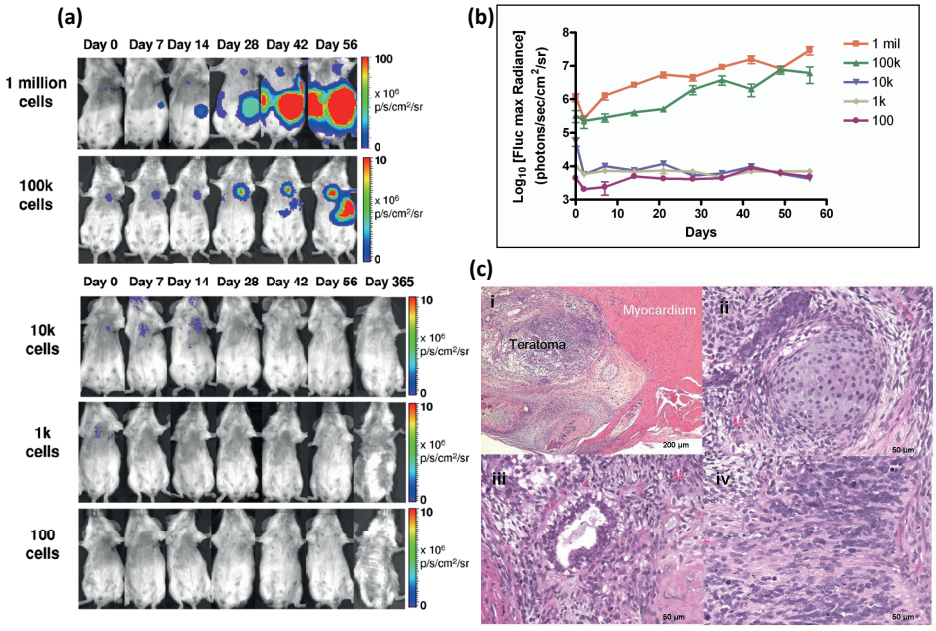


Figure 3. Potential for varying numbers of hESCs to form teratomas following intramyocardial injection. (a) Different numbers of undifferentiated Fluc-eGFP-positive hESCs were injected intramyocardially into SCID mice. BLI reveals tumour development in animals transplanted with 1×10^5 or 1×10^6 cells but not in animals receiving 1×10^4 cells or less. (b) Quantitative analysis of the kinetics of teratoma development using BLI. Orange squares, 1 million; green triangles, 100 000; violet inverted triangles, 10 000; grey diamonds, 1000; pink circles, 100. (c) Representative hematoxylin and eosin staining of intramyocardial teratoma: (i) low-power view of intramyocardial teratoma, (ii) cartilage (mesoderm), (iii) mucinous glandular epithelium (endoderm), and (iv) neural tissue (ectoderm) confirm the presence of cellular derivatives from all three germ layers. Reprinted with permission from Lee et al. (2009).

In addition, BLI together with PET imaging have provided insights into teratoma ablation using a reporter– suicide gene construct (figure 4; (Cao et al. 2007). However, Fluc is not suited for clinical application because of the limited penetration of the signal through tissue in larger animals. Furthermore, BLI only gives a two-dimensional image and reveals little spatial information. In contrast, MRI and PET provide a higher spatial resolution and can be used in clinical imaging (Hinds et al. 2003, Kraitchman et al. 2003, Yaghoubi et al. 2009), but with significantly lower detection threshold. Taking into account that every imaging modality has its advantages and drawbacks, combining two or several imaging modalities may provide a better solution. This multimodality approach together with the continuing technological advances will help scientists take tissue engineering and cell-replacement therapies into the clinical phase in the near future.

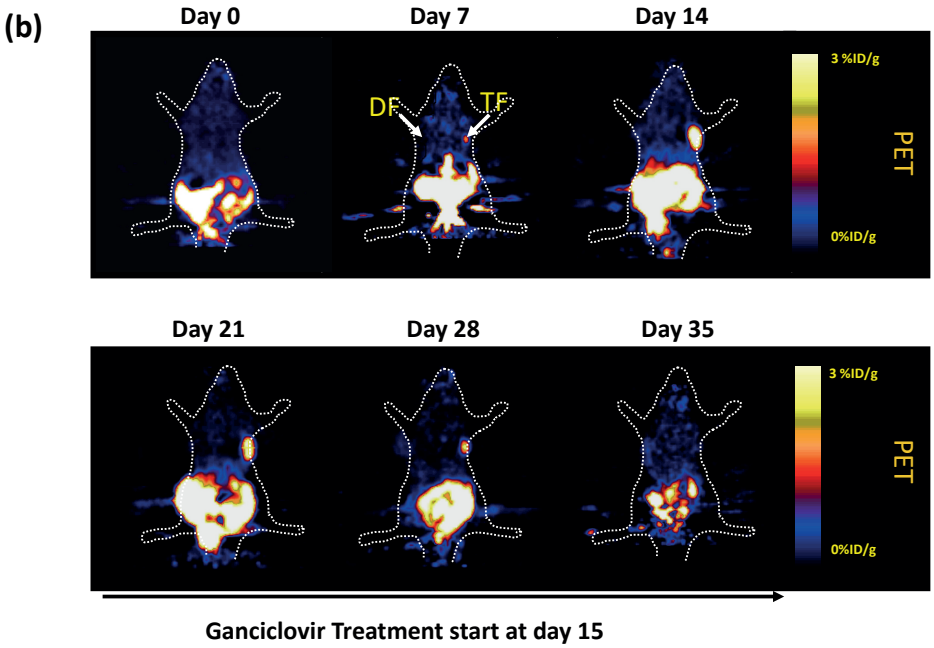


Figure 4. Ablation of teratoma formation using HSVttk reporter and suicide gene. mESCs were stably transduced with a triple-fusion (ESC-TF) reporter gene that consisted of monomeric red fluorescence protein (mRFP), Fluc and HSVttk or a double-fusion (ESC-DF) reporter gene that consisted of enhanced GFP and Fluc. Stably transduced ESC-TF and ESC-DF cells (1×10^6 each group) were transplanted into right and left shoulders of adult nude mice, respectively. (a) BLI and (b) PET imaging were performed at various time points using d-luciferin and [^{18}F]-FHBG reporter probes, respectively. The marked difference in PET activities is consistent with the expression of *HSVttk* reporter gene in ESC-TF cells but not ESC-DF cells. Ganciclovir (GCV) treatment was started at week 2 and continued until week 5. After three weeks, ESC-TF cells (right shoulder) were completely ablated by GCV treatment, whereas ESC-DF cells were not affected as they lack *HSVttk*. Reprinted with permission from Cao et al. (2007).

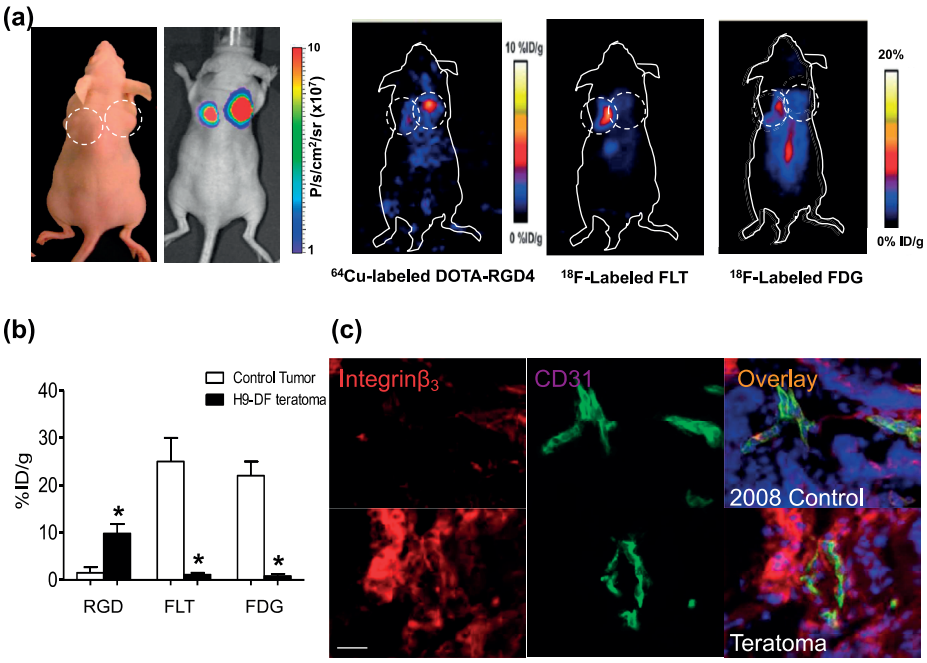


Figure 5. Non-inasive de novo imaging of hESC-derived teratoma formation. MicroPET imaging of 2-deoxy-2-[^{18}F]fluoro-d-glucose ([^{18}F]-FDG), 3'-deoxy-3'-[^{18}F]-fluorothymidine ([^{18}F]-FLT) and ^{64}Cu-DOTA-RGD4 on ESC-derived teratoma. (a) Static photograph and bioluminescence imaging show teratoma formation by H9 hESC-DF cells at the right shoulder and tumour formation by the control 2008 cell line at the left shoulder, which were confirmed by bioluminescence imaging ($7.3 \pm 2.5 \times 10^7$ versus $4.5 \pm 1.6 \times 10^7$ photons s^{-1} cm^{-2} sr^{-1}, respectively, p = n.s.). Specific and prominent uptake of 64Cu-DOTA-RGD4 was found in vascularized teratoma, but not in control human ovarian carcinoma cell line (2008) tumour with low integrin expression ($p < 0.01$). By contrast, hESC-derived teratomas had low uptake of [^{18}F]-FDG and [^{18}F]-FLT, whereas the 2008 ovarian cancer xenografts had both high [^{18}F]-FDG and [^{18}F]-FLT uptake. (b) Quantification of different microPET imaging patterns between ESC-derived teratoma (filled bars) and control human ovarian carcinoma (unfilled bars). *$p < 0.01$. (c) Higher expression of β3 integrin (red) was observed in ESC-derived teratoma (bottom) than that in control 2008 tumour (upper), which can be partly co-localized with CD31 staining (green; blue: DAPI; scale bar = 50 μm). Reprinted with permission from Cao et al. (2009).

DISCUSSION

The field of regenerative medicine using pluripotent stem cells holds great promise if clinical hurdles can be overcome. One significant problem is the tumorigenic property of pluripotent cells. This is highlighted by a recent case report involving a child that received foetal neural stem cells as a treatment for the neurodegenerative disease ataxia telangiectasia but later developed multifocal glioneural tumor from these transplanted neural stem cells (Amariglio et al. 2009). As gene expression of pluripotent cells becomes widely investigated, more and more correlations in gene expression between pluripotent cells and cancer cells

are being found. Not only are some of the pluripotent markers used in the creation of iPSCs directly oncogenic, other pluripotent genes are found to be highly associated with tumor differentiation as well. Because of the tumorigenicity of pluripotent cells, tracking them in vivo is of high importance for future clinical application, and several imaging modalities can be used for this purpose. To make regenerative medicine therapies safe, one option is to use a reporter–suicide gene mechanism that would allow for the in vivo tracking of the transplanted pluripotent cells and would target these cells for elimination in the case of tumor formation (figure 4; (Cao et al. 2007)). Although this study showed ablation of teratomas formed from ESCs, the construct is still based on genetically modifying the pluripotent cells by viral transduction, which has tumorigenic potential as well. Future approaches therefore should focus on site-specific genomic integration approaches such as zinc finger nuclease (Hockemeyer et al. 2009) or phiC31 integrase (Liu et al. 2009) to minimize potential adverse effects to the cells. Alternatively, one could bypass the reporter gene technique by designing molecular probes that target cell surface receptors of teratoma, as was recently demonstrated using 64Cu-labelled RGD tetramer that targets avb3 integrin receptors on hESC-derived teratomas (figure 5; (Cao et al. 2009)). Ultimately, clear insights into the gene expression of pluripotent cells will allow researchers to select a pluripotent cell population with a reduced tumorigenic signature. In addition, the advances in the field of molecular imaging will allow for (i) labelling of these cells without adverse effects to cellular function, (ii) tracking them in vivo with high sensitivity, spatial resolution, and over long periods of time without loss of signal (Thomson et al. 1998), and (iii) targeting these cells upon tumor formation. These exciting novel developments will pave the way for safe regenerative medicine.

REFERENCES

Amado, L. C., A. P. Saliaris, K. H. Schuleri, M. St John, J. S. Xie, S. Cattaneo, . . . J. M. Hare (2005). "Cardiac repair with intramyocardial injection of allogeneic mesenchymal stem cells after myocardial infarction." Proc Natl Acad Sci U S A 102(32): 11474-11479.

Amariglio, N., A. Hirshberg, B. W. Scheithauer, Y. Cohen, R. Loewenthal, L. Trakhtenbrot, . . . G. Rechavi (2009). "Donor-derived brain tumor following neural stem cell transplantation in an ataxia telangiectasia patient." PLoS Med 6(2): e1000029.

Ambrosini, G., C. Adida and D. C. Altieri (1997). "A novel anti-apoptosis gene, survivin, expressed in cancer and lymphoma." Nat Med 3(8): 917-921.

Amit, M., M. K. Carpenter, M. S. Inokuma, C. P. Chiu, C. P. Harris, M. A. Waknitz, . . . J. A. Thomson (2000). "Clonally derived human embryonic stem cell lines maintain pluripotency and proliferative potential for prolonged periods of culture." Dev Biol 227(2): 271-278.

Andrews, P. W., M. M. Matin, A. R. Bahrami, I. Damjanov, P. Gokhale and J. S. Draper (2005). "Embryonic stem (ES) cells and embryonal carcinoma (EC) cells: opposite sides of the same coin." Biochem Soc Trans 33(Pt 6): 1526-1530.

Arai, T., T. Kofidis, J. W. Bulte, J. de Bruin, R. D. Venook, G. J. Berry, . . . P. C. Yang (2006). "Dual in vivo magnetic resonance evaluation of magnetically labeled mouse embryonic stem cells and cardiac function at 1.5 t." Magn Reson Med 55(1): 203-209.

Bae, K. M., Z. Su, C. Frye, S. McClellan, R. W. Allan, J. T. Andrejewski, . . . D. W. Siemann (2010). "Expression of pluripotent stem cell reprogramming factors by prostate tumor initiating cells." J Urol 183(5): 2045-2053.

Ben-Porath, I., M. W. Thomson, V. J. Carey, R. Ge, G. W. Bell, A. Regev and R. A. Weinberg (2008). "An embryonic stem cell-like gene expression signature in poorly differentiated aggressive human tumors." Nat Genet 40(5): 499-507.

Blasberg, R. G. and J. G. Tjuvajev (2003). "Molecular-genetic imaging: current and future perspectives." J Clin Invest 111(11): 1620-1629.

Blum, B., O. Bar-Nur, T. Golan-Lev and N. Benvenisty (2009). "The anti-apoptotic gene survivin contributes to teratoma formation by human embryonic stem cells." Nat Biotechnol 27(3): 281-287.

Blum, B. and N. Benvenisty (2008). "The tumorigenicity of human embryonic stem cells." Adv Cancer Res 100: 133-158.

Blum, B. and N. Benvenisty (2009). "The tumorigenicity of diploid and aneuploid human pluripotent stem cells." Cell Cycle 8(23): 3822-3830.

Cao, F., M. Drukker, S. Lin, A. Y. Sheikh, X. Xie, Z. Li, . . . J. C. Wu (2007). "Molecular imaging of embryonic stem cell misbehavior and suicide gene ablation." Cloning Stem Cells 9(1): 107-117.

Cao, F., Z. Li, A. Lee, Z. Liu, K. Chen, H. Wang, . . . J. C. Wu (2009). "Noninvasive de novo imaging of human embryonic stem cell-derived teratoma formation." Cancer Res 69(7): 2709-2713.

Cao, F., S. Lin, X. Xie, P. Ray, M. Patel, X. Zhang, . . . J. C. Wu (2006). "In vivo visualization of embryonic stem cell survival, proliferation, and migration after cardiac delivery." Circulation 113(7): 1005-1014.

Cao, F., R. A. Wagner, K. D. Wilson, X. Xie, J. D. Fu, M. Drukker, . . . J. C. Wu (2008). "Transcriptional and functional profiling of human embryonic stem cell-derived cardiomyocytes." PLoS One 3(10): e3474.

Chaudhry, G. R., C. Fecek, M. M. Lai, W. C. Wu, M. Chang, A. Vasquez, . . . M. T. Trese (2009). "Fate of embryonic stem cell derivatives implanted into the vitreous of a slow retinal degenerative mouse model." Stem Cells Dev 18(2): 247-258.

Chiou, S.-H., C.-C. Yu, C.-Y. Huang, S.-C. Lin, C.-J. Liu, T.-H. Tsai, . . . J.-F. Lo (2008). "Positive correlations of Oct-4 and Nanog in oral cancer stem-like cells and high-grade oral squamous cell carcinoma." Clin Cancer Res 14(13): 4085-4095.

Cowan, C. A., J. Atienza, D. A. Melton and K. Eggan (2005). "Nuclear reprogramming of somatic cells after fusion with human embryonic stem cells." Science 309(5739): 1369-1373.

D'Amour, K. A., A. G. Bang, S. Eliazer, O. G. Kelly, A. D. Agulnick, N. G. Smart, . . . E. E. Baetge (2006). "Production of pancreatic hormone-expressing endocrine cells from human embryonic stem cells." Nat Biotechnol 24(11): 1392-1401.

Draper, J. S., K. Smith, P. Gokhale, H. D. Moore, E. Maltby, J. Johnson, . . . P. W. Andrews (2004). "Recurrent gain of chromosomes 17q and 12 in cultured human embryonic stem cells." Nat Biotechnol 22(1): 53-54.

Dubertret, B., P. Skourides, D. J. Norris, V. Noireaux, A. H. Brivanlou and A. Libchaber (2002). "In vivo imaging of quantum dots encapsulated in phospholipid micelles." Science 298(5599): 1759-1762.

Eilers, M. and R. N. Eisenman (2008). "Myc's broad reach." Genes Dev 22(20): 2755-2766.

Evans, M. J. and M. H. Kaufman (1981). "Establishment in culture of pluripotential cells from mouse embryos." Nature 292(5819): 154-156.

Hinds, K. A., J. M. Hill, E. M. Shapiro, M. O. Laukkanen, A. C. Silva, C. A. Combs, . . . C. E. Dunbar (2003). "Highly efficient endosomal labeling of progenitor and stem cells with large magnetic particles allows magnetic resonance imaging of single cells." Blood 102(3): 867-872.

Hochedlinger, K., Y. Yamada, C. Beard and R. Jaenisch (2005). "Ectopic expression of Oct-4 blocks progenitor-cell differentiation and causes dysplasia in epithelial tissues." Cell 121(3): 465-477.

Hockemeyer, D., F. Soldner, C. Beard, Q. Gao, M. Mitalipova, R. C. DeKelver, . . . R. Jaenisch (2009). "Efficient targeting of expressed and silent genes in human ESCs and iPSCs using zinc-finger nucleases." Nat Biotechnol 27(9): 851-857.

Hofmann, M., K. C. Wollert, G. P. Meyer, A. Menke, L. Arseniev, B. Hertenstein, . . . H. Drexler (2005). "Monitoring of bone marrow cell homing into the infarcted human myocardium." Circulation 111(17): 2198-2202.

Jaiswal, J. K., H. Mattoussi, J. M. Mauro and S. M. Simon (2003). "Long-term multiple color imaging of live cells using quantum dot bioconjugates." Nat Biotechnol 21(1): 47-51.

Kang, W. J., H. J. Kang, H. S. Kim, J. K. Chung, M. C. Lee and D. S. Lee (2006). "Tissue distribution of 18F-FDG-labeled peripheral hematopoietic stem cells after intracoronary administration in patients with myocardial infarction." J Nucl Med 47(8): 1295-1301.

Keravala, A., S. Lee, B. Thyagarajan, E. C. Olivares, V. E. Gabrovsky, L. E. Woodard and M. P. Calos (2009). "Mutational derivatives of PhiC31 integrase with increased efficiency and specificity." Mol Ther 17(1): 112-120.

Kleinsmith, L. J. and G. B. Pierce, Jr. (1964). "Multipotentiality of Single Embryonal Carcinoma Cells." Cancer Res 24: 1544-1551.

Knoepfler, P. S. (2009). "Deconstructing stem cell tumorigenicity: a roadmap to safe regenerative medicine." Stem Cells 27(5): 1050-1056.

Kraitchman, D. L., A. W. Heldman, E. Atalar, L. C. Amado, B. J. Martin, M. F. Pittenger, . . . J. W. Bulte (2003). "In vivo magnetic resonance imaging of mesenchymal stem cells in myocardial infarction." Circulation 107(18): 2290-2293.

Laflamme, M. A., K. Y. Chen, A. V. Naumova, V. Muskheli, J. A. Fugate, S. K. Dupras, . . . C. E. Murry (2007). "Cardiomyocytes derived from human embryonic stem cells in pro-survival factors enhance function of infarcted rat hearts." Nat Biotechnol 25(9): 1015-1024.

Lee, A. S., C. Tang, F. Cao, X. Xie, K. van der Bogt, A. Hwang, . . . J. C. Wu (2009). "Effects of cell number on teratoma formation by human embryonic stem cells." Cell Cycle 8(16): 2608-2612.

Li, F., G. Ambrosini, E. Y. Chu, J. Plescia, S. Tognin, P. C. Marchisio and D. C. Altieri (1998). "Control of apoptosis and mitotic spindle checkpoint by survivin." Nature 396(6711): 580-584.

Li, Z., Y. Suzuki, M. Huang, F. Cao, X. Xie, A. J. Connolly, . . . J. C. Wu (2008). "Comparison of reporter gene and iron particle labeling for tracking fate of human embryonic stem cells and differentiated endothelial cells in living subjects." Stem Cells 26(4): 864-873.

Lin, S., X. Xie, M. R. Patel, Y. H. Yang, Z. Li, F. Cao, . . . J. C. Wu (2007). "Quantum dot imaging for embryonic stem cells." BMC Biotechnol 7: 67.

Liu, J., E. C. Cheng, R. C. Long, S. H. Yang, L. Wang, P. H. Cheng, . . . A. W. Chan (2009). "Noninvasive monitoring of embryonic stem cells in vivo with MRI transgene reporter." Tissue Eng Part C Methods 15(4): 739-747.

Liu, Y., B. Thyagarajan, U. LakshMiPathy, H. Xue, P. Lieu, A. Fontes, . . . J. D. Chesnut (2009). "Generation of platform human embryonic stem cell lines that allow efficient targeting at a predetermined genomic location." Stem Cells Dev 18(10): 1459-1472.

MacLaren, D. C., S. S. Gambhir, N. Satyamurthy, J. R. Barrio, S. Sharfstein, T. Toyokuni, . . . H. R. Herschman (1999). "Repetitive, non-invasive imaging of the dopamine D2 receptor as a reporter gene in living animals." Gene Ther 6(5): 785-791.

Malashicheva, A. B., T. V. Kisliakova, P. Savatier and V. A. Pospelov (2002). "[Embryonal stem cells do not undergo cell cycle arrest upon exposure to damaging factors]." Tsitologiia 44(7): 643-648.

Mantel, C., Y. Guo, M. R. Lee, M. K. Kim, M. K. Han, H. Shibayama, . . . H. E. Broxmeyer (2007). "Checkpoint-apoptosis uncoupling in human and mouse embryonic stem cells: a source of karyotpic instability." Blood 109(10): 4518-4527.

Martin, G. R. (1981). "Isolation of a pluripotent cell line from early mouse embryos cultured in medium conditioned by teratocarcinoma stem cells." Proc Natl Acad Sci USA 78(12): 7634-7638.

Miyagawa, M., M. Beyer, B. Wagner, M. Anton, C. Spitzweg, B. Gansbacher, . . . F. M. Bengel (2005). "Cardiac reporter gene imaging using the human sodium/iodide symporter gene." Cardiovasc Res 65(1): 195-202.

Mostert, M. C., A. J. Verkerk, M. van de Pol, J. Heighway, P. Marynen, C. Rosenberg, . . . L. H. Looijenga (1998). "Identification of the critical region of 12p over-representation in testicular germ cell tumors of adolescents and adults." Oncogene 16(20): 2617-2627.

Nakagawa, M., N. Takizawa, M. Narita, T. Ichisaka and S. Yamanaka (2010). "Promotion of direct reprogramming by transformation-deficient Myc." Proc Natl Acad Sci U S A 107(32): 14152-14157.

Nussbaum, J., E. Minami, M. A. Laflamme, J. A. Virag, C. B. Ware, A. Masino, . . . C. E. Murry (2007). "Transplantation of undifferentiated murine embryonic stem cells in the heart: teratoma formation and immune response." FASEB J 21(7): 1345-1357.

Okita, K., T. Ichisaka and S. Yamanaka (2007). "Generation of germline-competent induced pluripotent stem cells." Nature 448(7151): 313-317.

Oosterhuis, J. W. and L. H. J. Looijenga (2005). "Testicular germ-cell tumors in a broader perspective." Nat Rev Cancer 5(3): 210-222.

Palma, I., R.-Y. Peña, A. Contreras, G. Ceballos-Reyes, N. Coyote, L. Eraña, . . . G. Queipo (2008). "Participation of OCT3/4 and beta-catenin during dysgenetic gonadal malignant transformation." Cancer Lett 263(2): 204-211.

Pierce, G. B., Jr., F. J. Dixon, Jr. and E. L. Verney (1960). "Teratocarcinogenic and tissue-forming potentials of the cell types comprising neoplastic embryoid bodies." Lab Invest 9: 583-602.

Schachinger, V., A. Aicher, N. Dobert, R. Rover, J. Diener, S. Fichtlscherer, . . . A. M. Zeiher (2008). "Pilot trial on determinants of progenitor cell recruitment to the infarcted human myocardium." Circulation 118(14): 1425-1432.

Sperger, J. M., X. Chen, J. S. Draper, J. E. Antosiewicz, C. H. Chon, S. B. Jones, . . . J. A. Thomson (2003). "Gene expression patterns in human embryonic stem cells and human pluripotent germ cell tumors." Proc Natl Acad Sci USA 100(23): 13350-13355.

Stevens, L. C. (1964). "Experimental Production of Testicular Teratomas in Mice." Proc Natl Acad Sci U S A 52: 654-661.

Stevens, L. C. (1967). "Origin of testicular teratomas from primordial germ cells in mice." J Natl Cancer Inst 38(4): 549-552.

Stevens, L. C. (1968). "The development of teratomas from intratesticular grafts of tubal mouse eggs." J Embryol Exp Morphol 20(3): 329-341.

Stevens, L. C. and K. P. Hummel (1957). "A description of spontaneous congenital testicular teratomas in strain 129 mice." J Natl Cancer Inst 18(5): 719-747.

Tada, M., Y. Takahama, K. Abe, N. Nakatsuji and T. Tada (2001). "Nuclear reprogramming of somatic cells by in vitro hybridization with ES cells." Curr Biol 11(19): 1553-1558.

Takahashi, K., K. Tanabe, M. Ohnuki, M. Narita, T. Ichisaka, K. Tomoda and S. Yamanaka (2007). "Induction of pluripotent stem cells from adult human fibroblasts by defined factors." Cell 131(5): 861-872.

Takahashi, K. and S. Yamanaka (2006). "Induction of pluripotent stem cells from mouse embryonic and adult fibroblast cultures by defined factors." Cell 126(4): 663-676.

Thomson, J. A., J. Itskovitz-Eldor, S. S. Shapiro, M. A. Waknitz, J. J. Swiergiel, V. S. Marshall and J. M. Jones (1998). "Embryonic stem cell lines derived from human blastocysts." Science 282(5391): 1145-1147.

van der Bogt, K. E. A., R.-J. Swijnenburg, F. Cao and J. C. Wu (2006). "Molecular imaging of human embryonic stem cells: keeping an eye on differentiation, tumorigenicity and immunogenicity." Cell Cycle 5(23): 2748-2752.

Wilmut, I., A. E. Schnieke, J. McWhir, A. J. Kind and K. H. Campbell (1997). "Viable offspring derived from fetal and adult mammalian cells." Nature 385(6619): 810-813.

Wu, J. C., F. Cao, S. Dutta, X. Xie, E. Kim, N. Chungfat, . . . E. W. Wang (2006). "Proteomic analysis of reporter genes for molecular imaging of transplanted embryonic stem cells." Proteomics 6(23): 6234-6249.

Wu, J. C., J. M. Spin, F. Cao, S. Lin, X. Xie, O. Gheysens, . . . T. Quertermous (2006). "Transcriptional profiling of reporter genes used for molecular imaging of embryonic stem cell transplantation." Physiol Genomics 25(1): 29-38.

Xie, X., F. Cao, A. Y. Sheikh, Z. Li, A. J. Connolly, X. Pei, . . . J. C. Wu (2007). "Genetic modification of embryonic stem cells with VEGF enhances cell survival and improves cardiac function." Cloning Stem Cells 9(4): 549-563.

Xie, X., A. Hiona, A. S. Lee, F. Cao, M. Huang, Z. Li, . . . J. C. Wu (2010). "Effects of Long Term Culture on Human Embryonic Stem Cell Aging." Stem Cells Dev.

Yaghoubi, S. S., M. C. Jensen, N. Satyamurthy, S. Budhiraja, D. Paik, J. Czernin and S. S. Gambhir (2009). "Noninvasive detection of therapeutic cytolytic T cells with 18F-FHBG PET in a patient with glioma." Nat Clin Pract Oncol 6(1): 53-58.

Yang, D., Z. J. Zhang, M. Oldenburg, M. Ayala and S. C. Zhang (2008). "Human embryonic stem cell-derived dopaminergic neurons reverse functional deficit in parkinsonian rats." Stem Cells 26(1): 55-63.

Yu, J., M. A. Vodyanik, K. Smuga-Otto, J. Antosiewicz-Bourget, J. L. Frane, S. Tian, . . . J. A. Thomson (2007). "Induced pluripotent stem cell lines derived from human somatic cells." Science 318(5858): 1917-1920.

Zhao, X. Y., W. Li, Z. Lv, L. Liu, M. Tong, T. Hai, . . . Q. Zhou (2009). "iPS cells produce viable mice through tetraploid complementation." Nature 461(7260): 86-90.

Chapter 7

Immunogenicity of PSCs and PSC-derived cell grafts

Kooreman, N.G.[*]*, de Almeida, P.E.*[*]*, Meyer, E.H.*[*]*, Diecke, S., Dey, D., Sanchez-Freire, V., Hu, S., Ebert, A., Odegaard, J., Mordwinkin, N.M., et al. (2014). Transplanted terminally differentiated induced pluripotent stem cells are accepted by immune mechanisms similar to self-tolerance.* **Nature Communications,** *5, 3903.*
[*] *authors contributed equally*

ABSTRACT

The exact nature of the immune response elicited by autologous-induced pluripotent stem cell (iPSC) progeny is still not well understood. Here we show in murine models that autologous iPSC-derived endothelial cells (iECs) elicit an immune response that resembles the one against a comparable somatic cell, the aortic endothelial cell (AEC). These cells exhibit long-term survival *in vivo* and prompt a tolerogenic immune response characterized by elevated IL-10 expression. In contrast, undifferentiated iPSCs elicit a very different immune response with high lymphocytic infiltration and elevated IFN-γ, granzyme-B and perforin intragraft. Furthermore, the clonal structure of infiltrating T cells from iEC grafts is statistically indistinguishable from that of AECs, but is different from that of undifferentiated iPSC grafts. Taken together, our results indicate that the differentiation of iPSCs results in a loss of immunogenicity and leads to the induction of tolerance, despite expected antigen expression differences between iPSC-derived versus original somatic cells.

INTRODUCTION

Pluripotent stem cells can be artificially generated in vitro by introducing a combination of defined factors into somatic cells (Takahashi and Yamanaka 2006, Takahashi et al. 2007). These cells, termed induced pluripotent stem cells (iPSCs), can differentiate into essentially any somatic cells and thus hold exceptional potential as sources of therapeutic cells for personalized medical applications such as organ repair. From an immunological standpoint, this technology brings tremendous benefits because patients could be treated with autologous cells, thereby avoiding life-long immunosuppressive therapy currently required for preventing rejection of allografts, which is costly and associated with significant side effects. However, the unexpected immunogenicity of syngeneic iPSCs demonstrated by a previous study (Zhao et al. 2011) raised serious concerns about the value of these iPSCs as a source of autologous cellular therapeutics. Slight differences in antigen repertoire introduced by neoantigens arising from genomic alterations acquired during the reprogramming process, or during the differentiation of iPSCs into the desired tissue, can profoundly alter the immunogenicity profiles (Mullally and Ritz 2007, Nicholls et al. 2009, Boyd and Wood 2010, Ben-David et al. 2013). Hence, a thorough assessment of the immunological phenotype elicited by tissues derived from iPSCs is essential prior to the potential translation of this technology into clinics.

In this study, we sought to delineate the impact of terminal differentiation of iPSCs on immunogenicity of their progeny using an autologous mouse model of transplantation and to determine how closely the immunological phenotype elicited by these cells relates to that of corresponding self-somatic cells. We show that autologous endothelial tissues derived from iPSCs can elicit an immune response that resembles the one against self, as represented by the aortic endothelial cells (AECs). These cells exhibited long-term survival in vivo and elicited an immune contexture consistent with self-tolerance. By contrast, autologous undifferentiated iPSCs were rejected with hallmark features of lymphocytic infiltration accompanied by abundant expression of interferon-γ and cytotoxic factors (granzyme-B and perforin). To further examine the immunological relatedness among iECs, AECs, and undifferentiated iPSCs, we used high-throughput T cell receptor (TCR) sequencing analysis and found that the clonal structure of infiltrating T cells found in iEC grafts was statistically indistinguishable from that of AEC grafts, but was clearly different from that of undifferentiated iPSC grafts. Taken together, our results demonstrate that differentiation of iPSCs could result in a loss of immunogenicity and in immunological responses that are similar to the one elicited by a corresponding self somatic cell.

RESULTS

Murine iPSCs are rejected in syngeneic recipients

In order to determine the survival kinetics of iPSCs in vivo, fibroblasts from transgenic FVB mice ubiquitously expressing green fluorescence protein and luciferase (GFP.Luc+) were used to generate iPSC lines using two approaches. Reprogramming of fibroblasts was performed using a lentiviral-based or a minicircle plasmid-based approach (genome-integration free) for delivery of the 4 reprogramming factors (Klf4, Oct-4, Sox-2, and c-Myc) as described elsewhere (Takahashi and Yamanaka 2006, Jia et al. 2010). The resulting iPSCs were characterized for pluripotency (Supplementary Fig. 1) and their immunogenicity assessed in syngeneic versus immunodeficient recipients. Transgenic expression of the luciferase reporter gene allowed tracking of iPSCs in vivo by bioluminescence imaging (BLI) over the course of the experiment. Mouse iPSCs (1×10^6) were implanted intra-muscularly in the legs of syngeneic FVB mice. BLI tracking of cell survival revealed a complete loss of bioluminescence in both lentiviral- and minicircle-derived iPSCs by days 21 and 42, respectively (Fig. 1a). By contrast, bioluminescence of two iPSC lines persisted in immunodeficient NOD/SCID mice, showing a substantial increase over time consistent with teratoma development. These results suggest that the loss of iPSC bioluminescence observed in syngeneic recipients was due to immunological rejection. A consecutive challenge of iPSC-primed mice with syngeneic iPSCs resulted in the accelerated loss of bioluminescence signals, suggesting that antigen-specific immunological memory had developed (Fig. 1b). To rule out the possibility that the immune response against iPSCs was elicited by the expression of GFP and luciferase, endpoint survival of a lentiviral iPSC line (B6.129.F1) free of these reporter transgenes was also examined (Meissner et al. 2007). To facilitate graft explantation, these reporter transgene-free iPSCs were implanted subcutaneously in the dorsa of syngeneic and immunodeficient mice and removed after 30 days in vivo. Mouse iPSC grafts explanted from syngeneic mice did not show histological features consistent with teratomas (i.e., 3 germ-layer structure) (Supplementary Fig. 2a) and were significantly smaller in size compared to grafts extracted from immunodeficient animals (Supplementary Fig. 2b). To gain additional insight into the quality of the immune response elicited by the syngeneic reporter transgene-free iPSCs, splenocytes from iPSC-primed or naïve syngeneic (B6.129.F10) or allogeneic (BALB/c, C57BL/6, and FVB) mice were re-exposed to B6.129.F1 iPSCs ex vivo for 24h, and IFN-γ production was measured by ELISPOT. Production of IFN-γ by syngeneic mice was statistically undistinguishable to two allogeneic mouse strains (BALB/c and FVB) but significantly lower than the C57BL/6 allogeneic mouse strain (Supplementary Fig. 2c). To further examine the effect of IFN-γ on the rejection of these cells, a third iPSC line (C57BL/6) was implanted subcutaneously in the dorsa of syngeneic wild type or in IFN-γ knockout (IFN-γ−/−) C57BL/6 recipients. The status of the iPSC grafts was evaluated

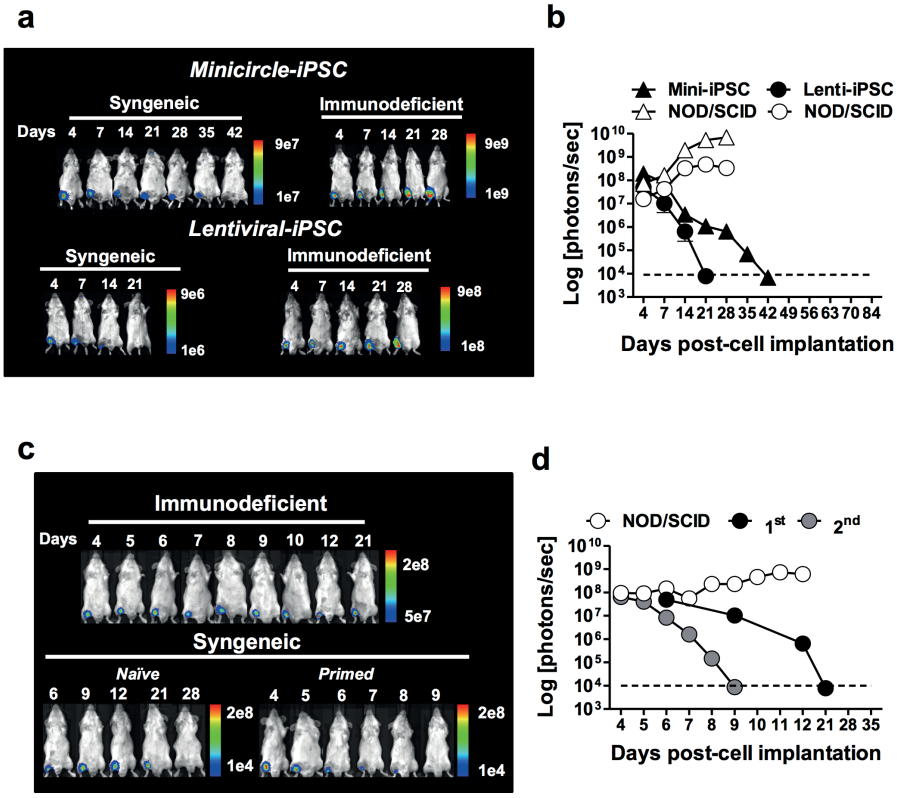


Figure 1. Undifferentiated iPSCs derived by LV or genome-integration-free strategies are rejected in syngeneic recipients. LV or minicircle-derived iPSCs expressing GFP and luciferase were injected intramuscularly in syngeneic or immunodeficient recipients, and their survival was monitored in vivo by bioluminescence imaging (BLI). (a) Representative BLI from one mouse per group demonstrating the longitudinal survival of minicircle- and LV-derived iPSCs in syngeneic and immunodeficient recipients. (b) Mean±s.e.m. bioluminescence of minicircle- versus LV-derived iPSCs in syngeneic and immunodeficient recipients demonstrating a progressive decay in bioluminescence to background levels by 42 days following implantation. After complete decay of bioluminescence signal, mice received a second injection of iPSCs. (c,d) Bioluminescence of iPSCs implanted in primed animals (2nd) had an accelerated decay compared with those receiving the first cell injection (1st). Data are representative of at least 10 animals and 3 independent experiments.

30 days post-implantation and, as expected, rejection of iPSCs was abrogated in IFN-γ−/− recipients (Supplementary Fig. 2d).

The contextual cellularity of iPSC grafts extracted from syngeneic and immunodeficient mice were drastically different (Supplementary Fig. 3a). Grafts from syngeneic mice comprised predominantly of pauricellular Matrigel and adipocytes but also contained small areas of undifferentiated iPSCs that could still be detected for up to 14 days post-implantation (Supplementary Fig. 3b). Surprisingly, large nodules of undifferentiated iPSCs could still be found in teratomas extracted from immunodeficient mice for at least 30 days post-cell implantation (Supplementary Fig. 3c). Differences in the contextual cellularity of grafts

extracted from syngeneic and immunodeficient mice support the premise that iPSCs, or the early progenitors that spontaneously differentiate upon transplantation, are immunogenic. The ability of iPSCs to elicit immune response in a syngeneic setting was also assessed by measuring ex-vivo cytokine responses by splenocytes from mice primed with syngeneic iPSCs. Primed splenocytes co-cultured with syngeneic iPSCs released significantly higher abundance of cytokines associated with innate as well as adaptive immune responses compared to naïve splenocytes (Supplementary Fig. 4). Although iPSCs did undergo certain level of differentiation during the 3 day-assay, 'terminal' differentiation of cells did not occur. Overall, these results support the premise that undifferentiated iPSCs or their early progenitors, which may still carry antigenic determinants from the parental iPSCs, are intrinsically immunogenic and elicit an immune response with strong pro-inflammatory and T-helper 1 (TH1) elements.

Terminal differentiation enables survival of iECs in syngeneic mice

GFP.Luc+ iPSCs generated by lentiviral-based reprograming were differentiated in vitro into endothelial cells as previously described (Li et al. 2007, Huang et al. 2010), and purified by FACS sorting, based on the expression of CD144 and CD31 (Supplementary Fig. 5a). Mouse iECs exhibited transcriptome (Supplementary Fig. 5b) and surface protein marker (Supplementary Fig. 5c–d) profiles that are consistent with endothelial cells. Furthermore, iECs displayed a functional phenotype consistent with endothelial cells, including the production of extracellular matrix material (Supplementary Fig. 5e), uptake of low-density lipoprotein (Supplementary Fig. 5f), and vasculogenesis (Supplementary Fig. 5g). Expression of major histocompatibility complex (MHC) molecules (class-I and class-II) was similar between iECs and AECs (Supplementary Fig. 5h). Functionality and tumorigenicity of iECs were also tested in vivo. In a hindlimb ischemia model, immunodeficient mice were injected with either iECs or vehicle. Engraftment of iECs as well as blood flow in the injured hindlimb were assessed by immunofluorescence staining and laser Doppler perfusion, respectively, 14 days post-cell implantation. iECs successfully engrafted and improved blood perfusion in the hindlimb ischemia model (Supplementary Fig. 6a). Histological evaluation of transplanted murine iECs in the ischemic hindlimb revealed muscle atrophy and degeneration, but no signs of teratoma formation (Supplementary Fig. 6b). Furthermore, immunofluorescence staining for CM-DiI labeled iPSC-ECs verified the localization and survival of iECs in the ischemic hindlimbs (Supplementary Fig. 6c). Assessment of syngeneic iECs' immunogenicity was then carried out in vivo and compared to the immunogenicity of the parental iPSC line and to the corresponding syngeneic somatic cell, AEC (Supplementary Fig. 7). To determine the kinetics of cell survival in vivo, cells ($1x10^6$) were mixed in Matrigel able to maintain graft integrity in situ, and implanted subcutaneously in the dorsa of syngeneic recipients. Survival was monitored by bioluminescence imaging over 63 days. Unlike iPSCs, bioluminescence signals of iECs and AECs were sustained throughout the entire period (Fig

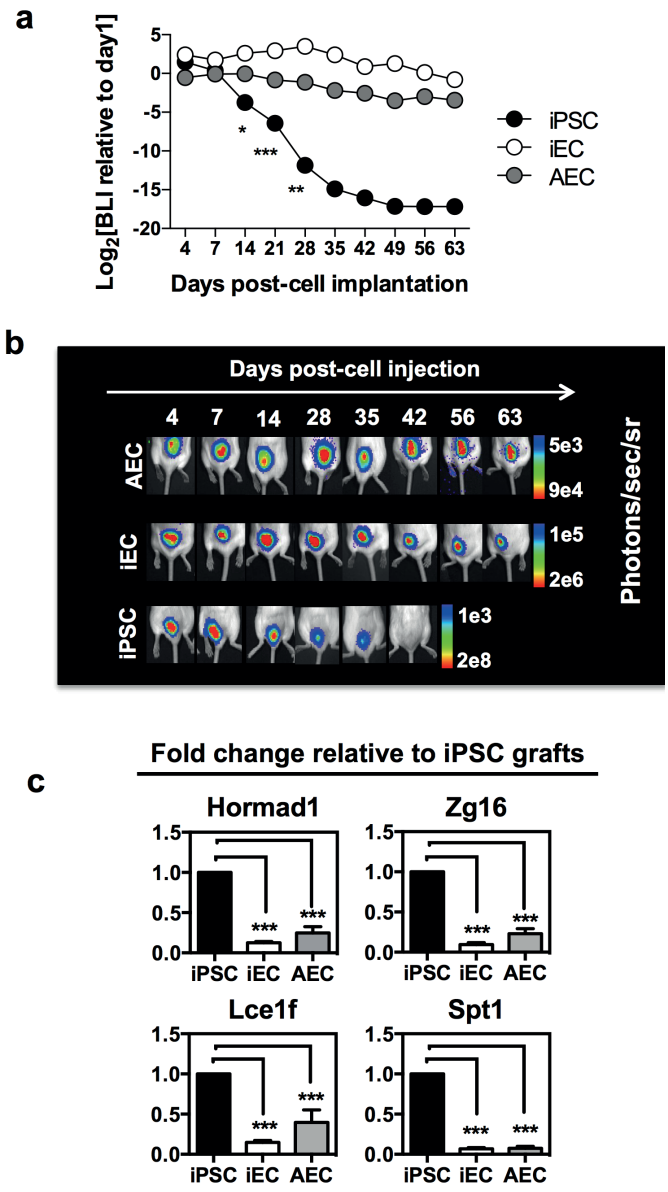


Figure 2. Terminal differentiation of iPSCs results in prolonged survival in vivo and in loss of antigenic determinants. (a) Cellular bioluminescence intensity normalized to day 1 demonstrate a prolonged survival of iECs and AECs relative to iPSCs. (b) Representative bioluminescence images from one animal from each of the three groups over 63 days. Bioluminescence data are representative of two independent experiments with 3–4 animals per group. (c) Gene expression fold-change in iEC and AEC grafts relative to iPSC grafts. Genes previously shown to elicit T-cell-mediated immunological rejection of iPSCs were significantly down- regulated in iEC and AEC grafts. Data are representative of mean±s.e.m. of eight biological replicates from three independent experiments. Significance of differences between series of results was assessed using analysis of variance with Tukey for multiple comparisons. *P < 0.05, **P < 0.01, ***P < 0.001.

2a–b). The long-term survival of iECs and AECs in syngeneic recipients provides additional evidence that rejection of iPSCs was not due to alloresponses directed against the reporter transgenes (GFP and luciferase). The survival of iECs and AECs was accompanied by a down-regulation of genes previously shown to elicit T cell-mediated rejection of iPSCs in syngeneic mice 3, including HORMA domain-containing protein 1 (Hormad1) and zymogen granule protein 16 (Zg16) (Fig. 2c).

Immune response elicited by iECs is similar to the one elicited by self

In order to elucidate and compare the nature of the immune response elicited by different cell types, we next implanted subcutaneously lentivirally-derived iPSCs devoid of reporter transgenes (B6.129.F1), their progeny iECs, and AECs. Cellular grafts were explanted at day 14 and digested enzymatically for cell retrieval. Flow cytometric analysis of the retrieved cells revealed a prominent lymphocytic infiltration in iPSC grafts compared to iEC, AEC, and sham (Matrigel only) grafts (Fig. 3a). T cell infiltration was detected in all graft types but was negligible in sham grafts. This suggests that the vehicle used for cell injection had a minimal effect on the immunological response that developed against the different cellular grafts. iECs and AECs elicited similar T cell infiltration (~4–5% of $CD45^+$ leukocytes), with $CD4^+$ T cells being the most prevalent T cell type found in these grafts (accounting for ~80% of the $CD3^+$ infiltrating T cells) (Fig. 3b–c). Overall, macrophages ($F4/80^+$) represented the majority of the leukocytes infiltrating iECs, AECs, and sham grafts (Supplementary Fig. 8a). The percentage of FoxP3-expressing $CD4^+$ T cells detected in iEC grafts was statistically undistinguishable from the one found in AECs but was significantly lower than in iPSC (Fig. 3d). At the transcript level, FoxP3 expression in iEC and AEC grafts were elevated compared to iPSC but these differences did not reach statistical significance (Supplementary Fig. 8b). By contrast, a much more hostile immune response was elicited by iPSCs, with significantly higher infiltration of T cells, and $CD8^+$ T cells representing ~50% of the T cell infiltrates (Fig. 3b–c). To further characterize the immunobiology of iECs compared to 'self' (AECs) and the parental iPSC lines, mRNA expression of cytokines and cytolytic factors known to be important in rejection responses was measured intra-graft. Expression analysis revealed a significant up-regulation of granzyme-B, perforin, and IFN-γ in iPSC grafts compared to iEC and AEC grafts (Fig. 3e). These results suggest that with terminal differentiation, iECs may approach a state of 'self' and are tolerated by the immune system.

iPSC immunogenicity is not dictated by reprogramming method

In order to determine the potential immunologic effects associated with residual viral DNA in the iPSCs and iEC progeny, an additional integration-free iPSC line was generated. Reprogramming of murine tail fibroblasts was performed using a novel codon optimized mini-intronic plasmid (MIP) expressing the four reprogramming factors Oct4, KLF4, Sox2 and c-Myc. MIP-iPSCs were then differentiated to endothelial cells (MIP-iECs) and

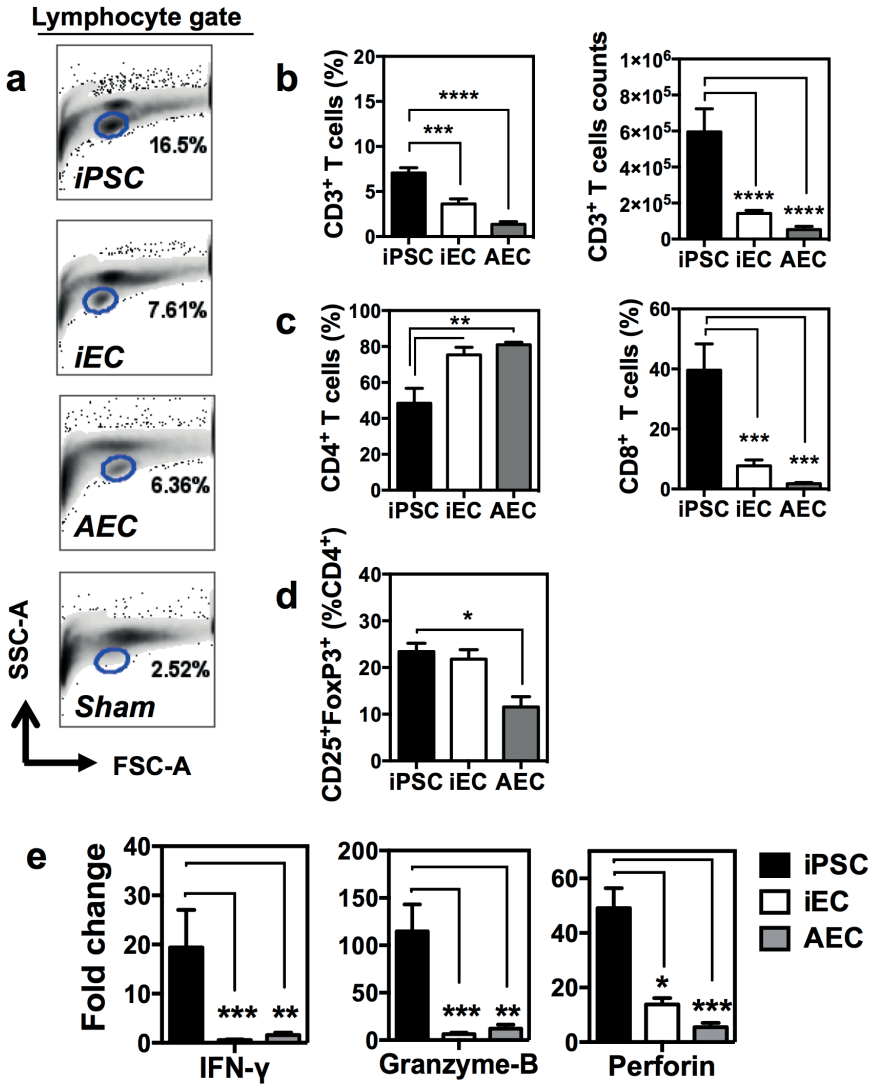


Figure 3. Immune response elicited by iECs resembled the one by AECs. Lymphocytic infiltration in cellular grafts was measured by FACS. (a) The iPSC graft displayed marked increase in lymphocytes compared with iEC, AEC and sham grafts. (b) Percentage (left) and absolute counts (right) of infiltrating $CD3^+$ T cells was reduced in terminally differentiated iECs and AECs. (c) Helper $CD4^+$ T cells were predominant among the T cells infiltrating iEC and AEC grafts. By contrast, cytotoxic ($CD8^+$) T cells were found at a much higher percentage in iPSC grafts. Percentages of $CD4^+$ and $CD8^+$ cells were calculated from CD3 parental gate. (d) Percentage of FoxP3 expression in $CD4^+$ T cells demonstrating higher prevalence in iPSC compared to AEC grafts. (e) Fold-change in gene expression relative to sham grafts demonstrating the differences in immunological milieu intragrafts, with iPSCs having significantly higher mRNA expression of Granzyme-B and Perforin factors compared with iEC and AEC grafts. Data are representative of mean±s.e.m. of eight animals per group from three experiments. Significance of differences between series of results was assessed using analysis of variance with Tukey for multiple comparisons. *P < 0.05, **P < 0.01, ***P < 0.001, ****P < 0.0001.

characterized for endothelial phenotype (Supplementary Fig. 9). Subsequently, MIP-iECs were implanted into syngeneic recipients and grafts characterized for elements of innate and adaptive immune response such as the percentages of infiltrating immunosuppressive versus pro-inflammatory cell types compared to endothelial cells derived from lentiviral-reprogrammed iPSCs (LV-iECs). Interestingly, our results suggest that transplantation of integration-free non-viral MIP-iECs may not be immunologically advantageous over its lentiviral counterpart. MIP-iECs elicited a 10% higher infiltration of neutrophils compared to LV-iECs (Fig. 4a). Among the $CD4^+$ and $CD8^+$ T cells infiltrating MIP-iEC grafts, a higher percentage had an effector memory phenotype ($CD44^+$) compared to LV-iEC (Fig. 4b,c). Among the $CD4^+$ T cells infiltrating the LV-iEC grafts, a higher percentage of them expressed the activation marker CD69 (Fig. 4c), but it is important to note that CD69 expression has also been reported in T regulatory cells known to suppress T cell prolifera-

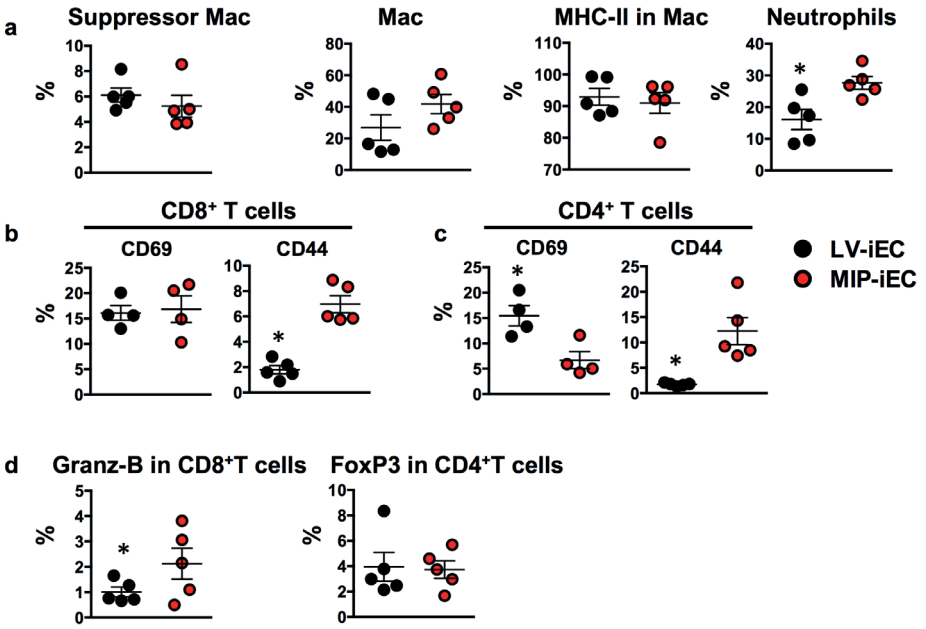


Figure 4. FACS analysis of digested LV-iEC and MIP-iEC grafts show differences in immune response elicited in syngeneic recipients. (a) Among the leukocytes infiltrating MIP-iEC and LV-iEC grafts, macrophages (Mac) with either suppressor ($CD3^-$ $CD11b^+$ $CD11c^-$ $Gr1^+$) or activated ($CD3^-$ $CD11b^+$ $CD11c^+$ $MHC\text{-}II^+$ $Gr1^-$) phenotype were present at similar proportions. MIP-iEC grafts had a significantly higher prevalence of neutrophils ($CD3^-$ $CD11b^-$ $CD11c^-$ $Gr1^+$) compared with LViEC. (b,c) A higher percentage of $CD8^+$ and $CD4^+$ T cells infiltrating MIP-iEC grafts expressed CD44 effector memory marker compared with the ones infiltrating LV-iEC grafts. (d) $CD8^+$ T cells infiltrating MIP-iEC grafts had a significantly higher expression of granzyme-B (Granz-B) compared with the ones infiltrating LV-iEC grafts. The percentage of $FoxP3^+$ -expressing CD4+ T cells infiltrating the MIP-iEC and LV-iEC grafts was indistinguishable. Data are representative of mean±s.e.m. of 4–5 animals per group from one experiment. Significance of differences between series of results was assessed using two-tailed unpaired Student's t-test; $^*P < 0.05$.

tion among other suppressive functions (Han et al. 2009). Furthermore, the percentage of $CD8^+$ T cells-expressing granzyme-B, a serine protease released with cytotoxic activity, was significantly higher in MIP-iEC compared to LV-iEC grafts (Fig. 4d). Finally, the percentage of $FoxP3^+$-expressing $CD4^+$ T cells was undistinguishable between MIP- and LV-iEC grafts. Taken together, these data suggest that viral-based methods of iPSC reprogramming may not be any less advantageous than non-viral integration-free-based methods in the context of establishing non-immunogenic iPSC derivatives. We believe that other factors, such as partial reprogramming or genetic instabilities, are likely to play a much more relevant role in dictating the immunological fate of iPSC progeny.

Terminally differentiated iECs elicit tolerance intra-graft

In order to better characterize the events that led to the acceptance of iECs, the expression of 84 genes linked to T cell quiescence and tolerance was quantified in iEC and iPSC grafts. Expression analysis revealed a panel of 19 genes that were significantly up-regulated in iEC compared to iPSC grafts (Supplementary Table 1). Hierarchical clustering revealed that some of these genes were part of a prominent aggregate in iEC grafts (Fig. 5a). This cluster contained genes known to be negative regulators of T helper 1 (TH1) cell-mediated inflammation (STAT3) (Welte et al. 2003, Wang et al. 2004, Kortylewski et al. 2005), transducers of apoptosis signals (TNFRSF10b)(Peppa et al. 2013), mediators of TGF-β _signaling (Fos) (Zhang et al. 1998), and potent regulators of adaptive immunity (IL-10 and TGF-β) (Rubtsov et al. 2008, Le Texier et al. 2012). More importantly was the striking up-regulation of genes that encode the immunoregulatory cytokines IL-10 and TGF-β found in iEC grafts compared to iPSC grafts which was validated on a larger biological sample size (Fig. 5b). Furthermore, immunofluorescence staining supported these findings by demonstrating a significant presence of IL-10 in iEC grafts compared to other grafts (Fig. 5c and Supplementary Fig. 10a). To rule out the possibility that the abundant IL-10 in iEC grafts originated from cellular infiltrates and not from the iECs themselves, staining of IL-10 was performed in conjunction with an endothelial-specific marker, von Willebrand Factor (vWF). No association between IL-10 and vWF was found, suggesting that this cytokine originated from the cellular infiltrates rather than the iECs themselves (Supplementary Fig. 10b). Next, to determine the role of IL-10 in promoting iEC acceptance, antibody-based neutralization of IL-10 was performed. Treatment with anti-IL-10 resulted in a reduction of iEC bioluminescence in syngeneic recipients by 3 weeks after cell implantation, suggesting that IL-10 was required for tolerance to iECs (Supplementary Fig. 11a). Finally, in order to exclude the possibility that the effects mediated by anti-IL-10 were due to antibody-dependent cell death, anti-IL-10 cytotoxicity to iECs was examined in vitro. Our results showed that anti-IL-10 did not induce iEC cytotoxicity (Supplementary Fig. 11b).

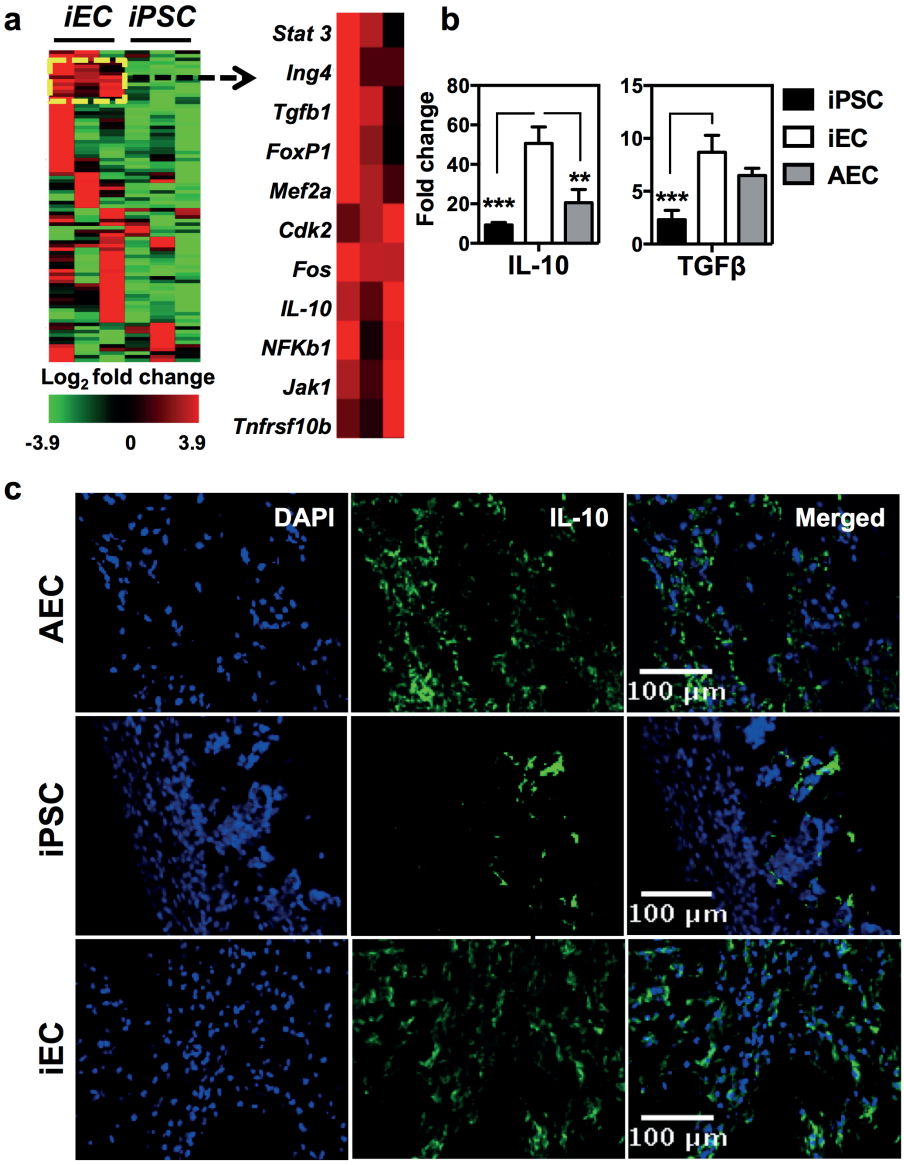


Figure 5. iECs elicited activation of a tolerogenic transcriptome network. (a) Hierarchical clustering revealed a group of nine genes (right panel) consistently upregulated in iEC grafts and with similar expression levels. These genes are known members of a pathway involved in regulation of IL-10. Data are representative of three animals per group. (b) Fold-change in gene expression relative to sham grafts confirming the pro-tolerogenic phenotype of iEC and AEC grafts. Data are representative of mean±s.e.m. of 3–4 animals per group from three independent experiments. Significance of differences between series of results was assessed using analysis of variance with Tukey for multiple comparisons. (c) Immunofluorescence staining demonstrating IL-10 abundance in iPSC, iEC and AEC grafts. Quantification of IL-10 expression was performed in five random fields from each graft type (x40 magnitude). Data are representative of mean±s.e.m. of a minimum of 1,000 cells from five randomly selected fields. $^{**}P < 0.01$, $^{***}P < 0.001$.

Immune cell infiltrates in differentiated grafts are tolerogenic

The tolerogenic effect associated with terminal differentiation of iPSCs on the elicited immune response was further characterized directly on graft infiltrating immune cells. For this, T cells ($CD4^+$ and $CD8^+$) and suppressor macrophages ($CD11c^-CD11b^+Gr1^+$) were isolated from the different grafts by FACS. The expression analysis of a panel of 14 genes, well described in the literature to be associated with suppression of T cell function and peripheral tolerance (Schietinger et al. 2012), were analyzed using the Fluidigm single cell-PCR platform (Narsinh et al. 2011). Expression analysis of the immune cells supported our results by demonstrating that induction of immunological self-tolerance accompanies terminal differentiation of iPSCs (Fig. 6). In the three immune cell types analyzed, up-regulation of a tolerogenic network of genes was found in T cells and macrophages infiltrating iEC and AEC compared to iPSC grafts. Protein-encoding genes associated with the suppressor function of regulatory T cells (Tregs) and type-1 regulatory T cells (Tr1), such as IL-10 and TGF-β, were consistently up-regulated in $CD4^+$ T cell isolated from iEC and

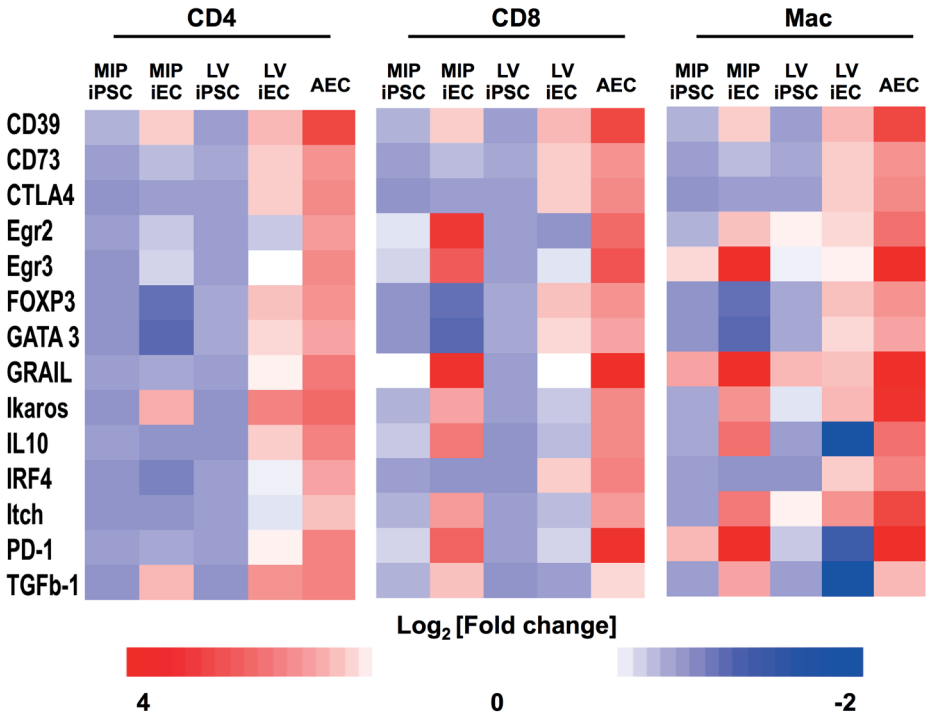


Figure 6. Heatmaps illustrating the patterns of expression of genes associated with tolerance and anergy in $CD4^+$ T cells, $CD8^+$ T cells and suppressor macrophages (Mac; $CD3^-$ $CD11c^-$ $CD11b^+$ $Gr1^+$) extracted from grafts. Fold-change in gene expression of immune cell infiltrates in iEC and AEC grafts relative to undifferentiated iPSC grafts, demonstrating a more tolerogenic and anergic phenotype of immune cells infiltrates from iEC and AEC grafts compared with iPSC grafts. Data are representative of five animals per group.

AEC grafts. The up-regulation of IL-10, which was accompanied by an overexpression of FoxP3 in $CD4^+$ T cells, further strengthens the notion that regulatory T cells may be key players in modulating acceptance of iECs. Additional protein-encoding genes associated with suppression function as well as with anergy of T cells, such as CD39, CD73 (Deaglio et al. 2007), and CTLA4 (Perez et al. 1997), were also similarly up-regulated in iECs and AECs. These similarities were particularly evident when comparing AECs to LV-iECs, supporting the flow cytometric results demonstrated in Fig. 5. Interestingly, MIP-iECs induced a different set of genes to similar levels as the AECs, especially in $CD8^+$ T cells and macrophages. Among these are Egr2 and Egr3 that increase E3 ubiquitin ligases, thereby inhibiting T cell activation. Furthermore, the induction of PD-1, as well as GRAIL and Itch, which was more evident in MIP-iECs compared to LV-iEC-infiltrating $CD8^+$ T cells and macrophages, are known to result in T cell inhibition (Keir et al. 2008, Nurieva et al. 2010) and suppression of pro-inflammatory cytokines (Shembade et al. 2008). Taken together, our results support the notion that terminal differentiation towards iECs induces a tolerogenic network that is also induced by self.

T cell clonality of iEC grafts is fundamentally different from iPSCs

To further examine similarities among grafts, we next used high-throughput T cell receptor (TCR) sequencing analysis of genomic DNA isolated from the tissue grafts to elucidate differences in the clonal structure of T cells infiltrating iPSC, iEC, and AEC grafts. We first examined the distribution of CDR3 lengths obtained by sequencing, which yielded results very similar to those of a conventional spectratyping method of measuring T cell repertoire diversity. This produced a restricted skewing in the distribution of CDR3 lengths in iPSC-infiltrating T cells versus iEC- or AEC-infiltrating T cells (Fig. 7a). This pattern of restriction in the distribution of CDR3 lengths correlates closely with oligoclonal or monoclonal cells (Gagne et al. 2000, Guillet et al. 2002, Zilberberg et al. 2008). One major limitation of CDR3 spectratyping has been the difficulty in statistically comparing samples or quantifying T cell clones by sequence identity. We next compared the clonal T cell repertoire structure in iPSC-, iEC-, and AEC-infiltrating T cells. We found that the iPSC-infiltrating T cell repertoire showed a remarkable expansion of only a few clones when compared to iEC- or AEC-infiltrating T cell repertoires. We found that the top five dominant T cell clones accounted for 30–55% of the total TCR diversity of T cell infiltrates in iPSC grafts, making this T cell response highly skewed towards a few clones in comparison to the fraction of diversity of the top five clones in iEC (15–20%) or AEC (10–25%) grafts. Therefore, relatively few clones dominated the T cell infiltrates of iPSC grafts, a pattern that was statistically different from that seen in iEC grafts (Fig. 7b; $p<0.001$; two-tailed unpaired Student t-test). Control experiments with splenic samples from the same mice showed no repertoire skewing in the spleens of mice with iPSC grafts, which suggests that the skewed clonality is a property of the grafts themselves and not a biased sampling of the repertoire (Supplementary Fig.

12). These data are consistent with the observation that oligoclonal expansion of a limited number of T cell clones is a hallmark of adaptive immune recognition that has been characterized as a reproducible feature of tissue rejection and is regarded as a measure of skewness in TCR repertoire (Dietrich et al. 1992, Matsutani et al. 2000).

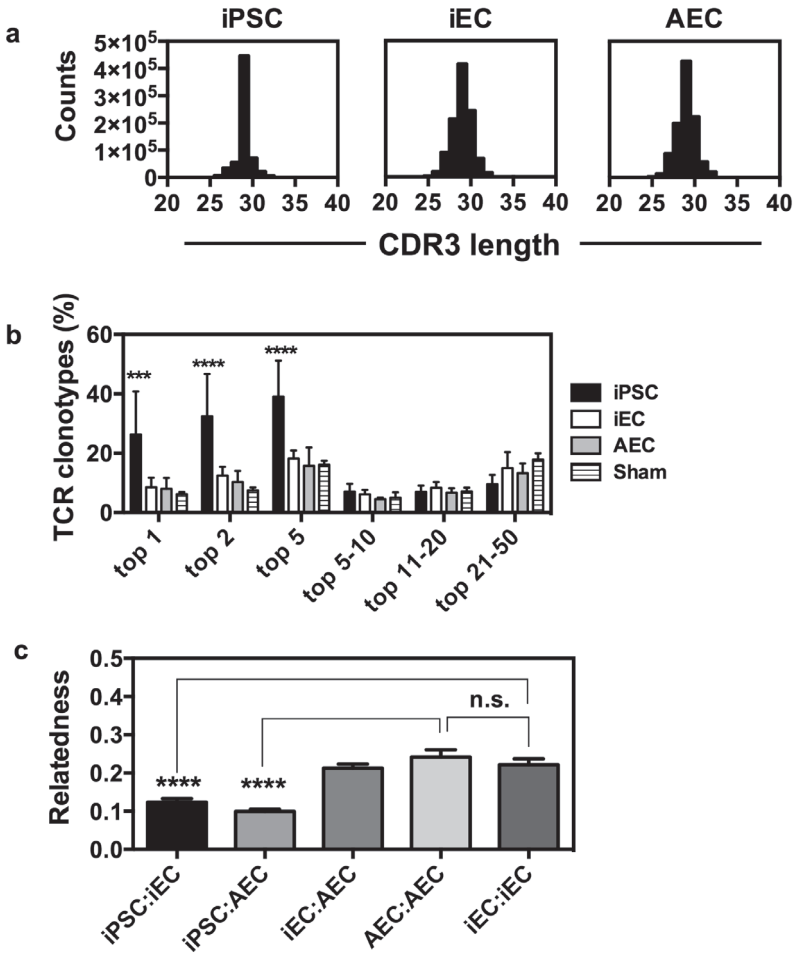


Figure 7. T-cell repertoire studies of graft infiltrates. (a) T cells infiltrating iPSC grafts show repertoire restriction. CDR3 length distribution of TCR sequences obtained from a representative syngeneic-rejected iPSC graft (left panel), accepted iEC graft (central panel) and accepted AEC graft (right panel). (b) T cells infiltrating iPSC grafts show a statistically significant expansion of a few dominant T-cell clones compared with iEC- or AEC-infiltrating cells. Results are pooled from two experiments, n = 3 mice per group. (c) The T-cell repertoires of iEC and AEC grafts are statistically indistinguishable but different from iPSC repertoires. BCs of relatedness averaged for comparisons within experimental groups. Data are representative of mean±s.e.m. of three animals pxer group from two independent experiments are reported here. Significance of differences between series of results was assessed using unpaired two-tailed Student's t-test; ***P < 0.001, ****P < 0.0001.

One remaining question is whether the same T cell clones were expanding within the grafts. We examined this in two ways: the first was to look at how the top 50 T cell clones within the graft were shared, and the second approach used statistical methods of whole repertoire comparison. We compared all of the mice within each experiment for the number of shared clones in the top 50 by rank order. We found that very few T cell clones were shared overall (Supplementary Table 2), with iPSC to iPSC comparisons averaging 3.7 shared clones in the top 50 between any two mice within experiments, versus iEC to AEC (11.1 shared clones), iEC to iEC (8.7 shared clones), and AEC to AEC (12.3 shared clones). Importantly, while the exact CDR3 sequence of the top T cell clones was not the same among grafts for different mice within and between each experiment, the proportion of T cell expansion was similar.

Using an information theory-based metric of similarity, the Bhattacharyya coefficient (BC) of relatedness that takes into account sequence identity and relative frequency of clones between samples (Bhattacharya 1943), we next examined the similarity in the entire TCR repertoires of T cells infiltrating the different grafts. A comparison of the grafts derived from the same tissue type among mice (iEC versus iEC or AEC versus AEC) showed values between 0.20 and 0.24, whereas the iPSC to iPSC comparison showed a value 0.15 to 0.18. The comparison of iEC to AEC tissues was statistically indistinguishable from iEC versus iEC, or AEC versus AEC, comparisons (Fig. 7c; p=0.66; two-tailed unpaired Student t-test). By contrast, comparisons of iPSC to iEC and AEC showed less relatedness with values of 0.12 for iPSC versus iEC and 0.10 for iPSC versus AEC. These results indicate that the TCR repertoire of iPSC-infiltrating T cells is statistically distinguishable from that of iEC- or AEC-infiltrating T cells (Fig. 7c). Since AEC and iEC relatedness cannot be distinguished between themselves or from one another, but can be distinguished for comparisons to iPSC, we conclude that the T cell response to iPSCs is fundamentally different from that of AEC or iEC tissues at a clonal level.

DISCUSSION

Transplantation of tissues derived from autologous iPSCs has the potential to treat many medical conditions, but a major concern for this approach is whether the immune system will accept iPSC-derived terminally differentiated tissues. Recent research has demonstrated that iPSCs retain epigenetic artifacts from the parental cells and from the reprogramming process (Kim et al. 2010, Bar-Nur et al. 2011). These changes can affect iPSCs' ability to efficiently differentiate into functional somatic cells, and most importantly, their ability to persist in their differentiated state after terminal differentiation (Lister et al. 2011). These factors can have serious implications for the safety and sustainability of iPSC derivatives in vivo, including tumorigenicity (Cunningham et al. 2012) and immunogenicity (Zhao et

al. 2011, Araki et al. 2013, Guha et al. 2013). Here we show that iPSCs generated by either lentiviral or genome integration-free methods are immunogenic in syngeneic recipients, which supports previous findings by Zhao et al. (Zhao et al. 2011). Moreover, our results support recent studies demonstrating that terminal differentiation of iPSCs can result in a loss of immunogenicity (Araki et al. 2013, Guha et al. 2013) and show for the first time that terminally differentiated iPSCs elicit immune responses consistent with self-tolerance.

Although the lack of rejection of transplanted tissues derived from iPSCs demonstrated here supports findings by Araki et al. (Araki et al. 2013) and Guha et al. (Guha et al. 2013), there are critical differences in the experimental methodologies in these studies with respect to this current study. Here we used a mouse model of autologous transplantation to assess the immunogenicity of cells implanted subcutaneously, similar to the mouse model used by Zhao et al. and Araki et al. We observed that undifferentiated lentiviral iPSCs and genome integration-free iPSCs elicited a robust immune response in syngeneic recipients that resulted in bioluminescence signal decay over-time and failure to form teratomas. However, the identity of the antigenic determinants in iPSC grafts was not addressed in our study and it remains unclear whether the robust immune response observed was elicited by the pluripotent cells themselves or by early progenitors that originate from spontaneous differentiation of iPSCs upon transplantation. Our results support the findings described by Zhao et al. but not by Araki et al. In the study by Guha et al., cells were implanted in the sub-renal capsule and rejection of undifferentiated iPSCs was not reproduced. The vascularity and niche of the graft are important factors determining cell survival, immune cell homing and engraftment. The sub-renal capsule is a highly vascularized site that has been vastly used for testing cellular tumorigenicity and has been known to support the growth of tumors that are unable to grow when implanted subcutaneously (Sun et al. 2005). Secondly, the endpoint for the experiments in Guha et al.' study was 30 days post-cell implantation. While histological evidence of cell survival was provided at the study end-point, no information that addresses a possible immunogenicity-associated decay in graft viability over the time-course of the study is shown.

In regard to the immunogenicity of terminally differentiated iPSC progeny, our findings support both Guha et al. and Araki et al. who demonstrate that terminally differentiated cells are immunologically accepted when transplanted syngeneically. Similar to our study, Guha et al. transplanted iPSC derivatives (endothelial, neuronal, hepatocytes) differentiated in vitro, while Araki et al. transplanted dermal and bone marrow tissues from highly chimeric mice developed from iPSC and ESC, a strategy that is arguably unrepresentative of a clinical setting. In both studies, grafts were deemed immunogenic based on one endpoint assessment of cell survival in histological tissue sections collected at 4 to 5 weeks post-transplantation and based on the amount of T cell infiltration found in grafts. Both studies demonstrated survival of iPSC derivatives at 4 to 5 weeks post-cell transplantation, with minimal to no T cell infiltration. However, while the abundance of T cell infiltration

provides important information regarding the involvement of adaptive immune responses on the status of the grafts, relying exclusively on this one parameter to assess the immunogenicity of grafts can be misleading. For instance, regulatory (Woo et al. 2001), anergic (Blank et al. 2004) or exhausted (Baitsch et al. 2011) T cells are often found in thriving tumors. These T cells are known to facilitate tumor survival and tumor growth by supporting an immunosuppressive environment. Hence utilizing T cell infiltration as main evidence for graft immunogenicity may not be ideal.

In contrast to the undifferentiated parental iPSCs, the endothelial progeny exhibited long-term survival in syngeneic recipients and produced a shift in immunological response consistent with self-tolerance and tissue acceptance. Contrary to previous reports correlating iPSC-derived tissue acceptance to the presence or absence of T cell infiltration (Zhao et al. 2011), our results indicate that T cell infiltration is common to both somatic and iPSC-derived cell grafts. The infiltration of T cells into early grafts may be in response to immune rejection, or in response to the trauma of graft introduction and intra-graft cell death of some tissue that invariably occurs. Importantly, while T cells infiltrating grafts early on was a common theme among iPSC, iEC, and AEC grafts, we found that the cytokine milieu was very different among grafts. Undifferentiated iPSC grafts possessed hallmark elements of cytotoxic T cell responses, whereas iEC and AEC grafts elicited a much more "benign" immune phenotype that was dominated by immunoregulatory cytokines such as IL-10 and TGF-β. The highest IL-10 responses were elicited by iEC grafts, suggesting that while the immune acceptance of iEC grafts is similar to AEC grafts, iECs may still have a certain level of antigen disparity with the recipient. Similar situation occurs for tolerance-inducing approaches in solid organ transplantation where IL-10 is needed for the immune protection of MHC-matched, minor-mismatched, or major-mismatched grafts in many animal models. In these systems, the production of IL-10 in the graft environment is critical for peripheral tolerance and graft acceptance. A key question in the field is how similar to 'self' must a graft be in order to be tolerated by the immune cells. Our work shows that iECs are sufficiently similar to 'self' tissue to be tolerated. At this point, how similar iECs must be to self remains an open question; hence the mechanism that led to the differences in tolerogenic response elicited by iEC and AEC grafts warrants further investigation. Finally, it is important to consider that the self-tolerogenic response elicited by terminally differentiated endothelial cells may also facilitate the survival of cells with oncogenic potential. Thus, the realization that self-tolerance may potentiate tumorigenesis of autologous iPSC-derived cells needs to be carefully considered and evaluated prior to clinical translation. Finally, the percentage of FoxP3-expressing $CD4^+$ T cells detected in iEC grafts was statistically undistinguishable from the one found in AECs but was significantly lower than in iPSC. Increases in FoxP3 expression have been noted in active immune rejection and may not be as reliable as a marker of tolerance in this setting as measuring effector molecules (Batsford et al. 2011,

Miyao et al. 2012). Similarities in FoxP3 expression between iEC and AEC grafts were also present at the mRNA level in total graft tissue as well as in T cell infiltrates.

We also examined the TCR clonal structure of rejecting tissue. Until very recently, oligoclonal and monoclonal T cell responses in tissue rejection were measured using spectratyping and V- and J-chain usage restriction, which is a relatively low-resolution method for tracking specific T cell clones mediating rejection. Alternatively, exhaustive studies have identified specific antigen responses in allogeneic transplants. In some of these cases, the expansion of dominant allo-reactive T cells was found. Using a higher-resolution method for tracking clonal T cell responses of repertoire sequencing, we found that relatively few oligoclonal T cells are greatly expanded in iPSC graft infiltrates versus AEC or iEC grafts. This suggests that iPSC graft infiltrating repertoire has a pattern of immune rejection. Importantly, the same T cell clones do not appear to dominate tissue rejection responses, likely because iPSCs can rapidly and stochastically divide into any number of differentiating tissues and the resulting T cell responses are variable. Our analysis offers novel ways to use TCR repertoire sequencing to help distinguish graft rejection from graft tolerance. Although there is potential for PCR bias in the TCR amplification, all experiments were performed such that all samples from each group—iPSC, iEC, AEC, sham control—were processed at the same time and had the same primers and reagents. Given that the iPSC grafts clearly had different dominant clonal sequences amongst themselves in the grafts, we believe these results are less likely due to the artificial overstating of a clone that appears in iPSC grafts and not in other grafts. In addition, control experiments with splenic samples from the same mice showed no repertoire skewing in the spleens of mice with iPSC grafts, which suggests that the skewed clonality is a property of the grafts themselves and not a biased sampling of the repertoire. While correction of PCR amplification bias should be a goal of the field, so far this is an underappreciated point in the current literature. Researchers are still trying to optimize methods to control for PCR amplification bias and disseminate these methods which is a highly innovative approach not previously available and not tested for murine or other animal models, as recently pointed out by Carlson et al. (Carlson et al. 2013) study. PCR amplification bias is very important for questions such as the detection of minimal residual disease, and statistical analysis can now be applied without bias correction as discussed in Meyer et al. (Meyer et al. 2013). Overall, our statistical analysis explicitly examines the probability of a chance event that a specific clone is somehow amplified better in one sample versus another, but our p-values suggest this is not the case.

In summary, our results indicate that iPSC-derived tissues can be accepted by the immune system without immunosuppressive therapy in a tolerant manner very similar to autologous tissues. Our results also suggest that viral-based reprogramming of iPSCs may not be critical in dictating downstream immunogenicity of iPSC progeny. Prior to clinical translation of iPSC-derived cellular therapy, it will be critical to determine the level of permissible dis-

similarity that allows these therapeutic cells to be seen as 'self' in autologous transplantation settings. Moreover, establishing the "ground" state of iPSCs (at the epigenome, genome, and proteome levels) required for derivation of safe cellular therapeutics that act as 'self' upon transplantation is imperative for the eventual clinical adoption of this technology.

METHODS

Mice

Six- to eight-week-old female FVB, NOD-SCID IL2Rgamma^{null}, C57BL/6 and IFN-/- were obtained from The Jackson Laboratory. B6.129.F1 females were obtained from Taconic. Transgenic FVB mice expressing luciferase and GFP were generated at the transgenic animal facility in the Department of Pathology at Stanford University by pronuclear injection of the reporter gene construct. Mice were maintained at the Stanford University Research Animal Facility in accordance with Stanford University's Institutional Animal Care and Use Committee guidelines.

Derivation and characterization of iECs

iECs were derived using a three- dimensional approach with modifications10. In brief, to initiate differentiation, iPSCs were cultured in ultra-low, non-adhesive dishes to form embryoid body (EB) aggregates in EBM2 media (Lonza) in the absence of leukaemia inhibitor factor. After 4 days of suspension culture, the EBs were reattached onto 0.2% gelatin-coated dishes and cultured in EBM2 medium supplemented with vascular endothelial growth factor (VEGF)-A165 (50 ng/ml; PeproTech). After 3 weeks of differentiation, single-cell suspensions were obtained using a cell dissociation buffer (Life Technologies, Grand Island, NY, USA) and labelled with APC-conjugated CD31 (eBiosciences) and PE-conjugated CD144 (BD Biosciences) anti-mouse antibodies. iECs were purified by FACS of CD31^{+} CD144^{+} population. iECs were maintained in EBM2 media supplemented with recombinant murine vascular endothelial growth factor (50 ng/ml).

Isolation of AECs

B6.129.F10 mice were killed and the ascending and descending aorta segments were harvested. The aorta was cleaned from surrounding adipose tissue under dissecting microscope. Subsequently, the aorta was mechanically and enzymatically dissociated in Collagenase II (1 mg/ml) by incubating at 37°C for 45 min. The digestion mix was triturated every 10 min to ensure complete dissociation. At the end of 45 min, the cell suspension was filtered through a 70-mm strainer to attain a single-cell suspension. Cell suspension was centrifuged at 1,200 r.p.m. for 5 min. The pellet obtained was subjected to red blood cell lysis, followed by a wash with phosphate-buffered saline (PBS) and centrifugation at 1,200 rpm for 5 min. The pellet

enriched in ECs was immediately seeded on a 0.2% gelatin-coated plate in EGM2 media (Lonza). After 2 weeks of in vitro expansion, ECs were further purified by FACS based on the expression of CD144 and CD31.

Cell graft implantations

Cell injection was conducted under the guidelines of Stanford University Administrative Panel of Laboratory Animal Care. Mice were placed in an induction chamber and anaesthesia was induced with 2% isoflurane (Isothesia, Butler Schein) in 100% oxygen with a delivery rate of 2 l min 1 until loss of righting reflex. Cells ($1x10^6$) were mixed in 200 ml BD Matrigel High Concentration (1:2; BD Biosciences) and injected subcutaneously in the lower dorsa of mice using a 28-G syringe.

In vivo BLI

Transplanted cell survival was longitudinally monitored via BLI using the Xenogen In Vivo Imaging System (Caliper Life Sciences). In brief, D-luciferin (Promega) was administered intraperitoneally at a dose of 375 mg kg 1 of body weight. Animals were placed in a light-tight chamber, and photons emitted from luciferase-expressing cells were collected with integration times of 5 s to 2 min, depending on the intensity of the bioluminescence emission. BLI signal was quantified in maximum photons s^{-1} cm^2 per steradian and presented as Log10(photons s^{-1}).

Graft explantation and cell isolation

Grafts were explanted, chopped into small fragments and digested with Liberase (27 WU ml^{-1}; Roche, Indianapolis, IN, USA) and DNase I (0.1%; Roche) in Dulbecco's modified Eagle medium (DMEM) media at room temperature for 30 min followed by incubation at 37°C for 15 min. Digested grafts were passed through a 100-mm strainer and centrifuged at 300 g for 10 min at 4°C. Cells were counted and prepared for flow cytometry or snap frozen for RNA and DNA extractions.

Flow cytometric analysis of graft-infiltrating lymphocytes

Fluorophore-con- jugated monoclonal antibodies against mouse CD3, CD4, CD8, CD25, FoxP3, CD11c and NK1.1 (1:100; BD Bioscience or eBioscience) were used in various combinations to stain cells extracted from grafts. For staining, $1x10^6$ cells were used. The Fc receptor was blocked by CD16/32 antibody. Cells were fixed and permeabilized using BD Cytofix/Cytoperm fixation and intracellular staining was performed. Cells were assayed using a LSRII flow cytometer (BD Biosciences) and further analyzed with FlowJo software (Tree Star, Ashland, OR, USA).

T-cell tolerance and anergy PCR array

Cell grafts harvested from syngeneic recipients 14 days post implantation were enzymatically dissociated to a single-cell suspension and washed with PBS for total RNA extraction by Qiagen RNeasy Mini kit. The RT2Profiler PCR Array kits were purchased from SA Bioscience Corporation (Frederick, MD, USA), and all assay procedures were conducted in accordance with the user kit manual. In brief, 1 mg of total RNA from iPSCs or iECs was transcribed into first strand cDNA and loaded into 96-well PCR array plates with 25 ml quantitative PCR master mix per well. After performing quantitative PCR, resulting threshold cycle values for all genes were exported into the company- provided data analysis template Excel files for comparison of gene expression between iPSC and iEC grafts.

Immunocytochemistry for iEC characterization

Primary antibodies for mouse vWF (1:150; Millipore), laminin (1:100; Abcam, Cambridge, MA, USA) and CD144 (1:100; Abcam) were used for iEC characterization. iECs were grown in 0.2% gelatin-coated coverslips and fixed in 4% paraformaldehyde when they reached 80% confluence. Before immunostaining, cells were blocked with 1% BSA for 1 h at room temperature. Subsequently, primary antibodies were maintained overnight at 4°C. Coverslips were washed in PBS and incubated with goat anti-rabbit Alexa Fluor 594 (Invitrogen) for 1.5 h at room temperature. For intracellular staining of vWF, cells were permeabilized with 0.2% Triton X-100 then subjected to BSA blocking and incubation with the antibody diluted in 1% BSA and 0.1% Triton X-100. Confocal images were taken using Carl Zeiss, LSM 510 Meta (Göttingen, Germany) using a 63 plan apochromat (oil) objective microscope. Images were analyzed using the ZEN software (Carl Zeiss).

LDL uptake

Acetylated LDL (ac-LDL) uptake was performed by incubating iEC monolayers in rhodamine-conjugated ac-LDL (10 mg/ml; Biomedical) for 4 h at 37°C. Subsequently, the medium was removed and cells were washed with a probe-free medium and harvested for flow cytometric characterization.

Histological analysis

Grafts were harvested and cryo-embedded directly in Tissue Tek O.C.T. (Sakura Finetek) or fixed in 10% buffered formalin overnight after which they were transferred to a 15% w/v sucrose solution until tissue processing and paraffin embedding. Multiple 5 mm tissue sections from each sample were cut at mid-teratoma and stained with haematoxylin and eosin for histological analysis. Frozen blocks were mounted on a Leica cryostat CM3050 S (Leica Microsystems) and 8 mm sections were transferred to Superfrost/Plus adhesive slides (Fisher brand) and stored at 80 °C. For characterization of cellular contexture of grafts, a pathologist, blinded to the to sample assignment, measured the total surface area of each

graft cross-section, assigned lineage differentiation to each of the morphologic components, and determined the representation of each component as a percentage of the total mid-tumor cross-sections area.

IL-10 immunoassaying

Immunostaining was performed using antibodies against IL-10 (1:100; Abcam) and Alexa-488-conjugated (Life Technologies) secondary antibodies (1:1,000). Frozen sections were fixed in acetone followed by blocking in 5% horse serum for 60 min at room temperature. Sections were then incubated with primary antibody in blocking solution overnight at 4°C. Nuclei were stained with Hoechst 33342 (Life Technologies). Fluorescent images were taken with a Leica SP2 AOBS (Acousto-Optical Beam Splitters) Confocal Laser Scanning Microscope with 20, 40 and 63 oil objectives. For resolution of nuclei- dense regions, Z-stacked confocal images were rendered into three dimensions using Volocity 6.0.1 software. For IL-10^{+} cell counts, one independent blinded observer examined five random fields at 40 magnitude. Quantification of IL-10 staining was determined by planar association of stain and nuclei.

IL-10 neutralization in vivo

Neutralization of IL-10 was performed using anti-IL- 10 antibody (JES5-2A5, BioXCell) or isotype control anti-Rat IgG1 (BioXCell). Mice received 250 mg of antibody intraperitoneally on days 1, 1, 3, 6, 9 and 12 relative to cell implantation.

Cell viability assay

Cell viability upon treatment with JES5-2A5 antibody was analyzed using an XTT-based in vitro toxicology assay kit (Sigma-Aldrich). Cells were grown in a 96-well plate (Corning) to about 50% confluency, and subsequently subjected to 48 h treatment of different concentrations of JES5-2A5 anti- body. During the last 12 h, control cells were treated with 50 nM Antimycin A, a Complex III inhibitor of the mitochondrial electron transport chain, as a positive control for cytotoxicity. Cells at a final density of ~80% were incubated for 4 h in the presence of a 20% XTT reagent diluted in culture medium, protected from light. Absorbance at 450 nm was measured using a plate-reader (Promega).

Derivation and culture of non-viral murine iPSCs

Murine tail tip fibroblasts of mice were dissociated and isolated with collagenase type IV (Life Technologies) and maintained with DMEM containing 10% fetal bovine serum, L-glutamine, 4.5g/l glucose, 100U/ml penicillin and 100mg/ml streptomycin at 37°C, 20% O2 and 5% CO2 in a humidified incubator. Murine fibroblasts (1x10^{6} m) were then reprogrammed using a CoMiP (10–12 mg of DNA) expressing the four reprogramming factors Oct4, KLF4, Sox2 and c-Myc using the Neon Transfection system (unpublished data). After

transfection, fibroblast were plated on a MEF feeder layer and kept in fibroblast media with the addition of sodium butyrate (0.2 mM) and 50 mg/ml ascorbic acid. When ESC-like colonies appeared, media was changed to murine iPSC media containing DMEM, 20% fetal bovine serum, L-glutamine, non-essential amino acids, b-mercaptoethanol and 10 ng/ml leukemia inhibitory factor. After two passages, the murine iPSCs were transferred to 0.2% gelatin-coated plates and further expanded. With every passage, the iPSCs were sorted for the murine pluripotency marker SSEA-1 using magnetic-activated cell sorting.

Immunofluorescence staining of cultured cells

Cells were fixed with 4% paraformaldehyde for 20 min, permeabilized with 0.2% Triton X-100 in PBS for 30 min and blocked with serum in PBS for 1 h. Cells were then stained with appropriate primary antibodies and Alexa Fluor-conjugated secondary antibodies (Life Technologies) and costained with 40,6-diamidino-2-phenylindole (DAPI) (Vector Laboratories, Burlingame, CA, USA). The primary antibodies for CD31 and CD144 (Abcam) were used in the staining. All murine iECs were also incubated with 10 mg/ml DiI ac-LDL (Life Technologies) at 37°C for 6 h. After washing twice with PBS, DiI ac-LDL uptake was detected with fluorescence microscopy. Imaging was performed on a Leica DFC500 inverted microscope.

Quantitative real-time PCR analysis

Total RNA was purified from iPSCs and teratomas using RNeasy Mini kit (Qiagen, CA, USA). RNA (1 mg) was reverse transcribed using a high-capacity cDNA transcription kit (Applied Biosystems), followed by high-throughput quantitative gene expression analysis using the Syber green-based assay system on the StepOne Plus Realtime PCR platform (Applied Biosystems). Primer sequences for Hormad1, Zg16, Lce1f and Spt1 were the same as previously described (Zhao et al. 2011). GAPDH was used as the internal control gene for all samples and the ΔΔCt method was used to calculate fold-change of gene expression. For characterization of the intragraft immunological milieu, Taqman- based real-time PCR was carried out using the same platform as described above. The following Taqman probes were used: IFN-c (Mm01168134_m1), FoxP3 (Mm00475162_m1), GAPDH (Mm99999915_g1), IL-10 (Mm00439614_m1), TGF-b1 (Mm01178820_m1), Perforin (Mm00812512_m1) and granzyme-B (Mm00442834_m1). For characterization of iECs, the following Taqman probes were used: vWF (Mm00550376_m1), CD144 (Mm03053719_s1), and FLK1 (Mm01222421_m1).

TCR sequencing

Genomic DNA was obtained from explanted grafts using Qiagen DNA extraction kits (Qiagen). Multiplex sets of sequencing tagged primers were used to PCR-amplify all the members of the TCRb repertoire present in a sample using multiplexed primers consisting

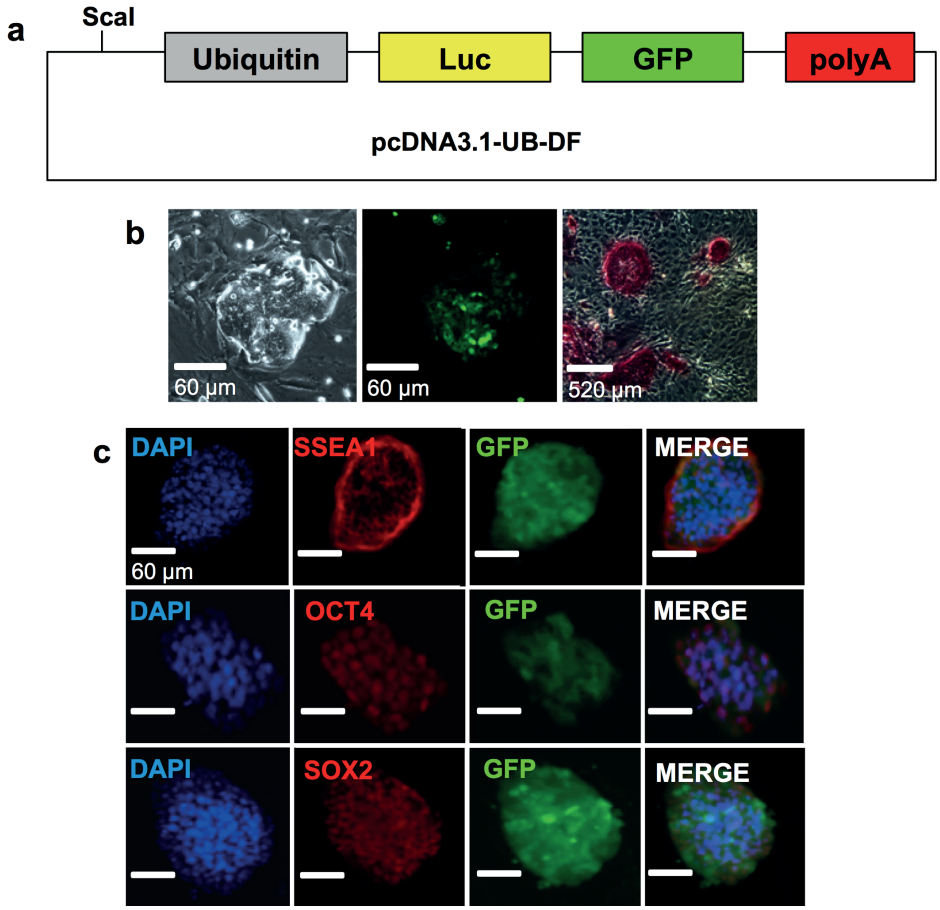
of 21 V segment primers and 11 J segment primers designed by Gigagen Inc. (South San Francisco, CA, USA). Pooled (AEC, iPS, iEC and sham) samples were run on an Illumina MiSeq (Illumina, San Diego, CA, USA) to a depth of 2 million sequence reads. The sample sorted fastq files were analyzed using the custom coded in Practical Extraction and Report Language (PERL) with bash scripting automation. Only error-free TCR sequences occurring at 42 copies were included in analysis. The BC measures the amount of overlap between two statistical samples, each with a finite number of distinct partitions and probabilities, corresponding to unique clonotypes and their frequencies. It is calculated as:

$$\sum_{j=1}^{n} \sqrt{f_{j,1} \times f_{j,2}}$$

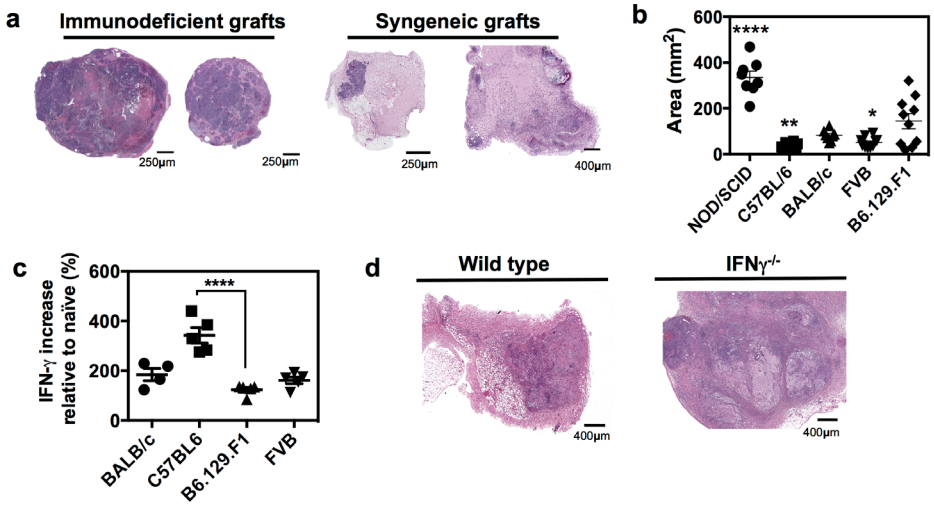
where $f_{j,1}$ and $f_{j,2}$ are the frequencies of clonotype j in samples 1 and 2, respectively, and n is the number of unique clonotypes present across samples 1 and 2. A BC of 1 between two Rep-Seq samples would mean that the samples are identical in number, sequence and frequency of unique clonotypes. A value of 0 would mean that no clonotypes are present in both samples, although a value of 0.0 would not be informative about the number of clonotypes or frequencies in either sample. The coefficient was calculated using customize PERL scripts. Statistical evaluation of the comparison of Bhattacharya distances was performed using a standard T-test with GraphPad Prism.

Statistical methods

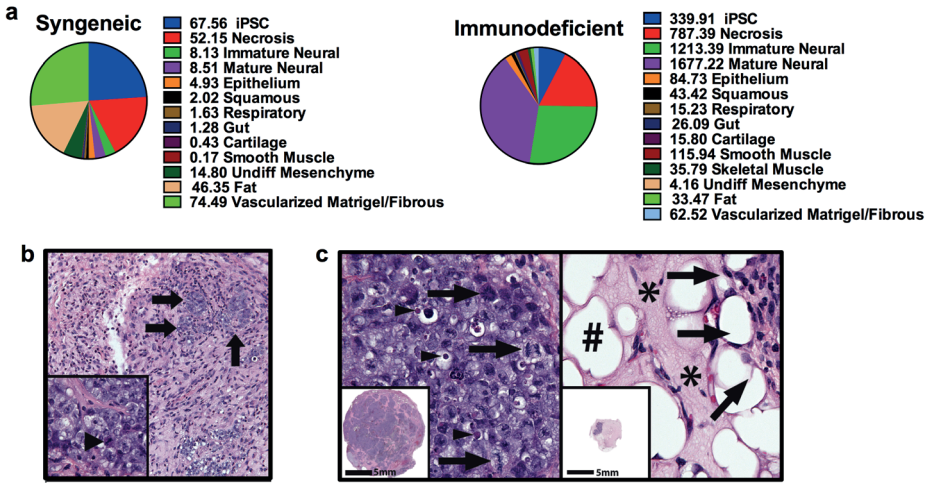
Differences between groups were assessed by two-way analysis of variance or Student's t-test using GraphPad Prism software. Bar graphs represent the mean and s.e.m. for each group.



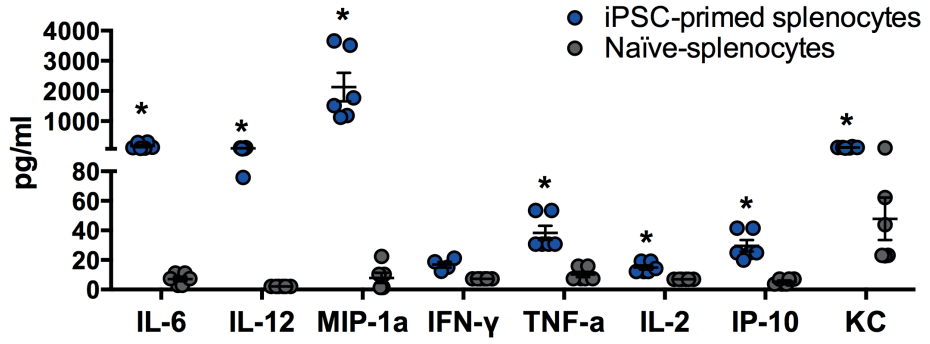
Supplementary Fig. 1. Characterization of lentiviral-reprogrammed iPSC line derived from a GFP-Luciferase transgenic FVB mouse fibroblast. (a) Map of the plasmid carrying GFP and luciferase (Luc) genes under control of the ubiquitin promoter. (b) Undifferentiated iPSCs had typical ESC-like colony morphology (left), expressed GFP (mid), and alkaline phosphatase (AP) (Right). (c) iPSCs stably expressed the embryonic markers such as SSEA1, Oct4, and Sox2.



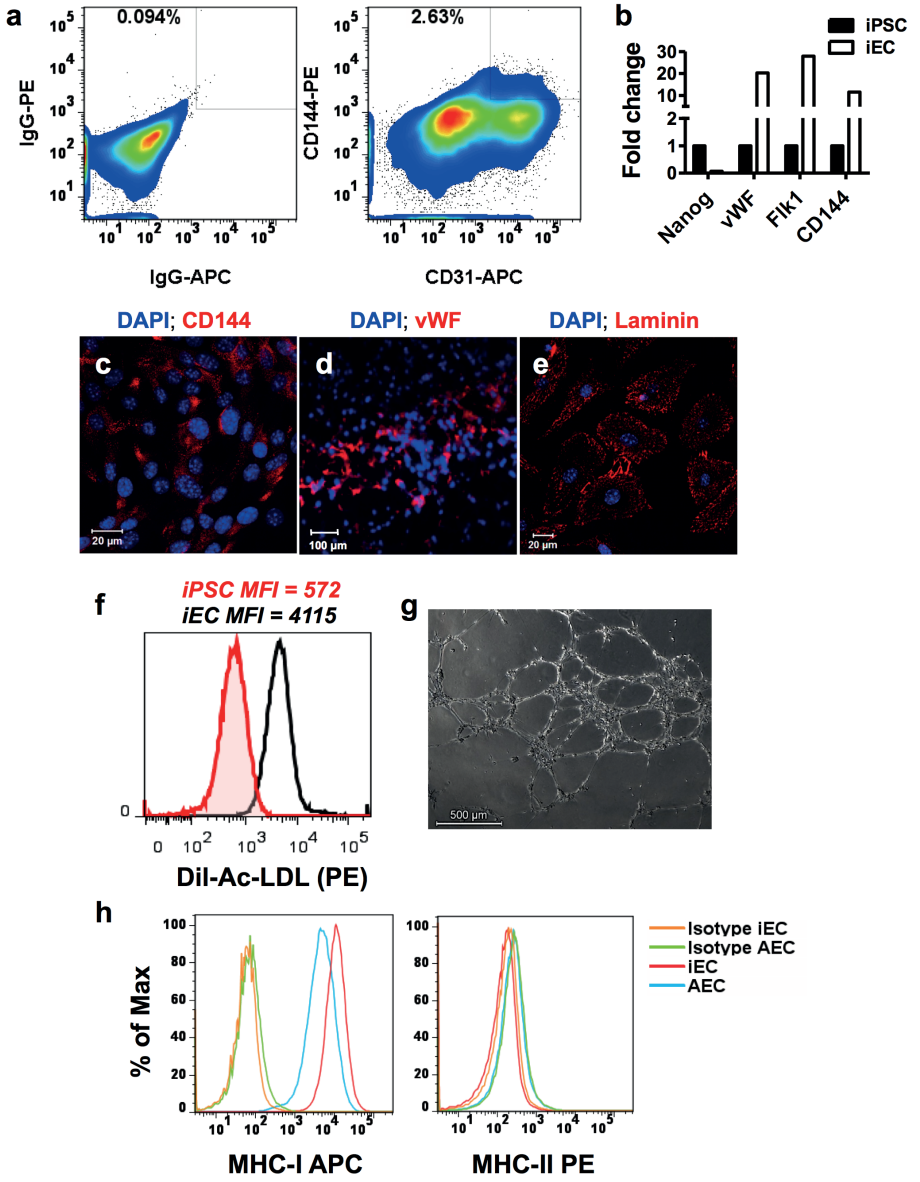
Supplementary Fig. 2. Immunological rejection of lentiviral-derived syngeneic iPSCs is not due to reporter transgene expression. (a) Two representative histopathological sections (H&E) of B6.129.F1 iPSC (free of GFP and luciferase expression) grafts per group explanted from immunodeficient (left; 1x magnification) and syngeneic mice (right; 5x magnification). Data are representative of at least 9 animals and 3 independent experiments. (b) iPSC graft areas measured 30 days post-intramuscular injection of iPSCs in immunodeficient (NOD/SCID), allogeneic (BALB/C, C57BL6, FVB), and syngeneic (B6.129.F1) mice. Data are representative of mean ± s.e.m. of at least 8 animals per group from 2 independent experiments. (c) IFN-γ ELISPOT demonstrating the percent production of IFN-γ by syngeneic (B6.129.F1) and allogeneic primed splenocytes (from BALB/c, C57BL/6, and FVB) relative to the respective naïve splenocytes in response to iPSCs (B6.129.F1). Data are representative of mean ± s.e.m. of 5 mice per group. (d) Histopathological views of iPSC grafts harvested 30 days after implantation in syngeneic C57BL/6 wild-type or C57BL/6 IFN-γ-/- mice. Significance of differences between series of results was assessed using ANOVA with Tukey for multiple comparisons. *p<0.05, **p<0.01, ****p<0.0001.



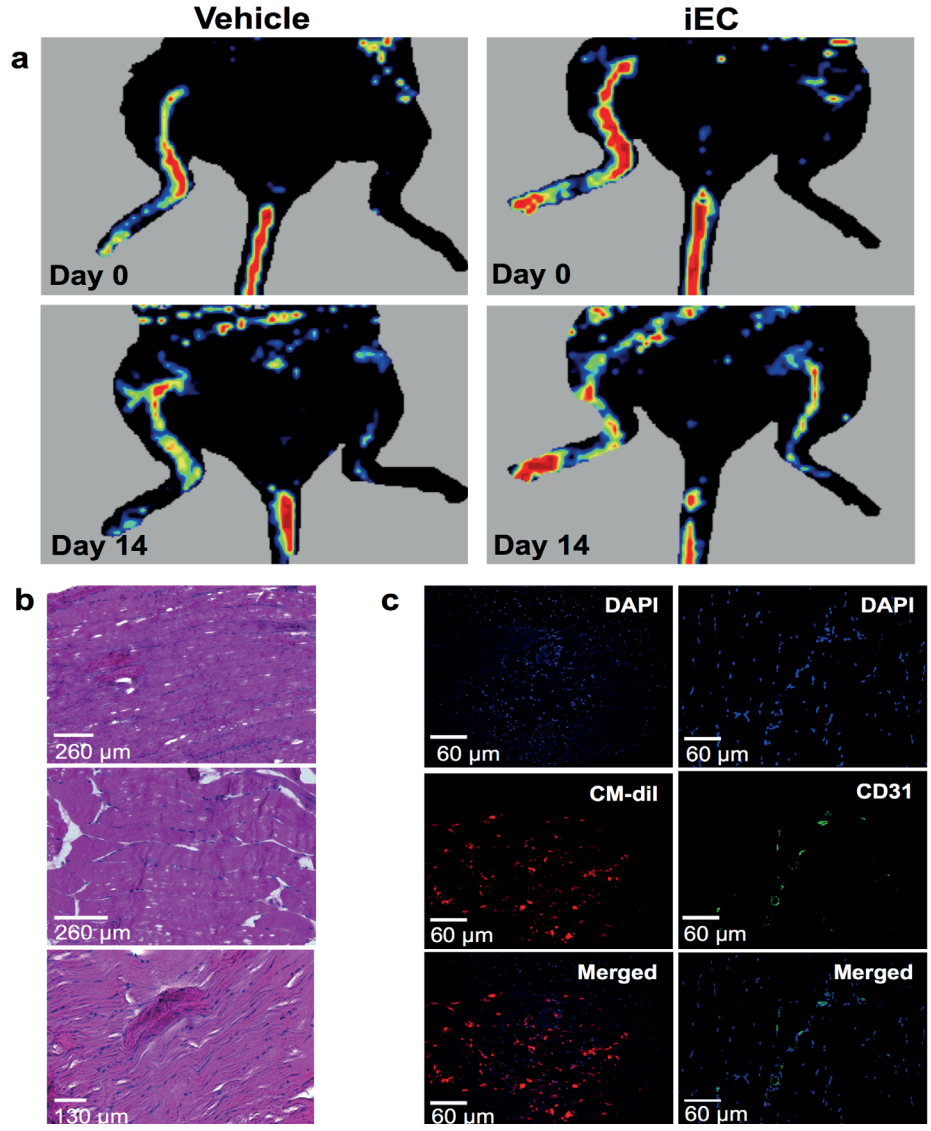
Supplementary Fig. 3. Undifferentiated iPSCs were still present in the grafts at the time of immunological analysis. (a) Pie charts demonstrating the dimensions of the areas (mm2) in which the listed cell types occupied grafts extracted from syngeneic (n=10) and immunodeficient (n=6) mice 14 days post-implantation. (b) A syngeneic iPSC graft extracted from mouse at 14 days post-implantation demonstrate the presence of undifferentiated cells (arrows). iPSCs were identifiable based on high nuclear-to-cytoplasmic ratios, frequent mitotic features (arrow head, inset), and the absence of any morphologic evidence of differentiation. (c) iPSCs injected into immunodeficient mice formed large subcutaneous tumors that persist for at least 30 days post- implantation (left panel, inset). These cells were identifiable based on high nuclear-to- cytoplasmic ratios, frequent mitotic features (arrows) and apoptotic bodies (arrowheads), and the absence of any morphologic evidence of differentiation. In contrast, iPSCs injected into syngeneic wild-type mice were mostly eliminated, resulting in much smaller tumors (right panel, inset) comprising predominantly of pauricellular Matrigel (right panel, *) and adipocytes (#) with lymphohistiocytic infiltrate (demarcated by arrows).



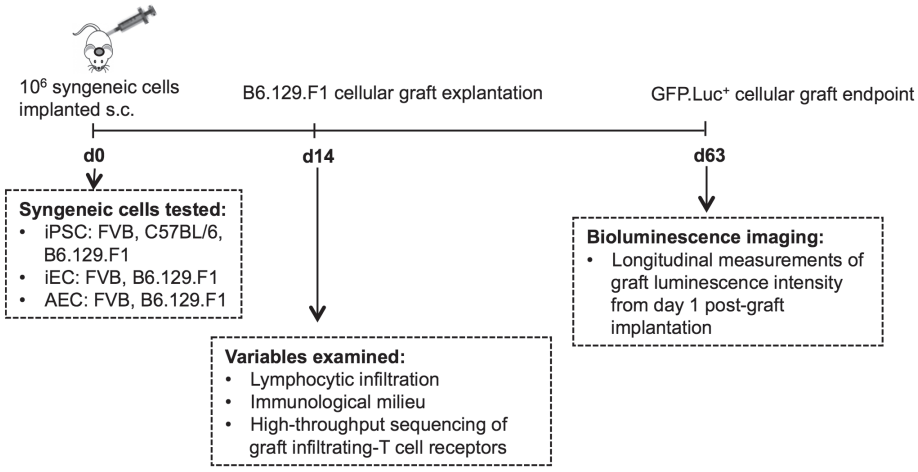
Supplementary Fig. 4. Syngeneic iPSCs elicit a pro-inflammatory immune response when co- cultured with syngeneic iPSC-primed splenocytes in vitro. Splenocytes ($2x10^5$) isolated from mice (n=6) primed with syngeneic iPSCs (10^5) or splenocytes from naïve mice (n=6) were co- cultured with syngeneic iPSCs for 72 hr in vitro. Various pro-inflammatory cytokines were measured in the culture supernatant by Luminex. Data are representative of mean ± s.e.m. of 6 mice per group. Significance of differences between series of results was assessed using two- tailed unpaired Student t-test. * $p<0.05$.



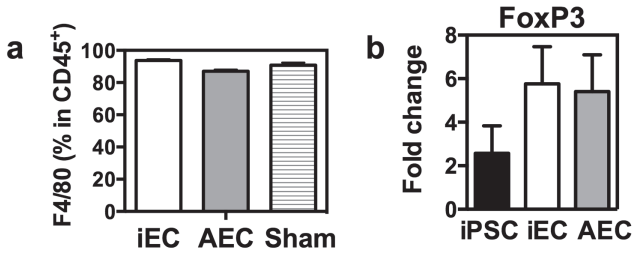
Supplementary Fig. 5. Purification and characterization of iECs. (a) Gating strategy for purification of differentiated iECs ($CD144^+/CD31^+$) by FACS. (b) Fold-change in transcript expression relative to undifferentiated iPSCs. Purified iECs showed up-regulation of endothelial transcripts (vWF, Flk1, CD144) as well as down-regulation of the pluripotency marker Nanog, consistent with terminal differentiation to endothelial lineage. Endothelial phenotype was characterized by immunofluorescence staining of endothelial-specific markers such as (c) CD144 and (d) von Willebrand factor. Functional phenotype of iECs was characterized by the production of (e) extracellular matrix laminin, (f) uptake of low-density lipoprotein, and (g) angiogenesis by means of tube-formation assay. (h) Expression of MHC-I and MHC-II in iECs and AECs by FACS.



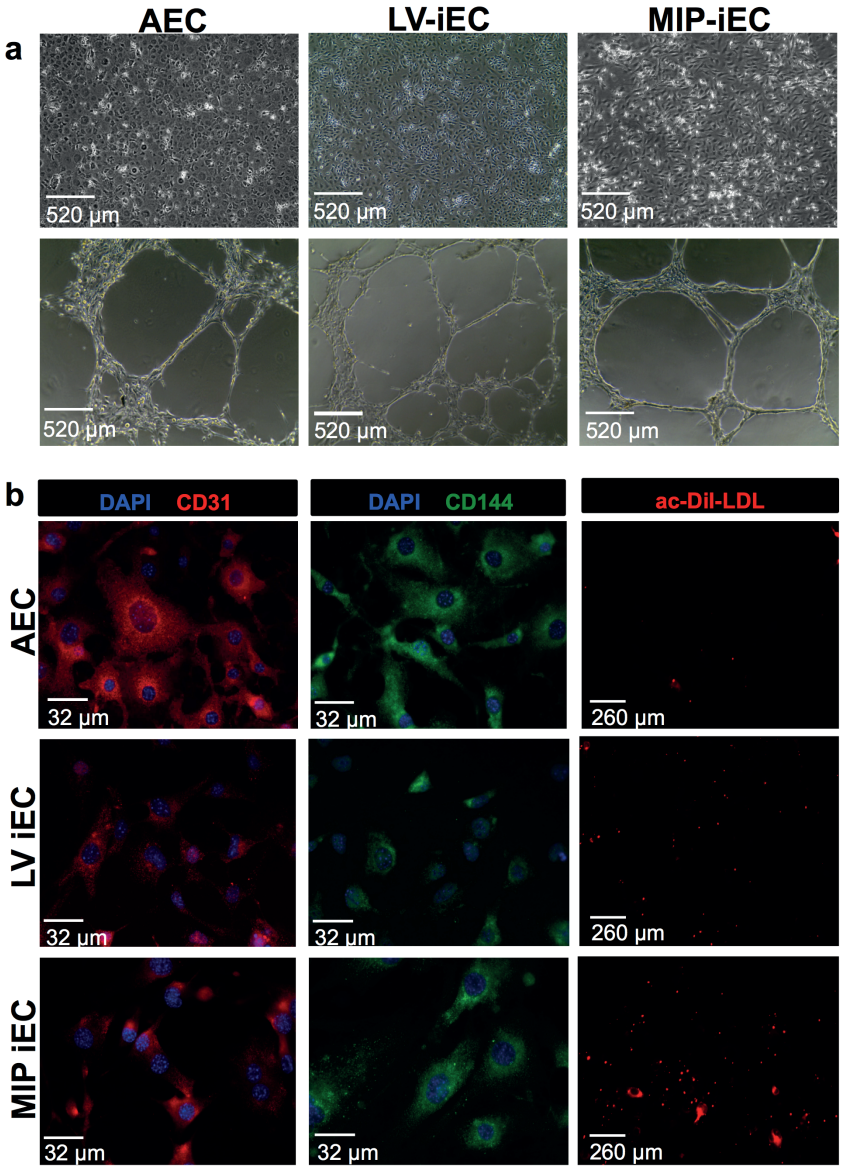
Supplementary Fig. 6. In a model of ischemia injury, iECs engrafted and promoted re- vascularization of the hindlimb of immunodeficient mice without any evidence of tumor formation. (a) Laser Doppler imaging of blood perfusion 1 hr after left hindlimb ischemia demonstrate a severe reduction of blood flow in mice treated with vehicle or iEC injection (top panels). Hindlimbs of mice at 14 days post-ischemia (bottom panels) demonstrate iEC injection promoted re-vascularization compared to control vehicle injection. (b) Histological evaluation of ischemic hindlimb at 14 days after iEC injection. No evidence of tumor formation was found in iEC grafts. (c) Immunofluorescence staining of hindlimbs at 14 days after iEC injection. CM-DiI labeled (red; left panel) iECs show localization and survival of iECs in the ischemic hindlimbs. Cell surface staining for CD31 (green) demonstrate structural organization of iECs in vascular- like structures.



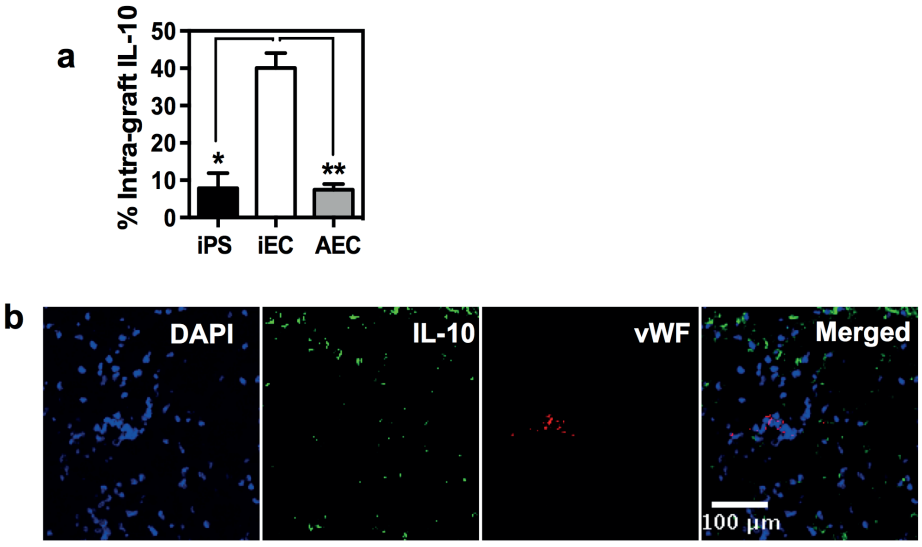
Supplementary Fig. 7. Schema of experimental design used to assess the immunogenicity of iPSC, iECs, and AECs.



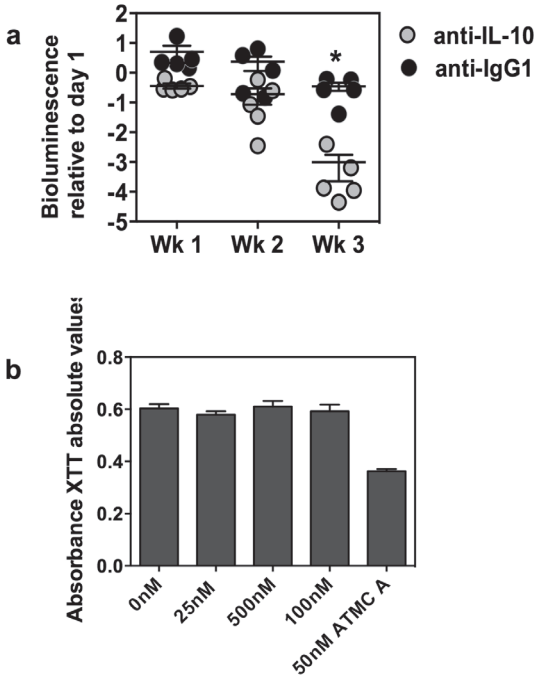
Supplementary Fig. 8. Assessment of macrophage infiltration and FoxP3 mRNA expression in different grafts. (a) Macrophages represented the predominant immune cell population infiltrating iEC, AEC, and sham grafts. Macrophage ($F4/80^+$) infiltration was quantified by FACS. Data are representative of mean ± s.e.m. of 5 animals per group. (b) Fold-change in FoxP3 expression relative to sham grafts demonstrating no statistically significant differences among iPSC, iEC, and AEC grafts. Data are representative of mean ± s.e.m. of eight animals per group.



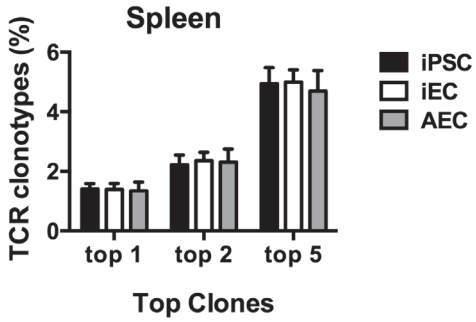
Supplementary Fig. 9. Characterization of murine AECs and iECs. (a) Brightfield overview of aortic endothelial cells (AEC), lentiviral-derived endothelial cells (LV-iEC), and mini-intronic plasmid-derived endothelial cells (MIP-iECs) (top panel). Formation of tube-like structures on Matrigel characteristic of endothelial cells (bottom panel). (b) Nuclear staining with DAPI (blue) and cell surface staining for CD31 (red) and CD144 (green). Uptake of ac-Dil-LDL (red) by endothelial cells.



Supplementary Fig. 10. IL-10 in iEC grafts originated from cellular infiltrates. (a) Quantification of IL-10 expression was performed in 5 random fields from each graft type (40x magnitude). (b) IL-10 expression was not associated with endothelial cells. Von Willebrand factor (vWF) was used to label endothelial cells and to determine association with IL-10. Data are representative of mean ± s.e.m. of a minimum of 1,000 cells from 5 randomly selected fields. Significance of differences between series of results was assessed using ANOVA with Tukey for multiple comparisons. *$p<0.05$, **$p<0.01$



Supplementary Fig. 11. Neutralization of IL-10 promoted rejection of iECs in syngeneic recipients. (a) Longitudinal survival of iECs was monitored in syngeneic mice by means of bioluminescence imaging. Data are representative of mean ± s.e.m maximum bioluminescence radiance relative to day 0 (n=5). Significance of differences between series of results was assessed using two-tailed unpaired Student t-test. Antibody-based neutralization of IL-10 promoted loss of iECs' bioluminescence signal within 3 weeks of cell implantation, consistent with cell death due to immune rejection. (b) Anti-IL-10-mediated cytotoxicity was examined in iECs in vitro. Actinomycin A (ATMC A) was use as a positive control for cytotoxicity. Data are representative of mean ± s.e.m of 3 technical replicates. *p<0.05



Supplementary Fig. 12. T cell repertoire of spleens from mice with iPSC, iEC, and AEC grafts. Contrary to T cells infiltrating iPSC grafts, splenic T cells of mice with iPSC grafts showed no repertoire skewing. Data are representative of mean ± s.e.m of 3 mice per group and two independent experiments.

Table S1 Genes found to be significantly up-regulated in iEC compared to iPSC grafts.

Symbol	Unigene	Refseq	Description
Ccl3	Mm.1282	NM_011337	Chemokine (C-C motif) ligand 3
Cdk2	Mm.111326	NM_016756	Cyclin-dependent kinase 2
Csf1	Mm.795	NM_007778	Colony stimulating factor 1 (macrophage)
Fas	Mm.1626	NM_007987	Fas (TNF receptor superfamily member 6)
Fos	Mm.246513	NM_010234	FBJ osteosarcoma oncogene
Foxp1	Mm.234965	NM_053202	Forkhead box P1
Icam1	Mm.435508	NM_010493	Intercellular adhesion molecule 1
Il10	Mm.874	NM_010548	Interleukin 10
Il7r	Mm.389	NM_008372	Interleukin 7 receptor
Ing4	Mm.262547	NM_133345	Inhibitor of growth family, member 4
Jak1	Mm.289657	NM_146145	Janus kinase 1
Mef2a	Mm.132788	NM_001033713	Myocyte enhancer factor 2A
Nfatc3	Mm.383185	NM_010901	Nuclear factor of activated T-cells, cytoplasmic, calcineurin-dependent 3
Nfkb1	Mm.256765	NM_008689	Nuclear factor of kappa light polypeptide gene enhancer in B-cells 1, p105
Notch1	Mm.290610	NM_008714	Notch gene homolog 1 (Drosophila)
Stat3	Mm.249934	NM_011486	Signal transducer and activator of transcription 3
Stat6	Mm.121721	NM_009284	Signal transducer and activator of transcription 6
Tgfb1	Mm.248380	NM_011577	Transforming growth factor, beta 1
Tnfrsf10b	Mm.193430	NM_020275	Tumor necrosis factor receptor superfamily, member 10b

Table S2 Number of TCR clones (among the top 50 most prevalent clones) shared between different graft types. Data is representative of two independent experiments (Exp1 and Exp2).

	Shared TCR clones													
Comparison	**Exp1**	**Exp1**	**Exp1**	**Exp1**	**Exp2**	**Exp2**	**Exp2**	**Exp2**	**Exp2**	**Exp2**	**Exp2**	**Exp2**	**Exp2**	**Mean ± s.e.m**
iPSC to iPSC	3				5	3								3.7 ± 0.38
iPSC to iEC	0	1	3	4	4	7	0	4	10	0	2	1	5	3.1 ± 0.33
iPSC to AEC	7	5	0	4	0	0	6	4	2	6	5	0	0	3 ± 0.30
iEC to iEC	12				6	8								8.7 ±1.01
iEC to AEC	11	8	8	16	12	8	15	15	6	19	10	5	11	11.1 ± 0.46
AEC to AEC	15				8	14								12.3 ± 1.26

REFERENCES

Araki, R., M. Uda, Y. Hoki, M. Sunayama, M. Nakamura, S. Ando, . . . M. Abe (2013). "Negligible immunogenicity of terminally differentiated cells derived from induced pluripotent or embryonic stem cells." Nature 494(7435): 100-104.

Baitsch, L., P. Baumgaertner, E. Devevre, S. K. Raghav, A. Legat, L. Barba, . . . D. E. Speiser (2011). "Exhaustion of tumor-specific CD8(+) T cells in metastases from melanoma patients." The Journal of clinical investigation 121(6): 2350-2360.

Bar-Nur, O., H. A. Russ, S. Efrat and N. Benvenisty (2011). "Epigenetic memory and preferential lineage-specific differentiation in induced pluripotent stem cells derived from human pancreatic islet beta cells." Cell stem cell 9(1): 17-23.

Batsford, S., M. Dickenmann, U. Durmuller, H. Hopfer, F. Gudat and M. Mihatsch (2011). "Is monitoring of FOXP3 Treg cells in renal transplants during acute cellular rejection episodes useful?" Clin Nephrol 75(2): 101-106.

Ben-David, U., N. Nudel and N. Benvenisty (2013). "Immunologic and chemical targeting of the tight-junction protein Claudin-6 eliminates tumorigenic human pluripotent stem cells." Nature communications 4: 1992.

Bhattacharya, A. (1943). "On a measure of divergence between two statistical populations defined by their probability distribution." Sankhyā: The Indian Journal of Statistics 7(4): 401-406.

Blank, C., I. Brown, A. C. Peterson, M. Spiotto, Y. Iwai, T. Honjo and T. F. Gajewski (2004). "PD-L1/B7H-1 inhibits the effector phase of tumor rejection by T cell receptor (TCR) transgenic CD8+ T cells." Cancer research 64(3): 1140-1145.

Boyd, A. S. and K. J. Wood (2010). "Characteristics of the early immune response following transplantation of mouse ES cell derived insulin-producing cell clusters." PloS one 5(6): e10965.

Carlson, C. S., R. O. Emerson, A. M. Sherwood, C. Desmarais, M. W. Chung, J. M. Parsons, . . . H. Robins (2013). "Using synthetic templates to design an unbiased multiplex PCR assay." Nat Commun 4: 2680.

Cunningham, J. J., T. M. Ulbright, M. F. Pera and L. H. Looijenga (2012). "Lessons from human teratomas to guide development of safe stem cell therapies." Nature biotechnology 30(9): 849-857.

Deaglio, S., K. M. Dwyer, W. Gao, D. Friedman, A. Usheva, A. Erat, . . . S. C. Robson (2007). "Adenosine generation catalyzed by CD39 and CD73 expressed on regulatory T cells mediates immune suppression." The Journal of experimental medicine 204(6): 1257-1265.

Dietrich, P. Y., A. Caignard, A. Diu, C. Genevee, J. L. Pico, M. Henry-Amar, . . . T. Hercend (1992). "Analysis of T-cell receptor variability in transplanted patients with acute graft-versus-host disease." Blood 80(9): 2419-2424.

Gagne, K., S. Brouard, M. Giral, F. Sebille, A. Moreau, M. Guillet, . . . J. P. Soulillou (2000). "Highly altered V beta repertoire of T cells infiltrating long-term rejected kidney allografts." J Immunol 164(3): 1553-1563.

Guha, P., J. W. Morgan, G. Mostoslavsky, N. P. Rodrigues and A. S. Boyd (2013). "Lack of immune response to differentiated cells derived from syngeneic induced pluripotent stem cells." Cell stem cell 12(4): 407-412.

Guillet, M., S. Brouard, K. Gagne, F. Sebille, M. C. Cuturi, M. A. Delsuc and J. P. Soulillou (2002). "Different qualitative and quantitative regulation of V beta TCR transcripts during early acute allograft rejection and tolerance induction." J Immunol 168(10): 5088-5095.

Han, Y. M., Q. L. Guo, M. G. Zhang, Z. B. Chen and X. T. Cao (2009). "CD69(+)CD4(+)CD25(-) T Cells, a New Subset of Regulatory T Cells, Suppress T Cell Proliferation through Membrane-Bound TGF-beta 1." Journal of Immunology 182(1): 111-120.

Huang, N. F., H. Niiyama, C. Peter, A. De, Y. Natkunam, F. Fleissner, . . . J. P. Cooke (2010). "Embryonic stem cell-derived endothelial cells engraft into the ischemic hindlimb and restore perfusion." Arteriosclerosis, thrombosis, and vascular biology 30(5): 984-991.

Jia, F., K. D. Wilson, N. Sun, D. M. Gupta, M. Huang, Z. Li, . . . J. C. Wu (2010). "A nonviral minicircle vector for deriving human iPS cells." Nat Methods 7(3): 197-199.

Keir, M. E., M. J. Butte, G. J. Freeman and A. H. Sharpe (2008). "PD-1 and its ligands in tolerance and immunity." Annual review of immunology 26: 677-704.

Kim, K., A. Doi, B. Wen, K. Ng, R. Zhao, P. Cahan, . . . G. Q. Daley (2010). "Epigenetic memory in induced pluripotent stem cells." Nature 467(7313): 285-290.

Kortylewski, M., M. Kujawski, T. Wang, S. Wei, S. Zhang, S. Pilon-Thomas, . . . H. Yu (2005). "Inhibiting STAT3 signaling in the hematopoietic system elicits multicomponent antitumor immunity." Nature medicine 11(12): 1314-1321.

Le Texier, L., P. Thebault, M. Carvalho-Gaspar, V. Vignard, E. Merieau, C. Usal, . . . E. Chiffoleau (2012). "Immunoregulatory function of IL-27 and TGF-beta1 in cardiac allograft transplantation." Transplantation 94(3): 226-233.

Li, Z., J. C. Wu, A. Y. Sheikh, D. Kraft, F. Cao, X. Xie, . . . J. P. Cooke (2007). "Differentiation, survival, and function of embryonic stem cell derived endothelial cells for ischemic heart disease." Circulation 116(11 Suppl): I46-54.

Lister, R., M. Pelizzola, Y. S. Kida, R. D. Hawkins, J. R. Nery, G. Hon, . . . J. R. Ecker (2011). "Hotspots of aberrant epigenomic reprogramming in human induced pluripotent stem cells." Nature 471(7336): 68-73.

Matsutani, T., T. Yoshioka, Y. Tsuruta, S. Iwagami, T. Toyosaki-Maeda, T. Horiuchi, . . . M. Hirokawa (2000). "Restricted usage of T-cell receptor alpha-chain variable region (TCRAV) and T-cell receptor beta-chain variable region (TCRBV) repertoires after human allogeneic haematopoietic transplantation." British journal of haematology 109(4): 759-769.

Meissner, A., M. Wernig and R. Jaenisch (2007). "Direct reprogramming of genetically unmodified fibroblasts into pluripotent stem cells." Nature biotechnology 25(10): 1177-1181.

Meyer, E. H., A. R. Hsu, J. Liliental, A. Lohr, M. Florek, J. L. Zehnder, . . . R. S. Negrin (2013). "A distinct evolution of the T-cell repertoire categorizes treatment refractory gastrointestinal acute graft-versus-host disease." Blood 121(24): 4955-4962.

Miyao, T., S. Floess, R. Setoguchi, H. Luche, H. J. Fehling, H. Waldmann, . . . S. Hori (2012). "Plasticity of Foxp3(+) T cells reflects promiscuous Foxp3 expression in conventional T cells but not reprogramming of regulatory T cells." Immunity 36(2): 262-275.

Mullally, A. and J. Ritz (2007). "Beyond HLA: the significance of genomic variation for allogeneic hematopoietic stem cell transplantation." Blood 109(4): 1355-1362.

Narsinh, K. H., N. Sun, V. Sanchez-Freire, A. S. Lee, P. Almeida, S. Hu, . . . J. C. Wu (2011). "Single cell transcriptional profiling reveals heterogeneity of human induced pluripotent stem cells." J Clin Invest 121(3): 1217-1221.

Nicholls, S., K. P. Piper, F. Mohammed, T. R. Dafforn, S. Tenzer, M. Salim, . . . B. E. Willcox (2009). "Secondary anchor polymorphism in the HA-1 minor histocompatibility antigen critically affects MHC stability and TCR recognition." Proceedings of the National Academy of Sciences of the United States of America 106(10): 3889-3894.

Nurieva, R. I., S. Zheng, W. Jin, Y. Chung, Y. Zhang, G. J. Martinez, . . . C. Dong (2010). "The E3 ubiquitin ligase GRAIL regulates T cell tolerance and regulatory T cell function by mediating T cell receptor-CD3 degradation." Immunity 32(5): 670-680.

Peppa, D., U. S. Gill, G. Reynolds, N. J. Easom, L. J. Pallett, A. Schurich, . . . M. K. Maini (2013). "Up-regulation of a death receptor renders antiviral T cells susceptible to NK cell-mediated deletion." The Journal of experimental medicine 210(1): 99-114.

Perez, V. L., L. Van Parijs, A. Biuckians, X. X. Zheng, T. B. Strom and A. K. Abbas (1997). "Induction of peripheral T cell tolerance in vivo requires CTLA-4 engagement." Immunity 6(4): 411-417.

Rubtsov, Y. P., J. P. Rasmussen, E. Y. Chi, J. Fontenot, L. Castelli, X. Ye, . . . A. Y. Rudensky (2008). "Regulatory T cell-derived interleukin-10 limits inflammation at environmental interfaces." Immunity 28(4): 546-558.

Schietinger, A., J. J. Delrow, R. S. Basom, J. N. Blattman and P. D. Greenberg (2012). "Rescued tolerant CD8 T cells are preprogrammed to reestablish the tolerant state." Science 335(6069): 723-727.

Shembade, N., N. S. Harhaj, K. Parvatiyar, N. G. Copeland, N. A. Jenkins, L. E. Matesic and E. W. Harhaj (2008). "The E3 ligase Itch negatively regulates inflammatory signaling pathways by controlling the function of the ubiquitin-editing enzyme A20." Nature immunology 9(3): 254-262.

Sun, B., M. Chen, C. L. Hawks, O. M. Pereira-Smith and P. J. Hornsby (2005). "The minimal set of genetic alterations required for conversion of primary human fibroblasts to cancer cells in the subrenal capsule assay." Neoplasia 7(6): 585-593.

Takahashi, K., K. Tanabe, M. Ohnuki, M. Narita, T. Ichisaka, K. Tomoda and S. Yamanaka (2007). "Induction of pluripotent stem cells from adult human fibroblasts by defined factors." Cell 131(5): 861-872.

Takahashi, K. and S. Yamanaka (2006). "Induction of pluripotent stem cells from mouse embryonic and adult fibroblast cultures by defined factors." Cell 126(4): 663-676.

Wang, T., G. Niu, M. Kortylewski, L. Burdelya, K. Shain, S. Zhang, . . . H. Yu (2004). "Regulation of the innate and adaptive immune responses by Stat-3 signaling in tumor cells." Nature medicine 10(1): 48-54.

Welte, T., S. S. Zhang, T. Wang, Z. Zhang, D. G. Hesslein, Z. Yin, . . . X. Y. Fu (2003). "STAT3 deletion during hematopoiesis causes Crohn's disease-like pathogenesis and lethality: a critical role of STAT3 in innate immunity." Proceedings of the National Academy of Sciences of the United States of America 100(4): 1879-1884.

Woo, E. Y., C. S. Chu, T. J. Goletz, K. Schlienger, H. Yeh, G. Coukos, . . . C. H. June (2001). "Regulatory CD4(+)CD25(+) T cells in tumors from patients with early-stage non-small cell lung cancer and late-stage ovarian cancer." Cancer research 61(12): 4766-4772.

Zhang, Y., X. H. Feng and R. Derynck (1998). "Smad3 and Smad4 cooperate with c-Jun/c-Fos to mediate TGF-beta-induced transcription." Nature 394(6696): 909-913.

Zhao, T., Z. N. Zhang, Z. Rong and Y. Xu (2011). "Immunogenicity of induced pluripotent stem cells." Nature 474(7350): 212-215.

Zilberberg, J., D. McElhaugh, L. N. Gichuru, R. Korngold and T. M. Friedman (2008). "Inter-strain tissue-infiltrating T cell responses to minor histocompatibility antigens involved in graft-versus-host disease as determined by Vbeta spectratype analysis." J Immunol 180(8): 5352-5359.

Chapter 8

Modeling PSC alloimmunity using humanized mice

Kooreman N.G.[*]*, de Almeida P.E.*[*]*, Stack J.P.*[*]*, Nelakanti R.V., Diecke S., Swijnenburg R.J., Sanchez-Freire V., Shao N., Matsa E., Hamming J.F., Quax P.H.A., Brehm M.A., Greiner D.L., Shultz L.D., Wu J.C.,(2017) Alloimmune responses of humanized mice to human pluripotent stem cell therapeutics.* **Cell Reports,** *20, 8; 1978-1990.*
[*] *authors contributed equally*

SUMMARY

There is growing interest in using embryonic stem cell (ESC) and induced pluripotent stem cell (iPSC) derivatives for tissue regeneration. However, an increased understanding of human immune responses to stem cell-derived allografts is necessary for maintaining long-term graft persistence. To model this alloimmunity, humanized mice engrafted with human hematopoietic and immune cells could prove to be useful. In this study, an in-depth analysis of graft-infiltrating human lymphocytes and splenocytes revealed that humanized mice incompletely model human immune responses toward allogeneic stem cells and their derivatives. Furthermore, using an "allogenized" mouse model, we show the feasibility of reconstituting immunodeficient mice with a functional mouse immune system and describe a key role of innate immune cells in the rejection of mouse stem cell allografts.

INTRODUCTION

Since the first isolation of human embryonic stem cells (hESCs) (Thomson et al. 1998) and creation of induced pluripotent stem cells (iPSCs) (Takahashi and Yamanaka 2006, Takahashi et al. 2007), the field of regenerative medicine has been investigating the therapeutic potential of these cells for cardiac diseases (Nguyen et al. 2016), neurological diseases (Barberi et al. 2003), hepatic failure (Soto-Gutierrez et al. 2006), diabetes (Pagliuca et al. 2014), and macular degeneration (Homma et al. 2013). Human clinical trials in immune-privileged areas, such as the eye for macular degeneration, are ongoing for ESC derivatives (Schwartz et al. 2012) or iPSC derivatives (Mandai et al. 2017). However, the immunological responses toward these derivatives in less immune-privileged sites are still poorly understood (de Almeida et al. 2013). Recently, advances have been made in tolerizing mice to accept human ESC- and iPSC-derived progenitor grafts for long-term monitoring of graft behavior (Lui et al. 2014). However, to date, it is still not clear how the human immune system would respond to allogeneic human ESC or iPSC grafts. This question would need to be answered before pluripotent stem cell (PSC) therapy, including both ESCs and iPSCs, could be widely implemented in clinical practice.

To model human immune responses, researchers have been studying immunodeficient mice engrafted with human immune cells and their progenitors, such as peripheral blood mononuclear cells (PBMCs) and hematopoietic stem cells (HSCs). The first description of these "humanized mouse models" dates back to 1983, when it was reported that the *Prkdc*^{scid} (severe combined immunodeficiency, *scid)* mutation in CB17 mice caused B and T cell deficiency (Bosma et al. 1983) and suggested that CB17-*scid* mice would be permissive for human HSC and PBMC engraftment. However, because of the high levels of host natural killer (NK) cell activity and the spontaneous generation of mouse B and T cells, this model supported only low levels of human HSC engraftment (Greiner et al. 1998). With the expression of human-like SIRPA in the non-obese diabetic (NOD)-*scid* strain, the levels of murine NK cells decreased (Shultz et al. 1995, Takenaka et al. 2007), resulting in heightened engraftment of human PBMCs (Hesselton et al. 1995). However, residual activity of NK cells as well as other innate immune system functions interfered with human HSC engraftment. Moreover, NOD-*scid* mice developed spontaneous thymic lymphomas, resulting in a shortened lifespan. It was not until the NOD-*scid* mouse strain with the interleukin-2 receptor gamma chain (*IL2rg*)-targeted mutation (NOD.Cg-*Prkdc*^{scid} *IL2rg*^{tm1Wjl}/Sz, NOD scid gamma [NSG]) and related NOD/shi-scid/γc ^{null} (NOG) strain mice were repopulated with human HSCs (*scid*-repopulating cell, *hSRC* mouse), that superior human hematopoietic and immune cell engraftment was achieved (Ito et al. 2002, Ishikawa et al. 2005, Shultz et al. 2005).

Despite enhanced engraftment of human HSCs in immunodeficient *IL2rg*^{null} mice, a robust human T cell-mediated immune response could not be established (Traggiai et al.

2004). The relatively weak T cell response was hypothesized to be due to the lack of human leukocyte antigen (HLA) on the murine thymus that is necessary for the positive selection of human T cells. To address this, a new model was created by subcapsular renal implantation of human liver and thymus fragments as well as intravenous injection of autologous (human liver-derived) HSCs in sublethally irradiated immunodeficient mice and was termed the human bone marrow, liver, and thymus (*hBLT)* model (Lan et al. 2006, Melkus et al. 2006). The superior engraftment of human immune cells combined with positive selection of T cells in the autologous human thymus has made this the preferred model for studying human immune responses to infection (Brehm et al. 2014).

An emerging field where humanized mice could prove to be useful is the study of human immune responses to allogeneic PSC transplants to assess the efficacy and safety of PSCs and guide effective immunosuppressive therapies. Here we describe the use of *hSRC* and *hBLT* humanized NSG mice to model the human immune response to allogeneic hESCs and their derivatives. We track allograft survival over time using bioluminescence imaging (BLI). In addition, we provide large transcriptome data as well as single-cell immunological analysis of human graft-infiltrating T cells and splenocytes isolated from humanized mice. Furthermore, using a similar implantation of mouse liver, thymus, and bone marrow, we developed an "allogenized" mouse model as a surrogate to assess allogeneic immunological responses to murine PSC allografts in vivo and ex vivo.

RESULTS

Human Immune-Engrafted NSG Mice Are Unable to Completely Reject Allogeneic hESCs

We used both the *hSRC* (NSG mice engrafted with HLA-A2^{neg} HSCs) and *hBLT* (NSG mice engrafted with HLA-A2^{neg} HSCs and fetal tissue) to model the allogeneic human immune responses to HLA-mismatched (HLA-A2^{pos}) hESCs. The hESCs were stably transduced with a reporter construct containing the ubiquitin promoter driving firefly luciferase (Luc) and EGFP. Allogeneic HLA-A2^{pos} hESCs (1×10^5) were implanted either subcutaneously (s.c.) or intramuscularly (i.m.) into *hSRC* mice. The hESC survival in these mice, as well as in control non-engrafted NSG and immunocompetent C57BL/6 mice, was longitudinally monitored in vivo using BLI. Both the *hSRC* and non-engrafted NSG mice were unable to completely reject allogeneic hESCs implanted at either injection site, whereas the immunocompetent C57BL/6 mice completely rejected the hESC grafts within 2 weeks (Figures S1A, S1C, S1D, and S1F).

To investigate whether low expression of major histocompatibility complex class I (MHC class I) in hESCs played a role in the failure of *hSRC* mice to reject these cells, hESCs were treated with interferon gamma (IFN-γ) for 24 hr prior to implantation into *hSRC* mice

to increase expression of MHC class I and cell immunogenicity (Drukker et al. 2002). MHC class I, encompassing HLA A, B, and C in humans, encodes the main molecular targets of allograft rejection as well as MHC-associated incompatibilities between donor and recipient. It is also responsible for almost all acute rejection. Indeed, upregulation of MHC class I, as well as multiple other co-stimulatory molecules, was seen in hESCs upon stimulation with IFN-γ (Figure S2). However, even the IFN-γ-stimulated hESCs were not rejected by *hSRC* mice (Figures S1B, S1C, S1E, and S1F). To address the possibility that the inability to reject these hESCs may be due to the hESCs modulating the immune response locally and enforcing tolerance, we transplanted *hSCR* mice with murine ESCs (mESCs), which should normally be rejected by human immune cells. However, these humanized mice were unable to reject murine cells as well (Figures S1G and S1H).

Having provided evidence for the inability of the *hSRC* model to mount strong PSC-directed immune responses, we moved to the *hBLT* model. *hBLT* mice support robust human cell engraftment of mouse lymphoid tissues and development of functional human T lymphocytes (Lan et al. 2006, Melkus et al. 2006). Indeed, total human leukocyte engraftment in *hBLT* mice in peripheral blood 12 weeks after humanization showed superior engraftment of B cells and $CD4^+$ T cells compared with the *hSRC* model (Figures S3A and S3B).

We next tested the ability of *hBLT* mice to reject human and mouse PSCs. Similar to the *hSRC* model, *hBLT* mice were transplanted with mouse iPSC (miPSC) grafts, generated from fibroblasts of a transgenic FVB mouse ubiquitously expressing EGFP and Luc (de Almeida et al. 2014); Figure 1A), or with human IFN-γ-stimulated hESC allografts (Figure 1B) by intra-splenic (i.s.) injection. The survival of the grafts was again monitored using BLI, with the signal normalized to the maximum radiance on day 1 of transplantation (Figure 1C). Despite superior engraftment of human immune cell subsets in *hBLT* mice compared with *hSRC* mice, the murine and human grafts were not rejected and underwent proliferative growth that resulted in large teratoma formation by week 4 and week 3, respectively (Figure S3C).

hBLT Mice Showed a Correlation between Pro-inflammatory Graft Infiltration and Graft Loss but Were Unable to Fully Reject Differentiated hESC-EC Grafts

Next, we derived mature endothelial cells from the labeled hESC line (hESC-ECs) to upregulate MHC class I molecules on ESCs, which has been described during differentiation of hESCs (Drukker et al. 2002). Upregulation of MHC class I molecules as well as several other co-stimulatory molecules was confirmed by differentiating hESCs using the embryoid body method (Figure S2). hESC-ECs (1×10^5) were then either transplanted s.c. in the back or i.m. in the gastrocnemius muscle of *hBLT* mice at 20 weeks after humanization, and graft survival was measured over time using BLI (Figure 2A). An initial decline in signal, representative of non-immune-mediated cell stress and loss during injections, was

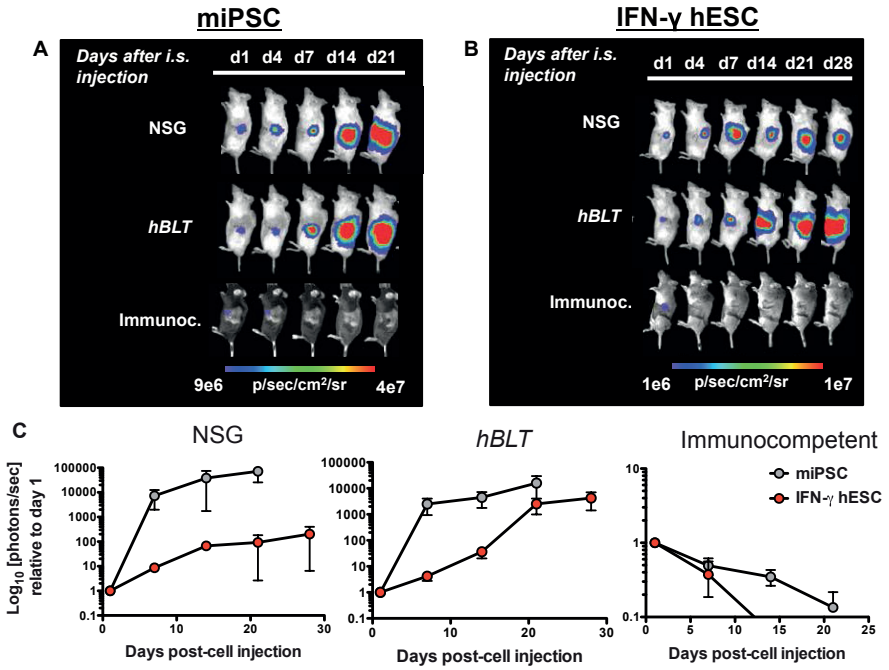


Figure 1. hBLT Mice Fail to Completely Reject Mouse iPSC Grafts and Allogeneic Human ESC Grafts (A and B) Representative BLI from one mouse per group, demonstrating the proliferation of miPSCs (A), and IFN-g-hESCs (B) after i.s. injection in NSG (n = 3) and *hBLT* mice (n = 5) and rejection of these cells in the immunocompetent (C57BL/6) recipients (n = 4). (C) Quantification of the BLI data normalized to the maximum radiance on day 1, showing intensification of the signal over time for transplanted miPSCs as well as IFN-g-hESCs in NSG and *hBLT* mice, respectively, resulting in teratoma formation (left and center). In contrast, complete immune rejection of miPSCs and IFN- g-hESCs occurred in immunocompetent C57BL/6 mice by 21 and 14 days, respectively (right). BLI data are represented as mean ± SEM of two independent experiments.

followed by stabilization of the signal and persistence of the graft for the duration of the study. Within the grafts, there appeared to be minimal immune cell infiltration (Figures S3D and S3E). The signal kinetics of hESC-ECs in *hBLT* mice were very similar or, in some cases, even improved compared with those in non-engrafted NSG mice, indicating that the reconstituted immune system might even favor graft persistence. In contrast, the signal in immunocompetent FVB mice returned to baseline within 2 weeks, indicating complete rejection of the hESC-EC grafts (Figure 2B). To be sure that the limited immune response was not the result of possible immune-evasive properties of hESC-ECs, we performed an additional experiment by transplanting labeled somatic human umbilical vein endothelial cells (HUVECs) into 16-week-old *hBLT* mice. Similar to the hESC-EC experiment, *hBLT* mice were unable to fully reject the HUVECs with graft persistence over a course of 3 weeks, whereas immunocompetent FVB mice rejected the cells within a week after transplantation (Figure S4).

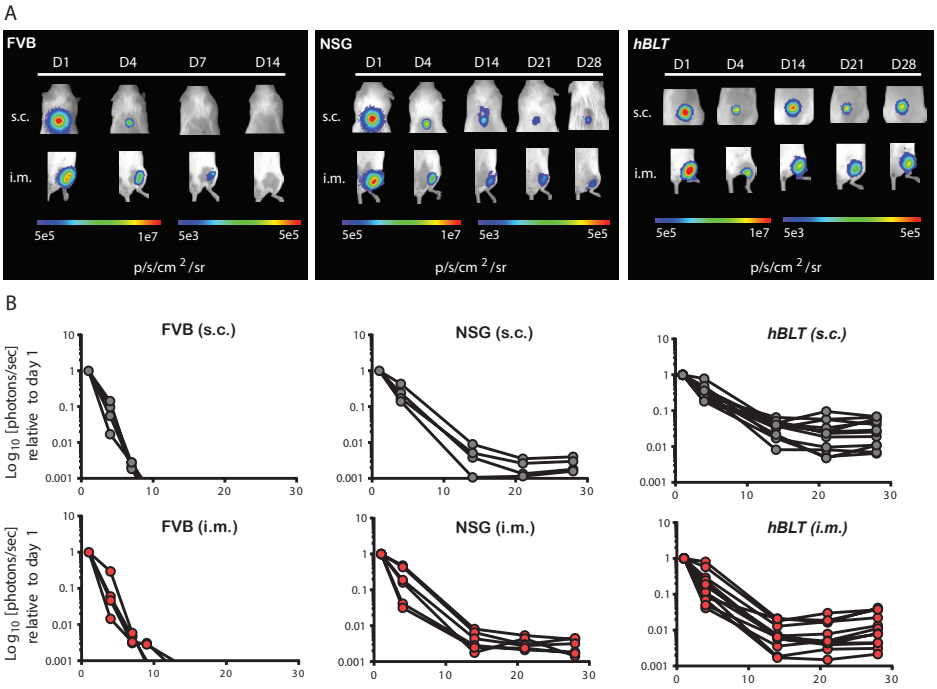


Figure 2. hBLT Mice Are Unable to Reject hESC-EC Grafts (A) Representative BLI from one animal per group over the course of 4 weeks, showing persistence of hESC-ECs after s.c. and i.m. injection in NSG (center, n = 5) and *hBLT* (right, n = 12) mice, whereas the immunocompetent FVB mice (left, n = 4) completely rejected the grafts by day 14. (B) Quantification of the BLI data normalized to the maximum radiance on day 1, showing initial non-immune-mediated graft loss followed by graft persistence in the subcutaneous (top) and gastrocnemius muscle (bottom) injection sites in NSG and *hBLT* mice and complete rejection by the FVB mice.

It is important to note that, over the course of the 4-week experiments, the condition of the *hBLT* mice deteriorated, with decreased body weight, fur loss, and lessened physical activity. For three *hBLT* mice, this necessitated euthanization. Uncertain about the cause of this increased morbidity and mortality, we analyzed the blood, spleen, draining inguinal lymph nodes (dLNs), and PSC grafts for human immune cell populations in the remaining 12 *hBLT* mice at 4 weeks (Table S1). Blood analyses of total $CD4^+$ helper T cells showed the presence of 64.5% ± 5.2% naive ($CD45RA^+$) T cells, 11.9% ± 2.8% activated memory helper T cells ($CD45RO^+$), and 7.6% ± 3.6% effector memory ($CD44^+$) helper T cells (Figure 3A, left). For $CD8^+$ cytotoxic T cells, the levels of naive cells decreased to 53.4% ± 6.4%, and they gained a more activated memory function with $CD45RO^+$ T cell levels at 20.6% ± 2.9% and cytotoxic effector memory cells at 21.0% ± 6.3% (Figure 3A, right). Only a very small percentage of human $CD3^+$ cells (0.4% ± 0.1%) was found in the dLNs, indicating that active human cells found in the systemic circulation were unable to traffic or localize appropriately to the dLNs (Figure 3B). In addition, the dLNs contained very few human B

cells or antigen-presenting cells. Analysis of the spleens showed substantial engraftment of human B and T lymphocytes but few monocytes or NK cells (Figure 3C). The subpopulations of $CD3^+$ lymphocytes consisted mainly of helper T cells and few cytotoxic T cells that were largely naive, with very few effector memory cells observed. Within the grafts, the human immune cells mainly retained a naive phenotype, with small percentages of effector memory $CD4^+$ (1.3% ± 0.3%) and $CD8^+$ (7.0% ± 1.3%) cells (Figure 3D). However, there was a strong correlation between graft loss, as indicated by the relationship between the decay in BLI signal, a reduction in the number of regulatory $FoxP3^+$ T cells and naive T cells (Figure 3E, left and center), and an increase in the amount of activated immune cells in the graft (Figure 3E, right). Again, the presence of inactive and immunosuppressive immune cells in the graft environment might favor graft persistence, whereas activated immune cells facilitated graft loss.

Taken together, our data suggest that these mice had an activated systemic immune system in the blood, but these active immune cells were not seen in similar quantities in the spleen, dLNs, or graft. Nevertheless, the limited numbers of activated graft-infiltrating T cells correlated strongly with graft loss. This revealed some functionality of the immune system in *hBLT* mice but also showed that they are incapable of mounting an effective alloimmune response to completely reject hESC-ECs.

In-depth Analyses of Immune Cells from hESC-EC-Engrafted hBLT Mice Show a "Non-stimulated" T Cell Phenotype

Immune cells isolated from spleens, dLNs, and Matrigel plugs from hESC-EC-engrafted mice were used for mixed lymphocyte reactions to assess the effectiveness of the different lymphoid structures in mounting an immune response. First, immune cells isolated from the blood and spleen of *hBLT* mice were stimulated with phorbol ester (phorbol myristate acetate [PMA])/ionomycin, and their activation was compared with positive control samples of HiCK-1 cells and PBMCs isolated from human whole blood (Figure S5A). Even though some pro-inflammatory responses were seen in the splenocytes of *hBLT* mice, this was reduced compared with the positive control samples. Second, immune cells isolated from the Matrigel plugs and dLNs were incubated with hESC-EC lysate or HUVEC lysate to compare specific and non-specific immune responses (Figure S5B*)*. In this experiment, neither hESC-EC nor HUVEC lysate exposure resulted in immune cell activation. Moreover, non-antigen stimulation by PMA/ionomycin also did not result in T cell activation. We next analyzed the gene expression profile of the small population of activated graft-infiltrating lymphocytes. As negative and positive controls for T cell activation, PBMCs from a healthy human donor remained unstimulated or were stimulated in vitro with PMA/ionomycin for 72 hr. After 72 hr, the PBMCs were harvested and, together with the *hBLT* lymphocytes, stained for murine and human CD45 markers and human CD3, CD4, CD8, CD45RA, and CD45RO. Human lymphocytes with an activated memory surface marker

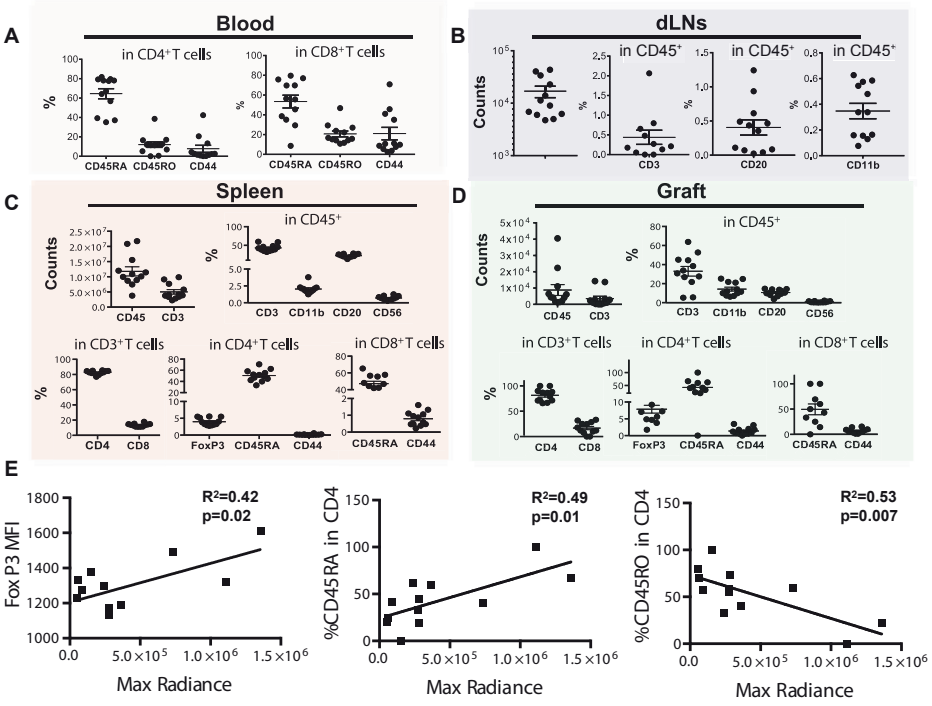


Figure 3. hBLT Mice Reveal Systemic Immune Activation, with a Strong Correlation between Small Numbers of Human Graft-Infiltrating Cells and Rejection of Allogeneic hESC-ECs (A and B) FACS analysis of (A) blood shows an active ($CD45RO^+$; $CD44^+$) systemic cytotoxic T cell ($CD8^+$) response but (B) little population of T cells as well as B cells and macrophages in the inguinal dLNs.

(C) Analysis of the spleen reveals larger populations of B cells ($CD20^+$) and T cells ($CD3^+$), but subpopulations of the latter show relatively high numbers of naive (CD45RA) and few effector memory ($CD44^+$) T cells. (D) Limited numbers of graft-infiltrating lymphocytes consist mainly of naive T cells with few effector memory cells. (E) The decrease in BLI signal (Max Radiance) in the graft was significantly correlated with a lower number of regulatory T cells (FoxP3, left) and naive T helper cells (CD45RA, center) and an increase in activated T helper cells (CD45RO, right).

Data are displayed as percentage (%) or number of cells (counts) within the parent population, e.g. in CD45/CD3/CD4/CD8 cells. Data are represented as mean ± SEM from one experiment (n = 12).

profile ($CD4^+CD45RO^+$; $CD8^+CD45RO^+$) were isolated using fluorescence-activated cell sorting (FACS), and their gene expression was analyzed with the Fluidigm single-cell PCR platform using a panel of 92 genes known to be involved with human Th1, Th2, and Th3 immune responses (Table S2).

Principal-component analysis (PCA) of the fold changes of all 92 genes revealed that *hBLT* $CD3^+$ lymphocytes isolated from the grafts grouped with the unstimulated control human T lymphocytes (Figure 4A). Activated human helper T cells ($CD4^+CD45RO^+$) and cytotoxic T cells ($CD8^+CD45RO^+$) isolated from *hBLT* spleens showed a similar grouping to their unstimulated counterparts from the healthy control (Figures 4B and 4C). These

activated memory graft-infiltrating lymphocytes and splenocytes had an "unstimulated" phenotype upon allogeneic antigen stimulus. However, the strong correlation between graft loss and the presence of $CD45RO^+$ lymphocytes seems to indicate that the graft-infiltrating lymphocytes were properly stimulated to target the grafts earlier in the response but that the immune response had subsided. Therefore, we analyzed gene expression profiles in *hBLT* splenocytes associated with T cell anergy and exhaustion. T cell exhaustion is described in cases of chronic infection and continuous exposure to foreign antigens and is associated with the upregulation of genes such as *CTLA4*, *LAG3*, and *TIM3*(Wherry 2011). Human activated memory helper T cells ($CD4^+CD45RO^+$) and activated memory cytotoxic T cells ($CD8^+CD45RO^+$) isolated from the spleen showed higher expression levels of these genes compared with unstimulated and stimulated PBMCs from the healthy human control (Figure S5C), providing initial signs for exhaustion of the human lymphocytes. A full-scale immune response cannot be mounted by these $CD4^+CD45RO^+$ and $CD8^+CD45RO^+$ lymphocytes, potentially explaining the inability of the *hBLT* model to fully reject allogeneic hESC grafts.

To assess where in the development of the *hBLT* model the failure in graft rejection occurs, we next analyzed the immune cells of *hBLT* mice (n = 5) at different time points during the humanization process. Blood samples from five *hBLT* mice were drawn at week 8 (p0), 16 (p3), and 20 (p4) after humanization, and human T cells were isolated for RNA sequencing (RNA-seq). The immune profile was then compared with T cells from a healthy control human blood sample (ctrl). The immune profile of human immune cells within the *hBLT* model at week 8 post-humanization reveals an immune profile similar to the human control sample, but, by weeks 16 and 20, this immune profile starts to diverge and shows significant upregulation of immune profiles associated with T cell anergy and upregulation of inhibitory molecules (Figures 4D and 4E).

Allogenized Mice Have a More Organized Lymphoid Architecture Than Humanized Mice and Can Reject Xenogeneic and Allogeneic iPSCs

Our data so far have demonstrated the superior engraftment of human immune cells in the *hBLT* model, but the model appears to have a limited ability to mount a robust full-scale allogeneic immune response to human PSCs over time. To determine whether this is "model-dependent," we next created allogenized mouse models by reconstituting NSG mice with allogeneic C57BL/6 mouse bone marrow (*aBM* mice) as well as mouse bone marrow, liver, and thymus (*aBLT* mice). Donor immune cells, as well as fetal liver and thymus transplanted in the abdomen, remained viable for up to one year in these models (Figure S6A).

Engraftment of donor immune cells in allogenized NSG mice was assessed by flow cytometry 12 weeks post-HSC transplantation. Donor cells were identified based on the CD45 allelic disparity between donor C57BL/6 (CD45.2) and recipient NSG (CD45.1) mice. Both the *aBM* and the *aBLT* allogenized mouse models had high levels of donor immune cell

engraftment. The percentages of total leukocytes, T cells, B cells, and NK cells in peripheral blood were similar between the two models and did not differ from wild-type C57BL/6 mice (Figure S6B).

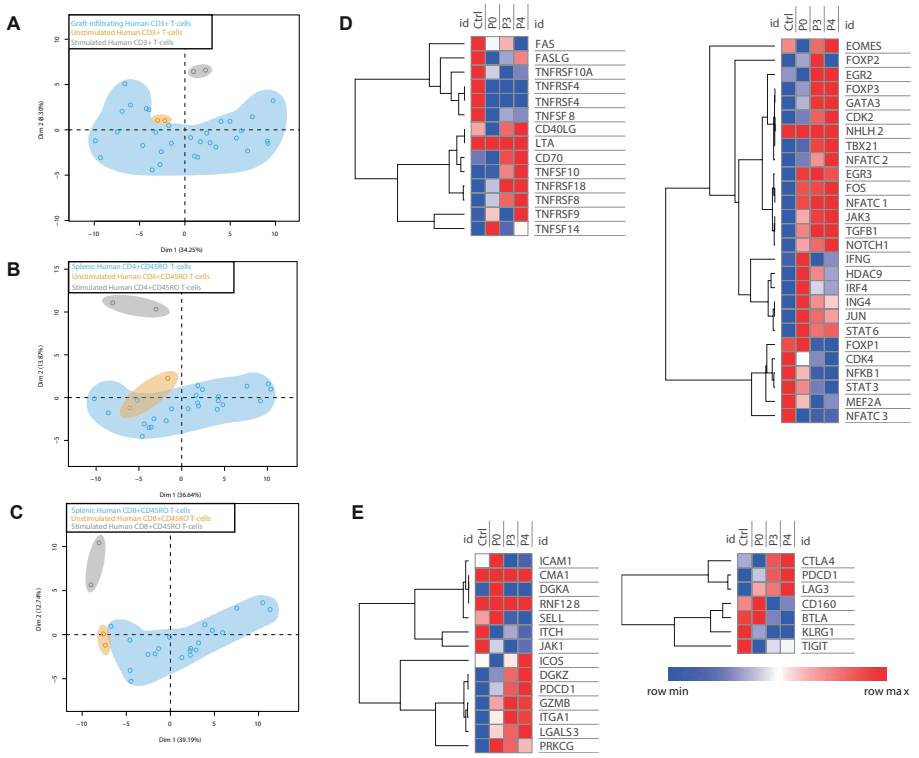


Figure 4. Single-Cell PCR Analysis and RNA-Seq of hBLT Graft-Infiltrating T Lymphocytes, dLNs, and Splenocytes Reveals the Unstimulated Phenotype (A) Graft-infiltrating lymphocyte ($CD3^+$, blue) group with unstimulated human PBMCs (yellow) and wide separation of PMA/ionomycin-stimulated human PBMCs (gray). (B and C) A similar trend was seen for activated helper T cells ($CD4^+CD45RO$, B) and activated cytotoxic T cells ($CD8^+CD45RO$, C) isolated from the spleens of *hBLT* mice. (D) Human immune cells isolated from *hBLT* mice show an impaired immune profile compared with the human control samples. Human T cells were isolated from *hBLT* blood at week 8 (p0), week 16 (p3), and week 20 (p4) (n = 5 mice per time point) after humanization, and the RNA expression profile was compared with T cells isolated from healthy human blood samples. At p0, the immune profile of *hBLT* T cells is most similar to control T cells, despite some marked increases in pro-inflammatory cytokine profiles at that time point. In contrast, other genes involved in T cell inhibition (*FOXP3*, *TGFB1*) are hardly expressed at baseline, but their expression increases over time during the aging of the mice. Interestingly, at p3, the ESC-derived ECs and HUVECs were engrafted, but this did not result in changes in the immune profile at p4. (E) Human T cells isolated from *hBLT* mice develop T cell anergy and senescence upon aging. At p0, the T cell anergy gene profile of human T cells is similar to human control T cells. However, upon aging of the *hBLT* mice, the anergic profile becomes increasingly present (left). A similar result was seen for the inhibitory molecules (right). Also, the engraftment of allogeneic cells at p3 did not result in an alteration from an inhibitory to a pro-inflammatory immune profile.

We examined the lymphoid structures in *aBLT* mice and compared these with the lymphoid structures in the *hBLT* mice, wild-type C57BL/6 mice, and unmanipulated negative control NSG mice (Figure 5A). H&E analysis of the spleens of *hBLT* mice revealed marked hematopoiesis but minimal periarteriolar lymphocyte migration (Figures 5C and 5E, center). Interestingly, this splenic architecture does mature over time with the development of a marginal zone by week 24 after humanization (Figure S7). In dLNs, human lymphocytes were found in minimal quantities at week 12 compared with the wild-type mouse (Figure 5F, left and center). In contrast, the spleen of the allogenized mouse at week 12 after humanization had a very similar architecture as the wild-type C57BL/6 mouse (Figures 5B and 5E), with periarteriolar lymphoid sheaths but without apparent germinal center B cell areas. In addition, the lymphoid areas of allogenized mouse spleens had irregular margins, consistent with missing marginal zone-type cell development or paucity of the perilymphoid macrophage-rich collections that are part of the specialized open and closed circulation (Figures 5D and 5E, right). Analysis of the dLNs in the allogenized mouse

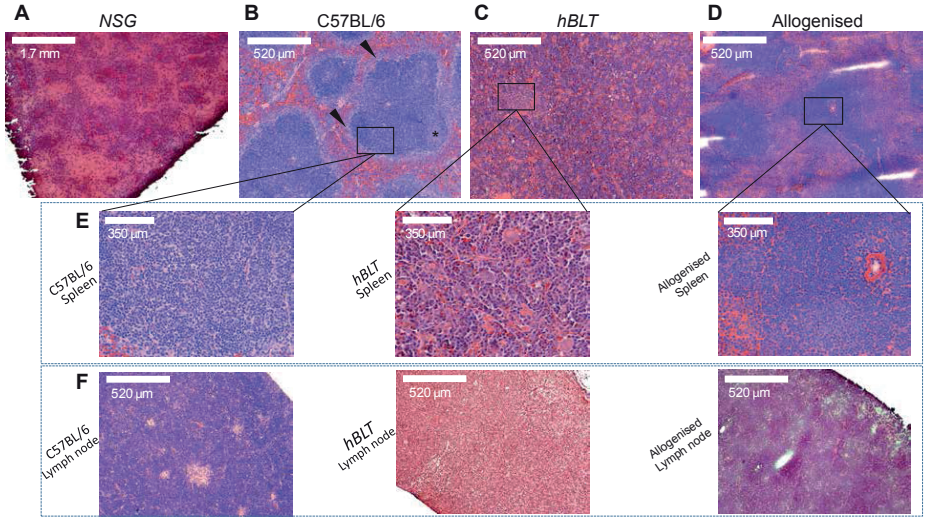


Figure 5. Allogenized Mice Have a More Organized Lymphoid Architecture that Is Similar to Wild-Type Mice (A) Overview of splenic tissue in NSG mice with poorly developed splenic architecture (H&E, 2x magnification). (B) Normal splenic architecture in a wild-type C57BL/6 mouse with a periarteriolar T cell area, B cell area (asterisk), and marginal zone (arrowheads) (H&E, 10x magnification). (C) *hBLT* mice show a high degree of hematopoiesis in the spleen but little periarteriolar T cell migration and an overall disorganized splenic architecture (H&E, 10x magnification). (D) Allogenized mice have an architecture more similar to the wild-type C57BL/6 mouse, with periarteriolar lymphoid sheets. However, apparent germinal center B cell areas as well as marginal zones are missing, giving the periarteriolar margins an irregular shape (H&E, 10x magnification). (E) Higher-magnification images (40x) of sites of interest in (B)–(D). (F) Overview of inguinal dLNs, showing high levels of lymphocyte infiltration in wild-type C57BL/6 (left) and allogenized mice (right) compared with the *hBLT* mouse model (center) (H&E, 40x magnification).

revealed high levels of lymphocytes, indicating migration of the lymphocytes to peripheral lymphoid organs (Figure 5F, right).

Next, allograft responses in the *aBM* and *aBLT* models were examined in vivo against allogeneic miPSCs. Allogenized mice were injected with 1×10^5 labeled miPSCs i.m. or i.s., and the survival of miPSC grafts was monitored longitudinally using BLI. The allogenized mice showed robust rejection of miPSC implanted i.m., similar to immunocompetent C57BL/6 mice, although rejection was delayed by ~7 days compared with that observed in C57BL/6 mice (Figures 6A and 6C). In contrast, the PSC survival kinetics in the spleens of allogenized mice were indistinguishable from immunocompetent mice (Figures 6B and 6D), and no differences were observed between the *aBM* and *aBLT* models with respect to their capacity to reject allografts (Figure S6C). Allogenized mice also developed robust

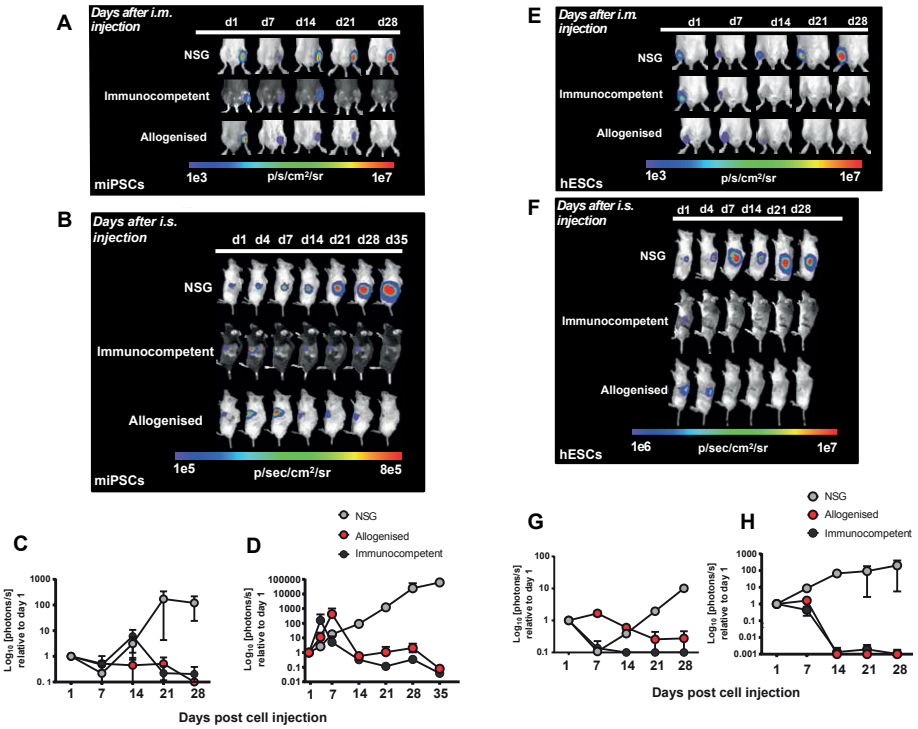


Figure 6. Allogenized Mice Show Robust Rejection of Allogeneic miPSC Grafts and Xenogeneic Human IFN-g-Stimulated ESC Grafts (A) Robust but somewhat delayed rejection of miPSC allografts injected i.m. (B) miPSC allografts injected i.s. were rejected at a similar rate as in immunocompetent C57BL/6 mice. (C and D) Quantification of the BLI data from (A) and (B), respectively, normalized to the maximum radiance on day 1. (E and F) More rapid rejection of xenogeneic hESCs injected (E) i.m. and (F) i.s. but, again, delayed by ~7 days compared with immunocompetent mice. (G and H) Quantification of the BLI data from (E) and (F), respectively, normalized to the maximum radiance on day 1. BLI data are represented as mean ± SEM from four independent experiments (n = 3).

immune responses that resulted in rapid rejection of hESCs, although rejection of hESCs injected i.m. or i.s. was again slightly delayed by 4–7 days compared with that of immunocompetent mice (Figures 6E–6H). Overall, these findings suggest that the allogeneic thymus offers an adequate microenvironment for appropriate mouse T cell development that leads to a robust allograft response. Furthermore, these data suggest that allograft responses can be modeled in reconstituted NSG mice, although there was a delay in rejection of the PSCs at some sites in the allogenized mice compared with wild-type C57BL/6 mice.

Allogenized Mice Demonstrate Impaired Immune Responses to Minor Histocompatibility-Mismatched Stem Cell Grafts

To investigate the ability of allogenized mice to reject minor histocompatibility-mismatched grafts, we next implanted mESCs with an immunological mismatch at the minor histocompatibility antigen (mHA). The mESCs from the 129S1/SvlmJ strain ($H2K^bD^b$) were injected i.m. or i.s. into allogenized mice (donor cells from C57BL/6J mice, $H2K^bD^b$). In contrast to immunocompetent mice (C57BL/6), allogenized mice were unable to reject mHA-mismatched mESCs at either implantation site. The rate of tumor growth in allogenized mice was slightly slower than in non-engrafted NSG mice. Nevertheless, large teratomas without signs of regression developed within 30 days in allogenized and NSG mice (Figures 7A–7D).

To gain insights into the defective immune responses found in the allogenized mice in response to mHA-mismatched grafts, we next examined cytokine production of splenocytes from mHA-mismatched allogenized mice. Production of IFN-γ by splenocytes in response to short-term PMA and ionomycin stimulus was found to be significantly diminished compared with immunocompetent C57BL/6 mice (Figure 7E). Overall, the slower growth of mHA grafts in our allogenized mice shows limited effectiveness in rejecting mHA cells. However, the significant reduction of IFN-γ levels in response to PMA and ionomycin reveals an inability of the reconstituted immune system to respond appropriately to mHA grafts.

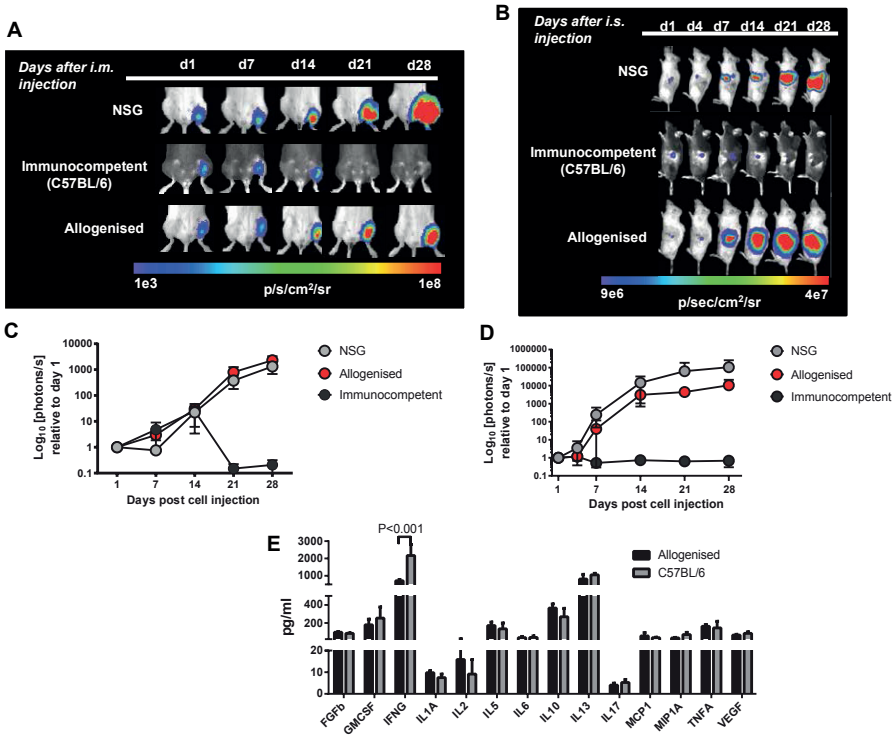


Figure 7. Allogenized Mice Fail to Reject mHA-Mismatched ESC Murine Allografts and Have Reduced IFN-g Responses (A and B) Allogenized mice were unable to reject mHA-mismatched 129S1/SvImJ mESCs injected (A) i.m. (n = 5) or (B) i.s. (n = 5), and their BLI signal was similar to unmanipulated NSG mice (n = 4), whereas immunocompetent mice (n = 4, n = 5) rapidly rejected these grafts at both implantation sites. (C and D) Quantification of the BLI data from (A) and (B), respectively, normalized to the maximum radiance on day 1. (E) Significantly reduced production of IFN-g from allogenized mouse splenocytes exposed to mHA-mismatched mESCs using a multiplex-Luminex platform. Cytokine data are represented as mean ± SEM from one experiment (n = 3).

DISCUSSION

Preclinical trials using humanized mice could prove to be crucial in addressing the efficacy and safety of supportive therapies necessary for the maintenance of PSC grafts. One report addressed the immunogenicity of CTLA4-Ig- and PD-L1-overexpressing PSC grafts using the *hBLT* model (Rong et al. 2014). An immune response to hESCs, marked by lymphocyte infiltration and necrosis of teratomas, was observed. However, solely relying on T cell infiltration is an insufficient measure of graft rejection because infiltrates may, in fact, be suppressing the immune response (de Almeida et al. 2014). This is supported by our observation of T cell infiltration in our humanized mice that did not result in graft rejection. We therefore utilized in vivo BLI to track graft survival over time instead of relying solely on

histopathology. In addition, central necrosis of tumors formed after injection of PSCs can also occur when proliferative growth is too high or too many PSCs are injected, as has been described in performing teratoma assays (Nelakanti et al. 2015).

We tested two humanized mouse models, *hSRC* and *hBLT*, to assess human immune responses to human allogeneic undifferentiated ESCs and ESC derivatives. Comparing these two mouse models, our results suggest that a functional full-scale immune response capable of rejecting human PSCs and their derivatives does not develop in these mice. We demonstrated this by first transplanting undifferentiated hESCs into *hSRC* mice. Because of the limitations of the *hSRC* mouse to properly educate human T cells in the murine thymus, we transplanted these cells in the *hBLT* model. Even though these *hBLT* mice were better reconstituted with human immune cells, the *hBLT* model still presents with abnormal reconstitution of certain subsets, such as $CD8^+$ T cells as well as NK cells and other innate immune cells (Rongvaux et al. 2014). Similar to the *hSRC* model, the *hBLT* model was unable to reject miPSCs, allogeneic hESCs, differentiated hESC-ECs, and somatic HUVECs. In some *hBLT* mice, with higher numbers of intra-graft naive and regulatory T cells, graft survival even improved compared with NSG mice. Conversely, we would like to note that humanized mice have proven to be useful in the modeling of rejection of skin grafts and human islet grafts (Xiao et al. 2014). In our model, there was a strong correlation between activated immune cells and graft loss, indicating that an effective immune response to the hESC-EC grafts developed at some point. However, the limited presence of immune cells in the dLNs and allografts suggests reduced clonal expansion of effector T cells in these tissues. This was confirmed by FACS analysis and H&E staining of the dLNs, which showed limited presence of lymphocytes and macrophages as well as disorganized lymphoid structures, respectively. Both negatively influence adequate antigen presentation and subsequent stimulation of T cells.

Single-cell PCR analysis of the small percentage of activated ($CD45RO^+$) lymphocytes found in the grafts, as well as splenocytes isolated from *hBLT* mice, showed a similar immunological phenotype to unstimulated PBMCs isolated from a healthy human donor, which contrasted sharply with PMA and ionomycin-stimulated healthy donor PBMCs. Even though the amount of $CD45RO^+$ T cells was small in the spleens and PSC grafts of humanized mice, $CD45RO^+$- and $CD44^+$-expressing $CD8^+$ lymphocytes in the blood were increased to ~20%, providing evidence for a systemically activated immune system. Additional RNA-seq data, derived from *hBLT* immune blood cells at different time points during humanization, further show the development of an anergic or exhausted T cell phenotype over time after an initial activated immune profile. In vivo testing of the different immune cells from the lymphoid organs was performed after the transplant studies by re-exposing them to antigens from the transplanted cells, unencountered antigens, or a non-antigen-specific stimulus with PMA/ionomycin. However, none of the conditions described above

resulted in the upregulation of pro-inflammatory cytokines and an overall inability to be activated.

We hypothesized that the education of human immune cells in the human fetal thymus failed to completely tolerize the developing human T cells to murine antigens, leading to an activated systemic immune system and a subsequent increase in morbidity and mortality in *hBLT* mice. This development of a wasting disease-like syndrome in *hBLT* mice has been described previously (Greenblatt et al. 2012, Covassin et al. 2013, Lockridge et al. 2013), but not in all laboratories (Onoe et al. 2011), and is correlated with a decrease of naive human CD45RA cells in the blood, as seen in our *hBLT* mice. The *hBLT* mice in our study were screened for chimerism 12 weeks after humanization, the transplant studies were initiated 20 weeks after humanization, and the mice were euthanized 4 weeks later. Having supporting RNA-seq and single-cell PCR data that show exhaustion of the human lymphocytes, combined with data showing impaired cytokine production during that time, indicates that there is a limited time frame for modeling human immune responses in these mice.

To test the feasibility of reconstituting an NSG mouse with a functional immune system that is capable of rejecting allogeneic PSC grafts, we next created an allogenized mouse model with allogeneic murine fetal bone marrow, thymus, and liver. This allogenized mouse model and the transplanted allogeneic hematopoietic and immune system remained viable for up to a year. Functionally, our allogenized mouse was able to fully reject the human grafts and allogeneic murine grafts. However, the allogenized mouse was unable to reject the mHA-mismatched mESCs, and these cells proliferated without signs of rejection. Cytokine profile analysis of their spleens revealed significantly lower levels of IFN-γ, which has important immunostimulatory effects and is critical for effective innate and adaptive immune responses. IFN-γ is produced predominantly by NK and NK T (NKT) cells as part of the innate immune response and by $CD4^+$ T helper (Th) type 1 and $CD8^+$ cytotoxic T cells when antigen-specific immunity develops. Under normal circumstances, NK and NKT cells show markedly increased IFN-γ secretion within hours after stimulation (Schoenborn and Wilson 2007), which did not occur in our allogenized mice. The presence of a more organized lymphoid structure in the allogenized mouse compared with the humanized mouse, as well as these immune cells' ability to be activated by allogeneic cytokines (Manz 2007), might provide an explanation for why the allogenized mouse was able to reject allogeneic and human grafts. However, the absence of a fully functional innate immune system, as indicated by the lower levels of IFN-γ, resulted in a delayed immune response to human and allogeneic murine grafts and an inadequate response to mHA-mismatched grafts.

In summary, we have shown, with the allogenized mouse, that reconstitution of an immunodeficient mouse with a functional immune system is feasible and would allow for the modeling of PSC alloimmunity. However, current humanized mouse models suffer from inadequate reconstitution of the innate immune system and the development of a wasting disease-like syndrome that renders them inadequate for long-term PSC transplant studies.

To limit the development of this syndrome, future efforts will focus on genetic modification of the SIRPA-CD47 pathway (i.e., providing a "don't eat me signal") (Lavender et al. 2013) as well as the continuing development of NSG mice that transgenically express HLA molecules in their thymus (Shultz et al. 2010, Babad et al. 2014), therefore allowing HLA-restricted T cell selection for both human and murine antigens. Moreover, NSG mice expressing important human cytokines for innate and adaptive immune responses, such as macrophage colony-stimulating factor (M-CSF), IL-3/granulocyte macrophage colony-stimulating factor (GM-CSF), and TPO, already exist (Rongvaux et al. 2014), and combination of one or more properties of these mice could result in a more effective model with which to conduct studies of the immunobiology of PSC therapeutics.

EXPERIMENTAL PROCEDURES

Humanized and Allogenized Mouse Development

All experiments were performed with approval of the Animal Care and Use Committee at Stanford University and the Institutional Animal Care and Use Committee (IACUC) committee at University of Massachusetts Medical School. Humanized *hSRC* mice (12 weeks old) were developed by γ-irradiating, 100 centigray (cGy), NOD.Cg-*Prkdc*^{scid} *IL2rg*^{tm1Wj1}/Sz (NSG) mice (3-4 weeks old) and transplanting them with lineage depleted HSCs (100,000 CD34^{+} HSC). Humanized *hBLT* mice (12 weeks old; male) were developed by γ-irradiating (200 cGy) NSG mice (6–8 weeks old), surgically implanting HLA-A2^{neg} human fetal liver and thymus under the kidney capsule, and injecting autologous HSCs (100,000 CD34^{+} HSC). All mice were screened for human cell chimerism levels 12 weeks post-engraftment. Allogenized mice were generated at Stanford University using a similar methodology as that used for generating *hBLT* mice (Supplemental Experimental Procedures). Control female mice, FVB/NJ mice, and C57BL/6J mice were purchased from The Jackson Laboratory at 6–8 weeks of age and aged to match our humanized and allogenized mice.

Labeling of hESCs and miPSCs for Bioluminescence Imaging

Human ESCs (H9 cell line, HLA-A2pos; obtained from WiCell, Madison, WI) were cultured on Matrigel-coated plates in mTeSR1 medium (Stem Cell Technologies, Vancouver, BC, Canada) as described previously (Ludwig et al., 2006). Mouse iPSCs were created by reprogramming of fibroblasts using a lentiviral based approach for delivery of the four reprogramming factors (Klf4, Oct4, Sox2 and c-Myc)(Takahashi and Yamanaka, 2006). Both cell lines were stably transduced with a reporter construct containing the ubiquitin promoter driving firefly luciferase and EGFP as previously described (Pearl et al., 2011).

Differentiation and Characterization of hESC-derived Endothelial Cells (hESC-ECs)

Transgenic hESCs were differentiated into ECs by culturing EBs with culture media containing DMEM (Invitrogen) containing 20% knockout serum (Invitrogen), 4.5 g/L L-glutamine (Invitrogen), 1% nonessential amino acids (Invitrogen), 0.1 mM 2-mercaptoethanol (Invitrogen), 50 units/ml penicillin (Invitrogen), 50 µg/ml streptomycin (Invitrogen), 10 ng/ml Activin A (R&D Systems), and 20 ng/ml bone morphogenetic protein-4 (BMP-4) (R&D Systems). The differentiation medium was supplemented with 25 ng/mL vascular endothelial growth factor (VEGF) (R&D system) and 8 ng/mL bFGF (R&D system). At day 4, the EBs were then seeded onto Matrigel-coated dishes and cultured for another 10 days in differentiation media without BMP-4. On day 14, plated EBs were digested and sorted by fluorescence activated cell sorting (FACS) for CD31-positive cells. The $CD31^{+}$cells were collected and seeded into a six-well plate, coated with 0.2% gelatin, and cultured in EGM-2 medium (Lonza). Characterization of the hESC-ECs was done by immunofluorescence staining for the EC markers CD31, CD144, and laminin and their ability to take up ac-Dil-LDL and form tubes on Matrigel (Huber et al., 2013).

Induction of MHC-I upregulation in hESCs by IFN-γ Stimulation or Differentiation

For in vitro stimulation of hESCs with IFN-γ, 25 ng/ml of the cytokine was added to the growth mediafor 48 hr. After 48 hr, hESCs were harvested and labelled with antibodies for MHC-I (BD Pharmingen, Cat. nr: 555553), SSEA4 (R&D systems, Cat. nr: MAB1435), B2-m (BD pharmingen, Cat. nr: 551337), MHC-II (BD Pharmingen, Cat. nr: 555557), ICAM-1 (BD Pharmingen, Cat. nr: 555511), LFA-3 (BD Pharmingen, Cat. nr: 555921), B7-1 (eBiosciences, Cat. nr: 11-0809), B7-2 (eBiosciences, Cat. nr: 12-0869), B7-H1(eBiosciences, Cat. nr: 12-5983), and CD40 (eBiosciences, Cat. nr: 11-0409) and analyzed using FACS. To measure MHC-I and other co-stimulatory molecules during differentiation, EBs were harvested at day 14 of differentiation and digested to a single-cell suspension. Cells isolated from these EBs were then stained with the same antibodies as for the IFN-γ stimulation assay and analyzed using FACS.

Cell Graft Implantation

Mice were placed in an induction chamber and anesthetized using 1-2% isoflurane (Isothesia, Butler Schein) and 98-99% oxygen at a delivery rate of 2 l/min. Cells were mixed with Matrigel High Concentration (BD biosciences) and PBS on a 1:2 ratio and injected s.c. in the lower dorsa, i.m. in the hindlimb, or i.s. in the spleen.

Graft Explantation and Cell Isolation

Grafts were explanted, minced and digested with Liberase (27 WU ml−1; Roche, Indianapolis, IN, USA) and DNase I (0.1%; Roche) in Dulbecco's modified Eagle medium (DMEM) media at 37 °C for 30 min with slight agitation. Digested grafts were passed through a 100-μm strainer and centrifuged at 300g for 10 min at 4°C. Cells were counted and prepared for flow cytometry.

Flow Cytometric Analysis of Cytokine Production

Cells were isolated from explanted grafts as described above, as well as from murine and human whole blood. Mixed lymphocyte reactions were performed using the Human Intracellular Cytokine Staining Starter Kit (BD Pharmingen). Briefly, the reactions were performed in a 96 well plate, with 5 x 10^5 cells used per reaction. Cells were incubated in one of the following conditions: PMA/ionomycin (10 μL per well), HUVEC lysate (25 μg/well), or hESC-EC lysate (25 μg/well) for 4 hours. The cells were then fixed, permeabilized, and stained with PE-conjugated antibodies for IL-2, IFN-γ, and TNF. Flow cytometry was performed using a FACSAria II SORP flow cytometer (BD Biosciences), and analysis was performed using FlowJo software.

Immunohistochemistry of Explanted Grafts

Gastrocnemius muscle containing hESC-EC grafts were explanted, fixed overnight in 4% paraformaldehyde, and transferred to 70% ethanol for 24 hr. Fixed samples were embedded in paraffin and 5μm sections were cut and stained with hematoxylin and eosin (H&E) for histological analysis. In addition, 10μm sections were prepared for immunohistochemistry using heat induced epitope retrieval. In brief, paraffin embedded gastrocnemius slides were deparaffinized using 2 washes of 5 min each in Histoclear II (EMS Diasum, PA, USA) followed by an ethanol rehydration series of 100%, 90%, 75%, and 50% EtOH for 3 min each. Antigen unmasking was then performed in 10mM sodium citrate pH 6.0 in a water bath set to 98°C for 20 min. After antigen retrieval, these sections were blocked with mouse on mouse blocking reagent (Vector Laboratories) and stained with anti-human CD3 (1:100; Abcam), CD31 (1:50; Invitrogen), and anti-GFP (1:500; Abcam). For the CD3 and GFP staining, Alexa-594-conjugated secondary antibodies (1:200; Life Technologies) were used, respectively. An anti-mouse IgG (biotin) and subsequent streptavidin Alexa-488 conjugate was used as a secondary antibody against the anti-CD31 (1:500; Life Technologies). After 3 washes with PBS, slides were mounted with DAPI-containing mounting media (Vectashield, Vector labs) and immunofluorescent images were taken by fluorescent microscopy.

In Vivo BLI

Survival of transplanted hESC-ECs was longitudinally monitored with BLI using the Xenogen In Vivo Imaging System (Caliper Life Sciences). After i.p. injection of the reporter probe

D-luciferin (375 mg/kg body weight), the mice were placed in the light-tight chamber and imaged with integration times of 5 s to 2 min, depending on emission intensity. Quantification of the BLI signal was performed by using the maximum photons per square centimeter and is presented as Log10 (photons s^{-1}).

Flow Cytometric Analysis of Graft-Infiltrating Lymphocytes

Cells were isolated from s.c. and i.m. injected grafts and resuspended in FACS buffer (phosphate-buffered saline [PBS] containing 2% fetal bovine serum [FBS] and 2 mM EDTA), and the Fc receptor was blocked by anti-human Fc receptor-blocking antibody (Miltenyi Biotec). Samples were then stained with fluorophore-conjugated monoclonal antibodies against murine CD45 and the following human markers: CD45, CD3, CD4, CD8, CD25, FoxP3, CD11b, and NK1.1 (1:100; BD Biosciences, eBioscience, BioLegend, and Thermo Fisher). Cells were fixed and permeabilized using BD Cytofix/Cytoperm fixation, and intracellular staining was performed. Cells were assayed using an LSRII flow cytometer (BD Biosciences) and further analyzed with FlowJo software (Tree Star, Ashland, OR, USA).

RNA-Seq

$CD45^+$ and $CD3^+$ cells were isolated by flow cytometry using a FACSAria II special order research product (SORP) flow cytometer (BD Biosciences). Total RNA was extracted and quantified using the miRNeasy Kit (QIAGEN) according to the manufacturer's protocol. Ten nanograms of total RNA was used to generate index-tagged paired-end cDNA libraries. Briefly, mRNAs were purified and then amplified to cDNA using the Ovation RNA-Seq System V2 (NuGEN). Libraries were prepared and indexed using the NEBNext Ultra DNA Library Prep Kit for Illumina and NEBNext Multiplex Oligos. Sequencing was performed with Illumina's HiSeq4000 platform using paired-end reads at an average length of 100 bp (2×100).

RNA-Seq Analysis

The sequenced reads were aligned to the human genome (hg19, downloaded from University of California, Santa Cruz [UCSC]) by HISAT2 (https://ccb.jhu.edu/software/hisat2/index.shtml; (Pertea et al. 2016)). We then used FeatureCounts (http://bioinf.wehi.edu.au/featureCounts/; (Liao et al. 2014) to quantitate the transcriptome with genome annotation GENCODE 19 (hg19, version 19). DESeq2 (https://bioconductor.org/packages/release/bioc/html/DESeq2.html; (Love et al. 2014) of Bioconductor was applied to the raw reads of the transcriptome to normalize and generate the table of differentially expressed genes (DEGs) (likelihood ratio test [LRT], $p < 0.05$). Hierarchical clustering was then implemented on the DEGs. Function enrichment analyses of the DEG clusters were then implemented by GeneAnswers from Bioconductor (https://www.bioconductor.org/packages/release/bioc/html/GeneAnswers.html).

Single-Cell PCR Analysis

Gene expression of single cells was done using a 96.96 Dynamic Array chip (M96, Fluidigm). Single cells were sorted into each well of a 96-well PCR plate. After cell sorting and brief PCR plate centrifugation, the plate was placed in a thermocycler for reverse transcription into cDNA, followed by pre-amplification for 18 cycles. Finally, samples and assays were loaded in the M96 Fluidigm plate using a NanoFlex integrated fluidic circuits (IFC) controller (Fluidigm), followed by real-time PCR in the BioMark high-definition (HD) system (Fluidigm). The results were analyzed using the Fluidigm real-time PCR analysis software.

Multiplex-Luminex Cytokine Assay

Production of various cytokines was measured in cell culture supernatant using a multiplex-Luminex (LabMap200 system, Luminex) together with Panomics antibodies at the Human Immune Monitoring Center at Stanford University.

Statistical Methods

Statistical tests were performed using GraphPad Prism software. Bar graphs represent the mean and SEM for each group. R package FactoMineR (http://cran.r-project.org/web/packages/FactoMineR/index.html) was applied for PCA and visualization of gene expression. The statistical method used in Figure 3 for the correlation analysis was a Pearson correlation test. In Figure 7E, the mean levels of IFN-γ between two groups were compared using an unpaired Student's t test. The engraftment data in Figure S3B were analyzed by comparing the mean percentage of cells between two groups using multiple t tests.

Accession Numbers

The accession number for the raw and processed data from the next-generation RNA-seq experiments reported in this paper is NCBI GEO: GSE100791.

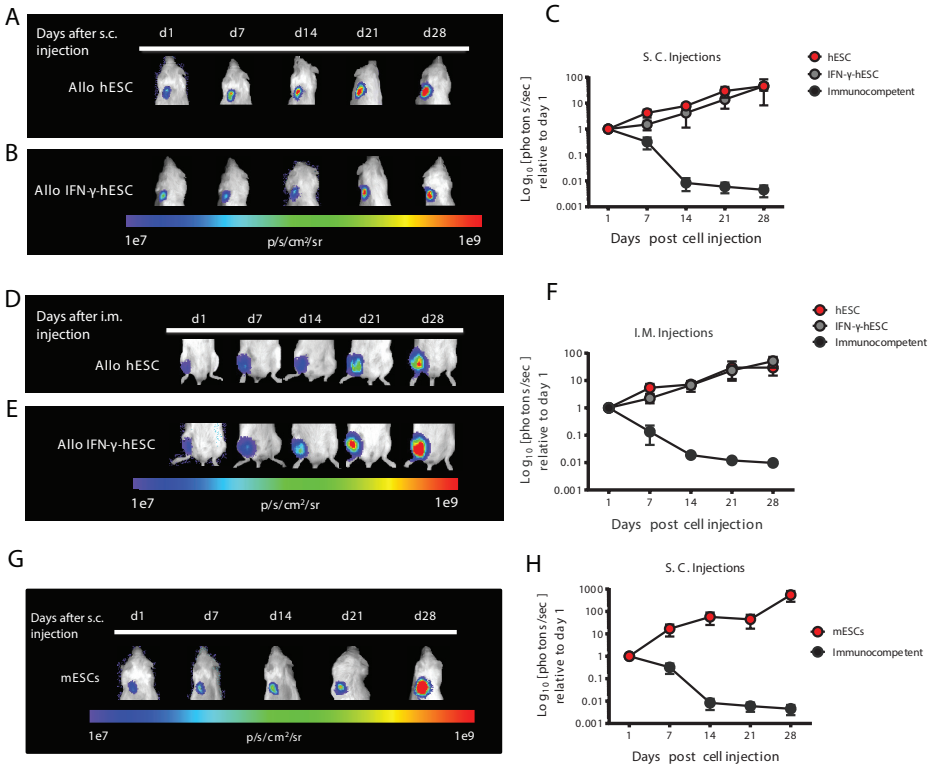


Figure S1. *hSRC* mice fail to reject allogeneic unstimulated, IFN-γ- stimulated hESCs and murine ESCs. (A) hESCs (Allo hESCs) and (B) IFN-γ-stimulated hESCs (IFN-Allo hESCs), implanted subcutaneously (s.c.), proliferated and showed no sign of immunological rejection as assessed by BLI. (C) Quantification of BLI data for s.c. injections of (A) allogeneic hESCs (n=10) and (B) IFN-γ-hESCs (n=8) in hSRC model and immunocompetent C57BL/6 mice (n=5). (D) hESCs (Allo hESCs) and (E) IFN-γ-stimulated hESCs (IFN-Allo hESCs), implanted intramuscularly (i.m.), proliferated and showed no sign of immunological rejection as assessed by BLI. (F) Quantification of BLI data for i.m. injections of hESCs (n=10) and IFN-γ-hESCs (n=8) in *hSCR* model and immunocompetent C57BL/6 mice (n=3) (*Figure 6*). Quantitative data are represented as mean ± SEM. (G) mESCs (129S1/SvJ strain; mESCs), implanted s.c., proliferated and were not rejected by hSRC mice (n=4) as assessed by BLI. In contrast, immunocompetent (C57BL/6) mice (n=5) rejected allogeneic (129S1/SvJ) mESCs within 2 weeks after cell implantation. (H) Quantification of the BLI data from (G) normalized to the maximum radiance at day 1. Data are represented as mean ± SEM.

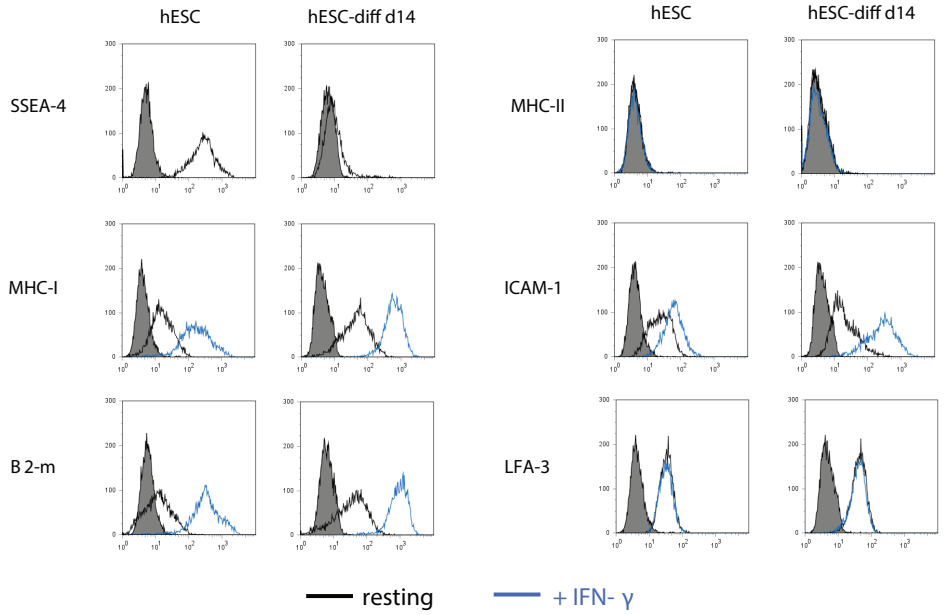


Figure S2. IFN-γ stimulation and differentiation of hESCs increases MHC-I expression and potential immunogenicity. FACS analysis of $1x10^6$ hESCs after 48 hr in vitro IFN-γ stimulation (blue line) increases cell surface expression of MHC-I, B2-m and ICAM-1 compared to the resting state (black line). A similar trend of upregulation of these molecules is seen after 14 days of differentiation (hESC-diff D14, n=20 EBs). Reduction in expression of the pluripotency marker SSEA-4 at day 14 of EB formation indicates adequate induction of differentiation.

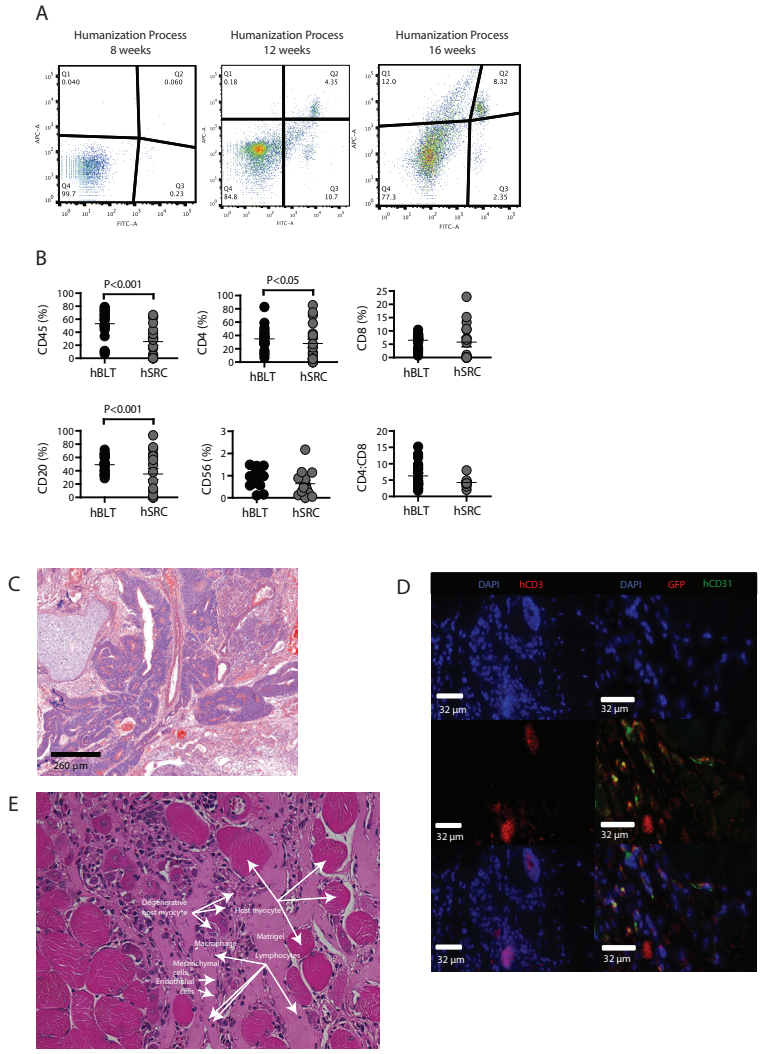


Figure S3. Superior engraftment of human immune cell subsets in hBLT mice did not result in the rejection of hESCs and their derivatives. (A) Beginning at 8 weeks after engraftment of human fetal bone marrow, liver and thymus, the presence of human immune cells ($CD3^+$: FITC, $CD45^+$: APC) can be detected in the *hBLT* circulation at 12 weeks. (B) Percentage of human $CD45^+$ immune cells and the proportion of each human cell subset of human $CD45^+$ cells in the peripheral blood 12 weeks after human immune cell engraftment of *hSRC* (n=18) and hBLT (n=21). Analysis was performed prior to the transplantation of hESCs. Data are presented as individual mice (dots) with mean ± SEM. (C) Representative H&E image of teratoma developed in the spleen of hBLT mouse 4 weeks after hESC transplantation. (D) Grafts isolated from hBLT mice 4 weeks after hESC-EC transplantation shows presence of human $CD3^+$ cells (hCD3; red) (left panel) and hESC-ECs (right panel) by co-staining for nuclei (blue), anti-GFP (red), and anti-human CD31 (hCD31; green). (E) Analysis of the Matrigel plugs reveals very little immune cell activity with a low presence of T-cells and macrophages. Even in comparison to a syngeneic transplant setting, the numbers are very low. Within the grafts the presence of spindle shaped cells that were forming tubes is indicative of endothelial cells, as confirmed by the immunohistochemistry staining in *Figure S3D*.

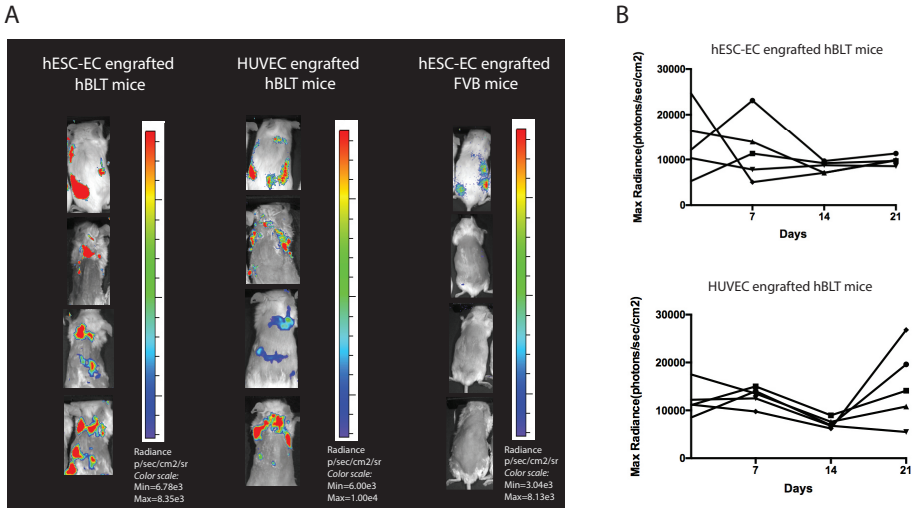


Figure S4. *hBLT* mice demonstrate an impaired ability to reject grafts derived from both somatic cells and ESCs. (A) Luciferase-labeled hESC-derived endothelial cells (hESC-ECs) (left panel) and HUVEC cells (middle panel) engrafted into humanized mice show graft persistence and proliferation over time, whereas hESC-ECs engrafted in immunocompetent FVB mice (right panel) are rejected within one week. (B) Quantification of the BLI signal (max. radiance) of the transplanted cells displayed in Figure S4A at day 7, 14 and 21.

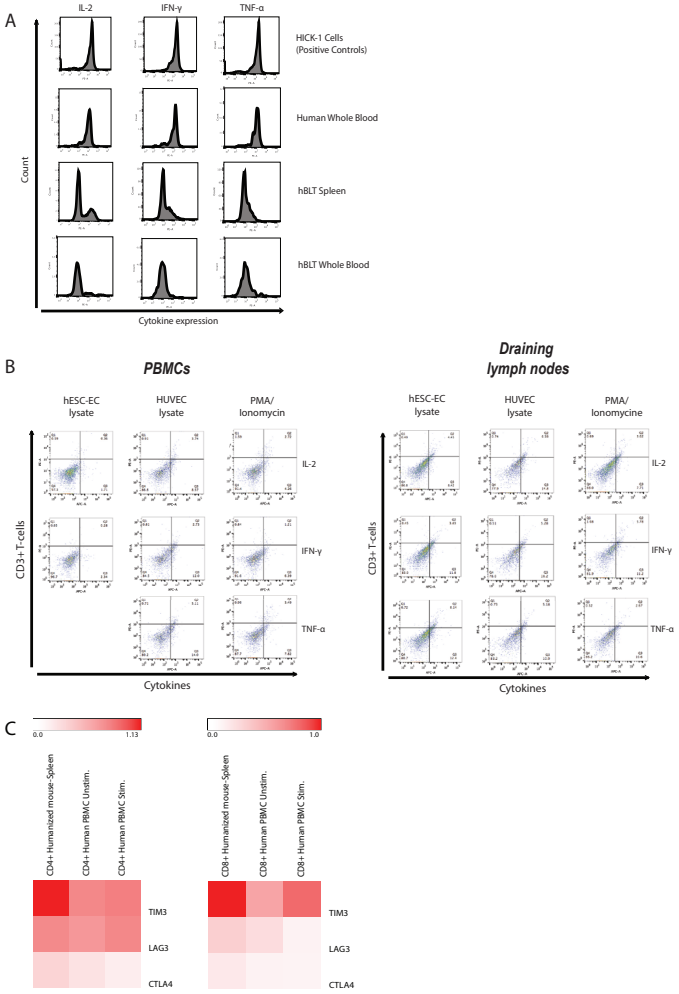


Figure S5. Inability of the *hBLT* immune cells to mount an effective immune response and high expression of T-cell anergy/exhaustion genes. (A) Human immune cells isolated from *hBLT* mice are incapable of mounting a pro-inflammatory immune response with IL2, IFN-γ and TNF-α release. Peripheral human immune cells (*hBLT Whole blood*) in 16-week old hBLT mice are anergic to PMA/Ionomycin stimulation. In contrast, splenic human immune cells (*hBLT Spleen*) reveal a limited response, but this response is limited as compared to the control samples (*HiCK-1; Human whole blood*). Data representative of three experiments. (B) Human immune cells isolated from Matrigel plugs of hESC-EC engrafted mice show low cytokine production upon stimulation with hESC-EC lysate. These results were comparable to stimulation with an antigen (HUVEC lysate) the immune cells had not been previously exposed to. Even upon non-antigen specific positive control stimulation with PMA/Ionomycin, hESC-EC engrafted human immune cells from the Matrigel plugs show very limited pro-inflammatory cytokine production. Similar results are found when performing these experiments on human immune cells isolated from lymph nodes from hBLT mice. In these mixed-lymphocyte reactions the percentage of cytokine producing immune cells is limited, especially when comparing the results to the positive control sample of whole human blood in *Figure S5A*. PE: (Cytokines, APC: CD3). (C) Splenocytes isolated from hBLT mice (n=12), 4 weeks after transplantation of hESC-ECs, show upregulation of *TIM3, LAG3* and *CTLA4* genes in $CD4^+$ and $CD8^+$ lymphocytes compared to unstimulated and PMA/Ionoycin stimulated control human PBMCs (n=4).

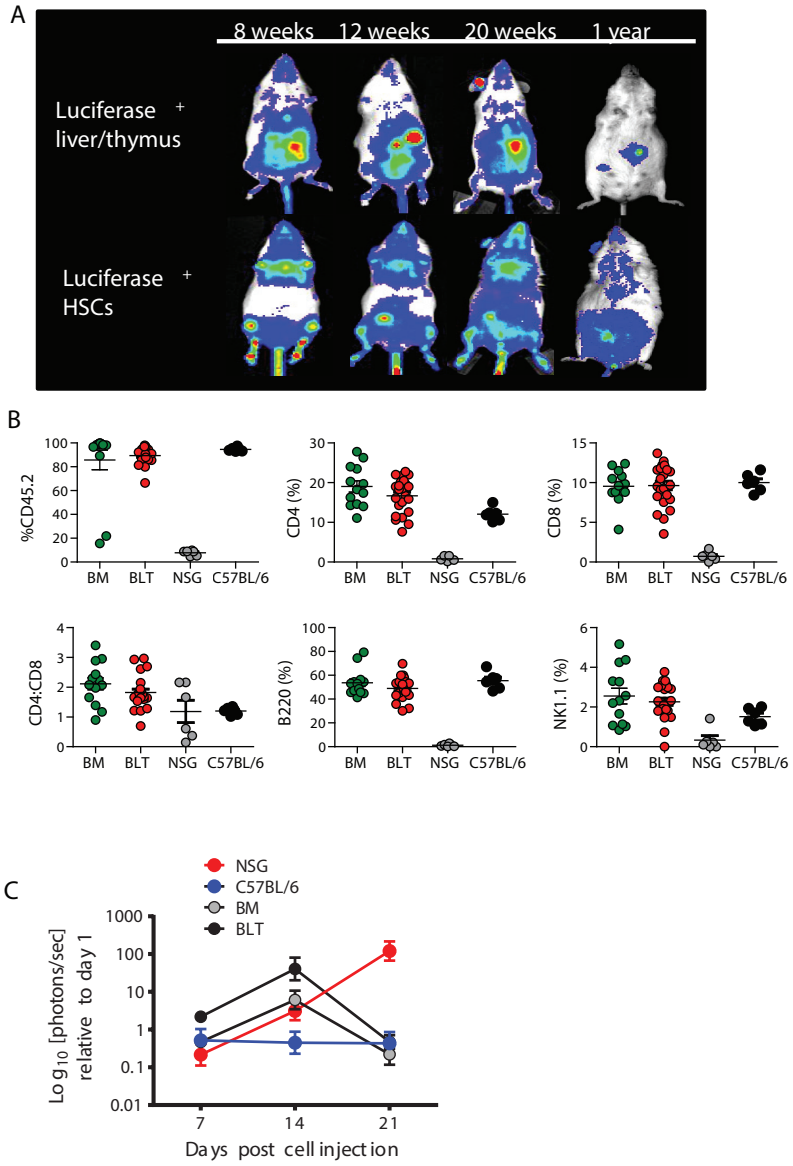


Figure S6. Allogenised BLT mice show sustained viability of grafted donor tissue, high levels of immune cell engraftment, and similar functionality between *BM* and *BLT* models. (A) BLI demonstrating sustained engraftment of luciferase positive allogeneic immune cells in bone marrow compartments and sustained viability of luciferase positive allogeneic liver and thymus transplanted in the abdomen of NSG mice. (B) Similar engraftment of C57BL/6 total leukocytes (CD45.2), helper and cytotoxic ($CD8^+$) T cells, B cells ($B220^+$), and NK cells ($NK1.1^+$) in *mBM* (n=13) and *mBLT* (n=23) NSG models compared to wild-type C57BL/6 mice (n=6). (C) Quantification of BLI data relative to the maximum radiance at day 1 shows that *BM* (n=3) and *BLT* (n=3) allogenised mice have similar effectiveness in the rejection of miPSC allografts (n=3), although the rate of rejection was delayed by ~7 days compared to wild-type C57BL/6 mice (n=3). Data are presented as individual mice (dots) with mean ± SEM.

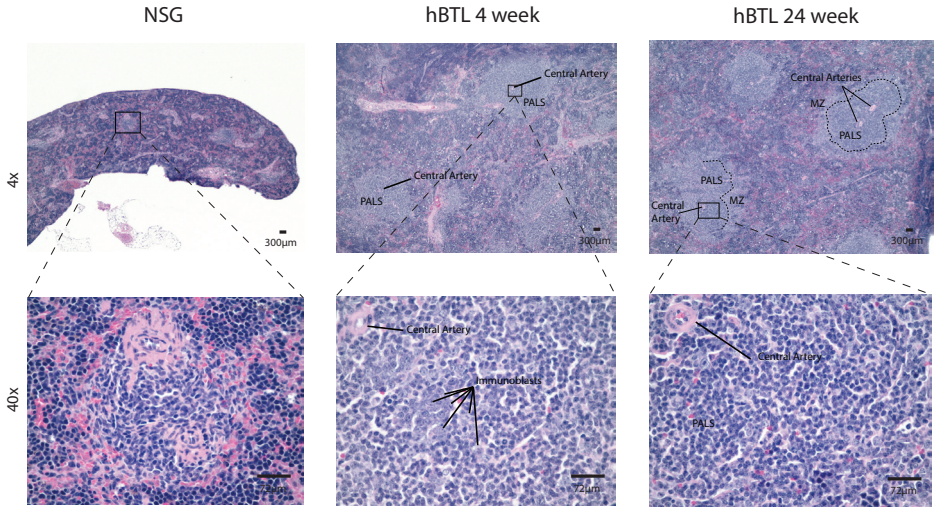


Figure S7. Older *hBLT* mice have a more mature splenic architecture compared to young *hBLT* mice. Compared to the NSG background mouse strain, *hBLT* mice at one week after humanization have abundant periarteriolar lymphatic sheaths (PALS), comprised of mononuclear cells. Some of these are small lymphocytes interspersed with clumps of larger cells, likely to be immunoblasts, as well as the lack of a marginal zone (MZ). Both aspects indicating an immature architecture. By week 24 after humanization, the numbers of periarteriolar small lymphocytes have increased and a marginal zone containing macrophages surrounds them, indicating maturation.

Table S1. FACS antibody panel used for analyzing and sorting human PBMC samples isolated from *hBLT* mice.

Antibody	Fluorophore Conjugate	Company
CD3	APC	BD Bioscience
CD3	APC	ThermoFisher
CD4	Pe-Cy7	BioLegend
CD8	FITC	BD Bioscience
CD45RA	PE	BioLegend
CD45RO	Pacific Blue	BioLegend
mouse CD45.1	PerCP/Cy5.5	BD Bioscience
human CD45	Pacific Orange	Life technologies
Human CD45	PerCP	ThermoFisher
FoxP3	FITC	eBioscience
CD56	FITC	BioLegend
CD20	Pe-Cy7	BD Bioscience
CD44	Pacific Blue	BioLegend
CD11b	APC	eBioscience
Fixable Viability Dye	AlexaFluor 780	Life Technologies

Table S2. Primer sequences used in single-cell PCR analysis. Gene sequences for human Th1, Th2, and Th3 immune responses (92 sequences) and 3 housekeeping gene sequences were provided by Origene Technologies Inc.

	Gene	Forward Primer	Reverse Primer
1	BCL2L1	GCCACTTACCTGAATGACCACC	AACCAGCGGTTGAAGCGTTCCT
2	CCL11	GCTACAGGAGAATCACCAGTGG	GGAATCCTGCACCCACTTCTTC
3	CCL5	CCTGCTGCTTTGCCTACATTGC	ACACACTTGGCGGTTCTTTCGG
4	CCL7	ACAGAAGGACCACCAGTAGCCA	GGTGCTTCATAAAGTCCTGGACC
5	CCR2	CAGGTGACAGAGACTCTTGGGA	GGCAATCCTACAGCCAAGAGCT
6	CCR3	TACTCCCTGGTGTTCACTGTGG	ACGAGGAAGAGCAGGTCCGAAA
7	CCR4	CTCTGGCTTTTGTTCACTGCTGC	AGCCCACAGTATTGGCAGAGCA
8	CCR5	TCTCTTCTGGGCTCCCTACAAC	CCAAGAGTCTCTGTCACCTGCA
9	CCR7	CAACATCACCAGTAGCACCTGTG	TGCGGAACTTGACGCCGATGAA
10	CD247	CTGCCTTGTTCCTGAGAGTGAAG	CATCGTACTCCTCTCTTCGTCC
11	CD27	ACTACTGGGCTCAGGGAAAGCT	GGATCACACTGAGCAGCCTTTC
12	CD28	GAGAAGAGCAATGGAACCATTATC	TAGCAAGCCAGGACTCCACCAA
13	CD3G	GCATTTTCGTCCTTGCTGTTGGG	GGTCATCTTCTCGATCCTTGAGG
14	CD4	CCTCCTGCTTTTCATTGGGCTAG	TGAGGACACTGGCAGGTCTTCT
15	CD40LG	GCGGCACATGTCATAAGTGAGG	GTCCTTGTCTTTTAACGGTCAGC
16	CD8	ACTTGTGGGGTCCTTCTCCTGT	TGTCTCCCGATTTGACCACAGG
17	CD80	CTCTTGGTGCTGGCTGGTCTTT	GCCAGTAGATGCGAGTTTGTGC
18	CD86	CCATCAGCTTGTCTGTTTCATTCC	GCTGTAATCCAAGGAATGTGGTC

Table S2. Primer sequences used in single-cell PCR analysis. Gene sequences for human Th1, Th2, and Th3 immune responses (92 sequences) and 3 housekeeping gene sequences were provided by Origene Technologies Inc. (*continued*)

	Gene	Forward Primer	Reverse Primer
19	CEBPB	AGAAGACCGTGGACAAGCACAG	CTCCAGGACCTTGTGCTGCGT
20	CREBBP	AGTAACGGCACAGCCTCTCAGT	CCTGTCGATACAGTGCTTCTAGG
21	CSF2	GGAGCATGTGAATGCCATCCAG	CTGGAGGTCAAACATTTCTGAGAT
22	CTLA4	ACGGGACTCTACATCTGCAAGG	GGAGGAAGTCAGAATCTGGGCA
23	CXCR3	ACGAGAGTGACTCGTGCTGTAC	GCAGAAAGAGGAGGCTGTAGAG
24	CXCR4	CTCCTCTTTGTCATCACGCTTCC	GGATGAGGACACTGCTGTAGAG
25	FASLG	GGTTCTGGTTGCCTTGGTAGGA	CTGTGTGCATCTGGCTGGTAGA
26	GATA3	ACCACAACCACACTCTGGAGGA	TCGGTTTCTGGTCTGGATGCCT
27	GFI1	GCTTCAAGAGGTCATCCACACTG	ACCTGGCACTTGTGAGGCTTCT
28	GLMN	GCTGGAATCTCGTTGGTCCTGT	GCTCTTCAATCAGTTCAAGCAAAC
29	GPR44	TGGAGTCATCCTCTTCGTGGTG	AGTAGGTGAAGAAGGGCAGGGA
30	HAVCR2	GACTCTAGCAGACAGTGGGATC	GGTGGTAAGCATCCTTGGAAAGG
31	ICOS	CCCATAGGATGTGCAGCCTTTG	GGCTGTGTTCACTGCTCTCATG
32	IFNG	GAGTGTGGAGACCATCAAGGAAG	TGCTTTGCGTTGGACATTCAAGTC
33	IGSF6	GCGAGAGCTAAACAGACAGGAG	CGGTCACATAGACAGAGAGCAG
34	IL10	TCTCCGAGATGCCTTCAGCAGA	TCAGACAAGGCTTGGCAACCCA
35	IL12B	GACATTCTGCGTTCAGGTCCAG	CATTTTTGCGGCAGATGACCGTG
36	IL12RB2	AGACCTCAGTGGTGTAGCAGAG	TGATGACCAGCGGTTCAGGATC
37	IL13	ACGGTCATTGCTCTCACTTGCC	CTGTCAGGTTGATGCTCCATACC
38	IL13RA1	CCTGAATGAGAGGATTTGTCTGC	CAGTCACAGCAGACTCAGGATC
39	IL15	AACAGAAGCCAACTGGGTGAATG	CTCCAAGAGAAAGCACTTCATTGC
40	IL17A	CGGACTGTGATGGTCAACCTGA	GCACTTTGCCTCCCAGATCACA
41	IL18	GATAGCCAGCCTAGAGGTATGG	CCTTGATGTTATCAGGAGGATTCA
42	IL18R1	GGAGGCACAGACACCAAAAGCT	AGGCACACTACTGCCACCAAGA
43	IL1R1	GTGCTTTGGTACAGGGATTCCTG	CACAGTCAGAGGTAGACCCTTC
44	IL1R2	GGCTATTACCGCTGTGTCCTGA	GAGAAGCTGATATGGTCTTGAGG
45	IL2	AGAACTCAAACCTCTGGAGGAAG	GCTGTCTCATCAGCATATTCACAC
46	IL23A	GAGCCTTCTCTGCTCCCTGATA	GACTGAGGCTTGGAATCTGCTG
47	IL2RA	GAGACTTCCTGCCTCGTCACAA	GATCAGCAGGAAAACACAGCCG
48	IL4	CCGTAACAGACATCTTTGCTGCC	GAGTGTCCTTCTCATGGTGGCT
49	IL5	GGAATAGGCACACTGGAGAGTC	CTCTCCGTCTTTCTTCTCCACAC
50	IL6	AGACAGCCACTCACCTCTTCAG	TTCTGCCAGTGCCTCTTTGCTG
51	IL7	GACAGCATGAAAGAAATTGGTAGC	CAACTTGCGAGCAGCACGGAAT
52	IL9	GACCAGTTGTCTCTGTTTGGGC	TTTCACCCGACTGAAAATCAGTGG
53	INHA	TCCCAAGCCATCCTTTTCCCAG	TCACCTGGCGGCTGCGTGTAT
54	IRF1	GAGGAGGTGAAAGACCAGAGCA	TAGCATCTCGGCTGGACTTCGA
55	IRF4	GAACGAGGAGAAGAGCATCTTCC	CGATGCCTTCTCGGAACTTTCC

Table S2. Primer sequences used in single-cell PCR analysis. Gene sequences for human Th1, Th2, and Th3 immune responses (92 sequences) and 3 housekeeping gene sequences were provided by Origene Technologies Inc. (*continued*)

	Gene	Forward Primer	Reverse Primer
56	JAK1	GAGACAGGTCTCCCACAAACAC	GTGGTAAGGACATCGCTTTTCCG
57	JAK2	CCAGATGGAAACTGTTCGCTCAG	GAGGTTGGTACATCAGAAACACC
58	LAG3	GCAGTGTACTTCACAGAGCTGTC	AAGCCAAAGGCTCCAGTCACCA
59	LAT	ATCCTGGAGCGGCTAAGACTGA	GTTCAGCTCCTGCAGATTCTCG
60	LEFTY2	CCGCGGAAAGAGGTTCAGCCA	GCTGCTCCATGCCGAACACCA
61	LTA	ACACCTTCAGCTGCCCAGACTG	TCCGTGTTTGCTCTCCAGAGCA
62	MAF	AGAAGTTGGTGAGCAGCGGCTT	CACTGATGGCTCCAACTTGCGA
63	MAP2K7	GACCTGGATGTGGTGCTGAAGA	TCTTGAGCTTCTCAGCGCAGGT
64	MAPK8	GACGCCTTATGTAGTGACTCGC	TCCTGGAAAGAGGATTTTGTGGC
65	NFAT5	CCTAATGCCCTGATGACTCCAC	GTTTGCTGAGTTGATCCAACAGAC
66	NFATC1	CACCAAAGTCCTGGAGATCCCA	TTCTTCCTCCCGATGTCCGTCT
67	NFATC2	GATAGTGGGCAACACCAAAGTCC	TCTCGCCTTTCCGCAGCTCAAT
68	NFATC3	AGACAGTCGCTACTGCAAGCCA	GCGGAGTTTCAAAATACCTGCAC
69	NFATC4	GCACCGTATCACAGGCAAGATG	TCAGGATTCCCGCGCAGTCAAT
70	PCGF2	CACTATCGTGGAGTGCCTGCAT	GGTTTTATGGACCTGCACGTCAC
71	PTPRC	CTTCAGTGGTCCCATTGTGGTG	CCACTTTGTTCTCGGCTTCCAG
72	SFTPD	GGACAAAGGCATTCCTGGAGAC	TGAGAGAAAGCAGCCTGGAGGT
73	SOCS1	TTCGCCCTTAGCGTGAAGATGG	TAGTGCTCCAGCAGCTCGAAGA
74	SOCS2	GGTCGGCGGAGGAGCCATCC	GAAAGTTCCTTCTGGTGCCTCTT
75	SPP1	CGAGGTGATAGTGTGGTTTATGG	GCACCATTCAACTCCTCGCTTTC
76	STAT1	ATGGCAGTCTGGCGGCTGAATT	CCAAACCAGGCTGGCACAATTG
77	STAT4	CAGTGAAAGCCATCTCGGAGGA	TGTAGTCTCGCAGGATGTCAGC
78	STAT6	CCTTGGAGAACAGCATTCCTGG	GCACTTCTCCTCTGTGACAGAC
79	TBX21	ATTGCCGTGACTGCCTACCAGA	GGAATTGACAGTTGGGTCCAGG
80	TGFB1	TACCTGAACCCGTGTTGCTCTC	GTTGCTGAGGTATCGCCAGGAA
81	TGFB2	AAGAAGCGTGCTTTGGATGCGG	ATGCTCCAGCACAGAAGTTGGC
82	TGFB3	CTAAGCGGAATGAGCAGAGGATC	TCTCAACAGCCACTCACGCACA
83	TLR4	CCCTGAGGCATTTAGGCAGCTA	AGGTAGAGAGGTGGCTTAGGCT
84	TLR6	ACTGACCTTCCTGGATGTGGCA	TGACCTCATCTTCTGGCAGCTC
85	TMED1	CTTTGACAGCCTCCAGGATGAC	TAGCGTGAGCATCTGGATGCTG
86	TNF	CTCTTCTGCCTGCTGCACTTTG	ATGGGCTACAGGCTTGTCACTC
87	TNFRSF8	ATCTGTGCCACATCAGCCACCA	AAGGTGGTGTCCTTCTCAGCCA
88	TNFRSF9	TCTTCCTCACGCTCCGTTTCTC	TGGAAATCGGCAGCTACAGCCA
89	TNFSF4	CCTACATCTGCCTGCACTTCTC	TGATGACTGAGTTGTTCTGCACC
90	TYK2	GGTTGACCAGAAGGAGATCACC	TCCTCGTCATCCATCTTGCCCT
91	YY1	GGAGGAATACCTGGCATTGACC	CCCTGAACATCTTTGTGCAGCC

Table S2. Primer sequences used in single-cell PCR analysis. Gene sequences for human Th1, Th2, and Th3 immune responses (92 sequences) and 3 housekeeping gene sequences were provided by Origene Technologies Inc. (*continued*)

	Gene	Forward Primer	Reverse Primer
92	FoxP3	GGCACAATGTCTCCTCCAGAGA	CAGATGAAGCCTTGGTCAGTGC
93	ACTB	CACCATTGGCAATGAGCGGTTC	AGGTCTTTGCGGATGTCCACGT
94	GAPDH	GTCTCCTCTGACTTCAACAGCG	ACCACCCTGTTGCTGTAGCCAA
95	HPRT1	CATTATGCTGAGGATTTGGAAAGG	CTTGAGCACACAGAGGGCTACA

REFERENCES

Aryee, K.E., Shultz, L.D., and Brehm, M.A. (2014). Immunodeficient mouse model for human hematopoietic stem cell engraftment and immune system development. Methods in Molecular Biology 1185, 267-278.

Babad, J., G. Mukherjee, A. Follenzi, R. Ali, B. O. Roep, L. D. Shultz, . . . T. P. DiLorenzo (2014). "Generation of beta cell-specific Human Cytotoxic T Cells by Lentiviral Transduction and Their Survival in Immunodeficient HLA-transgenic Mice." Clin Exp Immunol.

Barberi, T., P. Klivenyi, N. Y. Calingasan, H. Lee, H. Kawamata, K. Loonam, . . . L. Studer (2003). "Neural subtype specification of fertilization and nuclear transfer embryonic stem cells and application in parkinsonian mice." Nat Biotechnol 21(10): 1200-1207.

Bosma, G. C., R. P. Custer and M. J. Bosma (1983). "A severe combined immunodeficiency mutation in the mouse." Nature 301(5900): 527-530.

Brehm, M.A., Cuthbert, A., Yang, C., Miller, D.M., DiIorio, P., Laning, J., Burzenski, L.,Gott, B., Foreman, O., Kavirayani, A., et al.(2010). Parameters for establishing humanized mouse models to study human immunity: analysis of human hematopoietic stem cell engraftment in three immunodeficient strains of mice bearing the IL2rgamma(null) mutation. Clinical Immunology 135, 84-98.

Brehm, M. A., M. V. Wiles, D. L. Greiner and L. D. Shultz (2014). "Generation of improved humanized mouse models for human infectious diseases." J Immunol Methods 410: 3-17.

Covassin, L., S. Jangalwe, N. Jouvet, J. Laning, L. Burzenski, L. D. Shultz and M. A. Brehm (2013). "Human immune system development and survival of non-obese diabetic (NOD)-scid IL2rgamma(null) (NSG) mice engrafted with human thymus and autologous haematopoietic stem cells." Clin Exp Immunol 174(3): 372-388.

de Almeida, P. E., E. H. Meyer, N. G. Kooreman, S. Diecke, D. Dey, V. Sanchez-Freire, . . . J. C. Wu (2014). "Transplanted terminally differentiated induced pluripotent stem cells are accepted by immune mechanisms similar to self-tolerance." Nat Commun 5: 3903.

de Almeida, P. E., J. D. Ransohoff, A. Nahid and J. C. Wu (2013). "Immunogenicity of pluripotent stem cells and their derivatives." Circ Res 112(3): 549-561.

Drukker, M., G. Katz, A. Urbach, M. Schuldiner, G. Markel, J. Itskovitz-Eldor, . . . N. Benvenisty (2002). "Characterization of the expression of MHC proteins in human embryonic stem cells." Proc Natl Acad Sci U S A 99(15): 9864-9869.

Greenblatt, M. B., V. Vrbanac, T. Tivey, K. Tsang, A. M. Tager and A. O. Aliprantis (2012). "Graft versus host disease in the bone marrow, liver and thymus humanized mouse model." PLoS One 7(9): e44664.

Greiner, D. L., R. A. Hesselton and L. D. Shultz (1998). "SCID mouse models of human stem cell engraftment." Stem Cells 16(3): 166-177.

Hesselton, R. M., D. L. Greiner, J. P. Mordes, T. V. Rajan, J. L. Sullivan and L. D. Shultz (1995). "High levels of human peripheral blood mononuclear cell engraftment and enhanced susceptibility to human immunodeficiency virus type 1 infection in NOD/LtSz-scid/scid mice." J Infect Dis 172(4): 974-982.

Homma, K., S. Okamoto, M. Mandai, N. Gotoh, H. K. Rajasimha, Y. S. Chang, . . . M. Takahashi (2013). "Developing rods transplanted into the degenerating retina of Crx-knockout mice exhibit neural activity similar to native photoreceptors." Stem Cells 31(6): 1149-1159.

Huber, B.C., Ransohoff, J.D., Ransohoff, K.J., Riegler, J., Ebert, A., Kodo, K., Gong, Y., Sanchez-Freire, V., Dey, D., Kooreman, N.G., et al.(2013). Costimulation-adhesion blockade is superior to cyclosporine A and prednisone immunosuppressive therapy for preventing rejection of differentiated human embryonic stem cells following transplantation. Stem Cells 31, 2354-2363.

Ishikawa, F., M. Yasukawa, B. Lyons, S. Yoshida, T. Miyamoto, G. Yoshimoto, . . . M. Harada (2005). "Development of functional human blood and immune systems in NOD/SCID/IL2 receptor {gamma} chain(null) mice." Blood 106(5): 1565-1573.

Ito, M., H. Hiramatsu, K. Kobayashi, K. Suzue, M. Kawahata, K. Hioki, . . . T. Nakahata (2002). "NOD/SCID/gamma(c)(null) mouse: an excellent recipient mouse model for engraftment of human cells." Blood 100(9): 3175-3182.

Lan, P., N. Tonomura, A. Shimizu, S. Wang and Y. G. Yang (2006). "Reconstitution of a functional human immune system in immunodeficient mice through combined human fetal thymus/liver and CD34+ cell transplantation." Blood 108(2): 487-492.

Lavender, K. J., W. W. Pang, R. J. Messer, A. K. Duley, B. Race, K. Phillips, . . . K. J. Hasenkrug (2013). "BLT-humanized C57BL/6 Rag2-/-gammac-/-CD47-/- mice are resistant to GVHD and develop B- and T-cell immunity to HIV infection." Blood 122(25): 4013-4020.

Liao, Y., G. K. Smyth and W. Shi (2014). "featureCounts: an efficient general purpose program for assigning sequence reads to genomic features." Bioinformatics 30(7): 923-930.

Lockridge, J. L., Y. Zhou, Y. A. Becker, S. Ma, S. C. Kenney, P. Hematti, . . . J. E. Gumperz (2013). "Mice engrafted with human fetal thymic tissue and hematopoietic stem cells develop pathology resembling chronic graft-versus-host disease." Biol Blood Marrow Transplant 19(9): 1310-1322.

Love, M. I., W. Huber and S. Anders (2014). "Moderated estimation of fold change and dispersion for RNA-seq data with DESeq2." Genome Biol 15(12): 550.

Ludwig, T.E., Levenstein, M.E., Jones, J.M., Berggren, W.T., Mitchen, E.R., Frane, J.L., Crandall, L.J., Daigh, C.A., Conard, K.R., Piekarczyk, M.S., et al.(2006). Derivation of human embryonic stem cells in defined conditions. Nature Biotechnol 24, 185-187.

Lui, K. O., D. Howie, S. W. Ng, S. Liu, K. R. Chien and H. Waldmann (2014). "Tolerance induction to human stem cell transplants with extension to their differentiated progeny." Nat Commun 5: 5629.

Mandai, M., Y. Kurimoto and M. Takahashi (2017). "Autologous Induced Stem-Cell-Derived Retinal Cells for Macular Degeneration." N Engl J Med 377(8): 792-793.

Manz, M. G. (2007). "Human-hemato-lymphoid-system mice: opportunities and challenges." Immunity 26(5): 537-541.

McCune, J.M., Namikawa, R., Kaneshima, H., Shultz, L.D., Lieberman, M., and Weissman, I.L. (1988). The SCID-hu mouse: murine model for the analysis of human hematolymphoid differentiation and function. Science 241, 1632-1639.

Melkus, M. W., J. D. Estes, A. Padgett-Thomas, J. Gatlin, P. W. Denton, F. A. Othieno, . . . J. V. Garcia (2006). "Humanized mice mount specific adaptive and innate immune responses to EBV and TSST-1." Nat Med 12(11): 1316-1322.

Nelakanti, R. V., N. G. Kooreman and J. C. Wu (2015). "Teratoma formation: a tool for monitoring pluripotency in stem cell research." Curr Protoc Stem Cell Biol 32: 4A 8 1-4A 8 17.

Nguyen, P. K., J. W. Rhee and J. C. Wu (2016). "Adult Stem Cell Therapy and Heart Failure, 2000 to 2016: A Systematic Review." JAMA Cardiol 1(7): 831-841.

Onoe, T., H. Kalscheuer, N. Danzl, M. Chittenden, G. Zhao, Y. G. Yang and M. Sykes (2011). "Human natural regulatory T cell development, suppressive function, and postthymic maturation in a humanized mouse model." J Immunol 187(7): 3895-3903.

Pagliuca, F. W., J. R. Millman, M. Gurtler, M. Segel, A. Van Dervort, J. H. Ryu, . . . D. A. Melton (2014). "Generation of functional human pancreatic beta cells in vitro." Cell 159(2): 428-439.

Pearl, J.I., Lee, A.S., Leveson-Gower, D.B.,Sun, N., Ghosh, Z., Lan, F., Ransohoff, J., Negrin, R.S., Davis, M.M., and Wu, J.C. (2011). Short-term immunosuppression promotes engraftment of embryonic and induced pluripotent stem cells. Cell Stem Cell 8, 309-317.

Pertea, M., D. Kim, G. M. Pertea, J. T. Leek and S. L. Salzberg (2016). "Transcript-level expression analysis of RNA-seq experiments with HISAT, StringTie and Ballgown." Nat Protoc 11(9): 1650-1667.

Rong, Z., M. Wang, Z. Hu, M. Stradner, S. Zhu, H. Kong, . . . X. Fu (2014). "An effective approach to prevent immune rejection of human ESC-derived allografts." Cell Stem Cell 14(1): 121-130.

Rongvaux, A., T. Willinger, J. Martinek, T. Strowig, S. V. Gearty, L. L. Teichmann, . . . R. A. Flavell (2014). "Development and function of human innate immune cells in a humanized mouse model." Nat Biotechnol 32(4): 364-372.

Schoenborn, J. R. and C. B. Wilson (2007). "Regulation of interferon-gamma during innate and adaptive immune responses." Adv Immunol 96: 41-101.

Schwartz, S. D., J. P. Hubschman, G. Heilwell, V. Franco-Cardenas, C. K. Pan, R. M. Ostrick, . . . R. Lanza (2012). "Embryonic stem cell trials for macular degeneration: a preliminary report." Lancet 379(9817): 713-720.

Shultz, L. D., B. L. Lyons, L. M. Burzenski, B. Gott, X. Chen, S. Chaleff, . . . R. Handgretinger (2005). "Human lymphoid and myeloid cell development in NOD/LtSz-scid IL2R gamma null mice engrafted with mobilized human hemopoietic stem cells." J Immunol 174(10): 6477-6489.

Shultz, L. D., Y. Saito, Y. Najima, S. Tanaka, T. Ochi, M. Tomizawa, . . . F. Ishikawa (2010). "Generation of functional human T-cell subsets with HLA-restricted immune responses in HLA class I expressing NOD/SCID/IL2r gamma(null) humanized mice." Proc Natl Acad Sci U S A 107(29): 13022-13027.

Shultz, L. D., P. A. Schweitzer, S. W. Christianson, B. Gott, I. B. Schweitzer, B. Tennent, . . . et al. (1995). "Multiple defects in innate and adaptive immunologic function in NOD/LtSz-scid mice." J Immunol 154(1): 180-191.

Soto-Gutierrez, A., N. Kobayashi, J. D. Rivas-Carrillo, N. Navarro-Alvarez, D. Zhao, T. Okitsu, . . . I. J. Fox (2006). "Reversal of mouse hepatic failure using an implanted liver-assist device containing ES cell-derived hepatocytes." Nat Biotechnol 24(11): 1412-1419.

Takahashi, K., K. Tanabe, M. Ohnuki, M. Narita, T. Ichisaka, K. Tomoda and S. Yamanaka (2007). "Induction of pluripotent stem cells from adult human fibroblasts by defined factors." Cell 131(5): 861-872.

Takahashi, K. and S. Yamanaka (2006). "Induction of pluripotent stem cells from mouse embryonic and adult fibroblast cultures by defined factors." Cell 126(4): 663-676.

Takenaka, K., T. K. Prasolava, J. C. Wang, S. M. Mortin-Toth, S. Khalouei, O. I. Gan, . . . J. S. Danska (2007). "Polymorphism in Sirpa modulates engraftment of human hematopoietic stem cells." Nat Immunol 8(12): 1313-1323.

Thomson, J. A., J. Itskovitz-Eldor, S. S. Shapiro, M. A. Waknitz, J. J. Swiergiel, V. S. Marshall and J. M. Jones (1998). "Embryonic stem cell lines derived from human blastocysts." Science 282(5391): 1145-1147.

Traggiai, E., L. Chicha, L. Mazzucchelli, L. Bronz, J. C. Piffaretti, A. Lanzavecchia and M. G. Manz (2004). "Development of a human adaptive immune system in cord blood cell-transplanted mice." Science 304(5667): 104-107.

Wherry, E. J. (2011). "T cell exhaustion." Nat Immunol 12(6): 492-499.

Xiao, F., L. Ma, M. Zhao, G. Huang, V. Mirenda, A. Dorling, . . . G. Lombardi (2014). "Ex vivo expanded human regulatory T cells delay islet allograft rejection via inhibiting islet-derived monocyte chemoattractant protein-1 production in CD34+ stem cells-reconstituted NOD-scid IL2rgammanull mice." PLoS One 9(3): e90387.

Chapter 9

Utilizing the tumorigenic and immunogenic properties of iPSCs into a cancer vaccine

Kooreman N.G[*]., Kim Y. [*], de Almeida P.E., Termglichan V., Diecke S., Shao N., Dey D., Nelakanti R.N., Brouwer T., Barfi I., Han A., Quax P.H.A., Hamming J.F., Levy R., Davis M.M., Wu J.C. (2018) iPSC-Based Cancer Vaccination: An Autologous Stem Cell Vaccine against Cancer. **Cell Stem Cell,** *Apr 5;22(4):501-513.e7*
[*] *authors contributed equally*

SUMMARY

Cancer cells and embryonic tissues share a number of cellular and molecular properties, suggesting that induced pluripotent stem cells (iPSCs) may be harnessed to elicit anti-tumor responses in cancer vaccines. RNA sequencing revealed that human and murine iPSCs express tumor-associated antigens, and we show here a proof of principle for using irradiated iPSCs in autologous anti-tumor vaccines. In a prophylactic setting, iPSC vaccines prevent tumor growth in syngeneic murine breast cancer, mesothelioma, and melanoma models. As an adjuvant, the iPSC vaccine inhibited melanoma recurrence at the resection site and reduced metastatic tumor load, which was associated with fewer Th17 cells and increased $CD11b^{+}GR1hi$ myeloid cells. Adoptive transfer of T cells isolated from vaccine treated tumor-bearing mice inhibited tumor growth in unvaccinated recipients, indicating that the iPSC vaccine promotes an antigen-specific anti-tumor T cell response. Our data suggest an easy, generalizable strategy for multiple types of cancer that could prove highly valuable in clinical immunotherapy.

INTRODUCTION

Nearly a century ago, researchers observed that immunization with embryonic materials led to the rejection of transplanted tumors (Brewer et al. 2009). More recently, studies identified shared transcriptome profiles and antigens on various tumor cells and embryonic cells (Ben-Porath et al. 2008, Ghosh et al. 2011). This has led to the hypothesis that embryonic stem cells (ESCs) could be used as immunization agents to promote an anti-tumor response. A major advantage of whole-cell vaccination over traditional vaccines, which consist of inactivated organisms or protein products, is that a broad range of antigens can be presented to T cells, including unknown antigens (Palena et al. 2006, Yaddanapudi et al. 2012). However, the use of fetal and embryonic materials as vaccines to induce anti-tumor immunity has not yet advanced beyond animal models, owing largely to ethical challenges surrounding these therapies. Since the discovery of induced pluripotent stem cells (iPSCs) (Takahashi and Yamanaka 2006, Takahashi et al. 2007), pluripotent cells from a patient's own tissues can be created that share nearly identical gene expression and surface markers profiles with ESCs (Soldner et al. 2009, Bock et al. 2011, Mallon et al. 2013, Mallon et al. 2014), circumventing a major ethical roadblock. Additionally, the tumorigenic (Kooreman and Wu 2010, Lee et al. 2013) and immunogenic (Zhao et al. 2011, de Almeida et al. 2014) properties of iPSCs with autologous transplantation suggest potential efficacy in cancer vaccination. Importantly, autologous iPSCs may provide a more accurate and representative panel of patient's tumor immunogens than non-autologously derived ESCs. Here, we test the hypothesis that iPSCs may work as a whole cell-based vaccine that presents the immune system with a broad heterogeneity in cancer-related epitopes.

RESULTS

Human and Murine iPSCs Express Tumor-Specific and Tumor-Associated Antigens

We first performed RNA sequencing on 11 different human iPSC clones to compare expression profiles from a selected cancer-related gene list to human ESCs (hESCs), cancer tissues, and healthy tissues (Figure S1A). Based on this gene list, we found that human iPSCs cluster with hESCs and the cancer tissues, revealing important gene expression overlap in cancer genes between different cancer types and iPSCs. The upregulation of a subset of these genes was then also validated in murine iPSCs and ESCs (Figure S1B). These findings suggest the possibility of using iPSCs in different species to prime the host in developing immunity against known and, perhaps, unknown tumor-specific antigens (TSAs) and tumor-associated antigens (TAAs).

iPSC-Vaccine-Primed Mice Mount Strong B and T Cell Responses against Breast Cancer In Vitro and In Vivo

Using FVB strain iPSCs (Figures S2A and S2D) and the adjuvant CpG, proven to be successful in tumor vaccination (Mor et al. 1997, Gilkeson et al. 1998, Mukherjee et al. 2007, Goldstein et al. 2011), we observed an effective immune response to a murine breast cancer (DB7) with a CpG and iPSCs (C+I) combination. In brief, we first established the effect of CpG and an optimal vaccination schedule. We primed FVB mice with iPSCs or C+I for 2 weeks or 4 weeks and found the strongest in vitro T cell responses to DB7 tumor lysate in the C+I 4-week group (Figures S2E and S2F). In addition, a vaccination schedule of 4 weeks with the C+I combination resulted in the highest immunoglobulin G (IgG) binding (80.0% ± 3.4%) to DB7 and was therefore used for subsequent vaccination rounds (Figures 1A and 1B). After optimizing the schedule (Figure 1C), we proceeded with the vaccination of 40 FVB mice divided into four groups: (1) PBS, (2) CpG only, (3) iPSCs only, and (4) C+I. After four once-weekly vaccinations, $5x10^4$ DB7 cancer cells were injected subcutaneously, and tumor size was monitored using caliper measurement. After 1 week, all mice presented with a similar lesion at the injection site that regressed in 7 out of 10 C+I-treated mice and progressed to larger tumors in the other groups (Figures 1D, S3A, and S3B). Four weeks after tumor inoculation, five mice per group were sacrificed to analyze the immune profiles in blood, spleen, and draining lymph nodes (dLNs). The other five mice per group were used for long-term survival studies for up to 1 year. Most were sacrificed in the first 2 weeks after the end of the experiment when their tumor exceeded 1 cm^3. However, two mice in the C+I treatment group survived 1 year and had antibody titers against iPSCs and DB7 similar to the start of the experiment and were able to fully reject $5x10^4$ cancer cells upon reintroduction (Figures S3C and S3D). The control mice in this experiment, primed with iPSC-derived endothelial cells, were unable to mount IgG responses to the DB7 cell line, thereby ruling out the possibility that the culturing conditions with FBS-containing media could be responsible for the cross-reactivity or endogenous murine leukemia viral antigens.

C+I Vaccination Provides Breast Cancer and Melanoma Immunity by Upregulating Antigen Presentation and T-Helper/Cytotoxic T Cell Activity

To test the effectiveness of our vaccine in targeting multiple cancer types, an additional experiment was performed using the melanoma cell line B16F0, which is syngeneic to the C57BL/6 mouse strain. C57BL/6 iPSCs were generated (Figures S2B and S2D), and 40 mice were again divided into PBS, CpG, iPSCs, and C+I groups and treated for 4 weeks. Following this, $5x10^4$ B16F0 cells were subcutaneously injected in the lower back. Tumor growth assessment by caliper measurement showed significantly lower tumor progression by week 2 in the C+I group (Figures 1E, 1F, S3E, and S3F). Due to large tumor sizes in the control groups, the mice were sacrificed 2 weeks after tumor injection. Afterward, the immune cell profiles in blood, dLNs, and spleens were analyzed using flow cytometry. Cytometric

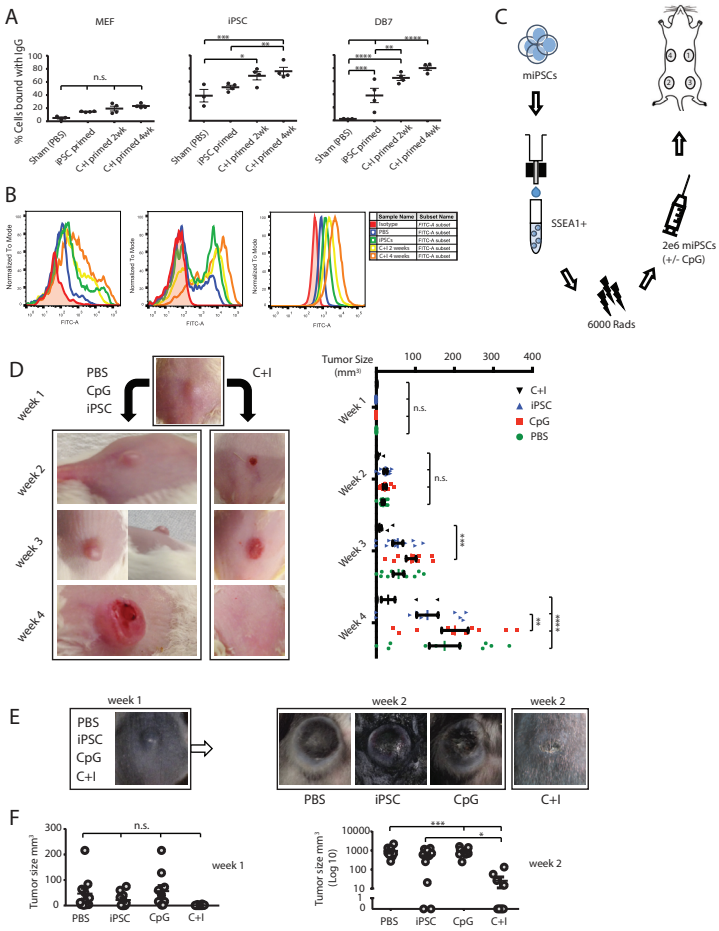


Figure 1. Assessing the Optimal Vaccination Schedule, followed by Successful Prophylactic Treatment of Breast Cancer and Melanoma in Mice. (A) Optimal vaccination was set to C+I vaccination for 4 weeks, as assessed by percent IgG binding to DB7, without a significant increase in non-specific mouse embryonic feeder (MEF) binding (n = 3 control animals, n = 4 iPSC primed animals, n = 4 C+I primed 2 week, and n = 4 C+I primed 4 week animals, mean ± SEM, ANOVA with Tukey's multiple comparison test). (B) Representative FACS plot of serum IgG binding of PBS 4-week, iPSC 4-week, C+I 2-week, or C+I 4-week vaccinated mice to embryonic fibroblasts (left panel), iPSCs (middle panel), and DB7 cancer cells (right panel). As a control sample for differentiated cells, a partly differentiated cell culture was included in the iPSC analysis. This is shown by IgG-positive and negative cells, indicating that the IgG binding is specific to the undifferentiated portion of the analyzed cells. C+I 4-week-vaccinated mice showed the best IgG binding to DB7 breast cancer cells. (C) Schema showing vaccine preparation consists of sorting murine iPSCs for pluripotency, irradiation, resuspension in adjuvant solution, and subcutaneous injection in the flank (sites 1–4). (D) Vaccination of FVB mice with C+I resulted in a complete rejection of the cancer cells in 7 out of 10 mice by 4 weeks and overall reductions in DB7 tumor size (n = 10 per group; representative images; left). Quantification of the data presented (right). (E) Vaccination of C57BL/6 mice with C+I resulted in significant reduction of melanoma sizes initiated by the aggressive B16F0 melanoma cell line by week 2 (n = 8 PBS, n = 9 iPSC primed, n = 10 CpG primed, and n = 9 C+I primed). (F) Quantification of the tumor size data presented in (E). Data in (D) and (F) represent mean ± SEM (ANOVA with Tukey's multiple comparison test). $^{*}p < 0.05$, $^{**}p < 0.001$, $^{***}p < 0.001$, $^{****}p < 0.0001$.

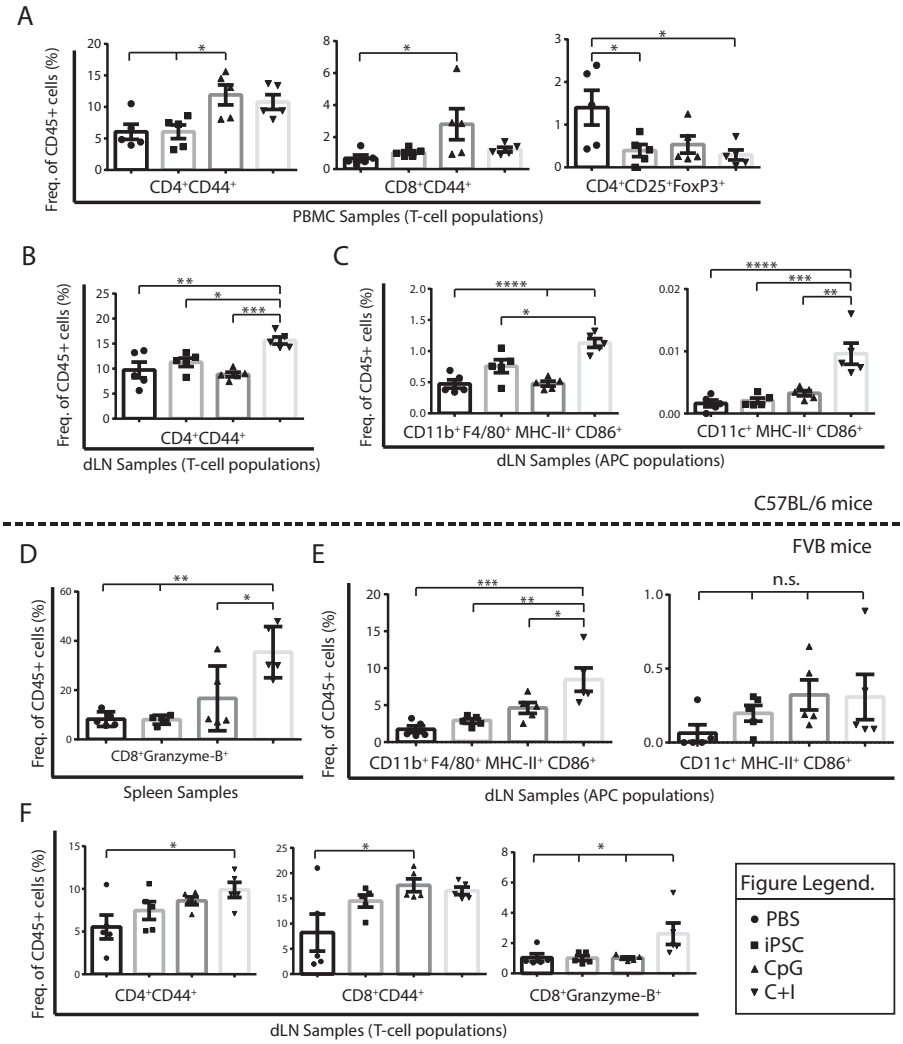


Figure 2. Prophylactic Vaccination Leads to Increased Antigen Presentation in dLNs and Subsequent Effector/Memory T Cell Responses in dLNs and Spleen

(A) 2 weeks after B16F0 introduction, iPSC- and C+I-vaccinated C57BL/6 mice showed a significant reduction in percentages of regulatory T cells ($CD4^+CD25^+FoxP3^+$) and an increase in effector/memory helper T cells ($CD4^+CD44^+$) in the peripheral blood of C+I-vaccinated mice. At that point, only limited upregulation of effector/memory cytotoxic T cells ($CD8^+CD44^+$) was seen.

(B and C) The dLNs in the C+I group had significantly higher percentages of effector/memory helper T cells (B) and increased antigen presentation by mature antigen-presenting cells (APCs) such as macrophages ($CD11b^+F4/80^+MHC\text{-}II^+CD86^+$) and dendritic cells ($CD11c^+MHC\text{-}II^+CD86^+$) (C). (D) C+I-vaccinated FVB mice showed increased percentages of activated cytotoxic T cells ($CD8^+$granzyme-B^+) in spleens 4 weeks after DB7 introduction. (E and F) dLNs of these mice revealed an increased frequency of mature antigen-presenting macrophages (E) as well as effector/memory helper T cells and cytotoxic T cells (F). Data represent mean ± SEM (n = 5 per group; ANOVA with Tukey's multiple comparison test). $^*p < 0.05$, $^{**}p < 0.001$, $^{***}p < 0.001$, $^{****}p < 0.0001$.

analysis showed a significant decrease in $CD4^+CD25^+FoxP3^+$ regulatory T cells (T-regs) in blood and an increase in effector/memory helper T cells in dLNs 2 weeks after tumor injections in C57BL/6 mice (Figures 2A and 2B), as well as increased percentages of mature antigen-presenting cells (APCs) (Figure 2C). At 4 weeks, FVB mice in the C+I-vaccinated group had significant increases in the effector/memory cytotoxic T cells in the spleen and dLNs (Figures 2D and 2F). The tumor specificity of these cytotoxic T cells was further confirmed by increased secretion of interferon-γ (IFN-γ) by splenocytes isolated from C+I-vaccinated mice in response to DB7 tumor lysate (Figures3A, 3B, S4A, and S4B). As with the C57BL/6 mice, upregulation of mature APCs and helper T cells was also seen in dLNs of FVB mice (Figures 2E and 2F). Both mouse strains remained healthy throughout the study and showed no signs of autoimmune responses due to the vaccine in serum and in tissues (Figures S4C–S4F). Lastly, the effectiveness of the C+I vaccine was assessed in the more clinically relevant orthotopic model of breast cancer. Significant tumor size differences were seen as early as 1 week after orthotopic transfer of cancer cells in C+I-vaccinated mice compared to vehicle control, followed by further tumor reduction over the course of 3 weeks (Figures 3C and 3E). Using an additional group of orthotopic breast cancer mice, in vivo tumor specificity was tested by adoptively transferring splenocytes from C+I vaccinated or vehicle (PBS+CpG) vaccinated mice into these tumor bearing mice (Figure 3D). This resulted in a significant reduction of tumor sizes in the C+I-vaccinated group compared to the vehicle-vaccinated group (Figure 3F).

Tumor Immunity in C+I-Vaccinated Mice Is the Result of Shared Epitopes between iPSCs and Cancer Cells

To test whether the C+I vaccine provides immunity against shared epitopes between iPSCs and cancer cells, we performed additional experiments to assess two-way immunity by demonstrating (1) cancer immunity by C+I primed T cells and (2) iPSC immunity by tumor-experienced lymphocytes (TELs). For the first experiment, isolated T cells from C+I-vaccinated or vehicle (PBS+CpG)-vaccinated mice were adoptively transferred to a group of tumor bearing orthotopic breast cancer mice (n = 7 per group), and tumor growth was measured over the course of 4 weeks (Figure 4A). This resulted in a significant reduction of tumor sizes in the C+I-vaccinated group compared to the vehicle-vaccinated group as early as 1 week after the adoptive transfer (Figure 4B). For the second experiment, another batch of mice vaccinated with C+I (n = 10) or vehicle (n = 10) were inoculated with breast cancer cells, and tumor growth was measured at 1 week (Figures 4C and 4D). Afterward, we extracted TELs from the dLNs near the tumor site (Torcellan et al. 2017). These TELs were then adoptively transferred to iPSC-inoculated non-obese diabetic severe combined immunodeficiency (NOD-SCID) mice ($5x10^6$ TELs per mouse; n = 4 per group), and teratoma development was measured for 4 weeks. Significant reduction in teratoma sizes was seen at 4 weeks in the NOD-SCID mice receiving TELs from C+I animals that were able to

reject the DB7 tumor cells, whereas mice receiving TELs from vehicle-vaccinated animals developed large teratomas (Figure 4E and 4F).

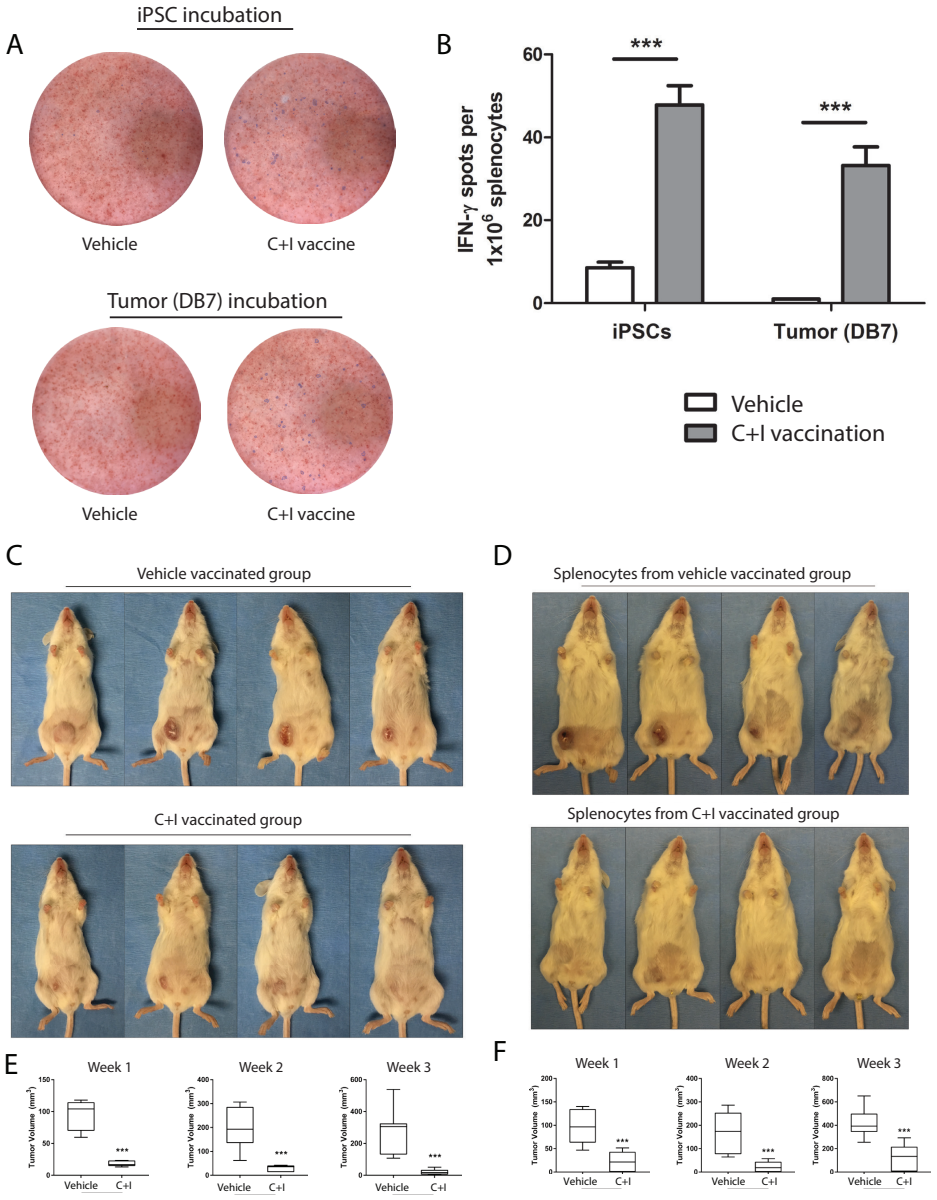


Figure 3. Tumor-Specific Properties of C+I Vaccine *In Vitro* and *In Vivo* in an Orthotopic Tumor Model of Breast Cancer.

Figure 3. Tumor-Specific Properties of C+I Vaccine *In Vitro* and *In Vivo* in an Orthotopic Tumor Model of Breast Cancer. (A) Dual ELISPOT assay (red, granzyme-β; blue, IFN-γ) for immune cell activation of splenocytes in the C+I-vaccinated group (n = 6) compared to CpG alone (vehicle; n = 4) group upon exposure to iPSC lysate and DB7 lysate (see also Figures S4A and S4B). (B) Significant increase of number of IFN-γ spots in the C+I-vaccinated group compared to the vehicle group. Spots were calculated using Adobe Photoshop software based on color differences. $^{***}p < 0.001$ (Student's t test). (C) Representative images of tumor volume in C+I-vaccinated mice compared to vehicle-vaccinated mice in an orthotopic tumor model of breast cancer 3 weeks after tumor inoculation. (D) Representative images of tumor volume in tumor bearing mice after receiving adoptive transfer of splenocytes from C+I-vaccinated mice compared to vehicle-vaccinated mice in an orthotopic tumor model of breast cancer 3 weeks after adoptive transfer. (E) Quantification of the results from (C) shows a significant reduction of tumor volume in C+I-vaccinated mice compared to vehicle-vaccinated mice in an orthotopic tumor model of breast cancer over the course of 3 weeks. $^{***}p < 0.001$ (one way ANOVA). (F) Significant reduction of tumor volume in tumor-bearing mice from (D) over the course of 3 weeks after adoptive transfer of splenocytes from C+I-vaccinated mice (n = 7) compared to mice receiving splenocytes from vehicle-vaccinated mice (n = 8). $^{***}p < 0.001$ (one way ANOVA). Mean ± SEM.

C+I Vaccination in a Mesothelioma Model Elicits a Pro-inflammatory Profile for Tumor-Infiltrating Lymphocytes

As an alternative model for prophylactic treatment, we selected the mesothelioma cell line AC29, syngeneic to CBA/J mice. Again, CBA/J iPSCs were created (Figures S2C and S2D), and mice were vaccinated for 4 weeks with PBS (P), CpG and iPSCs (C+I), or CpG with irradiated AC29 cancer cells (C+A) as a positive control. Afterward, $2x10^6$ AC29 cells (A) or $2x10^6$ iPSCs (I) were injected subcutaneously, and after 1 week, the TILs were analyzed for their immune profile and T cell receptor (TCR) sequences. Immune profiling was performed with cytometry by time of flight (CyTOF) analysis using a phenotype and intracellular staining kit, which revealed an increased presence of effector/memory $CD4^+$ (24.0%) and $CD8^+$ T cells (22.4%), with a reduction in T-regs in the C+I/A group (1.9%) compared to P/A control (21.1%, 14.2%, and 3.0%, respectively) (Figure 5A). Using Citrus (cluster identification, characterization, and regression) analysis (Bruggner et al. 2014), B cells and T cells expressing interleukin-2 (IL-2), IL-4, and IL-5 were found to be predictive of tumor regression in C+I-vaccinated mice compared to the PBS control group (Figures 5B, S5A, S5B, and S5D). Interestingly, systemic cytokine levels were significantly lower in the vaccinated group and were found to correlate with the positive control mice showing iPSC and tumor rejection (C+I/iPSC; C+A/AC29, respectively) (Figures 6A, S6A, and S6B). TCR sequencing in the PBS control group revealed an overlap in T cell clones that are commonly present in thymus and spleen (Figure S6C). In contrast, the TCRs in the C+I group were more diverse among different mice. In addition, there was a generally lower frequency of the clones in the thymus and more similar frequencies in the spleen, likely because of mouse-specific responses to the C+I vaccine (Figures 6B and S6D). Interestingly, there was one TCR clone that was shared by four of five mice in the C+I group but was not present in any of the other groups; this clone was also extremely rare in naive mice.

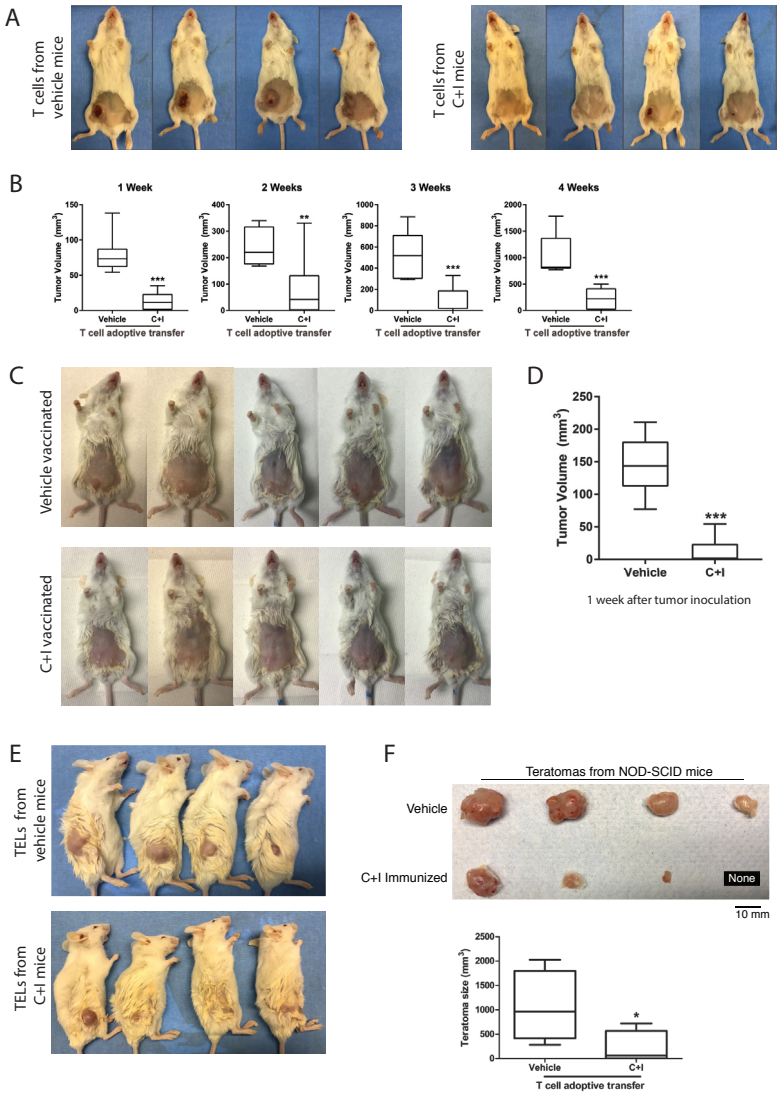
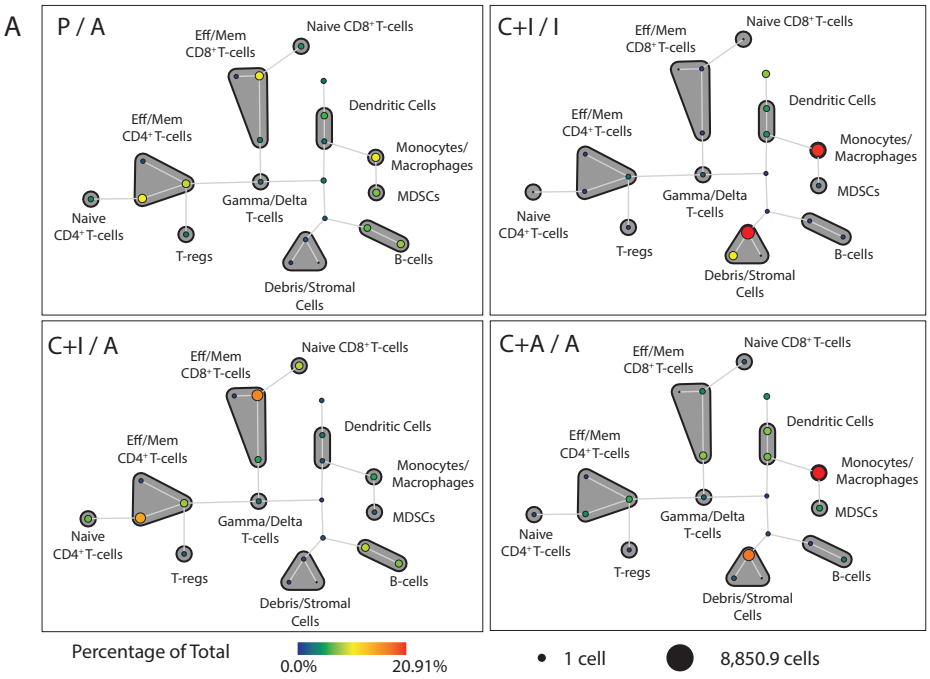


Figure 4. Shared Epitopes between Cancer Cells and iPSCs Provide T Cells with Two-Way Immunity. (A) Representative images from tumor-bearing mice 4 weeks after receiving T cells from either vehicle- or C+I-vaccinated mice. (B) Quantification of the tumor sizes of tumor-bearing mice in (A) over the course of 4 weeks after receiving T cells from vehicle- or C+I-vaccinated mice, as measured by caliper. Significant reduction of tumor sizes was seen as early as 1 week after the adoptive transfer of T cells from C+I-vaccinated mice and remained significantly reduced during the course of the experiment ($^{**}p < 0.01$; $^{***}p < 0.001$; Student t test). (C) Representative images of vehicle (n = 10) and C+I-vaccinated mice (n = 10) 1 week after orthotopic tumor inoculation. (D) Quantification of the tumor sizes displayed in (C) shows robust rejection of the DB7 breast cancer cells ($^{***}p < 0.001$; Student t test). (E) Representative images of NOD-SCID mice receiving TELs from the dLNs from vehicle- or C+I-vaccinated mice from the experiment in (C) (n = 4 per group). (F) Images from the teratomas isolated from mice in (E, top). Quantification reveals a significant reduction in teratoma sizes (bottom) from the C+I-immunized group ($^{*}p < 0.05$; Student t test). Mean ± SEM.



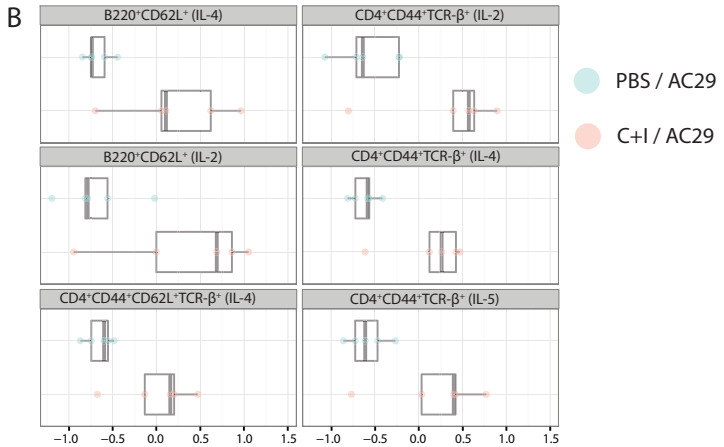


Figure 5. TILs Show a Pro-inflammatory Phenotype with B Cell and $CD4^+$ T Cell Anti-tumor Responses. (A) 1 week after 2×10^6 AC29 (A) mesothelioma cells were injected in CpG+iPSC (C+I)-vaccinated mice (n = 5), TILs in this C+I/A group showed an increase in the frequency of effector/memory $CD4^+$ and $CD8^+$ cells and a reduction in T-reg numbers compared to PBS (P)-vaccinated mice (n = 5; P/A group), as assessed by spanning tree progression analysis of density-normalized events (SPADE) of CyTOF data. The positive control groups, C+I-vaccinated and CpG+AC29 (C+A)-vaccinated mice, fully rejected iPSCs (n = 5; C+I/I) and AC29 cells (n = 5; C+A/A), respectively, with a subsequently enhanced presence of monocytes and macrophages and stromal cells. (B) Citrus analysis of CyTOF data revealed that higher levels of IL-2, IL-4, and IL-5 in B cell and helper T cell clusters in the C+I mice are responsible for the intra-tumoral immune response.

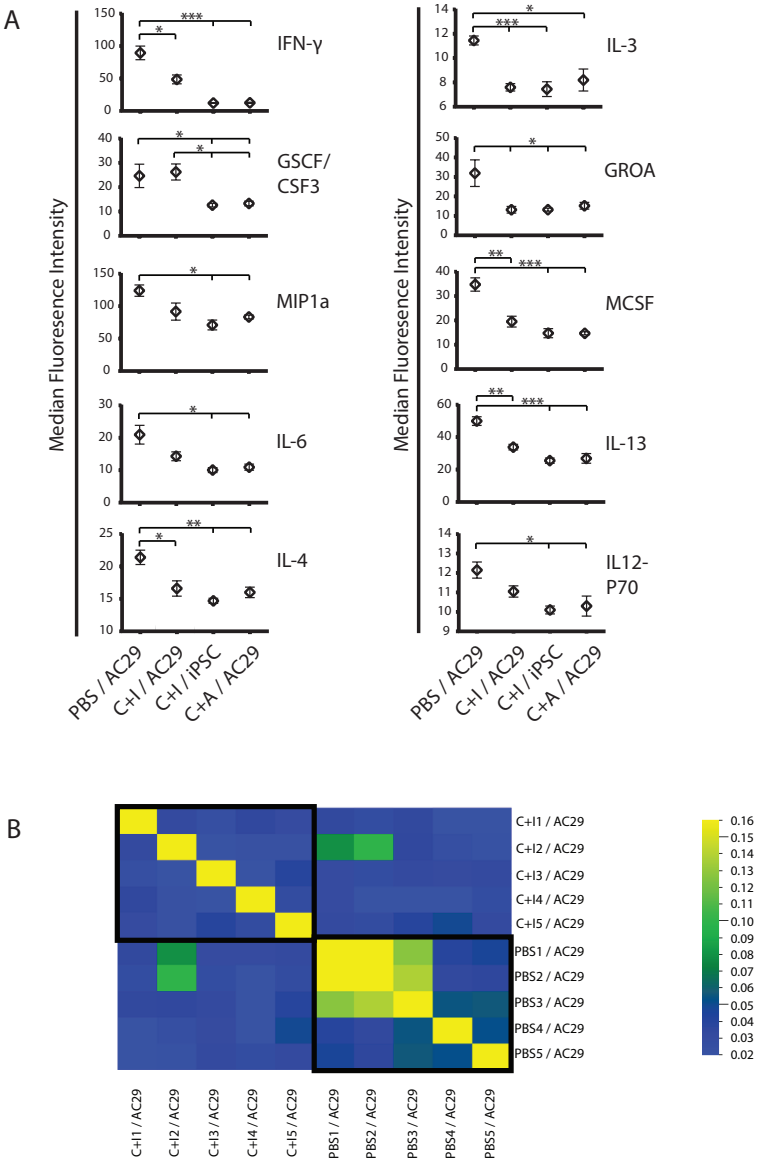


Figure 6. C+I Vaccination Leads to a Systemic Immune Profile Similar to Positive Control Groups of Tumor Rejection and Upregulation of Vaccine-Specific T Cell Clones. (A) Luminex analysis of serum from the different treatment groups 1 week after tumor cell introduction reveals a significantly lower presence of systemic cytokines in the positive control mice (C+I/iPSC, C+A/AC29) compared to PBS control mice (PBS/AC29). The C+I/AC29 group follows a similar trend as the positive control samples (C+I/iPSC and C+A/AC29; ANOVA with Tukey's multiple comparison test; $^{*}p < 0.05$, $^{**}p < 0.001$, $^{***}p < 0.001$). (B) Among C+I-vaccinated mice (C+I1 through C+I5/AC29), there was greater unique vaccine-associated variance within the TILs, whereas PBS-vaccinated mice (PBS1 through 5/AC29) demonstrated a higher uniformity among T cells that are commonly present in lymphoid organs (Figures S6C and S6D). Mean ± SEM.

C+I Adjuvant Therapy after Tumor Resection Leads to Decreased Tumor Load in Resection Areas and dLNs

To assess the effectiveness of the vaccine as an adjuvant therapy after tumor resection, we next injected $5x10^4$ B16F0 tumor cells subcutaneously in the lower back of C57BL/6 mice and R2- or R1-resected the tumors after 2 weeks. R2-resected mice had no visible recurrence of melanoma in the resection area (RA) after receiving two adjuvant rounds of C+I vaccine, whereas PBS-control-vaccinated mice had visible tumors within the RAs (Figure S7A). R1-resected mice were vaccinated for 4 weeks with the C+I vaccine (n = 10), CpG (n = 10), and PBS (n = 8) (Figure 7A), after which dLNs and RAs were analyzed using a tumor-specific primer designed to detect and quantify the B16F0 melanoma line (Figures S7B–S7G). Tumor load in the dLNs was reduced in both CpG-only and the C+I vaccine groups, indicating that CpG acted as a potent adjuvant to induce tumor degradation upon near tumor injection (Figure S7H). Interestingly, in areas more distant from the vaccination sites, only the C+I-vaccinated group had significantly lower tumor recurrence in the RA (Figure 7B). Systemically, this is explained by reactivation of the immune system (Numasaki et al. 2003, Dolcetti et al. 2010, Chung et al. 2013), as well as a reduction of B16 melanoma-promoting Th17 cells (Anders and Huber 2010) compared to the control groups (Figures 7C, S5C, and S5E).

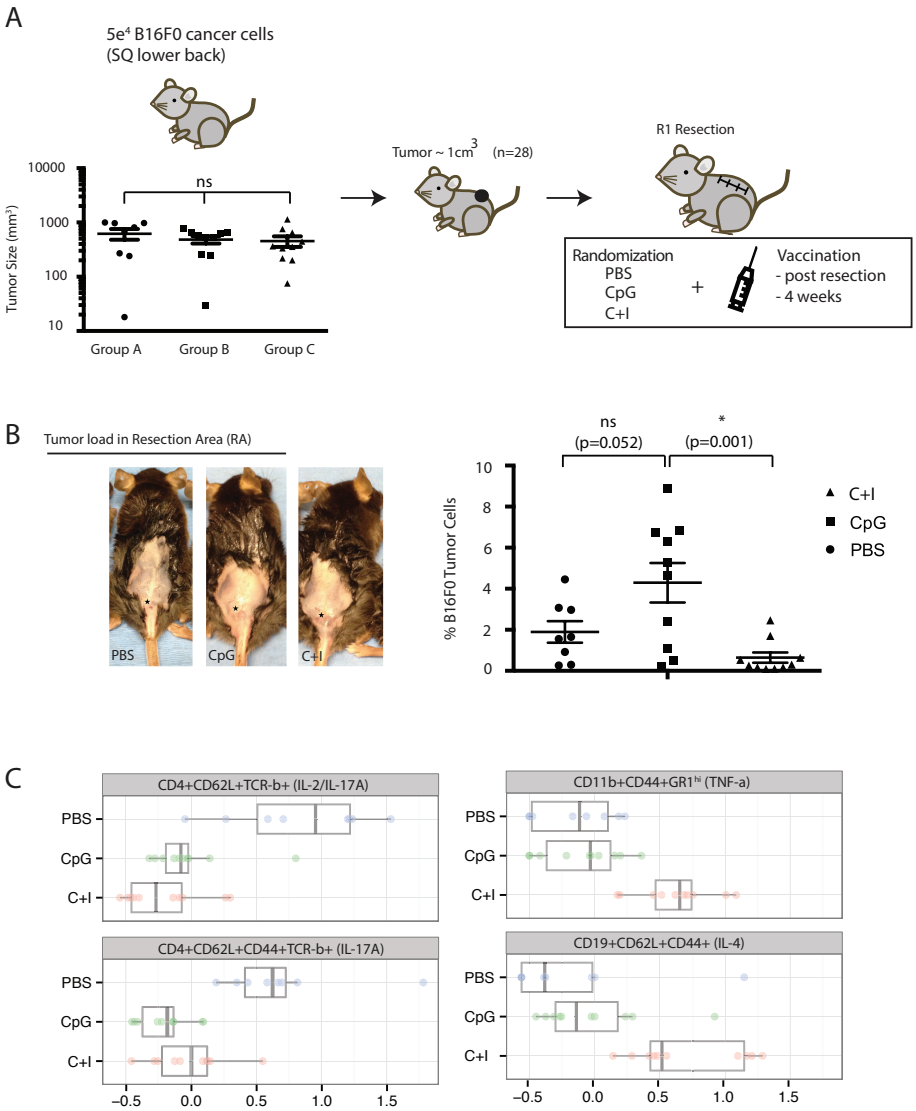


Figure 7. Adjuvant Vaccination after Tumor Resection Leads to Clean RAs and Reactivation of the Immune System to Target Cancer Cells. (A) B16F0 tumor-bearing mice underwent R1 tumor resection, were randomized into different treatment groups, and were vaccinated with C+I, CpG, or PBS for 4 weeks. (B) DNA from skin biopsy specimens (*) in resection areas (RAs) showed a significant reduction in the percentage of tumor cells after four vaccination rounds with the C+I vaccine, as assessed by ddPCR. (C) Vaccination post-tumor resection led to a reduction of Th17 cells ($CD4^+CD62L^+TCR\text{-}b^+$(IL-2/IL-17A); $CD4^+CD62L^+CD44^+TCR\text{-}b^+$(IL-17A)) and an increased presence of TNF-α-expressing myeloid cells ($CD11b^+CD44^+GR1^{hi}$(TNF-a)) and IL-4-expressing $CD19^+CD62L^+CD44^+$ B cells (n = 8 PBS, n = 10 CpG, n = 10 C+I). Mean ± SEM; ANOVA with Tukey's multiple comparison test; $^*p < 0.05$). SQ, subcutaneous injection.

DISCUSSION

Tumor establishment and progression involve highly proliferative hypoimmunogenic cells that evade the surveillance of the immune system. Therefore, new avenues within the field of cancer treatment are being pursued to target cancer by reactivating the immune system. One way researchers are trying to achieve this is by using chimeric antigen receptors (CARs), with promising results (Maude et al. 2014, Maus et al. 2014, Lee et al. 2015). The idea behind this therapy is to create a cancer-specific antigen receptor and couple this to an effector cell (e.g., T cell), with newer generations of CARs that might even incorporate the co-stimulatory pathways. However, thus far, results have been mixed, with some patients relapsing, possibly due to loss of expression of the targeted antigen (Grupp et al. 2013, Maude et al. 2014). One way to circumvent this would be to identify new tumor-specific antigens, but large numbers of tumor antigens are possibly still unknown. Pluripotent cells and tissues share known and likely also unknown TSAs and TAAs with cancer cells and therefore could be a potential agent to prime an immune system to target cancer. This modified cell would then function as a surrogate cell type that resembles the targeted cancer type. A few groups have pursued the use of pluripotent cells for priming the immune system in targeting cancer but thus far have not shown efficacy and safety for the treatment of various types of cancer (Li et al. 2009, Yaddanapudi et al. 2012). In addition, they still rely on the use of ethically concerning ESCs and/or a genetically modified cell line as an adjuvant (Yaddanapudi et al. 2012, Inoue 2013), making these treatments less suitable for personalized clinical translation. In this study, we showed that prophylactic immunization of several mouse strains with a non-genetically engineered iPSC-based vaccine produces an effective immune response to multiple cancer types by upregulation of mature APCs in the dLNs with a subsequent increase in helper T cells and cytotoxic T cells locally and, later on, systemically. Interestingly, this led to a systemically favorable T-effector/T-reg ratio, which has been found to reduce tolerizing conditions (Zou 2005). With our adoptive transfer data on transplantation of C+I-primed splenocytes into tumor-bearing mice, we demonstrated the tumor specificity of our iPSC vaccine, which, based on our in vitro data, was likely the result of IFN-γ^+ effector T cells. The lifespan of these IFN-γ^+ effector T cells (8–10 days) would also explain why there was tumor regression after the adoptive transfer of C+I-primed splenocytes in the orthotopic model of breast cancer for the first 2 weeks, after which a small increase in tumor size was seen (Dooms and Abbas 2002). To test whether the immunity created by the vaccine is the result of shared epitopes between iPSCs and cancer cells, we performed adoptive transfer of C+I-primed T cells to breast cancer-bearing mice and adoptive transfer of TELs to iPSC inoculated NOD-SCID mice. With these experiments, we were able show that C+I-primed T cells rejected the DB7 breast cancer cells and that the primed TELs were able to reduce teratoma size or stop teratoma formation altogether. This "two-way immunity" demonstrates shared epitopes between iPSCs and cancer cells. Looking into the

early intra-tumor immune response, we found mainly B cells and T cells expressing IL-2, IL-4, and IL-5 with a switch from common T cell clones to rarer vaccine-associated T cell clones. Most of these high frequency clones vary between the vaccinated mice, suggesting that each mouse mounts a cross-reactive immune response based on different epitopes from the iPSCs. This provides further evidence that iPSCs share a larger repertoire of cancer-related epitopes, indicating that this surrogate cell type could be a potential candidate to limit the chances of immune evasion by the cancer cells as has occasionally been reported in CAR therapy (Grupp et al. 2013, Maude et al. 2014). Another issue with CAR therapy is organ toxicity from cytokine storms upon transfusion of CAR T cells (Morgan et al. 2010). As we showed in our CBA/J mouse data using the Luminex assay, systemic cytokine levels are low; instead, there is a localized immune response within the tumor similar to the positive control group of tumor rejection. In addition, tissue analysis of our mice at different time points after vaccination did not show any increases in immune cells within heart and kidney tissues compared to negative control groups, nor were elevated levels of anti-nuclear antigen (ANA) IgG seen in serum from C+I-vaccinated mice. As a therapy for established melanomas, the C+I vaccine was not effective in reducing tumor growth, which is likely due to an established immunosuppressive tumor microenvironment that could potentially be remedied by combining the C+I vaccine with checkpoint blockade treatment (Le et al. 2015). However, as an adjuvant therapy after R1 resection of melanoma, we found that the C+I vaccine reactivated the immune system in rejecting remnant melanoma cells by the systemic upregulation of IL-4- expressing B cells and TNF-α-expressing $CD11b^{+}GR1^{hi}$ myeloid cells, as well as a reduction of tumor-promoting Th17 cells. In this setting, the cancer epitope heterogeneity of iPSCs, combined with the ease of their generation, may make this therapy readily available as adjuvant immunotherapy for multiple cancer types within weeks after diagnosis. This last point is crucial for immunotherapy, because it is commonly known that that the tumor microenvironment could limit effectiveness of tumor immunity by suppressive immune cells residing within the tumor. After debulking of the tumor and disrupting the tumor microenvironment to create an "inflamed" tumor site, immunotherapy should be more effective (Gajewski et al. 2013). This is demonstrated in our R1 resected melanoma model, which again emphasizes the need for a multi TSA- and TAA-based vaccine to be readily available at time of tumor resection. Having a surrogate whole cell vaccine with multiple known (and likely unknown) TSAs and TAAs available at such a short time after diagnosis would allow the priming of the immune system to target large numbers of cancer-specific antigens at a time when cancer cells are most vulnerable. Even though an overlap was seen in murine and human TAA genes, it is important to note the differences in murine and human immunology before extrapolating the above-mentioned data to humans (Mestas and Hughes 2004). Further testing of the C+I vaccine on human samples ex vivo should therefore be performed to show efficacy in humans. Taken together, our data show the feasibility of creating broad tumor immunity against multiple cancer types using

an iPSC- based vaccine that presents the immune system with large quantities of tumor antigens. Compared to current immunotherapy strategies, our iPSC vaccine is capable of reactivating the immune system to target cancers without therapy-associated adverse effects and can be created within a few weeks after diagnosis. These beneficial properties make this iPSC vaccine a potential option for personalized adjuvant immunotherapy shortly after conventional primary treatment of cancer.

EXPERIMENTAL MODEL AND SUBJECT DETAILS

Animal models

Young adult female FVB, C57BL/6J, and CBA/J mice (6-8 weeks old) were used. Animals were randomly assigned to the different treatment groups. Tumor-bearing mice were excluded from the experiment if their physical condition required euthanasia before the experimental deadline, due to criteria such as tumor sizes exceeding 1 cm^3, visible distress, pain, or illness. All experiments were approved by the Stanford University Administrative Panel of Laboratory Animal Care (APLAC).

Generation of murine iPSCs from fibroblasts

Fibroblasts from FVB, C57BL/6J, and CBA/J mice (The Jackson Laboratory, Bar Harbor, Maine) were grown in DMEM Glutamax (ThermoFisher Scientific, Waltham, MA, USA) with 20% fetal bovine serum (FBS) and 1x NEAA (ThermoFisher Scientific). Fibroblasts were dissociated using TrypLE Express (ThermoFisher Scientific) and $1x10^6$ fibroblasts were resuspended in electroporation buffer (Neon system, ThermoFisher Scientific). Cells were transfected with a codon-optimized mini-intronic plasmid (CoMiP) containing the four reprogramming factors Oct-4, Sox-2, c-Myc, and Klf4 (Diecke et al. 2015). After transfection, cells were plated on irradiated mouse embryonic feeder (MEF) cells and cultured in DMEM with 15% FBS, 1x NEAA, and 10 ng/ml murine leukemia inhibiting factor (mLIF; EMD Millipore, MA, USA). After iPSC colonies started to appear, they were manually picked and transferred to a fresh feeder layer. The iPSC colonies were grown for a few passages and then transferred to 0.2% gelatin-coated plates to be sorted for SSEA-1 using magnetic bead sorting (Miltenyi, Germany) to keep a pure undifferentiated population. For characterization, iPSCs were stained for Oct4, Nanog, Sox2 (Santa Cruz, CA, USA), SSEA1, and c-Myc (EMD Millipore) to assess pluripotency. In addition, a teratoma assay was performed on all iPSC lines by transplantation of $1x10^6$ iPSCs in the hindlimb of NOD-SCID mice (The Jackson Laboratory). All cell lines were tested for mycoplasma contamination and found to be negative.

Cancer cell lines and implantation

The breast cancer line DB7 was a gift from Dr. Joe Smith (University of Utah, USA). It was derived from FVB mice and is a non-metastatic cell line. The B16F0 melanoma cell line was purchased from ATCC (Manassas, VA, USA) and is syngeneic to C57BL/6 mice. It has low-grade lymphoid metastatic potential to the lungs. The AC29 mesothelioma cancer line was purchased from Sigma-Aldrich (St. Louis, MO, USA). The cancer lines were grown in DMEM, 10% FBS under normal culture conditions. For the C57BL/6 and FVB mice, $5x10^4$ cancer cells were resuspended in 100mL PBS and injected subcutaneously in the lower back of the mice. The CBA/J mice were injected with $2x10^6$ cancer cells. Tumor growth was

assessed weekly by caliper measurement. At the end of the study, tumors were explanted and gross examination of draining lymph nodes and lung tissue was performed for any metastases.

CpG + iPSC vaccine preparation and immunization

For each mouse, $2x10^6$ SSEA-1-sorted syngeneic murine iPSCs were irradiated at 6,000 rads prior to injection. Cells were suspended in 100mL of 5mM CpG (Invivogen, San Diego, USA), dissolved in PBS, and loaded into 1/4 cc insulin syringes (Terumo). Mice were placed in an induction chamber and anesthetized with 2% isoflurane (Isothesia, Butle Schein) in 100% oxygen with a delivery rate of 2 l/min until the loss of righting reflex, as per APLAC guidelines at Stanford University. Immunization was performed by subcutaneous injection of the vaccine in the flanks of the mice, with the injection site changing every week. Mice were monitored weekly for early signs of auto-reactivity to the vaccine by weight measurements and gross examination of overall appearance. Vaccination preparation and dosage were the same for the prophylactic and adjuvant treatment experiments. The prophylactic vaccination studies were replicated several times in the same mouse strain, different mouse strains and by different investigators. The investigator analyzing the tumor sizes and data from the adjuvant treatment experiment was blinded for the different treatment groups.

Mixed lymphocyte reaction (MLR)

Spleens were isolated, minced, and filtered through a 70μm strainer. After multiple washes with glucose-containing RPMI, the pellet was resuspended in ACK lysis buffer for removal of red blood cells. CFSE-labeled (ThermoFisher Scientific) splenocytes from C+I vaccinated mice were then plated at a density of $1x10^5$ cells per 100μL in a 96-well plate and incubated for 72 hr with another 100μL solution of DB7 tumor lysate, ranging from 1-10μg. After 72 hr, the plate was spun down and the supernatant isolated for cytokine analysis using the mouse Th1/Th2/Th17 Cytokines Multi-Analyte ELISArray kit (QIAGEN, Hilden, Germany), and the cell pellet was analyzed with the LSR-II Flow Cytometer to assess T cell proliferation.

IgG binding assay

Cells were washed multiple times with PBS and resuspended in 100μL FACS buffer with the addition of 2μL of serum from the vaccinated mice and incubated for 30 min on 4C. Following this, cells were washed multiple times and incubated with an anti- IgG FITC secondary antibody (ThermoFisher Scientific) for another 20 min on 4C. As an isotype control an IgG antibody, pre-adsorbed for murine IgG and IgM, was included. The cells were then analyzed using the LSR-II Flow Cytometer.

Histopathology of explanted organs

At time of sacrifice, the heart and kidneys were explanted from vaccinated mice and processed for histopathology. Briefly, the organs were fixed overnight in 4% paraformaldehyde and transferred to 70% ethanol for 24 hr. Fixed samples were embedded in paraffin and 5μm sections were cut and stained with hematoxylin and eosin (H&E) for histological analysis by a pathologist.

Isolation of inflammatory cells and serum from blood, spleen, tumor, and dLNs

FVB, C57BL/6, and CBA/J experimental mice were sacrificed at 4, 2, and 1 week(s), respectively, after tumor inoculation. Tissues were isolated from the mice and placed in a digestion buffer containing RPMI, FBS, collagenase, DNase, trypsin inhibitor and HEPES, then minced and placed in a shaker at 37°C for 45 min. Samples were than filtered through a 70μm strainer, spun down, and resuspended in ACK lysis buffer to remove any red blood cells. After lysis, the cell suspension was washed with PBS and used for subsequent analyses. Additionally, dissociated tumors were passed through a Percoll gradient to remove non-immune cells and isolate tumor-infiltrating leukocytes (TILs). Blood was collected in two separate tubes per mouse for PBMC (EDTA containing tube) and serum isolation (uncoated tube).

Staining of inflammatory cells for FACS analysis

Inflammatory cells isolated from blood and tissues were resuspended in 200μL FACS buffer (DPBS, 2% FBS and 200mM EDTA), blocked with a FcR-blocking Reagent (BD PharMingen, San Diego, CA, USA), and divided into 2 tubes. One tube was stained with a surface marker panel, containing CD3, CD4, CD25 (eBioscience), CD8a, CD44, CD45 (Biolegend), and the intracellular markers Granzyme-B (eBioscience) and FoxP3 (Biolegend). The second tube was stained for F4/80, MHC-II (eBioscience), CD86 (BD Biosciences), CD11b, CD11c, NK1.1, Ly6-G, and CD45 (Biolegend). A rat IgG2b κ isotype control was included for CD44, FoxP3 (Biolegend), and MHC-II (eBioscience). A rat IgG2ακ isotype was included for the Granzyme-β (eBioscience) and CD86 (BD Biosciences) staining. For CD25 staining, the IgG1 κ isotype (eBioscience) was included. In both panels, the fixable viability dye 780 (Invitrogen) was added to exclude dead cells from the analysis. Extracellular staining was performed prior to fixing and permeabilizing the samples for staining with intracellular markers. Samples were analyzed on the LSR-II Flow Cytometer analyzer in the Beckmann FACS facility (Stanford University).

Teratoma formation

Teratoma formation was performed as previously described (Nelakanti et al. 2015), with the exception of site of injection. For this manuscript, a flank injection was preferred over a hindlimb injection to ensure easier access for over-time measurements of teratoma size. In

brief, $1x10^6$ iPSCs were resuspended in growth factor reduced Matrigel (50µL per injection) and injected in the flank of immunodeficient mice (NOD-SCID IL2Rgamma null; NSG). Teratoma sizes at site of injection were measured over time using a caliper. After four weeks, mice were sacrificed and the teratomas harvested for final measurements.

Generation of tumor lysate

$1x10^7$ tumor cells were used from in vitro culture and resuspended in 1 mL of PBS. The cell suspension was frozen to -80°C for 45 min and then thawed on 37°C for 30 min. This process was repeated for a total of three times. Afterward, the suspension was spun down and the supernatant, containing tumor lysate, was isolated for protein concentration measurements using the Pierce BCA Protein Assay Kit (ThermoFisher Scientific).

Luminex multiplex cytokine assay

Production of various cytokines was measured in cell culture supernatant and serum samples using a multiplex-Luminex platform (LabMap200 System; Luminex) in conjunction with Panomics antibodies at the Human Immune Monitoring Center at Stanford University.

ELISPOT assay

Splenocytes ($5x10^5$) were isolated as described above and co-cultured with either iPSC or DB7 lysate (35µg) for the duration of 37 hr, after which the secretion of granzyme-β and IFN-γ was measured by Enzyme-Linked ImmunoSpot (ELISPOT) according to the manufacturer's instructions (cat# ELD5819, R&D Systems, Diaclone). Adobe Photoshop CS6 software was used for the calculation of size and number of IFN-γ positive spots.

Adoptive transfer of splenocytes and T cells

C+I vaccinated and vehicle vaccinated mice were sacrificed and their splenocytes isolated, as previously described (Sodhi et al. 1985, Naas et al. 2010, Galvan et al. 2015). In brief, the spleens were digested and passed through a 70µm strainer. Afterward red blood cells were lysed with ACK lysis buffer (cat# 118-156-101, Quality biology, INC.) and the remaining splenocytes washed with PBS. The splenocytes were then dissolved in 200µL PBS solution and intravenously injected in an orthotopic model of breast cancer by tail vein injection. For the adoptive transfer of T cells, the procedure is as described above, with the addition of a magnetic bead sorting using the Pan T cell isolation kit to acquire $CD3^+$ T cells (#130-095-130, Miltenyi, Germany) after the final washing step.

Orthotopic tumor model

FVB mice were injected with $2x10^6$ DB7 tumor cells directly into the mammary fat pad tissue, as previously described (Kocaturk and Versteeg 2015). The range of cancer cell number

was based on previous reports (Chen et al. 2011, Evans et al. 2014) and was set at $2x10^6$ DB7 cancer cells after validating the model and achieving a tumor incidence of 100%.

Isolation of TELs from draining lymph nodes

After sacrificing the C+I and vehicle-vaccinated mice, their dLNs were isolated, minced and passed through a 70μm strainer. After washing the cells with PBS, the T cell portion of the TELs were isolated using the Pan T cell isolation kit to acquire $CD3^+$ T cells (#130-095-130, Miltenyi, Germany).

Anti-nuclear antibody (ANA) ELISA

Murine blood was collected from PBS, CpG only, or CpG-iPSCs vaccinated mice and the plasma was separated from the blood via centrifugation for 15 min at 1000g. The plasma samples were diluted at 1:200 with sample dilution. The concentrations of anti-nuclear antibodies (IgG) were determined using an ELISA kit, according to the manufacturer's instructions (Antibodies-Online; antibodies-online.com). For this experiment, four biological replicates per group were used and for each biological replicate three technical replicates were included.

Cytometry by Time of Flight (CyTOF)

Immune cells were isolated from explanted tissues according to aforementioned methods. Cells were stained with the Mouse Spleen/Lymph Node Phenotyping kit, the Mouse Intracellular Cytokine I Panel kit, and the viability dye Cisplatin (Fluidigm, South San Francisco, CA). Cells were resuspended in MaxPar water at a concentration of $1x10^5$-$1x10^8$ cells per mL with the addition of normalization beads and ran on a CyTOF2 (Fluidigm) machine. Following this, the data were normalized using the normalization beads. The data were analyzed using the Cytobank online software for spanning tree progression analysis of density-normalized events (SPADE) (Qiu et al. 2011).

PCR detection of the large genomic deletion in Cdkn2a

Primers were designed to detect the junction of the large deletion in Cdkn2a of the B16 melanoma cell line (FigureS7B). Each 25μL PCR reaction solution contained 1.25 units of PrimeSTAR GXL DNA Polymerase (Clontech) and 50-100 ng of genomic DNA extracted by DNeasy Blood & Tissue Kit (QIAGEN) (Figure S7C). PCR products were then analyzed by Sanger sequencing and aligned with the gene database in NCBI (Figure S7D).

T cell Receptor (TCR) sequencing

The DNA from the TILs infiltrating the AC29 tumors was isolated using the DNeasy Blood & Tissue kit (QIAGEN). Samples were submitted to Adaptive Biotechnologies (Seattle, WA) for a survey level TCR sequencing. The minimum DNA content from the submitted samples

was 150 ng per sample with DNA quality A260/280 between 1.8 to 2.0. Data analysis as well as assessment of TCR clonality between samples were performed in collaboration with Adaptive Biotechnologies. In brief, a list of TCR clones within each sample and their frequencies within the DNA sample were provided. For the T cell overlap search, the amino acid sequences of the clones appearing in 4 or 5 of the samples in the two sample groups were compared. Data from the CI treatment group and the PBS control group were ruled comparable with similar average productive unique values (PBS: 3582.2, CI: 3005.4).

QUANTIFICATION AND STATISTICAL ANALYSES

All values are expressed as mean ± s.d. or mean ± s.e.m. as indicated. Intergroup differences were appropriately assessed by either unpaired two-tailed Student's t test or one-way/two-way analysis of variance (ANOVA) with Tukey's posthoc test using PRISM GraphPad software. * $P < 0.05$, ** $P < 0.01$, *** $P < 0.001$, **** $P < 0.0001$.

Cluster identification, characterization and regression (Citrus)

In brief, based on hierarchical clustering and a regularized regression model, Citrus generates a list of stratifying clusters and behaviors from multidimensional data. In addition, it can describe their features (e.g., intracellular cytokines) and provide a predictive model for newly acquired data or validation samples. The stratifying features from these clusters were plotted as median expression on the x axis (Figures 5B, 7C, and S5B). CyTOF data were analyzed using Cytobank and gated for viable single cells, after which the FCS files were uploaded in the GUI from Citrus 0.8 and the script was run in R (version 3.0.3). For the analysis of the splenocytes exposed to B16F0 tumor lysate, Citrus analysis was performed with 10,000 sampling events with 0.2% (567 events) minimum clustering. For the TILs, Citrus analysis was based on 1,000 sampling events with 500 events minimum clustering. Clustering features were found to be of interest with a cv.min and cv.fdr.constrained of less than 25.

Quantification of tumor load for melanoma by digital droplet PCR (ddPCR)

Primers and probe were designed to detect 3 SNPs (colored in red) that are specific to the B16 melanoma cell line. DNA was extracted from the tumor resection area and dLNs of C57BL/6 mice four weeks after R1 tumor resection using the DNeasy Blood & Tissue Kit (QIAGEN). Each ddPCR reaction solution was reconstituted to a final volume of 20μL using 40 to 50 ng of DNA template and ddPCR Supermix for Probes, without dUTP (BioRad). Each sample was quantified by using 2 probes: MT probe to assess the tumor load, and TaqMan Copy Number TFRC probe (Mm00000692_cn, ThermoFisher) to assess the cell amount (Figure S7E, F). The final primer and probe concentrations were 900 nM and 250 nM, respectively. Droplet formation was carried out using a QX100 droplet generator with 20μL of PCR reaction solution. A rubber gasket was placed over the cartridge and loaded

into the droplet generator. The emulsion (~35μL in volume) was then slowly transferred using a multichannel pipette to a 96-Well twin.tec PCR Plates (Eppendorf). The plate was then heat-sealed with foil and the emulsion was cycled to end point per the manufacturer's protocol with annealing temperature at 62.5C. The samples were then read using a BioRad QX100 reader. The standard curve was created for different amounts of tumor load, including 0%, 1%, 5%, 10%, 25%, 50%, 75%, 90%, 95%, 99%, and 100%, and linear regression equation was utilized to quantify the tumor load for each DNA sample (Figure S7G). Following are the sequences of the primers and probes for detecting tumor load:

Forward primer, 5'ACTAGCCAGAGGATCTTAAAGACT3';

Reverse primer, 5'GCCATCACTGGAAAGAGAGGC3';

Mutant Probe, 5'(HEX)CCTGCCCACCCACTCCCCCTTTTT (Blackhole Quencher)3';
(red indicating mutant-specific alleles).

Analysis of RNA-sequencing data

The pair-end human RNA-seq data from normal and cancer cell lines were downloaded from the GEO repository of ENCODE project (https://www.genome.gov/encode/) (Consortium 2011). The RNA-seq of iPSCs reprogrammed by different methods were generated from previous publication (Churko et al. 2017). The fastq files of the sequencing were aligned to the human genome (hg19) by Hisat (https://ccb.jhu.edu/software/hisat/index.shtml) (Kim et al. 2015). The aligned reads were assigned by HT-seq (http://www-huber.embl.de/users/anders/HTSeq) (Anders et al. 2015) to the gene annotation (version 19) provided by the GenCode project (http://www.gencodegenes.org/) (Harrow et al. 2012). The gene expression levels were estimated and normalized by DESeq (https://bioconductor.org/packages/release/bioc/html/DESeq.html) (Anders and Huber 2010, Anders et al. 2013). The gene expression levels were extracted from a curated selection of cancer-related genes described in seven datasets (allOnco; Bushman Lab, University of Pennsylvania) after which a heatmap was generated using GENE-E (https://www.broadinstitute.org/cancer/software/GENE-E).

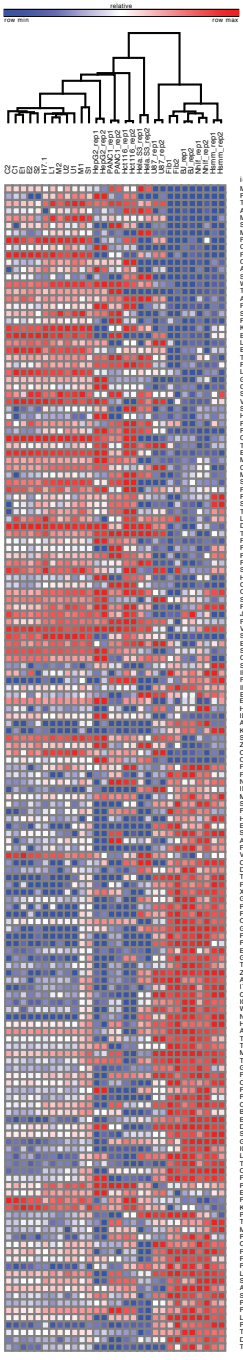
Analysis of murine RNA sequencing data

The pair-end/single-end RNA-seq data from tissues were downloaded from the mouse ENCODE project (http://mouseencode.org/). The mouse iPSC data were downloaded from GSE36294 (Chang et al. 2014). The fastq files of the sequencing were aligned to the mouse genome (mm10) by Hisat (https://ccb.jhu.edu/software/hisat/index.shtml). The aligned reads were assigned by HT-seq (http://www-huber.embl.de/users/anders/HTSeq) to the gene annotation (version M3) provided by the GenCode project (http://www.gencodegenes.org/). The gene expression levels were estimated and normalized by DESeq (https://bioconductor.org/packages/release/bioc/html/DESeq.html). The heatmap was generated using GENE-E (https://www.broadinstitute.org/cancer/software/GENE-E).

DATA AND SOFTWARE AVAILABILITY

T cell receptor sequencing data have been deposited in the immuneACCESS platform under the following accession number: https://doi.org/10.21417/B7B648.

A



B

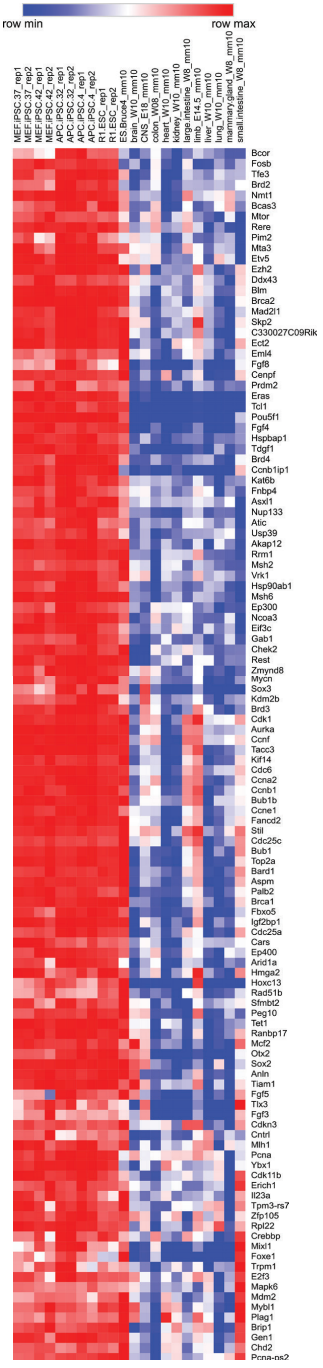


Figure S1. Heatmap analysis of RNA sequencing data from human and murine iPSCs, healthy tissues, and cancer tissues. (A) RNA sequencing from 11 human iPSC clones generated with different reprogramming methods (C, E, M, L, U, and S) reveals grouping with hESCs and different cancer types (Encode database) based on a selected list of cancer-related genes, described in seven datasets (allOnco; Bushman Lab, University of Pennsylvania). *Minicircle (C1, C2); Episomal (E1, E2); mRNA (M1, M2); Lentivirus (L1); microRNA (U1, U2); Sendai virus (S1, S2); hESCs (H7.1); Hepatocellular Carcinoma (HepG2); Pancreatic Carcinoma (PANC1); Cervical Carcinoma (Hela.S3); Glioblastoma/Astrocytoma (U87); fibroblasts (Fib); skin fibroblasts (BJ); lung fibroblasts (Nhlf); and Skeletal Muscle Myoblasts (Hsmm).* (B) Based on more than 2,000 human tumor-associated antigens (TAA) and tumor-specific antigens (TSA) RNA, we were able to identify the presence 116 of these tumor antigens in murine iPSCs (*MEF.iPSC and APC.iPSC*) and ESCs. Similar to the human data, these are highly expressed in the pluripotent populations but only lowly or not expressed in the somatic tissues. *MEF-derived iPSCs (MEF.iPSC); APC-derived iPSCs (APC.iPSC); murine ESCs (R1.ESC); murine ESCs (ES.Bruce4); brain tissue (brain_W10); central nervous system (CNS_E18); colon tissue (colon_W08); heart tissue (heart_W10); kidney tissue (kidney_W10); large intestines (large.intestine_W8); limb tissue (limb_E14.5); liver tissue (liver_W10); lung tissue (lung_W10); mammary gland tissue (mammary.gland_W8); and small intestines (small.intestine_W8).*

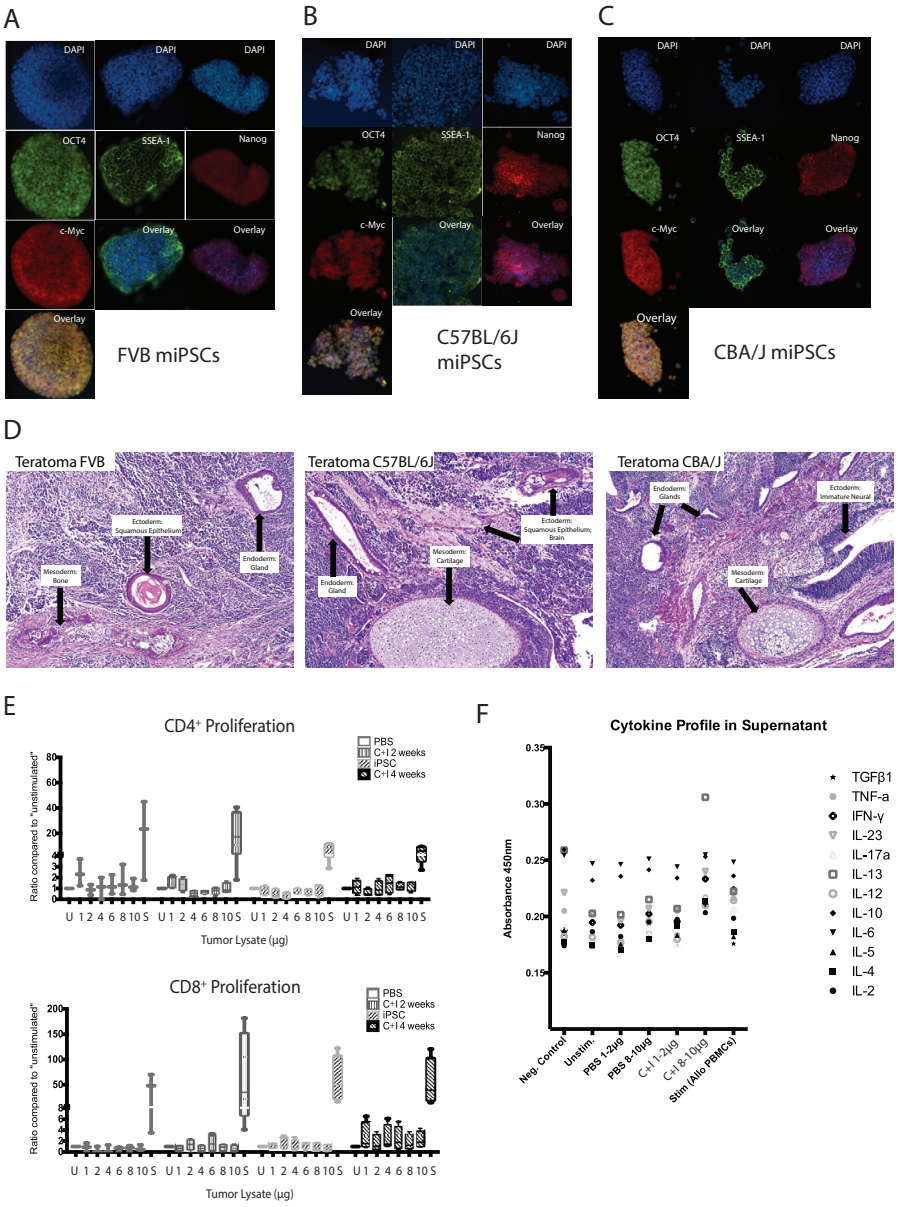


Figure S2. Characterization of iPSCs for pluripotency and *in vitro* optimization of the vaccination schedule using the adjuvant CpG. Pluripotency staining of (A) FVB, (B) C57BL/6, and (C) CBA/J murine iPSCs with pluripotency markers Oct4, c-Myc, Nanog, and SSEA-1. (D) All three cell lines were able to form teratomas *in vivo* upon transplantation of $1x10^6$ iPSCs in the hindlimb of NOD/SCID mice. (E) Using the adjuvant (CpG), most effective proliferation of CFSE-labeled splenocytes in response to DB7 lysate was seen in the $CD8^+$ T-cells in the C+I 4-week vaccination group (mean±s.e.m.). (F) This was also the only group with increased cytokine release in the supernatant with a higher dose of DB7 tumor lysate (*U*=unstimulated splenocytes; *S*=stimulated splenocytes with allogeneic C57BL/6 splenocytes).

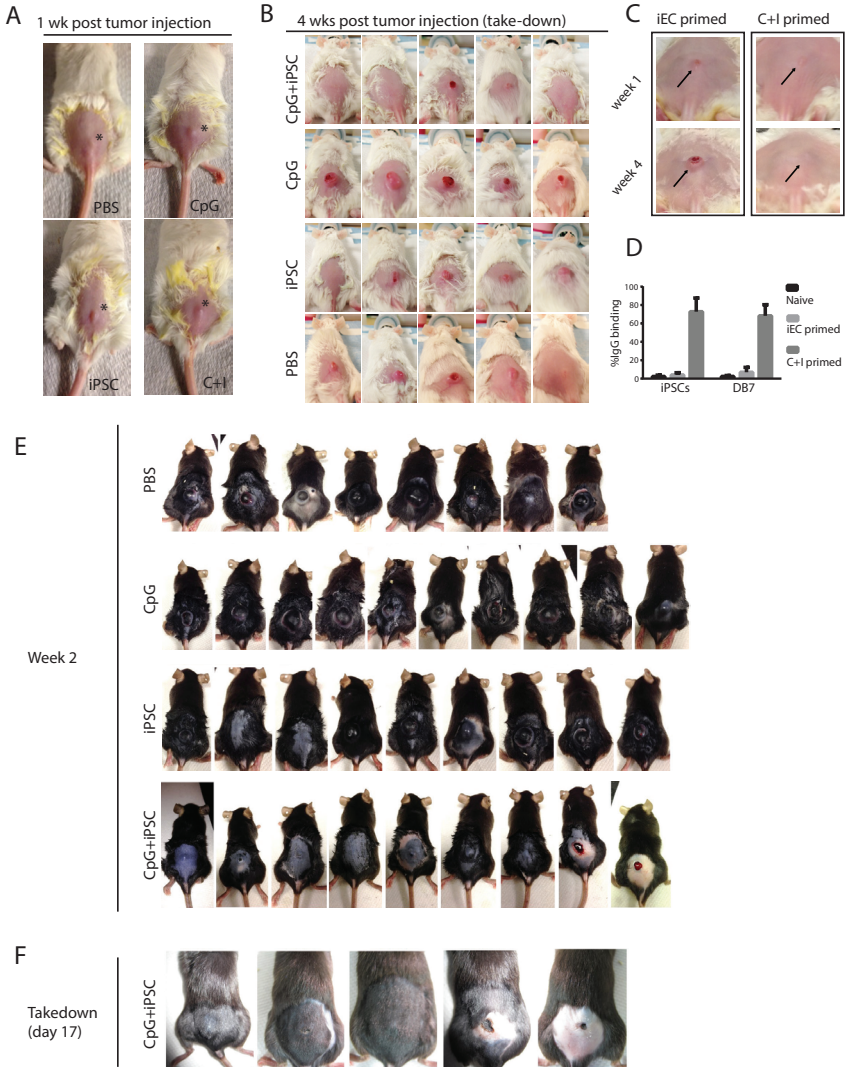


Figure S3. Tumor growth over time in FVB and C57BL/6 tumor-bearing mice. (A) Representative images of PBS, CpG only, iPSCs only, and CpG+iPSC (C+I) vaccinated mice one week after subcutaneous injection of $5x10^4$ DB7 cancer cells. (B) Images of five mice per group at four weeks after DB7 breast cancer cell injection that were selected for immune profile analysis of spleen, dLNs, and blood. (C) One year after the experiment in *Figure 1D*, C+I treated mice (n=2) were reintroduced with $5x10^4$ DB7 breast cancer cells and fully rejected the cancer cells by four weeks. In contrast, mice vaccinated with iPSC-derived endothelial cells (iECs; n=4) were unable to reject the cancer cells, which proliferated into large tumors. (D) One year after vaccination and full rejection of DB7 breast cancer cells, C+I primed animals still have high antibody titers against iPSCs and DB7, unlike mice that were vaccinated with iECs (mean±s.e.m.). (E) Images of all C57BL/6 mice in the four treatment groups two weeks after B16F0 melanoma cell injection. Several mice in the C+I group showed a regression of tumor sizes or inflammation as indicated by local swelling, redness, and, in some cases spontaneous bleeding. (F) Representative images showing mice in the C+I group that were used for immune profile analysis of spleens, dLNs, and blood at time of sacrifice.

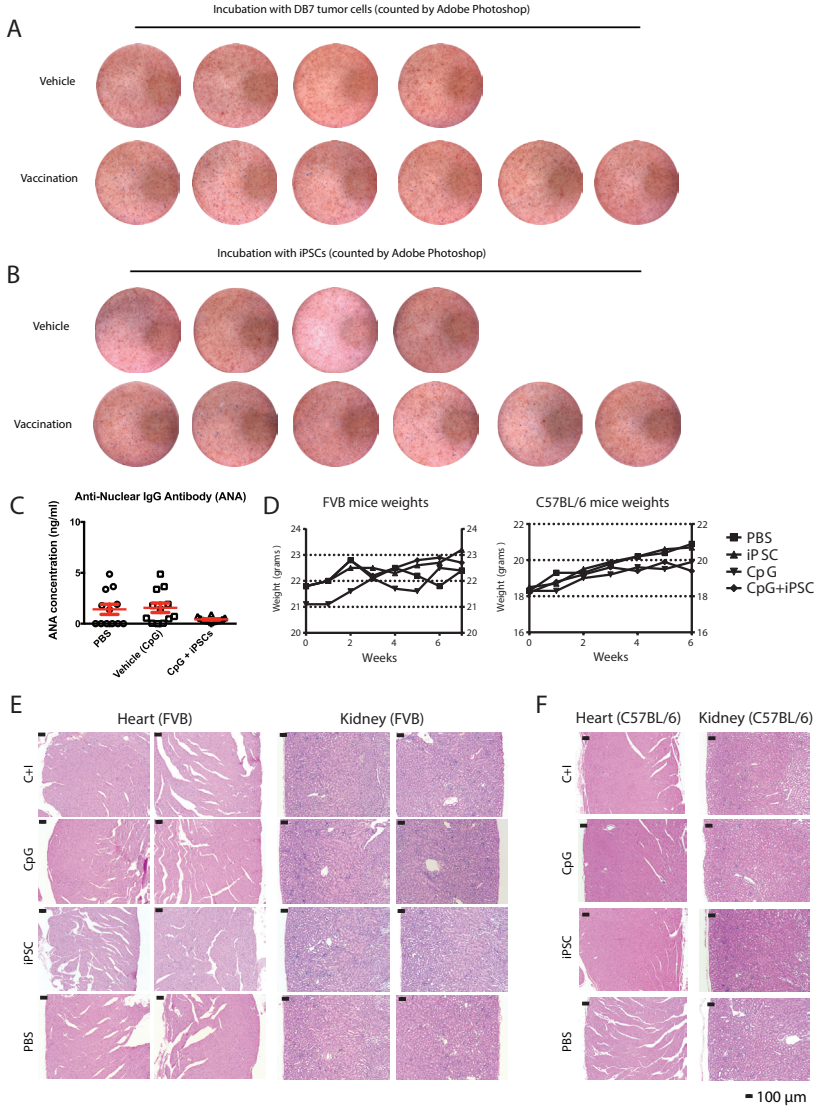


Figure S4. C+I vaccination leads to tumor specificity without causing auto-inflammatory responses. Cell culture images from splenocytes isolated from CpG only (vehicle; *n=4*) and C+I vaccinated mice (*n=6*) incubated with (A) DB7 tumor lysate or (B) iPSC lysate. Blue spots represent IFN-γ secretion by splenocytes and were identified with Adobe Photoshop software for each condition. (C) Serum from PBS (*n=4*), CpG (*n=4*), and CpG+iPSC (*n=4*) vaccinated mice was isolated after four rounds of vaccination. No significant differences were found in anti-nuclear antibody titers among the different groups (total samples: n=12 with three technical replicates for each sample) (mean±s.e.m.; one way ANOVA; p=0.29, ns). (D) For the duration of the experiment, FVB mice (left panel) and C57Bl/6 mice (right panel) were thriving with a healthy appearance and weight increase over time. (E) Representative images of heart (left panel) and kidney samples (right panel) from FVB mice in the three treatment groups revealed no increases in the numbers of inflammatory cells in any of the groups compared to PBS control. (F) Similar findings were seen in the heart (left panel) and kidney tissues (right panel) from C57BL/6 mice.

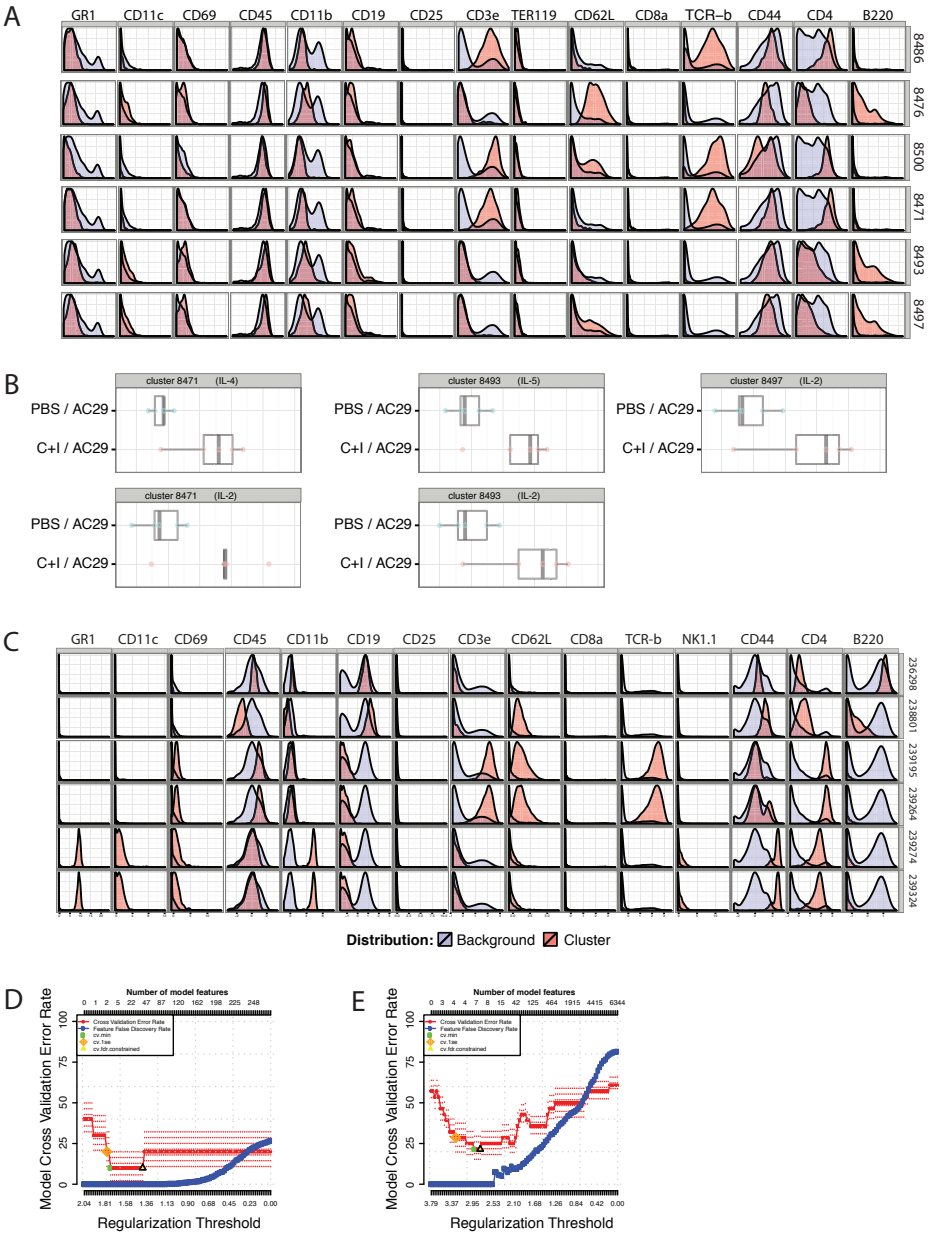
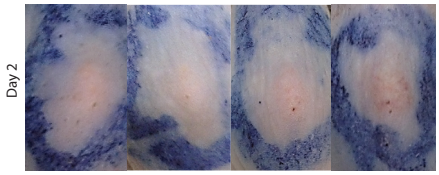
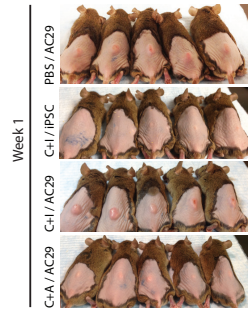


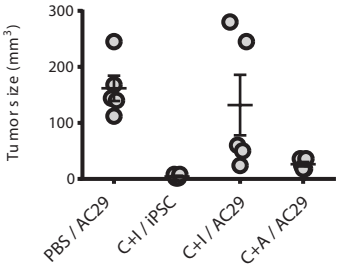
Figure S5. Citrus cluster description and features from tumor-infiltrating lymphocytes (TILs) of CBA/J mice and splenocytes from tumor-resected C57BL/6 mice. (A) Clustering analysis of the CyTOF data from *Figure 5B* using Citrus with their surface marker profile and (B) predictive features of the cytokine profiles from these clusters in the C+I vaccinated group compared to PBS control. (C) Citrus cluster description from *Figure 7C*. (D) Cross-validation error rate from Citrus analysis in *Figure 5B*. (E) Cross-validation error rate from Citrus analysis in *Figure 7C*.

A



B





C

Average Frequency	Sequence	CASGDARDW GSYEQYF	CASGDEGRE QYF	CASGDPGQG DSDYTF	CASGDTANSD YTF	CASGETAN TEVFF	CASGGQSSYE QYF	CASGGSQ NTLYF	CASRRDSN QAPLF	CASSDLGGRA EQFF
Mouse Strain										
BALB/c	Spleen			0.0023	0.0021	0.0015	0.0042	0.0029	0.0004	0.0008
	Thymus	0.0004	0.0013	0.0002	0.0010	0.0002	0.0025	0.0011	0.0003	0.0004
C57BL/6	Spleen	0.0023		0.0014	0.0025	0.0011	0.0020	0.0017		0.0020
	Thymus	0.0002	0.0004	0.0006	0.0007	0.0003	0.0012	0.0006	0.0004	0.0002
CD1	Spleen			0.0017	0.0031		0.0030	0.0039		0.0011
	Thymus	0.0007	0.0001	0.0002	0.0008	0.0004	0.0013	0.0019	0.0006	0.0001
NOD	Spleen	0.0010	0.0014	0.0006	0.0012	0.0012	0.0020	0.0021		0.0007
	Thymus	0.0002			0.0006	0.0002	0.0018	0.0016	0.0005	0.0004

	CASSDRGRDT QYF	CASSLSYEQY F	CASSPDRGDE RLFF	CASSQDNSY EQYF	CASSQDWGG YAEQFF	CASSQEANSD YTF	CASSQEDR DEQYF	CASSQEGASA ETLYF	CASSQEGG NSDYTF	CASSQEGG QDTQYF	CASSQEGG ETLYF	CASSQEGGSA
BALB/c	0.0023	0.0028		0.0034	0.0071	0.0012		0.0015	0.0010	0.0015	0.0029	
	0.0004	0.0086	0.0005	0.0046	0.0030	0.0009	0.0008	0.0003	0.0013	0.0010	0.0019	
C57BL/6	0.0005	0.0084		0.0050	0.0035	0.0014		0.0013	0.0013	0.0011	0.0042	
	0.0007	0.0118	0.0004	0.0022	0.0044	0.0006	0.0004	0.0004	0.0010	0.0008	0.0021	
CD1	0.0014	0.0165		0.0034	0.0039	0.0010		0.0010	0.0012	0.0021	0.0013	
	0.0004	0.0102	0.0007	0.0021	0.0043	0.0007	0.0007	0.0016	0.0008	0.0011	0.0018	
NOD	0.0015	0.0076		0.0050	0.0057	0.0063		0.0009	0.0009	0.0021	0.0011	
	0.0008	0.0103	0.0010	0.0026	0.0034	0.0013	0.0008	0.0011	0.0009	0.0011	0.0019	

	CASSQEGNQD TQYF	CASSQEGNSP LYF	CASSQEPNSO YTF	CASSQETGG AETLYF	CASSSGVSNE RLFF	CTCSADRPYE QYF	CTCSADW GGYAEQFF	CTCSAGQTNY AEQFF
BALB/c	0.0035	0.0010	0.0003	0.0021	0.0021	0.0048	0.0034	0.0004
	0.0008	0.0010	0.0010	0.0004	0.0024		0.0014	
C57BL/6	0.0016	0.0011	0.0018	0.0011	0.0017	0.0039	0.0037	
	0.0006	0.0007	0.0003	0.0008	0.0017		0.0008	
CD1	0.0012	0.0009	0.0018	0.0010	0.0033		0.0034	
	0.0007	0.0006	0.0009	0.0010	0.0035		0.0009	
NOD	0.0025	0.0012	0.0011	0.0019	0.0038		0.0022	
	0.0007	0.0009	0.0004	0.0007	0.0027	0.0005	0.0014	0.0006

0 0.0005 0.001 0.005 0.008 0.01 0.016

% Frequency of TCR-clone within T-cell population

D

Average Frequency	Sequence	CASGDAG DTQYF	CASGDAG GEQYF	CASSLTGG AYEQYF	CASSQEA NSDYTF	CASSQEGGGN YAEQFF	CASSQEGLGG YEQYF	CGARDAGG QDTQYF
Mouse strain								
BALB/c	Spleen	0.0019	0.0101	0.0013	0.0012	0.0001	0.0012	-
	Thymus	0.0007	0.0020	0.0015	0.0009	0.0002	0.0008	-
C57BL/6	Spleen	0.0026	0.0094	0.0039	0.0014	0.0002	0.0070	0.0005
	Thymus	0.0006	0.0014	0.0021	0.0006	0.0004	0.0011	-
CD1	Spleen	0.0035	0.0089	0.0071	0.0010			-
	Thymus	0.0008	0.0006	0.0026	0.0007	0.0003	0.0008	-
NOD	Spleen	0.0034	0.0054	0.0037	0.0063	0.0013	0.0036	-
	Thymus	0.0014	0.0018	0.0019	0.0013	0.0006	0.0012	-

0 0.0005 0.0008 0.001 0.003 0.005 0.01

% Frequency of TCR-clone within T-cell population

Figure S6. C+I vaccination in CBA/J mice leads to reduced tumor establishment and a reduction of commonly shared intra-tumor T-cell clones in favor of vaccine-specific clones. (A) Representative image at day 2 of CBA/J mice vaccinated with PBS, CpG+iPSC (C+I), or CpG+AC29 (C+A) and then introduced with either $2x10^6$ AC29 or $2x10^6$ iPSCs. (B) Image (left panel) and tumor sizes (right panel) of all mice at week 1 post-tumor injection, revealing a complete rejection of the iPSCs and cancer cells in the positive control groups (C+I/iPSC = CpG+iPSC vaccinated mice introduced with iPSCs, and C+A/AC29 = CpG+AC29 vaccinated mice introduced with AC29 cells). The last three mice in the C+I/AC29 already showed tumor regression, whereas the first two had severe erythema and swelling at the tumor sites (mean±s.e.m.). (C) Frequency of T-cell clones and their receptor sequences in the PBS+AC29 control group if they were shared by 4 or 5 out of 5 mice. 28 TIL clones were present in multiple mouse strains in spleen (n=3) as well as thymus (n=3). The larger public clone repertoire within the PBS group therefore likely consisted of shared TCR clones on the basis of chance. (D) Frequency of T-cell clones and their receptor sequences in the C+I/AC29 treatment group if they were shared by 4 or 5 out of 5 mice. Only six TIL clones were present in multiple mouse strains in spleen (n=3) as well as thymus (n=3). In these cases, the generally lower frequency of the clones in the thymus and more similar frequencies of the clones in the spleen suggest that the majority of the commonly shared clones in the vaccine group may be more important than public clones. In addition, clone CGARDAGGQDTQYF is extremely rare and was only present in 1 out of 3 spleens in the C57BL/6 mouse strain and was not present in the PBS, C+I/iPSC, or C+A/AC29 groups, indicating it was likely C+I vaccine-specific.

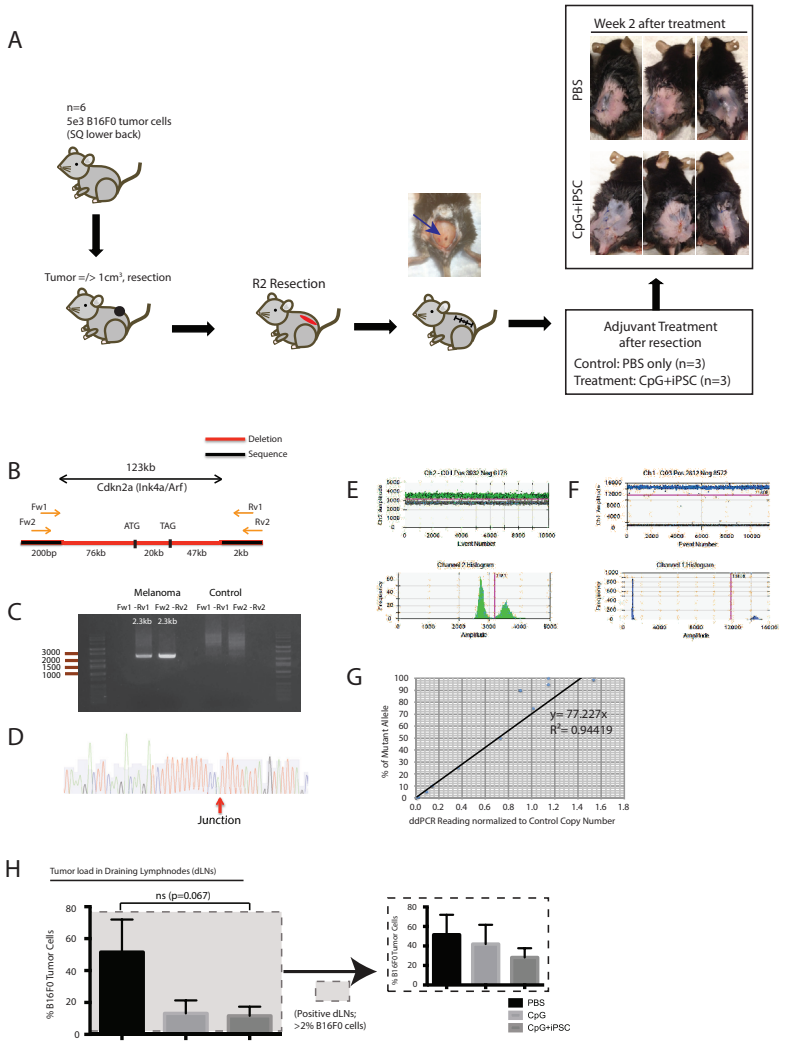


Figure S7. Adjuvant C+I vaccination prevents the recurrence of tumor after R2 resection of B16F0 melanoma and reduced tumor load in dLNs. (A) B16F0 tumor-bearing mice (*n*=6) with a tumor size ~1 cm^3 received a R2 resection where a small piece of tumor (blue arrow) was left behind in the resection area (RA). C+I vaccinated mice (*n*=3) had no visible tumor recurrence in the RAs after two rounds of vaccination, whereas the PBS control group (*n*=3) had visible and palpable tumors. (B) PCR/ddPCR primer development based on a large deletion in *Cdkn2a* in B16 melanoma cells (Fw1-Rv1, Fw2-Rv2). (C) B16 melanoma cell primers were designed to show the deletion by PCR in the melanoma samples without amplification in C57BL/6 wild type samples. (D) PCR products were then validated and analyzed by Sanger sequencing and aligned with the gene database in NCBI. (E-F) Using ddPCR with a mutant probe based on the *Cdkn2a* deletion and a TaqMan®Copy Number probe the quantity of tumor cells within each DNA sample could be assessed. (G) The standard curve was plotted using different concentrations of mutant DNA, revealing a good correlation between % of mutant DNA and the read-out from the BioRad QX100 reader. (H) Using ddPCR, a reduction of average tumor load in dLNs of R1 resected mice in the CpG and C+I groups was seen compared to PBS control. If dLNs were positive (>2% threshold), the C+I vaccinated group had the lowest percentage of tumor cells in dLNs (mean±s.e.m.).

Key Resouce Table

REAGENT or RESOURCE	SOURCE	IDENTIFIER
Antibodies		
PE/Cy7 anti-mouse CD3	eBioscience	25-0031-82; RRID: AB_469572
APC anti-mouse CD4	BD Bioscience	553051
PE anti-mouse CD4	eBioscience	12-0042-83; RRID: AB_465510
PerCP/Cy5.5 anti-mouse CD8	Biolegend	100734; RRID: AB_2075238
PE/Cy7 anti-mouse CD11b	Biolegend	101216; RRID: AB_312799
Pacific Blue anti-mouse/human CD44	Biolegend	103020; RRID: AB_493683
APC anti-mouse CD11c	Biolegend	117310; RRID: AB_313779
FITC anti-mouse CD86	BD Bioscience	553691
eFluor 450 anti-mouse F4/80	eBioscience	48-4801-82; RRID: AB_1548747
Alexa Fluor 488 anti-mouse FoxP3	Biolegend	126406; RRID: AB_1089113
PE anti-mouse Granzyme-B	eBioscience	12-8898-82; RRID: AB_10870787
Brilliant Violet 510 anti-mouse CD45	eBioscience	103137; RRID: AB_2561392
Alexa Fluor 700 anti-mouse CD25	eBioscience	56-0251-82; RRID: AB_891422
eFluor 780 Fixable Viability Dye	eBioscience	65-0865-14
Alexa Fluor 700 anti-mouse GR-1 Ly6	Biolegend	108422; RRID: AB_2137487
PerCP/Cy5.5 anti-mouse NK1.1	Biolegend	108728; RRID: AB_2132705
PerCP/Cy5.5 anti-mouse DX-5	Biolegend	108916; RRID: AB_2129358
PE anti-mouse MHC-II	eBioscience	12-5321-81; RRID: AB_465928
Alexa Fluor 488 anti-mouse IgG	Thermo Fisher Scientific	A-11001; RRID: AB_2534069
Anti-rabbit IgG Cross-adsorbed	Thermo Fisher Scientific	31213; RRID: AB_228376
Pacific Blue Rat IgG2b κ isotype control	Biolegend	400627
Alexa Fluor 488 Rat IgG2b κ isotype control	Biolegend	400625
PE Rat IgG2b κ isotype control	Thermo-Fisher Scientific	12-4031-82; RRID: AB_470042
FITC Rat IgG2a κ isotype control	BD Biosciences	553929
PE Rat IgG2a κ isotype control	eBioscience	12-4321-80; RRID: AB_1834380
Alexa Fluor 700 Rat IgG1 κ isotype control	eBioscience	56-4301-80; RRID: AB_494017
Anti SSEA-1 microbeads	Miltenyi Biotec	130-094-530

Key Resouce Table (*continued*)

REAGENT or RESOURCE	SOURCE	IDENTIFIER
Oct 3/4 anti-mouse	Santa Cruz Biotechnology	sc-5279
c-Myc anti-mouse	EMD Millipore	06-340
SSEA-1 anti-mouse	EMD Millipore	MAB4301
Nanog anti-mouse	Santa Cruz Biotechnology	sc-33760
Sox2 anti-mouse	Santa Cruz Biotechnology	sc-365823
Mouse on Mouse (M.O.M.) Basic Kit	Vector Laboratories	BMK-2202
Fc Block anti-mouse	BD Biosciences	553141
Chemicals, Peptides, and Recombinant Proteins		
DMEM, high glucose, GlutaMAX	Gibco	10569-010
Fetal Bovine Serum	Life Technologies	26140079
DPBS, no calcium, no magnesium	Gibco	14190250
MEM Non-Essential Amino Acids	Gibco	11140050
TrypLE Express	Gibco	12605-036
CpG ODN 1826	Invivogen	tlrl-1826-1
Murine Leukemia Inhibitory Factor (mLIF)	EMD Millipore	ESG1106
Gelatin	Sigma Aldrich	G1393-100ML
Isothesia	Henry Schein	029405
Matrigel™ matrix growth factor reduced	BD Biosciences	356231
RPMI medium 1640	Life Technologies	11875-119
ACK lysis buffer	Quality Biological	118-156-101
Collagenase D	Roche	11088882001
Deoxyribonuclease I from bovine pancreas	Sigma Aldrich	D4263-5VL
Trypsin Inhibitor	Sigma Aldrich	T9003-1G
HEPES 1M	Sigma Aldrich	H3662
Percoll GE Density Gradient Media	VWR	89428-524
UltraPure 0.5M EDTA	Life Technologies	15575-020
PrimeStar GXL DNA Polymerase	Clontech	R050A
ddPCR Supermix for Probes	Bio-Rad	1863024
Critical Commercial Assays		
Neon Transfection System 100µl Kit	Thermo Fisher Scientific	MPK10025
MycoAlert Detection Kit	Lonza	LT07-318
MycoAlert Assay Control Set	Lonza	LT07-518
CFSE Cell Trace staining	Thermo Fisher Scientific	C34554

Key Resouce Table (*continued*)

REAGENT or RESOURCE	SOURCE	IDENTIFIER
Mouse Th1/Th2/Th17 Cytokine Multi-Analyte ELISArray	Qiagen	MEM-003A
MaxPar Mouse Spleen/Lymph Node Phenotyping kit	Fluidigm	201306
MaxPar Mouse Intracellular Cytokine I Panel kit	Fluidigm	201310
Cisplatin viability dye	Fluidigm	201062
Cytofix/Cytoperm Permeabilization Solution kit	BD Biosciences	BDB554714
Pierce BCA Protein Assay Kit	Thermo Fisher Scientific	23225
Mouse IFN-gamma/Granzyme B Dual-Color ELISpot Kit	R&D Systems	ELD5819
Pan T-cell Isolation Kit II, mouse	Miltenyi Biotec	130-095-130
Anti-nuclear Antigen (IgG) mouse ELISA Kit	Antibodies-Online	ABIN366290
DNeasy Blood & Tissue kit	Qiagen	69504
Deposited Data		
TCRβ sequencing tumor-infiltrating lymphocytes	This paper	immunoACCESS: doi:10.21417/B7B648
RNA-seq from human somatic/cancer cell lines	ENCODE project	http://www.genome.gov/encode/
RNA-seq from human iPS cells	Churko et al., 2017	
RNA-seq form murine somatic cell lines	ENCODE project	http://mouseencode.org/
RNA-seq from murine iPS cells	Chang et al., 2014	N/A
Experimental Models: Cell Lines		
EmbryoMax® Primary Mouse Embryo Fibroblasts	EMD Millipore	PMEF-N
DB7 breast cancer cells	The University of Utah; Dr. Joe Smith	N/A
B16F0 melanoma cells	ATCC	CRL-6322
AC29 mesothelioma cells	Sigma Aldrich	10092308
Experimental Models: Organisms/Strains		
Mouse: FVB/NJ	The Jackson Laboratory	001800
Mouse: C57BL/6J	The Jackson Laboratory	000664
Mouse: CBA/J	The Jackson Laboratory	000656
NOD-SCID IL2Rgamma^{null} (NSG)	The Jackson Laboratory	005557
Oligonucleotides		

Key Resouce Table (*continued*)

REAGENT or RESOURCE	SOURCE	IDENTIFIER
TaqMan®Copy Number TFRC probe (Mm00000692_cn)	Thermo Fisher Scientific	4400291
5'ACTAGCCAGAGGATCTTAAAGACT3'	This paper	N/A
5'GCCATCACTGGAAAGAGAGGC3'	This paper	N/A
5'(HEX)CCTGCCCACCCACTCCCCCTTTTT (Blackhole Quencher)3'	This paper	N/A
Recombinant DNA		
Codon-optimized mini-intronic plasmid (coMIP)	Diecke et al., 2015	N/A
Software and Algorithms		
ImmunoSeq Analyzer	Adaptive Biotechnologies	https://clients.adaptivebiotech.com/
Prism GraphPad 7	GraphPad Software	https://www.graphpad.com/scientific-software/prism/
Cytobank	Cytobank, Inc.	https://stanford.cytobank.org/cytobank/login
Citrus 0.8	Nolan lab; Stanford, USA.	https://github.com/nolanlab/citrus/wiki/Installing-Citrus
R; version 3.0.3	The R Project	https://www.r-project.org/
Adobe Photoshop CS6	Adobe	http://www.adobe.com/nl/products/photoshop.html
Other		
29 Gauge x ½" needle 3/10cc	Terumo Medical	SS30M2913
Multiplex-Luminex platform (LabMap200 System)	HIMC; Stanford University, USA	N/A

REFERENCES

Anders, S. and W. Huber (2010). "Differential expression analysis for sequence count data." Genome Biol 11(10): R106.

Anders, S., D. J. McCarthy, Y. Chen, M. Okoniewski, G. K. Smyth, W. Huber and M. D. Robinson (2013). "Count-based differential expression analysis of RNA sequencing data using R and Bioconductor." Nat Protoc 8(9): 1765-1786.

Anders, S., P. T. Pyl and W. Huber (2015). "HTSeq--a Python framework to work with high-throughput sequencing data." Bioinformatics 31(2): 166-169.

Ben-Porath, I., M. W. Thomson, V. J. Carey, R. Ge, G. W. Bell, A. Regev and R. A. Weinberg (2008). "An embryonic stem cell-like gene expression signature in poorly differentiated aggressive human tumors." Nat Genet 40(5): 499-507.

Bock, C., E. Kiskinis, G. Verstappen, H. Gu, G. Boulting, Z. D. Smith, . . . A. Meissner (2011). "Reference Maps of Human ES and iPS Cell Variation Enable High-Throughput Characterization of Pluripotent Cell Lines." Cell 144(3): 439-452.

Brewer, B. G., R. A. Mitchell, A. Harandi and J. W. Eaton (2009). "Embryonic vaccines against cancer: an early history." Exp Mol Pathol 86(3): 192-197.

Bruggner, R. V., B. Bodenmiller, D. L. Dill, R. J. Tibshirani and G. P. Nolan (2014). "Automated identification of stratifying signatures in cellular subpopulations." Proc Natl Acad Sci U S A 111(26): E2770-2777.

Chang, G., S. Gao, X. Hou, Z. Xu, Y. Liu, L. Kang, . . . J. Tian (2014). "High-throughput sequencing reveals the disruption of methylation of imprinted gene in induced pluripotent stem cells." Cell Res 24(3): 293-306.

Chen, J. Y., Y. A. Tang, S. M. Huang, H. F. Juan, L. W. Wu, Y. C. Sun, . . . Y. C. Wang (2011). "A novel sialyltransferase inhibitor suppresses FAK/paxillin signaling and cancer angiogenesis and metastasis pathways." Cancer Res 71(2): 473-483.

Chung, A. S., X. Wu, G. Zhuang, H. Ngu, I. Kasman, J. Zhang, . . . N. Ferrara (2013). "An interleukin-17-mediated paracrine network promotes tumor resistance to anti-angiogenic therapy." Nat Med 19(9): 1114-1123.

Churko, J. M., J. Lee, M. Ameen, M. Gu, M. Venkatasubramanian, S. Diecke, . . . J. C. Wu (2017). "Transcriptomic and epigenomic differences in human induced pluripotent stem cells generated from six reprogramming methods." 1: 826-837.

Consortium, E. P. (2011). "A user's guide to the encyclopedia of DNA elements (ENCODE)." PLoS Biol 9(4): e1001046.

de Almeida, P. E., E. H. Meyer, N. G. Kooreman, S. Diecke, D. Dey, V. Sanchez-Freire, . . . J. C. Wu (2014). "Transplanted terminally differentiated induced pluripotent stem cells are accepted by immune mechanisms similar to self-tolerance." Nat Commun 5: 3903.

Diecke, S., J. Lu, J. Lee, V. Termglinchan, N. G. Kooreman, P. W. Burridge, . . . J. C. Wu (2015). "Novel codon-optimized mini-intronic plasmid for efficient, inexpensive, and xeno-free induction of pluripotency." Sci Rep 5: 8081.

Dolcetti, L., E. Peranzoni, S. Ugel, I. Marigo, A. Fernandez Gomez, C. Mesa, . . . V. Bronte (2010). "Hierarchy of immunosuppressive strength among myeloid-derived suppressor cell subsets is determined by GM-CSF." Eur J Immunol 40(1): 22-35.

Dooms, H. and A. K. Abbas (2002). "Life and death in effector T cells." Nat Immunol 3(9): 797-798.

Evans, M. S., J. P. Chaurette, S. T. Adams, Jr., G. R. Reddy, M. A. Paley, N. Aronin, . . . S. C. Miller (2014). "A synthetic luciferin improves bioluminescence imaging in live mice." Nat Methods 11(4): 393-395.

Gajewski, T. F., H. Schreiber and Y. X. Fu (2013). "Innate and adaptive immune cells in the tumor microenvironment." Nat Immunol 14(10): 1014-1022.

Galvan, D. L., R. T. O'Neil, A. E. Foster, L. Huye, A. Bear, C. M. Rooney and M. H. Wilson (2015). "Anti-Tumor Effects after Adoptive Transfer of IL-12 Transposon-Modified Murine Splenocytes in the OT-I-Melanoma Mouse Model." PLoS One 10(10): e0140744.

Ghosh, Z., M. Huang, S. Hu, K. D. Wilson, D. Dey and J. C. Wu (2011). "Dissecting the oncogenic and tumorigenic potential of differentiated human induced pluripotent stem cells and human embryonic stem cells." Cancer Res 71(14): 5030-5039.

Gilkeson, G. S., J. Conover, M. Halpern, D. S. Pisetsky, A. Feagin and D. M. Klinman (1998). "Effects of bacterial DNA on cytokine production by (NZB/NZW)F1 mice." J Immunol 161(8): 3890-3895.

Goldstein, M. J., B. Varghese, J. D. Brody, R. Rajapaksa, H. Kohrt, D. K. Czerwinski, . . . R. Levy (2011). "A CpG-loaded tumor cell vaccine induces antitumor CD4+ T cells that are effective in adoptive therapy for large and established tumors." Blood 117(1): 118-127.

Grupp, S. A., M. Kalos, D. Barrett, R. Aplenc, D. L. Porter, S. R. Rheingold, . . . C. H. June (2013). "Chimeric antigen receptor-modified T cells for acute lymphoid leukemia." N Engl J Med 368(16): 1509-1518.

Harrow, J., A. Frankish, J. M. Gonzalez, E. Tapanari, M. Diekhans, F. Kokocinski, . . . T. J. Hubbard (2012). "GENCODE: the reference human genome annotation for The ENCODE Project." Genome Res 22(9): 1760-1774.

Inoue, H., Watanabe, A., Sakamoto, C., Narusawa, M., Hiramoto, T., Miyamoto, S., Inoue, M., Takayama, K., Hasegawa, M., and Nakanishi, Y. (2013). "Vaccination With Irradiated Induced Pluripotent Stem Cells Genetically Engineered To Produce GM-CSF Confers Potent T Cells-Mediated Antitumor Immunity." Blood 122: 4492.

Kim, D., B. Langmead and S. L. Salzberg (2015). "HISAT: a fast spliced aligner with low memory requirements." Nat Methods 12(4): 357-360.

Kocaturk, B. and H. H. Versteeg (2015). "Orthotopic injection of breast cancer cells into the mammary fat pad of mice to study tumor growth." J Vis Exp(96).

Kooreman, N. G. and J. C. Wu (2010). "Tumorigenicity of pluripotent stem cells: biological insights from molecular imaging." J R Soc Interface 7 Suppl 6: S753-763.

Le, D. T., J. N. Uram, H. Wang, B. R. Bartlett, H. Kemberling, A. D. Eyring, . . . L. A. Diaz, Jr. (2015). "PD-1 Blockade in Tumors with Mismatch-Repair Deficiency." N Engl J Med 372(26): 2509-2520.

Lee, A. S., C. Tang, M. S. Rao, I. L. Weissman and J. C. Wu (2013). "Tumorigenicity as a clinical hurdle for pluripotent stem cell therapies." Nat Med 19(8): 998-1004.

Lee, D. W., J. N. Kochenderfer, M. Stetler-Stevenson, Y. K. Cui, C. Delbrook, S. A. Feldman, . . . C. L. Mackall (2015). "T cells expressing CD19 chimeric antigen receptors for acute lymphoblastic leukaemia in children and young adults: a phase 1 dose-escalation trial." Lancet 385(9967): 517-528.

Li, Y., H. Zeng, R. H. Xu, B. Liu and Z. Li (2009). "Vaccination with human pluripotent stem cells generates a broad spectrum of immunological and clinical responses against colon cancer." Stem Cells 27(12): 3103-3111.

Mallon, B. S., J. G. Chenoweth, K. R. Johnson, R. S. Hamilton, P. J. Tesar, A. S. Yavatkar, . . . R. D. McKay (2013). "StemCellDB: the human pluripotent stem cell database at the National Institutes of Health." Stem Cell Res 10(1): 57-66.

Mallon, B. S., R. S. Hamilton, O. A. Kozhich, K. R. Johnson, Y. C. Fann, M. S. Rao and P. G. Robey (2014). "Comparison of the molecular profiles of human embryonic and induced pluripotent stem cells of isogenic origin." Stem Cell Res 12(2): 376-386.

Maude, S. L., N. Frey, P. A. Shaw, R. Aplenc, D. M. Barrett, N. J. Bunin, . . . S. A. Grupp (2014). "Chimeric antigen receptor T cells for sustained remissions in leukemia." N Engl J Med 371(16): 1507-1517.

Maus, M. V., S. A. Grupp, D. L. Porter and C. H. June (2014). "Antibody-modified T cells: CARs take the front seat for hematologic malignancies." Blood 123(17): 2625-2635.

Mestas, J. and C. C. Hughes (2004). "Of mice and not men: differences between mouse and human immunology." J Immunol 172(5): 2731-2738.

Mor, G., M. Singla, A. D. Steinberg, S. L. Hoffman, K. Okuda and D. M. Klinman (1997). "Do DNA vaccines induce autoimmune disease?" Hum Gene Ther 8(3): 293-300.

Morgan, R. A., J. C. Yang, M. Kitano, M. E. Dudley, C. M. Laurencot and S. A. Rosenberg (2010). "Case report of a serious adverse event following the administration of T cells transduced with a chimeric antigen receptor recognizing ERBB2." Mol Ther 18(4): 843-851.

Mukherjee, P., L. B. Pathangey, J. B. Bradley, T. L. Tinder, G. D. Basu, E. T. Akporiaye and S. J. Gendler (2007). "MUC1-specific immune therapy generates a strong anti-tumor response in a MUC1-tolerant colon cancer model." Vaccine 25(9): 1607-1618.

Naas, T., M. Ghorbani, C. Soare, N. Scherling, R. Muller, P. Ghorbani and F. Diaz-Mitoma (2010). "Adoptive transfer of splenocytes to study cell-mediated immune responses in hepatitis C infection using HCV transgenic mice." Comp Hepatol 9: 7.

Nelakanti, R. V., N. G. Kooreman and J. C. Wu (2015). "Teratoma formation: a tool for monitoring pluripotency in stem cell research." Curr Protoc Stem Cell Biol 32: 4A 8 1-4A 8 17.

Numasaki, M., J. Fukushi, M. Ono, S. K. Narula, P. J. Zavodny, T. Kudo, . . . M. T. Lotze (2003). "Interleukin-17 promotes angiogenesis and tumor growth." Blood 101(7): 2620-2627.

Palena, C., S. I. Abrams, J. Schlom and J. W. Hodge (2006). "Cancer vaccines: preclinical studies and novel strategies." Adv Cancer Res 95: 115-145.

Qiu, P., E. F. Simonds, S. C. Bendall, K. D. Gibbs, Jr., R. V. Bruggner, M. D. Linderman, . . . S. K. Plevritis (2011). "Extracting a cellular hierarchy from high-dimensional cytometry data with SPADE." Nat Biotechnol 29(10): 886-891.

Sodhi, A., P. Tandon and S. Sarna (1985). "Adoptive transfer of immunity against solid fibrosarcoma in mice with splenocytes and peritoneal exudate cells obtained after in vitro sensitization and in vivo immunization with cis-dichlorodiamine platinum(II) treated fibrosarcoma cells." Arch Geschwulstforsch 55(1): 47-61.

Soldner, F., D. Hockemeyer, C. Beard, Q. Gao, G. W. Bell, E. G. Cook, . . . R. Jaenisch (2009). "Parkinson's disease patient-derived induced pluripotent stem cells free of viral reprogramming factors." Cell 136(5): 964-977.

Takahashi, K., K. Tanabe, M. Ohnuki, M. Narita, T. Ichisaka, K. Tomoda and S. Yamanaka (2007). "Induction of pluripotent stem cells from adult human fibroblasts by defined factors." Cell 131(5): 861-872.

Takahashi, K. and S. Yamanaka (2006). "Induction of pluripotent stem cells from mouse embryonic and adult fibroblast cultures by defined factors." Cell 126(4): 663-676.

Torcellan, T., H. R. Hampton, J. Bailey, M. Tomura, R. Brink and T. Chtanova (2017). "In vivo photolabeling of tumor-infiltrating cells reveals highly regulated egress of T-cell subsets from tumors." Proc Natl Acad Sci U S A 114(22): 5677-5682.

Yaddanapudi, K., R. A. Mitchell, K. Putty, S. Willer, R. K. Sharma, J. Yan, . . . J. W. Eaton (2012). "Vaccination with embryonic stem cells protects against lung cancer: is a broad-spectrum prophylactic vaccine against cancer possible?" PLoS One 7(7): e42289.

Zhao, T., Z. N. Zhang, Z. Rong and Y. Xu (2011). "Immunogenicity of induced pluripotent stem cells." Nature 474(7350): 212-215.

Zou, W. (2005). "Immunosuppressive networks in the tumor environment and their therapeutic relevance." Nat Rev Cancer 5(4): 263-274.



Part IV

General Discussion

Chapter 10

General Discussion and Summary

As was described in the introduction of this thesis, the continuing increase in life expectancy of humankind will likely result in an accompanying increase in chronic illnesses (Union 2012), which can largely be attributed to damage in organs with limited regenerative capacity. To address this, researchers have been exploring various avenues to regenerate different tissues with gene or cell therapies, among others, which are described in **Chapter 2.** This thesis mainly focuses on the use of different types of regenerative therapies for the treatment of vascular diseases.

REGENERATIVE THERAPIES

Starting nearly two decades ago, cell therapies have focused on the transplantation of progenitor cells or adult stem cells in diseased tissues (Prockop 1997; Pittenger et al. 1999; Amado et al. 2005; Dezawa et al. 2005). These therapies have shown promising results in preclinical animal models and are now being explored in large numbers of phase I-III clinical trials (Boncoraglio et al. 2010; Fisher et al. 2016). Some of the mechanisms by which these cells could regenerate tissue include: 1) paracrine factors being released by the adult stem cells to aid the damaged tissues and 2) transdifferentiation and integration of the adult stem cells into a beneficial cell type within the diseased tissue. However, the latter mechanism is controversial because of the low rates of engraftments observed in experiments thus far (van Berlo et al. 2014). For now, adult stem cells should mainly be regarded as multipotent and lineage-restricted.

Since the first isolation of human embryonic stem cells (hESCs) in 1998, researchers have been working with this cell type that could potentially be differentiated into every cell of the human body, and explored the potential of these pluripotent cells for regenerative therapies (Trounson and McDonald 2015). Although many cell lines have been derived from these ESCs, ethical concerns surrounding the use of embryonic tissue or cells persist that limit their therapeutic potential for regenerative medicine.

In 2006, Shinya Yamanaka reprogrammed adult somatic murine cells to a pluripotent state with a set of pluripotency genes. Similar to ESCs, these cells can give rise to cell types from all three germ layers by testing the gene expression profile of ESCs to distill from them key regulators that were important to maintain pluripotency (Takahashi and Yamanaka 2006). By overexpressing these genes (Oct4, cMyc, KLF4, and Sox2) in somatic cells using a lentiviral vector, they were able to push the somatic cells into a pluripotent state. These induced pluripotent stem cells (iPSCs) are similar to ESCs in morphology, key characteristics, and potential to form cells from all three germ layers. A year later, Yamanaka's group showed the same process to be true for human cells (Takahashi et al. 2007), giving rise to a whole new field with potential for regenerative medicine. Together, ESCs and iPSCs are referred to as pluripotent stem cells (PSCs).

In **Chapter 3,** two gene vectors are described that can be used for gene therapy and the reprogramming of somatic cells into iPSCs. First, we describe a new approach to overcome the relatively complex and time-consuming methods of generating vectors to reprogram somatic cells by using a user-friendly reprogramming plasmid, the codon-optimized mini-intronic plasmid (CoMiP). Using the 4-in-1 CoMiP, we were able to derive bonafide integration-free iPSCs from various donor tissue sources, including peripheral bone mar-

row cells (PBMCs). Compared to other DNA-based reprogramming methods, like the minicircle or the Yamanaka three individual plasmids system, the CoMiP construct is faster and less expensive for inducing pluripotency in somatic cell types. Secondly, as an appendix to Chapter 3, we describe the use of codon-optimized 4-in-1 minicircles (CoMiC) to reprogram somatic cells. Compared to conventional plasmids, a non-viral minicircle (MC) is smaller, consists of supercoiled DNA molecules, and lacks a bacterial origin of replication. Although faster reprogramming is possible with our CoMiP construct, MCs are ideal candidates for gene therapy because of 1) their smaller size compared to conventional plasmids, which increases their transfection efficiency, and 2) their reduced immunogenicity due to a lack of bacterial origin of replication.

For gene therapy purposes, we therefore used a MC to overexpress IL-10 in **Chapter 4** and systemically upregulated IL-10 to treat abdominal aneurysms in angiotensin II-infusion-ApoE-/- AAA mice. MC IL-10 transfusion significantly reduced average aortic diameter at day 28 and increased dissection free survival from 21.5% in control AAA mice to 62.3% in MC IL-10-treated AAA mice.

In addition to gene therapy, the possibilities of cell therapies for regenerative medicine are enormous and the use of PSCs in regenerative medicine has gained great interest over the past two decades. In **Chapter 5**, we focus on the use of iPSCs in the field of peripheral artery disease (PAD) in patients with diabetes. An important question that was answered here is whether the source of iPSCs influences the outcome of the cell product. Therefore, iPSCs from diabetic and non-diabetic mice were created and differentiated into endothelial cells (ECs) to assess their regenerative potential in an hindlimb ischemia (HLI) model. Interestingly, iPSC-ECs created from a diabetic source had a diminished regenerative potential compared to healthy cells. These findings are important in advancing the field of stem cell therapy, because it made clear that a healthy source of iPSCs has the best regenerative potential. However, the practical challenges of generating large quantities of patient-specific iPSCs due to cost and good manufacturing practices requirements (Turner et al. 2013) also means that "personalized iPSCs" may not always yield the best results in the clinical application of iPSC therapy.

Overall, it is clear that gene and PSC therapy have an important role to play in regenerative medicine. To that end, scientists have been evaluating the therapeutic and regenerative potential of PSCs in pre-clinical and clinical trials (Trounson and McDonald 2015; Mandai et al. 2017). However, PSCs' intrinsic properties and the method by which they are created, as well as challenges such as tumorigenicity and immunogenicity, raise potential safety concerns that need to be addressed before clinical implementation of these cells can be fully realized.

CLINICAL HURDLES ASSOCIATED WITH REGENERATIVE MEDICINE

Tumorigenicity

Gene and cell therapies have been used for regenerative medicine for several decades. Although both therapies have been around for a while, specific challenges persist, including the potential for inducing tumors or cancers in patients. Among these was an early report of the occurrence of leukemia after gene therapy with recombinant viral vectors to treat X-linked severe combined immune deficiency (Kohn et al. 2003). Such adverse events from the use of gene editing have attracted heightened scrutiny from regulatory authorities and the public. Subsequent studies examining the mechanism underlying these cases have led to a better understanding of the possible side-effects of these therapies (Thrasher et al. 2006; Woods et al. 2006; Thrasher and Williams 2017). However, despite years of additional mechanistic understanding, setbacks in regenerative medicine still occur. For instance, a more recent clinical trial in Riken Japan was halted in 2015 due to mutagenesis in the transplanted retinal pigment cells (derived from iPSCs) for the treatment of macular degeneration (Garber 2015).

As is described in **Chapter 6**, one key risk factor for both gene therapy as well as the generation of iPSCs is our insufficient knowledge of the effect that those incorporated genes have on the genome. Especially in cases where the vector integrates into the genome, the site of integration might result in the activation of pro-oncogenes. This is true for gene therapy as well as the generation of iPSCs, where the first generation of iPSCs resulted in the reactivation of the cMyc gene and subsequent tumorigenesis (Okita et al. 2007). Even the intrinsic properties of pluripotent cells may provoke safety concerns when they are used for regenerative medicine. For instance, reports of atypical cell configurations in transplanted grafts raise the question of whether these cells came from remnant undifferentiated cells or resulted from transdifferentiation of the differentiated portion due to plasticity in the epigenetic state of differentiated cells (Riegler et al. 2015).

Immunogenicity

One of the major limitations of gene and cell therapy is the immune response to vectors or cell types. As is described in this thesis, the immunogenicity of gene vectors can bring significant adverse effects, including death in rare cases such as the gene therapy trial of Jesse Gelsinger (Marshall 1999). In this trial, a retroviral vector was used to treat a neurodegenerative disorder. However, the vector caused a cytokine release storm in the patient that proved to be fatal. This immunogenicity is cause for concern with the vectors used in gene therapy as well as cell transplants. Most of the allogeneic stem cell-based therapies require immunosuppressive therapies (Kim et al. 2003; Schwartz et al. 2012; Selden et al. 2013), and

very good results have been achieved in preclinical animal models (Swijnenburg et al. 2008; Pearl et al. 2011). However, aside from these preclinical animal models, little is still known about the optimal immunosuppressive therapies in humans to enhance cell engraftment. Thus far, large animal models have revealed some improvements in the survival of PSC-derived cells after transplantation with the use of T-cell costimulatory blockade (Chong et al. 2014), indicating an important role of the immune system in the survival of transplanted cells.

The original premise of PSC therapies assumed that these could be performed without or with minimal immunosuppressive therapy. For ESCs, this is because of low expression of MHC molecules on ESCs. However, upon differentiation, ESCs seem to upregulate MHC class I (Drukker et al. 2002). With the discovery of iPSCs, researchers thought they had finally found a way to use autologous cells for regenerative therapies, abolishing the need for immunosuppressive therapies altogether. However, as we discuss in **Chapter 7,** this notion needs to be revised. We now know that iPSCs can be rejected, even in an autologous transplant setting. However, when iPSCs are differentiated to endothelial cells (iPSC-ECs), they may lose their immunogenicity and are accepted by the host immune system like the somatic aortic endothelial cells by local upregulation of the immunosuppressive cytokine IL-10.

In **Chapter 8**, we discuss our efforts to model this immunogenicity of PSCs in a human transplant setting using a humanized BLT mouse model. In this model, NOD-SCID IL2R/g knockout mice are sub-lethally irradiated and transplanted with fetal human bone marrow, liver, and thymus. This model has been described as having superior engraftment of human immune cells compared to earlier developed models (Lan et al. 2006; Melkus et al. 2006). This model has shown robust immune responses in HIV infections and other infectious diseases (Brehm et al. 2014), as well as in studies modeling skin and human islet graft rejection (Xiao et al. 2014). However, the model has not been extensively examined for stem cell transplant studies. One recent study confirmed the infiltration of immune cells within the grafts, but graft persistence was not assessed in an accurate way. It should be noted that $CD3^+$ immune cell infiltration does not necessarily equate graft rejection and may actually be the result of residing anergic or senescent immune cells. This phenomenon is also seen in cancer tissues in which immune cell infiltration occurs but does not result in rejection due to "tolerizing" effects (Zou 2005). However, as was seen in our BLT mice, the immune system was actually targeting host tissue, resulting in auto-immune responses and an inability of the mice to reject the stem cell grafts. T-cell presence was established in our grafts, but single-cell PCR analysis revealed T-cell exhaustion signs over time, further supporting the notion that T-cells can be present within the grafts without causing graft rejection.

PSC TUMORIGENICITY AND IMMUNOGENICITY: IT'S NOT ALL BAD…

Although a further understanding of PSC characteristics is needed to make these cells safe for transplantation, they have already proven useful in certain cases. For more than a century, there have been reports of the use of embryonic tissue and cells for priming the immune system to target cancer, with some promising results (Li et al. 2009; Yaddanapudi et al. 2012; Inoue 2013). However, as with regenerative therapies, the use of embryonic tissue has never moved passed the preclinical stages. As is described in **Chapter 9,** iPSCs have a great overlap in tumor-associated and tumor-specific antigens with various types of cancer. Combining a similar epitope profile of these cells with their immunogenicity could make them potent surrogate cells to prime the immune system for targeting various types of cancer. In this chapter, we show that this is indeed feasible for breast cancer, melanoma, and mesothelioma. Priming mice with iPSCs in combination with the adjuvant CpG resulted in increased antigen presentation within the draining lymph nodes with subsequent upregulation of effector/memory helper and cytotoxic T-cells. With this immune profile, mice were able to fully reject or significantly reduce tumor growth. Using CyTOF (cytometry by time of flight) analysis and the citrus algorithm we identified the intra-tumor immune profile responsible for this tumor immunity. We then demonstrated that the iPSC-based vaccine could be used to reactivate the immune system in mice that already had established cancer. These mice were treated with the vaccine after resection of their primary tumor and had a reduction in tumor recurrence in their resection areas and a diminished tumor load in their lymph nodes. This study shows the potential of iPSC-based tumor vaccines to prime the immune system and build immunity against cancer either prophylactically or therapeutically as a (neo) adjuvant therapy.

REFERENCES

Amado, L. C., A. P. Saliaris, K. H. Schuleri, M. St John, J. S. Xie, S. Cattaneo, . . . J. M. Hare (2005). "Cardiac repair with intramyocardial injection of allogeneic mesenchymal stem cells after myocardial infarction." Proc Natl Acad Sci U S A 102(32): 11474-11479.

Boncoraglio, G. B., A. Bersano, L. Candelise, B. A. Reynolds and E. A. Parati (2010). "Stem cell transplantation for ischemic stroke." Cochrane Database Syst Rev(9): CD007231.

Brehm, M. A., M. V. Wiles, D. L. Greiner and L. D. Shultz (2014). "Generation of improved humanized mouse models for human infectious diseases." J Immunol Methods 410: 3-17.

Chong, J. J., X. Yang, C. W. Don, E. Minami, Y. W. Liu, J. J. Weyers, . . . C. E. Murry (2014). "Human embryonic-stem-cell-derived cardiomyocytes regenerate non-human primate hearts." Nature 510(7504): 273-277.

Dezawa, M., H. Ishikawa, Y. Itokazu, T. Yoshihara, M. Hoshino, S. Takeda, . . . Y. Nabeshima (2005). "Bone marrow stromal cells generate muscle cells and repair muscle degeneration." Science 309(5732): 314-317.

Drukker, M., G. Katz, A. Urbach, M. Schuldiner, G. Markel, J. Itskovitz-Eldor, . . . N. Benvenisty (2002). "Characterization of the expression of MHC proteins in human embryonic stem cells." Proc Natl Acad Sci U S A 99(15): 9864-9869.

Fisher, S. A., C. Doree, A. Mathur, D. P. Taggart and E. Martin-Rendon (2016). "Stem cell therapy for chronic ischaemic heart disease and congestive heart failure." Cochrane Database Syst Rev 12: CD007888.

Garber, K. (2015). "RIKEN suspends first clinical trial involving induced pluripotent stem cells." Nat Biotechnol 33(9): 890-891.

Inoue, H., Watanabe, A., Sakamoto, C., Narusawa, M., Hiramoto, T., Miyamoto, S., Inoue, M., Takayama, K., Hasegawa, M., and Nakanishi, Y. (2013). "Vaccination With Irradiated Induced Pluripotent Stem Cells Genetically Engineered To Produce GM-CSF Confers Potent T Cells-Mediated Antitumor Immunity." Blood 122: 4492.

Kim, H. J., C. Y. Park, Y. H. Park, Y. J. Kim, D. W. Kim, W. S. Min and C. C. Kim (2003). "Successful allogeneic hematopoietic stem cell transplantation using triple agent immunosuppression in severe aplastic anemia patients." Bone Marrow Transplant 31(2): 79-86.

Kohn, D. B., M. Sadelain and J. C. Glorioso (2003). "Occurrence of leukaemia following gene therapy of X-linked SCID." Nat Rev Cancer 3(7): 477-488.

Lan, P., N. Tonomura, A. Shimizu, S. Wang and Y. G. Yang (2006). "Reconstitution of a functional human immune system in immunodeficient mice through combined human fetal thymus/liver and CD34+ cell transplantation." Blood 108(2): 487-492.

Li, Y., H. Zeng, R. H. Xu, B. Liu and Z. Li (2009). "Vaccination with human pluripotent stem cells generates a broad spectrum of immunological and clinical responses against colon cancer." Stem Cells 27(12): 3103-3111.

Mandai, M., Y. Kurimoto and M. Takahashi (2017). "Autologous Induced Stem-Cell-Derived Retinal Cells for Macular Degeneration." N Engl J Med 377(8): 792-793.

Marshall, E. (1999). "Gene therapy death prompts review of adenovirus vector." Science 286(5448): 2244-2245.

Melkus, M. W., J. D. Estes, A. Padgett-Thomas, J. Gatlin, P. W. Denton, F. A. Othieno, . . . J. V. Garcia (2006). "Humanized mice mount specific adaptive and innate immune responses to EBV and TSST-1." Nat Med 12(11): 1316-1322.

Okita, K., T. Ichisaka and S. Yamanaka (2007). "Generation of germline-competent induced pluripotent stem cells." Nature 448(7151): 313-317.

Pearl, J. I., A. S. Lee, D. B. Leveson-Gower, N. Sun, Z. Ghosh, F. Lan, . . . J. C. Wu (2011). "Short-term immunosuppression promotes engraftment of embryonic and induced pluripotent stem cells." Cell Stem Cell 8(3): 309-317.

Pittenger, M. F., A. M. Mackay, S. C. Beck, R. K. Jaiswal, R. Douglas, J. D. Mosca, . . . D. R. Marshak (1999). "Multilineage potential of adult human mesenchymal stem cells." Science 284(5411): 143-147.

Prockop, D. J. (1997). "Marrow stromal cells as stem cells for nonhematopoietic tissues." Science 276(5309): 71-74.

Riegler, J., M. Tiburcy, A. Ebert, E. Tzatzalos, U. Raaz, O. J. Abilez, . . . J. C. Wu (2015). "Human Engineered Heart Muscles Engraft and Survive Long Term in a Rodent Myocardial Infarction Model." Circ Res 117(8): 720-730.

Schwartz, S. D., J. P. Hubschman, G. Heilwell, V. Franco-Cardenas, C. K. Pan, R. M. Ostrick, . . . R. Lanza (2012). "Embryonic stem cell trials for macular degeneration: a preliminary report." Lancet 379(9817): 713-720.

Selden, N. R., A. Al-Uzri, S. L. Huhn, T. K. Koch, D. M. Sikora, M. D. Nguyen-Driver, . . . R. D. Steiner (2013). "Central nervous system stem cell transplantation for children with neuronal ceroid lipofuscinosis." J Neurosurg Pediatr 11(6): 643-652.

Swijnenburg, R. J., S. Schrepfer, J. A. Govaert, F. Cao, K. Ransohoff, A. Y. Sheikh, . . . J. C. Wu (2008). "Immunosuppressive therapy mitigates immunological rejection of human embryonic stem cell xenografts." Proc Natl Acad Sci U S A 105(35): 12991-12996.

Takahashi, K., K. Tanabe, M. Ohnuki, M. Narita, T. Ichisaka, K. Tomoda and S. Yamanaka (2007). "Induction of pluripotent stem cells from adult human fibroblasts by defined factors." Cell 131(5): 861-872.

Takahashi, K. and S. Yamanaka (2006). "Induction of pluripotent stem cells from mouse embryonic and adult fibroblast cultures by defined factors." Cell 126(4): 663-676.

Trounson, A. and C. McDonald (2015). "Stem Cell Therapies in Clinical Trials: Progress and Challenges." Cell Stem Cell 17(1): 11-22.

Turner, M., S. Leslie, N. G. Martin, M. Peschanski, M. Rao, C. J. Taylor, . . . I. Wilmut (2013). "Toward the development of a global induced pluripotent stem cell library." Cell Stem Cell 13(4): 382-384.

Union, E. (2012). "The 2012 Ageing Report." European Economy.

van Berlo, J. H., O. Kanisicak, M. Maillet, R. J. Vagnozzi, J. Karch, S. C. Lin, . . . J. D. Molkentin (2014). "c-kit+ cells minimally contribute cardiomyocytes to the heart." Nature 509(7500): 337-341.

Xiao, F., L. Ma, M. Zhao, G. Huang, V. Mirenda, A. Dorling, . . . G. Lombardi (2014). "Ex vivo expanded human regulatory T cells delay islet allograft rejection via inhibiting islet-derived monocyte chemoattractant protein-1 production in CD34+ stem cells-reconstituted NOD-scid IL2rgammanull mice." PLoS One 9(3): e90387.

Yaddanapudi, K., R. A. Mitchell, K. Putty, S. Willer, R. K. Sharma, J. Yan, . . . J. W. Eaton (2012). "Vaccination with embryonic stem cells protects against lung cancer: is a broad-spectrum prophylactic vaccine against cancer possible?" PLoS One 7(7): e42289.

Zou, W. (2005). "Immunosuppressive networks in the tumor environment and their therapeutic relevance." Nat Rev Cancer 5(4): 263-274.

Chapter 11

Future Perspectives

GENE AND PSC THERAPY FOR REGENERATIVE MEDICINE

The results of this thesis demonstrate the potential of gene and PSC therapy for vascular diseases but also point to the associated immunogenicity and tumorigenicity challenges. We show that regenerative therapies could benefit from the vector CoMiP to induce PSCs by reducing costs and decreasing the time of reprogramming, but this vector may induce an increase in immunogenicity. For clinical gene therapies, the MC vector may be a better candidate due to a high transfection efficiency and reduced immunogenicity (because of a lack of bacterial backbone). These advantages of MCs were confirmed *in vivo* in our experiments using an MC IL-10 to reduce the pro-inflammatory environment within aortic aneurysm tissue.

For iPSC therapies, the premise after their discovery was that they could be created from a patient's own tissue and transplanted back to them as a "personalized medicine" without the need for immunosuppressive regiments. This thesis, however, shows that the source of iPSCs is very important for the quality of the cells and that iPSCs from a diabetic source have a decreased regenerative potential. Additionally, we show that undifferentiated iPSCs are immunogenic upon transplantation into the same recipient but that this immunogenicity is abolished upon the differentiation of these cells. Both findings are important for the field of regenerative medicine because it could imply moving away from personalized cell therapies and focusing more on stem cell banks with iPSCs from healthy sources. This would in turn likely necessitate the use of some sort of immunosuppressive measures, given either to the cells or to the recipients. Even if our focus remains on personalized medicine, we need to make sure that we transplant fully differentiated cell grafts to avoid immunogenicity against remnant undifferentiated iPSCs. Another avenue that is being pursued to reduce immunogenicity is creating hypoimmunogenic pluripotent cell lines by genetically editing cells to limit HLA class I and II expression (Lu et al. 2013, Chen et al. 2015, Wang et al. 2015). Although HLA class I was successfully knocked out and the cell lines were able to avoid $CD8^+$ cytotoxicity, these cells were more susceptible to natural killer (NK) cell killing because of the "missing-self theory" (Bix et al. 1991, Liao et al. 1991). More recently, researchers were able to address this by overexpressing HLA-E to provide an inhibitory signal to NK cells, thereby reducing NK cell-mediated lysis (Gornalusse et al. 2017).

Immunogenicity, however, is not the only concern with undifferentiated PSCs. This thesis also provides a detailed description of some of the implicated tumorigenic properties, such as self-renewal, rapid proliferation, lack of contact inhibition, and telomerase activity. These properties, as well as similarities in their genetic profile, reveal similarities with cancer cells. These findings should caution us when preparing cell grafts for clinical use by making sure

they are devoid of undifferentiated cells or having built-in safety mechanisms, such as suicide genes that are incorporated in the transplanted cells (Cao et al. 2007, Jones et al. 2014).

The key findings of this thesis suggest that it is important to focus on alternative ways to increase the safety of regenerative therapies. For gene therapy, this could mean efforts to increase site-specificity with gene editing and using vectors with limited to no immunogenicity. One example is the use of "clustered regularly interspaced short palindromic repeats" (CRISPR), a technology that is based on the defense mechanism of prokaryotic organisms to use DNA strands of previously destroyed viral DNA sequences to help them destroy similar DNA sequences. Using this principle, CRISPR can be used to cleave specific strands of DNA. The addition of the Cas9 enzyme allows for the recognition of specific DNA sequences in this cleaving process to direct targeted gene editing. For vascular disease, this type of gene editing is being explored to reduce systemic cholesterol levels by reducing *in vivo* the PCSK9 gene that has been associated with LDL hypercholesterolemia (Ding et al. 2014, Chadwick et al. 2017). In addition, this technology can introduce heterologous DNA using the CRISP-assisted insertion tagging (CRISPaint) (Schmid-Burgk et al. 2016). In this setting, a minicircle could be used to introduce genetic material without the risk of inserting bacterial backbone DNA.

Although CRISPR-Cas9 has better precision than other gene-editing techniques, such as transcription activator-like effector nucleases (TALEN) and zinc finger nuclease (ZFN), with genetic alterations limited to the immediate vicinity of target sites and distal off-target sequences, recent studies have reported the occurrence of larger on-target deletions and genomic rearrangements (Kosicki et al. 2018). With numerous clinical trials underway using CRIPR-Cas9-edited cells, it is important to keep in mind that these genomic mutations may induce tumorigenicity in these cells. Therefore, extensive genomic screening on the edited cells should be required before using them in regenerative therapy.

Another challenge with gene therapy has been delivery. This is especially true for naked genetic molecules due to problems such as breakdown, reduced uptake, rapid renal clearance, and immunogenicity (Chen et al. 2015). To circumvent these issues, nanoparticles have proven effective for gene delivery (Yin et al. 2014). More recently, studies have developed organ-specificity for nanoparticles towards the liver (Dong et al. 2014) and endothelial cells (Khan et al. 2018) in pre-clinical primate models. The latter is particularly interesting for vascular disease by showing knockdown of a target gene with a small interfering RNA (siRNA) nanoparticle that was preferentially delivered to endothelial cells. However, although no direct adverse events were seen for the duration of the study, no long-term data have been obtained. Nevertheless, this was the first study to show the efficacy of cell-

directed gene therapy using nanoparticles in a non-human primate model that may pave the way to translating these therapies for multiple vascular diseases involving endothelial cells.

With regard to cell therapies, PSCs have the potential to become the focus of next-generation tissue regeneration. The premise of iPSC-derived cell transplantation was that these cells could integrate within the injured tissue to regenerate the damaged organ. However, intra-cardiac injection with PSC-derived cardiomyocytes has shown us that these cells sit within the heart, and despite their maturation over time, they do not couple with healthy tissue (Riegler et al. 2015). Additional preparation of the cells *in vitro* could potentially overcome this issue. For example, cells could be cultured in 3D conditions by creating scaffolds, perhaps in combination with vascularization, after which this *in vitro* generated tissue can be transplanted. Various laboratories are exploring these avenues for iPSC-based tissue generation and have been able to generate beating patches of heart tissue (Masumoto et al. 2014, Tiburcy et al. 2017), small liver buds (Takebe et al. 2014), and kidney organoids (Takasato et al. 2015). With recent advances in gene therapy, one could envision applying gene-editing the iPSCs to patients with genetic disorders, followed by *in vitro* generation of organs or tissues to replace the diseased ones. In this context, it will be important to map the immunogenic properties of iPSCs in more detail at different stages of the reprogramming and differentiation process to address the immunogenic properties of iPSCs and their derivatives. To do this, further optimization of the humanized mouse model could prove useful in modeling the human immune response towards allogeneic or syngeneic stem cell grafts. As was described in this thesis, this optimization should focus on the reconstitution of humanized mice with important human cytokines to allow for innate immune responses. Additionally, the development of NSG mice that transgenically express HLA molecules in their thymus will permit HLA-restricted T cell selection for both human and murine antigens, thereby limiting auto-immune responses in humanized mice. Having an adequate model for PSC immunogenicity would help optimizing immunosuppressive regiments and possibly reduce the duration of their administration.

IPSC TECHNOLOGY FOR DRUG SCREENING

Another focus of iPSC technology is *in vitro* drug screening. Here, iPSCs could be differentiated into the cell type of interest to test the efficacy of a specific drug (Liang et al. 2013, Zhang et al. 2014, Tzatzalos et al. 2016). In addition, iPSCs could be differentiated into various cells to assess off-target drug toxicity to different tissues (Burridge et al. 2016). In theory, it would be possible to assess which type of drug shows the best efficacy to the target organ without causing toxicity to other organs. This type of personalized medicine has the potential to select the optimal drug for a patient by assessing the efficacy and identify-

ing drug toxicity before it is given to the patient. This transformative drug screening can significantly expedite treatment and cut healthcare costs from drug-related toxicity.

In addition, iPSCs can be used as a cancer development model for cancer drug screening or as a renewable source of differentiated immune cells (Kooreman 2018). Firstly, they could be utilized for filling in the gaps in our understanding of the development of cancer, specifically the oncogenic mutations and epigenetic changes that lead to the malignant transformation of a cell. In this regard, pluripotent cells have already proven to be a useful platform (Hochedlinger et al. 2004). More recently, iPSC technology (Takahashi et al. 2007) has been used to model the development of several types of cancer. For instance, iPSCs derived from pancreatic ductal adenocarcinoma (PDAC) were transplanted into immunodeficient mice, which led to the generation of pancreatic intraepithelial neoplasia, a progenitor of PDAC. This progenitor later progressed to a metastatic stage that was influenced by the newly discovered HNF4a gene network (Kim et al. 2013). Similarly, iPSCs derived from Li Fraumeni Syndrome (LFS) patients were differentiated into osteoblasts that recapitulated the features leading to osteosarcoma (Lee et al. 2015). Based on this *in vitro* model of osteosarcoma modeling in LFS patients, researchers were able to identify the gene H19 as a mediator in suppressing LFS-associated osteosarcoma. Another cancer that iPSC-modeling has proven useful for is juvenile myelomonocytic leukemia (JMML), for which there is limited access to patient tissue. However, using iPSCs, scientists were able to generate a renewable source of myeloid cells that reconstituted the phenotype of JMML (Gandre-Babbe et al. 2013).

Additionally, iPSCs have provided important insights into the BCR-ABL mutation that drives cell expansion in chronic myeloid leukemia (CML). iPSCs generated from the human blast crisis stage CML (KBM7) revealed that, unlike the parental cancer line, KBM7-derived iPSCs lose their dependency on BCR-ABL signaling. An important clinical consequence of this finding is that these iPSCs are not susceptible to BCR-ABL inhibitor treatment, including Imatinib. This specific epigenetic stage may explain the heterogeneity in Imatinib drug responses and the limited effectiveness of the therapy for cells in a specific differentiated epigenetic stage (Carette et al. 2010). Another area of drug screening in which iPSCs have proven useful is in the modeling of glioma tumor-initiating cells (GTICs), which can originate from the transformation of neural progenitor cells (NPCs) (Sancho-Martinez et al. 2016). After validating the drug screening potential of iPSC-derived NPCs (iNPSCs), the model was used to test 101 anti-cancer compounds, several of which turned out to be strong therapeutics against iNPCs that were then validated on GTIC tumors. Using the iPSC-derived cancer model, one study conducted *in vitro* drug screening using an AKR1B10 inhibitor that demonstrated *in vitro* efficacy and safety for a patient with hepatocellular carcinoma. Based on these results, the patient was then treated with the AKR1B10 inhibitors, which led to a reduction of the tumor within three months (Moriguchi and Madson 2013).

IPSC TECHNOLOGY FOR CANCER IMMUNOTHERAPY

Finally, iPSCs could serve as a renewable source of differentiated immune cells that may help boost the host's immune system. Several immune cells have been created from iPSCs for cancer immunotherapy. For instance, iPSCs have been differentiated into myelomonocytic cells, including dendritic cells, macrophages, and Langerhans cells (Choi et al. 2009). These cells can be used for *in vitro* loading with cancer-related antigens to be introduced to patients for inducing cancer immunity (Sabado et al. 2017). Another way to boost the host immunity to fight cancer is by infusion with cancer-specific T cells. The idea is to isolate cancer-specific cytotoxic T cells (CTLs) from a patient, activate and expand them *in vitro* so that they can be given to the same patient later. iPSCs derived from cancer-specific CTLs can be differentiated back into CTLs in high yields that retain their antigen specificity (Nishimura et al. 2013, Vizcardo et al. 2013). iPSC-derived T-cells can even be modified to express chimeric antigen receptors (CARs), as Themeli et al. (2013) demonstrated with an anti-CD19 CAR to inhibit the growth of human Burkitt lymphoma in a xenogeneic tumor model. Similarly, NK cells can be differentiated from iPSCs for cancer therapy on a clinical scale (Knorr et al. 2013). In addition, NK T cells, a small subset of peripheral blood cells with NK cell properties but also expressing T cell receptors, have been successfully differentiated from murine iPSCs (Watarai et al. 2010), but the therapeutic roles of NKTs in cancer therapy and their clinical relevance are yet to be determined (Berzins and Ritchie 2014).

Furthermore, this thesis also describes the tumorigenic and immunogenic properties of iPSCs that could be harnessed to creating cancer vaccines. The overlap of various tumor-associated and tumor-specific antigens makes this cell type an ideal surrogate therapy for multiple cancers. For clinical applications, iPSCs could be generated from non-invasively acquired cells (Loh et al. 2009, Zhou et al. 2012). These iPSCs could then be expanded and made available as a vaccine several weeks after a cancer diagnosis. At the time of surgery or as an addition to adjuvant chemo- or radiotherapy, these iPSCs could be used to reactivate the immune system in targeting remnant cancer cells. As a true vaccine, another possible application could be priming the immune system from a certain age before tumor onset. With age, we now know that in many cases tumor growth or progression is the result of a diminished surveillance function of the immune system, either by evasion or overwhelming the immune system (Swann and Smyth 2007). This increase in the incidence of cancer from a certain age has led to several screening programs to detect cancer before clinical manifestation (e.g., Bowel Cancer Population Screening Programme, Breast Cancer Screening Programme, *Dutch National Institute for Public Health and Environment).* At the appropriate age, it may one day be possible to prophylactically administer iPSC vaccines to high-risk individuals, which will help boost their immune system to target a variety of cancers before development occurs or to treat them at an early stage.

REFERENCES

Berzins, S. P. and D. S. Ritchie (2014). "Natural killer T cells: drivers or passengers in preventing human disease?" Nat Rev Immunol **14**(9): 640-646.

Bix, M., N. S. Liao, M. Zijlstra, J. Loring, R. Jaenisch and D. Raulet (1991). "Rejection of class I MHC-deficient haemopoietic cells by irradiated MHC-matched mice." Nature **349**(6307): 329-331.

Burridge, P. W., Y. F. Li, E. Matsa, H. Wu, S. G. Ong, A. Sharma, . . . J. C. Wu (2016). "Human induced pluripotent stem cell-derived cardiomyocytes recapitulate the predilection of breast cancer patients to doxorubicin-induced cardiotoxicity." Nat Med **22**(5): 547-556.

Cao, F., M. Drukker, S. Lin, A. Y. Sheikh, X. Xie, Z. Li, . . . J. C. Wu (2007). "Molecular imaging of embryonic stem cell misbehavior and suicide gene ablation." Cloning Stem Cells **9**(1): 107-117.

Carette, J. E., J. Pruszak, M. Varadarajan, V. A. Blomen, S. Gokhale, F. D. Camargo, . . . T. R. Brummelkamp (2010). "Generation of iPSCs from cultured human malignant cells." Blood **115**(20): 4039-4042.

Chadwick, A. C., X. Wang and K. Musunuru (2017). "In Vivo Base Editing of PCSK9 (Proprotein Convertase Subtilisin/Kexin Type 9) as a Therapeutic Alternative to Genome Editing." Arterioscler Thromb Vasc Biol **37**(9): 1741-1747.

Chen, H., Y. Li, X. Lin, D. Cui, C. Cui, H. Li and L. Xiao (2015). "Functional disruption of human leukocyte antigen II in human embryonic stem cell." Biol Res **48**: 59.

Chen, J., X. Dong, T. Feng, L. Lin, Z. Guo, J. Xia, . . . X. Chen (2015). "Charge-conversional zwitterionic copolymer as pH-sensitive shielding system for effective tumor treatment." Acta Biomater **26**: 45-53.

Choi, K. D., M. A. Vodyanik and Slukvin, II (2009). "Generation of mature human myelomonocytic cells through expansion and differentiation of pluripotent stem cell-derived lin-CD34+CD43+CD45+ progenitors." J Clin Invest **119**(9): 2818-2829.

Ding, Q., A. Strong, K. M. Patel, S. L. Ng, B. S. Gosis, S. N. Regan, . . . K. Musunuru (2014). "Permanent alteration of PCSK9 with in vivo CRISPR-Cas9 genome editing." Circ Res **115**(5): 488-492.

Dong, Y., K. T. Love, J. R. Dorkin, S. Sirirungruang, Y. Zhang, D. Chen, . . . D. G. Anderson (2014). "Lipopeptide nanoparticles for potent and selective siRNA delivery in rodents and nonhuman primates." Proc Natl Acad Sci U S A **111**(11): 3955-3960.

Gandre-Babbe, S., P. Paluru, C. Aribeana, S. T. Chou, S. Bresolin, L. Lu, . . . M. J. Weiss (2013). "Patient-derived induced pluripotent stem cells recapitulate hematopoietic abnormalities of juvenile myelomonocytic leukemia." Blood **121**(24): 4925-4929.

Gornalusse, G. G., R. K. Hirata, S. E. Funk, L. Riolobos, V. S. Lopes, G. Manske, . . . D. W. Russell (2017). "HLA-E-expressing pluripotent stem cells escape allogeneic responses and lysis by NK cells." Nat Biotechnol **35**(8): 765-772.

Hochedlinger, K., R. Blelloch, C. Brennan, Y. Yamada, M. Kim, L. Chin and R. Jaenisch (2004). "Reprogramming of a melanoma genome by nuclear transplantation." Genes Dev **18**(15): 1875-1885.

Jones, B. S., L. S. Lamb, F. Goldman and A. Di Stasi (2014). "Improving the safety of cell therapy products by suicide gene transfer." Front Pharmacol **5**: 254.

Khan, O. F., P. S. Kowalski, J. C. Doloff, J. K. Tsosie, V. Bakthavatchalu, C. B. Winn, . . . D. G. Anderson (2018). "Endothelial siRNA delivery in nonhuman primates using ionizable low-molecular weight polymeric nanoparticles." Sci Adv **4**(6): eaar8409.

Kim, J., J. P. Hoffman, R. K. Alpaugh, A. D. Rhim, M. Reichert, B. Z. Stanger, . . . K. S. Zaret (2013). "An iPSC line from human pancreatic ductal adenocarcinoma undergoes early to invasive stages of pancreatic cancer progression." Cell Rep **3**(6): 2088-2099.

Knorr, D. A., Z. Ni, D. Hermanson, M. K. Hexum, L. Bendzick, L. J. Cooper, . . . D. S. Kaufman (2013). "Clinical-scale derivation of natural killer cells from human pluripotent stem cells for cancer therapy." Stem Cells Transl Med **2**(4): 274-283.

Kooreman, N. G., Wu, J.C. (2018). "How induced pluripotent stem cells can further cancer therapies." ResearchGate.

Kosicki, M., K. Tomberg and A. Bradley (2018). "Repair of double-strand breaks induced by CRISPR-Cas9 leads to large deletions and complex rearrangements." Nat Biotechnol **36**(8): 765-771.

Lee, D. F., J. Su, H. S. Kim, B. Chang, D. Papatsenko, R. Zhao, . . . I. R. Lemischka (2015). "Modeling familial cancer with induced pluripotent stem cells." Cell **161**(2): 240-254.

Liang, P., F. Lan, A. S. Lee, T. Gong, V. Sanchez-Freire, Y. Wang, . . . J. C. Wu (2013). "Drug screening using a library of human induced pluripotent stem cell-derived cardiomyocytes reveals disease-specific patterns of cardiotoxicity." Circulation **127**(16): 1677-1691.

Liao, N. S., M. Bix, M. Zijlstra, R. Jaenisch and D. Raulet (1991). "MHC class I deficiency: susceptibility to natural killer (NK) cells and impaired NK activity." Science **253**(5016): 199-202.

Loh, Y. H., S. Agarwal, I. H. Park, A. Urbach, H. Huo, G. C. Heffner, . . . G. Q. Daley (2009). "Generation of induced pluripotent stem cells from human blood." Blood **113**(22): 5476-5479.

Lu, P., J. Chen, L. He, J. Ren, H. Chen, L. Rao, . . . L. Xiao (2013). "Generating hypoimmunogenic human embryonic stem cells by the disruption of beta 2-microglobulin." Stem Cell Rev **9**(6): 806-813.

Masumoto, H., T. Ikuno, M. Takeda, H. Fukushima, A. Marui, S. Katayama, . . . J. K. Yamashita (2014). "Human iPS cell-engineered cardiac tissue sheets with cardiomyocytes and vascular cells for cardiac regeneration." Sci Rep **4**: 6716.

Moriguchi, H. and J. Madson (2013). "The reprogramming therapy for a patient with advanced hepatocellular carcinoma by using human-induced pluripotent stem (iPS) cells technology." BMJ Case Rep **2013**.

Nishimura, T., S. Kaneko, A. Kawana-Tachikawa, Y. Tajima, H. Goto, D. Zhu, . . . H. Nakauchi (2013). "Generation of rejuvenated antigen-specific T cells by reprogramming to pluripotency and redifferentiation." Cell Stem Cell **12**(1): 114-126.

Riegler, J., M. Tiburcy, A. Ebert, E. Tzatzalos, U. Raaz, O. J. Abilez, . . . J. C. Wu (2015). "Human Engineered Heart Muscles Engraft and Survive Long Term in a Rodent Myocardial Infarction Model." Circ Res **117**(8): 720-730.

Sabado, R. L., S. Balan and N. Bhardwaj (2017). "Dendritic cell-based immunotherapy." Cell Res **27**(1): 74-95.

Sancho-Martinez, I., E. Nivet, Y. Xia, T. Hishida, A. Aguirre, A. Ocampo, . . . J. C. Izpisua Belmonte (2016). "Establishment of human iPSC-based models for the study and targeting of glioma initiating cells." Nat Commun **7**: 10743.

Schmid-Burgk, J. L., K. Honing, T. S. Ebert and V. Hornung (2016). "CRISPaint allows modular base-specific gene tagging using a ligase-4-dependent mechanism." Nat Commun **7**: 12338.

Swann, J. B. and M. J. Smyth (2007). "Immune surveillance of tumors." J Clin Invest **117**(5): 1137-1146.

Takahashi, K., K. Tanabe, M. Ohnuki, M. Narita, T. Ichisaka, K. Tomoda and S. Yamanaka (2007). "Induction of pluripotent stem cells from adult human fibroblasts by defined factors." Cell **131**(5): 861-872.

Takasato, M., P. X. Er, H. S. Chiu, B. Maier, G. J. Baillie, C. Ferguson, . . . M. H. Little (2015). "Kidney organoids from human iPS cells contain multiple lineages and model human nephrogenesis." Nature **526**(7574): 564-568.

Takebe, T., R. R. Zhang, H. Koike, M. Kimura, E. Yoshizawa, M. Enomura, . . . H. Taniguchi (2014). "Generation of a vascularized and functional human liver from an iPSC-derived organ bud transplant." Nat Protoc **9**(2): 396-409.

Tiburcy, M., J. E. Hudson, P. Balfanz, S. Schlick, T. Meyer, M. L. Chang Liao, . . . W. H. Zimmermann (2017). "Defined Engineered Human Myocardium With Advanced Maturation for Applications in Heart Failure Modeling and Repair." Circulation **135**(19): 1832-1847.

Tzatzalos, E., O. J. Abilez, P. Shukla and J. C. Wu (2016). "Engineered heart tissues and induced pluripotent stem cells: Macro- and microstructures for disease modeling, drug screening, and translational studies." Adv Drug Deliv Rev **96**: 234-244.

Vizcardo, R., K. Masuda, D. Yamada, T. Ikawa, K. Shimizu, S. Fujii, . . . H. Kawamoto (2013). "Regeneration of human tumor antigen-specific T cells from iPSCs derived from mature CD8(+) T cells." Cell Stem Cell **12**(1): 31-36.

Wang, D., Y. Quan, Q. Yan, J. E. Morales and R. A. Wetsel (2015). "Targeted Disruption of the beta2-Microglobulin Gene Minimizes the Immunogenicity of Human Embryonic Stem Cells." Stem Cells Transl Med **4**(10): 1234-1245.

Watarai, H., S. Fujii, D. Yamada, A. Rybouchkin, S. Sakata, Y. Nagata, . . . M. Taniguchi (2010). "Murine induced pluripotent stem cells can be derived from and differentiate into natural killer T cells." J Clin Invest **120**(7): 2610-2618.

Yin, H., R. L. Kanasty, A. A. Eltoukhy, A. J. Vegas, J. R. Dorkin and D. G. Anderson (2014). "Non-viral vectors for gene-based therapy." Nat Rev Genet **15**(8): 541-555.

Zhang, M., C. D'Aniello, A. O. Verkerk, E. Wrobel, S. Frank, D. Ward-van Oostwaard, . . . M. Bellin (2014). "Recessive cardiac phenotypes in induced pluripotent stem cell models of Jervell and Lange-Nielsen syndrome: disease mechanisms and pharmacological rescue." Proc Natl Acad Sci U S A **111**(50): E5383-5392.

Zhou, T., C. Benda, S. Dunzinger, Y. Huang, J. C. Ho, J. Yang, . . . M. A. Esteban (2012). "Generation of human induced pluripotent stem cells from urine samples." Nat Protoc **7**(12): 2080-2089.

NEDERLANDSE SAMENVATTING

Zoals besproken in de introductie, zal de toename in de levensverwachting van de mens waarschijnlijk leiden tot een toename van chronische ziekten (Union 2012). Met name de weefsels van organen met weinig herstellend vermogen, zoals het brein en het hart, zullen bijdragen aan de verhoogde ziektelast. Om dit te bestrijden, zoeken onderzoekers al jaren naar verschillende manieren om weefsels te regenereren; zoals bijvoorbeeld gen- of celtherapie. Deze methoden worden in detail besproken in **Hoofdstuk 2,** waarbij dit proefschrift zich met name richt op de regeneratieve behandelingen voor aandoeningen van het vaatstelsel.

REGENERATIEVE THERAPIEËN

De afgelopen twee decennia bestonden celtherapieën uit het gebruik van progenitorcellen of volwassen stamcellen (Prockop 1997, Pittenger et al. 1999, Amado et al. 2005, Dezawa et al. 2005). De preklinische studies hadden veelbelovende resultaten, waardoor deze celtypen nu worden getest in diverse klinische studies (Boncoraglio et al. 2010, Fisher et al. 2016). Gedacht wordt dat het werkingsmechanisme van deze cellen lijkt te bestaan uit, 1) paracriene effecten die worden losgelaten door deze cellen in het beschadigde weefsel, of 2) transdifferentiatie en integratie van de volwassen stamcellen in het celtype wat beschadigd is geraakt. Dit laatste mechanisme is echter controversieel en lijkt maar in mindere mate daadwerkelijk voor te komen (van Berlo et al. 2014). Op dit moment worden volwassen stamcellen met name gezien als multipotent en kiemlaag-specifiek.

Sinds de eerste isolatie van menselijke embryonale stamcellen (hESCs) in 1998, hebben onderzoekers gekeken naar de diverse doeleinden waarvoor deze cellen gebruikt kunnen worden (Trounson and McDonald 2015). Alhoewel vele celtypen sindsdien zijn ontwikkeld uit deze hESCs, blijven de ethische bezwaren met betrekking tot het gebruik van embryonaal weefsel voor regeneratieve therapieën bestaan. Hierdoor zullen hESCs waarschijnlijk nooit hun volledige potentie bereiken.

In 2006 heeft Shinya Yamanaka ontdekt dat volwassen cellen konden worden geprogrammeerd naar een pluripotente staat, vanwaaruit, vergelijkbaar met ESCs, diverse typen cellen kunnen worden ontwikkeld (Takahashi and Yamanaka 2006). Deze ontdekking kwam tot stand door goed te kijken naar het genexpressie profiel van ESCs en die genen te vinden die verantwoordelijk zijn voor het behoud van pluripotentie. Door deze genen (Oct4, cMyc, KLF4 en Sox2) te verpakken als virale deeltjes en een volwassen cel daarmee te infecteren, was zijn groep in staat om deze volwassen cellen pluripotent te maken. Deze geïnduceerde pluripotente stamcellen (iPSCs) zijn vergelijkbaar met ESCs in morfologie, eigenschappen en potentie om alle cellen te vormen van de drie kiemlagen. Een jaar later liet dezelfde groep

zien dat het creëren van iPSCs ook mogelijk was voor menselijke cellen (Takahashi et al. 2007). Hiermee werd een compleet nieuw onderzoeksgebied geopend voor regeneratieve therapieën. Samen worden ESCs en iPSCs gezien als pluripotente stamcellen.

In **Hoofdstuk 3** beschrijven we twee genvectoren die gebruikt kunnen worden voor gentherapie en voor het reprogrammeren van somatische cellen tot iPSCs. Allereerst beschrijven we een nieuwe methode die het relatief complexe en tijdrovende reprogrammeren van somatische cellen vereenvoudigt door het reprogrammeren met een gebruiksvriendelijk plasmide; het codon-geoptimaliseerde mini-intronic plasmide (CoMiP). Door de vier reprogrammeringsgenen in een MIP te plaatsen (4-in-1 CoMiP), hebben we bona fide iPSCs weten te creëeren van verschillende donor cellen, waaronder PBMCs (bloedcellen). In vergelijking met andere DNA-gebaseerde reprogrammeringsmethoden, zoals minicircle of de Yamanaka individuele plasmiden, is de CoMiP methode sneller en goedkoper in het creëeren van pluripotente cellen van somatische cellen. Daarnaast, als appendix van hoofdstuk 3, wordt het gebruik van een codon-geoptimaliseerde 4-in-1 minicircle (CoMiC) beschreven voor het reprogrammeren van somatische cellen. In vergelijk met conventionele plasmiden, bestaan de non-virale minicircles (MC) uit dicht opgewonden DNA-moleculen die kleiner zijn dan een normaal plasmide en geen bacteriële replicatie cassette meer hebben. Deze eigenschappen maken MCs uitermate geschikt voor gentherapie omdat ze, 1) door hun kleine formaat een hogere transfectie efficiëntie hebben en, 2) zonder bacterieel DNA verminderd immunogeen zijn.

Ten behoeve van gentherapie, hebben we in **Hoofdstuk 4** een MC gebruikt voor de systemische overexpressie van IL-10 in het angiotensine II-infusie-ApoE-/- AAA muismodel van aortale aneurysma's. Infusie van MC IL-10 leidde tot significante reductie van de aorta diameter op dag 28 en verhoogde de dissectie-vrije overleving van 21.5% in controle muizen naar 62.3% in MC IL-10 behandelde muizen.

Naast gentherapie is er een extra gebied dat veel aandacht heeft gekregen in de laatste twee decennia: PSC therapie. In **Hoofdstuk 5** richtten we ons op het gebruik van iPSCs in een model van perifeer vaatlijden in patiënten met diabetes. Een belangrijke vraag die we hebben behandeld in dit hoofdstuk is of de bron van iPSCs belangrijk is voor de uiteindelijke effectiviteit van het celproduct. Om deze vraag te beantwoorden, zijn iPSCs van diabetische en niet-diabetische muizen gecreëerd en gedifferentieerd tot endotheelcellen (ECs) om het regeneratieve potentieel te bepalen in een achterpoot ischemie model. De bevindingen van deze studie lieten zien dat iPSC-ECs van diabetische donor cellen een verminderde regeneratieve capaciteit hadden in vergelijk met de iPSC-ECs van gezonde donoren. Deze resultaten zijn erg belangrijk voor het gebruik van gedifferentieerde cellen van iPSCs in de toekomst, omdat ze ons laten zien dat we deze cellen moeten creëren van gezonde donoren

voor het beste klinische resultaat. In de praktijk zal het gebruik van patiënt-specifieke iPSCs niet alleen gelimiteerd worden door de hoge kosten and "good manufacturing practices" (Turner et al. 2013), maar ook door het feit dat deze patiënt-specifieke iPSCs dus niet altijd zullen resulteren in de beste klinische resultaten.

Over het algemeen wordt het duidelijk dat regeneratieve therapieën met stamcellen grote potentie heeft. De therapeutische en regeneratieve mogelijkheden van deze cellen worden nu onderzocht in preklinische, maar ook klinische studies (Trounson and McDonald 2015, Mandai et al. 2017). Echter, de intrinsieke eigenschappen van deze cellen, alsmede de methode waarmee deze cellen worden gecreëerd, hebben gezorgd voor twijfel over de veiligheid van het gebruik van deze cellen. Deze worden geadresseerd in dit proefschrift.

KLINISCHE OBSTAKELS VOOR REGENERATIEVE THERAPIEËN

Tumorgeniciteit

Het gebruik van gen- en celtherapie voor regeneratieve therapieën is niet van de laatste tijd en de eerste onderzoeken dateren al van enkele decennia geleden. Hoewel deze therapieën al een tijd bestaan, heeft het gebruik hiervan ons over de tijd wel een aantal belangrijke lessen geleerd. Een voorbeeld hiervan is een rapport over het ontstaan van leukemie na behandeling met gentherapie (Kohn et al. 2003). Deze nadelige effecten hebben geleid tot een toename in de voorzichtigheid met betrekking tot gen- en celtherapie en diepgaander onderzoek in de effecten van beide therapieën. Echter, zelfs met de hieruit voortgevloeide regels en kennis over gen- en celtherapie, komen tegenslagen tot op de dag van vandaag voor. Een goed voorbeeld hiervan is de gestarte klinische trial in Riken, Japan voor het gebruik van retina pigmentcellen (gecreëerd vanuit iPSCs) in de behandeling van maculadegeneratie. Deze was kortdurend gestaakt in verband met mutagenese van de getransplanteerde cellen (Garber 2015).

Zoals beschreven in **Hoofdstuk 6,** is een risicofactor voor gentherapie en de ontwikkeling van iPSCs dat we nog onvoldoende weten wat de incorporatie van (gecorrigeerde) genen doen met de functionaliteit van het genoom. Zeker in de gevallen waar een vector integreert in het genoom kan de plaats waar integratie plaatsvindt leiden tot activatie van pro-oncogenen. Dit geldt voor gentherapie, maar ook voor de generatie van iPSCs, waarbij de eerste generatie iPSCs te maken hadden met reactivatie van het cMyc gen dat leidde tot tumorgenese (Okita et al. 2007). Maar ook de intrinsieke eigenschappen van pluripotente cellen eisen voorzichtigheid in hun gebruik voor regeneratieve therapieën. Want hoewel preklinische onderzoeken ons al hebben geleerd dat ongedifferentieerde PSCs teratomen vormen na transplantatie, hebben meer recente onderzoeken uitgewezen dat zelfs >90% pure gedifferentieerde grafts kunnen leiden tot tumor formatie (Riegler et al. 2015). En deze

bevindingen baren onderzoekers zorgen als er gekeken wordt naar verdere implementatie van deze therapieën voor de behandeling van patiënten.

Immunogeniciteit

Een van de grootste limitaties van gen- en celtherapie is de immuunrespons tegen vectoren en celtypen. Zoals beschreven in dit proefschrift, kan de immunogeniciteit van genvectoren zeer nadelige effecten hebben. Een voorbeeld hiervan is het overlijden van een patiënt aan een cytokinestorm, nadat deze met een retrovirale vector werd behandeld voor een neurodegeneratieve aandoening (Marshall 1999). Immunogeniciteit is niet alleen een nadelig effect van gentherapie, maar ook van celtherapie. De meeste allogene stamceltherapieën worden ondersteund door immuunsuppressie (Kim et al. 2003, Schwartz et al. 2012, Selden et al. 2013) en alhoewel goede resultaten zijn behaald in preklinische diermodellen (Swijnenburg et al. 2008, Pearl et al. 2011), is nog maar weinig bekend over de optimale immuunsuppressie om langdurige celoverleving te bevorderen in mensen. Tot dusver hebben preklinische onderzoeken in grotere diermodellen voordeel laten zien in het gebruik van T-cel co-stimulatoire blockade medicatie ter bevordering van de overleving van PSC-grafts (Chong et al. 2014). Deze resultaten laten zien dat er een belangrijke rol is voor het immuunsysteem in de overleving van getransplanteerde PSC-gerelateerde cellen.

De belofte van PSC-therapieën was dat de cellen konden worden gebruikt zonder, of met minimale immuunsuppressiva. Voor ESCs komt dit door de lage expressie van MHC moleculen op de ESCs. Echter, na differentiatie vindt er een upregulatie plaats van de MHC klasse I moleculen (Drukker et al. 2002). Na de ontdekking van iPSCs, hadden onderzoekers het idee dat ze een manier hadden gevonden om autologe cellen te gebruiken waardoor er helemaal geen noodzaak zou zijn voor immuunsuppressiva. Zoals in **Hoofdstuk 7** duidelijk is geworden, hebben we deze voorspelling enigszins moeten herzien. In dit hoofdstuk beschrijven we namelijk dat iPSCs worden afgestoten door het immuunsysteem, zelfs als deze autoloog worden getransplanteerd. Na differentiatie van iPSCs naar endotheelcellen (iPSC-ECs) verliezen deze cellen echter weer hun immunogeniciteit en werden geaccepteerd door het immuunsysteem op eenzelfde manier als somatische cellen door middel van upregulatie van het immuunsuppressieve cytokine IL-10.

In **Hoofstuk 8** proberen we vervolgens de immunogeniciteit van PSCs in de setting van een menselijk immuunsysteem te modelleren. Hiervoor gebruiken we een gehumaniseerde BLT muis. In dit model worden NOD-SCID IL2R/g knockout bestraald en getransplanteerd met foetaal menselijk beenmerg, lever en thyus (BLT). Humanisatie van het immuunsysteem van deze muizen is superieur aan eerdere beschreven muismodellen (Lan et al. 2006, Melkus et al. 2006). Vervolgens is met dit model al aangetoond dat er een robuuste immuunrespons kan worden opgewekt tegen HIV infecties en andere infectieuze ziekten (Brehm et al. 2014), alsmede in studies naar de afstoting van menselijke huid en pancreas eilandjes (Xiao et

al. 2014). Voor stamceltransplantatie studies is dit model echter nog niet uitvoerig getest. Een recente studie heeft infiltratie van immuuncellen in getransplanteerde menselijke grafts laten zien, maar graft overleving werd niet op een juiste manier geanalyseerd doordat T-cel infiltratie binnen de grafts niet automatisch betekent dat een graft wordt afgestoten. Ook "uitgeputte" of geïnactiveerde T-cellen kunnen aanwezig zijn binnen een graft, zoals bijvoorbeeld ook wordt gezien binnen kankerweefsel (Zou 2005).

Binnen onze BLT muizen werd het menselijk immuunsysteem echter wel geactiveerd, maar viel het hierbij het eigen weefsel van de muis aan wat resulteerde in een auto-immuunrespons. Deze langdurige activatie van het menselijk immuunsysteem tegen muis antigenen verhinderde hierdoor op een later moment een immuunrespons tegen de stamcel grafts. Binnen deze grafts waren T-cellen wel aanwezig, maar single-cell PCR analyse liet vermoeide en geïnactiveerde T-cellen zien. Met deze resultaten werd wederom aangetoond dat T-cellen binnen grafts aanwezig kunnen zijn zonder dat dat leidt tot afstoting.

PSC TUMORGENICITEIT EN IMMUNOGENICITEIT: NIET ALLEEN MAAR NADELEN...

Alhoewel er nog grote vooruitgangen moeten worden geboekt in ons begrip over de eigenschappen van PSCs om ze volledig veilig te maken voor transplantatie, kunnen ze nu al wel bruikbaar zijn voor bepaalde behandelingen. Al ruim een eeuw bestaan beschrijvingen over het gebruik van embryonaal weefsel om het immuunsysteem te activeren tegen kanker. Hiervan zijn een aantal met veelbelovende resultaten (Li et al. 2009, Yaddanapudi et al. 2012). Echter, vergelijkbaar met regeneratieve therapieën, zal het gebruik van embryonaal weefsel ook voor deze vorm van therapie niet snel voorbij de pre-klinische fase komen. Zoals wordt beschreven in **Hoofdstuk 9** hebben iPSCs ook een grote overlap in tumor-geassocieerde en tumor-specifieke antigenen met diverse typen kanker. De combinatie van het vergelijkbare epitopen profiel en de immunogeniciteit van iPSCs maken dat dit celtype als surrogaat kan worden gebruikt om het immuunsysteem te activeren tegen diverse kankertypen. In dit hoofdstuk laten we inderdaad zien dat dit het geval is voor borstkanker, melanoom en voor mesothelioom. Muizen vaccineren met iPSCs in combinatie met het adjuvant CpG resulteerde in verhoogde antigeen presentatie in de drainerende lymfeklieren waarop verhoging van het aantal effector/geheugen helper en cytotoxische T-cellen plaatsvond. Met dit immuunprofiel waren muizen in staat om de tumorgroei volledig of partieel te inhiberen. Met behulp van CyTOF analyses en het citrus algoritme hebben we vervolgens de immuuncellen geidentificeerd die verantwoordelijk waren voor deze kanker immuniteit. Hierna gingen we nog een stap verder door aan te tonen dat het iPSC vaccin gebruikt kon worden om het immuunsysteem te reactiveren tegen al bestaande kanker. De muizen in deze studie werden behandeld met het vaccin na resectie van de primaire tumor en hadden

minder terugkeer van kanker in het resectiegebied en verminderde tumor aanwezigheid in de drainerende lymfeklieren.

De resultaten van dit proefschrift beschrijven de potentie van gen- en celtherapie voor verschillende vaataandoeningen, maar geven ook een gedetailleerde beschrijving van de immunogeniciteit en tumorgeniciteit die hiermee geassocieerd zijn. Voor de verdere implementatie van deze therapieën zal hier rekening mee moeten worden gehouden door bijvoorbeeld de inbouw van "zelfmoord genen" in de getransplanteerde cellen, die voor celdood zorgen als er ongewenste groei of mutatie van het transplantaat plaatsvindt (Cao et al. 2007, Jones et al. 2014). Daarnaast zullen de nieuwe ontwikkelingen in het creëren van universele donorcellen, die het immuunsysteem niet activeren, waarschijnlijk een belangrijke rol gaan spelen (Lu et al. 2013, Chen et al. 2015, Wang et al. 2015, Bix et al. 1991, Liao et al. 1991, Gornalusse et al. 2017). Tot slot beschrijft dit proefschrift dat de immunogene en tumorgene eigenschappen van iPSCs ook gebruikt kunnen worden als vaccin tegen kanker. De overlap in tumor-specifieke en tumor-geassocieerde eiwitten maakt dit celtype een goede surrogaat om immuun activiteit tegen kankercellen te creëren.

REFERENCES

Amado, L. C., A. P. Saliaris, K. H. Schuleri, M. St John, J. S. Xie, S. Cattaneo, . . . J. M. Hare (2005). "Cardiac repair with intramyocardial injection of allogeneic mesenchymal stem cells after myocardial infarction." Proc Natl Acad Sci U S A 102(32): 11474-11479.

Bix, M., N. S. Liao, M. Zijlstra, J. Loring, R. Jaenisch and D. Raulet (1991). "Rejection of class I MHC-deficient haemopoietic cells by irradiated MHC-matched mice." Nature **349**(6307): 329-331.

Boncoraglio, G. B., A. Bersano, L. Candelise, B. A. Reynolds and E. A. Parati (2010). "Stem cell transplantation for ischemic stroke." Cochrane Database Syst Rev(9): CD007231.

Brehm, M. A., M. V. Wiles, D. L. Greiner and L. D. Shultz (2014). "Generation of improved humanized mouse models for human infectious diseases." J Immunol Methods 410: 3-17.

Cao, F., M. Drukker, S. Lin, A. Y. Sheikh, X. Xie, Z. Li, . . . J. C. Wu (2007). "Molecular imaging of embryonic stem cell misbehavior and suicide gene ablation." Cloning Stem Cells **9**(1): 107-117.

Chen, H., Y. Li, X. Lin, D. Cui, C. Cui, H. Li and L. Xiao (2015). "Functional disruption of human leukocyte antigen II in human embryonic stem cell." Biol Res **48**: 59.

Chong, J. J., X. Yang, C. W. Don, E. Minami, Y. W. Liu, J. J. Weyers, . . . C. E. Murry (2014). "Human embryonic-stem-cell-derived cardiomyocytes regenerate non-human primate hearts." Nature 510(7504): 273-277.

Dezawa, M., H. Ishikawa, Y. Itokazu, T. Yoshihara, M. Hoshino, S. Takeda, . . . Y. Nabeshima (2005). "Bone marrow stromal cells generate muscle cells and repair muscle degeneration." Science 309(5732): 314-317.

Drukker, M., G. Katz, A. Urbach, M. Schuldiner, G. Markel, J. Itskovitz-Eldor, . . . N. Benvenisty (2002). "Characterization of the expression of MHC proteins in human embryonic stem cells." Proc Natl Acad Sci U S A 99(15): 9864-9869.

Fisher, S. A., C. Doree, A. Mathur, D. P. Taggart and E. Martin-Rendon (2016). "Stem cell therapy for chronic ischaemic heart disease and congestive heart failure." Cochrane Database Syst Rev 12: CD007888.

Garber, K. (2015). "RIKEN suspends first clinical trial involving induced pluripotent stem cells." Nat Biotechnol 33(9): 890-891.

Gornalusse, G. G., R. K. Hirata, S. E. Funk, L. Riolobos, V. S. Lopes, G. Manske, . . . D. W. Russell (2017). "HLA-E-expressing pluripotent stem cells escape allogeneic responses and lysis by NK cells." Nat Biotechnol **35**(8): 765-772.

Inoue, H., Watanabe, A., Sakamoto, C., Narusawa, M., Hiramoto, T., Miyamoto, S., Inoue, M., Takayama, K., Hasegawa, M., and Nakanishi, Y. (2013). "Vaccination With Irradiated Induced Pluripotent Stem Cells Genetically Engineered To Produce GM-CSF Confers Potent T Cells-Mediated Antitumor Immunity." Blood 122: 4492.

Jones, B. S., L. S. Lamb, F. Goldman and A. Di Stasi (2014). "Improving the safety of cell therapy products by suicide gene transfer." Front Pharmacol **5**: 254.

Kim, H. J., C. Y. Park, Y. H. Park, Y. J. Kim, D. W. Kim, W. S. Min and C. C. Kim (2003). "Successful allogeneic hematopoietic stem cell transplantation using triple agent immunosuppression in severe aplastic anemia patients." Bone Marrow Transplant 31(2): 79-86.

Kohn, D. B., M. Sadelain and J. C. Glorioso (2003). "Occurrence of leukaemia following gene therapy of X-linked SCID." Nat Rev Cancer 3(7): 477-488.

Lan, P., N. Tonomura, A. Shimizu, S. Wang and Y. G. Yang (2006). "Reconstitution of a functional human immune system in immunodeficient mice through combined human fetal thymus/liver and CD34+ cell transplantation." Blood 108(2): 487-492.

Li, Y., H. Zeng, R. H. Xu, B. Liu and Z. Li (2009). "Vaccination with human pluripotent stem cells generates a broad spectrum of immunological and clinical responses against colon cancer." Stem Cells 27(12): 3103-3111.

Liao, N. S., M. Bix, M. Zijlstra, R. Jaenisch and D. Raulet (1991). "MHC class I deficiency: susceptibility to natural killer (NK) cells and impaired NK activity." Science **253**(5016): 199-202.

Lu, P., J. Chen, L. He, J. Ren, H. Chen, L. Rao, . . . L. Xiao (2013). "Generating hypoimmunogenic human embryonic stem cells by the disruption of beta 2-microglobulin." Stem Cell Rev **9**(6): 806-813

Mandai, M., Y. Kurimoto and M. Takahashi (2017). "Autologous Induced Stem-Cell-Derived Retinal Cells for Macular Degeneration." N Engl J Med 377(8): 792-793.

Marshall, E. (1999). "Gene therapy death prompts review of adenovirus vector." Science 286(5448): 2244-2245.

Melkus, M. W., J. D. Estes, A. Padgett-Thomas, J. Gatlin, P. W. Denton, F. A. Othieno, . . . J. V. Garcia (2006). "Humanized mice mount specific adaptive and innate immune responses to EBV and TSST-1." Nat Med 12(11): 1316-1322.

Okita, K., T. Ichisaka and S. Yamanaka (2007). "Generation of germline-competent induced pluripotent stem cells." Nature 448(7151): 313-317.

Pearl, J. I., A. S. Lee, D. B. Leveson-Gower, N. Sun, Z. Ghosh, F. Lan, . . . J. C. Wu (2011). "Short-term immunosuppression promotes engraftment of embryonic and induced pluripotent stem cells." Cell Stem Cell 8(3): 309-317.

Pittenger, M. F., A. M. Mackay, S. C. Beck, R. K. Jaiswal, R. Douglas, J. D. Mosca, . . . D. R. Marshak (1999). "Multilineage potential of adult human mesenchymal stem cells." Science 284(5411): 143-147.

Prockop, D. J. (1997). "Marrow stromal cells as stem cells for nonhematopoietic tissues." Science 276(5309): 71-74.

Riegler, J., M. Tiburcy, A. Ebert, E. Tzatzalos, U. Raaz, O. J. Abilez, . . . J. C. Wu (2015). "Human Engineered Heart Muscles Engraft and Survive Long Term in a Rodent Myocardial Infarction Model." Circ Res 117(8): 720-730.

Schwartz, S. D., J. P. Hubschman, G. Heilwell, V. Franco-Cardenas, C. K. Pan, R. M. Ostrick, . . . R. Lanza (2012). "Embryonic stem cell trials for macular degeneration: a preliminary report." Lancet 379(9817): 713-720.

Selden, N. R., A. Al-Uzri, S. L. Huhn, T. K. Koch, D. M. Sikora, M. D. Nguyen-Driver, . . . R. D. Steiner (2013). "Central nervous system stem cell transplantation for children with neuronal ceroid lipofuscinosis." J Neurosurg Pediatr 11(6): 643-652.

Swijnenburg, R. J., S. Schrepfer, J. A. Govaert, F. Cao, K. Ransohoff, A. Y. Sheikh, . . . J. C. Wu (2008). "Immunosuppressive therapy mitigates immunological rejection of human embryonic stem cell xenografts." Proc Natl Acad Sci U S A 105(35): 12991-12996.

Takahashi, K., K. Tanabe, M. Ohnuki, M. Narita, T. Ichisaka, K. Tomoda and S. Yamanaka (2007). "Induction of pluripotent stem cells from adult human fibroblasts by defined factors." Cell 131(5): 861-872.

Takahashi, K. and S. Yamanaka (2006). "Induction of pluripotent stem cells from mouse embryonic and adult fibroblast cultures by defined factors." Cell 126(4): 663-676.

Trounson, A. and C. McDonald (2015). "Stem Cell Therapies in Clinical Trials: Progress and Challenges." Cell Stem Cell 17(1): 11-22.

Turner, M., S. Leslie, N. G. Martin, M. Peschanski, M. Rao, C. J. Taylor, . . . I. Wilmut (2013). "Toward the development of a global induced pluripotent stem cell library." Cell Stem Cell 13(4): 382-384.

Union, E. (2012). "The 2012 Ageing Report." European Economy.

van Berlo, J. H., O. Kanisicak, M. Maillet, R. J. Vagnozzi, J. Karch, S. C. Lin, . . . J. D. Molkentin (2014). "c-kit+ cells minimally contribute cardiomyocytes to the heart." Nature 509(7500): 337-341.

Wang, D., Y. Quan, Q. Yan, J. E. Morales and R. A. Wetsel (2015). "Targeted Disruption of the beta2-Microglobulin Gene Minimizes the Immunogenicity of Human Embryonic Stem Cells." Stem Cells Transl Med **4**(10): 1234-1245.

Xiao, F., L. Ma, M. Zhao, G. Huang, V. Mirenda, A. Dorling, . . . G. Lombardi (2014). "Ex vivo expanded human regulatory T cells delay islet allograft rejection via inhibiting islet-derived monocyte chemoattractant protein-1 production in CD34+ stem cells-reconstituted NOD-scid IL2rgammanull mice." PLoS One 9(3): e90387.

Yaddanapudi, K., R. A. Mitchell, K. Putty, S. Willer, R. K. Sharma, J. Yan, . . . J. W. Eaton (2012). "Vaccination with embryonic stem cells protects against lung cancer: is a broad-spectrum prophylactic vaccine against cancer possible?" PLoS One 7(7): e42289.

Zou, W. (2005). "Immunosuppressive networks in the tumor environment and their therapeutic relevance." Nat Rev Cancer 5(4): 263-274.

ACKNOWLEDGEMENTS

Even though the completion of the above-mentioned research projects is partly the result of hard work, dedication and persistence; this thesis would not exist without the guidance and help of a special group of people over the years:

Dear Joe...as I am writing this section, I have come to realize that no amount of words is sufficient in thanking you for the opportunities and guidance you have provided me over the years. Having said that, please allow me to highlight some memorable moments for the readers of this thesis.

I have seen your lab grow from when I first joined it in 2010 to when I left the second time in 2015. During that period, the immense increase in the number of lab members has never stopped you from sitting down with me and discuss the projects I was working on. I have fond memories of those times scribbling on the whiteboard in your office to map out the next stages. In executing them, you always had my back and if needed, put me in contact with the right people to further the experiments.

Overall, I could not have wished for a better mentor.

Dear Jaap and Paul. Thank you both for the opportunities, support and guidance over the years. But most of all, thank you for providing me with a place to come home to upon my leaving Stanford. Without you both this transition would have been a lot harder.

To my "paranymfen", Joris and Maarten. You have been incremental at various stages leading up to the defense of this thesis. Joris, T4L is where it all started, and that philosophy is very much true today. Maarten, looking back at our time together, the most consistent thing has been "work hard, play hard". This was true for our time at Stanford, but also for our time in The Hague.

Both of you are great friends and I am proud to have you by my side during these memorable stages in my PhD.

To the Tsao boys. Uwe; During the rise and fall of Heisenberg you have become the best and most welcome distraction from the lab at times. And Matti, for our very...very early trips to Halfmoon Bay and Pacifica on the weekends and the love your family has shown me.

To Patricia. The voice in my head for a long time early on in the PhD programme. I cannot thank you enough for your advice and help in setting up some of the experiments. You are one of the smartest, meticulous and hardworking people I know and I owe a lot to your teachings.

To Craig and in loving memory of Ed. My family. Just referring to you as my landlords does not do you both justice. You were truly like family and I loved living in the cottage those few years and meeting up for Ed's infamous Martini's.

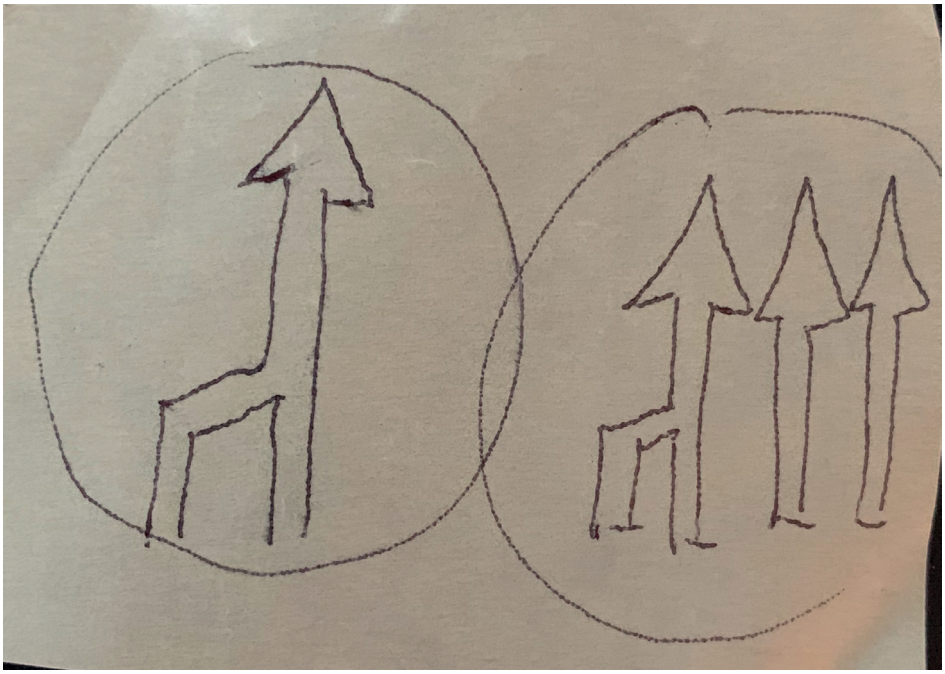
To the Peets girls. Having been customer of the week twice says it all. I loved coming in for coffee and spend some time hanging at the counter.

To the Wu-labbers. I have been most fortunate to have worked in a lab with such gifted people. I will never forget the collaborative spirit that made so much of the projects possible.

My colleagues and the surgeons in the HMC and the LUMC. A special thanks to Bert, Lex and Sven for creating an environment for me to develop myself as a HPB surgeon, as well as expanding my research efforts.

The Stanford connection. Dear Patrick and Jan; thank you for laying the foundations for such an amazing collaboration. Dear Koen and Rutger-Jan; many thanks for your guidance and advice.

And last, but not least. To my family and Veriene. Who were on the receiving end and shared in my laboratory ups and downs. Thank you for your love and support, and please know that you were incremental to every word in this thesis.



Road to Success.
Graphic description of opportunities and possible paths to take (G.J.D. van Acker)

CURRICULUM VITAE

The author of this thesis was born on March 4th, 1986 in Rotterdam, The Netherlands. He grew up in the small village of Hazerswoude-Dorp and attended the Stedelijk Gymnasium High School in Leiden. After graduating in 2004, he was accepted to medical school at the University of Leiden.

While attending medical school he was an active member of the student association Leidse Studenten Vereniging Minerva. In addition to his studies, he worked as an allocation officer at the Eurotransplant International Foundation. This further peaked his interest in surgery and resulted in him joining the Transplant Surgery research group at the Leiden University Medical Center, which ultimately led to the opportunity to do a research rotation within the laboratory of Joseph C. Wu at the Cardiovascular Institute at Stanford University. The experience within the Cardiovascular Institute was one of such excitement and personal development, that he decided to join dr. Wu's lab for a second term after finishing his clinical rotations and receiving his medical degree from Leiden University.

After receiving grants from the VSBfonds, the Prof. Michael-van Vloten Foundation, Ketel 1 funds and Hendrik Muller foundation, he moved back to Stanford University for a post-doctoral position, looking into the immunogenic and tumorigenic properties of pluripotent stem cells, such as ESCs and iPSCs. This utimately led to the development of the iPSC-based cancer vaccine, which was patented last year and further efforts are made at Stanford, as well as in Leiden to move testing of the vaccine to human conditions.

In addition to his research, he was a teaching assistent for the highschool summer program at the Cardiovascular Institute for three years.

At this point, he lives with his wife Veriene in The Hague and is in the fifth year of his surgical training in the Haaglanden Medical Center and Leiden University Medical Center. He still devotes time to science and is closely involved with furthering iPSC-based cancer therapies.

LIST OF PUBLICATIONS

2018 Autologous iPSC-based vaccines elicit anti-tumor responses in vivo.
Kooreman NG, Kim Y, de Almeida PE, Termglinchan V, Diecke S, Shao NY, Wei TT, Yi H, Dey D, Nelakanti R, Brouwer TP, Paik DT, Sagiv-Barfi I, Han A, Quax PHA, Hamming JF, Levy R, Davis MM, Wu JC. Cell Stem Cell. *2018 Apr 5;22(4):501-513. e7*

2018 Prolonged survival of transplanted stem cells after ischaemic injury via the slow release of pro-survival peptides from a collagen matrix.
Lee AS, Inayathullah M, Lijkwan MA, Zhao X, Sun W, Park S, Hong WX, Parekh MB, Malkovskiy AV, Lau E, Qin X, Pothineni VR, Sanchez-Freire V, Zhang WY, Kooreman NG, Ebert AD, Chan CKF, Nguyen PK, Rajadas J, Wu JC. Nature Biomedical Engineering. *2018; 2, 104-113*

2018 Systemic Upregulation of IL-10 (Interleukin-10) Using a Nonimmunogenic Vector Reduces Growth and Rate of Dissecting Abdominal Aortic Aneurysm.
Kooreman NG, Adam M, Jagger A, Wagenhäuser M, Mehrkens D, Wang Y, Kayama Y, Toyama K, Raaz U, Schellinger IN, Maegdefessel L, Spin JM, Hamming JF, Quax PHA, Baldus S, Wu JC, Tsao PS. Arteriosclerosis , Trombosis and Vascular Biology. *2018 Jun 7; 38:1796-1805*

2017 Alloimmune responses of humanized mice to human pluripotent stem cell therapeutics.
Kooreman NG, de Almeida PE, Stack JP, Nelakanti RV, Diecke S, Shao NY, Swijnenburg RJ, Sanchez-Freire V, Matsa E, Liu C, Connolly AJ, Hamming JF, Quax PHA, Brehm MA, Greiner DL, Shultz LD, Wu JC. Cell Reports. *2017 Aug 22; 20(8):1978-1990*

2015 Human engineered heart muscles engraft and survive long term in a rodent myocardial infarction model.
Riegler J, Tilburcy M, Ebert A, Tzatzalos E, Raaz U, Abilez OJ, Shen Q, Kooreman NG, Neofytou E, Chen VC, Wang M, Meyer T, Tsao PS, Connolly AJ, Couture LA, Gold JD, Zimmermann WH, Wu JC. Circulation Research. *2015 Sep 25; 117(8):720-30*

2015 Direct evaluation of myocardial viability and stem cell engraftment demonstrates salvage of the injured myocardium.

Kim PJ, Mahmoudi M, Ge X, Matsuura Y, Toma I, Metzler S, Kooreman NG, Ramanus J. et. al~ Yang PC. Circulation Research. *Stem Cell Biol. 2015 32: 4A.8.1 – 4A.8.x.*

2015 Novel codon-optimized mini-intronic plasmid for efficient, inexpensive, and xeno-free induction of pluripotency.
Diecke S, Lu J, Lee J, Termglinchan V, Kooreman NG, Burridge PW, Ebert AD, Churko JM, Sharma A, Kay MA, Wu JC. Scientific Reports. *2015 Jan 28;5:8081.*

2015 Teratoma Formation: A Tool for Monitoring Pluripotency in Stem Cell Research.
Nelakanti RV, Kooreman NG, Wu JC Current Protocols. Stem Cell Biol. *2015 32: 4A.8.1 – 17.*

2014 Transplanted terminally differentiated induced pluripotent stem cells are accepted by immune mechanisms similar to self-tolerance.
Kooreman NG, de Almeida PE, Meyer EH, Diecke S, Dey D, Sanchez-Freire V, Hu S, Ebert A, Odegaard J, Mordwinkin NM, Brouwer TP, Lo D, Montoro DT, Longaker MT, Negrin RS, Wu JC. Nature Communications. *2014 May 30;5:3903.*

2014 Tracking gene and cell fate for therapeutic gain.
Kooreman NG, Ransohoff JD, Wu JC. Nature Materials. *2014 Feb;13(2):106-9.*

2014 Pravastatin reverses obesity-induced dysfunction of induced pluripotent stem cell-derived endothelial cells via a nitric oxide-dependent mechanism.
Gu M, Mordwinkin NM, Kooreman NG, Lee J, Wu H, Hu S, Churko JM, Diecke S, Burridge PW, He C, Barron FE, Ong SG, Gold JD, Wu JC. European Heart Journal. *2014 Nov 2. pii: ehu411.*

2014 Second generation codon optimized minicircle (CoMiC) for nonviral reprogramming of human adult fibroblasts.
Diecke S, Lisowski L, Kooreman NG, Wu JC. Methods Molecular Biology. *2014;1181:1-13.*

2014 Short hairpin RNA gene silencing of prolyl hydroxylase-2 with a minicircle vector improves neovascularization of hindlimb ischemia.
Lijkwan MA, Hellingman AA, Bos EJ, van der Bogt KE, Huang M, Kooreman NG, de Vries MR, Peters HA, Robbins RC, Hamming JF, Quax PH, Wu JC. Human Gene Therapy. *2014 Jan;25(1):41-9.*

2013 Costimulation-Adhesion Blockade is Superior to Cyclosporine A and Prednisone Immunosuppressive Therapy for Preventing Rejection of Differentiated Human Embryonic Stem Cells Following Transplantation.
Huber BC, Ransohoff JD, Ransohoff KJ, Riegler J, Ebert A, Kodo K, Gong Y, Sanchez-Freire V, Dey D, Kooreman NG, Diecke S, Zhang WY, Odegaard J, Gold JD, Robbins RC, Wu JC. Stem Cells*, 2013 Nov;31 (11):2354-63*

2012 Validation of the Donor Risk Index (DRI) in orthotopic liver transplantation within Eurotransplant
Blok JJ, Braat AE, Adam R, Burroughs AK, Putter H, Kooreman NG, Rahmel AO, Porte RJ, Rogiers X, Ringers J. Liver Transplantation. *2012 Jan;18(1):112-9.*

2011 Preclinical Derivation and Imaging of Autologously Transplanted Canine Induced Pluripotent Stem Cells.
Lee AS, Xu D, Nguyen PK, Nag D, Lyons JK, Han L, Hu S, Lan F, Huang M, Liu J, Narsinh KN, Long CT, de Almeida P, Levi B, Kooreman NG, Bangs C, Pacharinsak C, Yeung AC, Gambhir SS, Longaker MT, Wu JC. Journal Biological Chemistry. *2011 Sep 16;286(37):32697-704*

2010 Tumorigenicity of pluripotent stem cells: biological insights from molecular imaging.
Kooreman NG, Wu JC Royal Society Interface *2010 7:S753-S763; doi:10.1098/rsif.2010.0353.focus*